The Geological Evolution of the DeGrussa volcanic-hosted massive sulfide deposit and the Eastern Capricorn Orogen, Western Australia

by

Margaret Louise Hawke

B.Sc (Hons), M. Sc (Econ. Geol.)

CODES, School of Physical Sciences

Submitted in fulfilment of the requirements for the

Doctorate of Philosophy (Geology)

University of Tasmania

August, 2016

Statement and Authority of Access

This thesis contains no material which has been accepted for a degree or diploma by the University or any other institution, except by way of background information and duly acknowledged in the thesis, and to the best of my knowledge and belief no material previously published or written by another person except where due acknowledgement is made in the text of the thesis, nor does the thesis contain any material that infringes copyright.

Margaret L. Hawke

8th August, 2016

This thesis is not to be made available for loan or copying for two years following the date this statement was signed. Following that time, the thesis may be made available for loan and limited copying and communication in accordance with the Copyright Act 1968.

Margaret L. Hawke

8th August, 2016

The publishers of the paper comprising Chapters 6 hold the copyright for that content, and access to the material should be sought from the respective journals. The remaining non published content of the thesis may be made available for loan and limited copying and communication in accordance with the Copyright Act 1968.

Margaret L. Hawke

8th August, 2016

Statement of Co-authorship

The following people and institutions contributed to the publication of work undertaken as part of this thesis:

Candidate:	Margaret L. Hawke (CODES School of Physical Science, University of Tasmania)
Author 1:	Sebastien Meffre (CODES School of Physical Science, University of Tasmania)
Author 2:	Holly Stein (AIRIE Program, Department of Geosciences, Colorado State University and CEED, Centre for Earth Evolution and Dynamics, University of Oslo, Norway)
Author 3:	Paul Hilliard (Sandfire Resources NL, West Perth, W.A., Australia)
Author 4:	Ross Large (CODES School of Physical Science, University of Tasmania)
Author 5:	J. Bruce Gemmell (CODES School of Physical Science, University of Tasmania)

Author details and their roles:

Paper 1: HAWKE, M. L., MEFFRE, S., STEIN, H., HILLIARD, P., LARGE, R. & GEMMELL, J. B. 2015. Geochronology of the DeGrussa Volcanic Hosted Massive Sulfide Deposit and Associated Mineralization of the Yerrida, Bryah and Padbury Basins, Western Australia. *Precambrian Research,* 267, 250-284.

Located in chapter 6.

Candidate was the primary author and with author 4 and author 5 contributed to the conception and design of the research project. Candidate contributed approximately 75% to the planning, execution, interpretation and preparation of the work for the paper. Author 1 contributed to the analytical work for zircon U-Pb and galena/pyrite Pb isotope sample preparation and analysis. Author 2 contributed to the analytical work for molybdenite Re-Os sample preparation and analysis. Author 3 contributed to the understanding of the regional and deposit geology.

Supervisor and Head of School Declaration:
We the undersigned agree with the above stated "proportion of work undertaken" for the above published peer-reviewed manuscript contributing to this thesis:

Signed	Signed
J. Bruce Gemmell	Leonid Danyushevsky
Supervisor	Head of School
CODES, School of Earth Science	School of Earth Sciences
University of Tasmania	University of Tasmania
Date:	Date:

ABSTRACT

The Paleoproterozoic DeGrussa copper-gold–silver, volcanic-hosted massive sulfide (VHMS) deposit is located in the eastern part of the Capricorn Orogen of central Western Australia. The DeGrussa deposit, discovered in 2009, occurs within the c. 2000 Ma Karalundi Formation equivalent sedimentary and mafic rocks (DeGrussa Formation), the lowermost stratigraphy of the Bryah Group. DeGrussa is a siliciclastic - mafic style, VHMS deposit located on the northern limb of the Robinson Range syncline and consists of four primary ore lenses (DeGrussa, Conductor 1, Conductor 4 and Conductor 5), with supergene enrichment of copper, providing a total resource of 12.4Mt @ 4.7% Cu and 1.8g/t Au.

The host rock sequence is turbiditic quartz-rich sandstone and siltstone to fine-grained mudstone rocks. Peperitic basalt intruded the sedimentary rock sequence. The footwall Magazine Member is hematitic, mudstone-rich turbidites, carbonate-dolomite megabreccia and volcanic conglomeritic rocks. The entire sequence is intruded by dolerite sills which postdate the VHMS mineralisation. The DeGrussa host sedimentary rocks overlie the Yerrida Group (Bubble Well Member and Johnson Cairn Formation), with the mafic rocks of the Johnson Cairn Formation interpreted to have formed in a continental rift setting similar to the Guaymas Basin or Red Sea Rift. Geological and geochemical evidence supports the DeGrussa deposit forming in a submarine continental rift.

Dolerites within the host sedimentary rock sequence are tholeiitic, of MORB composition, and have slight REE enrichment suggesting association with seamount and/or hot spot magmatism. The comparable mafic rocks of the Bryah Group, in particular the Narracoota Formation, have a large geochemical variation encompassing tectonic environments from a back arc basin rift to island arc settings. There was a change in basin dynamics from east to west within the Bryah and Yerrida Basins, where an initial continental rift may have progressed into a more open oceanic-rift or back arc tectonic setting. Subduction along margins of the Bryah basin is possible given the boninitic affinities of some mafic rocks of the Narracoota Formations.

The DeGrussa deposit displays mineral zonation atypical of most VHMS deposits, perhaps evident of its replacement style of formation. Magnetite forms in the hottest, central core of the deposit in association with pyrite and lesser chalcopyrite and pyrrhotite. Sphalerite and galena form in rare horizons throughout the ore lenses. Replacement textures indicate parts of the deposit were formed in the sub seafloor environment, although seafloor textures and chimney structures are present.

The Shiraz fault, with reverse sinistral displacement of 500-600m, truncates the southern side of the DeGrussa and Conductor 1 ore lenses, separating them from Conductor 4 and Conductor 5.

The Merlot Fault splays off the Shiraz Fault in a south-westerly direction, approximately 500 m north east of the DeGrussa and C1 ore lenses.

Alteration proximal to the DeGrussa deposit includes chlorite and talc-carbonate. Chlorite schist surrounds the massive sulfide lenses and is generally strongly sheared, although less deformed areas contain disseminated pyrite and chalcopyrite. Talc-chlorite-carbonate (± pyrite ± chalcopyrite) schist occurs within the ore deposit and as lenses along both the upper or lower contacts of the ore bodies where it is separated from mineralisation by chlorite schist.

The pyrite-chalcopyrite-pyrrhotite mineral assemblage and geological evidence suggests that the emplacement of reduced, magmatic-hydrothermal, mineralising fluids, at temperatures of 250-350°C and pH of 5-7, led to replacement of existing sedimentary and basaltic rocks via fault controlled feeder structures. The $\delta^{34}S$ values of +0.3 to +6.3‰ for DeGrussa sulfide is interpreted to represent leached igneous rock sulfur and/or magmatic-hydrothermal sulfur, mixed with minor seawater sulfate to produce the heavy $\delta^{34}S$ tail for pyrite up to +9.8‰. The lack of sulfate minerals in the ore, but the presence of peripheral jasper, suggests that DeGrussa formed in a sub-oxic to oxic, low sulfate oceanic sub-basin from reduced, metal-bearing fluids. Lead isotopes indicate a crustal source of lead.

New age dating indicates the DeGrussa VHMS mineralisation formed between 2011 - 2027 ± 7 Ma (Re-O; n=3) and 2060 - 2075 ± 50 Ma (Pb model ages; n=2) constraining the maximum deposition age for the Bryah Group rocks at c. 2075 Ma. Dolerites (2003 to 1991 ± 7 Ma; n=3) post-date the DeGrussa mineralisation, and regional granodiorites provide the first age for the Narracoota Formation of 2014 - 2018 ± 9 Ma (n = 2). A new model age of 2000 ± 35 Ma for the Horseshoe Lights VHMS deposit suggests it may have developed at a similar time to DeGrussa.

District mineralisation correlates with the major regional orogenic events: the Glenburgh Orogeny from 2005-1960 Ma (DeGrussa and Horseshoe Lights VHMS and Peak Hill and Fiveways orogenic gold deposits), the Capricorn from 1830-1780 Ma (Labouchere, Mt. Pleasant and Nathans orogenic gold deposits) and the Edmundian Orogeny from 1030-955 Ma (Fortnum-Starlight orogenic gold deposit).

These new ages assist in constraining stratigraphy and mineralising events of the Paleoproterozoic Yerrida, Bryah and Padbury Groups and their associations with regional orogenic events. Identification of prospective time periods and stratigraphy associated with major mineralising events will assist in exploration for significant gold and base metal mineralisation in the Capricorn Orogen.

TABLE OF CONTENTS

TABLE OF FIGURES

Chapter 4

Chapter 8

LIST OF TABLES

~ ACKNOWLEGEMENTS ~

Sandfire Resources staff, past and present, including John Evans, Paul Hilliard, Shannan Bamforth, Ian O'Grady, Murray Thompson, Rita Care, Karl Simich, Paul Lauricella, Allan Wynne, Jo Condon, Ernie Schmidt, Andy Hansen, Emine Hussein, Lynley Rattray, Kath Gray, Vivienne Buckle, the original and best field team Rob Sinclair and Clinton Shay, and the rest of the exploration team between 2007-2012.

To the geologists at various companies, for the interesting discussions: Bob Jeffery (Sandfire) who provided the maps, and proof reading of early drafts; Peter Neumayr (SIPA); Graeme, Oliver Judd (Talisman Mining); Cam McCuaig and John Reeves (UWA) for access to Horseshoe Lights samples; David Reid (Ventnor Resources); Albert Thamm, David Jones, Miles Kennedy, Duncan Foster (RNI); and other geologists I have encountered along the way including Bryan Krapez, Sue Thornett, Sandi Occhipinti and Kath Grey (GSWA); Simon Johnson (GSWA) for editorial comments on the paper (chapter 6) which made not only the paper awesome, but improved the thesis substantially; at UTas my supervisors Bruce Gemmell, Ross Large, Garry Davidson, and Sebastien Meffre, plus other UTas staff Tony Crawford, Sasha Stepanovic, Paul Olin, Elena Lounejeva, Sarah Gilbert, Izzy Von Lichten and Karin Orth. As well as all my other supportive friends in both Perth and Hobart who have been persistent with my constant promise of 'six more months!', for their proof reading abilities and ability to distract me at the times when I needed it most - Jeni Savage, Tom Less, Cat Matus, Ben McCormack, Sid Brown, Barbara Millner, Nat Bonnici, Sarah Howe, Rowena Salter, Tristan King, Indrani Mukerjee, Richelle Pascual, James Hyatt, Jodi Fox, Sean Johnson, Alex Cherry and Moochi.

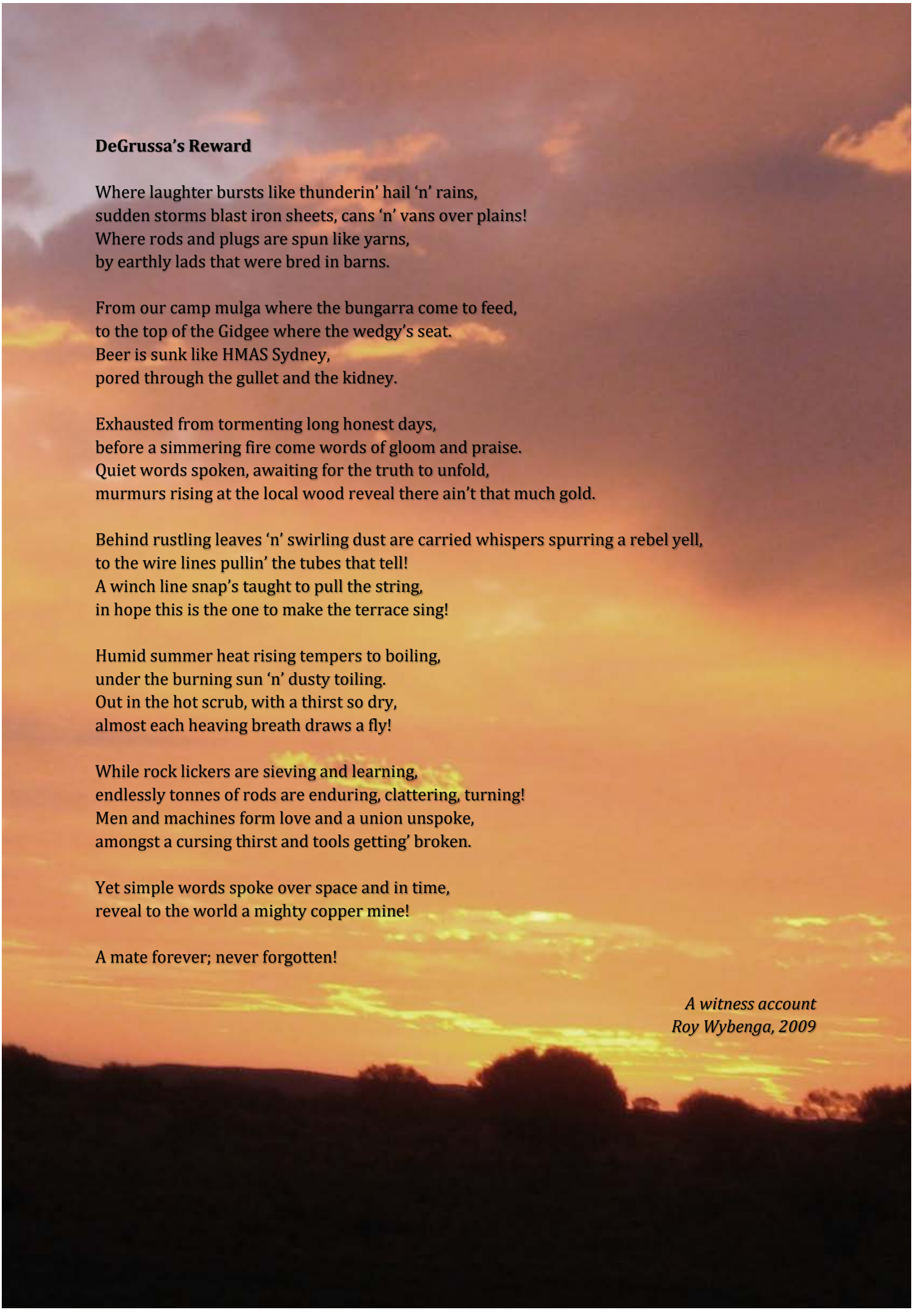

DeGrussa's Reward

Where laughter bursts like thunderin' hail 'n' rains,
sudden storms blast iron sheets, cans 'n' vans over plains!
Where rods and plugs are spun like yarns,
by earthly lads that were bred in barns.

From our camp mulga where the bungarra come to feed,
to the top of the Gidgee where the wedgy's seat.
Beer is sunk like HMAS Sydney,
pored through the gullet and the kidney.

Exhausted from tormenting long honest days,
before a simmering fire come words of gloom and praise.
Quiet words spoken, awaiting for the truth to unfold,
murmurs rising at the local wood reveal there ain't that much gold.

Behind rustling leaves 'n' swirling dust are carried whispers spurring a rebel yell,
to the wire lines pullin' the tubes that tell!
A winch line snap's taught to pull the string,
in hope this is the one to make the terrace sing!

Humid summer heat rising tempers to boiling,
under the burning sun 'n' dusty toiling.
Out in the hot scrub, with a thirst so dry,
almost each heaving breath draws a fly!

While rock lickers are sieving and learning,
endlessly tonnes of rods are enduring, clattering, turning!
Men and machines form love and a union unspoke,
amongst a cursing thirst and tools getting' broken.

Yet simple words spoke over space and in time,
reveal to the world a mighty copper mine!

A mate forever; never forgotten!

A witness account
Roy Wybenga, 2009

The author with drill core from DGDD001 in 2009

"The most exciting phrase to hear in science, the one that heralds new discoveries, is not 'Eureka!' but 'That's funny…."

-Isaac Asimov

Chapter 1. Introduction

1.1. Project Location and Description

The Paleoproterozoic DeGrussa copper-gold–silver, volcanic-hosted massive sulfide (VHMS) deposit is located in the eastern part of the Capricorn Orogen of central Western Australia. The DeGrussa deposit was discovered in 2009 within an interfingering sequence of sedimentary and mafic volcanic rocks, equivalent to the c. 2000 Ma Karalundi Formation and Narracoota Formation of the Bryah Group. These rocks also host the Red Bore VHMS and Horseshoe Lights VHMS deposits. The DeGrussa deposit consists of four primary sulfide ore lenses in conjunction with supergene enrichment of copper. Production to February 2015 totalled 137,000 tonnes of copper and 98,000 ounces of gold. The resource estimate consists of an underground primary sulfide of 9.5Mt @ 5.7% Cu, and 2.0g/t Au, for a contained metal content of 546,000 tonnes Cu and 616,000 ounces of Au; stockpiled oxide resource estimate of 2.8Mt @ 1.2% Cu and 1.0g/t Au, for a total metal resource of 33,000t Cu and 88,000 ounces Au; contributing to a total resource of 12.4Mt @ 4.7% Cu and 1.8g/t Au, with a metal resource of 579,000t Cu and 704,000 ounces Au (Taylor and Hastings, 2015).

Lateritisation, uplift and erosion has affected most of Western Australia since the Tertiary. These processes produced a broad plateau that was subject to deep weathering in the early Tertiary and subsequently eroded leaving only minor remnants of this plateau. The major divide between the exterior drainage system of the headwaters of the Gascoyne and Murchison Rivers trends north-west across the western half of the tenement package (Fig. 1.1.). The topography has a generally low relief, with mean elevation of about 550 metres. More resistant units form ridges and hills with elevations up to 640 metres (Jeffery, 2011).

Alluvial floodplains of the northward flowing branch of the Gascoyne River are present across the northern parts of the exploration area. This is characterised by the development of groundwater calcrete mounds that are a cryptocrystalline mixture of carbonate and opaline silica formed by precipitation below the water-table under conditions of low irregular rainfall

and high evaporation (Jeffery, 2011). The climate is semi-arid to arid with low and irregular rainfall between 200-240 mm per year. The weather is controlled by a succession of eastward moving anti-cyclones. Troughs between the anticyclones occasionally deepen to form rain-bearing depressions of tropical origin during the summer months and of southern origin during the late autumn and winter. Tropical cyclones, which occur in some years, are of considerable importance because they are usually accompanied by widespread heavy rain. Summers are hot, with temperatures commonly exceeding 40°C, whereas winters are mild, with temperatures ranging from 6 to 20°C in the months of June to August (Jeffery, 2011).

Vegetation consists of abundant mulga (*Acacia aneura*), eucalyptus (river red gum, *Eucalyptus camaldulensis)* in the major water courses, and other drought resistant shrubs dominantly including. *Eremophila forrestii* and other *Eremophila sp* and species of the *Cassia* group, such as *Cassia helmsii* and *Cassia luersenii* (Jeffery, 2011).

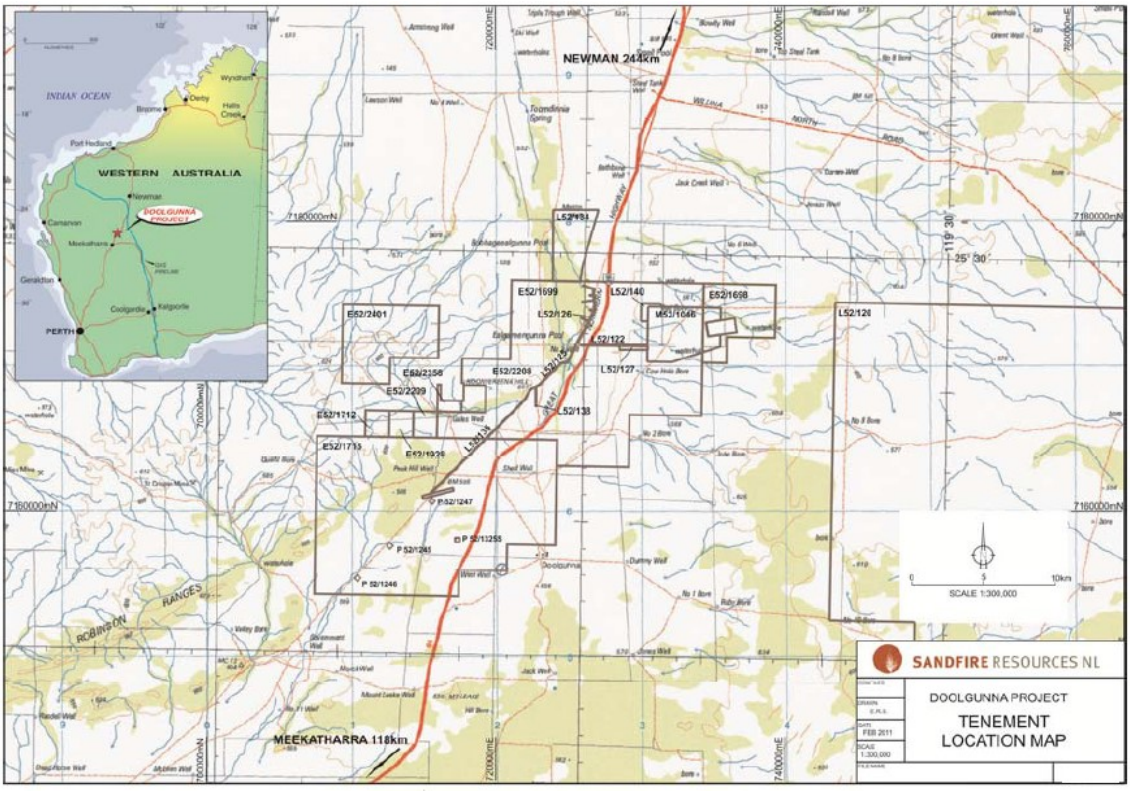

Figure 1.1. Location of the DeGrussa Copper-Gold Volcanic Massive Sulfide Deposit, Western Australia (from Jeffery (2011))

1.2. Discovery of the DeGrussa Deposit

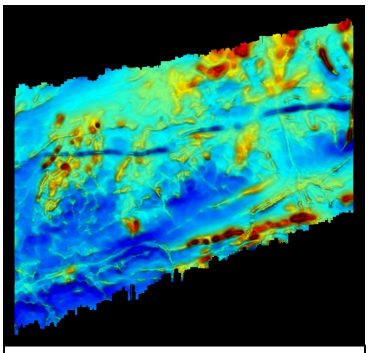

Figure 1.2. Troy Resources Aeromagnetic survey over the DeGrussa area.

Traditionally, exploration in the Bryah Basin (former Glengarry Basin) has targeted gold. High grade copper mineralisation exists at the Horseshoe Lights Cu-Au mine, approximately 70kms to the west of the DeGrussa mine, within Narracoota Formation volcanic and sedimentary rocks. The Thaduna Copper mine, largely mined for its copper oxide mineralisation is located ~ 50 kms to the east of DeGrussa within the Thaduna Formation turbiditic sediments of the Yerrida Basin.

Great Australian Resources NL completed limited percussion drilling on the Red Bore prospect between 1987-1988, located ~2km to the southeast of the present day DeGrussa mine. Here they drilled 3 iron stone gossans. The best results were RB2: 8m @ 1.3g/t Au and 2.03% Cu from 18m, and RB3 – 7m @ 1.09g/t Au and 7.25% Cu from 20m. Western Mining Company later held these two small copper-gold rich, malachite-azurite gossans (now Thunderlarra's Red Bore project containing a total indicated resource of 48,000 tonnes @ 3.6% Cu and 0.4g/t Au (Anonymous, 2015)).

In 1994-1995 Sabminco NL completed soil sampling and rock chip sampling across the area. An aeromagnetic survey (Fig. 1.2.) at 50m line spacing was completed by Troy Resources NL in 1998 (Dixon, 2000) before Sandfire Resources NL acquired the tenement as vacant ground in 2003.

Soil sampling and shallow vacuum drilling was completed across the tenement package including the DeGrussa area between 2004 and 2006. This identified areas of anomalous Au (>5ppb to 99ppb) across the tenements. RAB (Rotary Air Blast) drilling begun across prospective targets

As a follow up to results returned from vacuum drilling and soil sampling, one line of shallow RAB drilling was carried out in December 2007 across an anomalous value of 20ppb Au in soil sampling and corresponding 96ppb Au in vacuum. Drill hole DGRB2233 returned an

intersection of 10m with an average grade of 5.67g/t Au. RAB drilling in 2008 completed several lines along the strike of the DeGrussa gold anomaly returning favourable grades (Fig. 1.3). Multi-element analysis of drill holes indicated highly anomalous geochemistry (elevated Cu, As, Bi, Ag, Sb, Te and Zn) consistent with the mineralised gold zone.

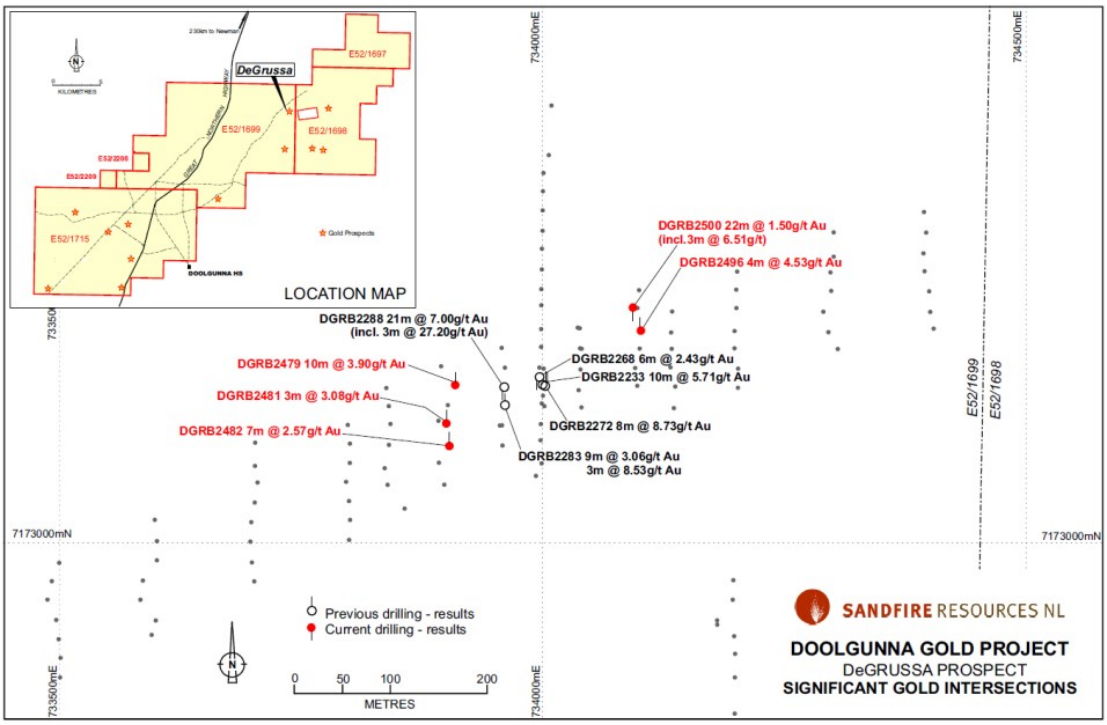

Figure 1.3. The developing supergene ore deposit.

In April 2008, a follow up RC drill programme of 60 degree angled holes, initially targeting bedrock hosted shear hosted gold mineralisation, failed to identify anything that could explain the anomalous supergene mineralisation. At the completion of the programme, one vertical stratigraphic hole was positioned central to the prospect area, where earlier angled drilling failed to intersect any significant bedrock mineralisation below the Au rich supergene mineralisation. This new drill hole (DGRC101) intersected massive sulfide (chalcocite, pyrite and chalcopyrite) intersected between 98m and 200m depth. A subsequent vertical drill hole (DGRC102), 20m to the north intersected a further ~100m of massive sulfide mineralisation

with additional drill holes intersecting both native copper, malachite and azurite in the supergene zone (Fig 1.4).

Airborne and downhole geophysics identified 3 electromagnetic conductors; 1. an oxide native copper horizon; 2. DeGrussa VHMS mineralisation, and, 3. the larger Conductor 1 ore body. Limited RC drilling in June 2009 confirmed the existence of Conductor 1.

Diamond drilling commenced in July 2009 with the first drill hole producing a combined intersection of 53.2m @ 17.3% Cu for the DeGrussa deposit. DeGrussa has a strike length of approximately 200m and Conductor 1 of 400m. The deeper and flat lying Conductor 4 and Conductor 5 ore lenses were later discovered with subsequent diamond drilling, downhole and surface geophysics.

Figure 1.4. Native copper and malachite from the supergene zone in RC chips.

DGDD-001: **8m averaging 27.3% Copper (Cu), 1.9g/t Gold (Au) and 34.9g/t Silver (Ag) from 146m**

- Assay results from this first intersection (Intersection 1) confirm field reports of abundant visible chalcopyrite, with individual 1 metre intersections including:
  - 550002 0.9m@ **32.0% Cu**
  - 550003 1m @ **31.3% Cu**
  - 550004 1m @ **30.2% Cu**
  - 550005 1m @ **25.6% Cu**

Excerpt from the initial Sandfire ASX report (Evans, 2009).

1.3. Classification of VHMS deposits

VHMS deposits are found in submarine or subsea floor environments, in a range of tectonic settings. Several classification schemes are in use for VHMS deposits including the Barrie and Hannington (1999) classification by host rock type, base metal composition (Large, 1992, Franklin et al., 2005, Galley et al., 2007), emplacement style (e.g. sea floor or sub sea floor (Doyle and Allen, 2003)), or type location (e..g. Cypress, Besshi, Kuroko, Urals, (Eastoe and Gustin, 1996, Ohmoto, 1996, Eldridge et al., 1983)). The DeGrussa deposit may be referred to as a 'Besshi'-type deposit although it has several differences. The classification scheme preferred for this study is that of Barrie and Hannington (1999) which describes the DeGrussa deposit as a siliciclastic-mafic style deposit, although the high copper grades within the DeGrussa (17.3% Cu over a combined intersection of 53.2m in DGDD001) and the Conductor 1 (2.7m @ 15.4% Cu) ore bodies, is considered unusual.

Although there is much overlap between the types of deposit described here as well as between the classification schemes, the following describes the five different types of VHMS deposit and their characteristics as determined by host rock composition (Barrie and Hannington, 1999):

Mafic: Mafic type VHMS deposits are generally Cu-rich and Pb-poor with enrichment in Au compared with Ag and Zn. Mineralogy is dominantly pyrite, chalcopyrite and sphalerite. Host rocks are mafic (tholeiitic basalts and boninites) (>75%) with rare or absent (<1%) felsic volcanic rocks. Siliciclastic rocks and/or ultramafic rocks form a minor (<10%) component in stratigraphy. Alteration is typically characterised by an Fe-Mg chlorite-quartz core and sericite rim (Franklin et al., 2005). Epidote-albite-actinolite alteration and local silicification may be present (Franklin et al., 1981). Mafic-hosted VHMS deposits are commonly found in ophiolitic and oceanic rift tectonic settings (Franklin et al., 2005).

Bimodal mafic: Bimodal-mafic type deposits are typically Cu-rich, with lesser Zn and Pb. They can also contain significant amounts of Au and Ag and are the most common type of VHMS deposit found in the world. Host rocks are typically >50% mafic rocks (basaltic, tholeiitic, and

calc-alkaline), with >3% felsic rocks (generally intermediate felsics) with subordinate siliciclastic rocks (Barrie and Hannington, 1999). Alteration is characterised by an Fe-chlorite and sulfide core, Mg-chlorite and sericite margin and local silicification. Pods of talc±magnetite may be present (Franklin et al., 2005). Bimodal mafic deposits can be found in primitive volcanic arc and rifted primitive volcanic arc settings (Franklin et al., 2005). The copper-rich VHMS deposit, Horseshoe Lights, situated approximately70 km west of DeGrussa in Bryah Group rocks may fit this style of mineralisation.

Mafic-siliciclastic: Pyrite, chalcopyrite and pyrrhotite form the dominant minerals in the mafic-siliciclastic VHMS deposit. Metal content is dominantly Zn and Cu with lesser Pb, Ag and Au. Host rocks are equal proportions of mafic volcanic and intrusive rocks, and turbiditic sedimentary rocks. Felsic rocks are minor or absent (Barrie and Hannington, 1999). This style of deposit is closely associated with Besshi-type with alteration consisting of a zoned Fe-Mg chlorite and sericite core. There is a significant amount of carbonate in host sediments. Chlorite, albite, muscovite, tourmaline, epidote, amphibole, and graphite are also common. Barium is elevated in hanging wall.

These deposits are typically found in rifted continental margins, oceanic rifts and back-arc basins with the Besshi deposit in Japan and the Windy Craggy deposit in British Colombia, Canada being the best examples of this type (Peter and Scott, 1999). As will be discussed throughout this thesis, the DeGrussa deposit shares many of the characteristics listed above, and is considered to belong to this group of deposits.

Bimodal-felsic: Bimodal-felsic type deposits are Zn and Ag rich with lesser Pb, Cu and Au increasing in the deposits through geological time. They may also contain some Sp and Gn. Host rocks are >50% felsic volcanic rocks (calc-alkaline, rhyolites), <15% siliciclastic rocks and lesser mafic and intrusive rocks (calc-alkaline, tholeiitic basalts) (Barrie and Hannington, 1999). Alteration is characterised by silicification and a sericite, zoned Fe-Mg core, with sericite rim (Galley et al., 2007). Bimodal-felsic deposits are found in mature and rifted volcanic arcs and are most abundant in the Phanerozoic (Franklin et al., 2005).

Bimodal-siliciclastic: Bimodal-siliciclastic deposits, typical of the Iberian Pyrite Belt of Portugal and Spain, are typically Cu poor, but contain large quantities of Zn and Pb. Dominant minerals are pyrite and pyrrhotite. Rocks are equal proportions of volcanic and siliciclastic rocks with felsic volcanics (calc-alkalic) more dominant than mafic volcanic rocks (tholeiitic with rare alkaline basalts) (Barrie and Hannington, 1999). Alteration is characterised by sericitic, silicic alteration, and Fe-chlorite. Ore deposits have semi-conformable K-rich upper zones, and Na-rich (epidote, actinolite) lower zones (Barrie and Hannington, 1999).

These deposits are found in continental arc or rifted continental arc tectonic settings (Franklin et al., 2005).

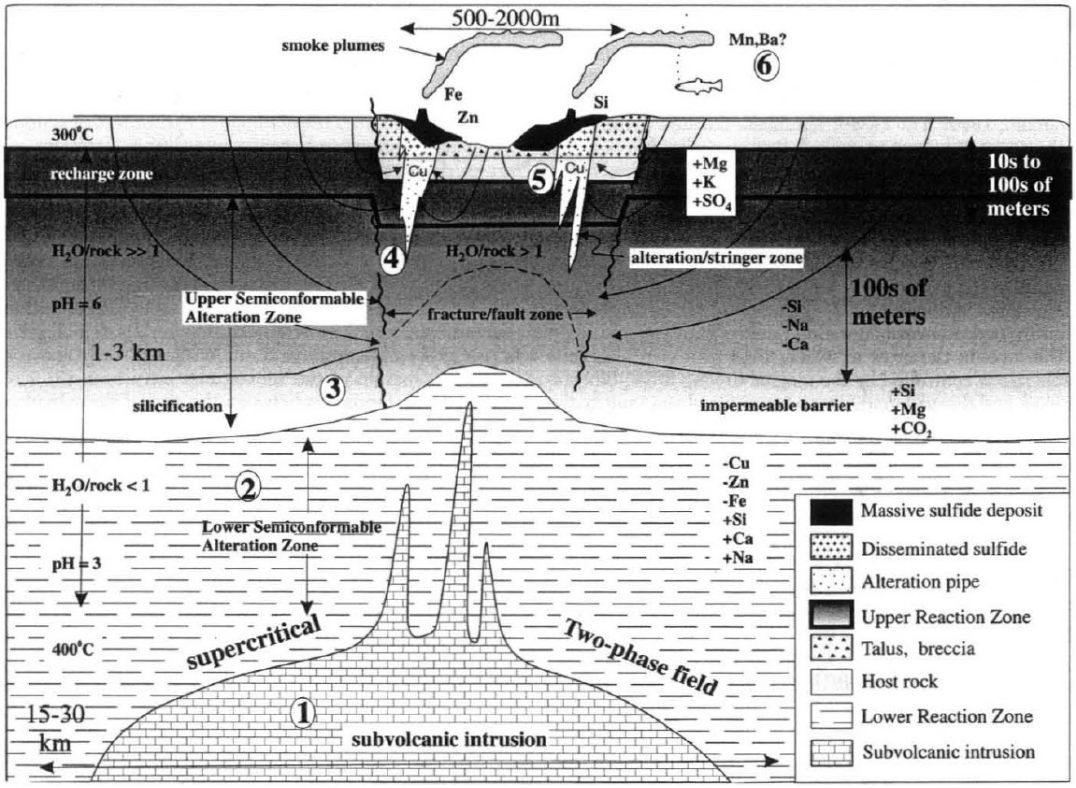

Figure 1.5. Formation of VHMS deposits displaying the basic components of a high temperature VHMS hydrothermal system from Franklin et al. (2005). 1. A heat source to drive the hydrothermal convective system, 2. high-temperature reaction zone from which some metals are leached from volcanic and sedimentary rocks, 3. synvolcanic faults and fissures that focus hydrothermal fluids, 4. footwall and hanging wall alteration zones produced by high-temperature fluid-rock reaction involving mixtures of ascending hydrothermal fluids and ambient seawater, 5. the massive sulfide deposit, and 6. distal products.

1.4. Formation of VHMS deposits

Metal source is generally derived from sea water circulation and leaching of surrounding sedimentary and volcanic rocks (Fig. 1.5). In most models of formation, in particular for Pb, Zn dominant VHMS deposits, hydrothermal leaching of country rock is the preferred method of metal accumulation (e.g. the Panorama district of Western Australia (Huston et al., 2001); Aljustrel in Portugal (Inverno et al., 2008); Ducktown, Tennessee (LeHuray, 1984); Windy Craggy in British Columbia (Peter and Scott, 1999)). Fewer deposits (e.g. Neves Corvo in the Iberian Pyrite Belt (Relvas et al., 2001, Huston et al., 2001); Trondheim and Sulitjelma districts of Norway (Fox et al., 1988) and parts of Kidd Creek in the Abitibi Belt (Huston et al., 2010)) are suggested to involve a significant magmatic-hydrothermal component contributing anomalous metal contents especially where there are higher grades of tin, copper, gold, molybdenite and other rare metals.

The heat source in all cases is likely to be derived from the upper mantle and related sub-volcanic intrusions (Barrie and Hannington, 1999). VHMS deposits are the result of hot, metal bearing fluids being deposited at the sea floor, or sub seafloor due to either a redox and/or temperature change. Deposits occur within both mafic and felsic submarine volcanic centres and can form at either deep (>1000m) or shallow (<1000m) water depths. They are spatially associated with syn-volcanic faults and commonly occur within volcanic vents that are localised along syn-volcanic structures (Gibson et al., 1999). Precipitation occurs when there is a change of temperature or redox state. Temperature generally defines the metal zonation with classic zonation of a volcanic massive sulfide consists of a central core of chalcopyrite + pyrite ± pyrrhotite with outer layers of pyrite ± sphalerite ± galena and sphalerite ± galena ± pyrite ± barite (Fig. 1.6.).

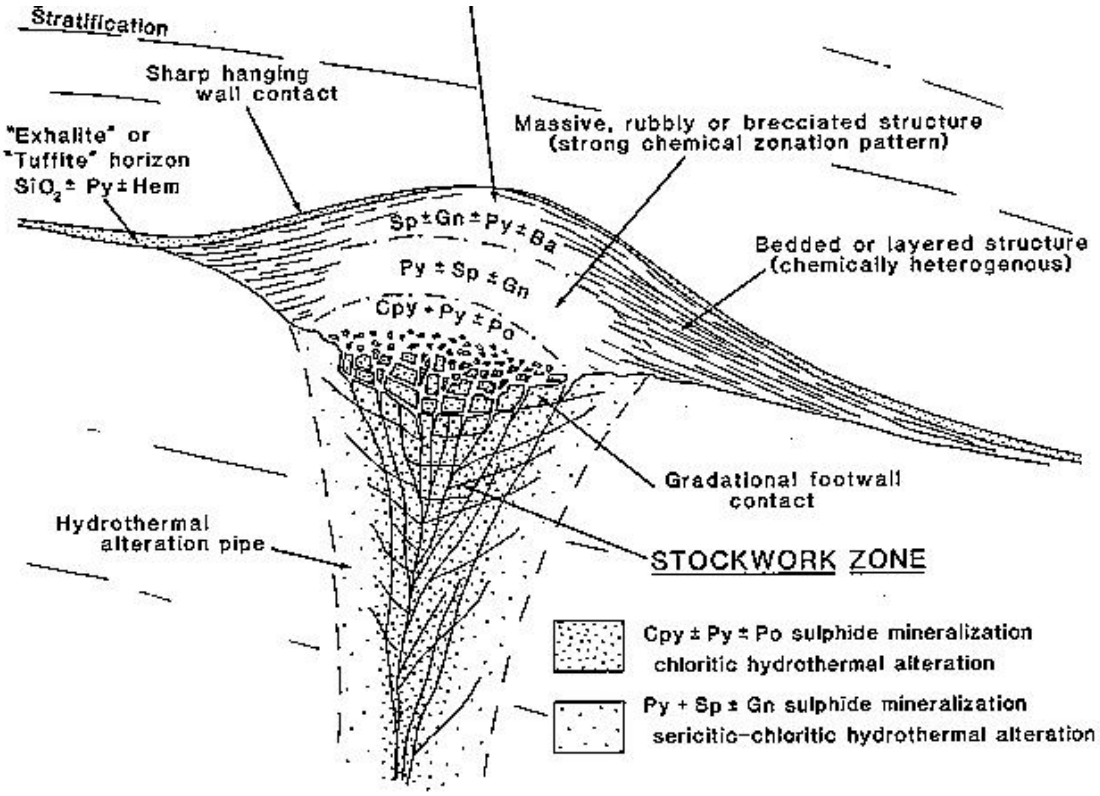

Figure 1.6. Classic zonation of massive sulfide deposits from Lydon (1984)

Subsea floor replacement provides a more efficient mechanism to trap a higher proportion of metals and may be responsible for forming larger, tabular VHMS deposits (Doyle and Allen, 2003). Some components of the hydrothermal fluid can still escape and become trapped in hanging wall sediments and sea floor precipitates (Franklin et al., 2005). A number of styles of VHMS deposit emplacement have been identified by Doyle and Allen (2003) of which several have similarities to textures seen in the DeGrussa deposit (Fig 1.7). Sedimentary rocks, in particular turbidites, are less permeable than volcanic rocks, and in the absence of abundant faulting, a turbidite-rich setting can effectively insulate a hydrothermal cell and its heat source from rapid advective cooling, thus allowing for a longer-lived hydrothermal system, and relatively efficient, subsea floor metal deposition (Barrie and Hannington, 1999).

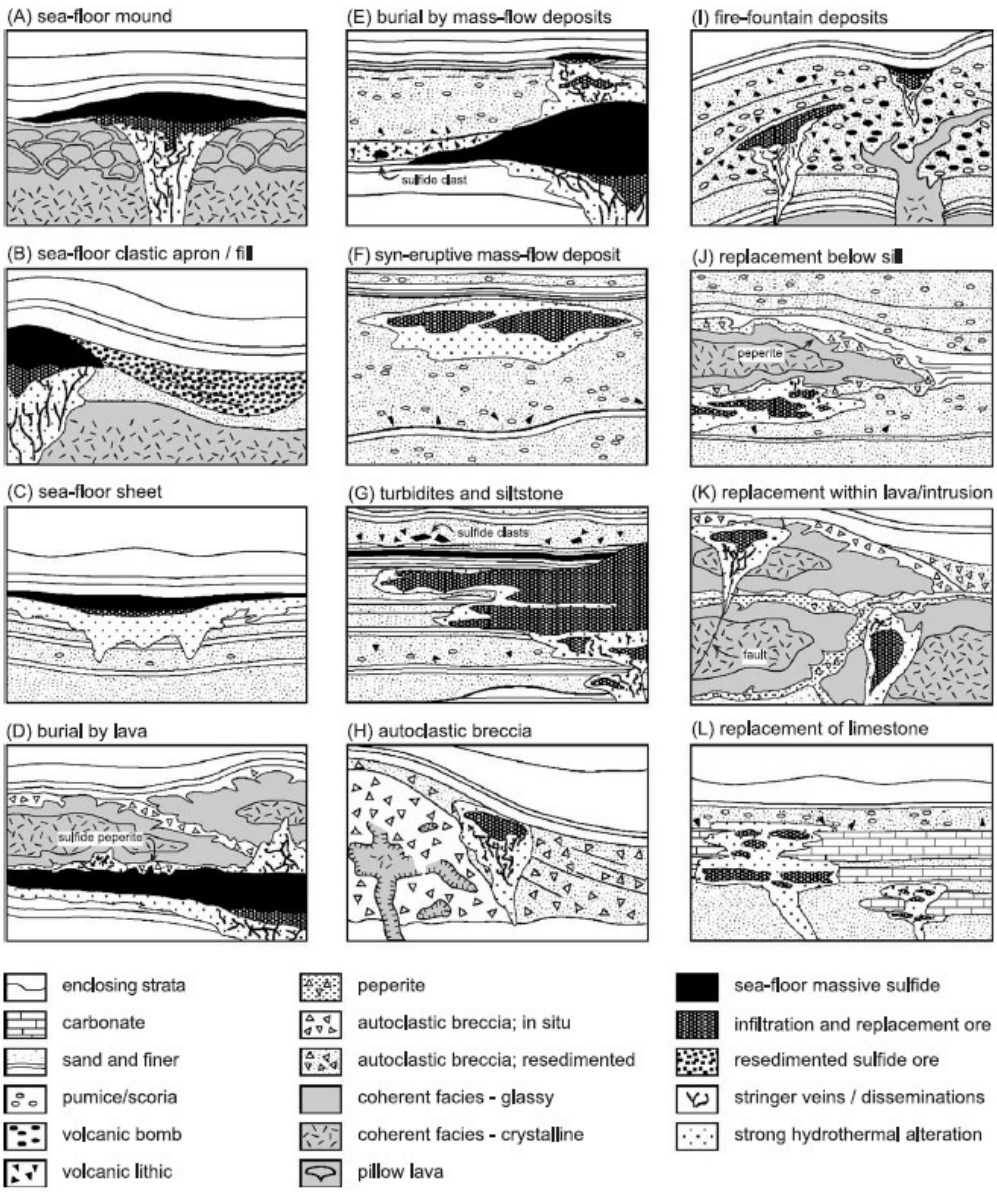

Figure 1.7. Sea floor and subsea floor replacement style VHMS deposit types, a number of which may be present in the DeGrussa deposits (Doyle and Allen, 2003).

1.5. Prior studies

The eastern Capricorn Orogen has had a long history of exploration and academic studies owing to its endowment in gold deposits. Since the discovery of DeGrussa, several major bodies of work have been completed. These include;

1. An Honours thesis by Adamczyk (2013) on the stratigraphy and mineralisation of the Conductor 5 ore lens. Adamczyk (2013) interpreted of parts of the mineralisation as subsea floor replacement

2. A Masters thesis by Condon (2015) which distinguished the different types of mineralisation textures, metal zonation and geometallurgy for a sequence of samples through the DeGrussa and Conductor 1 ore lodes.

3. An Honours thesis by Baker (2015) assessing the nature of the footwall sequence and it's relationship and importance to the DeGrussa mineralisation. Attempts to locate any feeder structures were also made as part of this study. However, perhaps due to the lack of drill holes and underground exposure, this was not successful.

4. Numerous internal Sandfire studies regarding the geochemistry of the host rock package and the identification of a regional marker unit, such as those by Cranney (2011), and Loiseau (2014). Data from some of these reports was available for this study, and is referenced herein as needed.

Regionally there have been many studies of the geology, with these discussed in detail throughout Chapter 2. Most prior studies of mineralisation within the Bryah Basin focused on gold. With the exception of the Horseshoe Lights Cu-Au deposit, prior to the discovery of DeGrussa in 2009, there was no significant VHMS mineralisation known within the Bryah Basin. Copper mineralisation in the district appears to be higher grade in comparison to most VHMS deposits mined in the world. Gold grades are also anomalous. Despite these studies, the Yerrida and Bryah basins have not been a major focus for research and exploration. Studies of note include:

1. Early geochemical studies by Hynes and Gee (1986) and the Geological Survey of Western

Australia (e.g. Pirajno et al. (2000)). However, these were limited across the Glengarry Basin (combined Yerrida, Bryah and Padbury Group rocks) and new geochemical techniques can now be utilised.

2. A limited amount of geochronological work had been completed, with definitive ages for only the Bubble Well Member given by Woodhead and Hergt (1997) and some sedimentary rock units by Halilovic et al. (2004).

3. Work by Occhipinti et al. (1997) restructured the stratigraphy for the original geology of Gee (1979) and Gee and Grey (1993), dividing the larger Glengarry basin into the Yerrida and Bryah Basins. This was designed to reflect the differing lithologies and provinces of the units and their source.

The main focus of this thesis will be the DeGrussa deposit. Research will concentrate on the geochronology, lead isotopes and geochemistry of the regional and DeGrussa host stratigraphy and mineralisation, to form comparisons of the tectonic and geological setting and identify the nature of copper mineralisation. Furthermore, geochronological constraints on the Yerrida, Bryah and Padbury Basins are poor and thus, regional geochronology where possible will contribute to the knowledge of the region.

1.6. Aims and Thesis structure

This study began as a Masters of Economic Geology thesis soon after the discovery in 2009. It was transferred to a PhD in 2012 when it became clear that the amount of work required would deem it thus. Hence, this thesis is a result of field and analytical work conducted between 2009 and 2015. Access to the Sandfire database including drill hole logs, geochemical assays and drill hole photos was kindly provided by Sandfire Resources. This thesis has the following aims:

1. Describe the stratigraphy of the host rock sequence and place the deposit into its regional context.

2. Characterise the DeGrussa mineralisation, including textures, metal relationships, zonation and emplacement styles. Geochemically characterise the mineralisation using Pb isotopes, S isotopes and trace elements on pyrites. Assess the nature of the ore forming fluids (magmatic-hydrothermal, sea water, leached sedimentary or volcanic rocks).

3. Geochemically assess the host rock package. Determine the tectonic setting of the deposit from mafic rock geochemistry and comparisons with existing mafic rock geochemistry.

4. Determine the age of the DeGrussa deposit and the host rock package using Re-Os geochronology (molybdenite), U-Pb (zircon) and Pb-Pb (galena and pyrite). Reassess existing ages of basin mineralisation and consolidate mineralisation with regional orogenic events.

5. Compare the mineralisation characteristics of DeGrussa with major mineralisation in the district, using S isotopes and Pb isotopes. Determine any characteristics that could be used for exploration.

6. Provide a geological model for the formation of the DeGrussa VHMS deposit.

To address the above aims, this thesis is divided into seven chapters encompassing the following topics:

Regional Geology – Chapter 2 provides an overview of the geology and stratigraphy of the eastern Capricorn Orogen, in particular the units of the Yerrida and Bryah Groups, with discussion of their stratigraphic and tectonic relationship to the greater Capricorn Orogen (notably the Glenburgh Terrane) and nearby Palaeoproterozoic and Archaean Terranes. The major mineralisation occurrences within the Yerrida and Bryah Groups mentioned throughout this thesis are also described in this chapter.

Stratigraphy of the DeGrussa mine sequence – Chapter 3 provides detailed descriptions, including petrographic and physical observations, of the units hosting and surrounding the DeGrussa mineralisation. Stratigraphic relationships are determined and where possible, comparisons to regional stratigraphic units are made. Structural features, including major faulting and post-mineralisation faulting, veining and shearing are also discussed.

Stratigraphy is determined from a combination of downhole drill core logging, drill core photos, underground and open pit observations, thin section petrographical observations, geochemical assays and compilation of cross sections and Leapfrog™ 3D modelling. Its position in a regional setting was assisted by geological mapping conducted by R.G. Jeffery between 2011 and 2013 (Jeffery, 2011, Jeffery, 2013), as well as existing GSWA maps (Bunting et al., 1977, Gee, 1979, Gee, 1986, Gee, 1987, Gee, 1990, Pirajno and Occhipinti, 1998, Pirajno and Adamides, 2000, Pirajno et al., 2000, Sheppard et al., 2010).

DeGrussa mineralisation – Chapter 4 provides an overview of the mineral textures and features at both macro and micro-scale, metal and geochemical characteristics and zonation throughout the deposit and in relation to surrounding host rocks. This chapter also discusses the location of the feeder zone and alteration features, including the chlorite schist and talc-carbonate exhalite, and their relationship to mineralisation. Sulfur isotopes and Pb isotopes are also presented elucidate the nature of mineralising fluids.

Geochemistry - Chapter 5 attempts to use geochemical features of the mafic dolerites and basalts within the DeGrussa mine sequence to characterise the tectonic setting of emplacement. Mafic geochemistry of the DeGrussa dolerites are compared with GSWA open file geochemical data from the larger Narracoota and Killara Formations in order to determine the overall tectonic setting of the Bryah and Yerrida Basins. Comparisons of the DeGrussa mafic geochemistry with that of varied tectonic settings around the world, and present day analogies are discussed.

Geochronology – Chapter 6 provides geochronological constraints on the host rock package and regional mineralising stratigraphy using U-Pb on zircons, Pb-Pb on pyrite and galena and Re-Os on molybdenite. The differences in the Pb model curves of Stacey and Kramers (1975) and Cumming and Richards (1975) are discussed and revised ages are provided for several deposits in the region. Results from this chapter were published in Precambrian Research (Hawke et al., 2015).

Source of Fluids – Chapter 7 describes the characteristics of the mineralising fluids and compares the DeGrussa mineralisation with deposits across the region using Pb isotopes, pyrite trace elements and $\delta^{34}S$ isotopes.

Genetic model - Chapter 8 consolidates the information drawn from the previous chapters to provide a genetic model of formation for the DeGrussa mineralisation.

Conclusions –Chapter 9 presents the main conclusions of the thesis and the implications of this work for further exploration in the DeGrussa district. Limitations of this study are discussed and ideas are provided for further work.

1.7. Funding

Funding for this project is courtesy of Sandfire Resources NL. Site access, as well as access to drill core and sample material has additionally been provided by Talisman Mining NL, Resource and Investment NL, Ventnor Resources NL and SIPA Resources NL. This thesis incorporates collaborative work on trace element geochemistry of pyrites between the University of Tasmania and the Geological Survey of Western Australia. Samples of Horseshoe Lights mineralisation were kindly loaned from the University of Western Australia.

The author, sieving and logging RAB chip samples over the DeGrussa prospect area, 2007

Chapter 2. Regional and Local Geology of the Capricorn Orogen

Sunset over the Doolgunna scrub

2.1. Introduction

The Capricorn Orogen of Western Australia is a ~1000 km long, 500 km wide region of variably deformed rocks located between the Pilbara and Yilgarn Cratons (Fig. 2.1.). It records the Paleoproterozoic rifting and collision of these Archean continental terranes during three main tectonic events (the Opthalmian, Glenburgh and Capricorn) which led to deposition, uplift and deformation of the sedimentary basins between the Yilgarn and Pilbara cratons to form the West Australian Craton (Cawood and Tyler, 2004, Sheppard et al., 2010, Johnson et al., 2011a, Johnson, 2013). The Orogen includes the deformed margins of the Pilbara and Yilgarn Cratons and associated deformed continental margin rocks of the Fortescue, Hamersley, Turee Creek and lower Wyloo Groups in the Ophthalmia Fold Belt, as well as the Palaeoproterozoic Gascoyne Province, Errabiddy Shear Zone and the Yarlarweelor Gneiss Complex in the west, the Ashburton (2446-1799 Ma, Johnson et al. (2013)), Edmund and Collier Basins (1680-1465 Ma, Zi et al. (2015) and 1171-1070 Ma respectively, (Martin and Thorne, 2004) in the north, and the Yerrida, Bryah, Padbury and Earaheedy Basins (c. 2174 – c. 1800 Ma, Pirajno and Occhipinti (2000)) in the south-east (Figure 2.1, 2.2). The Yerrida, Bryah and Padbury basins are a series

of Palaeoproterozoic volcano-sedimentary basins (Fig. 2.2.) emplaced and sutured together during the Glenburgh (2005-1970 Ma) and Capricorn (1820-1770 Ma) Orogenies.

The Paleoproterozoic DeGrussa copper-gold–silver, volcanic-hosted massive sulfide (VHMS) deposit is located in the eastern part of the Capricorn Orogen of central Western Australia (Fig. 2.1, 2.2.). The DeGrussa deposit was discovered in 2009 within an interfingerring sequence of sedimentary and mafic volcanic rocks of time equivalent to the Karalundi Formation and Narracoota Formation of the Bryah Group (Fig. 2.3.). These rocks also host the Red Bore and the Horseshoe Lights VHMS deposits. The DeGrussa deposit consists of four primary sulfide ore lenses in conjunction with a supergene enrichment of copper.

This chapter summarises prior studies of the area, including the regional stratigraphy, mineralisation and tectonic evolution, providing a framework for the geological evolution of the DeGrussa deposit. Due to the complicated history of research through the field area, definitions of significant tectonic units are provided in Table 2.1.

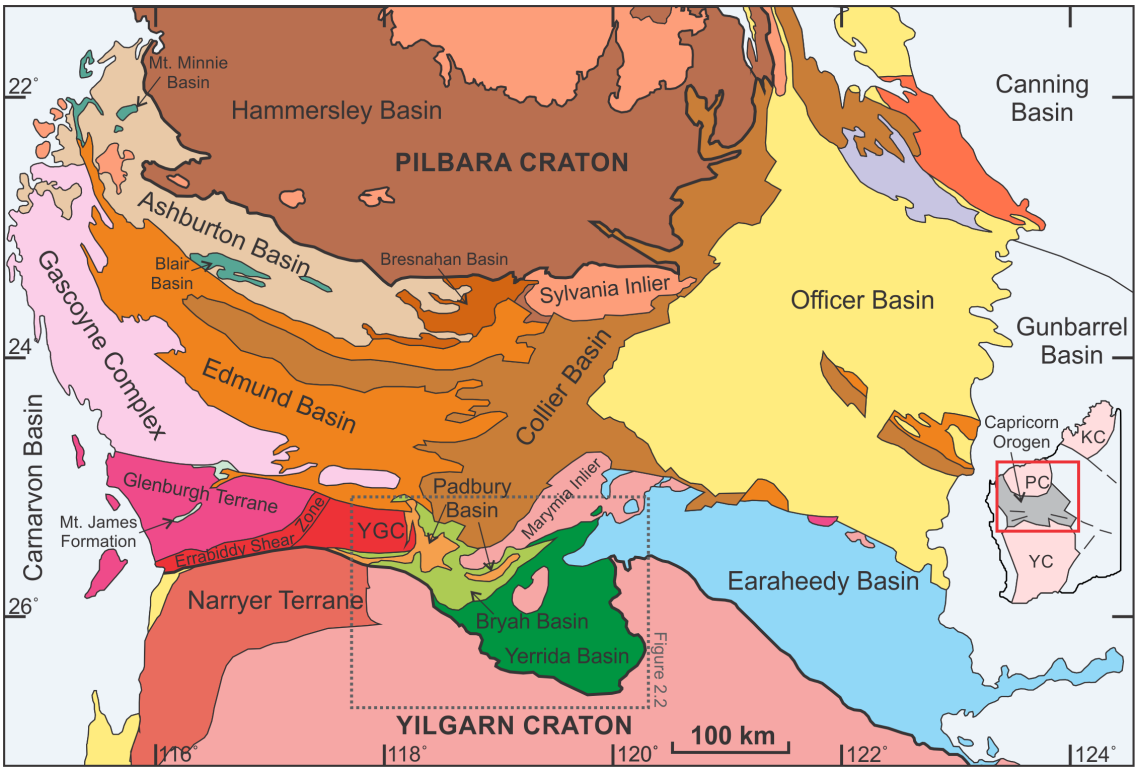

Figure 2.1. Geological Terranes of the Capricorn Orogen of Western Australia, a region of variably deformed rocks located between the Pilbara and Yilgarn Cratons which records Paleoproterozoic rifting and collision during the Opthalmian, Glenburgh and Capricorn Orogenies. It includes the deformed margins of the Pilbara and Yilgarn Cratons, as well as the Palaeoproterozoic Gascoyne Province, Errabiddy Shear Zone and the Yarlarweelor Gneiss Complex in the west, the Ashburton, Edmund and Collier Basins in the north, and the Yerrida, Bryah, Padbury and Earaheedy Basins in the south-east. Bold lines represent the extent of Palaeoproterozoic units. YGC = Yarlarweelor Gneiss Complex; KC = Kimberley Craton; PC = Pilbara Craton; YC = Yilgarn Craton. Adapted from Johnson et al. (2013).

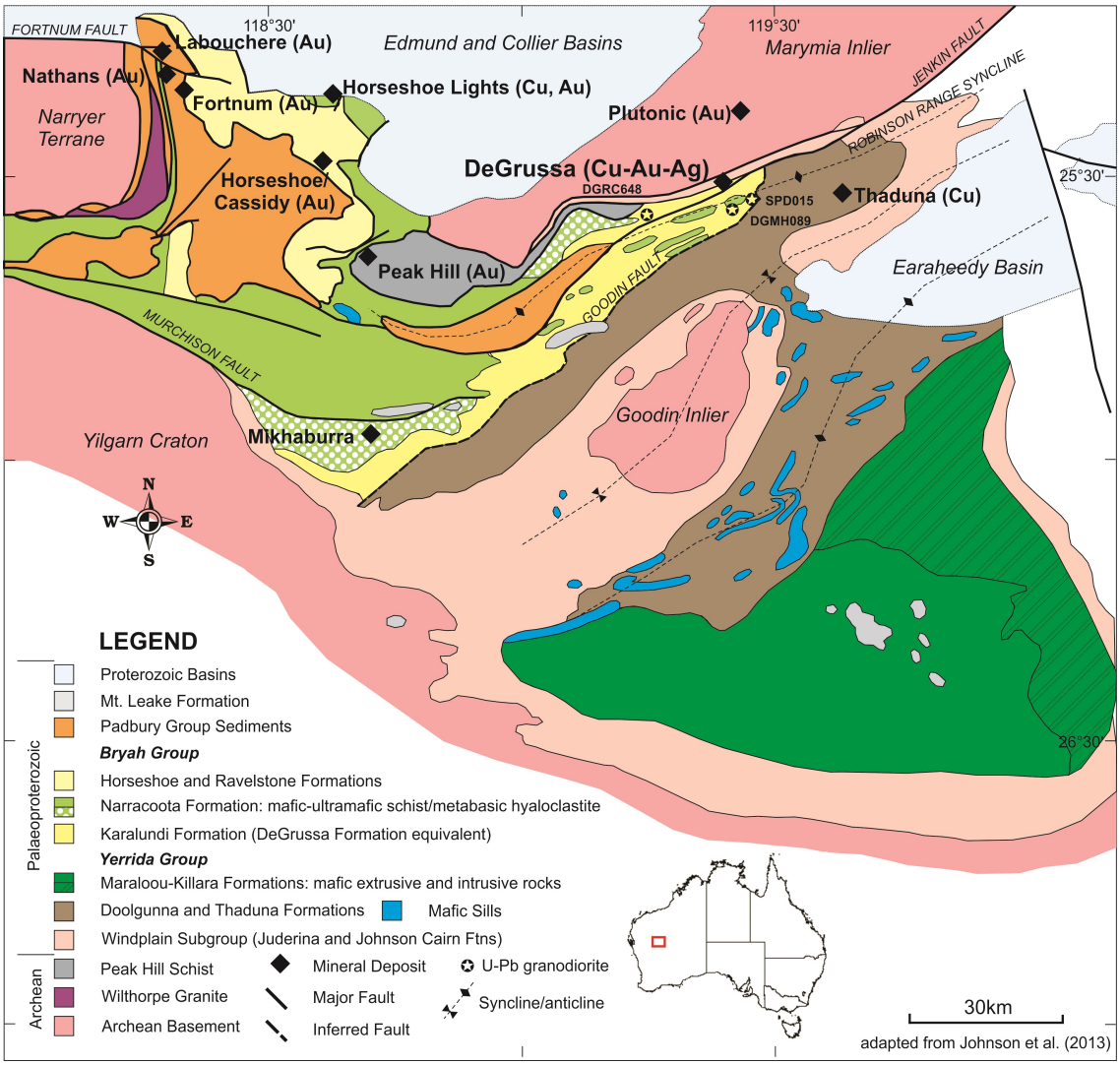

Figure 2.2. Regional Geology of the Yerrida, Bryah and Padbury groups with major mines and regional U-Pb zircon sample locations adapted from Johnson et al. (2013). The Bryah and Yerrida Groups are bounded to the south by the Archaean Yilgarn Craton, to the north by the Archaean Marymia Inlier and the Mesoproterozoic Edmund and Collier Basins, and to the west by the Narryer Terrane. They are unconformably overlain by the Paleoproterozoic Earaheedy Basin to the east. The Padbury Group unconformably overlies the Bryah Group. The Goodin Fault marks the southern boundary between Bryah and Yerrida Group sediments although this contact may be an unconformity (Jeffery, 2013). The DeGrussa deposit is located within sediments and mafic rocks of the DeGrussa Formation (lateral equivalent of the Karalundi Formation).

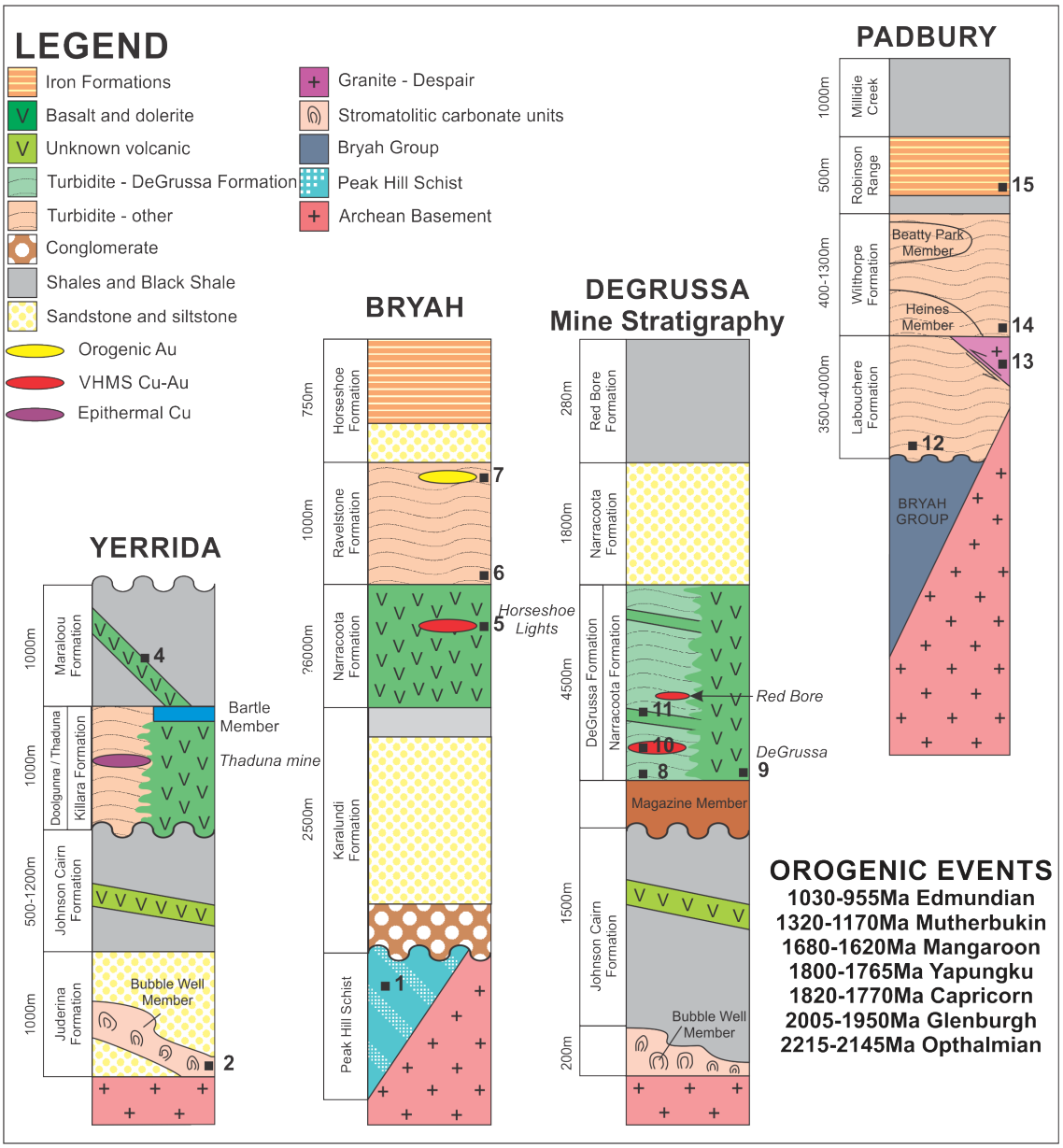

Figure 2.3. Stratigraphic column for the Yerrida, Bryah, and Padbury Group rocks with respect to the position of DeGrussa mine stratigraphy (adapted from Johnson (2013)). **1.** Peak Hill Mineralisation: main pit: 1610 Ma, 1620 Ma, 1705 Ma and 2070 ± 30 Ma; Fiveways: 1955 Ma; Mt. Pleasant: 1770 Ma (Thornett, 1995). **2.** The Bubble Well Member stromatolites at 2173 ± 64 Ma (Woodhead and Hergt, 1997). 3. Thaduna copper deposit mineralisation dated at 1475 ± 50 Ma hosted in the Thaduna Formation sediments. 4. The Maraloou Formation shales of age 1843 ± 10 Ma (Rasmussen and Fletcher, 2002). 5. Horseshoe Lights Cu-Au mineralisation, originally dated at 1922 ± 35 Ma (Windh, 1992) but reanalysed to 2000 ± 35 Ma and hosted at the top of the Narracoota Formation. Orogenic gold at Mikhaburra (Windh, 1992), located in Narracoota Formation hyaloclastite retains a mineralisation age of 1915 ± 30 Ma. 6. The Ravelstone Formation has a maximum age of <2014 Ma (Nelson, 1997) from detrital zircons. 7. Orogenic gold hosted within the Ravelstone Formation: Horseshoe/Cassidy 1940 ± 30Ma (Windh, 1992), Labouchere 1800 ± 30 Ma (Windh, 1992), Nathans 1820 ± 30 Ma (Windh, 1992) and Fortnum-Starlight 920 ± 50 Ma. 8. DeGrussa Formation/Karalundi Formation sediments detrital zircons with a maximum age of <2262 ± 40 Ma. 9. Regional granodiorites with a magmatic zircon age of 2018 ± 9 Ma. 10. DeGrussa deposit sulfides with a mineralisation age of 2027 ± 7 Ma from Re-Os on molybdenite. 11. Intrusive dolerite sills and dykes of the DeGrussa mine stratigraphy of 1991 ± 7 Ma to 2003 ± 7 Ma. 12. Labouchere Formation detrital zircons provide a maximum age of c. 1980 Ma (Johnson, 2013). 13. The Despair Granite, in faulted contact with the Padbury group with an Archean age of 2650 Ma (Occhipinti et al., 1998). 14. The Wilthorpe Formation with detrital zircons providing a maximum age of deposition at 1996 Ma (Nelson, 1997). 15. The Frere Formation iron formations in the Earaheedy Group were dated at 1891 ± 8 Ma by Rasmussen et al. (2012). Zircon ages from tuff interbedded between the iron formations, is extrapolated to also be the age of the Robinson Range Iron Formations of the Padbury Basin

Table 2.1. Terminology for the Capricorn Orogen, geological terranes and rock units.

Ashburton Basin	Consists of sediments and volcanic rocks of the Wyloo Group, Capricorn Formation, Mt. Minnie Group and Bresnahan Group, north of the Bryah/Padbury Basin.
Bryah Basin	Formerly part of the Glengarry Basin, it is the current name given to the basin sediments defined to be in tectonic contact with the underlying Yerrida Basin. It comprises the Karalundi Formation, Narracoota Formation, Ravelstone Formation and Horseshoe Formation.
Capricorn Orogen	A 300-400km wide belt of Palaeoproterozoic basin formation, plutonic magmatism and deformation between the Yilgarn and Pilbara Cratons. It consists of the Ashburton Basin, Gascoyne Complex, Nabberu Provinces and the Bangemall Group.
Earaheedy Basin	Part of the 'Nabberu Province'. A sedimentary basin unconformably overlying the Yerrida Basin with iron ore formations of the Frere Formation presumed contemporaneous with those of the Robinson Range Formation in the Padbury Basin. The Mt. Leake Formation is considered an outlier of the Earaheedy Basin, resting unconformably on top of the Yerrida, Bryah and Padbury Basin sediments and is considered equivalent to the basal Yelma Formation.
Gascoyne Complex	Basement gneisses and metamorphosed supracrustal rocks intruded by I and S type granitites.
Glenburgh Orogen	Collision of the Glenburgh Terrane and the Yilgarn Craton causing basin formation and widespread granitic magmatism at 2005-1996Ma.
Glengarry Basin	Former name for the newly assigned Yerrida, Bryah and Padbury Basins.
Glenburgh Terrane	A continental fragment exotic to both the Yilgarn and Pilbara Cratons. The crustal history ranges back to 3700Ma. It is interpreted to have collided with and accreted to the Pilbara Craton during the 2215-2145Ma Opthalmian Orogeny and later with the Yilgarn Craton at 2005-1996Ma.
Goodin Inlier	Tectonically activated and uplifted portion of the Archaean Yilgarn granites outcropping within the Yerrida Basin sediments, south of the DeGrussa mine. These granites form the basement of the Palaeoproterozoic Yerrida and Bryah Basins.
Marymia Inlier	Composed of and greenstones of late Archaean age, the Marymia Inlier is a rifted section of the Yilgarn Craton forming the northern boundary and basement rocks to the Proterozoic Yerrida/Bryah Basin in the vicinity of DeGrussa. It is host to gold mineralisation of Plutonic and Peak Hill.
Nabberu Province	Southern half of the Capricorn Orogen. Former name traditionally given to the Glengarry and Earaheedy basins with inliers of Archaean granite-greenstone basement, before these were subdivided into separate basins.
Narryer Terrane	Archaean age basement to the west of the Bryah/Padbury Basins and south of the Errabiddy Shear Zone
Padbury Basin	Unconformably overlying the Bryah Basin sediments it contains the Labouchere Formation, Wilthorpe Formation, Robinson Range Formation and the Millidie Creek Formation.
Paroo Platform	Refers to an area from Gee and Grey (1993) covering the Yerrida Basin sediments (Finlayson Sandstone, Juderina Formation, Narracoota Volcanics (renamed the Killara Formation by Pirajno and Adamides (2000a) and Maraloou Formation.
Peak Hill Schist	Formerly assigned to sedimentary rocks of the Glengarry Basin and known as the Peak Hill Metamorphic Suite, it is now identified as Archean and forms the southwestern portion of the Marymia Inlier.
Yapungku Orogen	Collision of the North Australia and West Australian Cratons at ca. 1790Ga.
Yarlarweelor Gneiss Complex	Deformed and metamorphosed granitic gneisses. Bounds the Bryah Basin to the northwest, north of the Errabiddy Shear Zone, west of the Bryah/Padbury sediments in the vicinity of the Labouchere and Nathan's gold deposits.
Yerrida Basin	Current name given to basal units of the former Glengarry Basin including the Juderina Formation, Johnson Cairn Shale, Thaduna Formation, Doolgunna Formation, Killara Formation (formerly Narracoota volanics of (Gee, 1987) that crops out in the Yerrida Basin) and the Maraloou Formation.

2.2. Previous Studies, Nomenclature and Stratigraphic Names

The earliest geological investigation of the Doolgunna area was completed by Talbot and Farquharson (1920). Despite many years of gold mining in the Peak Hill district, the first edition of the Peak Hill 1:250, 000 map sheet was not produced until 1970 by MacLeod (1970). MacLeod (1970) assigned sediments of the Doolgunna area to the Archaean as they appeared lithologically and structurally similar to other clastic-volcanic sequences of the Yilgarn block (Jeffery, 2011).

In 1973, BHP geologists completed a major study of the "Nabberu Basin" and its associated iron formations following the BMR publication of the aeromagnetic maps of the Stanley and Nabberu 1:250 000 map sheet (Hall and Goode, 1978). BHP extended their study into the Glengarry, Peak Hill and Robinson Range 1:250, 000 map sheets in 1974 and 1975. This work defined the Palaeoproterozoic Nabberu Basin as a major depocentre of sedimentary and mafic igneous rocks. The Nabberu Basin was subdivided into the Earaheedy, the Glengarry and the Padbury basins (Jeffery, 2011). This work defined the tectonic features of the northern Yilgarn margin.

The Peak Hill 1:250,000 map sheet was revised between 1977 and 1981 by the Geological Survey of Western Australia (GSWA) with a second edition provided by Gee (1987). This was the first comprehensive work completed in the Glengarry Basin (Gee, 1979, 1987). The initial stratigraphic column is provided in Figure 2.4.

The first geological evolution description of the Horseshoe Lights Cu-Au deposit (Gillies, 1988) included geochronological constraints on the mineralisation, stratigraphic and petrological studies. It concluded that this mineralisation was a syngenetic, VHMS-style copper deposit with a later overprint of epigenetic gold.

Windh (1992) completed a Ph.D. thesis on the tectonic evolution and metallogenesis of the Palaeoproterozoic Glengarry Basin. This study related known gold mineralisation to the tectonic evolution of the host terrane. This was in conjunction with Dyer's (1991) B.Sc. Hons. thesis of the alteration, fluid inclusions and stable isotopes of the Fortnum deposits.

On the basis of unconformable relationships, Gee and Grey (1993) elevated the Glengarry sub-basin to basin status, further subdividing the former Nabberu Basin into the Glengarry and Padbury Groups to the west and the Earaheedy to the east.

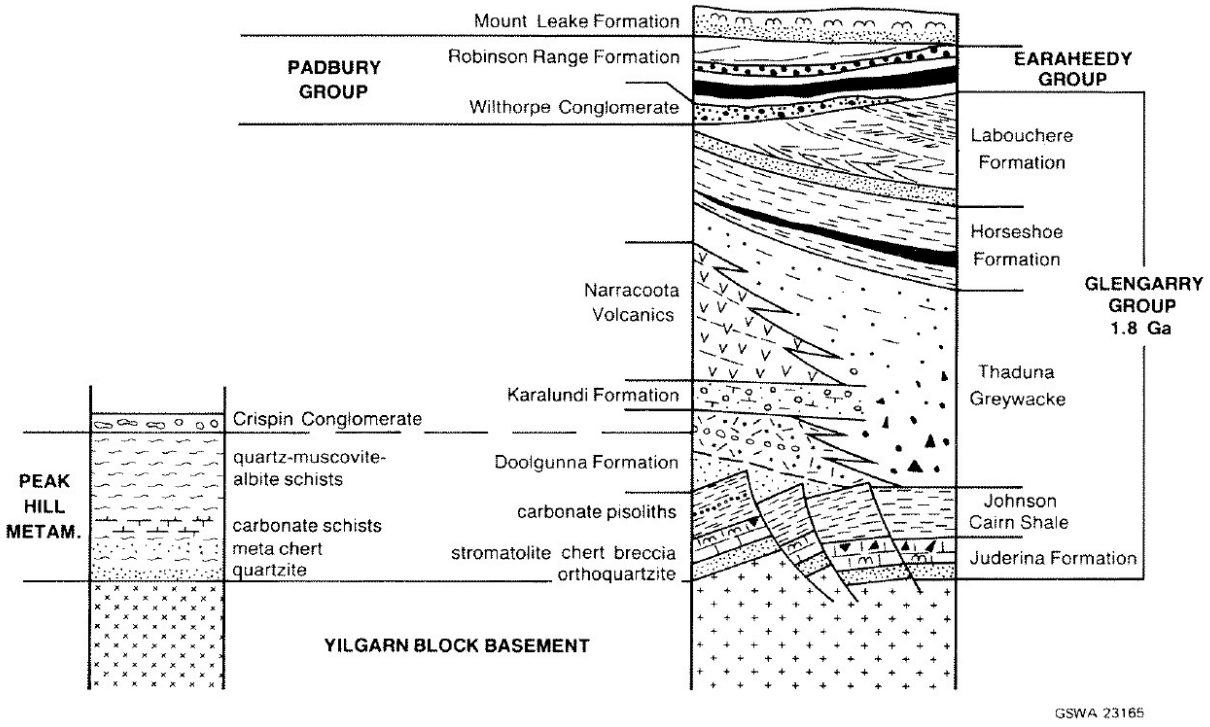

Figure 2.4. Stratigraphy of the Yerrida, Bryah and Padbury Basins from Gee (1987).

Thornett (1995) investigated the nature and timing of the gold mineralisation of the Peak Hill gold deposits as well as the Nathans and Labouchere deposits in the western Bryah. Her work included geochronological constraints on the mineralisation using lead (Pb) isotopes on sulfides and tellurides. It identified that the Peak Hill ores had a different Pb source to the Labouchere and Nathans deposits. Peak Hill ores were identified as originating from the same source composition as that of the Plutonic gold mine, leading to the Peak Hill Schist being amalgamated into the Archaean Marymia Inlier.

The Glengarry basin was discarded and superseded by the Yerrida and Bryah Basin by Pirajno et al. (1995), (Pirajno et al., 1996), Occhipinti et al. (1997a), and Pirajno et al. (2000).

The Padbury Basin remained as a separate basin unconformably overlying the Bryah Basin (Fig. 2.5). Despite the abandonment of the term "Glengarry Basin" studies of the Nabberu Province by Krapez and Martin (1999) were completed using sequence stratigraphy based on the classifications defined by Gee (1987). Krapez and Martin (1999)'s study focused on the tectonostratigraphy of the Yerrida, Bryah and Padbury Basin sedimentary rocks and extended to the larger Nabberu Basin and Palaeoproterozoic zone of orogensis. There are a much larger number of sub basins within the Glengarry basin, not clearly indicated from the remaining outcrop (Krapez, pers. comm.). Resulting from their studies during industry fieldwork, Krapez and Martin (1999) utilise nomenclature independent of that provided by the GSWA. They referred to the Yerrida and Bryah Basin sediments as the "Ned's Creek Basin". The Horseshoe Formation in the western portion of the Glengarry Basin was referred to as the "Horseshoe Basin". Krapez and Martin (1999) indicated that the Ned's Creek Basin may have been initially segmented by basement-cored fault blocks and they identified the sedimentary rocks as deposited in a marine environment formed by rifting of a continental margin, most likely forming a back arc rift basin.

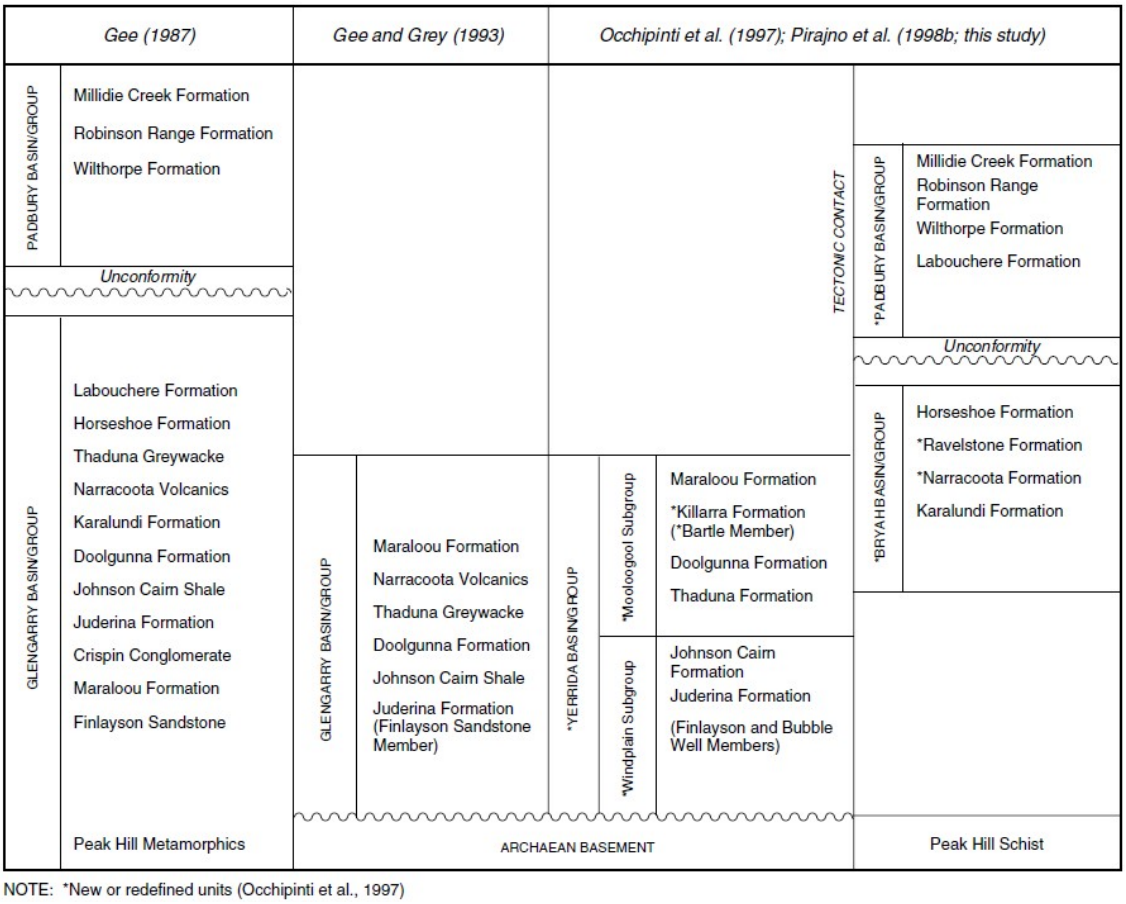

Figure 2.5. Summary of the GSWA's changing status of the Yerrida, Bryah and Padbury Basin sedimentary rocks (from Pirajno and Occhipinti (1998)).

The DeGrussa VHMS deposit is hosted in the lower mafic basalts/dolerites and sedimentary rocks of Karalundi Formation equivalence within the Bryah Basin. The accepted nomenclature and stratigraphy in use by exploration companies within the Yerrida, Bryah and Padbury Basins is that provided by the GSWA although their interpretation of the regions formation remains contentious.

There is little doubt among the many authors and field geologists working in the Doolgunna region that there are problems with the currently defined stratigraphy. Unless stratigraphy has been identified as differing, for the purpose of this study, regional stratigraphic units will be referred to using the currently assigned GSWA classification - the Yerrida, Bryah and Padbury basins - for ease of describing locations and position in the stratigraphy. The stratigraphic column and relationships presented in Figure 2.3 are used throughout this thesis.

2.3. Regional Geological Setting

In order to put the geology, geochemistry and geochronology presented in this thesis in context it is necessary to describe the major terranes and tectonic events that have formed the region. Of note is the Gascoyne Province, which comprises granitic and medium-high grade metamorphic rocks (Sheppard et al., 2010). The oldest rocks are found in the exotic Glenburgh Terrane (Fig. 2.1.) which contains the Dalgaringa Supersuite, similar in age to rocks associated with the DeGrussa Deposit. Additional units, the Bandee, Carlathunda, MacAdam and Yarraquinn Seismic Provinces, were also identified by Johnson et al. (2013) as distinct seismic terranes of unknown age and character, not exposed at surface and located north of the Glenburgh Terrane. These were all accreted to the Pilbara Craton before c. 2775 Ma (Johnson et al., 2013).

The Glenburgh Terrane consists of metamorphosed and variably deformed intermediate to felsic granitic rocks of the Halfway Gneiss (2550-2430 Ma) and Dalgaringa Supersuite (2005-1975 Ma), as well as meta-sedimentary rocks of the Moogie Metamorphics (2240-2125 Ma) and the Camel Hills Metamorphics (2000-1955 Ma) (Sheppard et al., 2010, Johnson et al., 2011a, Sheppard et al., 2004).

The Moogie Metamorphics overlie the Halfway Gneiss in the south of the Gascoyne Province, and contain detrital zircons (3510 – 2239 Ma) derived from the southern Pilbara and the Halfway Gneiss (Johnson et al., 2010, Johnson et al., 2011a). The unit is dominated by psammitic schists (the Mumba Psammite) and minor intercalated calc-silicate gneiss and marble. The unit was deposited between c. 2240 and c. 2125 Ma, likely as part of the Opthalmian foreland basin system (Johnson et al., 2011a)

The Dalgaringa Supersuite comprises massive, foliated and gneissic granitic rocks. It forms, and is exposed in, the southern part of the Gascoyne Province. Recent magnetotelluric data obtained by Dentith et al. (2014) suggests an unknown unit beneath the Edmund and Collier Basins may correlate to the Dalgaringa Supersuite. The Dalgaringa Supersuite formed during two episodes of magmatism, which are separated by a regional high-grade tectonometamorphic

event. The rocks consist of 2005-1985 Ma foliated and gneissic diorite to monzogranite with interleaved amphibolite, and c. 1975 Ma tonalite and granodiorite plutons of the Nardoo Granite (Sheppard et al., 2004). The granites have whole rock major, trace and rare earth element concentrations consistent with formation in a supra-subduction zone setting. Whole-rock Nd isotopic signatures indicate the involvement of late Archean granitic gneisses, suggesting that magmatism occurred in a continental margin arc as an Andean-type batholith (Sheppard et al., 2004). This is supported by Hf isotope data which demonstrates that the Yilgarn Craton crust cannot be involved in the generation of these magmatic rocks instead fitting a two component system of depleted mantle and Halfway Gneiss Johnson et al. (2010), Johnson et al. (2011b).

The Camel Hills Metamorphics form fault-bounded units within the Errabiddy Shear Zone between the Gascoyne Province and Narryer Terrane of the Yilgarn Craton. The unit comprises the Quartpot Pelite and the Petter Calc-silicate, as well as undivided amphibolite and metamorphosed banded iron-formation, with all units affected by amphibolite to granulite facies metamorphism. The Quartpot Pelite consists largely of biotite– plagioclase–quartz (–K-feldspar–garnet–sillimanite) pelitic gneiss, migmatitic pelitic gneiss, and psammitic schist, interlayered with minor quartzite, calc-silicate gneiss, and amphibolite. U–Pb SHRIMP dating of detrital zircons yield a range of ages between c. 2892 and c. 1985 Ma, but are dominated by zircons in the 2080 – 2000 Ma range (Johnson et al., 2010). The package was deposited sometime after 2001 ± 26 Ma or 1985 ± 28 Ma, but before the growth of metamorphic zircon rims at 1955 ± 7 Ma and 1952 ± 14 Ma.

The Petter Calc-silicate is composed of clinopyroxene–plagioclase (–epidote– quartz ± hornblende ± grossular) calc-silicate schist and gneiss, interlayered with quartzite and quartz–diopside rock, and minor pelitic schist or migmatitic pelitic gneiss and amphibolite. The peak mineral assemblages have been overprinted and retrogressed during the Capricorn Orogeny. The unit has solely Archean detritus (c. 3148 and c. 2603 Ma) and may have been deposited along the Yilgarn Margin sometime after 2608 ± 4 Ma (Johnson et al., 2011a).

Rocks of the Camel Hills Metamorphics are interpreted to have formed in a forearc or backarc basin setting along the margin of the Glenburgh Terrane in response to uplift of the southern margin of the Pilbara during continental collision between c. 2240 and 2125 Ma (Johnson et al., 2011a). The Camel Hills Metamorphics are the meta-sedimentary rocks equivalent to the intrusive rocks of the Dalgaringa Supersuite.

The Errabiddy Shear Zone separates the Glenburgh Terrane from early to late Archean granitic gneisses and foliated granites of the Narryer Terrane (3730 – 2920 Ma)(Fig 2.1) and marks the northern limit of the Yilgarn Craton. Subduction in a northerly direction occurred along this margin until ca. 1970 Ma (Sheppard et al., 2004).

2.4. East Capricorn Geology and the Yerrida, Bryah and Padbury Basins

The Yerrida, Bryah and Padbury Basins form the eastern part of the Capricorn Orogen and are relatively understudied in comparison with the western parts of the Capricorn Orogen. The Yerrida Basin forms a ~4 km thick succession of mixed siliciclastic and carbonate rocks and although poorly dated, appears to be the oldest. It is both unconformably and structurally overlain by the Bryah and Padbury Basins. The Bryah Basin represents a 10km thick sequence of intrusive and extrusive volcanic rocks, volcanoclastic rocks and sedimentary rocks which host significant amounts of gold and copper mineralization. The Padbury Basin (~6 – 7 km thick) developed as a foreland basin, unconformably overlying the Bryah Basin and consists of a succession of clastic and chemical sedimentary rocks.

2.4.1. The Archean Marymia and Goodin Inliers

The Marymia Inlier is a fragment of Archean granite-greenstone basement. Rocks are mainly granitic but also include small enclaves of calc-silicate rock, ortho-amphibolite and minor metamorphosed banded iron formation. The south-western end of the Marymia Inlier comprises the Peak Hill Schist, a strongly deformed portion of Archean rocks comprising phyllonite, quartz-muscovite schist, calc-silicate schist, sericite (-quartz) schist, quartz-

muscovite-biotite-chlorite schist and mylonite. They are faulted and tectonically interleaved along the contact with Bryah group sedimentary rocks (Occhipinti et al., 1997a, Pirajno et al., 2000). The Peak Hill schist hosts the Peak Hill, Fiveways and Mt. Pleasant orogenic gold deposits. Rocks of the Yerrida and Bryah groups are mostly in tectonic contact with the Marymia Inlier, although north of the DeGrussa deposit it appears unconformable onto Archean basement (Jeffery, 2013).

The origin of the Marymia is controversial. Stratigraphic correlations between the Marymia Inlier and the Youanmi Terrane have been made, but more recent studies have favoured correlation with the Eastern Goldfields Superterrane (Gazley, 2011). The Marymia was suggested by Gee (1979) as an in situ remnant of Archean basement. Krapez and Martin (1999) suggested it as a rotated and separated portion of the Yilgarn. Pirajno et al. (2004) inferred it to be a stable remnant rifted from the northern margin of the Yilgarn during the Capricorn Orogeny. Most recent magnetotelluric transects of Dentith et al. (2014) show the Marymia Inlier as a wedge-shaped, fault bounded unit, the southern contact corresponding to the Jenkin fault (Fig. 2.2). In this interpretation, the Marymia Inlier is interpreted as a para-autochthonous fragment separated from the Eastern Goldfields Superterrane of the Yilgarn Craton during continental rifting and deposition of the Windplain Group of the Yerrida Basin at c. 2174 Ma (Dentith et al., 2014).

The Goodin Inlier (2624 ± 8 Ma (Nelson, 1997)) outcrops from within the Yerrida Group sedimentary rocks. It is interpreted as a tectonically reactivated block of the Archaean Yilgarn Craton on which the Yerrida Group unconformably lies (Pirajno and Adamides, 2000a). The Goodin Inlier is suggested to be a part of the Youanmi Terrane, implying that the Ida Fault, which divides the Youanmi and Eastern Goldfields Superterrane from each other, passes to the east of the Goodin Inlier (Dentith et al., 2014).

2.4.2. Yerrida Group

The Yerrida Group (Fig. 2.2, 2.3) consists of the Windplain Subgroup and the Mooloogool Subgroup (Pirajno and Adamides, 2000a). The Windplain Subgroup comprises the basal Finlayson sandstone, the carbonaceous and stromatolitic Juderina Formation and the siliciclastic siltstones and shales of the Johnson Cairn Formation. The overlying Mooloogool Subgroup (comprising siliciclastic sedimentary rocks of the Thaduna and Doolgunna Formations, the mafic Killara Formation and the black shale-rich Maraloou Formation) is absent from stratigraphy in the DeGrussa area. The Mooloogool Subgroup is suggested to represent a change to a rift-basin setting (Pirajno et al., 1996). Initially the contact between the two subgroups was identified as transitional by Pirajno et al. (1996). Later studies suggest there is a hiatus between the Windplain (2.17 Ga) and Mooloogool groups, due to a monazite age date of 1843 ± 10 Ma for intrusion of mafic sills of the Killara Formation into Maraloou Formation rocks (Rasmussen and Fletcher, 2002). Lower greenschist facies metamorphism has affected all rocks in the Yerrida group (Pirajno and Adamides, 2000a).

2.4.2.1. Juderina Formation

The Juderina Formation, as identified by Pirajno and Adamides (2000a) consists of quartz arenite and subordinate siltstone, chert breccia and pebble beds. It is largely observed as unconformable on Archean granite-greenstone basement and consists of the lower Finlayson member and upper Bubble Well Member. SHRIMP U-Pb analyses of detrital zircons in the Finlayson Member yield ages of 2.7Ga (Pirajno et al., 2004) indicating probable derivation from Archaean basement rocks. The Finlayson Member is not present in drill holes proximal to the DeGrussa Stratigraphy (Jeffery, 2011).

The Bubble Well Member consists of dolomite, cherty microbial laminites and stromatolitic carbonate with interbeds of dolomitic shale. In the DeGrussa area, the Bubble Well Member is located above the Archean Marymia Inlier and consist of approximately 100m of stromatolitic mats, mudstones and evaporate (Grey, 1984, Gee and Grey, 1993, Grey, 1994, Russell, 1992,

Grey and Pirajno, 2012). Pb-Pb dating of carbonate by Woodhead and Hergt (1997) provides an age of 2174 ± 64 Ma for the unit at the southern edges of the Yerrida Basin. The 2.22 to 2.06 Ga Lomagundi-Jatulian (Lomagundi) Event, a large positive C isotope excursion of up to +12‰, was preserved in these rocks (El Tabakh et al., 1999, Lindsay and Brasier, 2002, Melezhik et al., 2007, Bekker et al., 2008). The Lomagundi-Jatulian event occurred worldwide, and postdates a rise in atmospheric oxygen as carbon was biogenically fixed by photosynthesis and then sequestered between 2.47-2.32Ga (Melezhik et al., 2007). The Lomagundi-Jatulian event is recorded in rocks of Finland, South Africa, North America and Australia. The first major isotopic excursion followed the first appearance of basins (Hammersley Basin at 2.45-2.2Ga) on the Australian continent, raising the possibility of a causal connection between the Lomagundi excursion and the plate tectonic evolution of Earth's Crust (Lindsay and Brasier, 2002). Although there is no true consensus as to why the Lomagundi-Jatulian event occurred, one suggestion is the input of oxygen to the atmosphere due to photosynthsis of organisms following the break up of the icesheet due to tectonic activity.

2.4.2.2. Johnson Cairn Formation

The Johnson Cairn Formation consists of varicoloured, iron-rich shale with graded silty layers and dolomite bands (Pirajno and Adamides, 1998). The boundary with the underlying Juderina Formation is conformable and is taken as the topmost bed of quartz arenite. The Johnson Cairn Formation is present in stratigraphic drill holes within the footwall of the DeGrussa Deposit. The siliciclastic mudstone and pyritic organic rich shale of the Johnson Cairn Shale is suggested by Krapez and Martin (1999) to represent rapid deposition in a transgressive marine environment.

2.4.2.3. Thaduna Formation

Prior works have defined the Thaduna Formation by varied names and positions in stratigraphy across both the Bryah and Yerrida Basins (MacLeod, 1970, Gee, 1979, Gee, 1987).

Occhipinti et al. (1997a) defined the unit as the "Thaduna Formation" with the type locality at the Thaduna Copper Mine where it is host to the mineralization (Pirajno and Adamides, 2000a). Pirajno et al. (1996) sub-divided the Thaduna "Greywacke" into the Thaduna Formation within the Yerrida Basin, and similar sedimentary rocks of the Bryah Group into the "Ravelstone Formation". This is the currently accepted stratigraphy (Fig. 2.3.). The Thaduna Formation interfingers with the overlying Doolgunna Formation, Karalundi Formation and Narracoota Formation, suggesting that it is contemporaneous with these units. It eventually overlies the Narracoota Formation in the west of the basin.

The Thaduna Formation was described by Gee (1987) as a thick turbidite sequence of graded fine to coarse-grained lithic, feldspathic and mafic wacke with subordinate interbedded slaty mudstone, containing a variety of sedimentary structures (single and multiple-graded cycles, shale, intraclasts, flute masks, load casts, convolute lamination and slump folds). Lithic fragments are altered basalt, jasper and ferruginous shale. Field and petrographic analysis (Pirajno et al., 2004) provide evidence that the Thaduna and Doolgunna Formations are both composed of granite, greenstone and mafic volcanic lithic fragments. Detrital zircons have an Archaean age of 2.65 Ga (Pirajno et al., 2004).

The Thaduna Formation within the Yerrida Basin is interpreted as a product of a high energy environment, which resulted in a sequence of turbidites deposited in a deep northeast-trending rift concurrently with the volcanic activity that produced the adjacent Killara Formation (Gee, 1987, Pirajno and Adamides, 1998, Pirajno et al., 2004).

2.4.2.4. Doolgunna Formation

The Doolgunna Formation consists of thick bedded, arkosic sandstone, quartz siltstone, and subordinate pebble beds, conglomerates, arkosic turbidite rocks and megabreccia units (containing large blocks and fragments up to 3m across of Bubble Well Member rocks and Archean granitic rocks)(Pirajno and Adamides, 1998, Pirajno et al., 2004). All beds characteristically display angular to sub rounded quartz and subordinate chert clasts and

feldspar in a matrix of kaolinitic clays. Low-grade metamorphism resulted in the partial conversion of kaolinite to illite or fine grained sericite.

As with the Thaduna Formation, the Doolgunna Formation is interpreted to have been deposited in a northeast-trending rift (or 'Doolgunna Graben' (Pirajno, 1996)) concurrently with the volcanic activity of the Killara Formation (Pirajno and Adamides, 1998, Gee, 1987). Pirajno and Adamides (1998) suggest that these turbidite rocks are predominately the result of terrigenous sedimentation sourced from the uplifted Goodin Dome and Marymia Inlier. Mega-breccia units are suggested to be a result of mass-wasting. In comparison, Krapez and Martin (1999) suggest the Juderina Formation, Johnson Cairn Shale and the lower Doolgunna Formation resemble lagoonal mud and barrier bar sands and a late lowstand systems tract consistent with a shallow sea or large lake with barrier bar shorelines.

2.4.2.5. Killara Formation

The Killara Formation volcanic rocks are composed of flat lying to shallow dipping, low Ti subalkaline, unmetamorphosed intrusive and extrusive rocks as well as high-Fe, high-Mg tholeiitic to calc-alkaline basalts and basaltic andesites emplaced as subaerial and subaqueous lava flows, intrusive sheets, sills and dykes (Pirajno and Adamides, 1998, Pirajno and Adamides, 2000a, Pirajno et al., 2004). The dolerite and basalt contain augite, plagioclase, secondary epidote, quartz, leucoxene, carbonate, sericite, chlorite and sulfides (pyrite, pyrrhotite and lesser chalcopyrite, either replacing plagioclase crystals or forming along microfractures). Trace element geochemistry suggests crustal contamination or alternately an enriched mantle source (Pirajno, 1996, Pirajno and Occhipinti, 2000) possibly representing formation in a continental rift setting (Pirajno and Davy, 1996). The end of volcanic activity is marked by the Bartle Member, a chemical-evaporitic unit consisting of chertified microbial laminites with barite and anhydrite nodules, massive chert, and chert breccia (Pirajno and Adamides, 1998, Pirajno and Adamides, 2000a). The rocks are interpreted by Pirajno and Adamides (2000a) to have been volcanoclastic, chemical sedimentary rocks and evaporates indicative of an

evaporitic-pyroclastic-thermal-spring environment associated with rifting (Pirajno and Grey, 2002).

The Killara Formation is overlain conformably by the Maraloou Formation with peperitic contacts observed in eastern parts of the Yerrida Basin associated with dolerite emplacement. The Yelma Formation of the Earaheedy Group unconformably overlies in the east. The lower contact interfinger with the Johnson Cairn, Thaduna and Doolgunna Formations (Pirajno and Adamides, 2000a). The western extensions of the formation are lenses mainly of tholeiitic basalt intercalated with rocks of the Thaduna and Johnson Cairn Formations. The Killara Formation mafic rocks are possibly a time equivalent of the Narracoota Formation and mafic rocks associated with the DeGrussa deposit, however age dating of the Yerrida Group is scarce and correlations cannot be clearly defined.

2.4.2.6. Maraloou Formation

The Maraloou Formation is considered a basin-fill facies of the uppermost Yerrida Group, and could be laterally equivalent to the Labouchere Formation 150 km to the northwest (Gee, 1979, Gee, 1987, Gee and Grey, 1993). Lithologies range from siltstone, laminated siltstone, black sulfidic shale and ferruginous shale, intercalated with subordinate marl beds, dolostone, laminated chert and chert breccias deposited in below wave base conditions with evidence of microbial origin (Pirajno and Adamides, 2000a, Pirajno and Adamides, 1998). A small number of gossans with anomalous Cu, Pd, Ba and Zn are present throughout (Pirajno and Occhipinti, 2000).

The contact between the Killara and Maraloou Formations is transitional or locally discordant consisting of intercalated mafic lavas and sills and black shale. Rasmussen and Fletcher (2002) provide a minimum age of 1843 ± 10 Ma for the Maraloou Formation, based on SHRIMP U-Pb analysis of monazite in contact metamorphosed shale against a Killara Formation related dolerite sill in the southwest of the Yerrida Basin.

2.4.3. Bryah Group

The Bryah Group (Fig. 2.2, 2.3) preserves a sequence of intrusive and extrusive volcanic, volcanoclastic and sedimentary rocks (Pirajno et al., 2000). It consists of the Karalundi, Narracoota, Ravelstone and Horseshoe Formations. With the exception of the volcanic Narracoota Formation, all other formations consist of siliciclastic shales, siltstones and sandstone sequences. Additionally, the Horseshoe Formation contains a prominent iron formation which hosts the Horseshoe and Mt. Padbury Manganese deposits. Stratigraphy is often cross cut by late mafic dykes and sills of unknown age. The majority of the Bryah Group is affected by low to medium grade greenschist facies regional metamorphism as well as a retrogressive hydrothermal greenschist facies metamorphism (Pirajno et al., 2000).

The Bryah Group is in faulted contact with the Yarlarweelor Gneiss Complex, the Marymia Inlier, and the Palaeoproterozoic Yerrida Group. The Goodin Fault, a north easterly trending, high-angle reverse fault, marks the divide between the Bryah Group and the Yerrida Group (Pirajno et al., 2000, Dentith et al., 2014) (Fig. 2.2). However, more recent work by Jeffery (2013) indicates the contact as unconformable and in keeping with original geological interpretations of Gee (1987).

2.4.3.1. Karalundi Formation

The Karalundi Formation's position within stratigraphy and distribution across the basin is problematic. It was first described by Gee (1979) and Gee (1987) as a mixed sequence of clastic, carbonate, chert and tuff about 1500m thick in a stratigraphic position conformable between the underlying Doolgunna Formation and the overlying Narracoota Formation. Bunting (1986) went on to describe it as a shale sequence with minor amounts of quartz wacke, chert, tuff and carbonate. Gee and Grey (1993) recognised the unit in thrust slices around the southern margin of the Goodin Inlier and then, for the purposes of their study, amalgamated the Karalundi with the Doolgunna Formation although it was suggested that it could be present at depth within their field area.

Two distinctive rocks were assigned to this sequence by Gee (1979) and Gee (1987); 1. Medium to fine-grained, poorly sorted, ferruginous sandstone with upward-fining beds, convolute lamination and low-angle cross-bedding, and; 2. Hematite-magnetite jasper which occurs as steeply inclined pipes up to 20m in diameter, interpreted as colloidal hydrothermal deposits formed in fumarolic pipes associated with basic volcanism.

Pirajno et al. (2000) re-assigned the Karalundi Formation to form the base of the Bryah Basin. It is placed in faulted contact with the Doolgunna Formation to the south-east along the Goodin Fault although this contact is questionable (Jeffery, 2013). To the north it is in fault contact with the Peak Hill Schist. It is intercalated with volcanoclastic rocks of the Narracoota Formation in the western Bryah Basin. Pirajno et al. (2000) identified the Karalundi as an immature clastic with lesser siltstone, calcareous siltstone, cross-bedded arenite, ferruginous arenite, litharenite, minor dolomite and purple, green and black shales. Basaltic water-lain tuff and minor carbonated beds appear in the upper part of the formation. They also make note of the hematite-magnetite, jasperoidal chert and agree with the Gee (1979) interpretation. Overall the formation is interpreted to represent a transition from deep-water arkosic turbidites to shallow-water marine or even fluvial conditions and records the commencement of basaltic volcanism (Gee, 1987). SHRIMP U-Pb analyses of detrital zircons at the base of the Karalundi yield two ages of ca. 2.0 and 2.7Ga (Halilovic et al., 2004) indicating derivation of sediments from both the Yilgarn and possibly Dalgaringa Supersuite aged rocks.

2.4.3.2. Narracoota Formation

The 6000m thick Narracoota Formation forms the bulk of the Bryah Group and is intercalated with sedimentary rocks of the Karalundi Formation (Hynes and Gee, 1986). Its upper contact is both disconformable and interfingerring with the Ravelstone Formation. In places it is in tectonic contact with the Padbury Group and also the Horseshoe Formation (Pirajno et al., 2000).

The Narracoota Formation consists of peridotitic and high-Mg basalt, mafic volcanoclastic rocks including pillow structured meta-basalts, mafic intrusive rocks and mafic to ultramafic schists (Pirajno and Occhipinti, 1998). More felsic volcanic rocks (basaltic andesite, andesite and rhyolite) appear to be largely restricted to western portions of the basin proximal to the Horseshoe Lights and Fortnum mine sites (Pirajno, 1996) whereas mafic volcanic compositions predominate towards the east in the proximity of DeGrussa. Mid-greenschist and locally amphibolite facies metamorphism has affected the rocks, with almost complete replacement of the primary mafic mineralogy resulting in a mineral assemblage of albite + actinolite + chlorite + clinozoisite (epidote) + quartz + leucoxene (sphene) and relict pyroxenes. Mafic rocks are commonly aphyric, but pseudomorphs of actinolite after probable clinopyroxene and of albite/saussurite after plagioclase occur. Sheafs and plumose bundles of actinolite needles replacing former pyroxene and other metamorphic minerals including actinolite, epidote, clinozoisite, albite and calcite. Rocks have undergone sea floor metasomatism dominated by albitization (Hynes and Gee, 1986, Pirajno et al., 2000).

An oceanic depositional environment is supported by widespread occurrence of pillow structures and volcaniclastic rocks in eastern parts of the Bryah Basin around Noonyereena Hill and DeGrussa. Chemically, mafic rocks are similar to low-potash tholeiite from mid-ocean ridges but with slightly lower Ti and Zr contents representative of boninites (Hynes and Gee, 1986) This suggests that the Narracoota volcanics were erupted as an island arc, with rocks having more similarities to the boninites of forearc regions in the western Pacific than to any other modern tectonic environment. However, the current interpretations favour the Narracoota Formation as an oceanic plateau, accreted to the north-west margin of the Yilgarn Craton given the similar chondrite normalized REE patterns (Pirajno, 2004, Pirajno et al., 2004). Hyaloclastite in the southern Bryah Basin resulted from explosive volcanic activity in a shallow-water setting and were emplaced unconformably on the Archean granites of the Yilgarn (Hynes and Gee, 1986, Pirajno and Occhipinti, 2000) contrasting with the oceanic setting of the metabasites of the Narracoota Formation further north.

2.4.3.3. Ravelstone Formation

The 1000m thick Ravelstone Formation comprises a succession of lithic and quartz wacke, shale and siltstone with upwards fining graded bedding and a provenance from nearby granitic or felsic precursors, and mafic material derived from the underlying Narracoota Formation (Pirajno et al., 2000, Pirajno et al., 2004, Pirajno and Occhipinti, 2000). It contains lenses of chert in the north. SHRIMP U-Pb ages on detrital zircons give a maximum age of 2.01 Ga (Nelson, 1997). The Ravelstone Formation is interpreted to represent a rift-fill succession that was deposited on top of the Narracoota Formation (Pirajno et al., 2004). The lower contact with the Narracoota Formation is disconformable, and sometimes interfinger. The upper contact with the Horseshoe Formation is conformable (Pirajno et al., 2000).

2.4.3.4. Horseshoe Formation

The Horseshoe Formation is approximately 300m thick, defined as including finely laminated (hematitic) shale and siltstone, fine grained quartz-wacke with interleaved iron formation and chert, graded quartz wacke, manganiferous shale, garnetiferous biotite-chlorite schist and garnetiferous iron-formation (Pirajno et al., 2000, Pirajno et al., 2004) (Fig. 2.6). A prominent iron-formation member, host to the Horseshoe and Mt. Padbury manganese deposits (Pirajno et al., 2000), occurs in the stratigraphic centre of the unit consisting of three bands of 40m thick iron formation intercalated with alternating layers of chert-magnetite-stilpnomelane rock, chloritic shale and chert (Gee, 1987). The contact between the underlying Ravelstone Formation is gradational and conformable, although in places the Horseshoe Formation directly overlies the Narracoota Formation in conformable or tectonic contact.

Deposition of the Horseshoe Formation was interpreted by Gee (1987) and Pirajno et al. (2004), to mark deposition and filling of a deep submarine trough followed by a cessation of sedimentation and a period of quiet shallow-water sedimentation during which chemical sediments (Banded Iron Formations and manganese deposits) precipitated in isolated depressions.

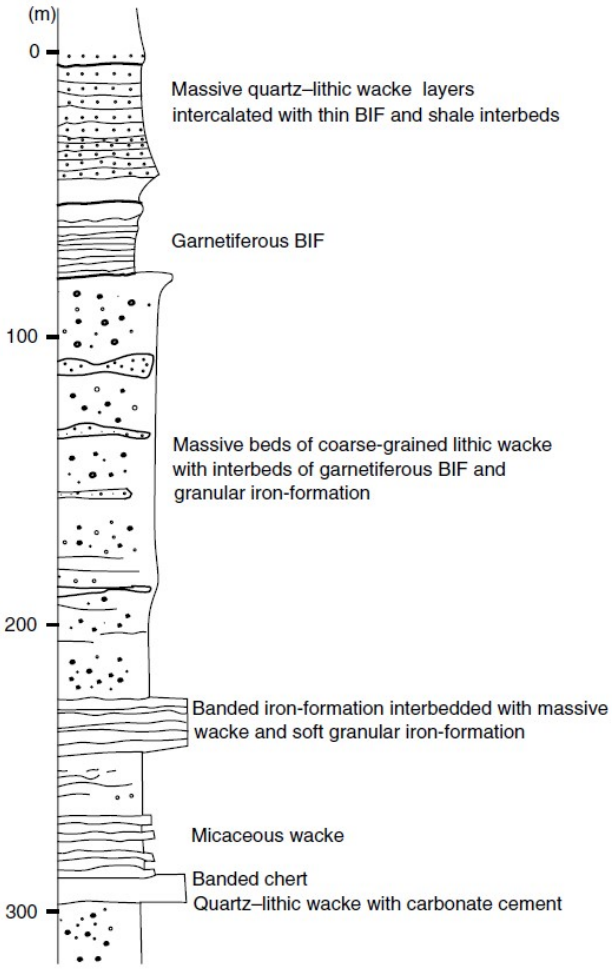

Figure 2.6. Schematic stratigraphy from Pirajno et al. (2000) of the Horseshoe Formation, from an area of outcrops ~12 km west-northwest of the Peak Hill mine.

2.4.4. Padbury Group

The Padbury Group (Fig 2.2, 2.3) unconformably overlies the Bryah Group and consists of a succession of clastic and chemical sedimentary rocks formed as a foreland structure (Pirajno et al., 2000). It consists of a sequence of tightly infolded conglomerate, iron-formation and calcareous sedimentary rocks (Gee, 1987). Stratigraphic units are the Labouchere, Wilthorpe, Robinson Range and Millidie Creek Formations. The Labouchere and Wilthorpe Formations consist of upwards coarsening deep water turbidites with detrital zircons dated at c. 1980 Ma (Pirajno et al., 2004). The Robinson Range and Millidie Creek Formations are fine grained

banded iron formations, ferruginous shales and siltstones deposited in a shallowing submarine environment. These iron formations could be correlated with the granular iron formation of the Frere Formation (Earaheedy Group) dated at 1891 ± 8 Ma (Rasmussen et al., 2012). The Padbury Group remains a clearly definable sequence of rocks separate from the Yerrida and Bryah Basin sedimentary sequences.

2.4.4.1. Labouchere Formation

Prior to Occhipinti et al's (1997) studies, the Labouchere Group was considered part of the Bryah Basin sedimentary succession. The Labouchere Group was incorporated into the Padbury Basin on the basis of an unconformable contact with the underlying Bryah Group sediments. Together with the overlying Wilthorpe Formation the sequence is estimated to be approximately 5000m thick (Pirajno et al., 2000).

The contact between the Labouchere Formation and underlying Horseshoe Formation is identified as unconformable., often marked by a conglomeratic unit, or as fault or shear zones (Windh, 1992, Pirajno et al., 2000). It is regionally inferred from the low-angle truncation of an iron-formation marker unit in the Horseshoe Formation by the lowermost quartz arenite of the Labouchere Formation (Pirajno et al., 2000). The Labouchere Formation is gradational and overlain conformably (Pirajno et al., 2000, Martin, 1994) by the Wilthorpe Formation despite the original interpretation (Gee, 1979) of an unconformable relationship.

Gee (1987) described the Labouchere Formation as quartz sandstones and sericitic quartz siltstone interpreted to have deposited on a stable marine shelf swept by sediment-dispersal currents. The lower sequence consists of medium grained, well-sorted quartz sandstone with sparse feldspar in siliceous cement with low-angle trough cross-bedding and linguoid ripple marks. Higher in the sequence interbeds of sericitic quartz siltstone and phyllitic shale occur, when the sandstone has an argillaceous and micaceous character.

2.4.4.2. Wilthorpe Formation

The Wilthorpe Formation is approximately 1300m thick and was formerly named the "Wilthorpe Conglomerate" by Gee (1987). Isolated exposures of shallow-dipping conglomerate were seen by Gee (1987) to sit unconformably over the steeply dipping Bryah Basin sediments. Conglomerate clasts consist predominately of vein quartz, coarse iron-cemented sandstone and fine grained silica-cemented sandstone identified as Bryah Basin sediments.

Pirajno et al. (2000) redefined the Wilthorpe Formation as comprising quartz- and chert-pebble conglomerate, quartz wacke, sericitic siltstone, chlorite-quartz shale, quartz-sericite-hematite schist, dolomitic sandstone and finely laminated chert lenses. The conglomeritic portion contains clasts of vein-quartz, chert, quartzite, quartz wacke and rare siltstone-mudstone clasts in a quartz wacke matrix. The siltstone forms a distinct horizon along the gradational contact with the overlying Robinson Range Formation.

Gee (1987) interpreted the Wilthorpe Formation as a fluvial deposit with shales recording the position of large rivers spreading across a peneplain surface. Shale, chert and terrigenous muds later covered the river sequence.

2.4.4.3. Robinson Range Formation

The 500m thick Robinson Range Formation consists of a lower banded iron formation and an upper granular cherty iron formation separated by chlorite-sericite-hematite shale. The granular iron formation is characterised by 10-20mm thick beds of granular and oolitic chert, red jasper, and 1m thick beds of clastic ironstone(Gee, 1987, Pirajno et al., 2000). The formation occurs as elongated outcrops that extend from east to west in the ventre of the Bryah-Padbury Basin, and isn a northerly direction of the eastern margin of the Yarlarweelor gneiss complex (Pirajno et al., 2000).

The Robinson Range Formation ironstones may be contemporaneous with iron formation in the Frere Formation within the Earaheedy Basin sediments. Bunting (1986) made a detailed petrographic study of Frere Formation ironstone. These were interpreted as chemical

precipitates of iron oxide, iron silicates and oolitic chert on a stable marine shelf. Banded varieties of the Robinson Range Formation formed in deeper water. Granular varieties represent deposition in a shallow, wave disturbed environment (Gee, 1987). The Frere Formation was dated at 1891±8 Ma (Rasmussen et al., 2012).

2.4.4.4. Millidie Creek Formation

The 1000m thick Millidie Creek Formation was originally defined by Gee (1979) and redefined by Occhipinti et al. (1997b). It consist of small outcrops in the cores of the Robinson Syncline and Fraser Syncline (Pirajno et al., 2000). Stratigraphy consists of ferruginous shale and siltstone, intercalated with irregularly banded manganiferous iron-formation, iron-rich shale and siltstone, dolomitic sandstone, ferruginous quartz wacke and chloritic siltstone, ferruginous shales with a well-developed pencil cleavage, sandstone, finely bedded micaceous siltstone-shale with interbedded quartz-dolomite siltstone layers and minor granular iron-formation. The unit hosts many manganese prospects (Gee, 1987, Pirajno et al., 2000). Based on its composition it is very likely to have formed in a shallow marine setting.

2.4.5. Regional Intrusive Rocks

Granodioritic intrusive rocks in the eastern parts of the Bryah Basin are related to the Narracoota Formation and result with Palaeoproterozoic U-Pb ages of 2012-2018 Ma (chapter 6/Hawke et al. (2015)). Both diamond and RC drill hole observations suggests that the Narracoota mafic dolerite and gabbro fractionated from these granodiorites and are possibly contemporaneous with mineralization at the DeGrussa deposit.

The 1965-1945 Ma Bertibubba Supersuite granites and dykes are the first common magmatic elements of the northern margin of the Yilgarn, Yarlarweelor Gneiss Complex, Errabiddy Shear Zone and the Glenburgh Terrane (Paradise Zone) (Sheppard et al., 2004, Sheppard et al., 2010). No intrusive rocks of this age have been yet identified in the eastern

Capricorn Orogen. Deformed rocks of the Padbury Group are intruded by granite (Martin, 1994) that are correlated with c. 1800 Ma granites (the Moorarie Supersuite) in the region.

2.5. Regional Tectonics

The DeGrussa deposit is located proximal to the Jenkin Fault, a large scale structure running in a southwest to northeast direction which splays and disappears towards the west. The Goodin Fault, a high-angle reverse fault forms the southern boundary between the Yerrida and Bryah Groups and merges with the Murchison Fault in the southern parts of the Bryah Basin. The Coolinbar Fault in the west forms the contact between the Yarlarweelor Gneiss Complex and the Bangemall Group sediments. The Fortnum Fault is a continuation of the Coolinbar Fault, crosscutting sediments of the Padbury and Bryah Basins (Fig. 2.7). Fortnum gold mineralisation at Yarlarweelor and Starlight/Trevs is proximal to this fault and related splays. The Labouchere and Nathans deposits are located proximal to the north-south oriented Kinders Fault, east of, and subparallel to, the Wilthorpe Fault but also close to the Fortnum Fault. Four deformation events have been identified by Pirajno et al. (2000) in the Bryah/Padbury basins.

D1 (North-south compression): The initial deformation event formed subhorizontal mylonites, thrusts and folds, mesoscale recumbent folds, and tight-isoclinal, rootless folds. It is rare to view these due to overprinting of later deformation events. F1 folds are apparent in the Peak Hill Antiform, Robinson Syncline, Fraser Syncline and the Millidie Syncline (Fig. 2.7) as well as at the Peak Hill mine. No indicators for the sense of movement were observed by Pirajno et al. (2000). The Goodin and Murchison Faults may be D1 faults, reactivated by D2 (Pirajno et al., 2000)

D2 (North-south compression): D2 structures largely overprint D1 events and include upright tight-isoclinal east-west folds and subvertical foliation, east-west shear zones and south-verging thrust faults (Pirajno et al., 2000). D2 folds include the Robinson Syncline and Padbury Syncline.

Pervasive S2 foliation is developed over large areas in the mafic schists of the Narracoota Formation. South of the Robinson and Fraser Synclines, regional anastomosing D2 shear zones are developed in the basaltic rocks of the Narracoota Formation (Pirajno et al., 2000).

The Fortnum Fault, proximal to the Fortnum Gold mines of Yarlarweelor and Starlight, is interpreted as a steeply dipping WNW-trending structure, with a steep west-pitching mineral lineation associated with D2 reverse-sinistral shearing. The dominant structural trends at Fortnum are associated with the D2 deformation event (Windh, 1992). Intrusion of Palaeoproterozoic course-grained granites is inferred to be associated with D2 (Pirajno et al., 2000).

D3 (East-west compression): North-south trending folds and subvertical foliation characterise D3 deformation. Subvertical faults or shear zones are localised east of the Narryer Terrane with increasingly disharmonic east-northeast trending folds eastwards (Pirajno et al., 2000). The D3 event was responsible for the doubly plunging nature of the Robinson Syncline and the Peak Hill Anticline. S3 foliations and moderate to steep, southerly plunging, small-scale F3 folds are well developed in the area of the Horseshoe Syncline.

D3 faults include the Kinders Fault (Fig. 2.7), a northerly trending fault separating a wedge of mafic volcanic schists of the Narracoota Formation (Bryah Group) from the Robinson Range, Wilthorpe, and Labouchere Formation rocks (Padbury Group) (Pirajno et al., 2000). The Fortnum Fault was reactivated by D3 (Windh, 1992) with 1 to 1.5km dextral movement indicated. Pirajno et al. (2000) suggest that D2 and D3 structures may not be two separate events and instead may have developed contemporaneously in different domains. Intense D3 folding is largely restricted to the area between the Yarlarweelor Gneiss Complex in the west and the Peak Hill Schist in the east with no evidence for D3 refolding of D2 within areas proximal to the Yarlarweelor Gneiss. In contrast, D2 features are preserved to the south and east and to a lesser extent to the west of the Peak Hill Schist.

D4 (North-northeast - South-southwest compression): D4 deformation overprints the earlier deformation events. It includes small-scale folds, subvertical foliation, shear zones,

faults and quartz blows with a common orientation of 280˚ to 310˚ in western parts of the basin. To the eastern side of the basin, in proximity to the DeGrussa Massive Sulfide deposit, structures associated to D4 are oriented in a northeast to south westerly direction, the most prominent feature of these being small boudinaged quartz veins often associated with gold mineralisation.

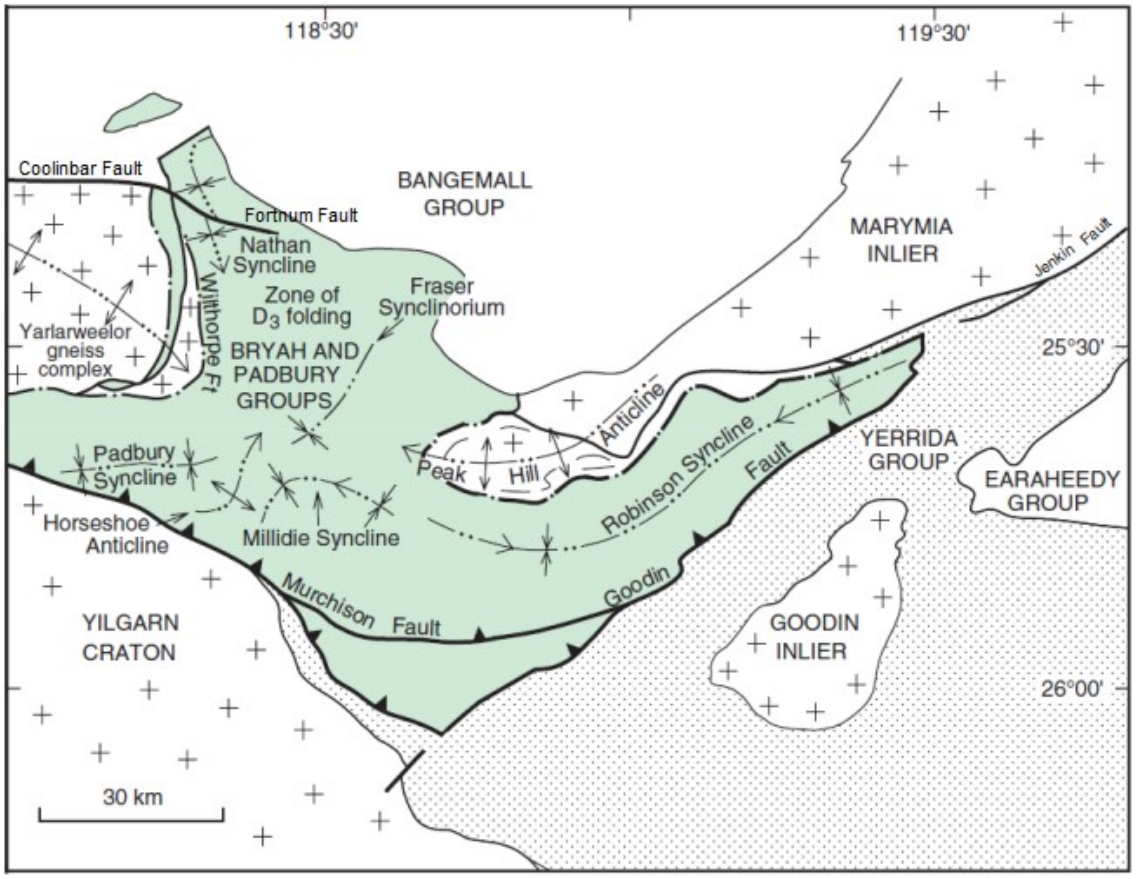

Figure 2.7. Deformation events across the Bryah/Padbury basin adapted from Pirajno et al. (2000). Highest metamorphic grades are located in fault contact zones with the Yarlarweelor Gneiss Complex. D1 deformation is no longer evident in the basin. D2 folds include the Robinson and Padbury synclines. D3 deformation is stronger in the western parts of the Bryah group, represented by the Kinders and Wilthorpe Faults. The Kinders Fault is 1.5km east and parallels the Wilthorpe Fault.

2.6. Metamorphism

The majority of the Bryah Group is affected by low to medium grade greenschist facies regional metamorphism. Within the Yerrida Group the metamorphic grade decreases to very low greenschist facies (Fig. 2.8).

The highest metamorphic grades within the Bryah Basin are located in the faulted contact zones between the Yarlarweelor Gneiss Complex and overlying metasedimentary rocks (Fig 2.8). These zones record upper greenschist to lower amphibolite facies conditions (Pirajno et al., 2000). Two main metamorphic events are identified by Pirajno et al. (2000) to have affected the basin:

M1 – a prograde regional greenschist facies metamorphic event which could have been related to D1 deformation in the Bryah and Padbury Basin sediments.

M2 – a retrogressive event throughout the Bryah and Padbury Basin sedimentary rocks which also included local hydrothermal alteration. It was possibly associated with metasomatism in high-strain zones that are aligned to D2 and D3 (Pirajno et al., 2000).

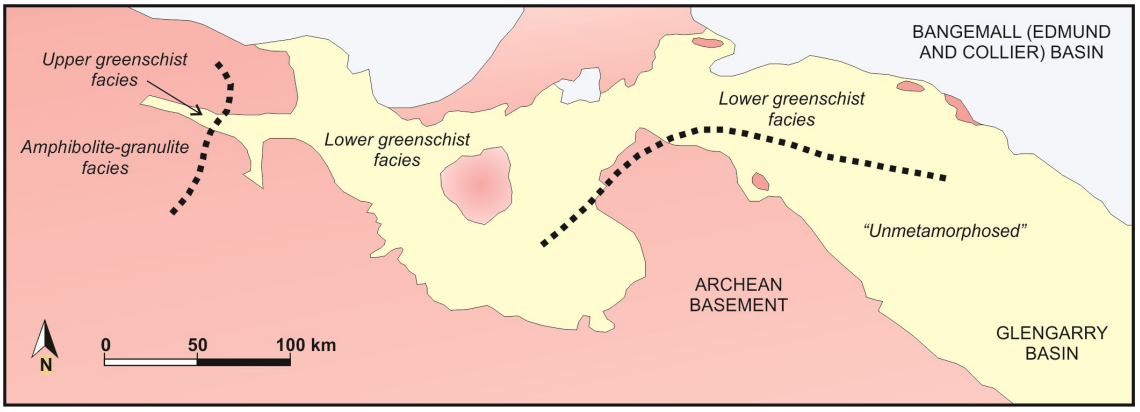

Figure 2.8. Bryah/Yerrida Group zones of metamorphism as identified by Hall and Goode (1978) and modified from Dyer (1991).

There are no constraining temperatures or pressures given for the bulk of metamorphic domains across the Yerrida/Bryah/Padbury Groups. Areas where metamorphic grades have been given are concentrated in highly deformed areas in the west of the Bryah/Padbury groups and along significant fault zones. The Peak Hill Schist was identified to have undergone amphibolite-facies metamorphism at temperatures between 500-620°C and pressures of 6.5-7kbar (Thornett, 1995), although metamorphic mineral assemblages observed commonly do not concur with these data (Pirajno et al., 2000). In western parts of the Bryah and Padbury Groups, adjacent to the Billara Fault, staurolite-andalusite-biotite-muscovite-quartz schist

developed from the metamorphism of Padbury Group sediments and indicates amphibolite grade metamorphism (Pirajno et al., 2000). On the contact between the Kerba Granite and the Narracoota Formation, a quartz-kyanite-tremolite-feldspar schist indicates upper greenschist-facies metamorphism, with pressures of 3-4kbar (Occhipinti and Myers, 1999). Domains of known metamorphic grades in the region as definied by Hall and Goode (1978) are given in Figure 2.8.

2.7. Geophysics

At the time of DeGrussa discovery, geophysical methods had been under-utilised across the region. Troy Resources had completed a small aeromagnetic survey across the DeGrussa area (Fig 2.9) and a SAM survey (Fig. 2.9) by Sandfire Resources for use in gold exploration was completed in 2008. Neither indicated a major deposit. No deep geophysical methods had been used on the area prior to the discovery. After the discovery, geophysical methods employed over the Doolgunna tenements included gravity, magnetics, radiometric and VTEM (Fig 2.9). These have all contributed to the identification of major structures and regional geological interpretation, however have not been successful in identifying clear targets for mineralisation.

A program of seismic traverses were undertaken by the GSWA across both the east and west of the Capricorn Orogen, with the eastern line passing to the east of the DeGrussa deposit (Fig 2.10). As previously discussed in Section 2.4.1. the magnetotelluric transects of Dentith et al. (2014) interpret the Marymia Inlier as a para-autochthonous fragment separated from the Eastern Goldfields Superterrane of the Yilgarn Craton during continental rifting and deposition of the Windplain Group of the Yerrida Basin at c. 2174 Ma. A transect completed across the western Gascoyne, through the Glenburgh Terrane, also identified several terranes previously unidentified from geological mapping of the region. The Glenburgh Terrane is postulated by Johnson et al. (2013) and Dentith et al. (2014) to be present in the eastern Capricorn as a block beneath the Edmund and Collier Basins, to the north of the Marymia Inlier (Fig. 2.10).

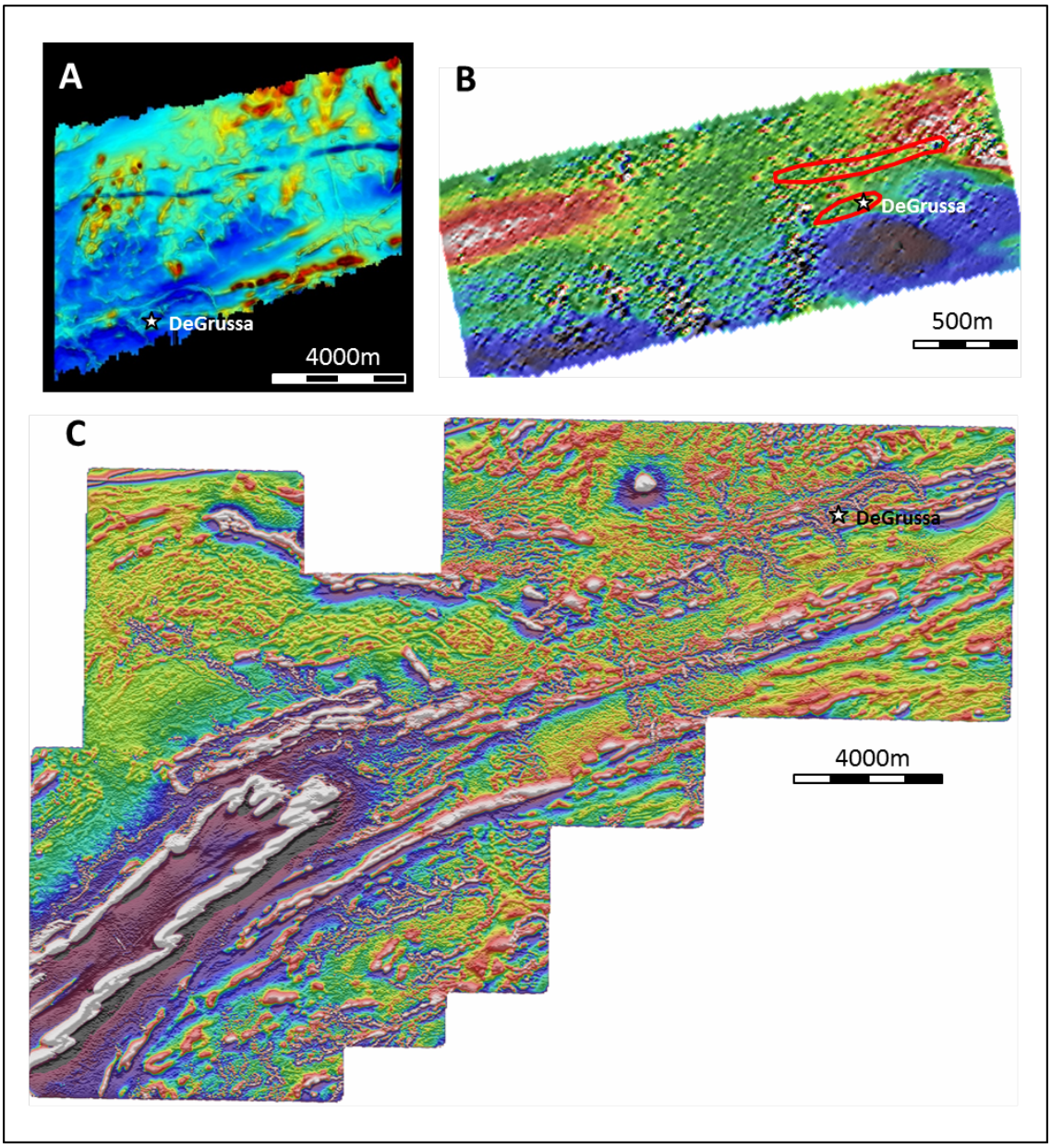

Figure 2.9A. Troy Resources Aeromagnetic survey over the DeGrussa area. **B.** Initial SAM survey over the DeGrussa project area EQMMR_Eshadel (image courtesy Sandfire Resources NL). **C.** Geophysics image from the DeGrussa project (image courtesy Sandfire Resources NL).

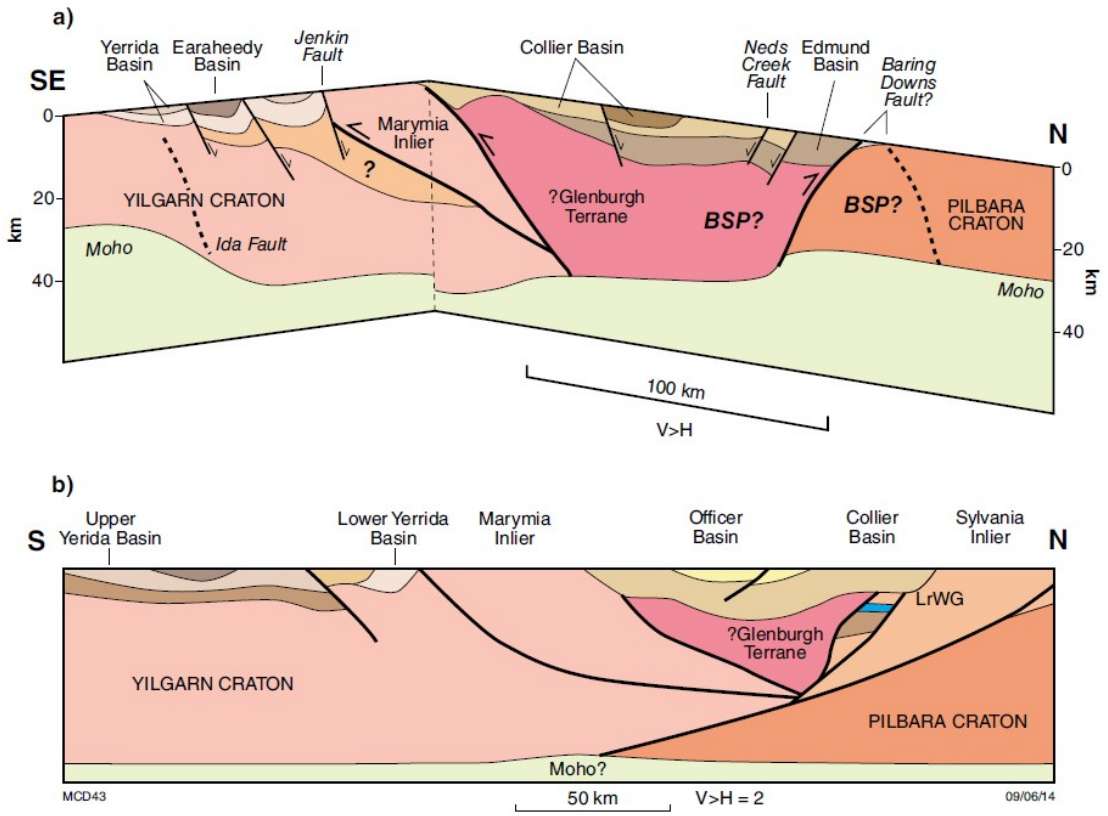

Figure 2.10A. Seismic traverse from across the eastern part of the Capricorn Orogen interpreted form magnetotelluric results (Dentith et al., 2014). BSP – Bandee Seismic Province; LrWG – Lower Windplain Group. **B.** The original geological cross-section of the same area of Cawood and Tyler (2004).

2.8. Tectonic and Orogenic Events across the Capricorn Orogen

The Glenburgh terrane is an exotic micro-continent to the Pilbara and Yilgarn Cratons. Collision with the Pilbara occurred during the Opthalmian Orogeny at c. 2240 and 2125 Ma. The Moogie Metamorphics meta-sedimentary rocks were deposited concurrently in a foreland basin system (Johnson et al., 2010, Johnson et al., 2011a). In the eastern Capricorn Orogen, continental rifting of the northern Yilgarn margin may have led to separation of the Marymia Inlier and subsequent deposition of Yerrida Group sediments in a sag basin setting (Pirajno et al., 1995, Pirajno and Adamides, 2000b, Dentith et al., 2014).

Continental-margin arc-magmatic activity was initiated along the southern margin of the combined Gascoyne-Pilbara Terranes with the intrusion of the Dalgaringa Supersuite magmatic rocks in a continental margin arc as an Andean-type batholith c. 2005 to 1975 Ma (Sheppard et

al., 2004). Oceanic plate subduction, and hence closure between the Gascoyne and Yilgarn, was initiated at c. 2080 Ma (Sheppard et al., 2004) along the proto-Dalgaringa arc, toward the north and under the southern leading edge, of the Glenburgh Terrane. This is opposite to the present-day dip of the suture zone (Johnson et al., 2011a). Rocks of the overlying Camel Hills Metamorphics (Petter Calc-silicate and Quartpot Pelite) are interpreted to have formed in a forearc or backarc basin setting along the southern margin of the Glenburgh Terrane, between approximately 2000 and 1955 Ma as the meta-sedimentary rocks equivalent to the intrusive rocks of the Dalgaringa Supersuite (Johnson et al., 2011a).

In contrast, rocks of the Bryah Group, in particular the Narracoota Formation, have most recently been interpreted to represent a fragment of oceanic plateau accreted to the Archean Yilgarn Craton margin during oceanic basin closure between the Pilbara and Yilgarn Cratons (Pirajno, 2004). Previous works, however, have suggested a range of tectonic environments from intracontinental basins to back arc rifts (Bunting et al. (1977), Gee (1979), Hynes and Gee (1986), Tyler and Thorne (1990), Windh (1992), Gee and Grey (1993), Myers (1993), Martin (1994), Pirajno et al. (1994), Myers et al. (1996), Pirajno (1996), Pirajno and Occhipinti (2000), Pirajno et al. (2000)). Myers et al. (1996) and Hynes and Gee (1986) suggested that the Bryah Group could represent a back-arc formed during south directed subduction beneath the northern margin of the Yilgarn Craton. Occhipinti et al. (2004) suggested that remnants of cordilleran-like magmatic suites related to this subduction, may be buried beneath the Edmund and Collier basins, to the north of the Bryah and Padbury Basins. Geochronological data presented in Chapter 6 suggests the DeGrussa Formation sedimentary rocks were deposited between c. 2080 and 2030 Ma coincident with deposition of the Camel Hills Metamorphics and magmatism within the Dalgaringa Arc. Closure and collision of the combined Pilbara Craton-Glenburgh Terrane and the Yilgarn Craton led to development of the Errabiddy Shear Zone and east directed emplacement of the Bryah Group over the Yerrida Group during the latter part of the Glenburgh Orogeny (c. 1965 and c. 1950 Ma)(Occhipinti et al., 2004, Sheppard et al., 2004, Johnson et al., 2011a).

Several later orogenic and tectonic events have affected the region. The 1820 – 1770 Ma Capricorn Orogeny, associated with granite plutonism, affected this margin and was coincident with the Yapungku Orogeny (c. 1790 Ma) which records the onset of collision between the West Australian Craton and the North Australian Craton (Johnson, 2013). The Mangaroon Orogeny (1680-1620 Ma) was related to reworking of crust in the northern Gascoyne and the coeval intrusion of voluminous granites, followed by reactivation of faults and shear zones and intrusion of granite plutons over a wide area of the Gascoyne Province (Sheppard et al., 2005) The Mutherbukin Tectonic Event (1320-1170 Ma, (Korhonen et al., 2015)) is a tectonothermal event with no significant magmatism or sedimentation and is largely confined to the Gascoyne Province and overlying parts of the Edmund Group. The event is characterized by faulting and amphibolite facies metamorphism (Korhonen et al., 2015). The Edmundian Orogeny (1030-955 Ma) was responsible for intracontinental reworking along a NW-SE striking corridor with greenschist-amphibolite facies metamorphism and deformation followed by pegmatite intrusion and coeval granite magmatism (Sheppard et al., 2007).

2.9. Regional Mineralisation

The Bryah Basin is well endowed and has been mined for a number of commodities, including copper, gold, manganese, iron ore and talc. Less mineralisation has been located in the Yerrida and Padbury Basins. For this study, a small number of copper and gold deposits in the Bryah and Yerrida basins will be used for comparison with the DeGrussa mineralisation. These are briefly discussed below, with more detail discussed in later chapters.

The DeGrussa VHMS deposit is the only substantial deposit of its kind discovered in the district. It is hosted in the lower mafic basalts/dolerites and sedimentary rocks of the Narracoota Formation of the Bryah Basin. The similar, but smaller Horseshoe Lights Cu-Au massive sulfide deposit is located in the Narracoota Formation but is associated with felsic volcanics approximately 70kms west of DeGrussa. Other pyrite associated gold deposits are located in varying stratigraphic units throughout the basin.

VHMS mineralisation at DeGrussa, hosted in the Narracoota Formation, has in previous studies, been presumed to have formed post the Glenbugh Orogeny (2005-1996Ma). However, new geochronological work presented in this thesis (Ch. 6) indicates DeGrussa mineralisation predates the Glenburgh Orogen. Regional ages for syngenetic intrusive dolerites and granodiorites within the Narracoota and DeGrussa Formation rocks are approximately 2014Ma. Furthermore, geochronological results presented in this thesis result in a galena Pb-Pb isotope model depositional age for the DeGrussa mineralisation of 2030-2040Ma and a Re-Os molybdenite age of 2027 ± 7 Ma. Given these new ages, which constrain the Narracoota Formation magmatism and sedimentary deposition at least in the eastern part of the basin, it is suggested that the Bryah Basin rifting was initiated earlier than previously believed (approximately 2030 Ma given the age of DeGrussa mineralisation, Chapter 6). This supports the original designation of basin stratigraphy by Gee (1987).

Widespread pyrite-related epigenetic/orogenic gold mineralisation is most likely associated dominantly with D4 deformation during the Capricorn Orogeny. Deposits of this style are located at Fortnum, Horseshoe/Cassidy/The Pod, Peak Hill/Fiveways, Labouchere, Horseshoe Lights (overprinting primary copper sulfide mineralisation) and Plutonic Gold mines (several stages of mineralisation since the Archean (Gazley, 2011)). Figure 2.11 shows the locations of mineral deposits referred to throughout this thesis and Table 2.2 give details of all known mineralisation in the basin.

The Thaduna Copper deposit is hosted in the Thaduna Formation of the Yerrida Basin. These sedimentary rocks are determined to have deposited at a similar time to that of the DeGrussa however the mineralisation is much later.

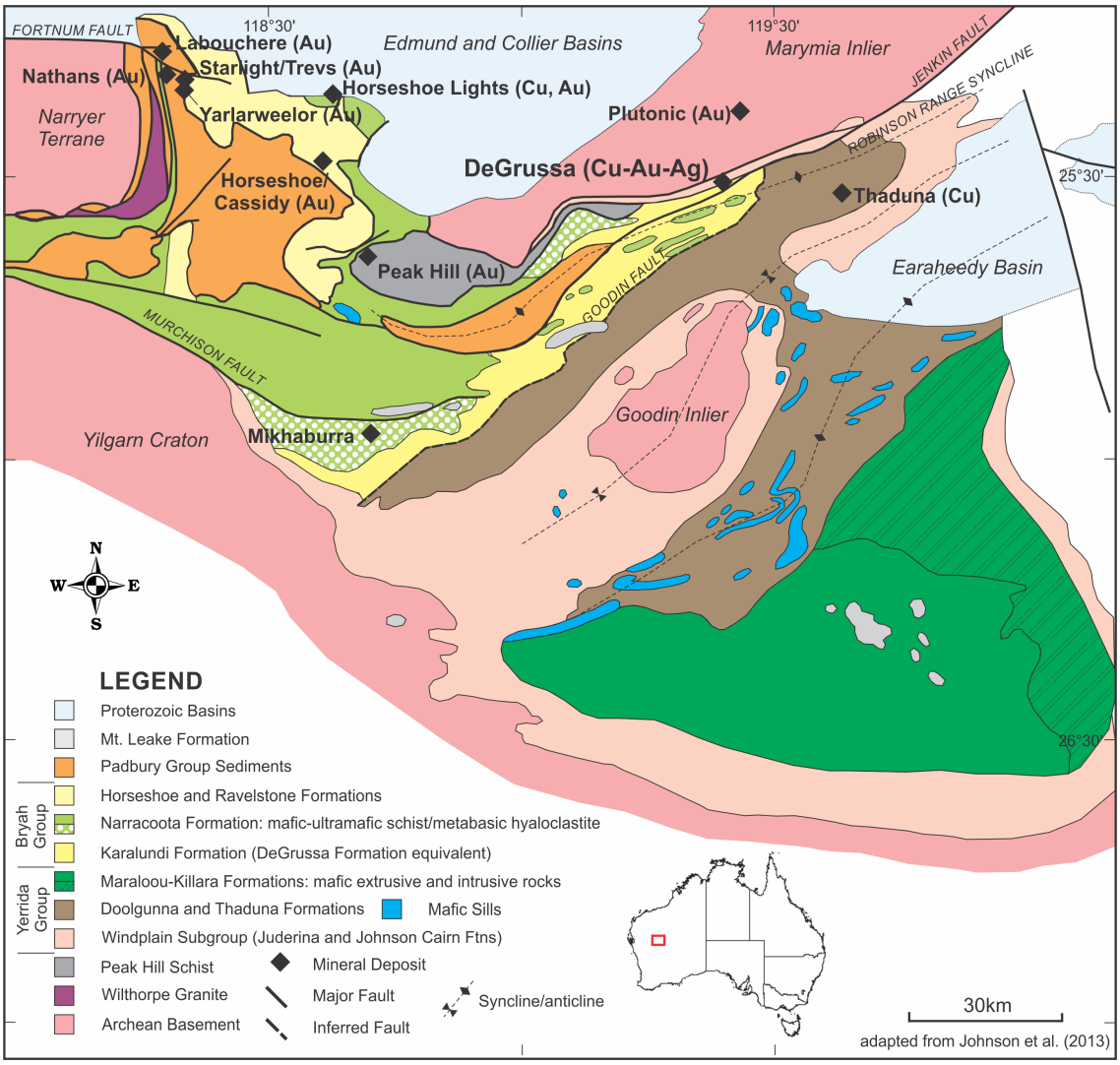

Figure 2.11. Location of major deposits of focus in this study in relation to Proterozoic Basins and regional geological units.

Table 2.2 Significant Mineral Deposits within the Bryah and Yerrida Basins.

Deposit	*Mine or Prospect*	*AMG coordinates*		*Commodity*	*Ore minerals*
		Easting	**Northing**		
Cashman	M	662129	7126994	Regolith-enrichment and mesothermal Gold	Gold
Durack	P	670440	7150520	Mesothermal Gold	Gold, pyrite, magnetite
Green Dragon	M	774787	7181073	Copper	Cuprite, chalcocite, malachite
Harmony	M	664145	7161267	Regolith-enrichment and mesothermal Gold	Gold, chalcopyrite, pyrrhotite, scheelite, pehtlandite, pyrite
Heines Find	P	682759	7145164	Mesothermal Gold	Gold
Horseshoe/Cassidy	P	661359	7183130	Vein hosted Copper-gold	Gold
Horseshoe Lights	M	662648	7193894	Copper-gold VHMS with supergene enrichment	Chalcocite, pyrite, chalcopyrite, native copper, and gold
Jubilee	M	671889	7165443	Mesothermal Gold	Gold, pyrite
Labouchere	M	627730	7204710	Mesothermal Gold	Gold, pyrite
Livingstone	M	567540	7171032	Talc (replacement)	Talc
Magellan	M	793340	7063440	Lead	Cerrusite, anglesite
Mikhaburra	P	656252	7130396	Vein-hosted Gold	Gold
Monty	P	743620	7171000	Copper-gold VHMS	Chalcopyrite, pyrite, bornite
Mount Pleasant	M	674287	7162089	Mesothermal Gold	Gold, pyrite
Mount Seabrook	M	572631	7168338	Talc (replacement)	Talc
Nathans Deep South	M	631713	7198812	Mesothermal Gold	Gold, pyrite
Peak Hill	M	672190	7163003	Mesothermal Gold	Gold, pyrite, altaite, chalcopyrite, bismuthotelluride, molybdenite, megnetite
Ravelstone	M	665734	7166777	Supergene Manganese	Mn oxides
Ravelstone	M	669313	7166423	Supergene Manganese	Mn oxides
Red Bore	P	735940	7172530	Copper-gold VHMS with supergene enrichment	Pyrite, chalcopyrite, pyrrhotite
St Crispin	P	691358	7158940	Mesothermal Gold	Gold
Thaduna Copper Deposit	M	772872	7176217	Copper-Silver	Chalcopyrite, Bornite, Chalcocite, Covelite
Trevs, Starlight	M	636412	7198887	Mesothermal Gold	Gold, pyrite
Unnamed	P	656664	7185310	Supergene Manganese	Mn oxides
Wembley	P	663983	7149044	Mesothermal Gold	Gold
Wilgeena	M	685369	7155622	Mesothermal Gold	Gold
Wilthorpe	M	630414	7176521	Mesothermal Gold	Gold, pyrite, galena, arsenopyrite
Yarlarweelor	M	636723	7196423	Mesothermal Gold	Gold, pyrite
DeGrussa	M	733840	7173045	Copper-Gold-Silver VHMS with supergene enrichment	Pyrite, chalcopyrite, pyrrhotite, sphalerite, marcasite, galena

2.9.1. Copper Mineralisation

Both oxide copper and primary sulfide copper are present in the region. Two main deposits, Horseshoe Lights and Thaduna, are used as a comparison to DeGrussa.

2.9.1.1. Horseshoe Lights

The Horseshoe Lights deposit is a gold-copper ore body (Fig. 2.12), approximately 70 kilometres to the west of the DeGrussa mine site in the west of the Bryah Basin. Here, the primary sulfide ore contains chalcopyrite and pyrite, with near surface supergene enrichment of chalcocite.

Of all Capricorn Orogen deposits, Horseshoe Lights, is the most similar to the DeGrussa deposit. It was determined by Gillies (1988) to be a copper-rich, volcanogenic massive sulfide with a later phase of epigenetic gold, although studies by Windh (1992) suggest that it is more likely that gold and copper were contemporaneous. Horseshoe Lights is located stratigraphically near the top of the Narracoota volcanic pile within ultramafic, mafic and felsic rocks (Gillies, 1988). A Pb isotope model age of 1922 ± 35 Ma was determined for pyrite in the mineralisation by Windh (1992) and is recalculated in Chapter 6 of this thesis as 2000 ± 35 Ma.

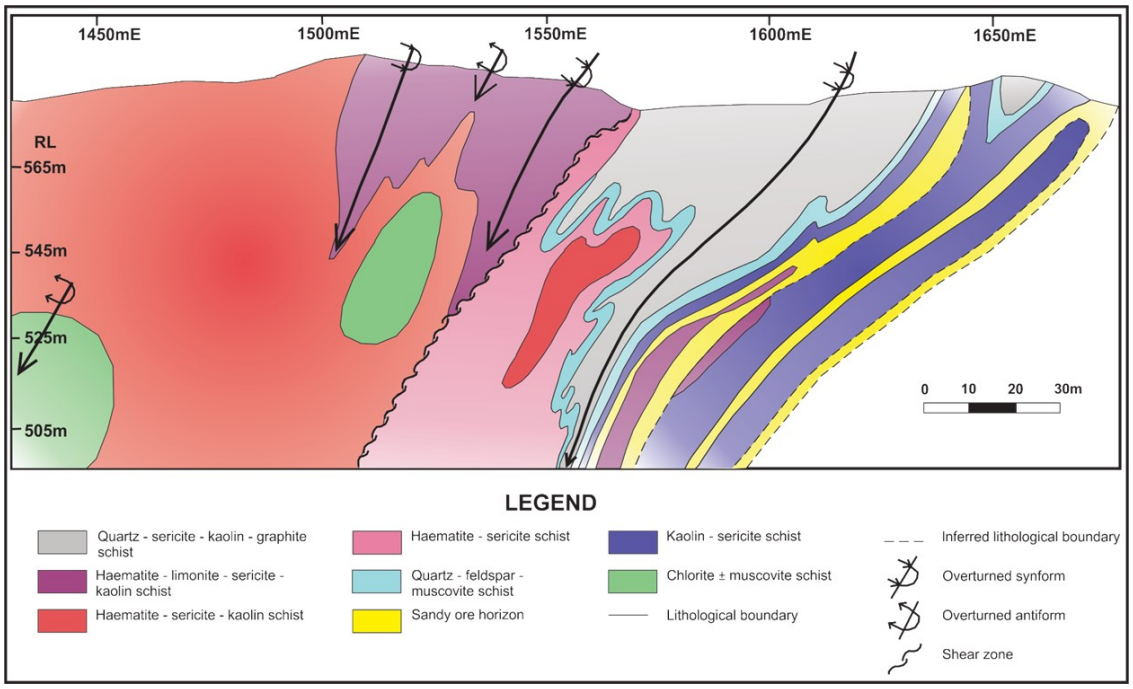

Figure 2.12. East-west cross section through the Horseshoe Lights Cu-Au massive sulfide deposit, adapted from Gillies (1988).

2.9.1.2. Thaduna Copper Deposit

Rocks of the Thaduna Formation host fault-controlled epigenetic copper deposits. The Thaduna (Fig. 2.13) and nearby Green Dragon deposits contain a combined resource of about 17 000 t of copper metal at an average grade of 3.4% (Pirajno and Adamides, 2000a). The copper lode follows the northwest trending Thaduna Fault with the majority of the lode consisting of sheared and brecciated sedimentary rock containing abundant hydrothermal graphite as a matrix to quartz and carbonate minerals.

Mineralisation is dominated by copper oxide ore (namely malachite, azurite, chrysocolla, cuprite and chalcocite) with chalcopyrite, bornite and chalcocite forming primary mineralisation at depth under both the Thaduna and Green Dragon pits (Reid, 2013).

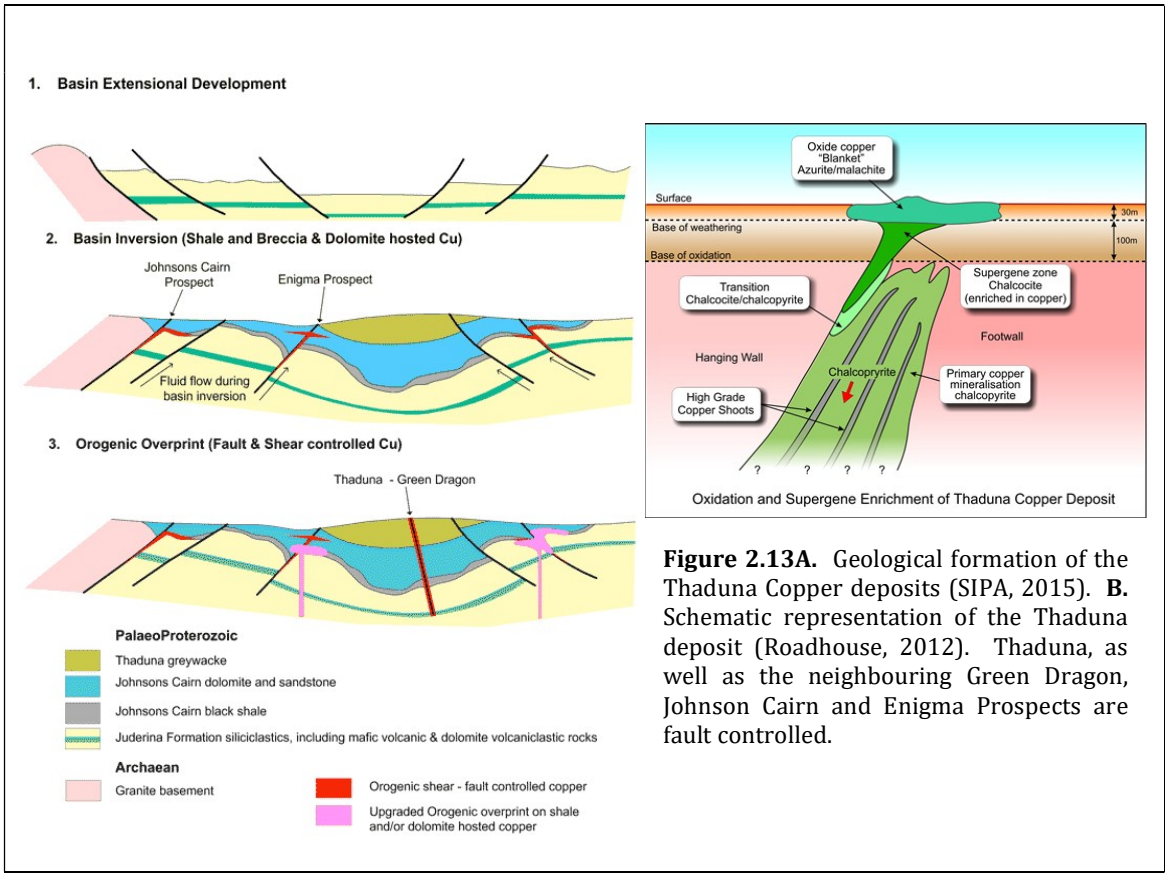

Figure 2.13A. Geological formation of the Thaduna Copper deposits (SIPA, 2015). **B.** Schematic representation of the Thaduna deposit (Roadhouse, 2012). Thaduna, as well as the neighbouring Green Dragon, Johnson Cairn and Enigma Prospects are fault controlled.

2.9.2. Gold mineralisation

Gold occurrences are widespread predominately hosted in sedimentary rocks throughout the Bryah and Padbury Basins and neighbouring Archean rocks of the Marymia Inlier. Most mining to date has been restricted to the Peak Hill, Fortnum and Horseshoe/Cassidy gold mining areas. The Peak Hill gold mines are hosted in the Peak Hill Schist, originally part of the former Glengarry Basin as identified by Gee (1987) but now is considered Archean and part of the Marymia Inlier. Despite this, the tectonic events associated with gold mineralisation at Peak Hill are of similar age to those of the Bryah and Padbury Basins.

Gold in the Bryah/Padbury Basins is associated with D4 structures, developed on the hinges of D4 folds, especially antiforms, and associated with D4 faults and shear zones (Harper et al., 1998). Gold formation is related to fluid flow during deformation, and both prograde and retrograde metamorphism (Pirajno and Occhipinti, 2000). There are no large gold deposits known in the eastern portions of the Bryah Basin, although it is present at a prospect level and

is frequently sought after at surface by gold prospectors. Within the western parts of the Basin, outside of the DeGrussa deposit area, gold mineralisation is related to quartz veins and shear zones, possibly associated with D4 folds.

For comparative work with DeGrussa mineralisation, samples from the major gold occurrences of Fortnum (Fig. 2.14), Horseshoe/Cassidy/The Pod (Fig. 2.15) within the Bryah/Padbury Basins are used. Previous data from studies of Labouchere and Nathans (Bryah Basin) as well as Peak Hill (Fig. 2.16) within the Marymia Inlier (Thornett, 1995) are also collated for comparison. These deposits are discussed briefly below.

2.9.2.1. Fortnum - Yarlarweelor and Starlight

The Fortnum Gold Project (Fig. 2.14) is located along the contact between mafic and ultramafic schists of the Narracoota Formation and the overlying sediments of the Ravelstone Formation (Bryah Basin). These deposits are located proximal to the east trending Fortnum Fault. Mineralisation is associated with large euhedral pyrite and south-east striking shears, quartz veins and red-grey chert-jasperoid pods (Pirajno et al., 2000).

At Yarlarweelor, mineralisation is hosted by lenses of jasperoid chert within variably schistose mafic and ultramafic volcanic rocks and interbedded fine tuffaceous and coarse fragmental layers. Cherts are interpreted as occurring within a west dipping reverse D3 shear zone. Gold bearing quartz-pyrite veins within chert pods and magnetite-bearing chlorite schist trend to 120˚, dip steeply north and are parallel to sinistral D4 faults (Windh, 1992, Pirajno et al., 2000). These form the main host with veins containing quartz, siderite, pyrite, chalcopyrite and native gold. Mineralisation is interpreted to be spatially associated with east-southeast-trending brittle faults formed during the D3 deformation event (Windh, 1992). At Starlight/Trevs, mineralisation is similar but also occurs in bedding parallel zones of pyrite alteration within volcanoclastic and sedimentary rocks (Windh, 1992). The Labouchere and Nathan's mines are interpreted by Windh (1992) to have formed in a similar way to Fortnum during D3 deformation.

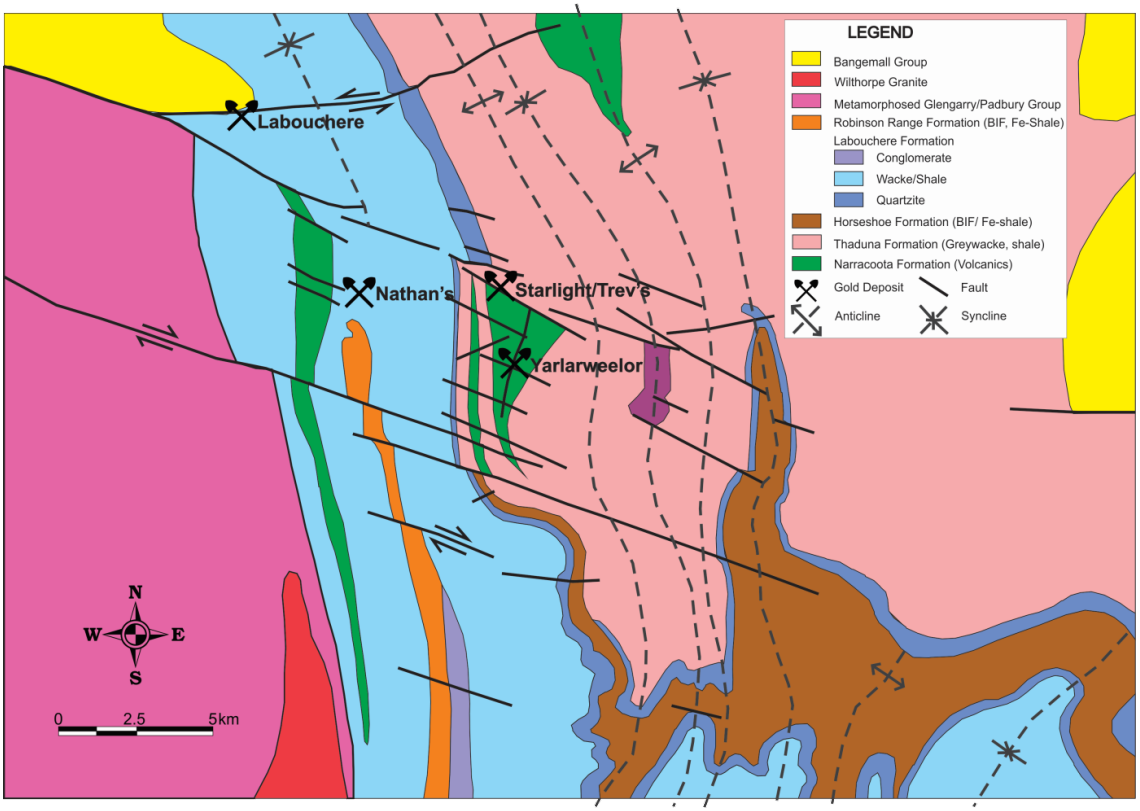

Figure 2.14. Location of mineralisation at Fortnum – Yarlarweelor, Starlight/Trevs, Labouchere and Nathans. Adapted from Windh (1992).

2.9.2.2. Horseshoe, Cassidy and The Pod

Horseshoe, Cassidy and The Pod (Fig. 2.15) are three deposits each mined by open pitting with depths of 85, 82 and 27 metres respectively. Host rocks are identified as ultramafic, high magnesian and mafic volcanic rocks assigned to the Narracoota Formation (Groves, 1996). Jasperlititc lenses and breccias, and minor tuffaceous beds accompany the mineralisation. The deposits are hosted by argillite, siltstone and minor greywacke assigned to the Ravelstone Formation. The Ravelstone Formation grades into the Labouchere Formation to the south. East-trending Proterozoic dykes are present in the region. Contrasting with this, a dyke of unknown age, intruded along one of the major north-east trending structures and truncates the western edge of the Cassidy and Horseshoe ore bodies (Groves, 1996).

Two major folds exist – an overturned syncline, and an anticline east of The Pod (Fig. 2.15). The deposits sit near the core of a south-westerly plunging anticline. Mineralisation is hosted in

quartz veins, oriented at 135-150˚, dipping 60˚to the north-east within the main zones of Horseshoe and Cassidy. The eastern parts of Cassidy and The Pod contain mineralised quartz veins that strike parallel to bedding (100˚) dipping 70-80˚to the south. Pyrite is the dominant mineral with lesser chalcopyrite and arsenopyrite in quartz veins, shear zones within jasperoid units, mineralised contacts and in cherty silica alteration and quartz veins in ultramafic rock (Groves, 1996). Mineralisation can be interpreted as related to structural deformation and alteration during D4 (Groves, 1996).

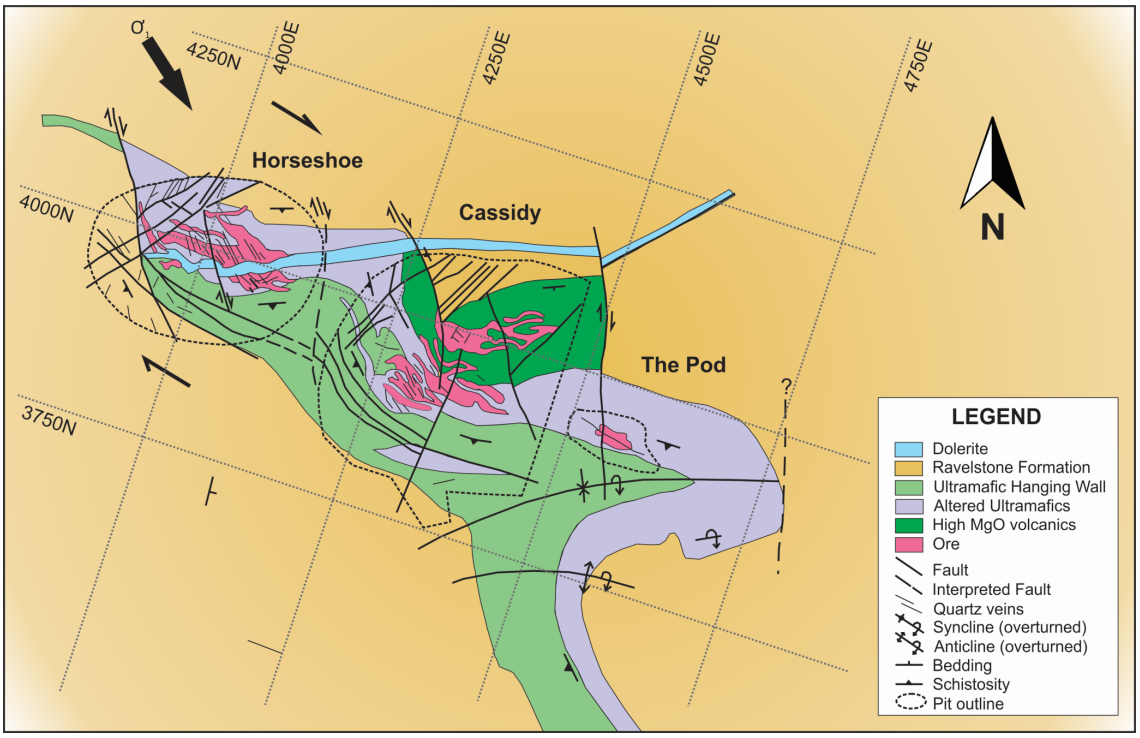

Figure 2.15. Mineralised lodes at the Horseshoe, Cassidy and The Pod mines (from left to right) with relation to major structures and stratigraphic units. Figure adapted from Groves (1996).

2.9.2.3. Peak Hill/Fiveways

The Peak Hill mining centre (Figure 2.16) is one of the oldest in the region. Mineralisation is hosted in highly deformed rocks of the Peak Hill Schist, regionally metamorphosed to amphibolite grade regional metamorphism. Retrograde alteration accompanies gold mineralisation in D4 shear zones and folds. Alteration assemblages consist of iron-chlorite,

biotite, white-mica, albite, garnet, pyrite, carbonate, tourmaline and fluorite. Gold is inferred by Thornett (1995) to have formed at temperatures between 250 and 375˚C.

The Peak Hill Schist was initially presumed to be part of the Bryah Basin sediments before being reassigned as a highly deformed part of the Archaean Marymia Inlier. Work by Thornett (1995) further enforced this with Pb isotope data identifying the Peak Hill Mine to have the same source as the Marymia Inlier hosted Plutonic Gold Deposit.

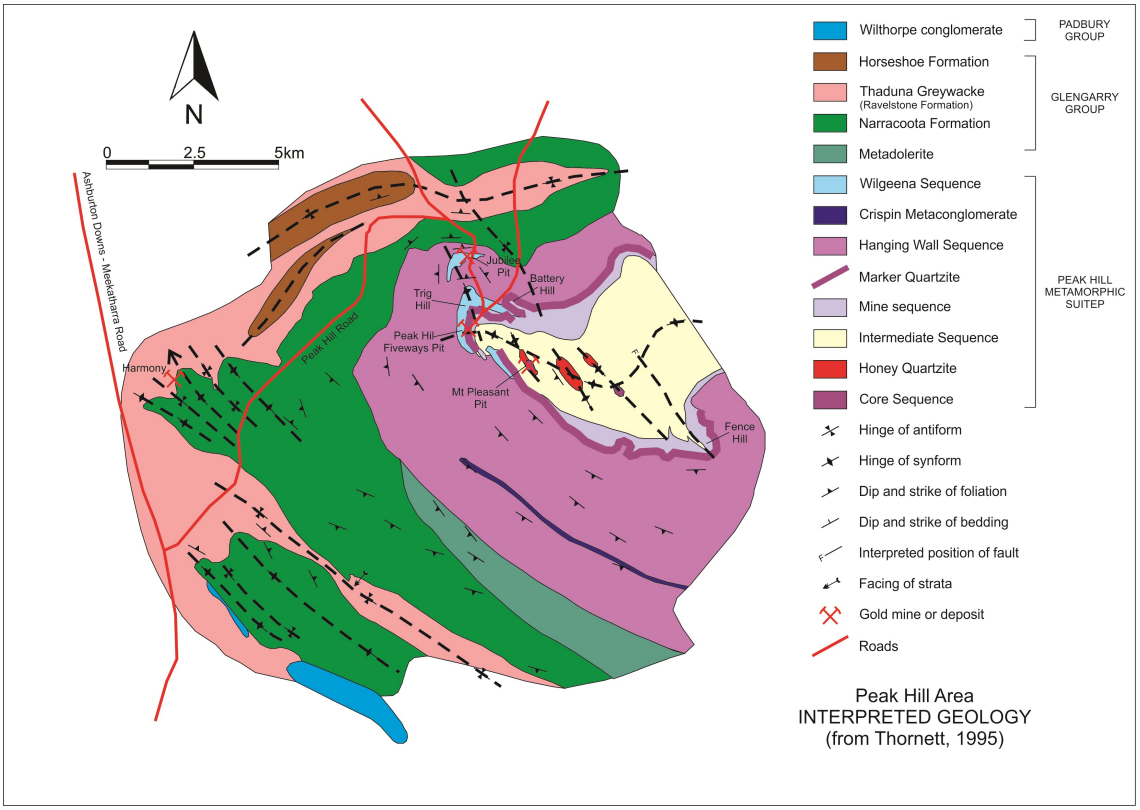

Figure 2.16. Peak Hill mine locations displaying Jubilee, Fiveways, Mt. Pleasant and Harmony deposits (Thornett, 1995).

2.9.2.4. Archean Plutonic gold Deposit

The Plutonic gold deposit (Fig. 2.17) is hosted in a sequence of metamorphosed mafic amphibolites (predominantly high Fe and Mg tholeiites), that is locally known as the Mine Mafic Package (Gazley, 2011), within the Archean Marymia Inlier approximately 40km to the north-northeast of the DeGrussa deposit (refer to section 2.4.1). The thickness of the package is variable, with eight deformation events recognised (Rowe et al., 2002). Gold mineralisation

(Plutonic brown-lode) typically occurs as thin (~ 1–3 m wide) lodes consisting of quartz-biotite-amphibole-titanite-epidote-carbonate-tourmaline-arsenopyrite-pyrrhotite ± chalcopyrite ± scheelite ± Au (Gazley, 2011). Petrographic and microstructural observations by Gazley (2011) suggest that stratigraphy was a dominant control on focusing Au-bearing fluids. Several other styles of gold have been identified by Fallon et al. (2010) throughout Plutonic and the larger Marymia Greenstone Belt including replacement and vein hosted lodes and shear related mineralisation. Four time intervals have been assigned to mineralisation events - ~2650 Ma, ~2200 Ma, ~1850 Ma and 1730 – 1660 Ma. The major mineralising event at Plutonic was ~2200 Ma. These ages will be discussed more in Chapter 6.

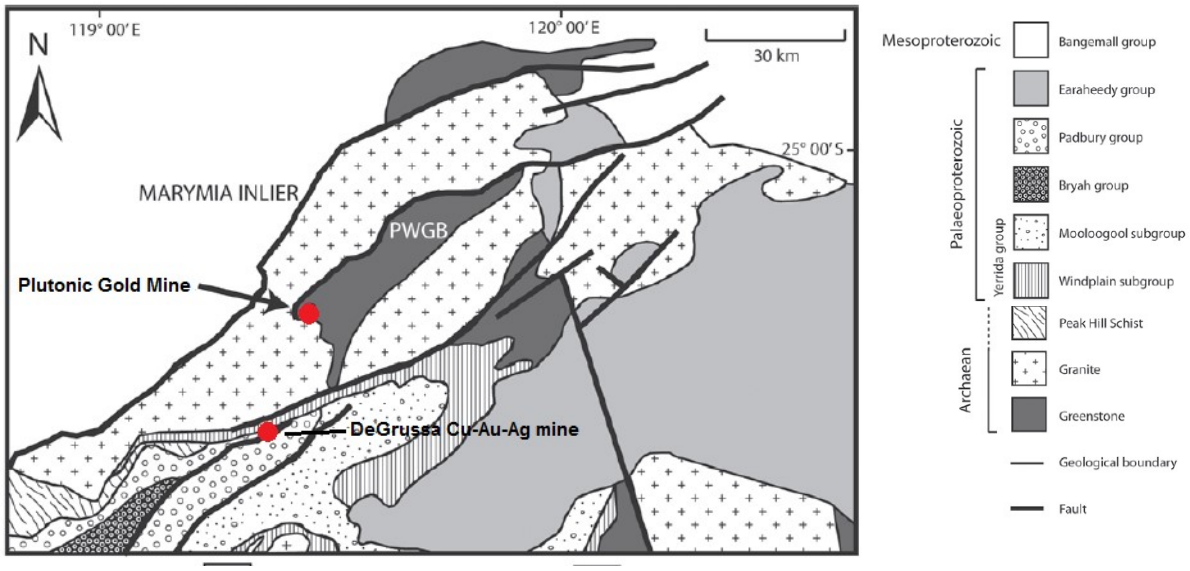

Figure 2.17. Location of the Plutonic gold deposit in relation to the DeGrussa deposit. Adapted from Bagas (1999).

Chapter 3. Deposit Geology: Stratigraphy of the eastern Bryah group and the DeGrussa host sequence.

DeGrussa Pit looking south

3.1. Introduction

Regional mapping of Sandfire Resources Doolgunna Project was completed by Bob Jeffery over the 2010-2011 field seasons (Jeffery, 2011). This map (Fig. 3.1) provides the framework for the mine geology presented in this thesis and is continually undergoing revision. Observations presented in this thesis are based on geology and drilling up to the end of 2013. Mapping and drill core logging has allowed stratigraphy to be examined in the DeGrussa area from the Archean basement, through the Yerrida Group and into the host rocks on the Bryah Group.

Stratigraphy can be divided into three main rock types which host the DeGrussa massive sulfide deposits.

1. Sedimentary rock – these include sandstones and siltstones deposited as turbidites and debris flows and conglomerate.
2. Basalt –Interlayered with the host sediments often displaying hyaloclastite and peperitic textures. Breccia, in the form of peperite and hyaloclastite, is present.
3. Dolerite – intrusive rocks varying in texture from fine grained microdoleritic-dolerite-gabbro in texture. There is no difference geochemically between basalts and dolerite.

This chapter will;

1. Identify and broadly characterise the major rock types hosting the DeGrussa ore.
2. Identify stratigraphic relationships between units
3. Identify the alteration assemblage related to each of the different rock types
4. Identify the major structures present in the mine sequence.

Observations made in this chapter are drawn from a combination of drill core logging, thin section observations and compilation of cross sections between 2009-2013. Where the author has not had the privilege of viewing stratigraphic contacts in the field, the mapping work of Jeffery (2011) has been used although the stratigraphy of the overall region (Fig. 3.2) is based on that of Occhipinti et al. (1997).

Figure 3.1. Map 1. The Bryah and Yerrida Basin with location of DeGrussa, Bubble Well Member (stromatolite) sampling site of Russell (1992), and THD001 drillhole**. Map 2.** The local DeGrussa area as mapped by Jeffery (2013) and location of schematic cross sections through the project area. Section A-B, C-D, forms a south-east to north-west cross section through the Robinson syncline and DeGrussa deposit area, transecting the Jenkin Fault to the south of the C4 and C5 ore lenses of the DeGrussa deposit**. Map 3.** Is a close up view of the ore deposits in plan view, with the footwall sedimentary rocks dolomitised and silicified below the DeGrussa deposit.

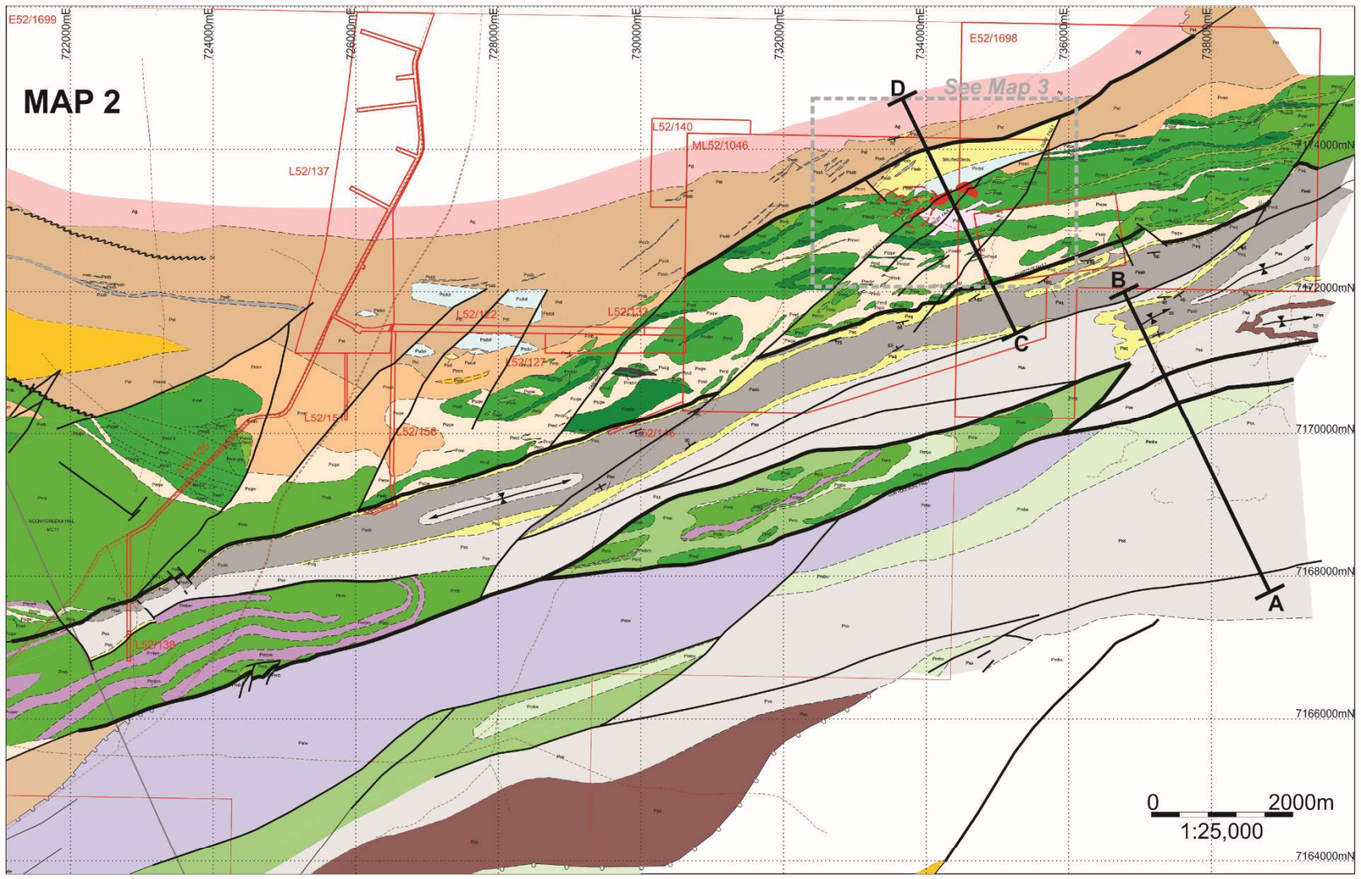

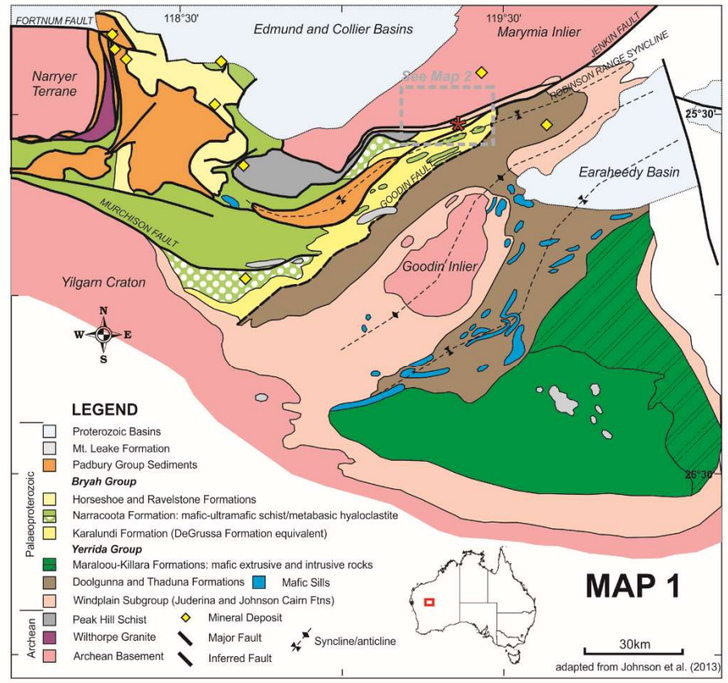

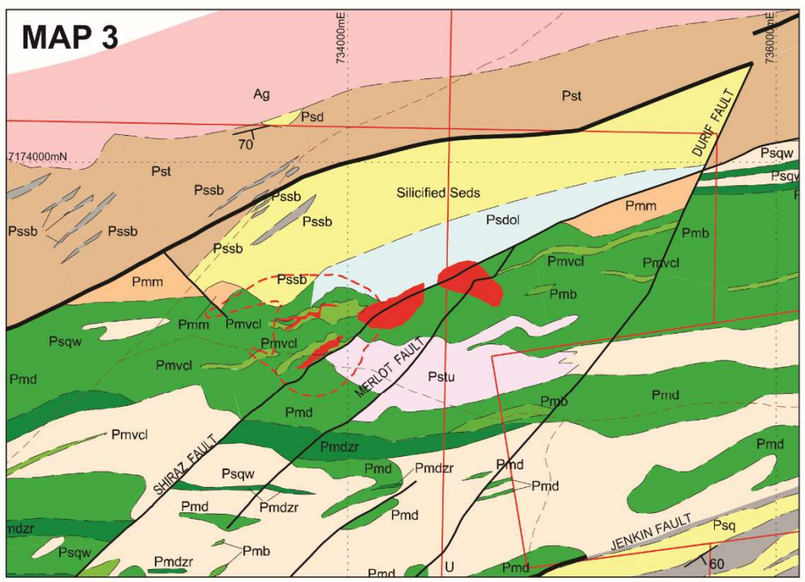

Schematic cross section of the eastern Bryah Group

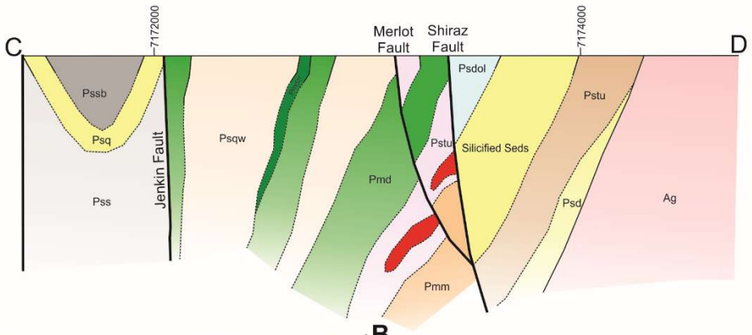

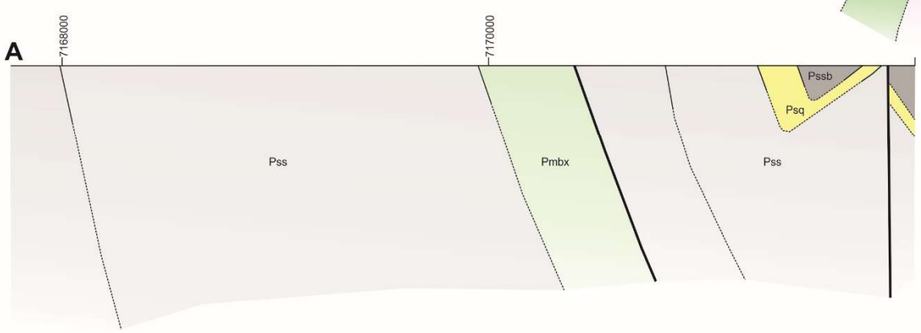

All information referred to in this chapter can be located in supplementary appendices. Sample thin section descriptions and photos can be located in Appendix 3.1. Cross sections are located in Appendix 3.2, drill hole logs in Appendix 3.3, and alteration (Terraspec and QXRD) located in Appendices 3.4 and 3.5 respectively.

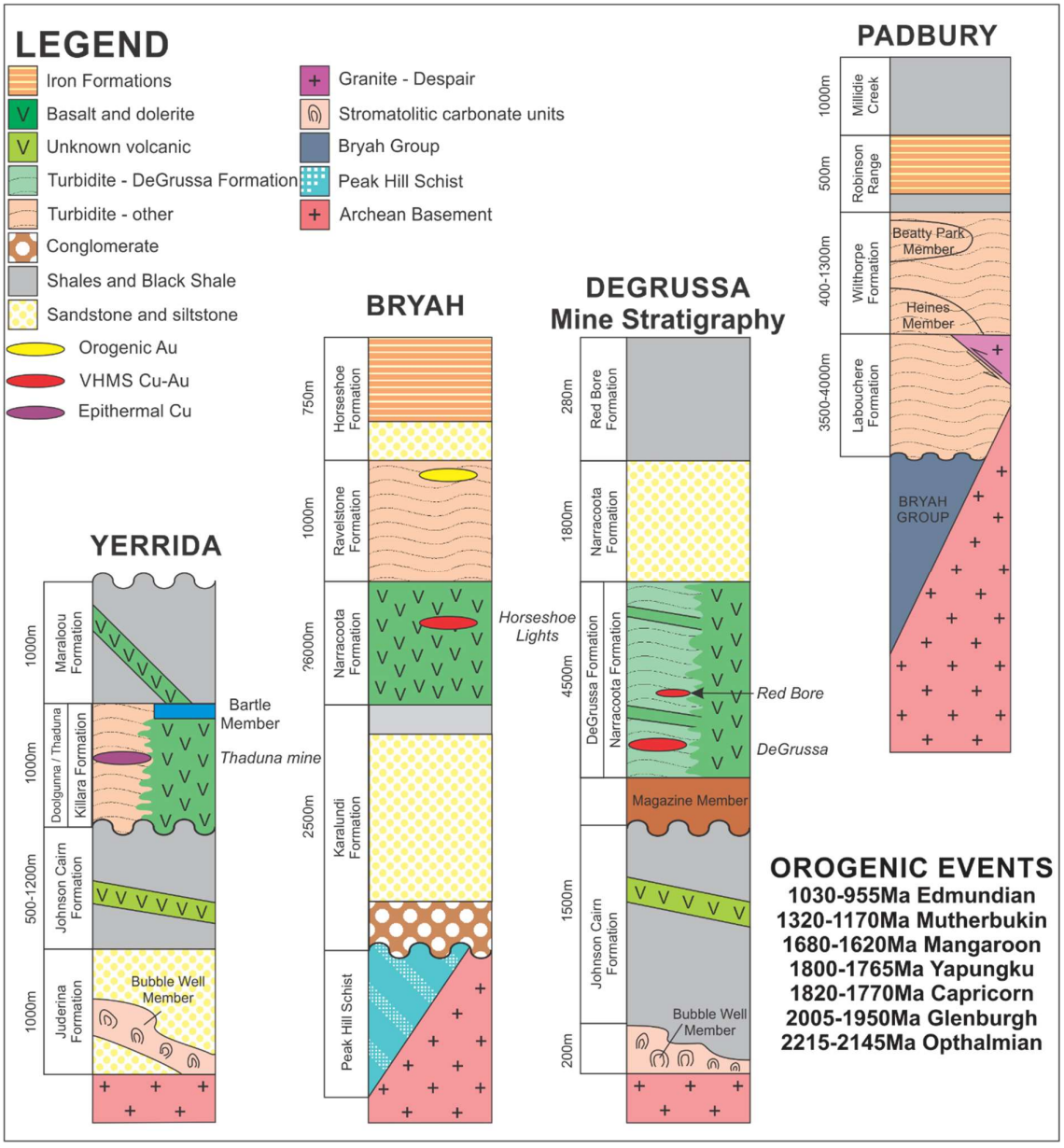

Figure 3.2. Simplified stratigraphic logs compiled from Occhipinti et al. (1997), Pirajno and Adamides (2000), Jeffery (2011) and drill hole observations undertaken during this thesis.

3.2. Geological Setting

3.2.1. Archean Basement (Marymia Inlier)

Archean basement in proximity to the DeGrussa deposit consists of a pink-cream, coarse grained granite with large (centimeters in size) intergrown crystals of feldspar (plagioclase and K-feldspar) and quartz with crosscutting carbonate, quartz and chlorite veins (e.g. DGMH113, DGMH115, Fig. 3.3). In thin section, the rock consists dominantly of feldspar (plagioclase with varying amounts of K-feldspar) and quartz (5-20%). Chlorite is interstitial to phenocrysts and sometimes pseudomorphs former amphibole and pyroxene grains. Carbonate is pervasive and present as felty masses along fractures and replacing entire phenocrysts of feldspar.

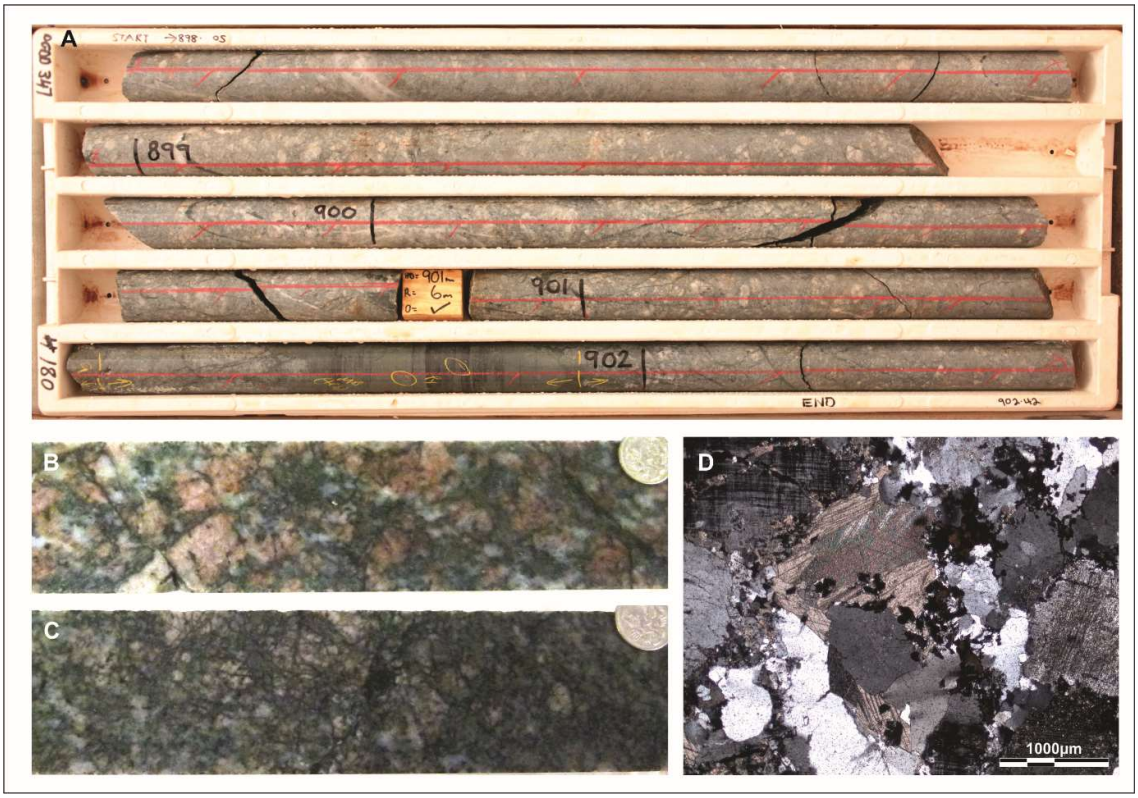

Figure 3.3 DGDD347, 898.05-902.42m (NQ core). **A.** Archean Granites with large plagiocalse laths and inclusion of ?basaltic unit approximately 901.7-902.0m. NQ core examples of the Archean Marymia Inlier, as basement to the DeGrussa deposit from **B.** DGDD347, 962.16-963.1m (DGMH113) and **C.** DGDD347, 1000.44-1001.78m (DGMH115). **D.** DGMH115, thin section under polarised light showing plagioclase dominated composition.

The Marymia Inlier is a fragment of Archean granite-greenstone basement providing zircon ages between 3.35 and 2.63 Ga (Vielreicher and McNaughton, 2002). Rocks are mainly granitic but also include small enclaves of calc-silicate rock, ortho-amphibolite and minor metamorphosed banded iron formation. They are faulted and tectonically interleaved along the contact with Bryah group sedimentary rocks (Occhipinti et al., 1997, Pirajno et al., 2000)

3.2.2. Juderina Formation (Bubble Well Member)

The Finlayson Member is not present at the base of the Juderina Formation below the DeGrussa mineralisation. Instead, the base of the Juderina is marked by 2m of mudstone and carbonate breccia, with a 40cm wide zone of chlorite schist directly onto the Archean basement. This underlies an approximately 150m sequence of stromatolites interbedded with evaporitic and mudstone facies with similar textures, as described by El Tabakh et al. (1999). This unit becomes progressively more silicic towards the base (observed in DGDD347, Appendix 3.3), belonging to the Bubble Well Member, part of the upper section of the Juderina Formation, Windplain Subgroup.

The Bubble Well Member in DGDD347 provides a stromatolitic assemblage typical of other occurrences in the Yerrida Basin. *Stromatolite form 1* and to a lesser extent, *Stromatolite form 2* are hosted towards the upper portions of the sequence (705.46m to 758.7m) with interbedded massive and featureless stromatolitic algal mats. Breaks in stromatolite growth are defined by ~5cm thick layers of sedimentary mudstone deposition. Doming and branching directions indicate upwards direction of stratigraphy. Isolated occurrences of *Stromatolite form 2* (Fig 3.4) and *Segosia finlaysoniensis* (Fig 3.4) are also present in this upper section. *Stromatolite form 1* varies from small domal structures to larger domes interpreted from the limited drillcore exposure at 769.64m depth, of up to 50cm in height (Grey, 2012a).

In thin section, primary stromatolites/carbonates indicate recrystalisation of the original rock. Layers of fine grained quartz alternate with layers of fine and coarse grained carbonate (Fig 3.5). Dark grey-black opaque layers are present along bedding planes. Sample DGMH139 preserves a

bedded stromatolitic mat texture in hand sample, however in thin section is now largely replaced by quartz with only remnant enclaves of carbonate.

The stromatolite sequence displayed here is in the reverse order progressing uphole compared with that described by Grey (1994) in which *Stromatolite form 1* and *Stromatolite form 2* formed the lower part of the sequence progressing up to *Segosia finlaysoniensis* at the top of the sequence. Younging direction is up-hole with branching direction in *Segosia finlaysoniensis* indicating way up in the lower section.

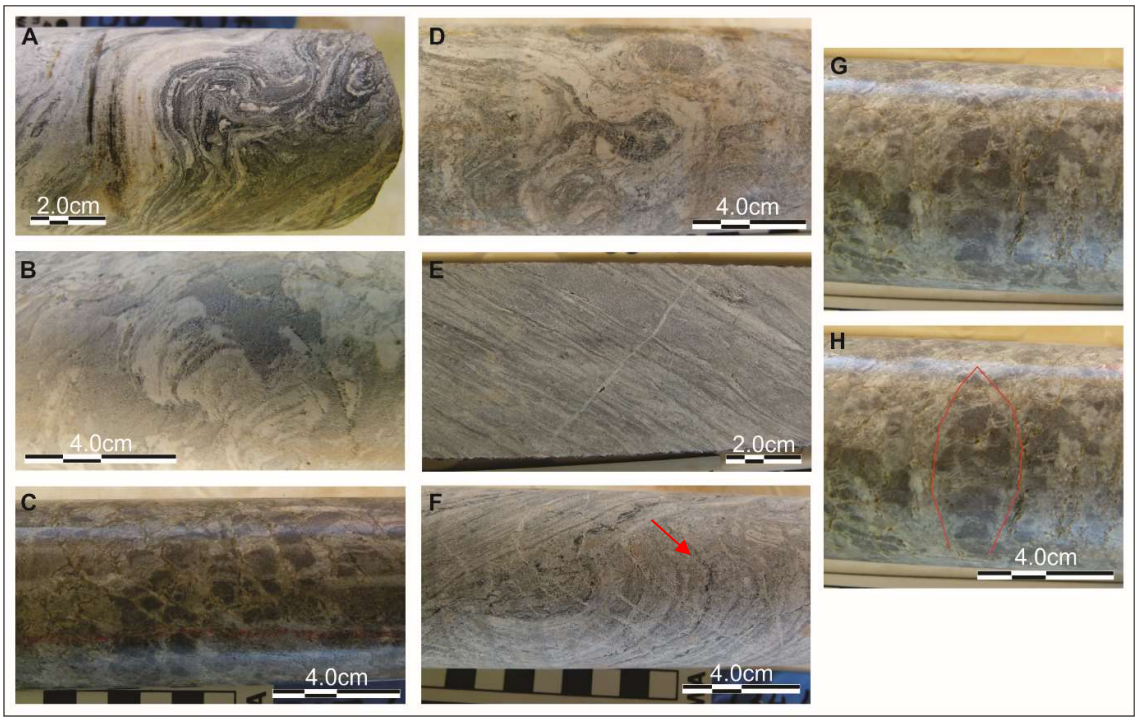

Figure 3.4.A. Domal *Stromatolite form 1* near top of stromatolite sequence (DGDD347, 706.99m). **B.** Possible *Segosia sp*, isolated occurrence in upper stromatolite sequence (DGDD347, 708.61m)**, C.** Highly silicified and deformed *Segosia sp.* in lower section of Bubble Well Member. **D.** Domal *Stromatolite Form 1*, with protrusion, **E.** Stromatolitic algal mats of the Bubble Well Member, Yerrida Formation. No identifiable features to determine species (DGDD347, 712.5m); **F.** Domal *Stromatolite Form 1*, growth direction determines 'way up' direction; **G.** Segosia finlaysoniensis oriented with upward growth in lower section of highly silicified and deformed Bubble Well Member, Juderina Formation. and **H.** second picture with outlined morphology.

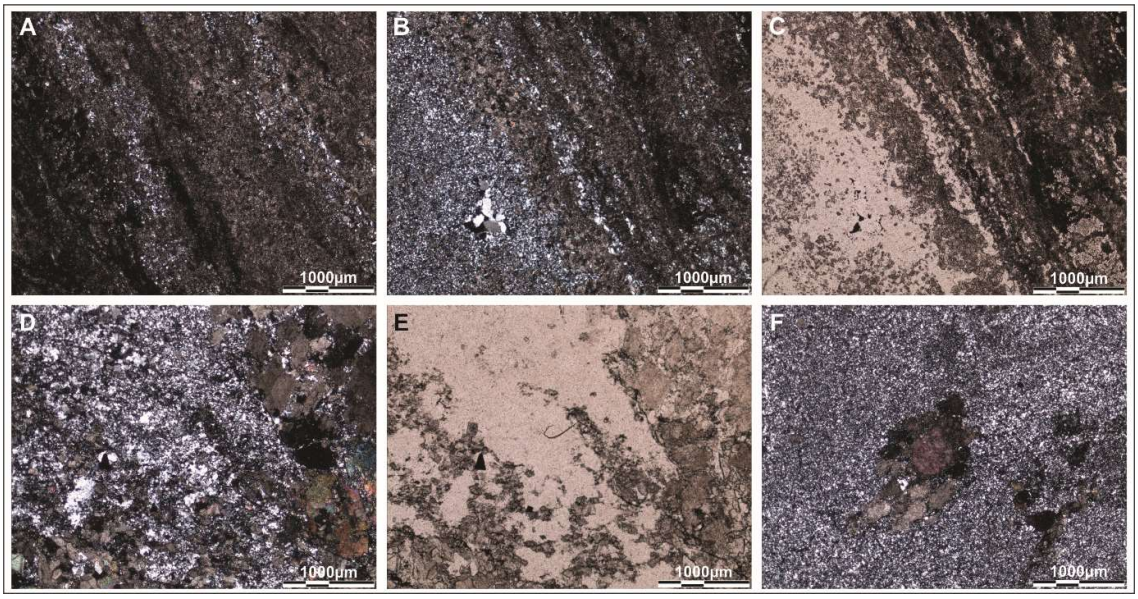

Figure 3.5. Textures of stromatolitic rock of the Bubble Well Member in thin section, **A.** and **B.** banded stromatolite layers showing carbonate and quartz in crossed polars (DGMH120), and **C.** in plane light. **D.** Recrystallised and pervasive quartz dominated stromatolitic rock with carbonate domain to the top right of image under polarised light (DGMH139), and **E**. in plane light. **F.** DGMH138 with occasional clasts of carbonate (~1mm) in a pervasive groundmass of quartz.

The strike/dip of bedding within the Juderina Formation with way up, as indicated by stromatolite growth is 240/60. Stromatolites typically grow in a flat and calm environment, hence it is inferred that significant tectonic movement has occurred since original deposition. It is suggested here that as rifting began, stromatolites were progressively dropped down into the rift basin in which deep water black shales later formed. No folding is indicated in the Juderina Formation. The top of the unit is marked by grey-black graphitic shales of the Johnson Cairn Formation and the occurrence of mafic basalts.

The lack of the Finlayson member at the base of the Yerrida Group, as seen in drilling proximal to the DeGrussa deposit, suggests a tectonic contact. However, the contact between the Bubble Well Member stromatolites at the base of the sedimentary rock sequence with the Marymia does not appear tectonic in drill core.

3.2.3. Johnson Cairn Formation

The Johnson Cairn Formation, as exemplified by drill hole DGDD347, consists of thick 10-50m stratigraphic units of fine-medium grained sandstones often with turbiditic sequences (e.g.

DGDD347, 360-370m), pale-dark grey siltstones, mudstones, and black shales (Fig. 3.6). Occasional green-grey mudstones of unknown origin are interbedded with the black shale units. Shear foliation and slump folding is visible in some parts of the core. Quartz and carbonate veins crosscut the units, dominantly in the units of siltstone and black shales. Black shales become the dominant lithology from approximately 440m to the lower contact with the Juderina Formation (at 705.5m). Coarser sandstones and siltstones dominate the top of the sequence. Mafic rocks are present within the black shale sequence from approximately 640m to the base of the unit (discussed in section 3.2.4). The Doolgunna and Maraloou Formations are not present in the vicinity of the DeGrussa deposit.

There are at least 2 thick dolomite units (±50-100m) in the Johnson Cairn Formation immediately below DeGrussa. Thin section investigations (Fig. 3.7) reveal that the Johnson Cairn Formation rocks are extensively carbonaceous. Siltstone units consist of patchworks of fine and coarse grained carbonate with minor quartz (10%) throughout. Mudstones are foliated and dominated by clays and opaque minerals (possibly pyrite) with occasional quartz grains. When carbonaceous, carbonate minerals are pervasive through the groundmass or sometimes appear as discreete clasts in a fine-grained matrix (DGMH133). Sample DGMH136 is characterised by a fine-grained matrix with large magnetite crystals (50μm) now infilled with secondary quartz. The rock is foliated with chlorite pervasive through the matrix with vugs of secondary quartz. In plane light, clay minerals appear to pseudomorph original feldspar crystals not visible under crossed polars (Fig 3.7). No chlorite alteration is present.

Figure 3.6. Johnson Cairn Shales, **A.** Green chlorite altered shale (DGDD020, 409.1-412.9m). **B.** Sandstones and siltstones with carbonate and quartz veining (DGDD020, 476.78-481.03m).

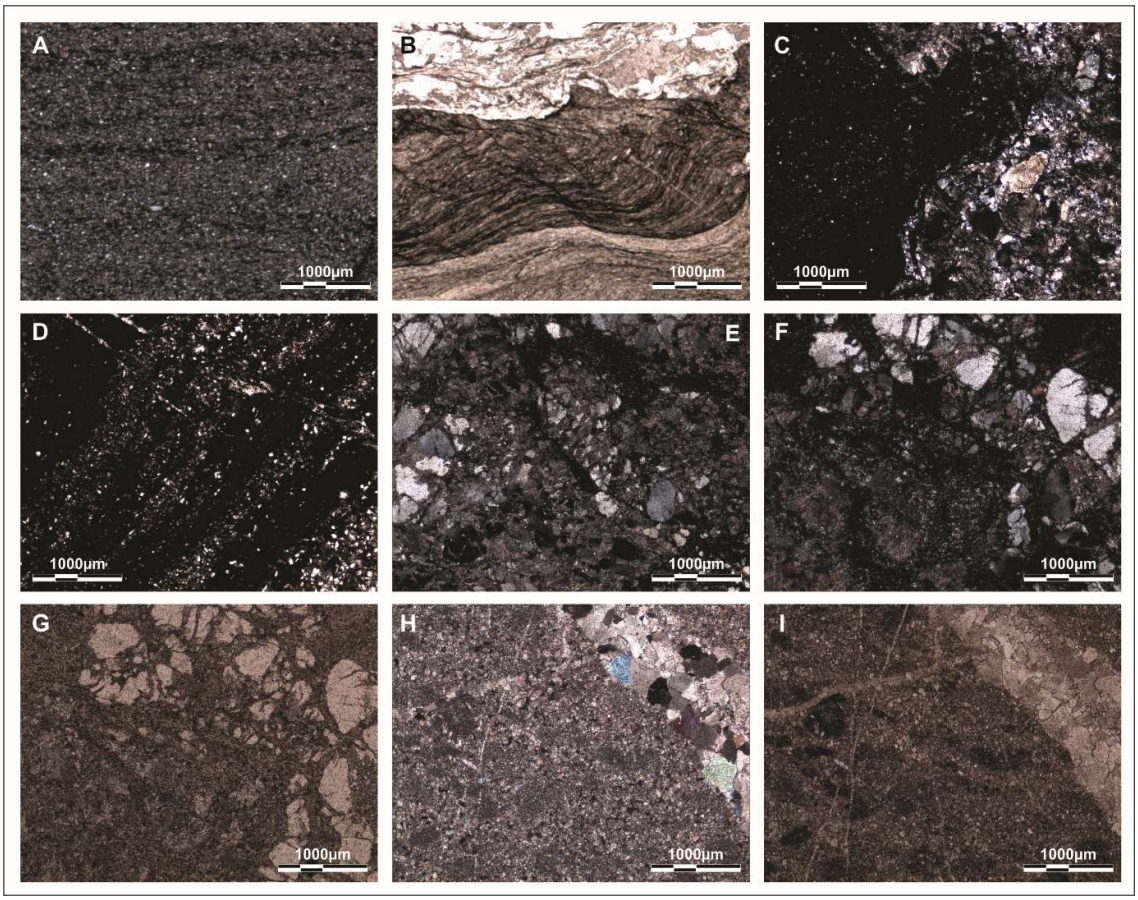

Figure 3.7. Johnson Cairn Formation thin sections. **A.** Polarised light and **B.** transmitted light of carbonate-rich, fine-grained siltstone with frequent angular-subangular quartz clasts (DGDD347, 705.2-705.5m, sample DGMH119). Foliated carbonate-rich zones are cross cut by quartz veins. **C.** and **D.** fine-grained black shale, same textures as sedimentary and turbiditic rocks in transmitted light. Coarse grained quartz, angular 40% + opaque (magnetite 20%, pyrite – cubic 5%), clay minerals forming matrix supported groundmass. Fine grained bands of quartz-rich sediment with epidote alteration throughout. Thin quartz veins crosscut. (DGDD020, 528.7-528.9, sample DGMH075). **E.** and **F.** Thin sections in polarised light and **G.** in transmitted light, showing carbonate breccia of the Magazine Member comprising subangular-subround quartz clasts to 30mm in size with shattered appearance and fractures infilled by dolomite mosaic. Minor elongated talc crystals occasional throughout and chlorite alteration as stringers along edges of clasts (DGDD020, 279.95-280.19m, sample DGMH072). Carbonate breccia fragment from the footwall sedimentary rocks in **H.** polarised light and **I.** transmitted light showing a mosaic of carbonate with occasional elongated talc crystals. Crosscutting veins of carbonate and quartz (DGMH098).

3.2.4. Lower Mafic Sequence – Johnson Cairn Formation

A previously unidentified unit of intrusive mafic rock is present within sedimentary rocks of the Johnson Cairn Formation (Fig 3.8). In drillhole THD001 (Fig 3.8) - a stratigraphic drillhole approximately 50 kilometers to the north west of DeGrussa, on the margins of the Yerrida Basin sedimentary rocks bounding the Marymia Inlier (Fig 3.1) – the same mafic rock unit is found within Johnson Cairn Formation sedimentary rocks, indicating its presence over a wide area (Table 3.1). In drillhole DGDD347, mafic rocks are present in the lower section of the Johnson Cairn Formation from 644-701m depth, interbedded with siltstones and black shales. Contacts are sheared and the basalts are difficult to identify in hand sample in comparison to sedimentary rocks. Basalt is fine-grained, light grey with pervasive chlorite alteration and quartz-carbonate veins visible in hand sample. In thin section (e.g. DGMH138), it consists of randomly oriented opaque and plagioclase phenocrysts in a fine grained clay altered matrix (Fig 3.9). Vugs (200μm) are filled with carbonate. Chlorite is anastomising through the rock. Quartz, carbonate and opaque-carbonate veins crosscut the unit.

Table 3.1. Summary of THD00l Lithostratigraphic Units (see appendix 3.3 for drill hole log and (Mueller, 2011))

Depth (from/to)	Lithology
0-48	Black shale (weathered) and chert
48-313.51	Pyritic black shale
313.51-335.4	Carbonaceous siltstone and black shale
335.4-359.8	Sandstone and conglomerate with authigenic carbonate
359.8-486.66	"Turbiditic" sandstone-siltstone-shale sequence - some authigenic carbonate in sandy layers
486.66-551.12	Breccia and basalt - marl (felsics?) - minor siltstone and sandstone, authigenic carbonate in breccia matrix
551.12-773.98	Carbonaceous siltstone and sandstone – some authigenic carbonate, minor marl/silty marl
773.98-785.98	Hematitic siltstone and marl
785.98-938.58	Basalt carbonate-chlorite altered, minor marl, siltstone, and hematitic siltstone
938.58-972.13	Siltstone - minor marl and hematitic sandstone/siltstone
972.13-1017.8	Pink limestone/dolomite - minor silty marl and chert

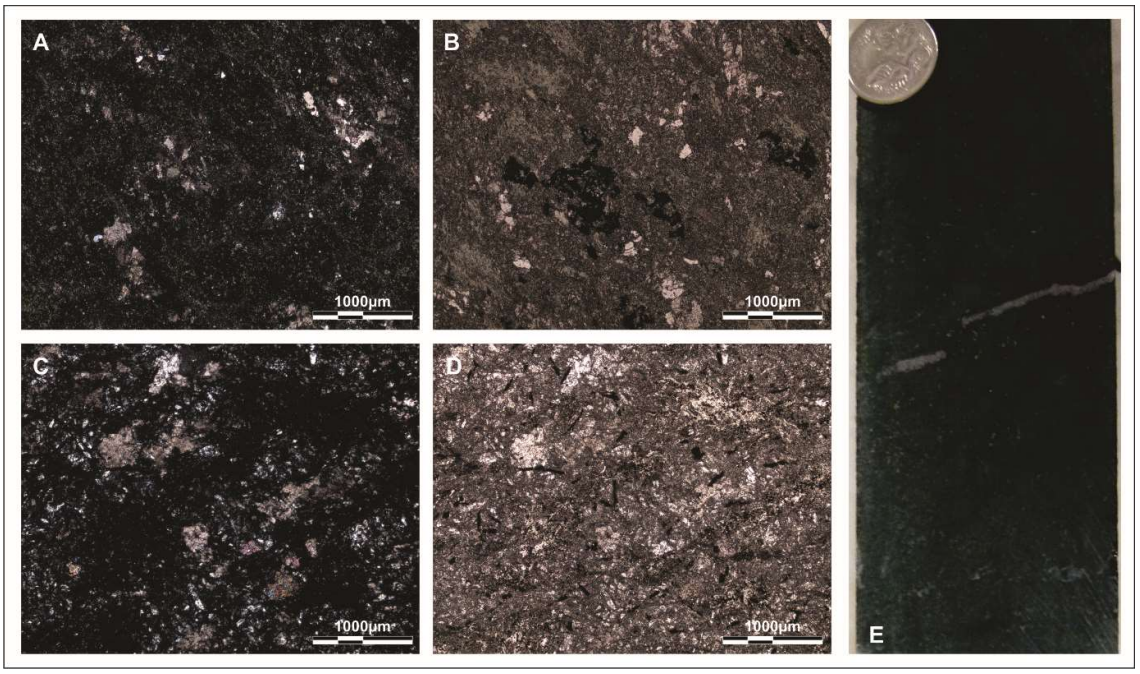

Figure 3.8. Johnson Cairn Formation basalt in thin section and core/hand sample. **A**. Polarised light and **B.** transmitted light showing strongly altered basalt dominated by calcite/carbonate which replaces feldspars and chlorite which replaces original amphibole/pyroxene (DGDD247, 1000.44-1001.78m, sample DGMH116). **C** and **D.** Randomly oriented opaque and plagioclase phenocrysts in a fine grained clay altered matrix. Vugs (200 µm) are filled with carbonate (DGDD347, 684.2-684.35m, sample DGMH138). **E.** Hand sample, fine grained basalt (DGMH116).

3.2.5. Footwall sedimentary rocks - Magazine Member (Informal Name)

The Doolgunna and Maraloou Formations are not identified, east of the Gascoyne along the northern Bryah Basin margin. The 150-230m thick Magazine Member marks the beginning of rifting and volcanic activity in the Bryah Group. It is in disconformable contact with the underlying dolomites and hematitic siltstones of the Johnson Cairn Formation. The upper portion of the Magazine Member is intruded by dolerite and it is separated from the DeGrussa host sedimentary rocks by a thick dolorite sill. An Honours thesis by Baker (2015) studied the Magazine member, and its extent and variation across the DeGrussa deposit region.

The unit consists of four main lithotypes;

1. Hematitic mudstone-rich turbidite forms the uppermost unit of the Magazine Member (Fig. 3.9) and consists of green-purple mudstone turbidite sedimentary rocks. Jasper clasts are often

found in horizons close to the base of mineralisation (e.g. below C4) and in association with disseminated sulfides. In thin section, it displays dominantly fine-grained clay minerals with sparse quartz/feldspar clastic grains. Chlorite and hematite alteration is strong and fine-grained pyrite is scattered throughout the groundmass. Graded bedding and small scale slump folds are visible. Chlorite veins crosscut the rock.

Figure 3.9. **A.** Hematitic siltstones of the Magazine Member. **B.** Volcaniclastic breccia. **C.** Magazine member polymictic breccia distal to the western edge of the DeGrussa deposit (DGDD398, 213.8-214m). Clasts include angular to subangular carbonate/dolomite clasts, red jasper, green basalt and brown vesicular basalt fragments with vesicles infilled with carbonate. All these in a matrix of fine-grained altered sediment matrix (chlorite-rich clays, carbonate). Crosscutting arbonate and ?sericite veins are observed.

2. Carbonate-dolomite megabreccia (Fig. 3.10) is characterised by subangular to subrounded dolomite clasts, millimetres to meters in size, in a fine-grained, foliated clay and chlorite–rich matrix. In hand sample, clasts are variably dominated by calcite (DGMH079) as identified by staining with Alizarin Red S and potassium ferricyanide (expected results: dolomite is stained purple, Fe-free calcite pink, Fe-free dolomite not stained, ferroan dolomite light blue, and ankerite dark blue.). The matrix also contains pervasive calcite, trace pyrite and chalcopyrite. Trace sulfides appear associated with chlorite alteration on the margins of calcite clasts. Fragments of what appear to be stromatolite are observed, suggesting derivation from the Bubble Well Member (Baker, 2015).

In thin section, clasts are formed from a mosaic of dolomite and/or calcite grains and minor amounts of clastic quartz grains. Occasionally, some clasts include clastic grains of quartz. The matrix is composed of subangular-subrounded, clastic quartz (0.5-1mm) and clay minerals with green chlorite flakes (DGMH069).

3. Volcanic conglomeritic rocks (Fig 3.9) are not present in stratigraphy below the DeGrussa deposit, and were not observed by the author, however are well developed in drill holes ~600m west of the deposit and described by Baker (2015). The unit comprises massive to very thickly bedded, variably matrix supported (60 - 90 %), subangular to angular, mafic volcanic-lithic, pebble (± cobble) breccias in a pervasively chlorite ± sericite ± carbonate altered sandstone, siltstone or shale cement. Clasts include amygdaloidal basalt (40 - 100 %), basalt (40 - 100 %), dolerite (0 - 50 %) and unidentified very fine- to medium- grained lithic fragments (10 - 20 %) (Baker, 2015).

4. Polymict Conglomerates are in gradational to abrupt contact with polymictic (basalt and sandstone) clast bearing interbedded sandstones and variably hematitic siltstones and shales (Baker, 2015). Dolomitic breccia and interbedded sandstone and siltstone in the western sequence are predominantly matrix supported (60 – 80 %) comprising poorly sorted, sand sized quartz and feldspar as well as grey-green to grey-purple, siltstone shale. Clast sizes range from 1 mm to 15 cm, with an average of 5 cm. There are highly variable proportions of sandstone (0 – 40

%), siltstone (40 – 80 %), shale (0 – 10 %), jasper (0 – 30 %), carbonate (5 – 40 %), mixed quartz (5 – 10 %), and mafic volcanic-lithic (5 – 20 %) clasts (Baker, 2015). Sedimentary clasts are subrounded to subangular, however the volcanic lithic clasts are subangular to angular. In comparison, rocks beneath the DeGrussa deposit (DGDD020) contain pebbles of carbonate, rare basalt fragments and granular mixed quartz and feldspar in a chlorite - sericite - carbonate altered, siltstone matrix (Baker, 2015).

Figure 3.10. Underground exposure of Carbonate Mega-breccia of the Magazine Member. Large clasts of dolomite and/or calcite occur in chlorite-sericite altered sediments within the footwall succession of the DeGrussa Deposit. Photo width ~5m.

3.3. DeGrussa Host Sequence

The DeGrussa host sedimentary rocks, or "DeGrussa Formation" as determined by Jeffery (2011), can be split into an eastern and western stratigraphy (with the division at the Gascoyne River) (Fig 3.11).

Western stratigraphy: West of the Gascoyne River the unit consists of tholeiitic pillow basalt and thin lava flows with sub-volcanic dolerite sills outcropping at Noonyereena Hill. The lowest stratigraphic unit is a mixture of schistose lapilli tuff and thin lava flows with overlying siltstone, shale, and black shale. Fine- to coarse-grained arkose layers occur within siltstones (Jeffery, 2011).

Pillow basalts are locally associated with lapilli tuff. Pyroclastic rocks of unknown environment, form a minor component of the volcanic pile. Coarse-grained, thick basalt flows are intercalated with ultramafic rocks, which become highly fissile talc-chlorite and talc-carbonate schists where tectonised. A 200m thick basaltic komatiite is present ~2kms stratigraphically below the upper ultramafic rocks (Jeffery, 2011).

Overall, the western succession of the DeGrussa Formation consists of a mafic volcanic sequence comprising tholeiite, magnesian-tholeiite and basaltic komatiite basalts that Jeffery (2011) interpreted to have extruded at high eruption rates due to their fine-grained, granular, re-crystallised appearance, paucity of phenocrysts and other magmatic textures.

The basal contact of the ~6700m thick DeGrussa Formation was considered by Jeffery (2011) be tectonic to the east and west of the DeGrussa deposit. Drill core observations suggest that it is disconformable or paraconformable with the underlying Johnson Cairn Formation below the Magazine Member. The top of the sequence is not seen as the formation is in structural contact with overlying units (Jeffery, 2011).

Fig.3.11. Map of the eastern Bryah Basin showing major geographic features and geological units. A major change in geology in comparison to that of the DeGrussa host sequence, to the west of the Gascoyne River. Adapted from Pirajno et al. (2000).

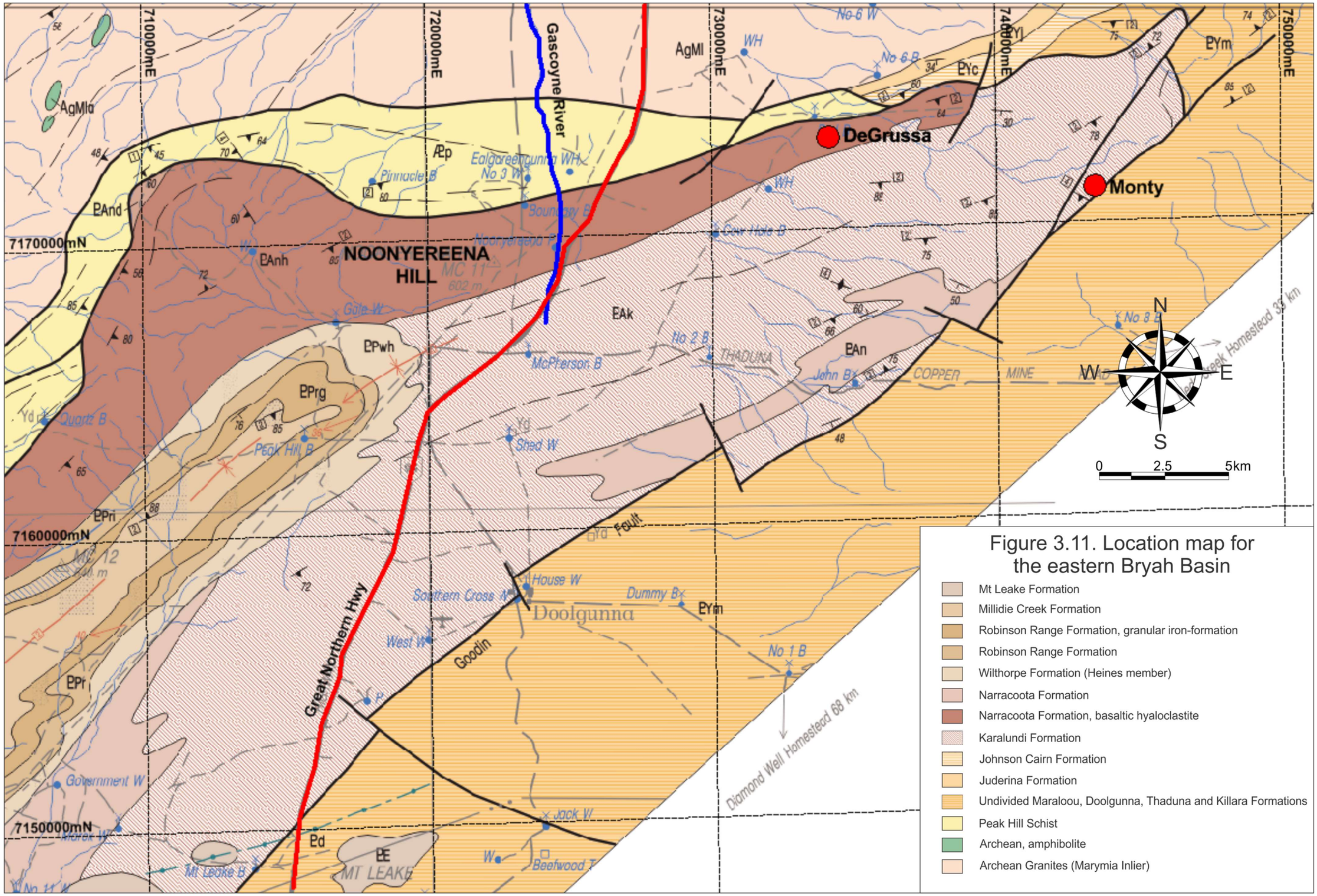

Figure 3.11. Location map for the eastern Bryah Basin

- Mt Leake Formation
- Millidie Creek Formation
- Robinson Range Formation, granular iron-formation
- Robinson Range Formation
- Wilthorpe Formation (Heines member)
- Narracoota Formation
- Narracoota Formation, basaltic hyaloclastite
- Karalundi Formation
- Johnson Cairn Formation
- Juderina Formation
- Undivided Maraloou, Doolgunna, Thaduna and Killara Formations
- Peak Hill Schist
- Archean, amphibolite
- Archean Granites (Marymia Inlier)

Eastern stratigraphy (DeGrussa host sedimentary rocks): East of the Gascoyne River, the DeGrussa host sedimentary rocks are fine-grained, argillaceous and arenaceous sedimentary rocks, turbidites and mass debris flows, carbonate rocks, conglomerate, with basalt and volcanic breccia.

Metamorphic minerals are seen to pseudomorph redundant primary minerals. Zoisite is interpreted by Jeffery (2011) to indicate hydration during metamorphism rather than sea floor alteration. Metamorphic tremolite and zoisite have partially replaced plagioclase. The rocks have characteristics of boninites in trace elements but do not have high Si and Mg. They are particularly characterised by low levels of Ti and Zr.

3.3.1. Host sedimentary rocks (DeGrussa Formation Informal)

DeGrussa host sedimentary rocks are turbiditic, consisting of graded units comprising quartz-rich sandstone, siltstone and mudstone (Fig. 3.12). Normal and reverse graded bedding can be correlated across several drill holes south of the Shiraz Fault. There are no black shales preserved in the sequence. Sedimentary rocks are generally intensely altered to chlorite and clay minerals, however some grainsize variation is observed. Due to the strong alteration of the sedimentary rocks, original crystal textures are largely destroyed.

In thin section (Fig 3.13), sedimentary rocks are dominated by quartz (5-40%) and lesser feldspar (30%) and opaques (10%) in a matrix of clay and carbonate minerals. Chlorite rims the clasts. Grains are subrounded to subangular and alternate between fine and coarse bands. Coarse-grained bands tend to be clast supported. Mineralogy of layers varies with some layers dominated by opaque iron minerals. Small scale microfaulting (reverse) and folding is visible in thin section (Fig 3.13). Coarse-grained rocks often occur at the base of turbidites, gradational from shale and siltstone units, and are of two forms. The first, sedimenatary breccia lenses (e.g. DGMH057:DGDD203, 94.78-94.95m), comprise turbiditic mudstone-siltstone and small basalt clasts (Fig. 3.12 and 3.13). Basalt clasts (0.5-7mm) consist of fine-grained, interlocking crystals of plagioclase (70%), opaque minerals (10%) and chlorite (20%). Additional clasts consist of

fragments of subround-angular quartz and opaques in a matrix of clay and opaque minerals, carbonate and chlorite. The second, coarse-grained sandstone comprise poorly-sorted, subround-round quartz <0.5mm (65%) and minor opaque minerals (5%) in a fine-grained ground mass consisting dominantly of clay mineral and chlorite (throughout the groundmass and rimming quartz clasts).

Jasper and disseminated pyrite occur in sedimentary rocks above and peripheral to the ore lodes (see Fig 3.14, section 733800). They are also seen in the Magazine Member footwall sedimentary rocks, below conductor 4 as discussed in Section 3.2.5.

Alteration is dominantly carbonate with lesser chlorite and sericite. Epidote is rare. Quartz, carbonate, and quartz-carbonate veins both laminar and stockwork, with or without sulfides (pyrite > chalcopyrite), cross cut and are preferentially developed in the sedimentary rock in comparison to dolerite and basalt.

Fig 3.12. Examples of turbidite rock from the DeGrussa host sediment sequence. **A.** Turbiditic mudstone-siltstone (DGDD106, 268.15-268.3m, sample DGMH014). **B.** Turbiditic carbonaceous siltstone-mudstone host rock to DeGrussa (DGDD173, 97.41-97.57m, sample DGMH018), **C.** Sedimentary breccia comprising clasts of basalt and a matrix of clay minerals (DGDD203, 94.78-94.95m, sample DGMH057). **D.** Host turbiditic siltstone-mudstone proximal to the Conductor 1 ore lens (DGDD173, 217.11-217.3m, sample DGMH022), **E.** Turbiditic mudstone with coarse clastic base (DGDD125, 165.98-166.19m, sample DGMH029).

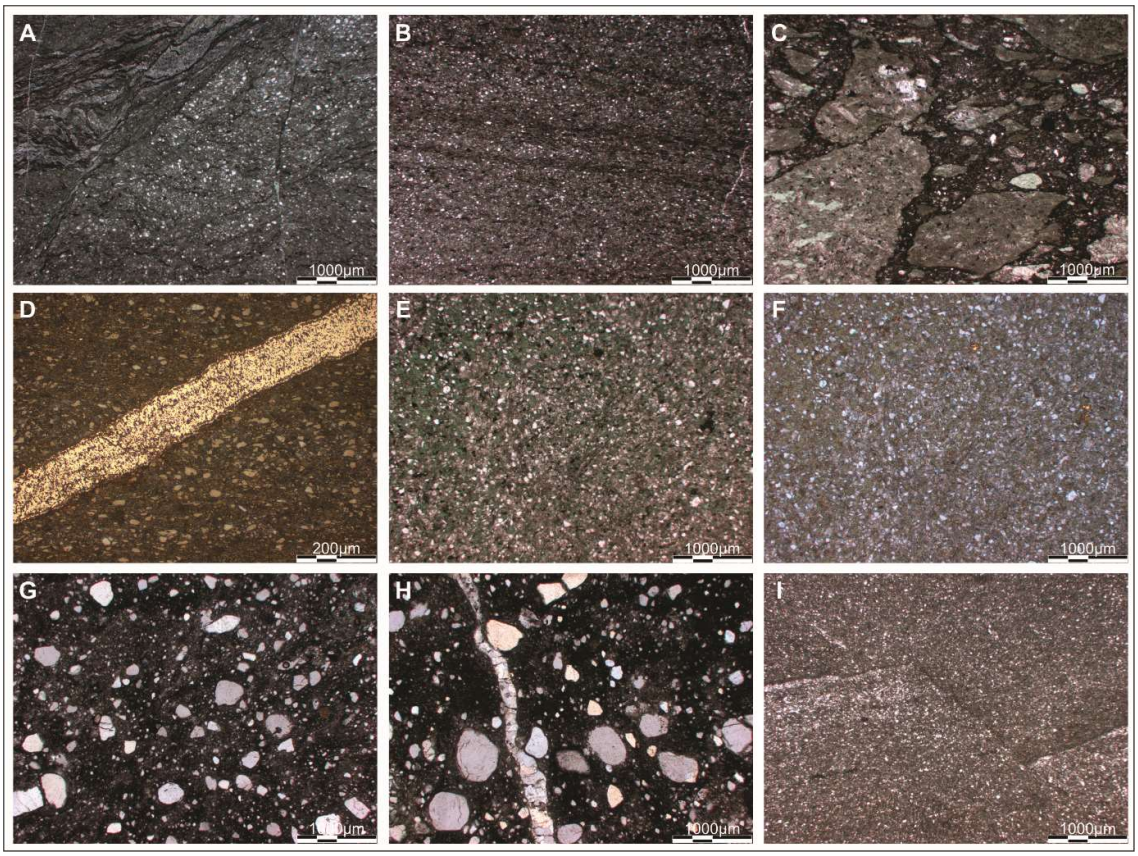

Figure 3.13. Thin sections from the DeGrussa host sedimentary rock sequence, **A.** Siliciclastic turbidite displaying fine- and medium-grained quartz rich layers. Clay minerals are sericite and chlorite dominated (DGMH014: DGDD106 275.55-275.75m). **B.** Laminar quartz-rich, turbiditic sedimentary rocks (DGMH018: DGDD173 97.57-97.41m). **C.** Basalt breccia in clay-rich turbidite matrix (DGDD057: DGDD203, 94.78-94.95m) (see also Fig. 3.17c)**. D.** Pyrite vein crosscutting turbidite sediments under plane light (DGMH018: DGDD173 97.57-97.41m). **E.** Fine-grained, quartz-rich turbidite with intense chlorite alteration (magnesium-chlorite) and **F.** with pyrite grains throughout, these are opaque in previous image (DGMH023: DGDD173, 242.75-243.0m). **G**, and **H.** . Coarse-grained with cross cutting carbonate vein (DGMH026: DGDD125, 79.6-79.75m). **I.** Microfaulting of sedimentary rock units (DGMH028: DGDD125, 165.98-166.19m).

Figure 3.14. Plan view and section through the DeGrussa ore lodes at 733800E. Drill hole logs referring to this section are located in Appendix 3.3.

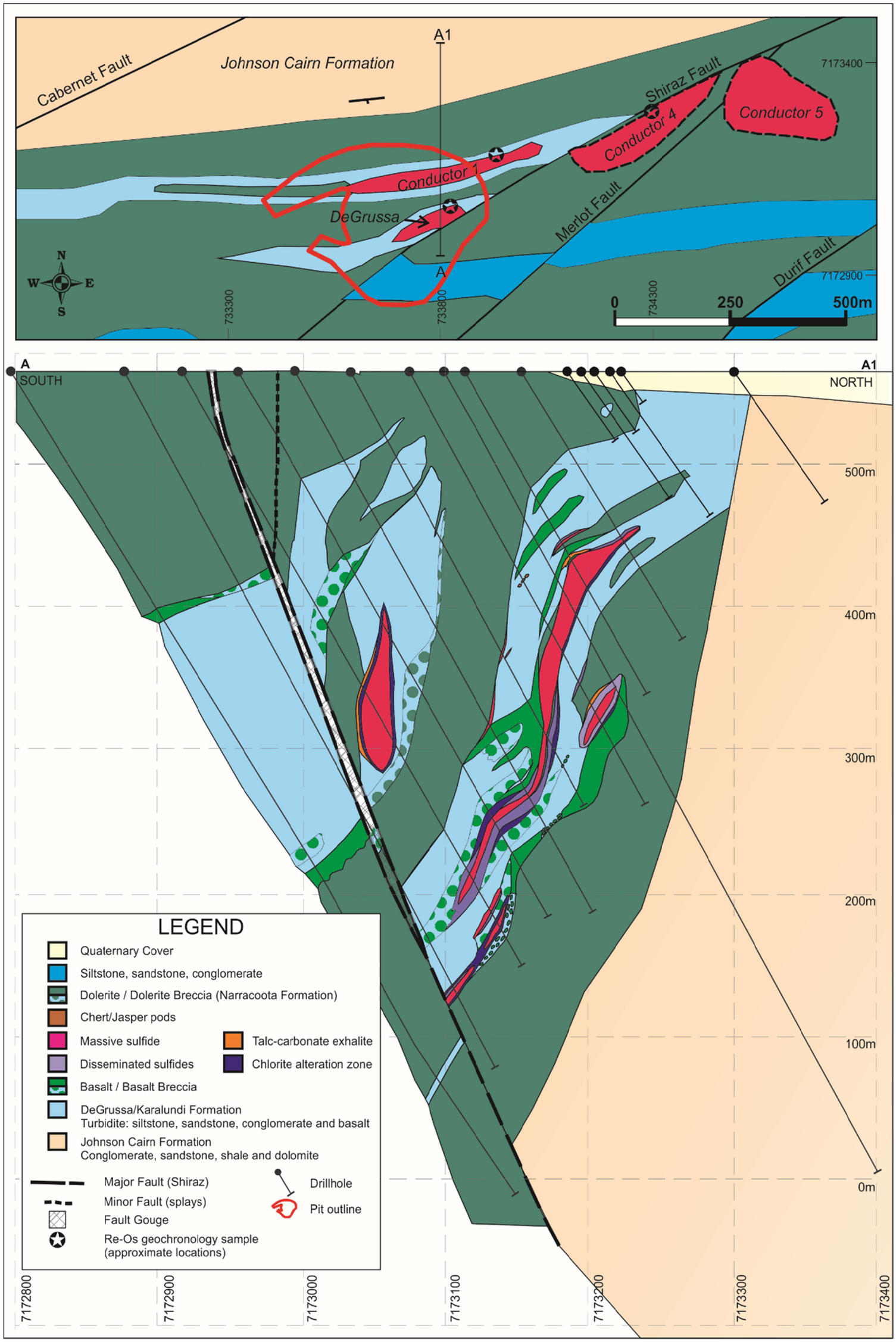
A1
Johnson Cairn Formation
Cabernet Fault
Shiraz Fault
Conductor 5
Conductor 4
Conductor 1
DeGrussa
Merlot Fault
Durif Fault
A
7173400
7172900
N
W
E
S
733300
733800
734300
0
250
500m
A
SOUTH
A1
NORTH
500m
400m
300m
200m
100m
0m
LEGEND
Quaternary Cover
Siltstone, sandstone, conglomerate
Dolerite / Dolerite Breccia (Narracoota Formation)
Chert/Jasper pods
Massive sulfide
Talc-carbonate exhalite
Disseminated sulfides
Chlorite alteration zone
Basalt / Basalt Breccia
DeGrussa/Karalundi Formation
Turbidite: siltstone, sandstone, conglomerate and basalt
Johnson Cairn Formation
Conglomerate, sandstone, shale and dolomite
Major Fault (Shiraz)
Minor Fault (splays)
Fault Gouge
Re-Os geochronology sample
(approximate locations)
Drillhole
Pit outline
7172800
7172900
7173000
7173100
7173200
7173300
7173400

3.3.2. Basalts

Large blocks of basalt, with no discernable contact metamorphism occur throughout the sedimentary rocks and may be large lithic clasts rolled downslope. Basalts intrude the sedimentary rock sequence directly above the C1 ore lode.

Drill core is often made up of approximately equal portions basalt and sedimentary rock. Basalt morphology includes peperite (Fig 3.15) and irregular deformation of adjacent sedimentary rock in the vicinity of DeGrussa. Pillow basalt has been observed west of the highway within the Narracoota Formation (Fig 3.15). In hand sample, basalts are pale green-grey to dark blue-black, fine grained and flecked with white-grey titanite crystals up to 0.5mm. Veining in basaltic units varies between quartz-carbonate±chlorite and lesser epidote.

In thin section, the basalts consist of plagioclase (50%) and pyroxene (30%) with lesser magnetite and/or leucoxene (10%). Basalt groundmass alters to Fe-Mg clays, chlorite and carbonate (e.g. DGMH002, DGMH003). Foliation is visible in fine grained alteration/metamorphic minerals but no flow banding is visible in either the macro or micro-scale. When basalts are in proximity to mineralisation they often include small amounts of chalcopyrite, pyrite, molybdenite and sphalerite.

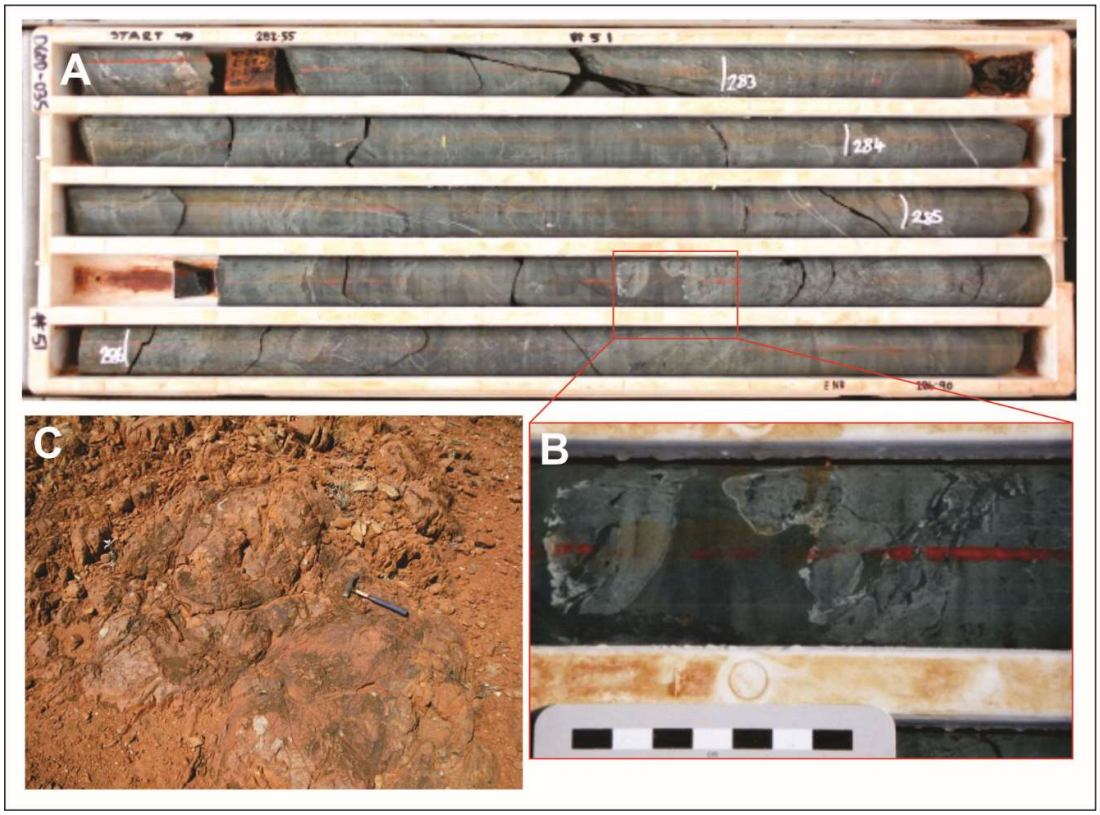

Figure 3.15 A. Basalt and sedimentary rock in core for DGDD035, 282.55-286.90m, **B.** Magnified image of basalt-sedimentary rock contact (peperite) showing finer grainsize (DGDD035, 285.5m). **C.** Outcropping pillow basalts indicating emplacement in a submarine environment west of the Great Northern Highway.

3.3.3. Mineralisation (see also chapter 4).

Descriptions of the mineralisation is presented in Chapter 4. The DeGrussa mineralisation is characterised by massive pyrite, chalcopyrite and pyrrhotite with lesser sphalerite, marcasite, galena and molybdenite. Ore textures vary and display primary features (eg. bedded sulfides, chimney structures, insitu sulfide breccia) and deformational textures (fragmental textures, remobilisation and recrystallisation, sheared contacts with host rocks and schists).

Massive sulfide mineralisation is bounded on its upper contact by chlorite altered wall rock between 1-3m wide and/or a rock comprised predominantly of talc-carbonate. Disseminated sulfides may or may not be present within these units. The lower contact is similarly bounded by chlorite and/or talc-carbonate schist. Basalt units are also common directly below mineralisation or alteration zones (see Fig. 3.14).

3.3.4. Dolerite

The stratigraphy in the mine area has been intruded by numerous layer sub-parallel dolerite sills. These sills are in the order of meters to hundreds of meters thick. Contacts are hyaloclastite breccia, sheared, or faulted. Grain size varies from finer grained and microdoleritic at the margins, gradational to medium-grained, coarse and sometime pegmatitic in the centre (Fig. 3.16).

The primary mineralogy of the gabbro/pegmatite rocks seen in thin section, consist of plagioclase (40-70%), hornblende (≤40%), clinopyroxene (≤30%), magnetite and/or titanate (sphene) and occasional trace sulfides (pyrite and chalcopyrite) (Fig 3.17). Rocks are altered to clay minerals (identified from Terraspec as Fe, Mg clays, see Appendix 3.4), chlorite (Fe, Mg chlorites – clinoclore and chamosite) and carbonate, lesser talc, actinolite, epidote, albite and stilpnomelane replacing primary phenocrysts and around grain margins. Titanite alters to leucoxene producing a flecked appearance to the rock in hand specimen. Clays and calcite dominantly replace plagioclase and chlorite. Talc and actinolite replace pyroxenes and amphibole.

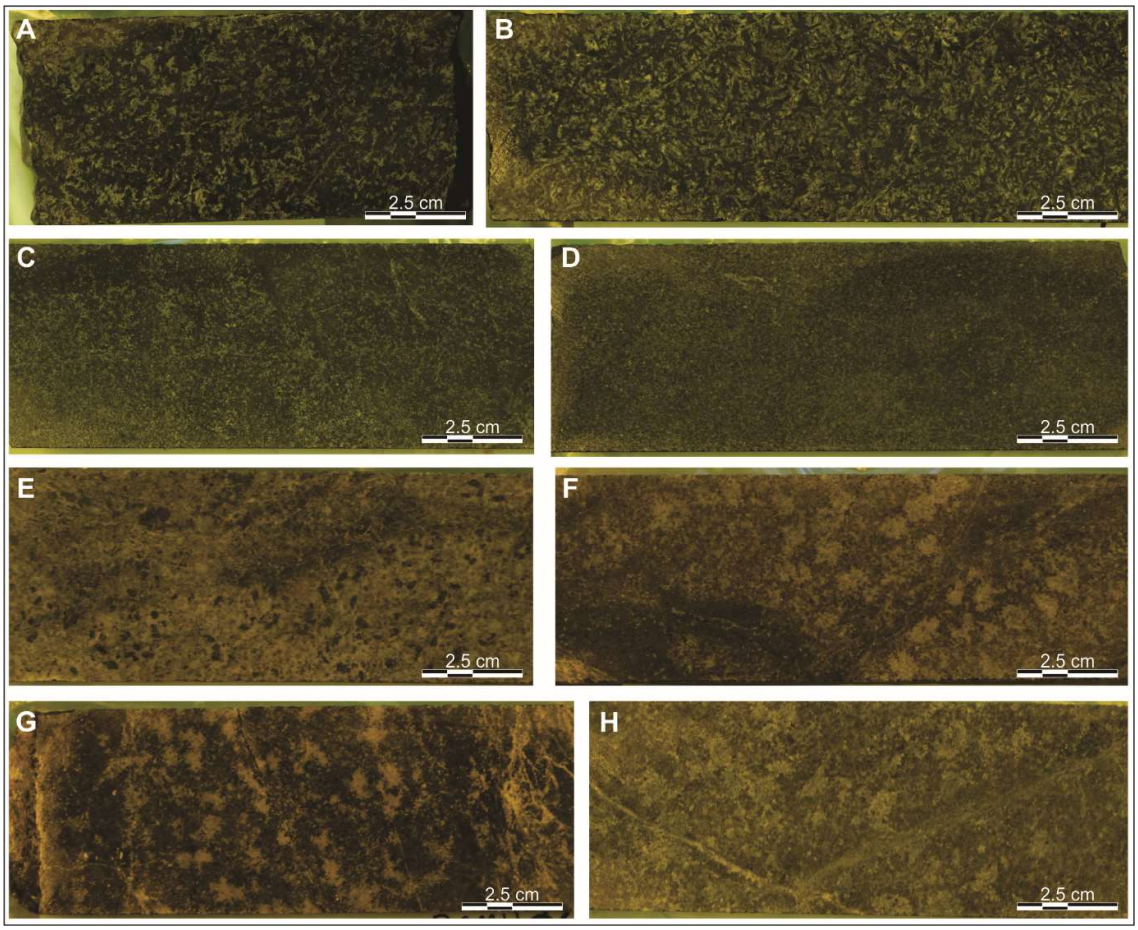

Figure 3.16. Examples of DeGrussa dolerites, in progressive stages of alteration. Coarse-grained dolerite in **A.** DGDD057, 306.57-306.7m (DGMH006), and **B.** DGDD219, 147.51-147.7m (DGMH044), **C.** Fine-grained dolerite from the footwall of the DeGrussa deposit (DGMH021: DGDD173, 330.72-330.9m), **D.** Fine-grained dolerite from sill between the DeGrussa and C1 ore lenses (DGMH045: DGDD219, 197.6-197.74m). **E.** Altered dolerite. Strong carbonate alteration (~70%) of plagioclase and hornblende (DGMH010: DGDD057, 118.33-118.5m). **F.** Altered dolerite consisting of original plagioclase (60%), pyroxene (20%) hornblende (10%) and opaque minerals (10%) now replaced by talc (DGMH020: DGDD173, 182.75-183.0m). **G.** Altered dolerite. Plagioclase (10%), amphibole (30%) + opaque (<5%), clay, chlorite and talc alteration throughout. Alteration is pervasive but small clusters visible in hand specimen (DGMH062: DGDD203, 533.03-533.2m), and **H.** Altered medium- to coarse-grained dolerite, plagioclase (40%) altered to clay, with pyroxene (45%) altered to chlorite and opaque minerals (5%) (DGMH047: DGDD219, 339.45-339.6m).

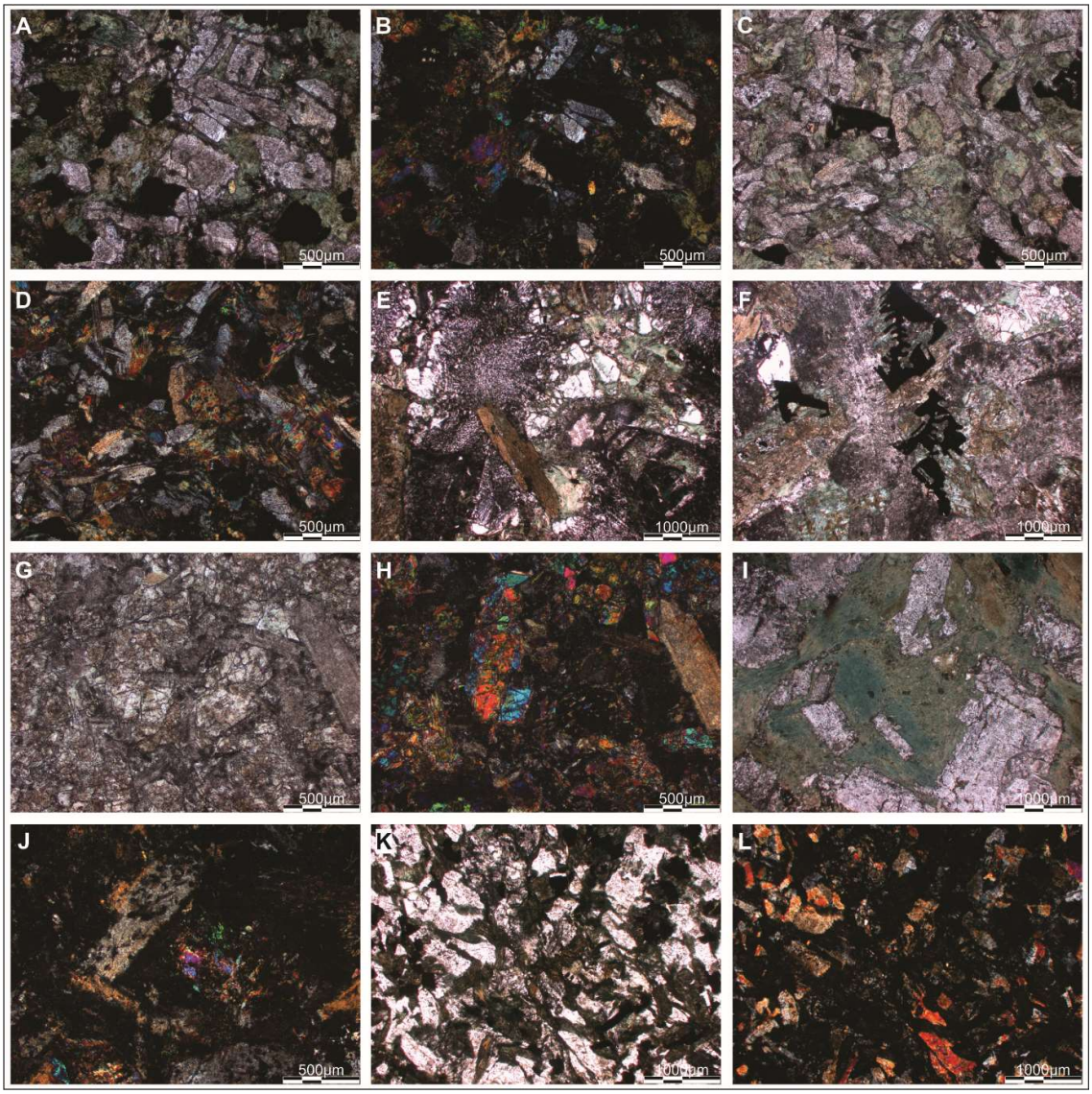

Figure 3.17. Examples of Dolerite in thin section **A.** Dolerite with moderate alteration of original mineralogy of plagioclase, hornblende and opaque pyrite and **B.** the same sample in polarised light (DGMH080, DGDD243, 161.7-161.88m). **C.** plane light image and **D.** polarised image showing weakly altered basalt with interlocking crystals of plagioclase. Chlorite and weak zoisite alteration within the footwall gabbroic unit (DGMH041: DGDD125, 603.31-603.25m). **E.** Plane light, coarse-grained host dolerite/gabbro displaying primary composition of hornblende, plagioclase and clinopyroxene, with alteration to zoisite and chlorite, and **F.** with original plagioclase and skeletal magnetite crystals and alteration minerals of actinolite, zoisite and chlorite (DGMH044: DGDD219 147.51-147.7m). **G.** Plane light, and **H.** crossed polars. Strongly altered dolerite with rounded globular alteration patterns and crosscutting epidote-carbonate veins, from host dolerite/gabbro unit. Much of the original mineralogy has been overprinted by sericite/zoisite, chlorite and epidote alteration. Original mineralogy estimated to consist of plagioclase (40%), hornblende and clinopyroxene (40%) and opaque magnetite (10%) (DGMH047: DGDD219, 339.45-339.6m). **I.** Coarse grained (up to 4mm), interlocking grains, plagioclase (40%), hornblende (30%) and opaque minerals (10%) with chlorite, epidote, talc and rare carbonate alteration (DGMH006: DGDD057, 306.57-306.7m). **J.** Plagioclase (50%), hornblende/pyroxene (40%) and opaque (chalcopyrite and pyrite) minerals (10%) with strong carbonate alteration (~70% of rock) and lesser chlorite and talc (DGMH010: DGDD057, 118.3-118.5m). **K** Transmitted light and **L.** under polarised light showing medium-coarse, interlocking crystals of plagioclase (50%), pyroxene (10%) and opaque (magnetite, minor chalcopyrite) (10%) altering to chlorite and clay (DGMH060: DGDD203, 417.91-418.11m).

Alteration intensity varies from rocks where textures are largely preserved (eg. DGMH219) to rocks where primary mineralogy is obliterated, yet original textures are still observable (eg. DGMH010, DGMH047) (Fig. 3.17).

Intense quartz-carbonate veining occurs proximal to faults and major contacts – i.e. the base of the lower footwall gabbro/dolerite in contact with the Magazine member.

Variations of the same mineralogy to that of the dolerites is retained in coarse-grained gabbro and pegmatite units (Fig. 3.16). These sections are often located central to dolerite intrusions with boundaries being either sharp and often defined by shearing or veins, or gradational where these is a progression from finer microdolerite at the margins, to medium-grained dolerite and coarse grained gabbro/pegmatite.

In thin section, primary mineralogy consists of interlocking crystals, up to 4mm in size, of plagioclase (~40%), amphibole and/or pyroxene (30-50%), opaque minerals (~10%) and minor quartz (≤5%) (Fig 3.17). Alteration minerals are chlorite, epidote and talc as well as trace amounts of chalcopyrite and pyrite and rare carbonate. Veins of carbonate, amphibole/actinolite and opaque minerals are present. An interesting globular alteration of gabbro is observed (eg. DGMH062, Fig 3.23.) where the original mineralogy of interlocking feldspar, amphibole, pyroxene and opaque minerals is pervasively altered to clay minerals, carbonate and epidote, but small clusters, dominated by pyroxene crystals, undergo stronger clay alteration.

Dominant alteration types vary depending on position in the sill. Carbonate and clay alteration dominates at the edges of intrusions, with chlorite, epidote and albite towards the centre. Veins follow a similar pattern. Carbonate veins are dominant at the edges. Epidote veins are found towards the centres of intrusions, also with occasional albite/prehnite veining. Chlorite cross cuts epidote veins as does albite in coarse-grained sections of gabbro and pegmatite (visible in DGDD014). Veins are often multistage with typical assemblages comprising (from edge to centre of vein) chlorite+carbonate+quartz, chlorite+carbonate+albite, chlorite+albite, carbonate+chlorite, epidote+chlorite. Carbonate veins of varying thicknesses often have associated halos of pervasive chlorite alteration (eg. DGDD125, Fig 3.18). Within this halo,

leucoxene crystal aggregates are visible (Figure 3.18). Sericite/epidote alteration becomes pervasive in the rock, away from the carbonate vein. Sulfide (eg. pyrite) appears related to chlorite-carbonate veins.

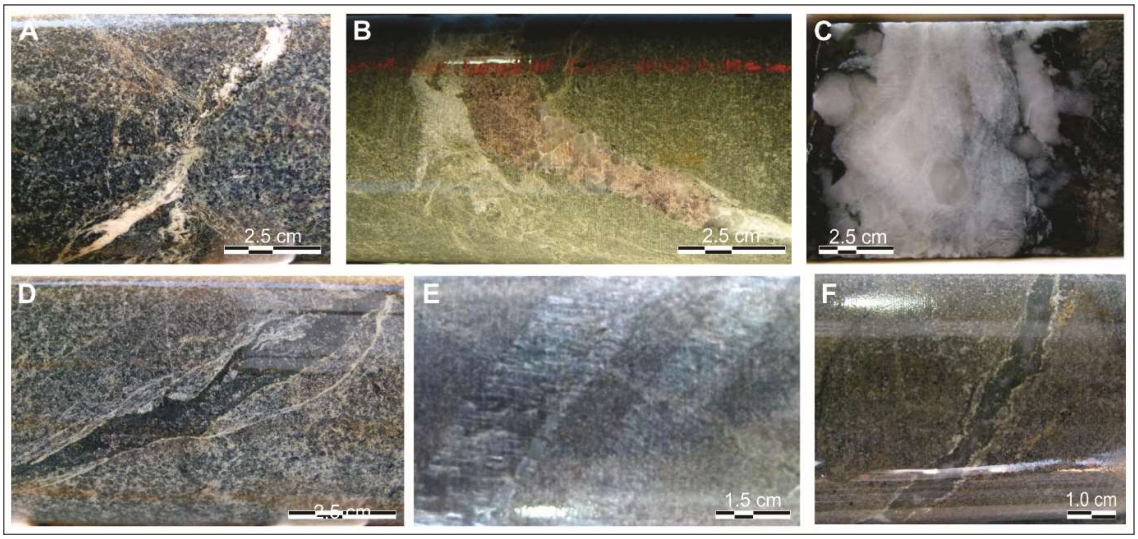

Figure 3.18. Veins in dolerite and basalt rocks. **A.** Plagioclase/feldspar vein crosscutting and offsetting epidote vein (DGDD014), **B.** Pink carbonate-quartz vein crosscutting epidote veins in dolerite (DGDD125), **C**. Chlorite-carbonate-quartz vein. Hexagonal quartz crystals within carbonate-dominated vein. Thin chlorite-dominated halo to the vein within dolerite host rock (DGDD125), **D.** Chlorite infill to vein with epidote rims (DGDD014), **E.** Extensional calcite-chlorite veins in dolerite host rock. Crystal direction parallel with direction of extension (DGDD125). **F.** Pyrite crystallisation related the chlorite-carbonate veins in dolerite (DGDD125).

3.4. Other Regional Units

3.4.1. Killara Formation

Basalts and dolerites in the Killara Formation outcrop, are blocky and more resistant to surface weathering processes than the DeGrussa dolerites. In thin section, mafic rocks of the Killara Formation are characterised by plagioclase (60%), quartz (10%), clinopyroxene (20%) and opaque minerals (10%)(Fig. 3.19). Rocks are often vesicular with vugs infilled with pale green epidote. Thin quartz veins occasionally cross cut.

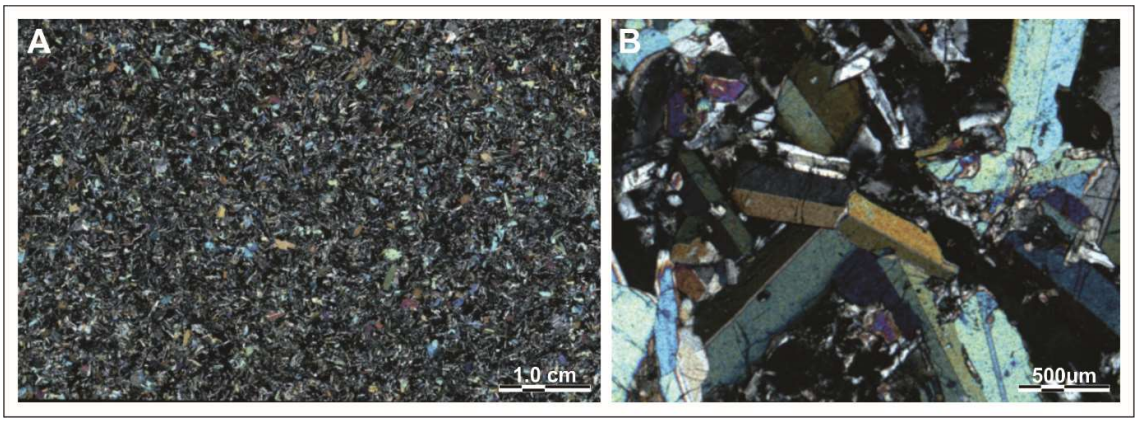

Figure 3.19 A. Polarised light microscope image of Killara Basalt displaying fine grained interlocking crystals (Sample KL003) at 795929mE, 7146403mN, outcrop along Ned's Creek Rd. **B.** Thin section showing interlocking nature of plagioclase and clinopyroxene crystals (KL003).

3.4.2. Narracoota Formation

A sample of a quartz-bearing mafic rock from the Narracoota Formation, west of the Great Northern Highway (DGMH084, was examined in thin section. This sample of Narracoota Formation mafic rock comprise fine grained clusters dominated by plagioclase (40%) and pyroxene (30%) with surrounding coarse-grained interlocking crystals of quartz (30%) and plagioclase, with plagioclase altering to clay minerals (e.g. sericite). Alteration of feldspar to clay minerals.

Other samples of the Narracoota Formation mafic rocks were proximal to the Fortnum and Cassidy gold deposits to the west of the Bryah Basin. These rocks are altered and deformed, those hosting the Fortnum mineralisation (FTMH004A, 636852mE, 7198710mN) comprising sheared/schistose bands of alternating quartz (40%) and tremolite (45%) dominant zones with minor chlorite (5%) and remnant feldspar (5%) clasts and opaque minerals (5%) scattered throughout but also concentrated in crosscutting veins. The altered mafic rocks associated with the Cassidy gold mineralisation (CS001 - 661799mE, 7182946mN; CS002 - 661473mE, 7182864mN) show large feldspar phenocrysts surrounded and resorbed by chlorite which is aligned/foliated around the feldspar, to rocks comprising very fine-grained foliated tremolite/talc and clay minerals.

3.4.3. Red Bore Formation (Padbury Group)

The Red Bore Formation was not studied by the author, but is described here for completeness. The "Red Bore Formation" as described by Jeffery (2011) has an estimated thickness of 300 metres and is in tectonic contact with the DeGrussa host sedimentary rocks along the Jenkin Fault. It mainly consists of quartzite, but varies from thin pebble-granule conglomerate near the unit base (containing vein quartz clasts in a sandy quartz matrix, interspersed with shale and thin planar bedded quartz arenite), to well bedded, laminated, and commonly cross-bedded quartzite. Black, banded graphitic shales overlie the quartzite and are regionally continuous and clearly identified in regional geophysical maps (Jeffery, 2011). Black shale may be a unit that was not previously identified.

The Red Bore Formation is considered to be part of the Padbury Group, a fault preserved block analogous to the Robinson Range Formation, rather than part of the Bryah Group (Hilliard, 2015).

3.4.4. Regional Intrusive Rocks

Several intrusive rocks have been identified from drilling across the region. These are compositionally granodioritic or leucogranitic with contacts gradational to dolerite suggesting that these are the fractionated portions of doleritic units. In hand sample, these are coarse-grained, plagioclase and quartz-phyric with dominant chlorite alteration and thin cross cutting quartz and chlorite veins. Epidote is patchy in hand sample. In thin section (e.g. SPD015, 75.2-78.9m, Fig. 3.20), plagioclase (70%) is twinned and intergrown with quartz (20%). Chlorite alteration (10%) is pervasive along fractures and grain boundaries.

Figure 3.20. Leucogranite from SPD015 in **A.** hand sample and **B.** Thin section under polarised light.

3.5. Structure

The Shiraz Fault is a splay from the long-lived, deep crustal Jenkin Fault. The Jenkin Fault places the upper contact of the DeGrussa host sedimentary rocks against the Red Bore Formation. The Jenkin Fault can be tracked from the southwest from the Robinson Range through the Bryah and Yerrida Groups to the Baumgarten Greenstone Belt. The DeGrussa deposit lies within a small ~2km long (east-west) graben structure in which footwall geology differs markedly from rocks to the east and west. To the east, this is marked by the Durif Fault, and to the west by a small, as yet unnamed, fault along which Conductor 1 mineralisation appears to terminate. The Magazine Member volcaniclastic conglomerate was not visible within this zone, and Johnson Cairn Formation sedimentary rocks are more intensely dolomitised and silicified than seen distally (Jeffery, 2013).

Several upright, large scale folds transect the Bryah Group rocks. The DeGrussa ore deposit sits on the northern limb of one of these folds - the Robinson Range syncline (Fig. 3.1, Map 1) – that plunges at approximately 30˚ to the southwest. No significant parasitic folding has been documented at the DeGrussa deposit. Lithological layering and mineralisation dips south at 55-70˚. Two large faults crosscut and displace the DeGrussa ore lodes from each other. The Shiraz fault (Fig. 3.1) is the most significant with reverse sinistral displacement of 500-600m. The Shiraz Fault truncates the southern side of the DeGrussa and C1 ore lodes, separating them from C4 and C5 which are on the south side of the fault. The Merlot Fault splays off the Shiraz Fault in a south-west direction, approximately 500 m north east of DeGrussa and C1 ore lenses. It displaces C5 from C4 by approximately 80m (Jeffery, 2011, Hilliard, 2013).

Stresses during deformation have largely been taken up by sediments and schistose units. In drill core, contacts between different units are mostly fractured and sheared, removing any primary textures from observation. Margins of the ore body, in underground exposure, are largely sheared contacts within the C1 and DeGrussa ore lodes. C4 and C5 are less deformed. Peperite is present where basalts have intruded wet sediments and form a large part of the host sequence.

The Robinson and Padbury synclines are interpreted by Pirajno et al. (2000) as formed during D2 deformation (D1, is rarely visible and overprinted by D2). D3 is characterised by north-south trending folds and sub-vertical foliations and was responsible for the doubly plunging nature of the Robinson Syncline and the Peak Hill Anticline. The intensity of D3 deformation lessens towards the eastern portions of the basin. D4 includes small-scale folds, sub-vertical foliation, shear zones, faults and quartz blows with a common orientation of 280˚ to 310˚ in western parts of the basin. To the eastern side of the basin, in proximity to the DeGrussa deposit, structures associated to D4 are oriented in a northeast to south westerly direction.

3.6. Discussion

3.6.1. Juderina Formation

The Juderina Formation, as identified by Pirajno and Adamides (2000) consists of quartz arenite and subordinate siltstone, chert breccia, dolomite and pebble beds. It is largely observed as unconformable on Archaean granite-greenstone basement and consists of the lower Finlayson member and upper Bubble Well Member. Unlike outcrop observed by previous authors (e.g. Grey (1984)), the Finlayson Member is not present at the base of the Juderina Formation below the DeGrussa mineralisation.

The contact with the Marymia Inlier and the Yerrida Group sedimentary rocks was considered by previous authors (Pirajno and Adamides, 2000, Johnson et al., 2011, Johnson et al., 2013, Dentith et al., 2014) to be tectonic. The lack of the Finlayson member at the base of the Yerrida Group, as seen in drilling proximal to the DeGrussa deposit, suggests a tectonic contact. However, the contact between the Bubble Well Member stromatolites at the base of the sedimentary rock sequence with the Marymia does not appear tectonic in drill core. This would be consistent with original interpretations by Gee (1986) who interpreted the Yerrida and Bryah Group sedimentary rocks to unconformably mantle the Marymia Inlier. Hence rifting of Archean crust to form a shallow marine shelf environment is possible.

Comprehensive studies of stromatolites and their stratigraphic location in the basins of the Capricorn Orogen have been completed by Grey (1994). Her work identified a number of stromatolite species in the Juderina Formation's Bubble Well Member to the south of the Yerrida Basin, proximal to Mt. Russell. A full list of stromatolites found in the region is provided in Table 3.2. Several of these species, *Segosia finlaysonensis*, *Stromatolite form 1* and *Stromatolite form 2* are also found in DGDD347 (DeGrussa diamond drillhole) and THD001 (co-funded diamond drill hole between SIPA and GSWA). The other species known to occur within the confines of the basins is *Eucapsiphora new form* at Mt. Leake although this unit unconformably overlies the Padbury Group sediments and is identified as being a similar age to the Earaheedy Basin further to the east. These stromatolites do not resemble any of the known forms in the Earaheedy and therefore provide no further basis for correlation (Gee and Grey, 1993).

Table 3.2 Summary of stromatolite species/forms and their location in stratigraphy

Basin	**Yerrida**	**Bryah and Padbury**	**Earaheedy**		**Mt. Leake**
Host Unit	Bubble Well Member, Juderina Formation	NA	Yelma Formation (Lower strom unit)	Yelma Formation (Upper strom unit)	Mt. Leake Sandstone
Species	*Conophyton form* *Kussoidella karalundiensis* *Segosia finlaysoniensis* *Willunella glengarrica* *Stromatolite form 1* *Stromatolite form 2*		*Yandilla meekatharrensis* *Yelma digitata* *Pilbara deverella*	*Ephyaltes from indet.*	*Eucapsiphora new form*
Age	2174±64Ma[1]	2027±7Ma		1946±71Ma[2]	
[1] Woodhead and Hergt (1997); [2] Russell (1992)					

Evaporites were identified by El Tabakh et al. (1999) in the stromatolitic succession of Bubble Well Member near Mt. Russell/Eagle's Roost (south-east margin fo the Yerrida Basin) where stromatolites are partially dolomitised with positive $\delta^{13}C$ values of up to +7.69±0.11‰ correlating with the Lomagundi-Jatulian event (Russell, 1992, El Tabakh et al., 1999, Grey, 2012b, Grey and Pirajno, 2012). At DeGrussa, stromatolites present in the Juderina Formation have similarly high C isotope values up to +7‰ (unpublished data, this study). Although highly deformed and silicified, suggestions of evaporitic textures exist interbedded with the stromatolite and mudstone horizons. These textures were identified by El Tabakh et al. (1999) as quartz

pseudomorphs of gypsum or anhydrite and further supported by inclusions of anhydrite in the quartz. They are believed to have grown within the then partially dolomitised stromatolitic beds in a restricted marginal marine environment. Early diagenetic alteration was associated with syn-sedimentary hydrothermal activity, perhaps indicating the beginnings of rift activity in the Yerrida basin. Environment of deposition of the Juderina stromatolites is indicated as a nearshore, shallow-marine to tidal-flat, sabhka environment (El Tabakh et al., 1999).

3.6.2. Johnson Cairn Formation sedimentary rocks and basalts

The Doolgunna and Maraloou Formations are not present in the vicinity of the DeGrussa deposit. This may be due to the non-deposition of these rocks in this area as suggested by Jeffery (2013).

Diamond drill hole THD001, (cofounded GSWA and SIPA resources drill hole) approximately 40kms to the northeast of DeGrussa within Yerrida Basin sedimentary rocks, provides an opportunity to examine and compare early sedimentation processes of basin rifting in the region and comprises similar stratigraphic units to that within the footwall of DeGrussa. Black shale of the Johnson Cairn Formation in THD001 is interpreted to have been deposited in a deep water setting in an anoxic water environment (Mueller, 2011). The basalt within the Johnson Cairn Formation at DeGrussa can be compared with basalts and volcanic rock found in THD001, likely to represent one of the first phases of volcanic activity related to rifting.

3.6.3. Magazine Member

The Magazine Member carbonate megabreccia may have developed from collapse of a carbonate shelf (i.e. the Bubble Well Member). The megabreccia unit is comparable to other carbonate megabreccia deposits in the world such as those of the Jurassic Tethys ocean of the eastern Alps of Switzerland (Eberli, 1987), the Arabian carbonate platforms in Oman (Watts, 1990), and the present day northern Nicaraguan Rise (Hine et al., 1992). Development of megabreccia in these locations is considered mainly to be the result of bank-margin collapse

triggered by seismic activity related to rifting events, although megabreccia development and slope instability is also likely to be related to sea level falls and low-stands, and the resulting pore water overpressure of confined aquifers beneath the sea floor initiation gravitational instability on slopes (Hine et al., 1992, Spence and Tucker, 1997, Hass, 1999). Most carbonate megabreccia deposits are located adjacent to fault scarps (Eberli, 1987, Watts, 1990, Hine et al., 1992, Spence and Tucker, 1997, Hass, 1999) suggesting that the Magazine member megabreccia is also located proximal to a shelf environment which was destabilised by seismic activity.

Baker (2015) interpreted turbidite sequences in the lower Magazine Member stratigraphy as deposited below storm wave base on a continental shelf or slope, and turbidite layers higher in stratigraphy, intercalated with dolomite clast mega-breccias, as mass-rock fall deposits which represent graben development prior to the onset of volcanism. Intrusive basaltic activity was contemporaneous with turbidity sedimentation evident from quench fragmented tops and bottoms of basalt intrusions (Baker, 2015). The sedimentary rocks were dewatered and lithified when they were intruded by dolerite, indicating that the footwall dolerites were emplaced subsequent to the intrusion of basalt into wet sediment (Baker, 2015).

Similiarities have been suggested between the Magazine Member, host sedimentary rocks and the Karalundi Formation. The position of the Karalundi Formation in stratigraphy as well as the descriptions provided by Gee (1987) and Pirajno et al. (2000) refer to hematite-magnetite jasperlitic rocks, clastic, carbonate, chert and tuffaceous rocks which mark the onset of rifting and volcanism within the Bryah Basin, suggesting that the Magazine Member is a likely an equivalent.

3.6.4. Host Sedimentary Rocks, basalt and dolerite (DeGrussa Formation)

Detrital zircons are present, with the youngest U-Pb age of 2173 Ma (see Chapter 6, Hawke et al. (2015)). This infers sedimentary rocks are derived from Archean basement rocks, the Dalgaringa Formation or equivalent aged rocks, and possibly basalts of the Johnson Cairn Formation.

The contacts between basalt and DeGrussa sedimentary host rocks are peperitic, suggesting intrusion of basalts into unconsolidated sedimentary rocks. Basalts and basaltic breccia is interbedded with the sedimentary rocks. When mineralisation is in contact with basalt breccia it often replaces basalt clasts. This suggests deposition of basalt was concurrent with sedimentary rocks and in some cases predated mineralisation.

Geochronological work presented in Chapter 6 suggests that dolerite postdates mineralisation. However, in drill core it is often difficult to determine the nature of the contacts between rock units (due to shearing and faulting), as well as any different phases of dolerite intrusion. Two interpretations are therefore possible for the timing of dolerite;

1. Dolerites were intruded at the same time as mineralisation, forming a source of heat for the hydrothermal system. Contacts between sedimentary rock and dolerite display characteristic peperite textures suggesting intrusion of mafic rock into unconsolidated wet sedimentary rocks.

2. The dolerites are intruded later than mineralisation and 'split' the DeGrussa and C1 mineral lodes. Geochronology (Ch. 6) supports a- syn to post-mineralisation age of emplacement although the three contrasting geochronological methods are all within error.

3.6.4.1. Association with the Narracoota Formation

It is possible that the mafic rocks at DeGrussa are associated with the Narracoota Formation of Gee (1987). Although initial mapping by Jeffery (2011) described the "Sandfire Formation" in the equivalent position as the Narracoota Formation, the "Sandfire Formation" is now considered to be part of Occhipinti et al. (1997) and Pirajno et al. (2000)'s Narracoota Formation. In the DeGrussa area, the Sandfire Formation comprises sedimentary rocks as well as basalts and intrusive dolerite. Turbiditic sedimentary rocks of the Sandfire Formation are juxtaposed via a faulted contact over the DeGrussa host sedimentary rocks (cross sections in Fig. 3.1 based on Jeffery (2013)).

The estimated thickness of the Sandfire Formation is 1800 metres (Jeffery, 2011). Drilling suggests the contact of the DeGrussa host sedimentary rocks and dolerite sills with the Sandfire

Formation is tectonic. The contact with the overlying "Red Bore Formation" (see Section 3.3.6) is not exposed but is considered tectonic. Sedimentary structures have been obliterated by the strong millimetre scale, penetrative slaty cleavage (Jeffery, 2011).

Jeffery (2011) describes the "Sandfire Formation" in the vicinity of DeGrussa as having two parts:

1. A lower, 800m thick sandstone-dominated unit of thin, planar bedded, well rounded and well-sorted, quartz arenites with a chloritic matrix, siltstone and minor shale with coarser felspathic grits and granule conglomerate lenses, and

2. An overlying, 1000m thick unit of variably sericitic and chloritic shale, containing thin lenticular bedded quartz arenites with less common conglomerate lenses. The conglomerate units contain well rounded quartz grains and granules of vein quartz, chert and sub-angular orange-coloured shale clasts set in a feldspathic sandy matrix.

Jeffery (2011) infers these conglomerates to have an uplifted Archaean provenance, and to be the equivalent of the GSWA mapped Karalundi Formation, south and southeast of the DeGrussa deposit, on the southern side of the Bryah basin, north of the Goodin Fault. However, as previously discussed, the Karalundi Formation may be a lateral equivalent to the DeGrussa host sedimentary rocks (DeGrussa Formation).

The Sandfire Formation is positioned in the same stratigraphic location, and has a similar description to that of the Ravelstone Formation (lithic and quartz wacke, shale and siltstone– see chapter 2), suggesting that these two units may be lateral equivalents. More work is required to clearly distinguish the complicated regional stratigraphy outside of the DeGrussa deposit mine area.

3.7. Summary

The development of the stratigraphy of the DeGrussa deposit (Fig. 3.21) and can be summarised as;

1. Continental rifting led to separation of the Marymia Inlier from the northern Yilgarn.

2. Deposition of Yerrida Group sedimentary rocks in an evaporitic sag basin setting from c. 2174 Ma. There is no deposition of the Finlayson Member sandstone in the DeGrussa area.

3. Stromatolite growth in the Bubble well member, interbedded with evaporite deposits indicate the saline, shallow water environment, in a similar setting to that of the present day

4. Progressive rifting of crustal material and deepening of the rift basin caused the deposition of the Johnson Cairn Formation's turbiditic sandstones, pale-dark grey siltstones, mudstones, and black shales in an anoxic submarine basin. Minor amounts of basalt related to early rifting are found in the Johnson Cairn Formation.

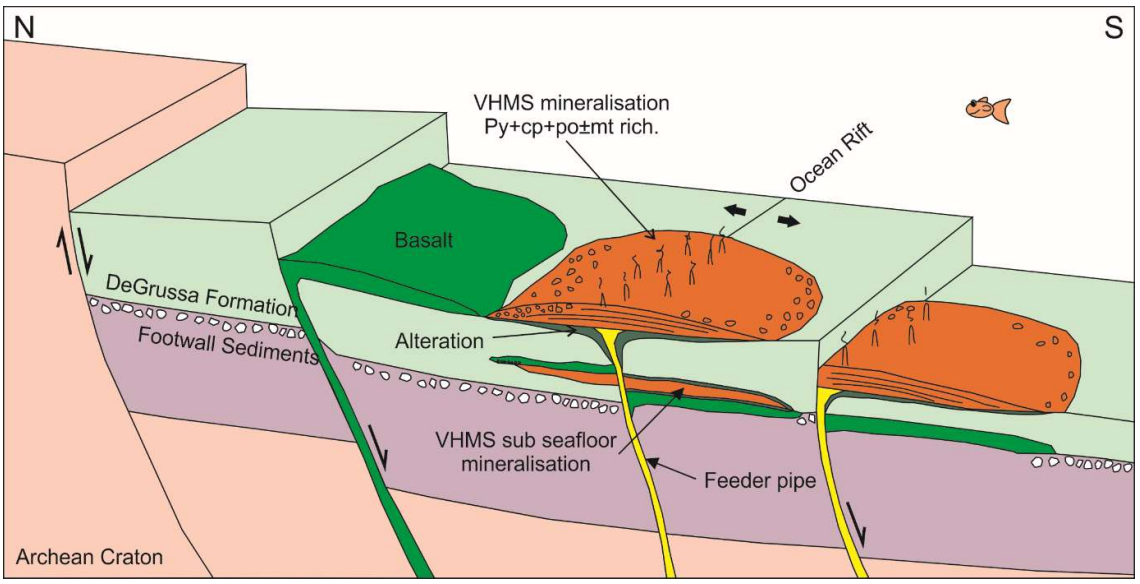

Figure 3. 21. Schematic representation of the DeGrussa host stratigraphy at time of mineralisation

5. The Magazine member (conglomerate (carbonate-dolomite breccia), hematitic, mudstone-rich turbidite rocks, volcanic conglomerate and polymict conglomerate) is deposited during continental rifting and extension along the northern margin of the Yilgarn Craton. The carbonate

megabreccia may have developed as the result of bank-margin collapse of a carbonate shelf triggered by seismic activity related to rifting events. The megabreccia is likely to be proximal to the continental shelf with limestone clasts derived from a shallow water marine setting, likely to have been the Bubble Well Member.

6. The DeGrussa mineralisation was deposited into a deep submarine setting (>1000m), below wave base, possibly in a constrained basin similar to the setting of hydrothermal sites in the northern trough of the Guaymas basin, at the bottom of horst blocks/ fault escarpments. Dolerite and basalts, syn- to post- DeGrussa mineralisation intruded into a sedimented rift setting (i.e. oceanic rift similar to the Red Sea rift or Guaymas Basin as it progresses from a continental to oceanic-rift).

7. Ore lenses were buried by turbidites and basalt flows, with occasional small ore lenses found higher in stratigraphy (e.g. the Red Bore deposit).

8. The Narracoota Formation was emplaced dominantly in western parts of the Bryah Basin, perhaps as a result of rifting progressing from east to west across the Bryah Basin.

9. The Red Bore Formation is tectonically emplaced in the DeGrussa area. It is the result of forearc sedimentation in the Padbury Basin.

10. Southwest to northeast directed deformation related to closure of the late Paleoproterozoic basins caused faulting and folding across the region. The DeGrussa deposit was folded and transected by three major SE-NW faults – the Shiraz, Merlot and Cabernet faults - dividing the deposit into three lenses.

Chapter 4. Deposit Geology: Mineralisation and Alteration

Micro-scale sulfide textures

4.1. Introduction

Ore minerals in the DeGrussa deposit are pyrite, pyrrhotite, chalcopyrite, arsenopyrite, sphalerite, marcasite and magnetite, with lesser galena and molybdenite. The ore deposit is fine-grained and cycles between layers dominated by massive chalcopyrite or pyrite with lesser pyrrhotite and sphalerite interbedded in chalcopyrite-dominated sections. Magnetite occurs predominately with pyrite lenses.

Supergene chalcocite forms one of the main ore minerals of the DeGrussa and Conductor 1 lenses to a depth of approximately 120m depth, and deeper along faults.. Oxide minerals consist of malachite, azurite, chrysocolla, atacamite, native copper and cuprite. Bornite and covelite are visible in thin section as rims around chalcopyrite in parts of the ore where partial oxidisation has occurred.

Only one internal company report on the mineralogy has been completed (Apr, 2010). More recently a masters thesis by (Condon, 2015) was completed on the textures and geometallurgy of the DeGrussa and Conductor 1 mineralisation.

4.1.1. Aims

The aims of this chapter are;

1. Describe the morphology of the ore lenses,
2. Describe the metals and their associations
2. Describe gangue minerals related to mineralisation
3. Identify any zonation throughout the deposit
4. Describe the alteration associated with mineralisation, with particular emphasis on the chlorite schist and talc-carbonate rock.
5. Suggest modes of transport and emplacement for the DeGrussa mineralisation.

The information presented in this chapter is the result of drill core logging, underground and thin section observations between 2009 and 2014. Drill core assays through ore horizons were provided by Sandfire Resources NL (Appendix 4.1) and allowed zonation of metals to be understood throughout the ore lode and surrounding host rocks. Underground drill holes believed to intersect feeder zones (Appendix 4.2) were drilled in 2014. Supporting drill hole graphic logs by the author are in Appendix 4.3 and core photos in Appendix 4.4.

4.2. Massive sulfide: Ore lens characteristics

The DeGrussa deposit has four ore lenses. Each of these lenses is elongated in shape with abrupt, sheared contacts between sulfide and surrounding host rocks. The orientation of the ore lenses (southeast to northwest) is consistent with the regional D4 deformation. Surrounding rocks generally comprise chlorite schist (see alteration section). The DeGrussa ore lens is vertical to sub-vertically oriented, up to ~40m thick, and truncated at the base by the Shiraz Fault (See Fig 3.14). The Conductor 1 (C1) ore lens is located to the north of the DeGrussa lens, is lower in stratigraphy, and separated from DeGrussa by a thick dolerite sill. The C1 lens is thinner than the DeGrussa lens and broken into several disconnected and lenticular pods of similar composition and texture (Fig. 4.1).

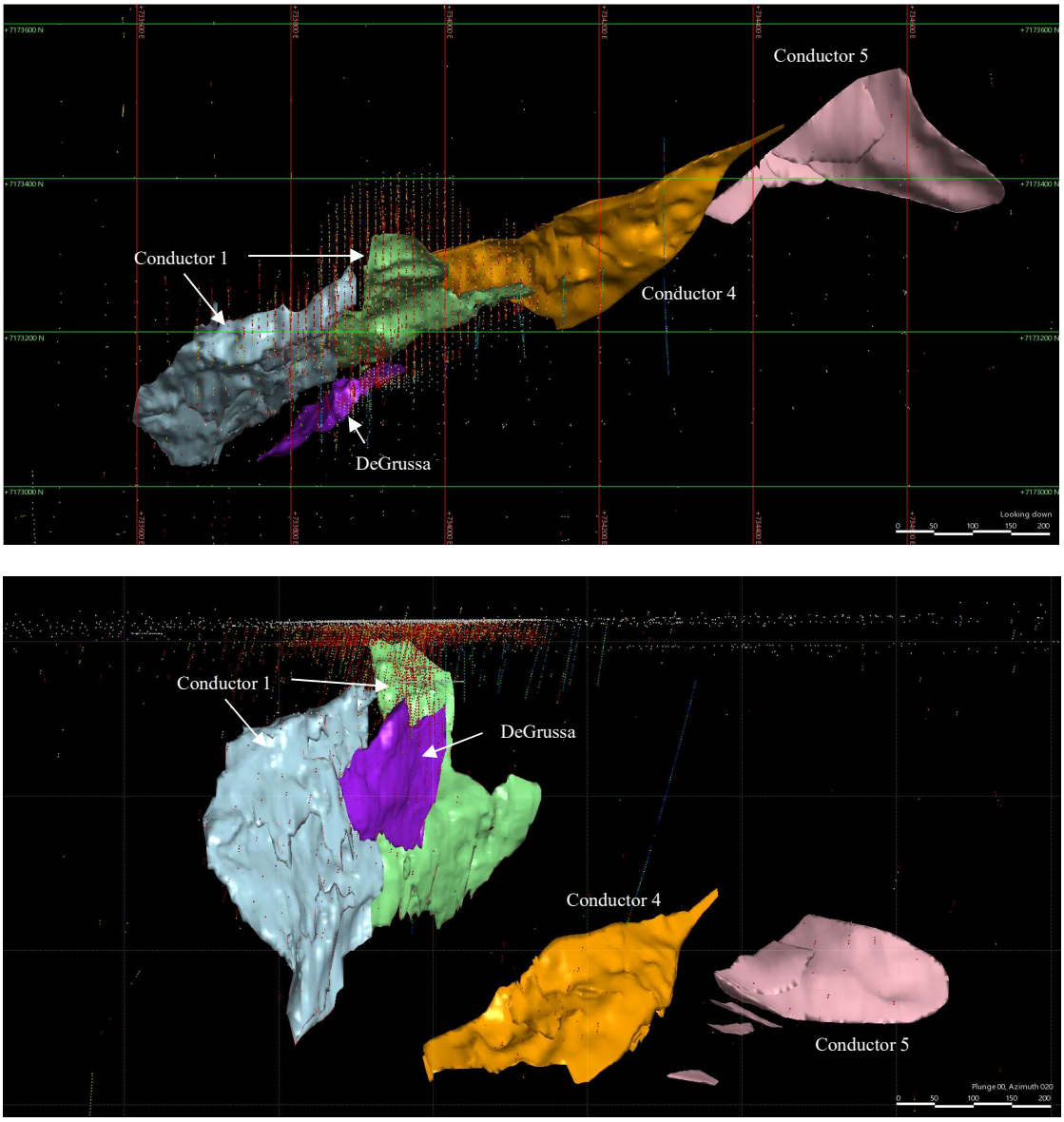

Figure 4.1. 3D representation of the DeGrussa ore lenses produced from logged geology where visible sulfide is >50% and modelled in Surpac using 5-10m spaced sectional strings (images courtesy of Sandfire Resources NL). **A.** Plan view, **B.** towards the north-east 020.

This section discusses the ore minerals and their relationships to each other, common micro-scale features, macro-scale features indicating both primary seafloor deposition and sub seafloor replacement, as well as deformation textures.

4.2.1. Primary ore metals

Pyrite is the dominant ore mineral. It is fine grained, but takes on a range of morphologies, including small globular aggregates, euhedral and fragmented crystals. Typical pyrite morphology is displayed in Figure 4.2. In thin section (Fig. 4.2, 4.3) it typically displays itself in bands of fine grained sulfides intermixed with chalcopyrite, pyrrhotite and sphalerite. It can form colloform rings enclosing minor fine chalcopyrite, rare magnetite and micas. 'Spongy pyrite' as described by Condon (2015) contains inclusions of sphalerite, galena, magnetite, pyrrhotite, clausthalite or cobaltite (McKnight, 2009). Pyrite also occurs as euhedral crystals of varying sizes within sedimentary banding and as clusters and solitary cubes within basalts and dolerites. These euhedral pyrites are a metamorphic feature within the sulfide lenses, commonly displaying localised fragmentation within more massive and consistent pyrite units.. Pyrite dominant units can be banded or brecciated. Banding is likely to be the result of original deposition textures although some units are likely to have taken up more strain during deformation resulting in microscopic fragmental textures of fine grained pyrite surrounded by more malleable chalcopyrite or gangue minerals,

Within basalts and dolerites, larger, zoned metamorphic pyrites are formed. Pyrite is also commonly found in veins (Fig. 4.3), associated with carbonate and quartz. Arsenopyrite is often present intergrown with pyrite and chalcopyrite. Marcasite is rare but forms globular clusters within the ore deposit (Fig. 4.4), occasionally forming on the margins of the ore body within massive pyrite units.

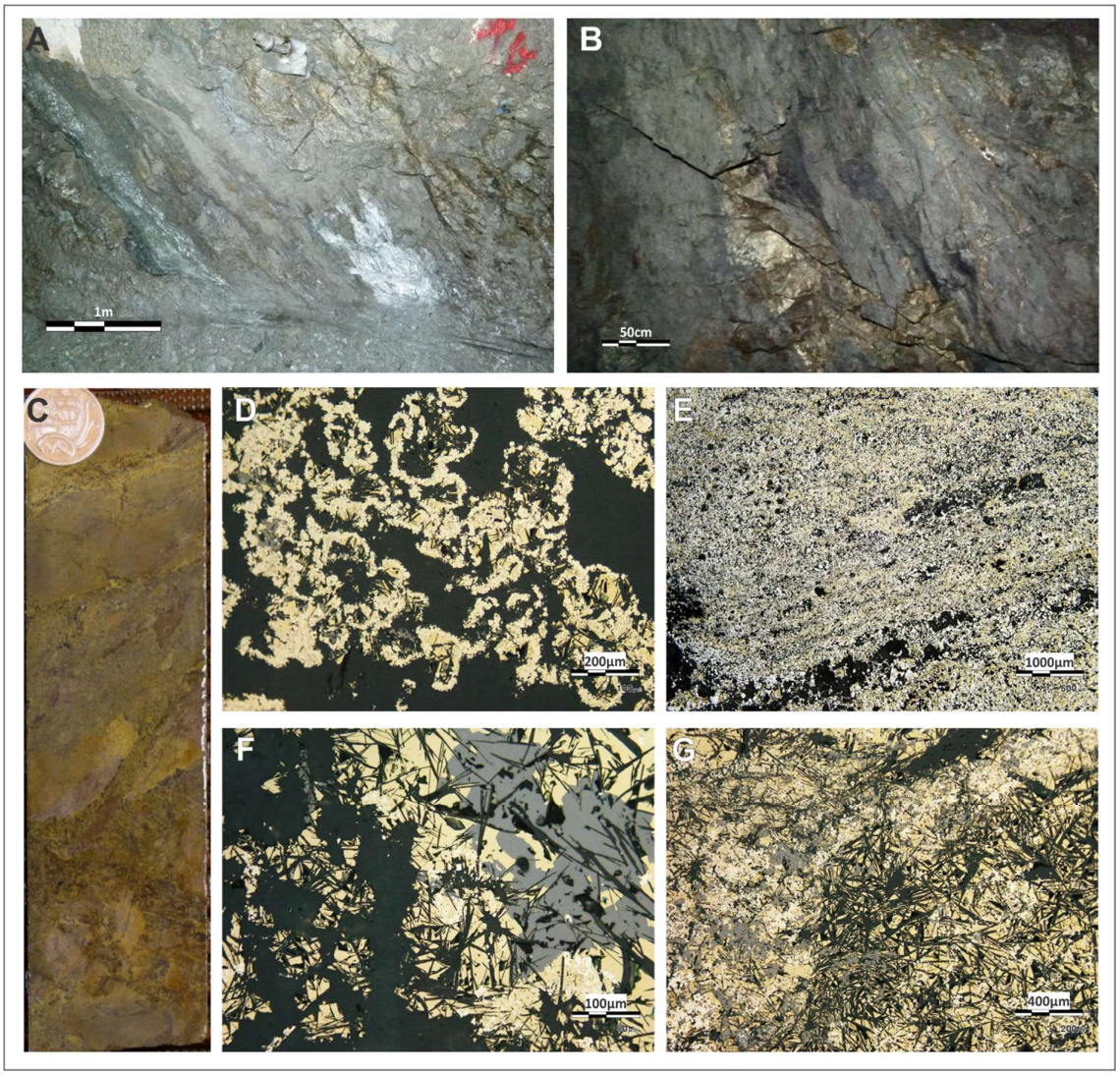

Figure 4.2. Macro and micro-scale pyrite textures. **A.** and **B.** Banded sulfide ore of Conductor 1 – alternating layers of massive pyrite, chalcopyrite and pyrrhotite. **C.** Pyrite dominant sulfide texture in DGDD219, 540.12-540.90m. **D.** Framboidal pyrite with centres of needles (DGRC104, 183-184m). **E.** Fine grained, banded massive sulfide (DGRC104, 120-127m). **F.** Coarse chalcopyrite, sphalerite, rare pyrite. Black crystals of minnesotaite/stilpnomelane in sulfides and forming veins (DGRC105, 138-140m). **G.** Low magnification showing gross characteristics of sulfide (+magnetite) mineralization. Left side of photo is intricately mixed, extremely fine chalcopyrite and pyrite enclosing patches of grey magnetite. Right hand is mixed chalcopyrite > pyrite incorporating random flakes/fibres of minnesotaite and rarer grey magnetite (DGRC104, 183-184m).

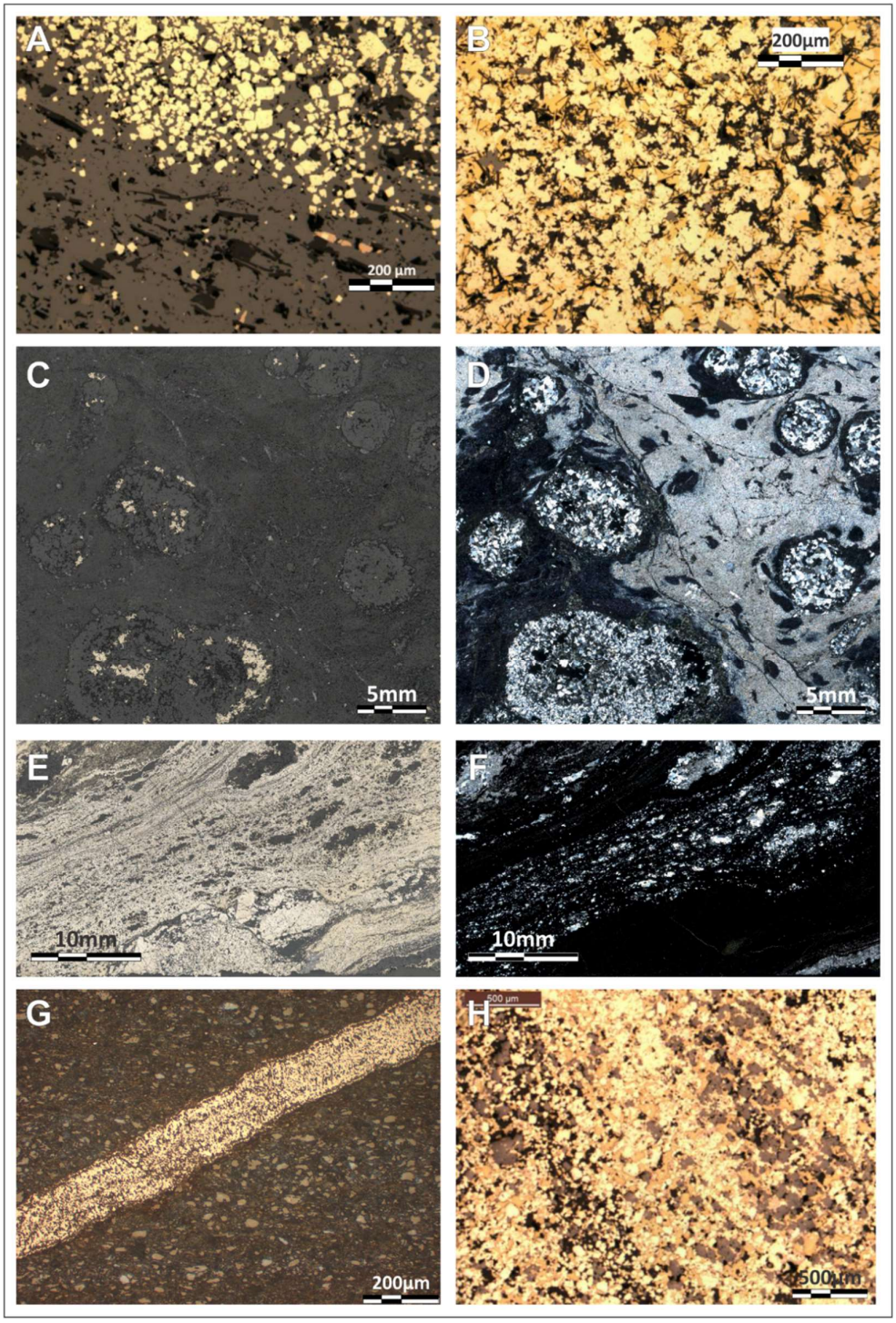

Figure 4.3. Pyrite textures. **A.** Massive blebby pyrite (MBP, see section4.2.2) with minor Semi-massive foliated pyrite (SMWS, section 4.2.2) showing euhedral pyrite to the top and sphalerite (brown) to the lower half of the image. Patches of quartz and stilpnomelane are present, with siderite veins crosscutting (DGJC013: DGDD014, 166.44-166.5m, Condon (2015)), **B.** Subhedral pyrite grains, with chalcopyrite remobilised around pyrite grains, and gangue of minnesotaite and chlorite (DGJC015: DGDD014, 199.5-199.65m; Condon (2015)), **C.** Quartz ± chalcopyrite framboids in reflected light. **D.** polarised light (DGJC063: DGDD080, 367.05-367.1m), **E.** Banded and brecciated euhedral 'spongy' pyrite in reflected light and **F.** transmitted light. Sulfides have a matrix of chlorite, minnesotaite and quartz. Boudinaged texture indicates recrystallisation as a result of extension (DGJC003: DGDD010, 317.2-317.25m (Condon, 2015)), **G.** Pyrite vein crosscutting sedimentary host rocks (DGMH018: DGDD173, 97.41-97.57m), **H.** Recrystallised sulfide ore consisting of inclusion-rich subhedral to euhedral spongy pyrite and magnetite with interstitial chalcopyrite and pyrrhotite (DGJC047: DGDD051, 355.6-355.75m).

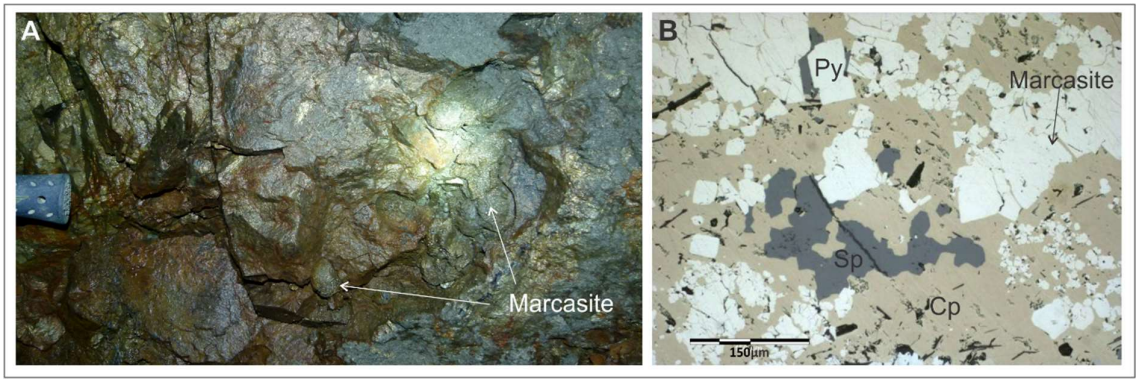

Figure 4.4. A. Marcasite nodules in Conductor 1 underground exposure. B. Thin section of sulfide ore showing intergrown nature of chalcopyrite (cream), sphalerite (grey), pyrite (white, euhedral crystals) and marcasite (white).

Chalcopyrite is the dominant copper bearing mineral within the DeGrussa ore lens. It forms in massive, fine-grained bands (Fig. 4.5), alternating with pyrite and pyrrhotite-rich bands. When ore is brecciated, chalcopyrite is more mobile than pyrite. Chalcopyrite rims pyrite in fractures and veins and has a close association with calcite, perhaps indicating that chalcopyrite has undergone remobilisation with the carbonate during subsequent deformation events. Furthermore, the ease of mobility of chalcopyrite during deformation is exemplified in the DeGrussa deposit by its presence in tension gashes (Fig 4.5). Digenite commonly replaces chalcopyrite along grain boundaries due to low grade supergene oxidation (Condon, 2015).

In fault zones, there may be pulverization of ore and gangue minerals, and the development of "ball textures," forming from fragments of foliated gangue (Craig and Vaughan, 1994). Framboids of chalcopyrite-quartz (see Fig. 4.3C and D) is the result of strong deformation to the ore minerals and gangue. Injection of more ductile ore minerals into fractures and cleavages in more brittle ore minerals and gangue minerals is common.

Sphalerite dominated horizons occasionally occur throughout the sulfide ore. Where present, it is often in close association with chalcopyrite (Fig. 4.6). Although is found in smaller quantity than pyrite, chalcopyrite and pyrrhotite, it is commonly localised in patches and more dominant in thicker parts of the ore deposit. In thin section, sphalerite is intricately intergrown with the other sulfides (Fig 4.2, 4.3, 4.4). Pyrrhotite is preserved as massive bands of fine-grained sulfides between chalcopyrite and pyrite-rich horizons. In thin section, crystals are intergrown with other

sulfides, forms as small inclusions within chalcopyrite, or partially replaces pyrite in places. Core samples taken from the Conductor 5 ore body, show bands of pyrrhotite and pyrite, which in hand sample appears to be primary sedimentary deposition of pyrrhotite, with larger metamorphic pyrite in a fine grained chlorite-clay matrix (Fig. 4.7).

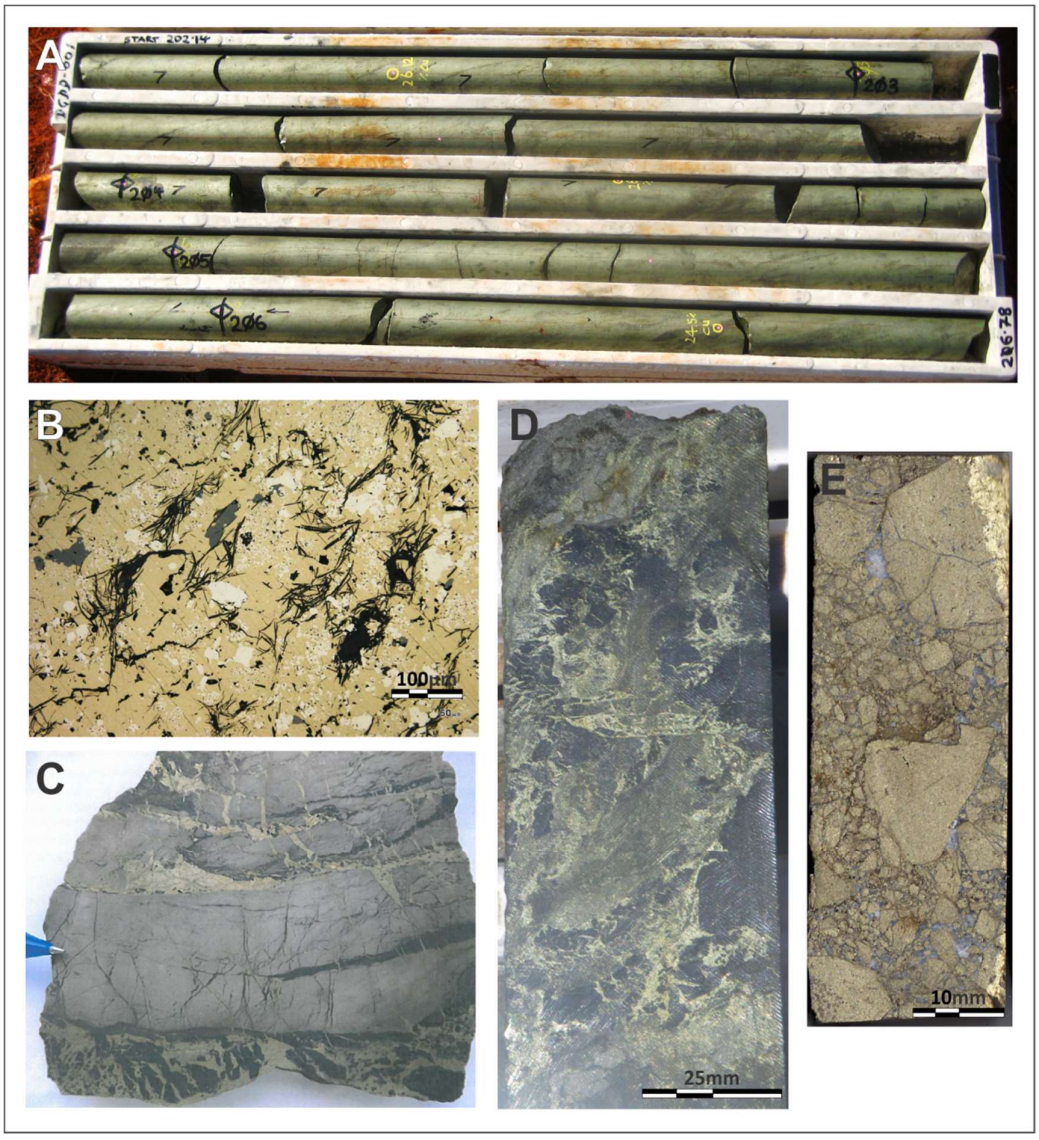

Figure 4.5. A. Massive chalcopyrite in the DeGrussa ore lens of DGDD001 (202.14-206.78m). **B.** Thin section, reflected light of chalcopyrite dominant massive sulfide ore with scattered pyrite and flakes of stilpnomelane (DGRC105, 138-140m). **C.** Cut slab of interbedded pyrite-rich ore, chalcopyrite-rich ore and mudstone from Conductor 1. Chalcopyrite and chlorite remobilised into tension gashes during deformation (photo: Anonymous (2014)). **D.** Blebs and stringers of pyrite and chalcopyrite in chlorite-altered host rock. Chalcopyrite is mobilised as veins and stringers throughout the host rock in comparison to the more massive blebs of pyrite. **E.** Jigsaw-fit, chalcopyrite breccia with infilling calcite matrix and patchy limonite alteration.

Figure 4.6. DGDD064, 175-192m, displaying a sphalerite-chalcopyrite rich interval along the upper contact of the Conductor 1 ore lens (Cu 7.3%, Zn 1.7% over 45m).

Inclusions of pyrrhotite, sphalerite, galena and sulfosalts in chalcopyrite, as well as galena and sulfosalts in pyrite occur throughout the ore deposit and are interpreted by Condon (2015) as paragenetic textural features. Additionally, crosscutting veinlets of chalcopyrite ± sphalerite occur through all sulfide and non-sulfide mineralogy, and partial replacement of pyrite by chalcopyrite and pyrrhotite, and of chalcopyrite by digenite occurs (Condon, 2015).

Magnetite has a close affiliation with pyrite and pyrrhotite. In drill hole DGDD141, magnetite correlates with pyrite units through the DeGrussa lode. In thin section, magnetite occurs as cubic crystals interlocking with other sulfide grains as well as larger needles with a texture resembling spinifex texture (Fig. 4.8). It can be either distributed evenly through the massive sulfide, but occasionally occurs as large clusters. It is associated with trace minerals of cobaltite, chalcopyrite and pyrite.

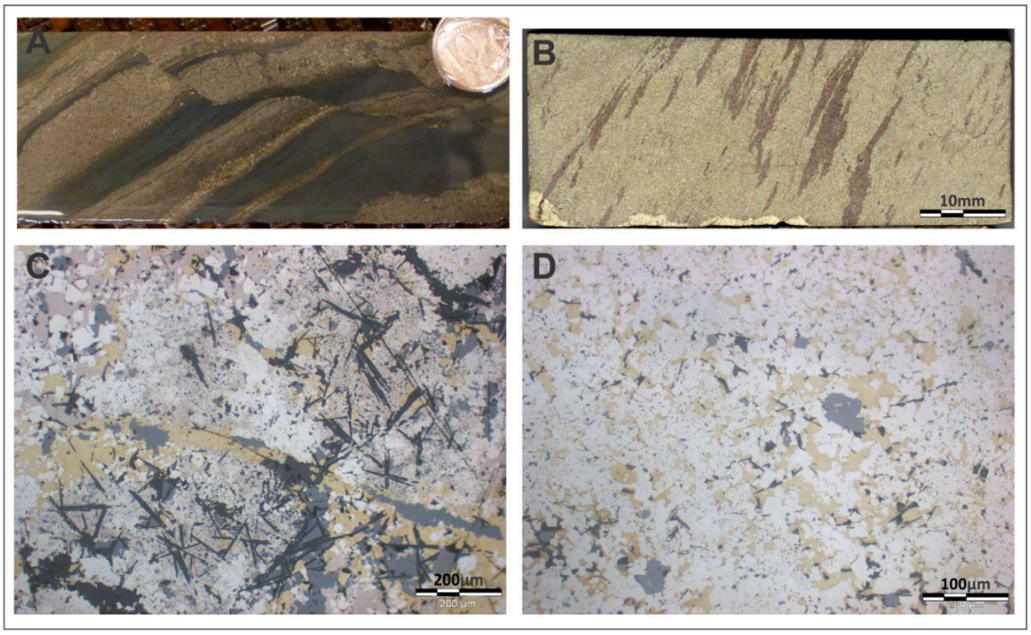

Figure 4.7 A. Banded pyrite and pyrrhotite in sedimentary host rocks from the Conductor 5 ore (DGDD219, 534.0-534.4m). **B.** Lenses of pyrrhotite define foliation in massive banded chalcopyrite (DGDD014, 320.9m). **C.** Light pink pyrrhotite intergrown with pyrite, chalcopyrite and stilpnomelane crystals from the Conductor 5 ore lode (DGMH091: DGDD219, 538.87-538.93m). **D.** Massive fine grained pyrite with chalcopyrite and minor stilpnomelane (DGMH090: DGDD047, 240.28-240.39m).

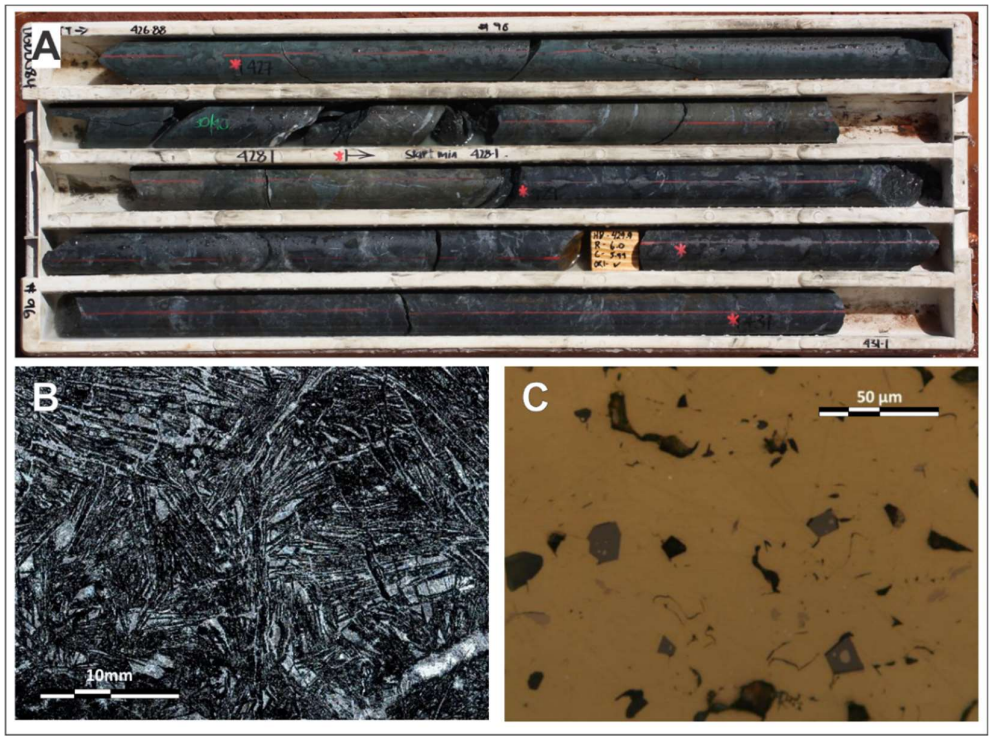

Figure 4.8. A. Massive magnetite ore in NQ core from the C1 ore lens (DGDD084, 426.88-431.1m). B. Thin section transmitted light of spinifex textured magnetite and stilpnomelane interpreted by Condon (2015) to replace magnesian-rich basalt (DGDD011, 333.55 to 333.65 m). C. Massive chalcopyrite with inclusions of euhedral magnetite crystals (DGDD012, 282.80 to 282.90 m)

Molybdenite typically occurs along the base, sometimes at the top, of massive sulfide ore lodes. Coarse-grained stringers of molybdenite are associated with chalcopyrite in strongly sheared and pervasively altered talc-chlorite schist at the base of the DeGrussa lode. Fine-grained molybdenite is distributed within fine grained sulfide bands, and associated and intergrown with pyrite, chalcopyrite and galena. Patchy molybdenite mineralisation is associated with chalcopyrite in basaltic meta-breccia proximal to the ore lodes (Fig. 4.9).

Where molybdenite is present in chlorite or talc-chlorite schist, it is associated with chalcopyrite-dominant, sulfide-sericite clusters. Feathery flakes of molybdenite (~20 μm) in size, are concentrated in small bundles and dense aggregates, intergrown with subhedral titanite crystals, near margins of the larger chalcopyrite aggregates (Fig. 4.9). Rare euhedral to subhedral pyrite crystals tend to occur within the margins of the chalcopyrite aggregates (Mason, 2011).

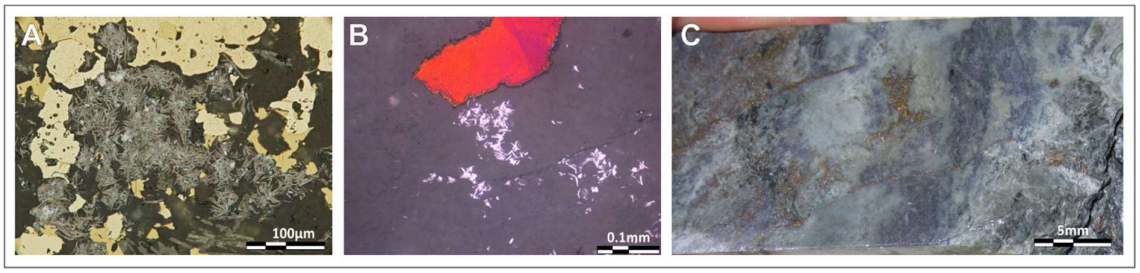

Figure 4.9. A. Thin section, reflected light showing small, grey, molybdenite flakes which form dense bundles and aggregates intergrown with sericite (dark grey background) near pyrite (cream) and chalcopyrite (yellow) (DGMH036: DGDD125, 569.45-569.55m)(PHOTO: Mason (2011)) . **B.** Thin section, reflected light, of small bundles of molybdenite from a sample of chlorite-sericite altered basalt (red is a tarnished sulfide). Molybdenite in this sample is often intergrown with titanate (DGMH002: DGDD141, 190.35m). **C.** Coarse-grained molybdenite within a talc-chlorite host with disseminated pyrite and chalcopyrite (DGDD141, 181.1-181.25m).

Galena is fine-grained and localised in thin horizons near the base of the ore body. In DGDD202, which intersects the margins of the Conductor 4 ore body, galena occurs in a 5cm thick horizon with pyrite and lesser chalcopyrite. This is the only occurrence of galena within this mineralised horizon. Galena is also found in late quartz-carbonate extensional veins, dated in chapter 6 at 1820Ma.

Electrum is the most important gold and silver-bearing phase (Fig 4.10), and is predominately associated with pyrite, occurring in cracks and along grain boundaries. Hessite (Ag_2Te) is an important host to silver and is intimately associated with composite Bi-tellurides and native Bi grains (Condon, 2015).

Minor amounts of covelite, bornite and chalcocite are found on the rims of grains within the shallower depths (<200m from surface) of the DeGrussa and Conductor 1 ore lodes or at depth where ore is proximal to weathered faults. The importance of bornite as a copper bearing mineral in the DeGrussa district may is evidenced with the recent discovery of the Monty VHMS deposit which hosts significant quantities (Anonymous, 2016), as well as the bornite-rich Thaduna copper deposit to the northeast. Supergene chalcocite is the dominant sulfide within the upper 50m of the DeGrussa deposit Tellurides were not viewed by the author, but were identified by McKnight (2010) and Condon (2015) throughout the ore deposit, as telluro-bismuth, and unnamed Au-Ag and Pb-Cu-Se tellurides (Fig. 4.10).

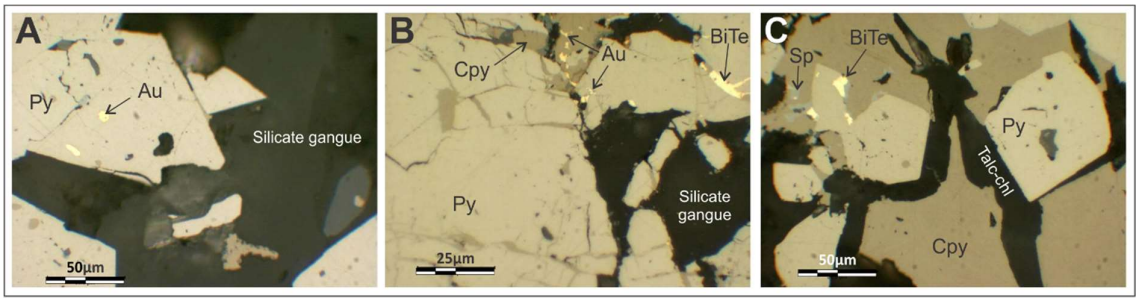

Figure 4.10. Au occurrences (electrum) and BiTe occurrence. **A.** and **B.** Reflected light images showing two different occurrences of gold. C. Telluro-bismuth is of minor but widespread occurrence throughout the ore lenses. Dark flakes are talc ((McKnight, 2011)

Minnesotaite, an iron-talc mineral, is present as needles between the sulfide crystals (Fig. 4.11). In other deposits, minnesotaite is usually associated with quartz, siderite, greenalite and magnetite in iron formations, interpreted as either an alteration mineral associated with sulfide-bearing veins or with low grade metamorphic banded iron formations (Gruner, 1944). Although minnesotaite is the dominant gangue mineral, stilpnomelane is widespread within and in proximity to the ore lenses. Stilpnomelane is a common mineral associated with banded iron formations, blueschist and greenschist facies of metamorphic rocks, metamorphosed massive sulfide deposits(Gruner, 1944, Miyano and Klein, 1989), and is typically found throughout dolerite rocks as indicated in QXRD (Appendix 3.5). Siderite, an iron-rich carbonate typical of hydrothermal deposits, is also a common constituent of the gangue. Quartz and calcite occur as vugs and veins, with calcite most closely associated with chalcopyrite.

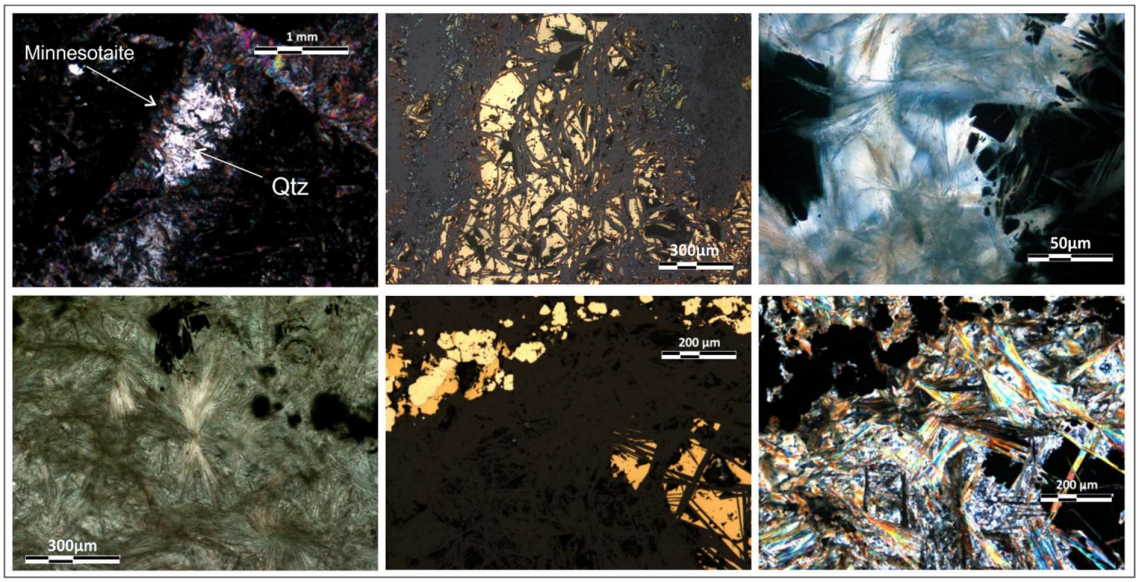

Figure 4.11. **A.** Minnesotaite and quartz vein crosscutting magnetite-chalcopyrite rich ore (DGJC007: DGDD011, 333.55 to 333.65 m, (Condon, 2015)). **B.** Stilpnomelane wrapping around pyrite (DGJC033, Photo: Condon (2015)). **C.** Detail of minnesotaite vein in polarised light (DGRC105, 138-140M: Photo (Pontifex, 2009)). **D.** Intergrowth of stilpnomelane and minnesotaite in transmitted light (DGDD035, 642.5m. Photo: McKnight (2009). **E.** Chalcopyrite and pyrite with interstitial stilpnomelane and siderite in reflected light and **F.** transmitted crossed polars (DGJC049: DGDD053, 401.35 to 401.50 m (Condon, 2015))

4.2.2. Major Ore Textures

Condon (2015) distinguished 23 different ore types defined by the total amount of sulfide in the rock, the ore textures, and the ore minerals. Her classification structure is described in Table 4.1. The four ore types by textural group (Level 2) of Table 4.1 are described in detail below (Condon, 2015):

Table 4.1. Ore Type Classification Structure (Condon, 2015)

Level 1: Sulfide %	Level 2: Texture		Level 3: Dominant Mineral(s)	Ore Type	Code
25-50% sulfide (semi-massive 'SM' code prefix)	Massive		Pyrite	Massive Pyrite	MASP
			Chalcopyrite	Massive chalcopyrite	MASC
			Pyrrhotite	Massive pyrrhotite	MASPO
			Magnetite	Massive magnetite	MASM
	Clastic	Blebby/Spotty	Chalcopyrite	Blebby/spotty chalcopyrite-dominant	(S)MBC
			Chalcopyrite>Pyrrhotite	Blebby/Spotty Chalcopyrite-Dominant with Pyrrhotite	(S)BCPO
			Pyrite	Blebby/Spotty Pyrite-Dominant	(S)MBP
			Chalcopyrite>Sphalerite	Blebby/Spotty Chalcopyrite-Dominant with Sphalerite	(S)MBCS
			Magnetite	Blebby/Spotty Magnetite-Dominant	(S)MBM
		Fragmental	Chalcopyrite	Fragmental Chalcopyrite-Dominant	(S)MFC
			Pyrite	Fragmental Pyrite-Dominant	(S)MFP
50-100% sulfide (Massive, 'M' code prefix)	Banded	Laminated	Chalcopyrite	Laminated Chalcopyrite-Dominant	MLC
			Chalcopyrite>pyrrhotite	Laminated Chalcopyrite-Dominant with Pyrrhotite	MLCPO
			Pyrite	Laminated Pyrite-Dominant	MLP
		Foliated	Chalcopyrite	Foliated Chalcopyrite-Dominant	(S)MWC
			Pyrite	Foliated Pyrite-Dominant	(S)MWP
			Sphalerite	Foliated Sphalerite-Dominant	(S)MWS
			Chalcopyrite + Pyrrhotite	Foliated Chalcopyrite and Pyrrhotite	(S)MWCPO
		Sheared	Chalcopyrite>Pyrrhotite	Sheared Chalcopyrite-Dominant with Pyrrhotite	(S)MSCPO
0-25% sulfide (Barren to minor)	REMNANT (Host)		Talc-Carbonate >> Sulfides	Talc-Carbonate-Altered Host with Sulfides	TCSE
			Talc-Carbonate	Talc-Carbonate-Altered Host	TCE
			Chlorite >> Sulfides	Chlorite-Altered Host with Sulfides	CSZ
			Chlorite	Chlorite-Altered Host	CAZ

1. *Massive: MASP, MASC, MASPO and MASM*

Massive textured ore types are texturally featureless rocks made up entirely of only one mineral (either Massive Pyrite 'MASP', Massive Chalcopyrite 'MASC', Massive Pyrrhotite 'MASPO', or Massive Magnetite 'MASM'), although sometimes possible clastic or sheared textures are discernible.

2. *Clastic: (S)MBC, (S)MBCPO, (S)MBP, (S)MBCS, (S)MBM, (S)MFC and (S)MFP*

Clastic textured ore types comprise two subgroups:

1. *Blebby/spotty:* Comprises Chalcopyrite-Dominant '(S)MBC', Chalcopyrite-Dominant with Pyrrhotite '(S)MBCPO', Pyrite-Dominant '(S)MBP', Chalcopyrite-Dominant with

Sphalerite '(S)MBCS' and Magnetite-Dominant '(S)MBM' ore types. This ore type occurs as both irregular and regular shaped aggregates within a matrix of either sulfide or host rock minerals. Regular-shaped aggregates lend to a 'spotty' texture.

2. *Fragmental:* Comprises Chalcopyrite-Dominant '(S)MFC' and Pyrite-Dominant '(S)MFP' ore types, defined by angular to rounded, monomict or polymict massive sulfide clasts in a matrix of either sedimentary rock or fine-grained sulfides. Fragmental textures are often difficult to distinguish as they sometimes overprint blebby textures.

3. *Banded: MLC, MLCPO, MLP, (S)MWC, (S)MWP, (S)MWS, (S)MWCPO, (S)MSCPO*

Banded textured are split into three ore types:

1. *Laminated:* Comprises Chalcopyrite-Dominant '(S)MLC', Chalcopyrite-Dominant with Pyrrhotite '(S)MLCPO' and Pyrite-Dominant '(S)MLP' ore types. This texture is defined by primary sulfide laminations or replacement bands of bedded siltstone.
2. *Foliated:* Comprises Chalcopyrite-Dominant '(S)MWC', Pyrite-Dominant '(S)MWP', Sphalerite-Dominant '(S)MWS' and Chalcopyrite and Pyrrhotite '(S)MWCPO'.
3. *Sheared:* Comprises Chalcopyrite-Dominant with Pyrrhotite, '(S)MSCPO' ore type. Both foliated and sheared groups represent deformed ore, where one more of the minerals form either a gentle or strong rock fabric, respectively.

Banded textured rocks require close inspection, as commonly laminated ore types can be difficult to distinguish from foliated and sheared ore types. Deformation of the DeGrussa ore has resulted in remobilisation of chalcopyrite across the deposit, and thus it is readily identified in foliated or sheared ore, but is more difficult to identify when replacing primary host sedimentary rock laminations (i.e. as in MLC). Pyrrhotite, is commonly associated with remobilised chalcopyrite, and thus, is difficult to identify as MLCPO.

4. *Remnant (Host): TC(S)E, CSZ and CAZ*

Remnant, or host rock textured ore types commonly have blebs and disseminations of pyrite and chalcopyrite and are of two main types:

1. *Talc-rich rocks ('Talc – chlorite – carbonate ± actinolite schist' of section 4.3.2):* Talc-Carbonate-Altered Host with Sulfides 'TCSE' (5-25% sulfide) and Talc-Carbonate-Altered Host 'TCE' (<5% sulfide)
2. *Chlorite-rich rocks (Chlorite (+sericite+sulfide) schist of section 4.3.1)*: Chlorite-Altered Host with Sulfides 'CSZ' (5-25% sulfide) and Chlorite-Altered Host 'CAZ (5-25% sulfide).

These ore types also form part of the alteration around the DeGrussa ore lenses. Characteristics of these two ore types are described in section 4.3.

4.2.3. Macro-scale ore features

The margins of the C1 ore lens have been clearly exposed in the underground workings, with sharp contacts existing between the massive sulfide and surrounding chlorite schist and sedimentary rocks. Figure 4.12 shows the variation where contacts are often convolute, saw-toothed and generally irregular and typically surrounded by chlorite schist, which displays sheared foliation and may or may not contain disseminated sulfides. The chlorite schist has shear contacts with talc-carbonate schist or host turbiditic sedimentary rocks.

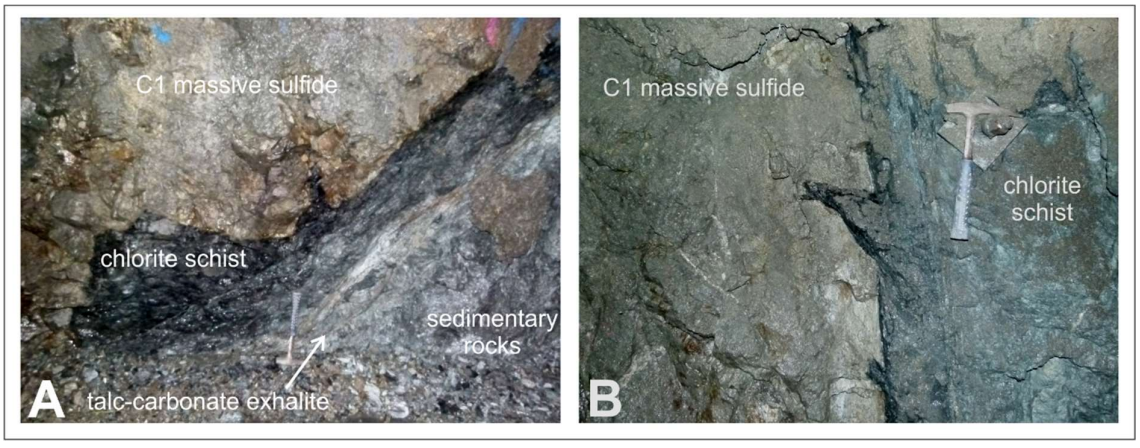

Figure 4.12. Underground exposure of the margins of the Conductor 1 ore lens illustrating **A**. convolute margins between the massive sulfide and chlorite, and an irregular but sharp, sheared contact between the chlorite schist, quartz-sericite-chlorite-carbonate schist and host sedimentary rocks. **B.** Saw-toothed margins with no talc-carbonate schist. Sulfides are dominantly chalcopyrite with lesser pyrite. Image B faces west through the deposit. Disseminated sulfides occur throughout the adjacent schists and host sedimentary rocks proximal to the ore contact.

The base of the DeGrussa ore lens, (Fig. 4.13), consists of disseminated blebs of chalcopyrite dominant sulfides in a sheared talc-carbonate. This is elongate in form and wraps around the lower contact of the DeGrussa ore lens. Upper contacts of the ore lenses are varied. In places they are similar to the contacts discussed above. In other places, angular sulfide (pyrite-chalcopyrite) breccia is present. Macro-scale features in both core and underground exposure are important for the type of emplacement of the ore lenses. Both seafloor and sub seafloor textures are evident.

Along the hanging wall contact of the C1 ore lens is a unit comprising angular fragments of sulfide (pyrite-chalcopyrite) within a matrix of chlorite-altered sedimentary rocks (Fig. 4.14) interpreted to be derived from the main sulfide orebody as sea floor breccia.

Textures formed in fine-grained massive chalcopyrite ore include banding, whispy secondary veining crosscutting other sulfides, disseminations in chlorite and talc-carbonate schist, and shear foliations. Shear textures are difficult to identify as they are very similar to massive and banded textures (Condon, 2015). The amount of shear and brecciation within the deposit depends on the amount of deformation and the mineral composition of the ore (e.g. pyrite in a pyrite only ore will fragment more than pyrite in a pyrite-pyrrhotite-chalcopyrite ore as the softer pyrrhotite and chalcopyrite in the later ore type will take up the strain (Fig. 4.14)). Minor brecciation grades into complex cataclasis with an increasing degree of fragmentation and disorientation, eventually involving both ore and gangue minerals, termed 'durchbewegung' texture (Craig and Vaughan, 1994) as seen in

Figure 4.13. Stringer zone below DeGrussa from DGDD001 (155.44-170.3m). Chalcopyrite-rich sulfide stringers dominate through a talc-clay altered section within the supergene zone.

hand sample in Figure 5.14D. Chalcopyrite is present in fractures that radiate from the fragmental pyrite clasts in the example from figure 5.14B. Chalcopyrite may have been remobilised into fractures as a result of later deformation and metamorphism.

Fragmental textures related to deformation are seen in pyrite due to pyrites more brittle nature under strain (Fig. 4.14). Recrystallisation of pyrite, due to metamorphic processes allows euhedral pyrite to form, often rimmed by sphalerite, chalcopyrite or other sulfide minerals, exsolved from the crystal structure during deformation.

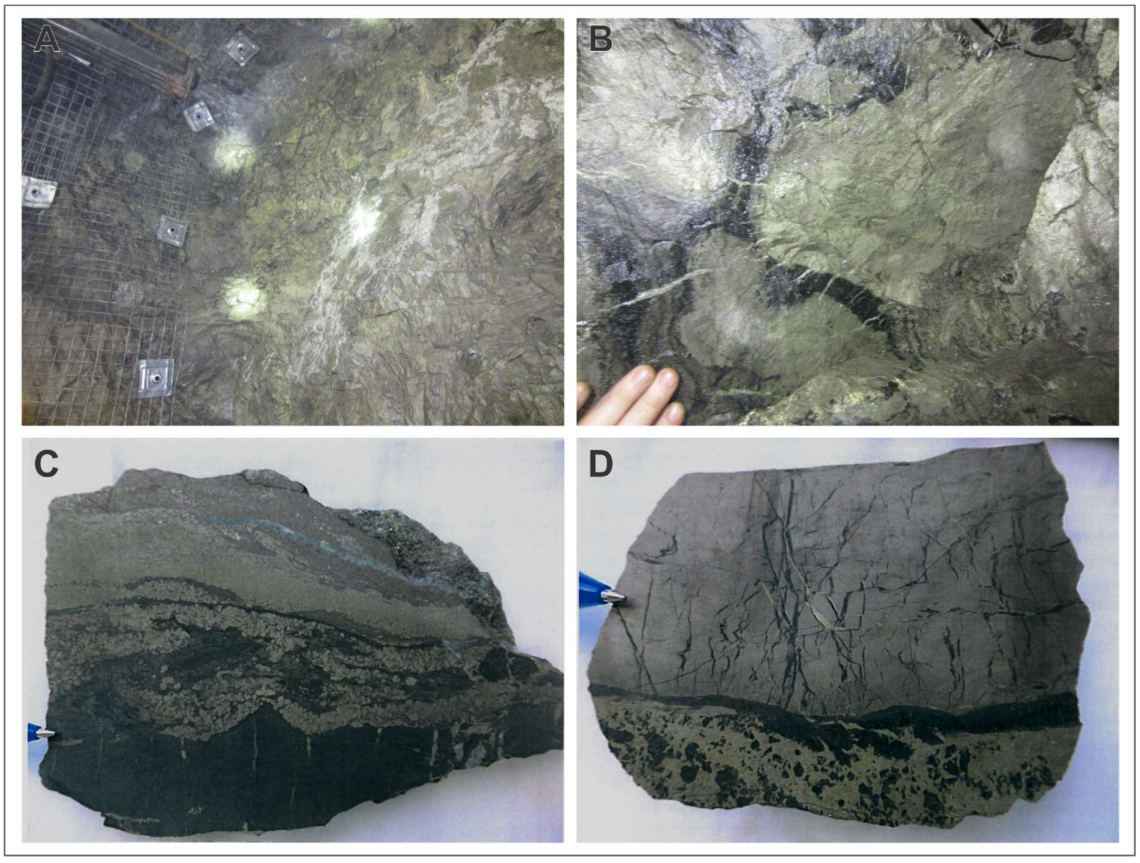

Figure 4.14. **A**. Massive sulfide breccia, upper contact of C1 ore lens. White is talc-chlorite-carbonate; and **B.** close up of sulfide (pyrite-chalcopyrite) clasts in chlorite matrix with chalcopyrite mobilised into fractures during deformation. **C.** Flame structures in mudstone beneath massive chalcopyrite-sphalerite ore (PHOTO:Anonymous (2014)). **D.** Example of ore showing possible durchbewegung texture in chalcopyrite-rich ore, and fragmental massive pyrite unit (PHOTO:Anonymous (2014))

Spheroidal zones of quartz and/or carbonate, chlorite or sphalerite, rimmed with pyrite and chalcopyrite have been identified in both drill core and underground exposures (Fig. 4.15). Chalcopyrite is concentrated in central bands, progressing to pyrite at the edges. Concentric

banding is visible in hand specimen (Fig. 4.15). These textures are interpreted to be pieces of mineralising conduits, similar to those interpreted as black smoker chimneys in the Urals VHMS deposit of Russia (Maslennikov et al., 2009, Maslennikov et al., 2013) (Fig. 4.16) and have been found in the C1 and DeGrussa ore deposits.

In deeper levels of the deposit, initial pyrite-rich ore may have been fractured by later ore-bearing hydrothermal fluids, creating new pathways along which chalcopyrite-rich mineralisation later precipitated (often associated with carbonate alteration).

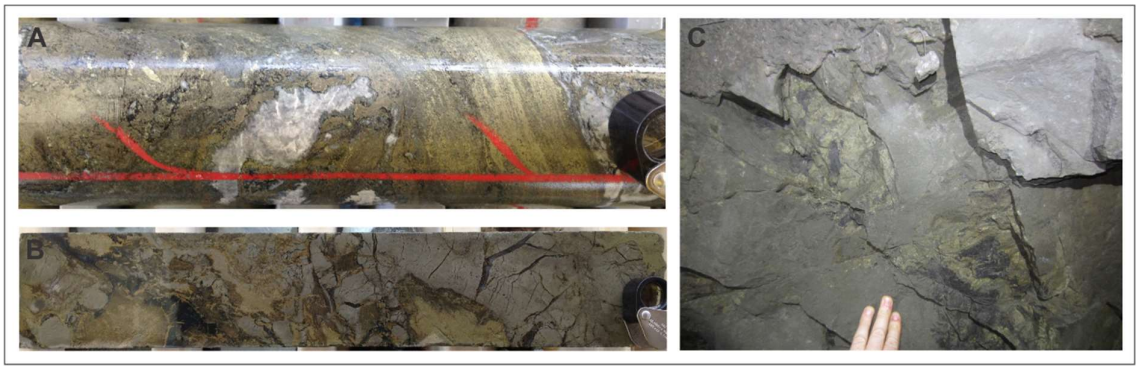

Figure 4.15 Examples of conduit structures in the underground exposure and drill core. A. Calcite filled conduit structures with pyrite and chalcopyrite rim. NQ drill core (DGUG0755). B. Chalcopyrite filled conduit with minor chlorite rimming within massive pyrite (DGDD277). C. Chalcopyrite-rich conduit structures in massive pyrite (Underground exposure, 2225 C1 ODL west drive).

Figure 4.16. A. Polished cross section through a sphalerite-chalcopyrite-pyrite-marcasite chimney structure (Maslennikov et al., 2009), B. Polished cross section through a sphalerite-pyrite-quartz-barite with chalcopyrite chimney (Maslennikov et al., 2009). C. Polished cross section through a sphalerite-chalcopyrite chimney (Maslennikov et al., 2013)Although different in mineralogy to the DeGrussa vent structures, there is a striking resemblance between the two deposits

One of the more interesting sulfide textures is in the Conductor 1 ore deposit which in DGDD173 displays a reversal in the pyrite and chalcopyrite relationships (Fig 4.17). Subrounded chalcopyrite clasts with a chlorite matrix are seen with a network of crystalline pyrite veins surrounding the clasts. This may have formed from an original basalt and/or sedimentary rock

breccia in which pyritic veins were emplaced between breccia clasts, and a later phase of Cu-rich fluid dissolved the basaltic clasts, replacing them with chalcopyrite and chlorite. These textures are similar to those initially described by Eldridge et al. (1983) for Kuroko VHMS deposits in which late stage chalcopyrite is introduced, replacing pyrite and sphalerite minerals, and in the Conductor 5 ore lens of DeGrussa where Adamczyk (2013) identified partially replaced fragments of both basalt and chert are found within mineralised zones. In the Conductor 5 ore lenses (Fig. 4.18), contacts between the sulfide zones and sedimentary rocks grade from massive to blebby and disseminated and where in contact with basalt, the contacts are either sharp, similar to those visible at the base of C1, or gradational into jigsaw-fit breccia textures (Adamczyk, 2013). No chimney structures, or a sub seafloor, disseminated, stock-work zone were observed in drill core in the C5 horizon by Adamczyk (2013), although later core observations (Fig. 4.16) indicate that mineralising conduits are likely present.

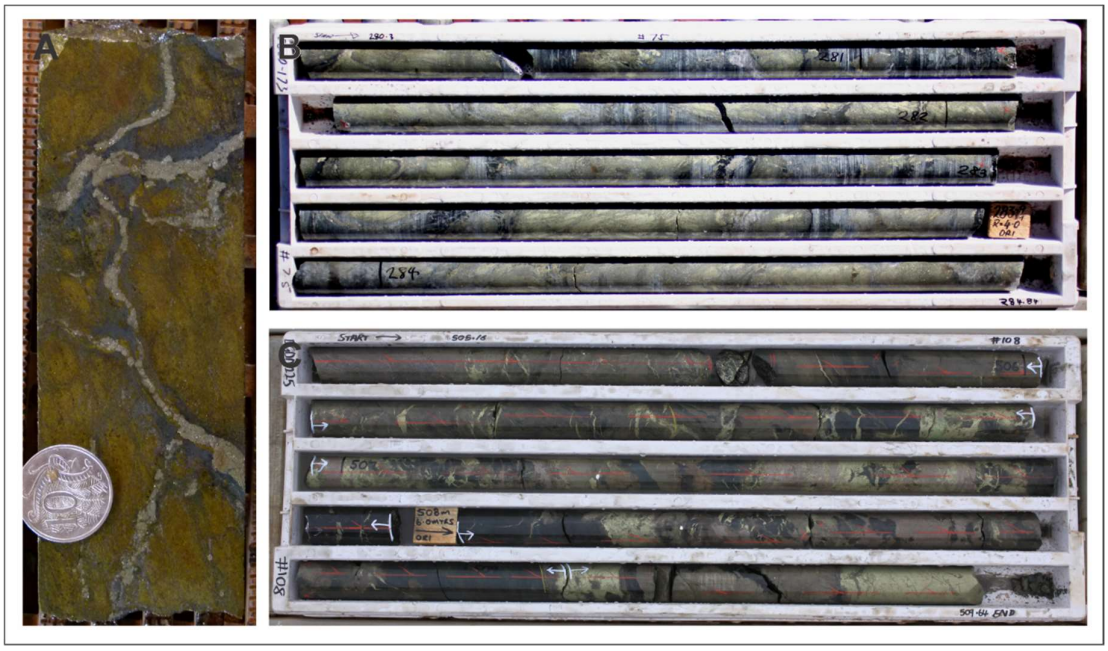

Figure 4.17. Sulfide in Conductor 1 and Conductor 5 interpreted by Adamczyk (2013) as replacement. **A.** Chalcopyrite-rich ore replacing basalt breccia. Pyrite and chlorite infills fractures. **B.** C1 chalcopyrite dominated sulfides replacing basalt clasts. Strong calcite alteration (DGDD173, 280.3-284.84m). **C.** Pyrrhotite and chalcopyrite replacing basalt. Chalcopyrite occurs as massive clasts and also as veins/stringers, cross cutting massive pyrrhotite, mobilised during deformation.

4.2.4. Stockwork/Feeder Zone

Alteration throughout the feeder zones (Fig. 4.18) is; 1) A central core of quartz + pyrite ± chalcopyrite, with remnant clast textures of banded sedimentary rock, now overprinted with siliceous alteration. Sulfides (pyrite and chalcopyrite) are disseminated throughout or occur as stringer veins. Grades are up to 3% Cu (P. Hilliard, pers comm, 2014); 2) A chlorite-rich alteration zone, similar to rocks found within the footwall and hanging wall of the ore lenses. Sulfides are disseminated throughout (cpy + py), with somesilica alteration as veins and throughout the groundmass. Flecks of leucoxene and remnant fragmental host rock textures, likely basalt, are preserved but strongly chlorite altered, and 3) A zone of chlorite-sericite altered rock is formed on the outer edge of the feeder zone, which is gradational into 4) a sericite altered unit, in which the sedimentary rocks are strongly sericitised, especially when in contact with peperitic basalt. Peperitic basalt with strong sericitic alteration is commonly observed around the ore lenses. Graphic logs through two feeder zone sections are presented in Figure 4.19.

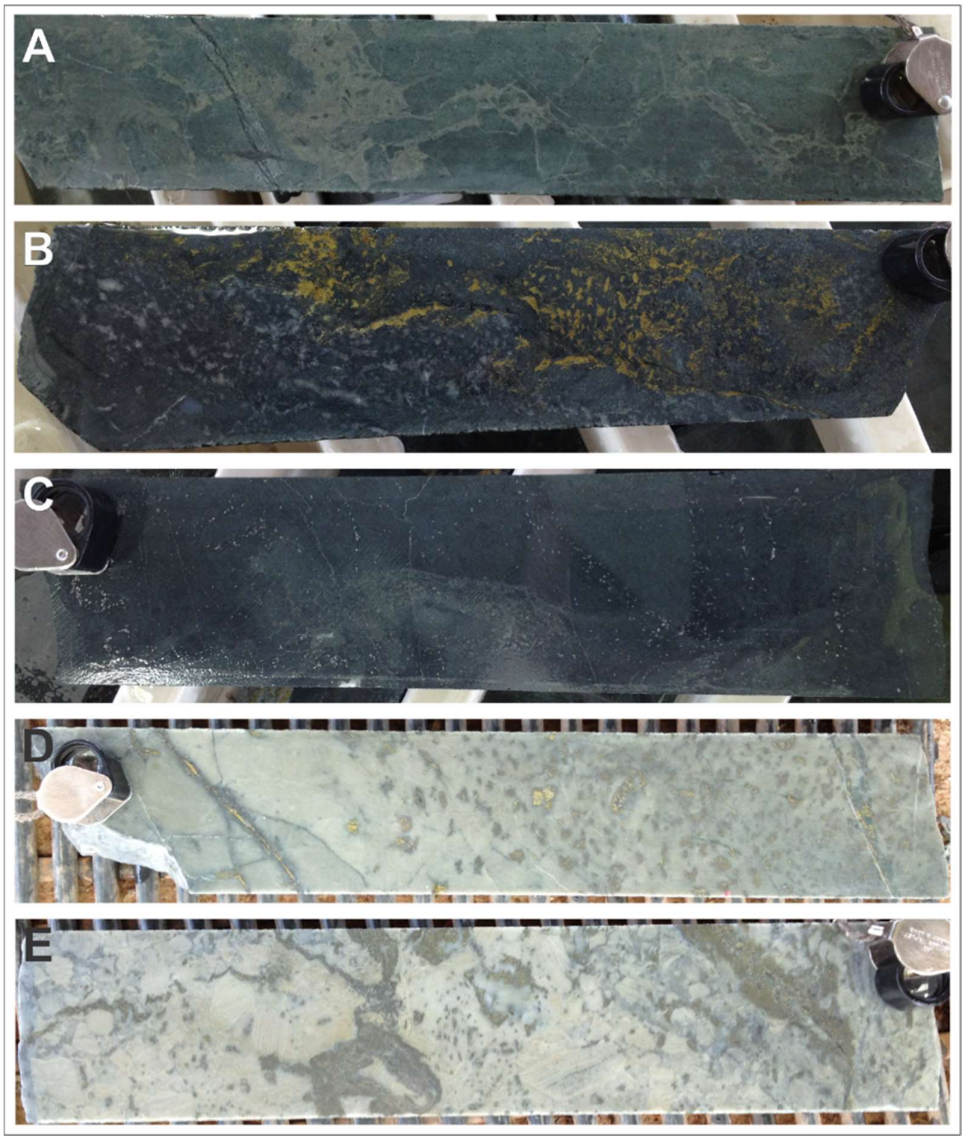

Figure 4.18 A. DGUG0569. Sericite + chlorite altered peperite; **B.** Chlorite + quartz + carbonate with stringers of chalcopyrite. Rock was originally a basalt-sediment peperite breccia now strongly overprinted with chlorite alteration; **C.** Fragmental peperite texture still visible in chlorite alteration zone. Clasts and sediments can be defined by the differing amounts of leucoxene in the rocks; **D.** Siliceous feeder zone to C1 mineralisation. Quartz extensively replaces the original rock. Minor chlorite and sericite is preserved in veins. Chalcopyrite and pyrite occurs as blebs, veins and stringers throughout; **E.** Siliceous feeder zone to C1 mineralisation. Displays fragments of silicified and bedded sediment with surrounding veins/infill of quartz, chlorite and sulfide (pyrite>chalcopyrite).

Stockwork/feeder zone alteration is discontinuously present in areas where sulfide ore is thickest, or along the edges of ore lenses. Three areas of quartz-sulfide stringer zone alteration have been identified:

1. The top western edge of the C1 ore lens (Fig. 4.20)
2. The lower western edge of C1 (Fig 4.21) and also within the hanging wall along the western edge (Fig. 4.22).
3. C1 central stringer zone (Fig. 4.23).

Unlike other VHMS deposits, where stringer zones can be large and widespread below the deposit (e.g. Hellyer (Gemmell and Fulton, 2001)), feeder zones at DeGrussa are narrow and restricted. At DeGrussa, quartz + pyrite stringer is rarely identified in the hanging wall of the deposits, but has been identified above the C1 ore lens. Generally, only chlorite and sometimes talc-exhalite occur in the hanging wall.

Figure 4.19. Graphic Logs for feeder zone. Main mineralised zone highlighted in yellow. Alteration surrounding the silicic core consists of chlorite, carbonate and sericite. Sericite is particularly strong in association with peperitic margins to basalt.

Feeder zone alteration: Conductor 1, drill hole DGUG0569

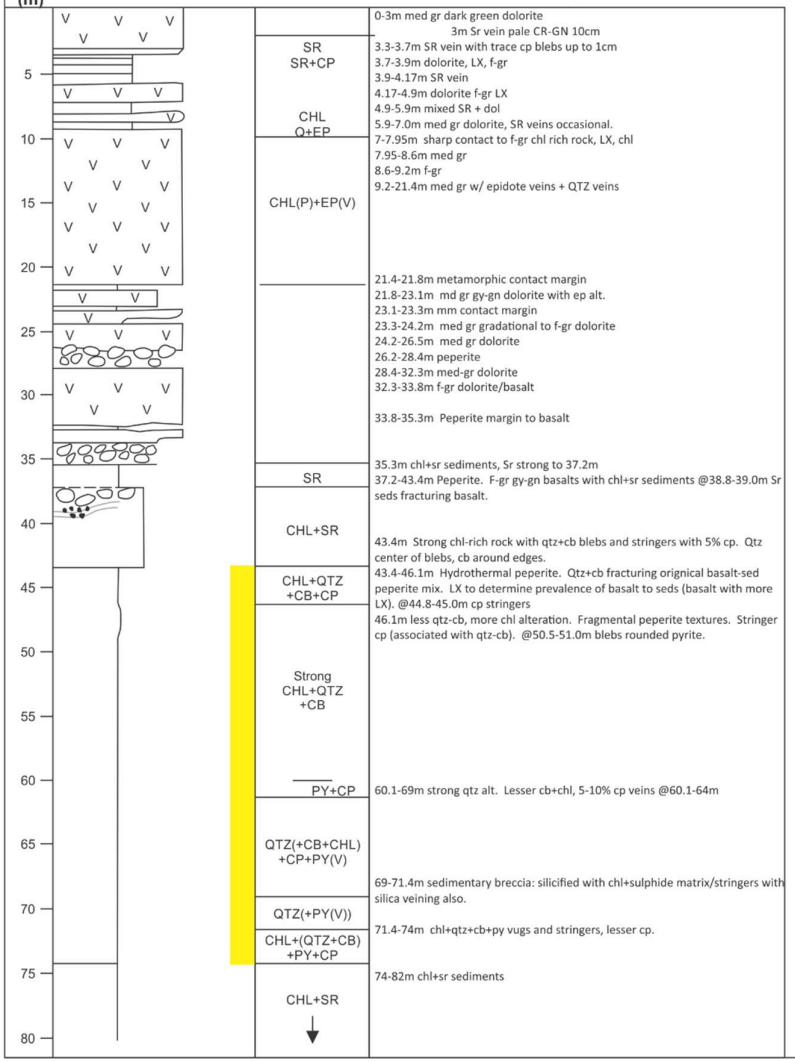

Feeder zone alteration: Conductor 4, drill hole DGUG0701

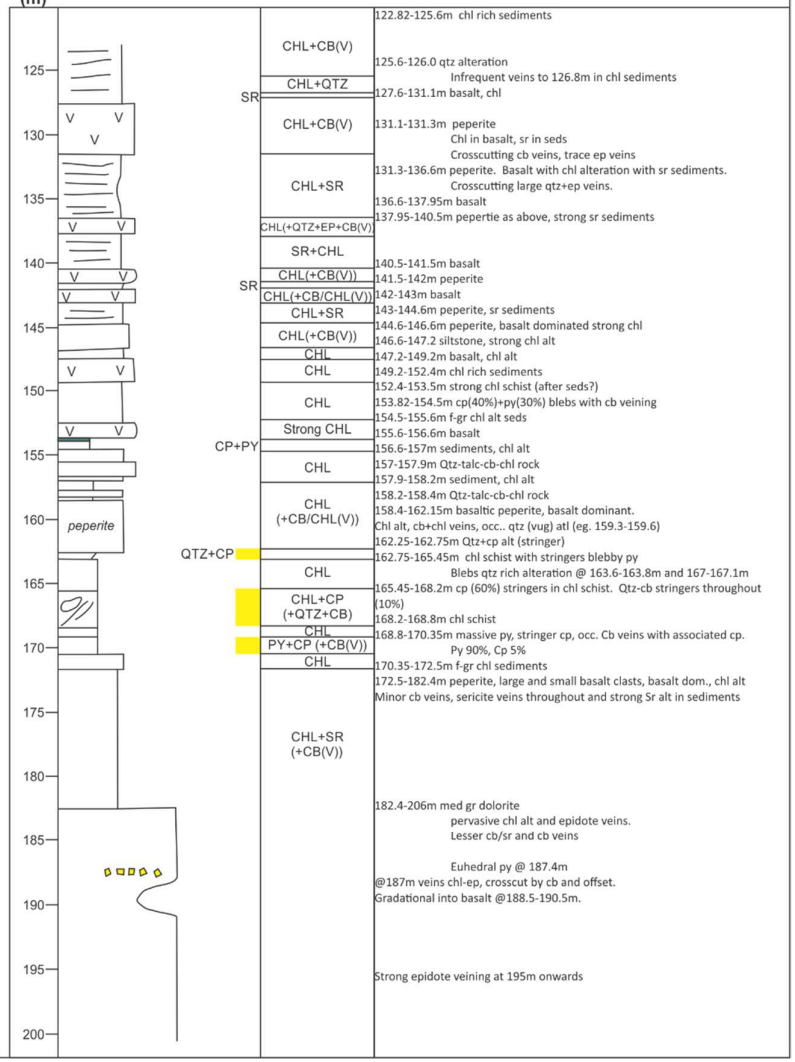

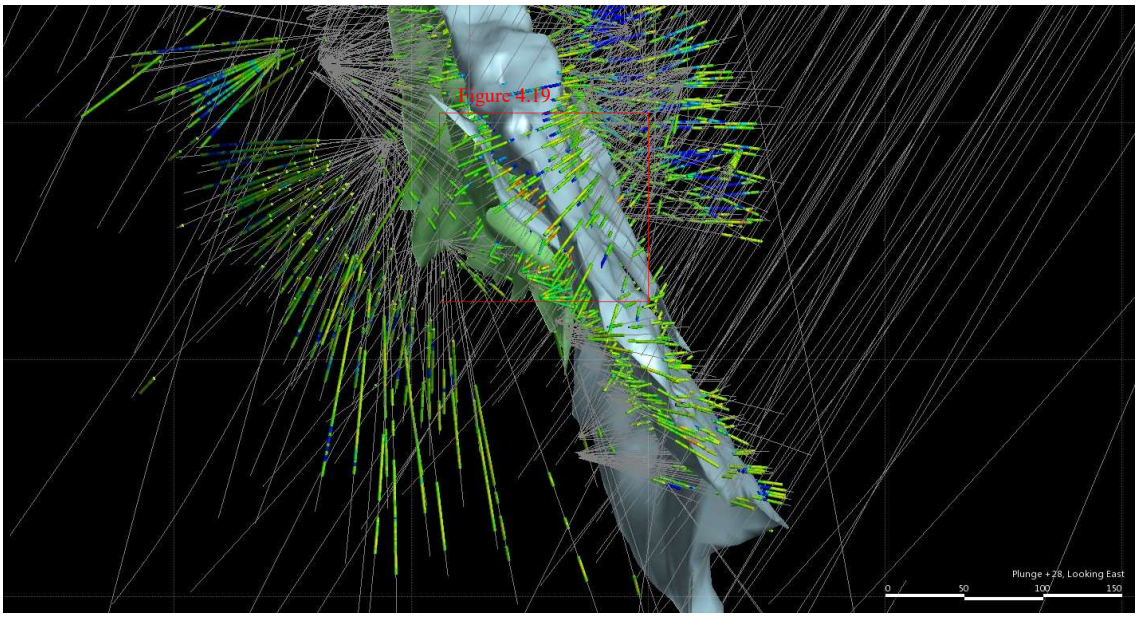

Figure 4.20. The Conductor 1 ore lens looking east. Light blue is the upper lens, and light green in the lower lens or Conductor 1. Drill holes show high (>50%) SiO2 (%) in orange, representing the silicified feeder alteration. Red box indicates area covered by Figure 4.22.

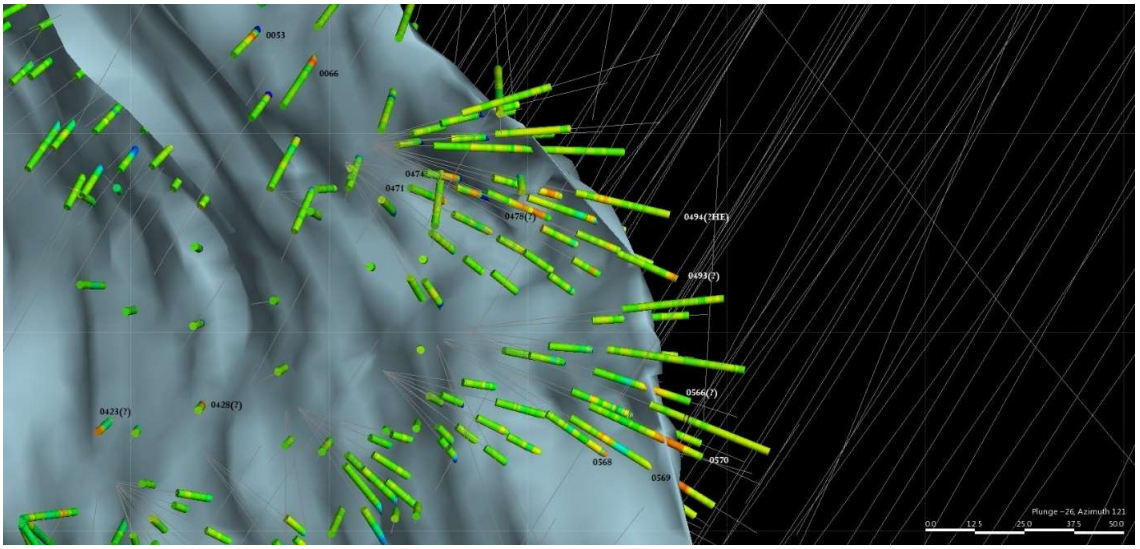

Figure 4.21. Western edge of the Conductor 1 ore lens and corresponding feeder zone silicic alteration. Graphic drill hole log for drill hole DGUG0569 is located in Figure 4.20. The restricted occurrence of silicic feeder zone material at the far western edge of the Conductor 1 ore lens suggests that fluids have been mobilised up fault structures, which also confined mineralisation deposition to the east.

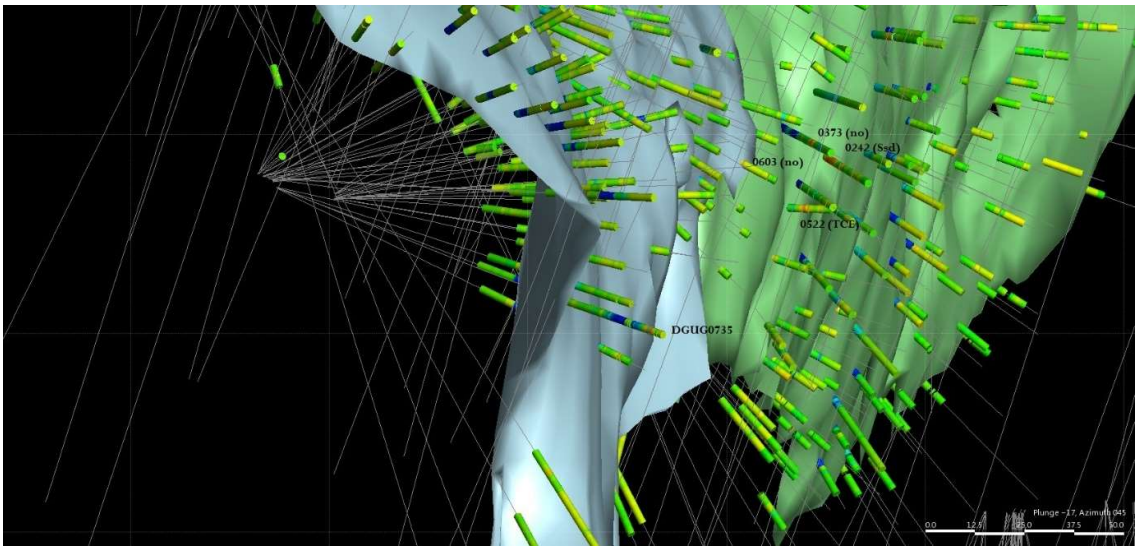

Figure 4.22. Hanging wall of Conductor 1 ore lens (above area shown in Figure 4.19). Visual inspection of core results with most intersections representing either sandstone-rich horizons or talc- exhalite.

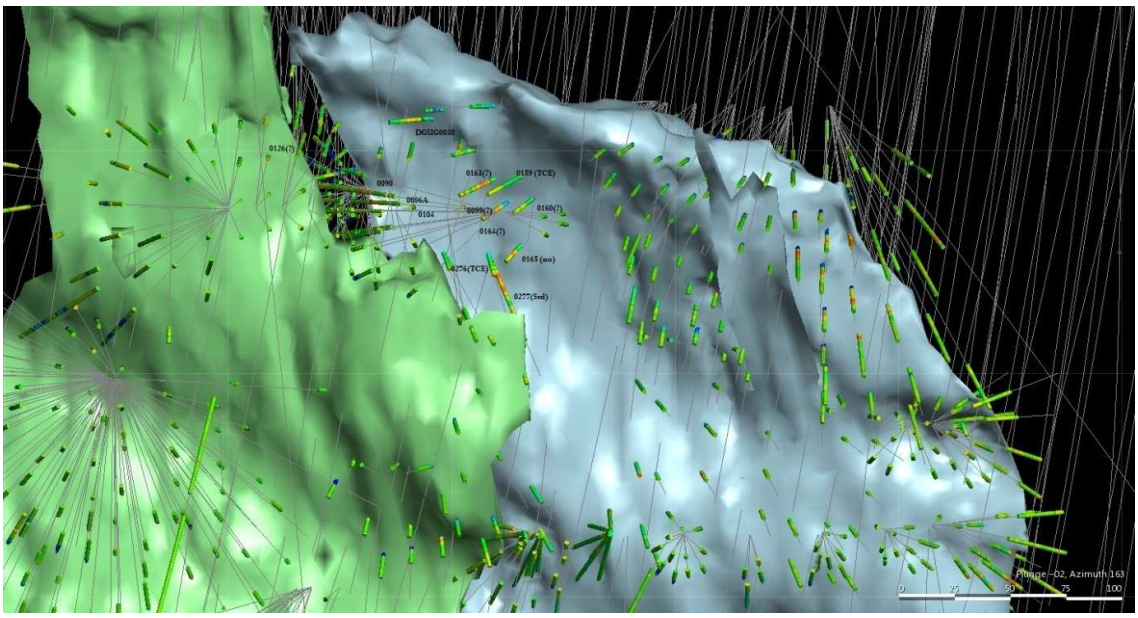

Figure 4.23. From the north, looking south at the underside of the Conductor 1 ore lens. High SiO_2 values to the centre of the deposit are one feeder zone for the ore lens. High SiO_2 to the western edge are sandstone rich sedimentary rock units.

4.2.5. Supergene Mineralisation

As the supergene mineralisation is not the focus of this thesis it will not be discussed in detail although has formed a significant component of ore in the DeGrussa deposit. The supergene mineralisation contributes to a stockpiled oxide resource estimate of 2.8Mt @ 1.2% Cu and 1.0g/t Au, for a total metal resource of 33,000t Cu and 88,000 ounces Au (Taylor and Hastings, 2015)

Upper portions of the DeGrussa deposit are exposed to surface weathering processes resulting in oxidation of sulfide minerals and dispersal of metals throughout the regolith environment (Fig. 4.24). Common minerals found in the surface environment include chalcocite, cuprite, tennantite, malachite, azurite, chrysocolla, and native copper (Fig 4.25).

Figure 4.24. Top of the Conductor 1 lode, DeGrussa Stage 2 pit, facing west showing dark chalcocite rich ore hosted in sedimentary rock.

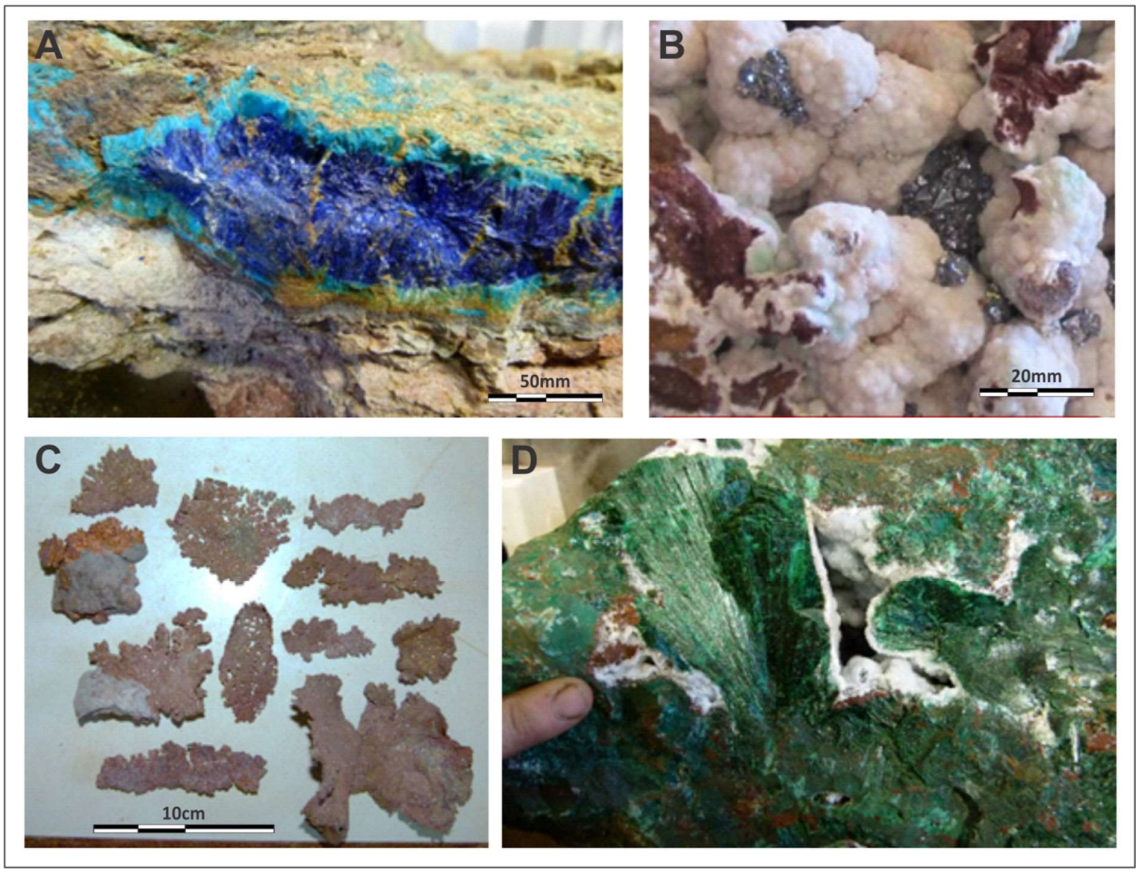

Figure 4.25. A. Azurite and chrysocolla pseudomorph in clay matrix. Image is ~30cm across. **B.** small cuprite crystals on calcite**. C.** Small, flattened native copper pieces from within shear and fault zones in the DeGrussa open cut. **D.** Radiating malachite with calcite.

4.3. Hydrothermal alteration

The DeGrussa VHMS deposit has undergone several periods of alteration, deformation and metamorphism. Initial alteration resulted from hydrothermal processes concurrent with emplacement of the rocks and deposition of the massive sulfide lodes during sea floor rifting at 2.05Ga. The second results from burial greenschist facies metamorphism of the deposit and later Capricorn age deformation at c. 1800 Ga (Pirajno et al., 2000). Greenschist facies regional metamorphism is dominant across the Bryah and Padbury Group rocks (Pirajno et al., 2000). Prehnite-pumpellyite metamorphism is present in the Yerrida Group (Pirajno and Adamides, 2000).

Characteristic metamorphosed mineral assemblages associated with the DeGrussa mineralisation include chlorite schist, talc-chlorite-carbonate schist, chert, jasper, and hematite (refer to Ch. 3). Other important alteration includes dolomite and quartz-carbonate veins which postdate but possibly reprecipitate some metals.

In thin section, alteration minerals of mafic rock consist of chlorite, epidote, talc, actinolite, albite, and clinozoisite/clay minerals. In sedimentary rocks, including argillaceous, shales and carbonaceous sedimentary rocks, alteration minerals are clay minerals (mica), carbonate (calcite and dolomite), minor talc and chlorite. Alteration assemblages are dependent on the host rock composition, temperature and pressure conditions and fluid chemistry that rock is subjected. The alteration box plot of Large et al. (2001) shows the effect of hydrothermal alteration on dolerite and basalt rocks, and the ACF metamorphism diagrams of Best (2002) display the possibility of prehnite-pumpellyite facies metamorphism (250-300˚C, 2-7kbars) and greenschist facies metamorphism (300-450˚C, 1-4kbars).

4.3.1. Chlorite (+sericite+sulfide) schist

Chlorite-sericite-sulfide alteration associated with massive sulfide mineralisation is dark green-black, foliated and formed as an alteration halo to the massive sulfide, in contrast to regional chlorite alteration which is a green-grey colour in hand sample (see Fig 4.26). The

original rock type is difficult to decipher in hand sample and thin section, although both basaltic and sedimentary precursor rocks are likely. The unit is generally strongly sheared although less deformed variations containing abundant disseminated sulfide (pyrite and chalcopyrite) are also observed.

In thin section, the rock is a patchwork of alteration minerals, with no primary minerals preserved (Fig 4.26). The majority of the rock is formed from fine-grained chlorite (80%) with lesser sericite (10%). Chalcopyrite and molybdenite as blebs and stringers are observed throughout the rock. Trace amounts of pyrite are present and the white-grey flecks visible in hand sample are rounded leucoxene/titanite crystals. Variations include alteration assemblages where the rock contains a higher proportion of quartz (35%) in a chlorite (50%) groundmass, with flecks of leucoxene/titanite, and trace calcite (Fig. 4.26).

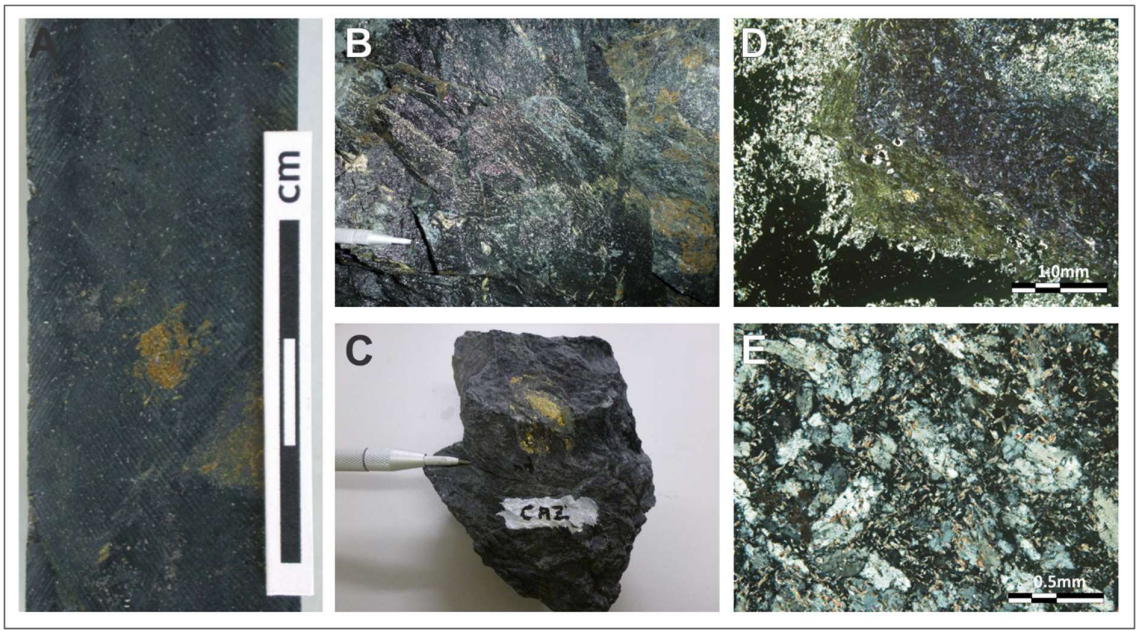

Figure 4.26. A. Chlorite-sericite-sulfide schist proximal to the C4 ore lens. White flecks are leucoxene (DGMH036: DGDD125, 569.45-569.55m) (photo courtesy Mason (2011)). Chlorite schist with disseminated chalcopyrite aggregates. B. 2400W Ore Drive 3 Sample ID UGB041B, **C.** 2375W Ore Drive 2, Sample ID: A004086. **D.** Transmitted light view of SAMPLE DGMH036 view of chlorite schist with ragged patches (bottom left, top right) composed of sericite (tiny bright flakes) and opaque sulfide (chalcopyrite, pyrite, molybdenite), fine-grained, dense chlorite (anomalous dull green, purple) (DGMH036) (photo: Mason (2011)). **E.** Crossed polarised view of chlorite schist (after basalt) showing massive assemblage of chlorite (dull grey background), quartz (white grains) and sericite (tiny bright flakes) (DGMH037) (photo: Mason (2011)).

Chlorite is Mg-Fe rich with likely compositions of clinochlore and more definitive analysis using QXRD of chamosite (see Appendix 3.4 and 3.5). These two likely compositions are formed via metasomatism of ferromagnesian minerals (e.g. hornblende) in the original rock.

4.3.2. Talc – chlorite – carbonate (± actinolite) schist

Talc-chlorite-carbonate-schist displays both strong schistosity (DGMH015, DGMH059) and pseudobreccia in a sheared matrix of calcite. The unit occurs as lenses, along either the upper or lower contacts of the ore bodies and separated from mineralisation only by chlorite schist. Occasionally, significant amounts of sulfide (dominantly pyrite and chalcopyrite) are present. Often the talc-chlorite-carbonate-schist occurs interbedded within the ore deposit. Composition varies with different quantities of calcite, tremolite, chlorite and talc. Sample DGMH015 (Fig. 4.27) consists almost entirely of calcite (95%) with incorporation of rounded to sub-rounded lithic clasts of feldspar and clay minerals derived from surrounding host sedimentary rocks. Larger carbonate crystals and fragments of fine-grained calcite and lithic clasts are in a matrix of calcite.

In comparison, sample DGMH059 (Fig. 4.27) contains calcite (77%), tremolite (20%) and minor chlorite (3%). Calcite is present as coarse-grained, rounded grains and aggregates in a matrix of foliated, fine-grained, micro-granular carbonate. Tremolite (~0.4-5mm) is preserved as bladed phenocrysts irregularly distributed and intergrown with calcite. Chlorite is patchy throughout the rock and clusters as small flakes which are elongated in the direction of foliation.

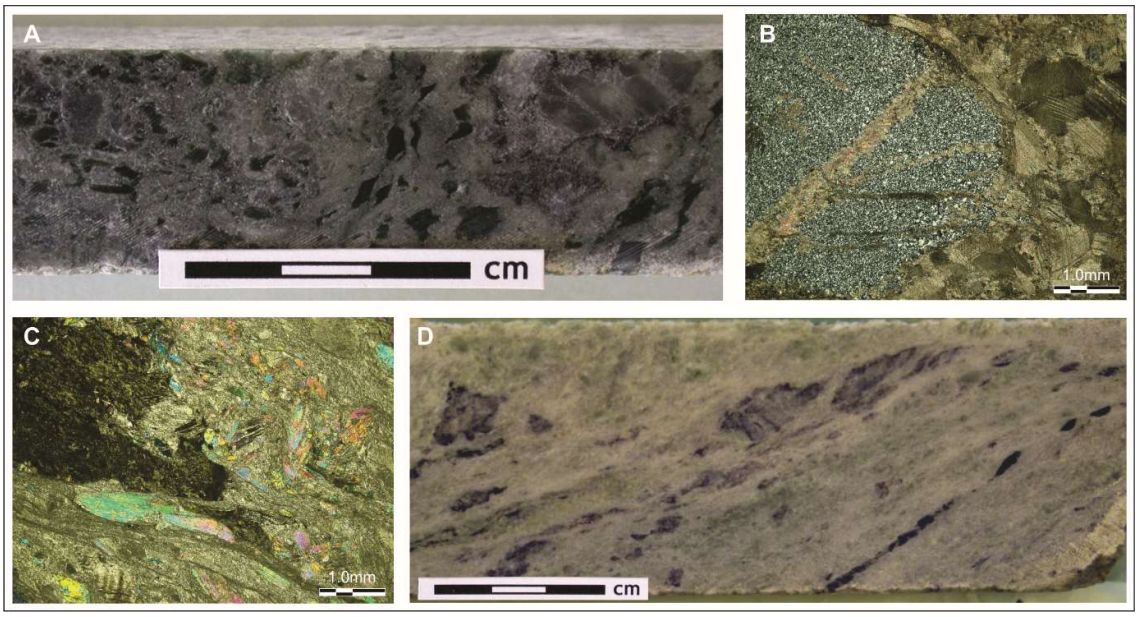

Figure 4.27. Examples of talc-carbonate alteration **A.** NQ quarter core of calcite-rich unit with irregular clasts of grey quartz, and **B.** the same rock in thin section (transmitted light, crossed polars). The quartz clasts are cherty (fine-grained, grey, left) in a matrix of recrystallised calcite (right of image). Sericite also occurs but is not shown in this image (DGMH015: DGDD173, 271.45-271.54m). **C.** This section of a similar calcite-rich rock comprising chlorite-altered basaltic lithic fragments (top left) in a foliated matrix of calcite and lesser tremolite (bright coloured crystals), and **D.** the same rock in hand sample (NQ half core) showing foliation of the rock, purple-grey fragments of altered basalt and green chlorite alteration throughout the calcite matrix (DGMH059: DGDD203, 200.58-200.73m).

4.3.3. Chert, Jasper and Hematite

Hematite and jasper horizons are primarily found in the footwall of the DeGrussa ore lenses, with the occasional jasper clast or thin hematite-altered horizon found in the hanging wall of the deposit. Adamczyk (2013) identified patchy zones of salmon-coloured hematite alteration above and below the C5 deposit and noted that it became increasingly more abundant east of C5 where it is associated with an increase in irregular-shaped, jasperoidal fragments and a decrease in talc-carbonate alteration (Fig. 4.28).

Silicification is widespread in the footwall sedimentary rocks of the Johnson Cairn and Juderina Formation (see Figure 3.1, Map 2 and Map 3) (Jeffery, 2013). The relationship to mineralisation is unclear, but it is possible that hydrothermal fluids related to mineralisation may have passed through these rocks.

Figure 4.28. Examples of hematite and jasperlitic units in the footwall of the DeGrussa host sedimentary rocks. **A.** Strong, orange-red hematite alteration below the C5 ore lens in DGDD231, 484.15-488.7m. **B.** Bright red jasper-chert clast and underlying dark purple hematite altered sedimentary rocks in DGDD219, 563.9-568.07m.

4.3.4. Dolomite and Carbonate rocks

In addition to the dolomitic breccia of the Magazine Member (described in chapter 3, section 3.2.6), persistent dolomitisation of rocks occurs, usually as small 1-10m thick units within the Magazine Member and Johnson Cairn Formation. These rocks are white to light-grey with dark stylolitic veins of chlorite or white milky veins of dolomite or quartz. Talc often forms a component of the rock, and sometimes hematite appears as a persistent groundmass component (Fig. 4.29). Dolomite and calcite commonly occur together, potentially in units that were originally limestone, and later altered to dolomite. Traces of pyrite are found throughout but is not abundant.

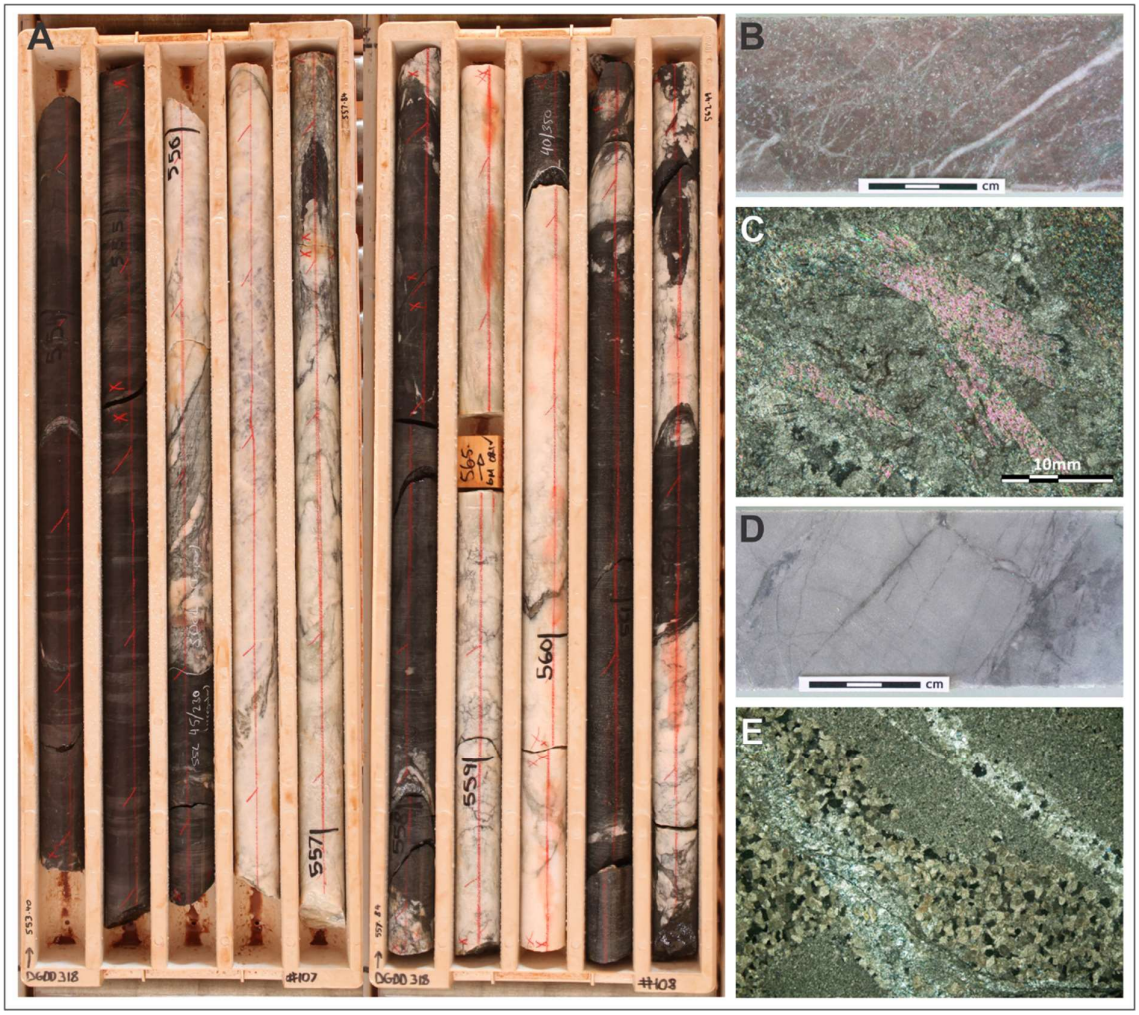

Fig. 4.29. Dolomite and carbonate rocks in the footwall of the DeGrussa deposit. **A.** Representative horizon of dolomitised rock in DGDD318 (553.40-562.69m). **B.** Hand sample of hematite-stained calcite-talc rock with dolomite veins (DGMH068: DGDD203, 621.49-621.65m), and **C.** Thin section of the same rock (DGMH068) under crossed polars showing fine-grained, calcite-dominant composition with brightly coloured talc plates. **D.** Hand sample of light grey, dolomitic rock with quartz-calcite-chlorite veins within the footwall of the DeGrussa ore lenses (DGMH071: DGDD020, 275.85-276.06m), and **E.** Thin section of the same rock (DGMH071) under crossed polars showing fine-grained (top right) and coarse-grained (middle) dolomite (high pastel colour). Thin veinlets are filled by calcite (pale crystals).

4.3.5. Quartz-carbonate-chlorite veins

There are a large number of gold-bearing quartz vein prospects across the Bryah-Padbury region. Quartz-carbonate–chlorite veins are associated with Capricorn age deformation, with underground exposure showing that these cross cut mineralisation. Galena bearing qtz-carbonate veins cross cut the deposit and have a date of 1820±50Ma (chapter 6).

Halos of chlorite around quartz veins (Fig. 4.30) suggest removal of silica from the dolerite and sedimentary rocks, most likely from the replacement of plagioclase and mafic minerals (amphibole and pyroxene), leaving a chlorite-rich margin.

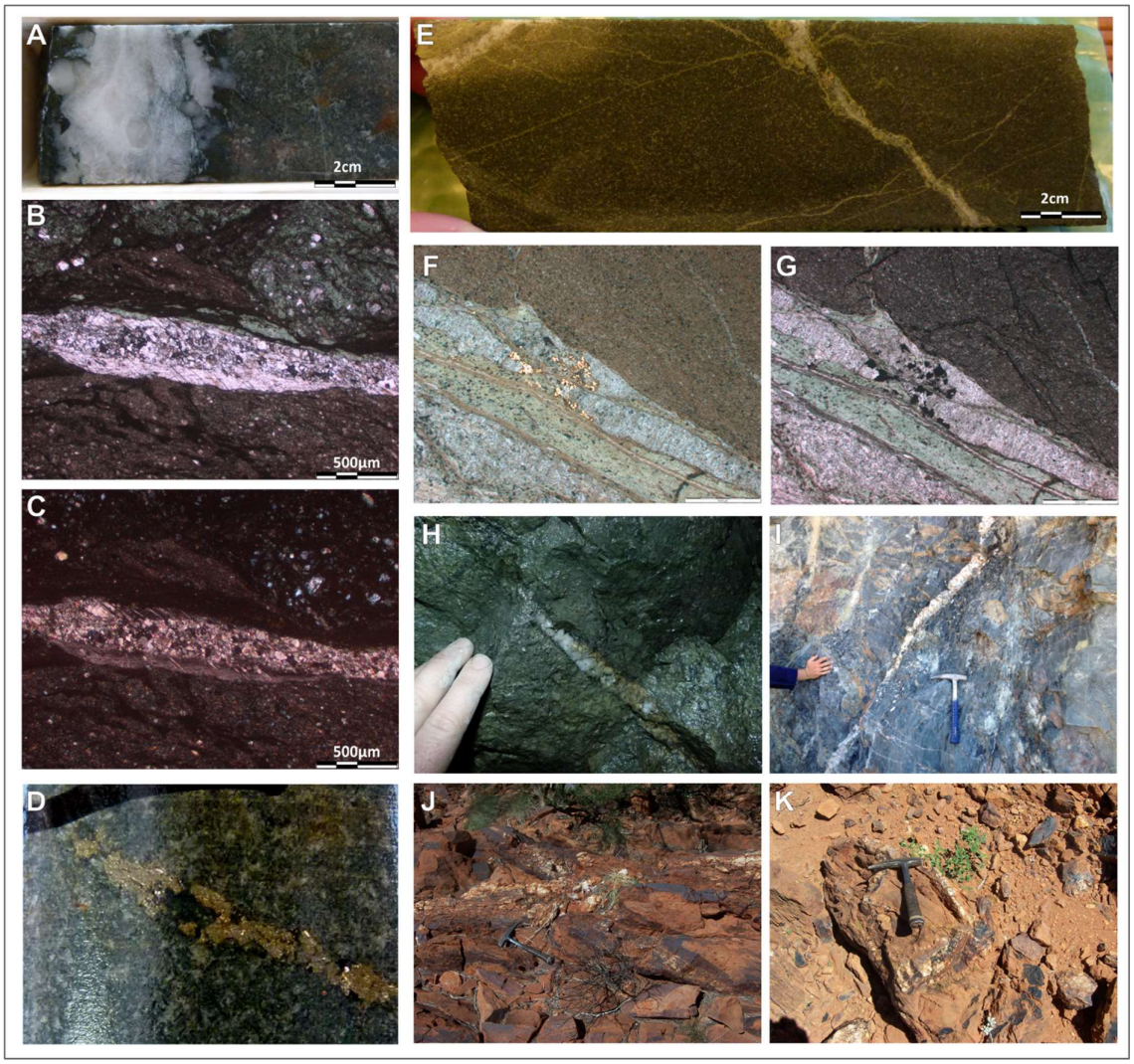

Figure 4.30. A. Chlorite-carbonate-quattz vein. Hexagonal quartz crystals within carbonate dominated vein. Chlorite halo to vein within dolerite host rock (DGDD125). **B.** Thin section, transmitted light and **C.** crossed polars of a calcite-quartz vein within sedimentary rock. Strong chlorite alteration is pervasive throughout the coarser grained groundmass. **D.** Chlorite-pyrite vein (vein is ~7mm wide), crosscutting dolerite rocks (DGDD125). **E.** Fine-grained dolerite with cross-cutting sericite-calcite vein withchalcopyrite/pyrite (DGDD203, 566.27-566.42m). **F.** Thin section, reflected light of a carbonate-chlorite-chalcopyrite vein in fine-grained sedimentary rock (DGMH029, DGDD125, 165.98-166.19m) and **G.** same thin section (DGMH029) under crossed polars. **H.** Underground exposure of a lensoid quartz vein in chlorite-altered sedimentary host rocks. **I.** DeGrussa open pit exposure of a quartz-carbonate vein within host sedimentary rocks. **J.** and **K.** Characteristic outcrop of ferruginous quartz-veins hosted in sedimentary rocks across the Doolgunna project area.

4.4. Metal Zonation and Trace Element Geochemistry

4.4.1. Downhole geochemistry

A selected amount of assay data for downhole geochemical plots (Appendix 4.6) were obtained from the Sandfire Resources database which were processed through Ultratrace Laboratory, Perth, Western Australia. These were then plotted with Microsoft Excel and the results compared to the geological units. Figures 4.31 to 4.36 show downhole geochemistry with reference to geological units for drill holes with most complete assay data through the ore lenses. The following important observations can be made from observations of drill core and assay data:

4.4.1.1. DGDD001 (DeGrussa and Conductor 1) (Fig. 4.31)

Cu, Au, Ag and Se are elevated in the DeGrussa and C1 ore zones. Cu (max. 30.2%) and Ag (39ppm) are elevated in the weathered upper section of the DeGrussa ore lens with respect to the rest of the drill hole mineralisation. There is less Pb and Zn in comparison to the other major ore metals (Cu and Au) increase together,. The DeGrussa ore lens has less Pb and Zn compared with the C1 ore lens (max. Pb 8050ppm and Zn 6.62% in C1 compared with max. Pb 2310ppm and Zn 1.12%in DeGrussa). C1 is higher in As, Sn and Sb compared with DeGrussa which is higher in Cu, Au and Ag.

Co, Cd, Mn, Ba, V and W are below detection limit in the ore lens. Ba increases in sedimentary rocks surrounding the ore (<81ppm within the ore lens and up to 545ppm in surrounding host rocks). Ba and V are elevated around the contact between dolerites and host sedimentary rocks in the hanging wall of C1. V is also elevated in dolerite units (320-430ppm) in comparison to host sedimentary rocks (90-140ppm).

Chlorite schist has elevated values of Mo (max. 659ppm), Cd (max. 44ppm), Te (max. 240ppm), W (max. 13ppm) and Re (max. 4.6ppm). Elevated Mo correlates with a spike in Pb (5900ppm) within schistose stringer rocks below DeGrussa (214m depth). Mo is elevated in the weathered upper portions of DeGrussa (up to 897ppm Mo), although is found in the hypogene zone also.

Tungsten (19ppm at 115m depth) is also elevated on the contact between sedimentary rocks and dolerite in the hanging wall of DeGrussa. Cd is elevated on contact with chlorite schist and turbiditic host sedimentary rocks above and below the DeGrussa ore lens. Ni, Cr and Ti are depleted through the ore zones.

4.4.1.2. DGDD015 (DeGrussa and Conductor 1) (Fig. 4.32)

A broad increase in Cu (up to 29.8%) at the base of the DeGrussa lens in DGDD015 at 294m depth, correlates with a spike in Au (82.8ppm) and Ag (90ppm), associated with a very fractured section of the ore lens but no discernible reasons why it is higher in Au and Ag. Zn is elevated (1.4%) near the top of the DeGrussa lens coincident with elevated As (2570ppm) and Sb (≤31.8ppm).

Bi (352ppm) and Te (179ppm) peak at 272m depth, in the centre of the DeGrussa ore lens, with correspondingly high levels of Se (248-285ppm). Sn peaks at 257.7m, near the top of the DeGrussa intersection, and at 275m, in the centre of the ore lens. The top peak is coincident with a small spike in Cu (10.3%), the second a decrease in Cu (2.26%).

4.4.1.3. DGDD057 (DeGrussa and Conductor 1) (Fig. 4.33)

Cu (>10%) occurs associated with Ag (17.5ppm) and Co (970ppm, steadily decreasing to 455ppm at the base of the ore lens, and 65ppm in disseminated sulfides below) and Sn (70ppm). Pb (0.2%) and Zn (≥3.8%) occurs with Cd (114ppm), As (1290-1730ppm), and Bi (110-138ppm). Te (74.4ppm), Se (150-180ppm) and Sb (39-51.2ppm) are consistent throughout the ore lens. Mo (up to 1440ppm) and Re (0.5-3ppm) peak in the hanging wall basalt/dolerite reflecting trace sulfides, probably in a shear or fault. W is highest on the lower contact between dolerite sill and host sedimentary rock. Ni is depleted in the ore lens (15-60ppm) in comparison with the surrounding host rocks (50-100ppm). No V occurs in the ore lens, with the highest values found in basalt and dolerite rocks (up to 350ppm).

4.4.1.4. DGDD106 (Conductor 1) (Fig 4.34)

Cu is coincident with elevations in Zn (0.9%), Te (290-466ppm), Re (13ppm), Mo (1880ppm), Co (>1220ppm) and Cd (37.5ppm). W is elevated at the top of the ore lens, within the peperitic contact (6.5ppm from background of 0.5-2ppm), possibly reflecting the derivation from the dolerite intrusive rock above. These elements may have been upgraded during dolerite intrusion (supported by increases in the upper portions of the ore lens, closest to the intrusion, with decreasing amounts towards the base).

Throughout lower parts of the ore lens, despite the elements above still being present, high Ag (95-100ppm), Au (≤40ppm) and Pb (≤2.2%) are coincident with elevated As (≤3450ppm), Bi (568ppm), Se (1130ppm), Sn (56ppm from lower 36ppm values associated with the copper rich zone), Ni (235ppm) and Sb (49ppm).

One possibility for these metal associations could be that all elements could have been spread throughout the ore lens evenly when first deposited. The intrusion of the basalt above the ore deposit may have mobilised chalcopyrite and associated magmatic trace elements, concentrating them in the hotter upper portions of the ore lens.

4.4.1.5. DGDD202 (Conductor 4) (Fig 4.35)

The intersection in DGDD202 through the Conductor 4 ore lens is split by basalt. Pyrite at the base of the ore lens provides an age of 1920Ma, suggested in Chapter 6 to reflect orogenic events. Sn (32ppm) and W (3ppm, background of 1ppm) are elevated along the contact between sedimentary rock and basalt breccia beneath the first ore horizon. These elevations may reflect shear or faulting.

Ore lenses are thin and have similar metal relationships. Increased Cu correlates with increased Ag, Bi, Te, Se, Mo, Re and Sb. The upper contact of the ore with chlorite schist contains elevated Au (19ppm) with Pb (2.6%), Zn (5%), As (4450ppm), Bi (26.3ppm), Sn (18ppm), Cd (113ppm) and Sb (38.4ppm). In the lower ore horizon, below the basalt, Cu-rich ore (14% Cu) is coincident with elevated Ag (23ppm), Bi (101ppm), Te (83.2ppm), Se (185ppm), Co (585ppm),

Sb (23.8ppm) and lesser Sn (11ppm) and Cd (35.5ppm). Pb (5270ppm) and Zn (7910ppm) are present but in lesser quantities to that of the upper ore horizon (2.6% Pb and 5% Zn).

Hematitic sedimentary rocks in the footwall show increased Ba (1240ppm) in comparison to ore and basalt proximal to the ore deposit (53-129ppm). Mn is elevated in chlorite schist directly under the lower ore lens (3310-3460ppm) and corresponds with enrichments in Ni (~600ppm) and Cr (850-950ppm) suggesting possible ultramafic affinities of the chlorite-schist.

4.4.1.6. DGDD219 (Conductor 5) (Fig. 4.36).

The highest Cu (12%) in the Conductor 5 lens correlates with Ag (25.5ppm). A secondary Cu spike (10%) lower in the ore intersection shares elevated Co (685-760ppm), Se (≤260ppm), Ag (≤24ppm), Au ≤5.3ppm) and coincident depletions in Cd (7.5pppm from highs of ≤250ppm), Bi (~60ppm), As, Zn and Pb. Au (5-6.7ppm) is elevated with Bi (200-325ppm) and Te (100-180ppm) reflecting that Au is likely held in a bismuth-telluride, probably with some Ag.

Mo (219ppm, from background ≤1ppm in surrounding rocks and ≤40ppm in ore intersections) and corresponding W (14.5ppm from background ≤5ppm in ore lens) peak within the main ore lens at 543m depth. This may be a primary feature, or as in the case of other elevated Mo results, reflect shear/faulting within the deposit. Values correlate with moderate values of Pb, Zn and Cd.

As (5060ppm) and Zn (2.7%) peak along the upper contact. However, highest values of Zn (3.2%) near the base of the ore lens do not correlate with high As. This indicates that there are no definite metal associations between the two elements. High Zn at the base of the ore lens correlates with high Pb (5610ppm).

Depletions in Ba, Ni and V are seen in association with the ore lens, although the three are comparatively elevated in surrounding host sedimentary rocks, basalt and dolerite.

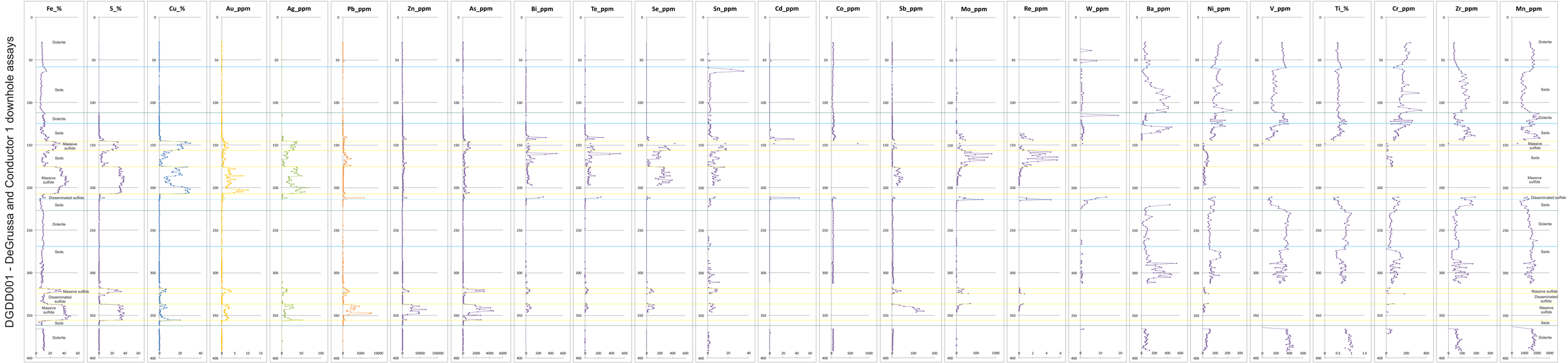
DGDD001 - DeGrussa and Conductor 1 downhole assays
Fe_%
S_%
Cu_%
Au_ppm
Ag_ppm
Pb_ppm
Zn_ppm
As_ppm
Bi_ppm
Te_ppm
Se_ppm
Sn_ppm
Cd_ppm
Co_ppm
Sb_ppm
Mo_ppm
Re_ppm
W_ppm
Ba_ppm
Ni_ppm
V_ppm
Ti_%
Cr_ppm
Zr_ppm
Mn_ppm
Dolerite
Seds
Massive sulfide
Disseminated sulfide

DGDD015 - DeGrussa downhole assays

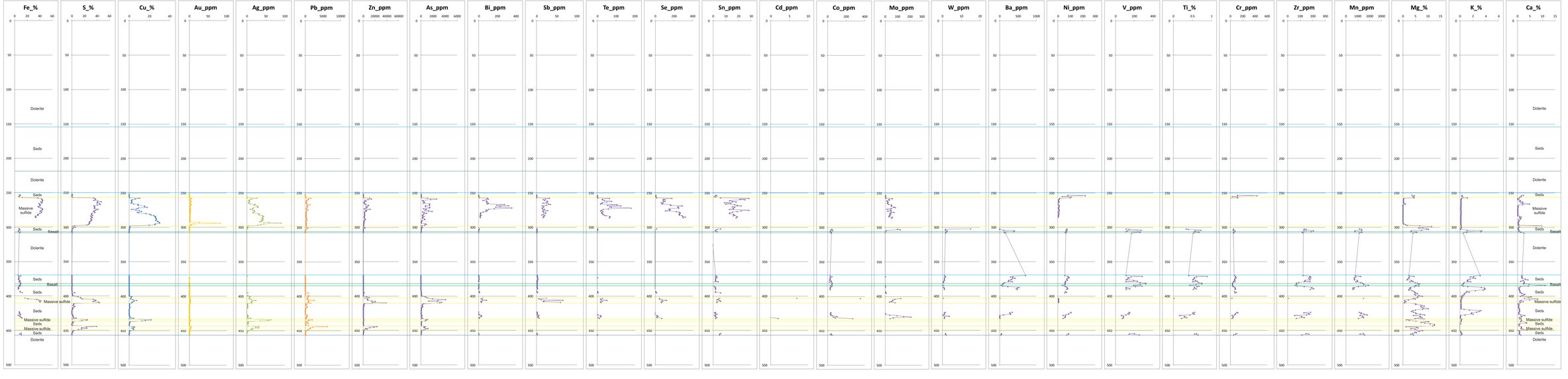

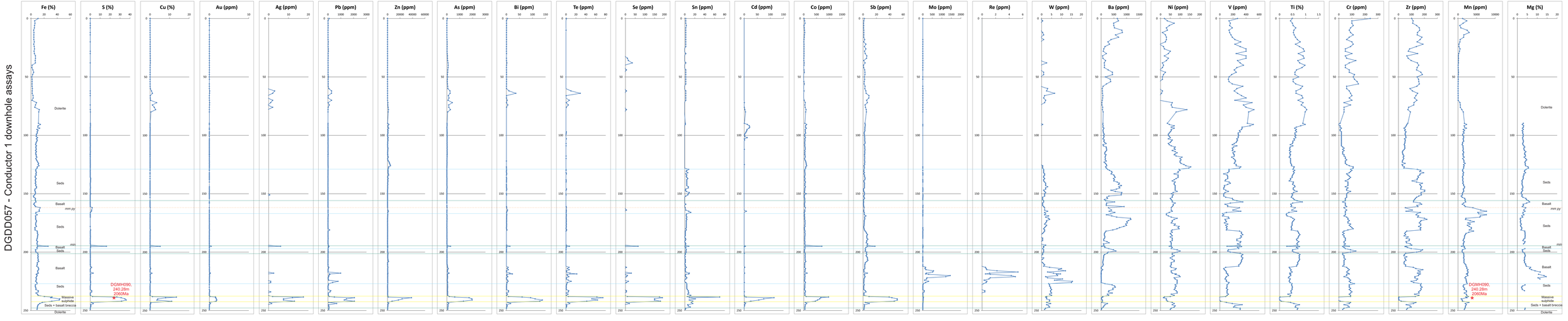
DGDD057 - Conductor 1 downhole assays
Fe (%)
S (%)
Cu (%)
Au (ppm)
Ag (ppm)
Pb (ppm)
Zn (ppm)
As (ppm)
Bi (ppm)
Te (ppm)
Se (ppm)
Sn (ppm)
Cd (ppm)
Co (ppm)
Sb (ppm)
Mo (ppm)
Re (ppm)
W (ppm)
Ba (ppm)
Ni (ppm)
V (ppm)
Ti (%)
Cr (ppm)
Zr (ppm)
Mn (ppm)
Mg (%)
Dolerite
Seds
Basalt
mm py
Seds
mm
Basalt
Seds
Basalt
Seds
Massive sulphide
Seds + basalt breccia
Dolerite
DGMH090, 240.28m 2060Ma

DGDD106 - Conductor 1 downhole assays

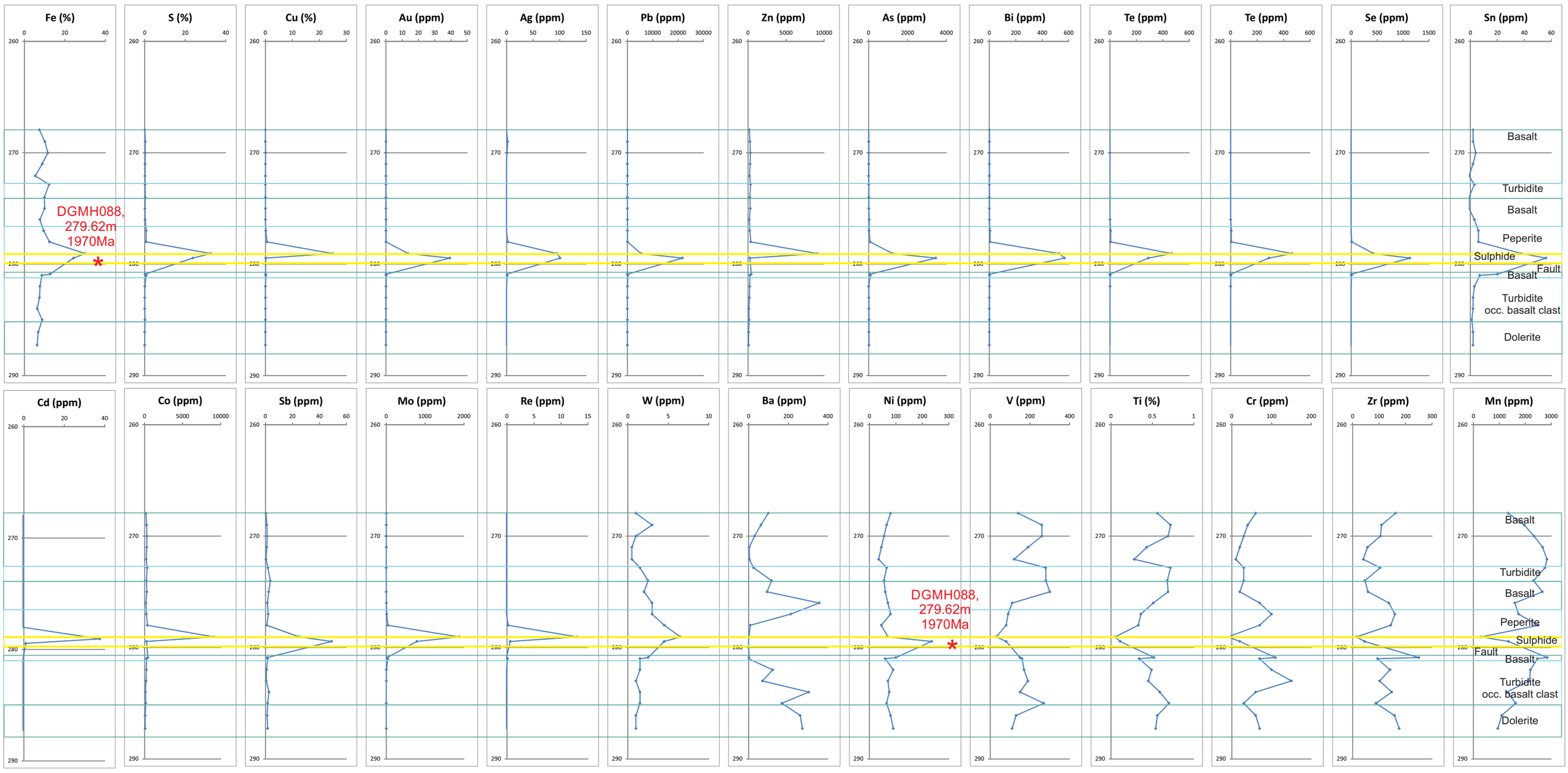

DGDD202 - Conductor 4 downhole assays

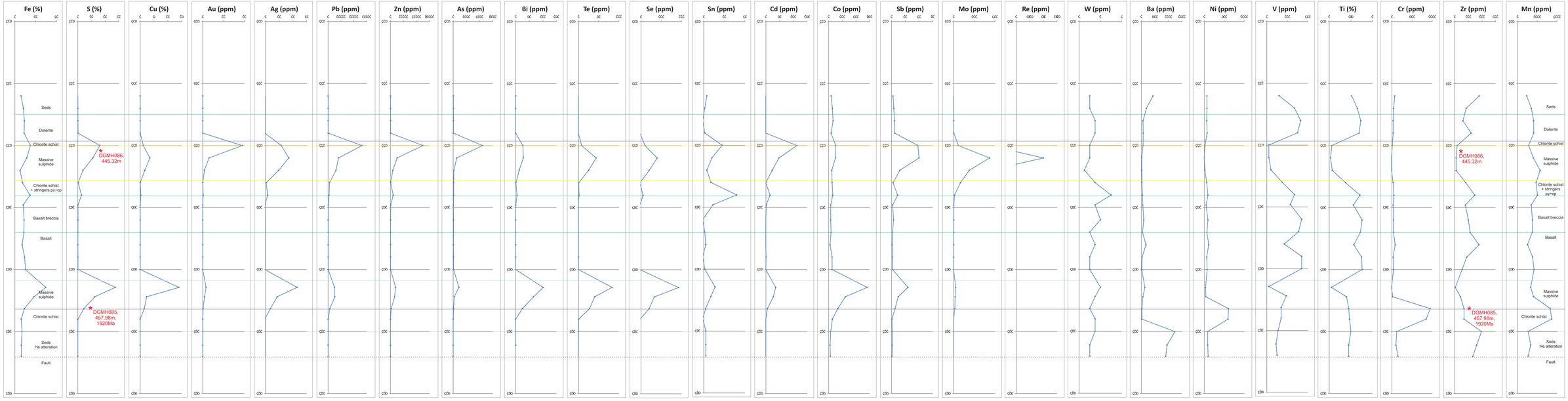

DGDD219 - Conductor 5 downhole assays

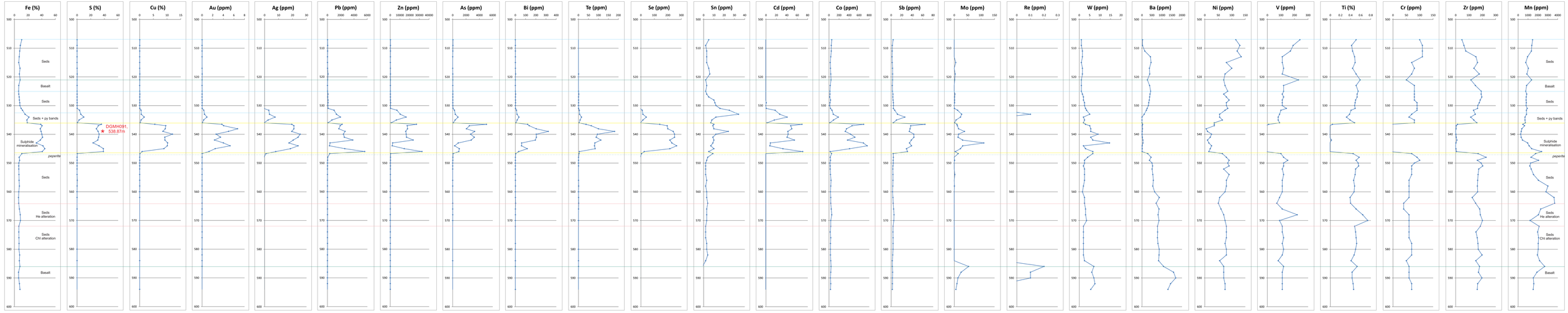

4.5. Discussion

4.5.1. Metal assemblage, deposit zonation and alteration

At DeGrussa, pyrite, chalcopyrite and pyrrhotite are the main ore minerals which cycle in banded layers up to meters in thickness, alternating between the massive and banded ore types described by Condon (2015). Banding may be due to changing physiochemical conditions of mineralising fluids, alternating through zinc, copper and iron-rich zones (de Ronde et al., 2011). The fine-grained and the intergrown nature of the different minerals suggests that ore minerals formed at the same time. Magnetite appears to form in the thicker and central parts of the deposit in association with pyrite, pyrrhotite and minnesotaite (Hilliard, 2013). Work by Sandfire geologists suggests that the magnetite-rich parts of the DeGrussa ore lens are located above the silicieous stringer zones, similar to observed pyrite-magnetite immediately over the footwall stringer zone at the base of the Currawong deposit (Bodon and Valenta, 1995). This is contrast to the classic zonation of a VHMS deposit consists of a central core of chalcopyrite+pyrite±pyrrhotite and outer layers of pyrite±sphalerite±galena and sphalerite±galena±pyrite±barite (Lydon, 1984) as well as the siliciclastic-mafic type (Besshi-type model)(Peter and Scott, 1999, Galley et al., 2007)(Fig. 4.37). The Cu-rich nature of the ore minerals has more in common with Cypress, or mafic/ophiolitic hosted VHMS deposits (Large, 1977, Galley and Koski, 1999), with the exception of the sediment-dominant strata the DeGrussa mineralisation forms in, compared with the mafic rock dominant strata described for Cypress style deposits.

Pyrite is the least mobile of the ore bearing minerals and becomes fragmented with post mineralisation deformation. Chalcopyrite, and to a lesser extent sphalerite, and associated calcite are remobilised to infill fractures in the pyrite ore. In the Mousoulos and Kokkinovia deposits of Cyprus, chalcopyrite and sphalerite fill spaces between pyrite clasts, deposited by late-stage hydrothermal fluids or remobilisation of the massive sulfide mound during successive and overprinting fluid pulses (Galley and Koski, 1999). In the Perseverance deposit, Matagami, Quebec, the distribution of chalcopyrite is interpreted to be due to mechanical remobilisation of

chalcopyrite throughout the ore lenses (Pierre et al., 2016). Spongy textures in the DeGrussa deposit could be similar to those of the Brothers VHMS which are interpreted by de Ronde et al. (2011) to be rapidly deposited. The ease at which chalcopyrite is redistributed throughout the ore is consistent with observations by Yui (1983) of chalcopyrite and sphalerite mobility during the growth of metamorphic pyrite (i.e. more sphalerite than chalcopyrite inclusions are retained in euhedral pyrite crystals). Reprecipitation of chalcopyrite and sphalerite, and recrystallisation of pyrrhotite may explain the metal distribution at DeGrussa. This is supported by geochronological work on pyrite and pyrrhotite (chapter 6) of several phases of metamorphic recrystallisation or remobilisation between c. 2030 and c. 1980Ma. Similar distributions are described for chalcopyrite, pyrrhotite, pyrite and sphalerite for the Whalesback deposit of Newfoundland, Canada (Cloutier et al., 2015).

The abundance of primary pyrrhotite at DeGrussa can be attributed to deposition of metals at high temperatures (>275°C). The stability of pyrrhotite at high temperatures is demonstrated at the pyrrhotite-rich deposits of the sedimented rift environments of the Escanaba Trough (Tormanen and Koski, 2005) and the Guaymas Basin (Lonsdale and Becker, 1985), where pyrrhotite-rich black smoker vent fluids were measured at 275-325°C. The Cypress-type Cu-rich Whalesback deposit also contains significant amounts of primary pyrite interpreted to have precipitated concurrently with pyrite at temperatures of >250 to 300° (Cloutier et al., 2015). Conversely, pyrrhotite presence may be due to deposition in a locally anoxic/reduced environment (Eastoe and Gustin, 1996, Marcoux et al., 2008). Some pyrrhotite is likely to precipitate from the breakdown of pyrite during metamorphism (Craig and Vokes, 1993), which is supported by the younger age dates provided in Chapter 6 of 1982 ± 7 Ma and 1984 ± 8 Ma for pyrrhotite. The presence of intergrown marcasite and pyrite in the DeGrussa ore lens may indicate an interaction with oxidised fluids (Eastoe and Gustin, 1996, Wright-Holfeld et al., 2010, de Ronde et al., 2011). Pyrrhotite is oxidised to marcasite, pyrite or iron hydroxides in the presence of seawater in modern and ancient deposits, commonly found on the outside margins of the massive sulfide and chimneys (Maslennikov et al., 2009).

Galena is scarce throughout the ore deposit, and found along the outer edges of the Conductor 4 ore lens where cooler temperatures dominate. Post-mineralisation quartz-carbonate-galena veins which crosscut the ore lenses may have remobilised lead sulfides from other parts of the deposit during the Capricorn Orogen, or stripped the Pb from the host rocks (see chapter 7).

Turbiditic sedimentary rocks are not as permeable as volcanic sedimentary and eruptive deposit, hence feeder zones may be restricted as hydrothermal fluids would preferentially utilise weaknesses in the rock to permeate through. The zonation in the stockwork/feeder zones at DeGrussa display similar characteristics to other VHMS deposits although on a much smaller scale. The Hellyer Zn-Pb-Cu-Ag-Au VHMS deposit of Tasmania displays: a central siliceous core (quartz-sericite), passing outwards into zones of chlorite, chlorite-carbonate, sericite-chlorite and sericite-quartz (Gemmell and Fulton, 2001).The restricted nature of the quartz-sulfide feeder zone at DeGrussa may be structurally controlled. Faults (such as the Jenkin, Shiraz or Durif faults at DeGrussa)in these areas, could have provided a conduit along which to focus hydrothermal, metal bearing fluids, precipitating sulfide onto the sea floor or replacing favourable horizons in the sub-sea floor similar to that seen in other VHMS deposit (e.g. Currawong, Bodon and Valenta (1995); Turner-Albright, Zierenberg et al. (1988) Perseverance, Matagami, Pierre et al. (2016)). However, the feeder zones have not been intersected in drill holes which pass into the footwall zone (Baker, 2015), and at the time of field work there were few drill holes located on the periphery of the mineralisation and so the nature of the feeders can not be confirmed. The feeder located along the western edge of Conductor 1 is coincident with the western most extent of the ore deposits. One possibility is that the feeder controlling mineralisation at the western edge may have been an active normal fault with the downthrown block to the east. As seen in Figure 3.1, there is a unit of silicified and dolomitic sediments restricted to the stratigraphy beneath the DeGrussa mineralisation, truncated on the east and west sides by fault contacts. These units of the Magazine member and Johnson Cairn Formation, are in paraconformable contact beneath the DeGrussa and Conductor 1 mineralisation, and tectonic contact beneath the Conductor 4 and 5 lenses. The up-thrown western block may have constrained mineralisation within a basin to the

east, trapping the exhalative hydrothermal plumes and sulfide. Fragmental peperite and hyaloclastite textures are now overprinted by feeder zone hydrothermal alteration suggesting that hydrothermal fluids may have used faults and zones of weakness, along the peperitic margins of dolerite and basalt intrusions, as conduits for deposition for mineralisation. Breccia pipes are suggested by Gibson et al. (1999) to be conduits for mineralising hydrothermal fluids at Sturgeon Lake.

A similar scenario to that of the DeGrussa mineralisation has been proposed on a much larger scale for the Rio Tinto deposit in Spain. At Rio Tinto, ore formed in a restricted basin, hosted in a sediment-sill package of rocks, in which sills are inferred to intrude unconsolidated wet sedimentary rocks and cap the mineralising system (Boulter, 1993). A similar, modern analogy can be found in the Guaymas basin, Gulf of California, where massive sulfide mineralisation is forming in response to the intrusion of mafic sills into a sedimentary rock package (Gieskes et al., 1982). The emplacement of sills likely helped to focus mineralising fluids and trap heat in the hydrothermal system with, small lenses of massive sulfide often deposited along the contacts of the dolerite.

Carbonate alteration is pervasive throughout the host sedimentary rock groundmass, throughout the sulfide ore lenses (in particular association with chalcopyrite, and as cross cutting veins), and along the edges of basalt and dolerite intrusions. This supports interaction with dolerite and basalt units only at the margins of the intrusions as they were emplaced into the sea floor environment. The chalcopyrite and carbonate association may have resulted from mixing of circulating Cu-rich hydrothermal fluids and seawater causing a temperature change in the hydrothermal fluid and subsequent deposition of chalcopyrite and carbonate.

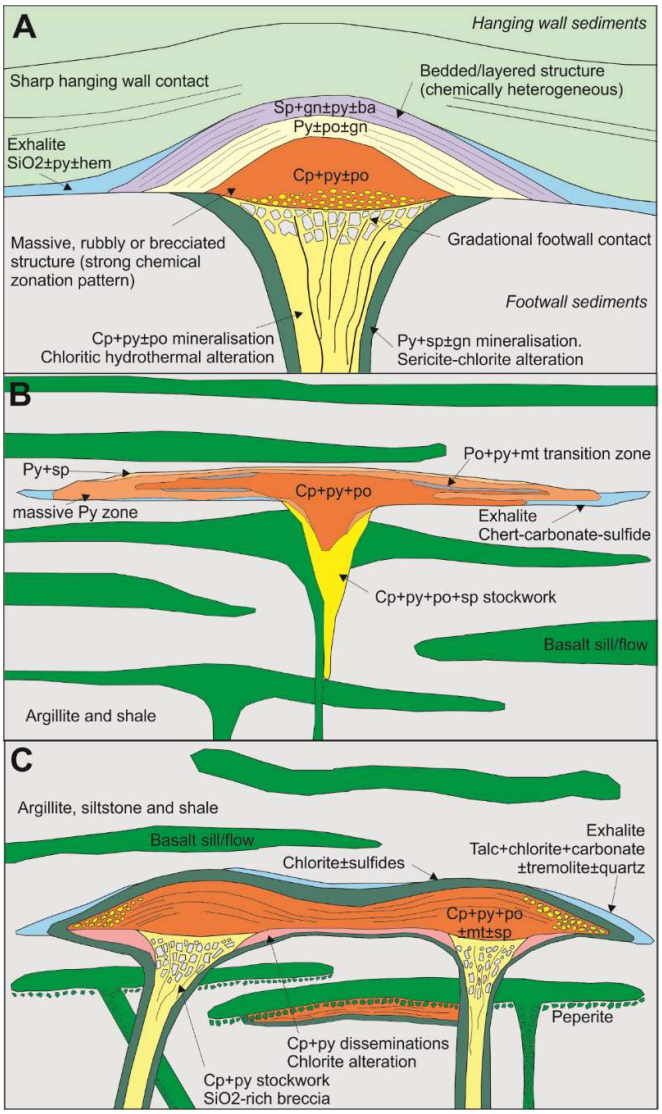

Figure 4.37. A. Typical VHMS model and zoning (Lydon, 1984). and **B.** VHMS zoning for a siliciclastic-mafic deposit (Galley et al., 2007). **C.** VHMS model for the DeGrussa deposit displaying characteristics of Besshi-type deposits and both sea floor and sub seafloor ore lenses.

4.5.2. Element associations

Major metals are hosted in likely minerals – copper in chalcopyrite, zinc in sphalerite, and lead in galena. More iron-rich zones are likely to reflect pyrite and marcasite dominant areas. Elevated cobalt (>800ppm) is likely associated with zones where traces of cobaltite are found as either inclusions in chalcopyrite and pyrite, as identified by Condon (2015), or rimming the mineral grains. Gold is associated with bismuth-tellurides and/or arsenopyrite (Condon, 2015). Silver has an association with copper and hence may form inclusions in chalcopyrite. Primary

molybdenite is associated with chalcopyrite mineralisation. Disseminated sulfides found throughout both the chlorite schist and talc-carbonate-schist rocks suggest a direct relationship with mineralising fluids as well as strong enrichments in trace element compositions such as Mo, Cd, Te, W and Re, although these trace element contents and mineral relationships appear inconsistent and may depend on the amount of sulfide. Huston et al. (2010) associates these elements with hydrothermal-magmatic fluids, however other authors (Franklin et al., 1981, Barrie and Hannington, 1999, Cloutier et al., 2015, Keith et al., 2016) indicate that most metals can be leached from the surrounding host sedimentary and volcanic rocks.

Cr and Ti are below detection limits through ore zones, but present in surrounding host rocks, and are inferred to reflect the geochemistry of the dolerite, basalt and mafic derived sedimentary host rocks. Ni is lower in the mineralisation compared with surrounding host rocks. Ore associated metals of Mo, Re, Sn and W are likely to be transported by hydrothermal fluids, along fault and shears where they are locally enriched proximal to the DeGrussa deposit. Elevated Cd may indicate substitution into sphalerite in place of Zn. Mn is often elevated on the lower contacts of the chlorite schist with ore. Mo in the deposit is likely to be derived from seawater, with fluid-seawater mixing at the seawater interface introducing the molybdenum into the ore assemblage. This scenario controls the presence of Mo in the Skouriotissa VHMS in Cyprus, with elevated Mo contents in pyrite interpreted to reflect fluid-seawater mixing associated with decreasing fluid temperatures and increasing oxygen fugacity (fO_2) (Keith et al., 2016).

4.5.3. Gold in the DeGrussa deposit

Gold in VHMS deposits may occur in four main mineralogical forms: 1. native gold, 2. electrum, 3. tellurides, and 4. “invisible” or refractory gold (Mercier-Langevin et al., 2010). Mineralisation throughout the Peak Hill, Fortnum and Horseshoe mining centres has focused on an epigenetic model for gold mineralisation. The Horseshoe Lights deposit was cited by Gillies (1988) to epigenetically overprint copper-rich sulfide mineralisation, with gold concentrated in the upper portions of the deposit.

In the DeGrussa deposit, gold appears to be associated with arsenopyrite, tellurides and electrum and widely dispersed throughout the ore lenses (Condon, 2015). Due to the disseminated nature of Au throughout the DeGrussa lenses, it is likely that gold is a primary ore mineral introduced during VHMS formation rather than a later overprinting epithermal event.

Sedimentary host rocks are inferred to be derived from the Au-rich Archean crustal rocks, as well as lower units of the Johnson Cairn Formation, hence are presumed to contain some quantity of Au. Leaching of sedimentary rocks may provide the source of gold in the DeGrussa deposit.

Au-rich VHMS deposits are found in modern day back-arc environments, such as the PACMANUS deposits of the Eastern Manus Basin, Papua New Guinea, with gold grades up to 58g/t (Herzig et al., 2003). At the Brothers VHMS, gold is found in all the Cu-rich chimneys (>30 ppm) with correspondingly high Bi (de Ronde et al., 2011). Similarly, primary Au is related to Bi-minerals, free gold and electrum in pyrrhotite-rich, high temperature deposits of the sedimented Escanaba Trough (Tormanen and Koski, 2005), with a second phase of Au precipitation occurring where pyrrhotite is oxidised and replaced by Fe oxyhydroxides, Fe sulfate and sulfur. The Bi-Au association at the Escanaba Trough is interpreted to be associated with interaction of hyudrothermal fluids with sediments (Tormanen and Koski, 2005). Ancient Au rich deposits include: Boliden in Sweden (Wagner et al., 2004), where Au is hosted in massive arsenopyrite (from which the Au is believed to be derived) and crosscut by later veins carrying a quartz-sulfosalt-sulfide assemblage; Currawong (Bodon and Valenta, 1995), where Au has 3 associations – 1. Au-Pb-As, 2. Au-Pb-Bi occurring in the footwall within chalcopyrite-chlorite stringer mineralisation, and 3. Au only, with Au forming within electrum.

Gold in VHMS deposit is suggested to form in a number of different ways (Mercier-Langevin et al., 2010):

1. Disseminated throughout massive or semi massive sulfide zones
2. High gold grades in stockwork zones, disseminations or in barite lenses around the massive sulfide lenses.

3. Remobilisation of gold into veins or veinlets peripheral to or within the VHMS deposit during deformation and metamorphism.
4. Late stage hydrothermal remobilisation.

Some deposits are thought to have formed in shallow submarine volcanic-dominated environments and have distinctive epithermal characteristics suggesting a hybrid VHMS-epithermal classification (e.g. Horseshoe Lights, (Gillies, 1988)) or even as intermediates between VHMS and porphyry (Mercier-Langevin et al., 2010).

4.5.4. Temperature and pH

Using the classification scheme of Large (1977), DeGrussa fits best into the Cu-rich model with minor Zn and negligible Pb. As a proxy for DeGrussa pyrite, chalcopyrite, pyrrhotite ± magnetite mineralisation assemblage, the best fit model (Fig. 4.38) indicates the temperature of hydrothermal vent fluids can be estimated at between 250-350°C, along a descending temperature gradient, although the reality probably involves fluctuating temperatures. This is consistent with observations of magnetite stability in the central, hot (>300°C) upwelling zones of the deposit.. The irregular zoning of the DeGrussa deposit, as well as the intergrown nature of all minerals indicates either 1. there were changing fluid compositions and temperatures (both hotter and cooler) throughout the growth of the deposit, 2. Mixing of two different metal bearing fluids (i.e. magmatic-hydrothermal + seawater derived hydrothermal), or 3. replacement of primary minerals during subsequent fluid pulses or metamorphism. However, it is important to note that these are only examples as the exact fluid compositions and conditions are not known. The suggested pH of 5-7 for the DeGrussa sulfides can be represented on the mineral stability fields provided by Hannington et al. (1999) at constant temperature of 250°C and varying pH and fO_2 (Fig. 4.38). Although this graph was developed for the Kidd Creek deposit, the mineral assemblage preserved is similar to that at DeGrussa.

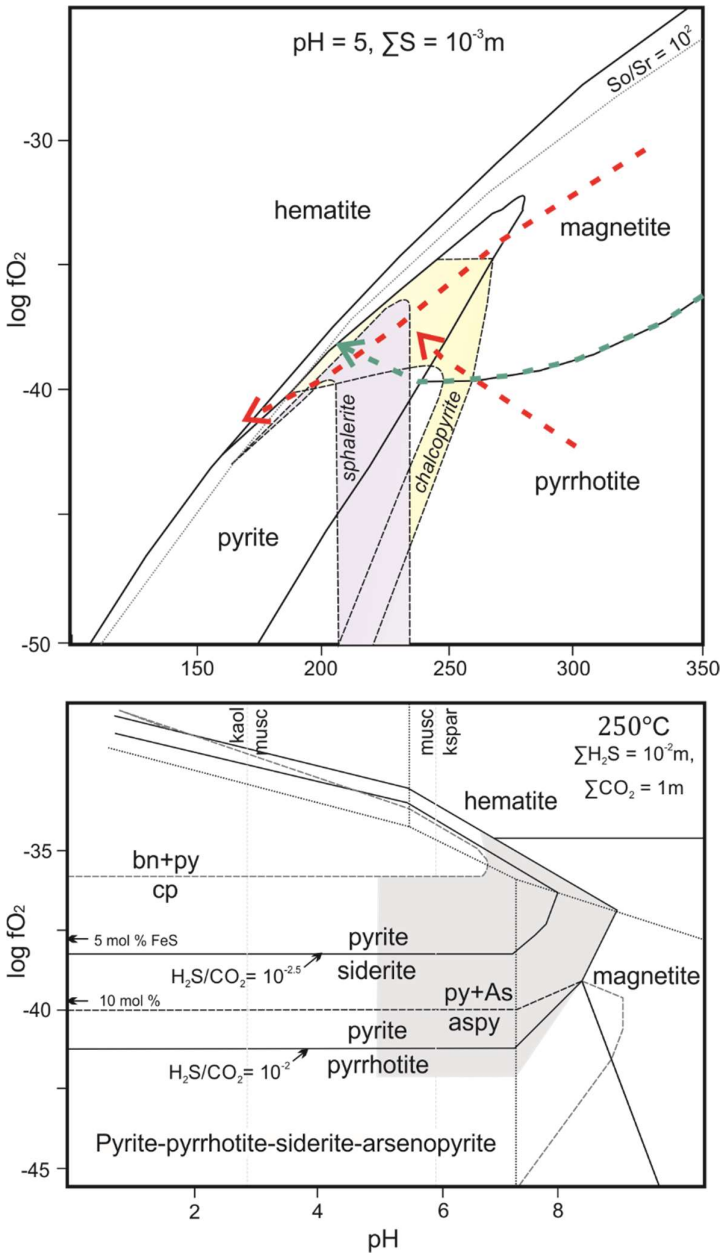

Fig. 4.38 **A.** A 1 M NaCl solution at a pH of 5, $\sum S = 10^{-3}M$ (adapted from Large (1977)) can precipitate the observed assemblage of DeGrussa sulfides at temperatures of >250°C. Red dotted lines show one scenario for the formation of sulfides from two potential fluid compositions, and green dotted line shows a second scenario which allows both magnetite and pyrrhotite to be precipitated together. It is likely that there were changing fluid compositions and temperatures during the growth of the deposit. **B.** The DeGrussa mineralisation assemblage is shown as a shaded area for pH 5-7 at constant 250°C on a stability diagram adapted from Hannington et al. (1999).

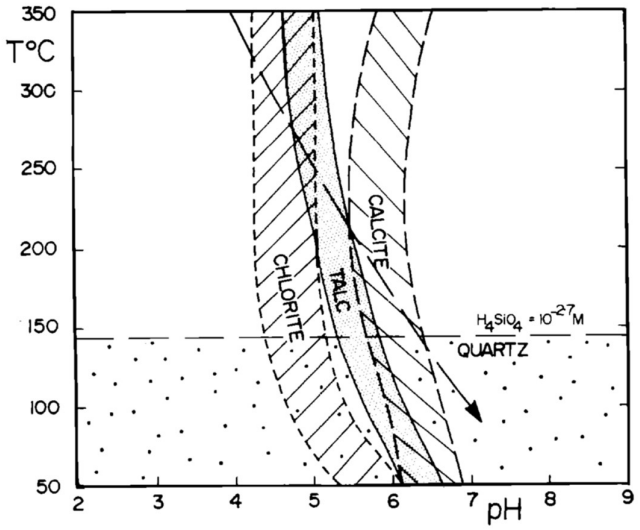

Figure 4.39. pH vs. temperature for stability of different gangue minerals associated with VHMS mineralisation. The presence of chlorite, talc, quartz and carbonate suggest pH varied between 5 and 7.

The alteration mineral assemblage consisting of sericite, chlorite, epidote, quartz, carbonate, talc and stilpnomelane (stable at temperatures of <500°C (Miyano and Klein, 1989)) indicates a pH ranging from 5-7 consistent with studies by Large (1977) (Fig. 4.39).

4.5.5. Hydrothermal alteration

The presence of strong hanging wall alteration, similar in style and intensity to footwall alteration is one characteristic described by Doyle and Allen (2003) to be associated with sub seafloor replacement style VHMS deposits. In this respect, the DeGrussa deposit has chlorite schist envelopes most of the ore deposit, and the talc-carbonate schist is inconsistent, but present in both the hanging wall and footwall of the deposit.

The chlorite schist is one of the most consistent features along the margins of the massive sulfide ore lenses. Bodon and Valenta (1995) interprets the Currawong VHMS of NSW to have formed in response to upwelling of hydrothermal fluids along faults and deposition of mineralisation replacing existing sedimentary and volcanogenic rocks in the sub seafloor environment (Fig. 4.40). As part of this model, chlorite and quartz-sericite-carbonate alteration

halos are interpreted to form in response to interaction between the hydrothermal fluid, unconsolidated rock and seawater within the sub seafloor rocks (Bodon and Valenta, 1995). The chlorite schist at DeGrussa probably formed in the same way, however, the presence of sea floor textures (chimneys) in some parts of the DeGrussa deposit indicates that at least some of the sulfide was deposited onto the seafloor. Mason (2011) suggests that chlorite and talc-chlorite schist, was invaded by a K-S-Cu-Mo-bearing hydrothermal fluid generating local patches of sericite + sulfides (chalcopyrite >> molybdenite > pyrite) which replaced the chloritic assemblage. Textural equilibrium between sulfides and titanite at the margins of the sulfidic aggregates suggests that all minerals may have formed more-or-less synchronously under the same pressure-temperature-composition (P-T-X) conditions (Mason, 2011).

It is possible that there was an anhydrite exhalite which was not preserved due to the retrograde solubility of anhydrite as convecting fluids through the sulfide mound cooled. The fine-grained units of sulfide, and brecciated sulfide may be the result of a dissolved anhydrite cap and matrix. If this was the case, the sulfide 'sand' may have been redistributed as sedimentary bands into distal parts of the ore deposit leaving textures such as that seen in Conductor 5 (Fig 4.7), and may form the sandy pyrite ore of the Horseshoe Lights Cu-Au VHMS in the western parts of the Bryah Basin. The TAG deposit along the Mid-Atlantic Ridge is characterised by anhydrite blocks at the base of black smoker chimneys with abundant coarse-grained disseminated pyrite and chalcopyrite which weathers out as the anhydrite dissolves Hannington et al. (1998). Anhydrite in the TAG deposit is stable at temperatures between 300-400°C (Hannington et al., 1998). However, no anhydrite-style replacement features were identified in the detailed mineralogical studies of Condon (2015). Conversely, if there was little to no SO_4 available in the oceans, anhydrite is unlike to precipitate. Ancient basins in which reduced anoxic conditions prevail would also favour anhydrite-free deposits.

The talc-chlorite-carbonate schist, and similarly composed units may represent areas of high heat flow in the DeGrussa deposit, as supported by its high temperature metal assemblage dominated by chalcopyrite and pyrite, and may result by altering a precursor rock of unknown

composition in the hanging wall and footwall. Similar talc-carbonate deposits are found associated with hydrothermal venting in the Guaymas basin, California (Lonsdale et al., 1980) or Logatchev on the Mid-Atlantic ridge (Melekestseva et al., 2013) interpreted to be alteration of ultramafic host rocks. In the northern trough of the Guaymas basin, hydrothermal sites are located at the bottom of horst blocks/ fault escarpments and talc deposits are identified as either a hydrothermal precipitate or, more likely, the result of hydrothermal alteration of an aluminium-poor mafic rock such as peridotite (Lonsdale et al., 1980). Ancient deposits which preserve a talc-carbonate unit include the Outokumpu Cu-Co-Zn deposit in Finland (Peltonen et al., 2008), and the Dergamysh, Ivanovka and Iskinino deposits of the Urals (Melekestseva et al., 2013), where talc is interpreted as an alteration product of ultramafic rocks. The presence of talc-carbonate and chlorite-schist in the Currawong deposit of New South Wales (see above), may be more similar to that of DeGrussa, given the sub seafloor location, and indications that temperature may be the control it's deposition.

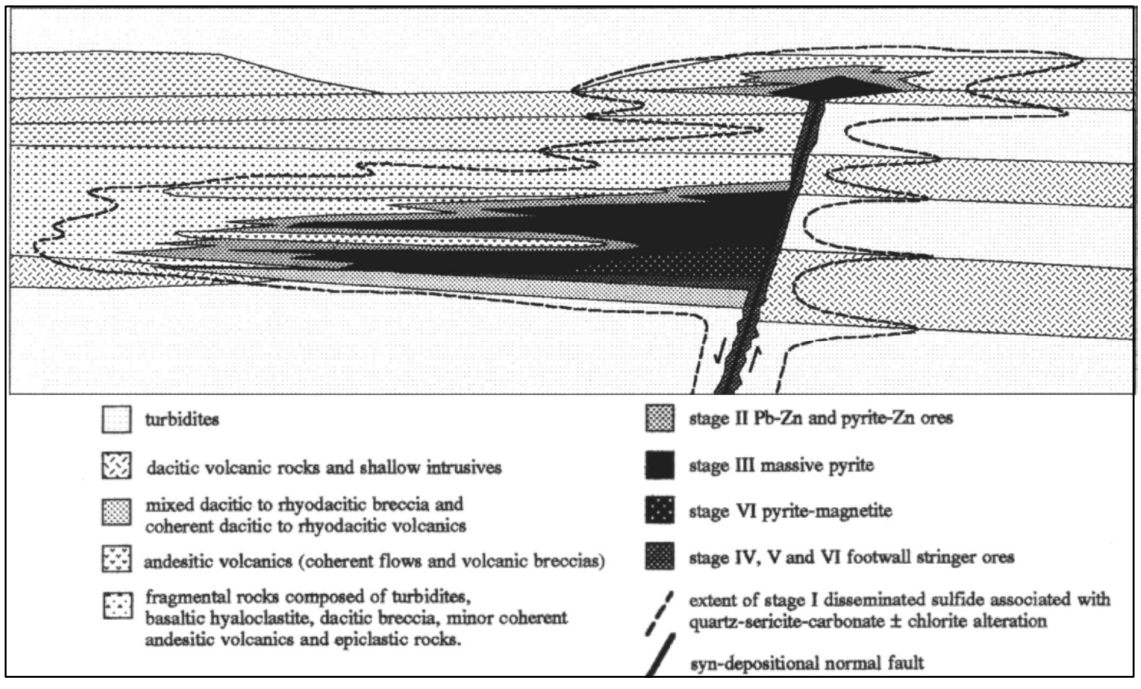

Figure 4.40. Schematic representation of the formation of the Currawong sub seafloor deposit, New South Wales (Bodon and Valenta, 1995). A similar mode of formation may have been active in the DeGrussa deposit.

Hematite and jasperlitic horizons within the footwall of the ore lenses, become increasingly present to the east (Adamczyk, 2013) indicating that an oxidised hydrothermal component was present at or slightly before the deposition of mineralisation or the hydrothermal fluid responsible for the hematite alteration was an oxidised fluid. The narrow and very localised feeder zones to DeGrussa mineralisation may have restricted the movement of reduced fluids, cross cutting the oxidised units, although evidence of this has not been observed. Interaction with sea water throughout the DeGrussa host sequence is indicated by the presence of pervasive carbonate alteration throughout the groundmass of sedimentary rocks. As described in chapter 3, basalts and dolerites display calcite veining and some pervasive groundmass calcite alteration on the edges of intrusions, entrained into the mafic rocks during emplacement. The pervasive carbonate throughout the host rocks may be due to the degassing of dolerite sills, but further work including multi-element geochemistry, carbon and oxygen isotopes would help to clarify the source of carbonate throughout the deposit and surrounding host rocks.

Whether the prehnite-pumpellyite facies metamorphism (250-300˚C, 2-7kbars) and greenschist facies metamorphism (300-450˚C, 1-4kbars) is associated with hydrothermal alteration related to mineralisation or not, the mineralogy of the DeGrussa deposit suggest high temperatures for deposition of mineralisation (pyrite and chalcopyrite at 250-350˚C). The lack of low temperature minerals (e.g. galena, sphalerite, barite), and the cyclical nature of pyrite, pyrrhotite and chalcopyrite dominant ore horizons, with a magnetite-rich core suggests that although deposit temperatures fluctuated, high hydrothermal-magmatic fluid temperature (>300°C) was maintained. Additionally, the occurrence of only minor galena suggests that there could be a lack of Pb in source hydrothermal fluids. Emplacement of the DeGrussa deposit, from multiple hydrothermal vents is represented schematically in figure 4.37. There is no exhalative unite preserved at DeGrussa..

4.5.6. Deposit morphology and emplacement

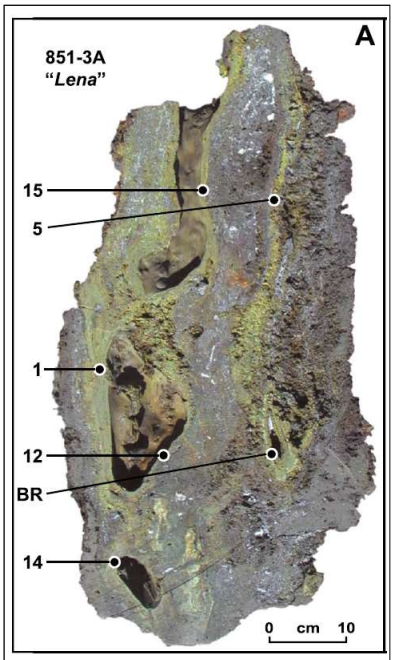

Figure 4.41. Chimney from the present day Brothers VHMS, Lau Basin. Similar chimney textures are seen in the DeGrussa deposit, reinforcing its VHMS character and sea floor depositional environment (Berkenbosch et al., 2015, Jan M. Peter and Scott, 1999).

The orientation (southwest-northeast) of the ore deposit is consistent with the regional deformation and may have reduced the thickness of the original deposit although preservation of conduit material suggests that deformation is relatively modest. Alteration halos are relatively thin, with talc-chlorite-carbonate schist lensing inconsistently along the upper and lower contacts of the ore. Chlorite schist forms a relatively thin but consistent alteration halo around the ore deposit, and primary features, such as seafloor breccia are retained. Primary angular sulfide breccia in the hanging wall of Conductor 1, as well as chimney structures and textures similar to that seen the Brothers VHMS deposit of the Lau Basin (Berkenbosch et al., 2015), massive sulfide of Middle Valley (Ames et al., 1993) and the Urals massive sulfide deposits of Russia (Maslennikov et al., 2009, Maslennikov et al., 2013) are evident in the C1 ore lens (Fig. 4.41), and considered to represent sulfide deposition directly into the sea floor environment. Typical chimney structures show mineralogical banding due to incremental growth (Galley et al., 2007). Conversely, chimneys may form from fragments cemented by later sulfide growth during mound collapse and subsequent invasion by hydrothermal fluid (Galley et al., 2007), and may explain the infiltration of chalcopyrite around pyrite clasts in the DeGrussa deposit.

Observations of sub seafloor deposition is evident by replacement style textures in the C1 and C5 ore lenses, as well as basalt breccia with a former chloritic matrix now replaced by sulfide minerals. Condon (2015) built on the textures observed in this study, interpreting the deposit to form predominantly by sub seafloor replacement of host rock and subsequent re-deposition by gravity flows into clastic ore lenses, which included accessory rock fragments collected by the parent sediment gravity flows during transport. A diversity of textures across the four ore lenses,

with some direct sea floor deposition is plausible due to the number of vent sites (as identified in section 4.2.4) and sea floor textures.

The exact depth of formation for the DeGrussa ore deposit cannot be determined, however the presence of turbiditic sedimentary host rocks and mass flow breccia suggests that the deposit formed below wave base in a deep sub-basin that was likely undergoing active subsidence. Present day analogies could include the Red Sea rift, or the Guyamas basin. Most present day VHMS deposits form in water depths of greater than 1000m (Binns, 2004).

Ore lenses were altered in shape, structure, composition and texture during regional metamorphic and deformation events. Since deposition, the DeGrussa mineralisation, has been intruded by several phases of dolerite (see chapter 3) and truncated by three faults – the Shiraz, Cabernet and Merlot faults. Where ore is in contact with these faults, sulfides are fragmented or sheared. Supergene weathering has affected the ore in proximity to the faults, leading to the formation of chalcocite and bornite on the rims of primary sulfide minerals.

Condon (2015) contrasts DeGrussa with modern an ancient VHMS systems which typically form by a sequence of early Stage 1 deposition of pyrite, sphalerite and quartz followed by pyrrhotite and chalcopyrite replacement at higher temperatures in both modern and ancient VHMS systems (Shanks III and Thurston, 2012). Incorporating the observations from work on the ore mineral composition and paragenesis by Condon (2015), the general sequence of mineral formation may be as follows:

1. Host rock mineral deposition;
2. Hydrothermal venting of metal-bearing fluids depositing pyrite + sphalerite + chlorite, talc (minnesotaite) and stilpnomelane during primary deposition;
3. Chalcopyrite + pyrrhotite + pyrite during primary deposition, including magnetite + pyrrhotite above multiple vents (evidence of feeder zones)
4. Cyclical pulses of hydrothermal fluids of varying temperatures, resulting in the distribution of mineral assemblages seen in the deposit;

5. Interaction of hydrothermal fluids with seawater at the hydrothermal fluid-seawater interface in chimneys, or the sea floor results in the precipitation of lower temperature minerals such as marcasite, galena, and trace elements such as Mo, Sb, W, Sn, which are likely to be entrained into the hydrothermal mineralising fluid as a result of seawater circulation.
6. During deformation and metamorphism of the deposit, pyrite + pyrrhotite are recrystallised and accompanied by extraction of trace elements and inclusions such as galena and sulfosalts. Chalcopyrite + sphalerite are remobilised through the deposit, and galena precipitated with quartz-carbonate veins.
7. Siderite + digenite precipitation during weathering alteration as well as supergene minerals including chalcocite and bornite.

4.6. Further work

This thesis is a preliminary study of the DeGrussa geology and mineralisation, and this chapter helps to put the context to the geochronology and geological evolution of the deposit. Additional work that would be beneficial may include:

- Detail studies of the sulfides with the aim to constrain the fluid sources, temperature, oxygen fugacity and pH, responsible for mineralisation.
- Multi-element geochemistry, carbon and oxygen isotopes to clarify the source of carbonate throughout the deposit, talc-carbonate schist and surrounding host sedimentary rocks and dolerite.
- Studies of the Au distribution throughout the deposit, its metal relationships and source.

4.7. Conclusion

The DeGrussa deposit displays mineral zonation atypical of most VHMS deposits, perhaps evident of its replacement style of formation. Magnetite forms in the hottest, central core of the

deposit in association with pyrite and lesser chalcopyrite and pyrrhotite. Sphalerite and galena form in rare horizons throughout the ore lenses.

The presence of seafloor breccia and chimney structures indicates that the DeGrussa deposit formed from both direct seafloor hydrothermal venting, as well as sub seafloor replacement, with the later likely to be the dominant mode of emplacement. Emplacement of hot, hydrothermal-magmatic, mineralising fluids, via fault controlled feeder structures (similar to the formation of the Currawong deposit) led to replacement of existing sedimentary and basaltic rocks at temperatures of 250-350°C and pH of 5-7. The lack of sulfate minerals in the ore, but the presence of peripheral jasper, suggests that DeGrussa either formed in either: 1. an reduced, oceanic sub-basin with an oxic top layer, or 2. from low-Ba, highly reduced fluids that were emplaced into a suboxic-oxic water column, which forms the barite-poor Cu-Zn deposits in modern mid-ocean ridge basins. Hydrospheric conditions of the deep basin water were Fe-rich and low sulfate, leading to the high content of Fe-rich minerals (pyrite, minnesotaite, stilpnomelane, Fe-Mg chlorite). The lack of a sulfate bearing and the lack of a sulfate-bearing exhalite although the reduction of seawater SO_4 during hydrothermal circulation may precipitate anhydrite at high temperatures (> 300°C) which was dissolved as the hydrothermal system cooled.

Chapter 5. Geochemistry

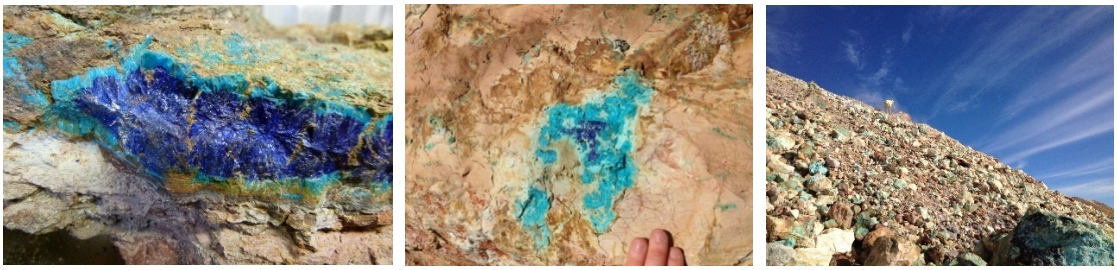

Chrysocolla and azurite, DeGrussa open pit

5.1. Introduction

VHMS deposits can form in a variety of tectonic environments including oceanic ridges, thickened oceanic crust, sedimented-oceanic ridges and continental margin rifts, nascent arcs, primitive volcanic arcs, mature volcanic arcs and continental arcs (Barrie and Hannington, 1999). Identifying which environment a deposit has formed in, can be difficult especially in ancient, deformed and metamorphosed terranes. Major and trace element geochemistry can assist in identifying rocks of different tectonic settings.

Rocks of the Bryah Group, in particular the Narracoota Formation, have most recently been interpreted to represent a fragment of oceanic plateau accreted to the Archean Yilgarn Craton margin during oceanic basin closure between the Pilbara and Yilgarn Cratons (Pirajno, 2004). Previous works however have suggested a range of tectonic environments from intracontinental basins to back arc rifts (Bunting et al. (1977), Gee (1979), Hynes and Gee (1986), Tyler and Thorne (1990), Windh (1992), Gee and Grey (1993), Myers (1993), Martin (1994), Pirajno et al. (1994), Myers et al. (1996), Pirajno (1996), Pirajno and Occhipinti (2000), and Pirajno et al. (2000)). Myers et al. (1996) and Hynes and Gee (1986) suggested that the Bryah Group could represent a back-arc formed during south directed subduction beneath the northern margin of the Yilgarn Craton. Occhipinti et al. (2004) suggested that remnants of cordilleran-like magmatic suites related to this subduction, may be buried beneath the Edmund and Collier Basins, to the north of the Bryah and Padbury Basins. Geochemical studies by Pirajno (2004) of the Narracoota

Formation identified rocks that were likely part of an ancient oceanic plateau, created by a 2.0 Ga mantle plume with REE patterns indicating the similarity to modern oceanic plateaux.

5.1.1. Aims

This chapter investigates the geochemistry of the mafic rocks and it's relationships to known mineralisation and discusses possible tectonic settings. Here the geochemistry of the DeGruss mafic rocks and their relationship to the Killara, Narracoota and Johnson Cairn Formation, and to known mineralisation It will:

1. Identify any alteration affecting the rocks,

2. Analyse and interpret the major and trace element geochemistry of mafic rocks within the DeGrussa host sequence.

3. Compare the mafic rocks in the DeGrussa host sequence, with regional mafic rocks of the Yerrida and Bryah Groups, and

4. Determine the likely tectonic setting for DeGrussa mineralisation and the larger Yerrida and Bryah Groups.

5.2. Previous Studies

Most geochemical studies in the Yerrida, Bryah and Padbury Groups have been undertaken by the Geological Survey of Western Australia. These have focused on distinguishing different rock units and the tectonic environment using geochemical analysis. Rocks of the Narracoota Formation identified as komatiite-picrite to basalt and basaltic andesite by Pirajno et al. (2000), with a small number of samples classified as bonninite and andesite.

The first detailed study of the Narracoota Formation mafic rocks was undertaken by Hynes and Gee (1986) in which several transects of the unit were made across the Bryah Group for geochemical analysis. Hynes and Gee (1986) interpreted the Narrocoota Formation mafic rocks in the south are a chemically uniform succession of tholeiites, differing from MORB only in their slightly low Ti/Fe and Zr/Fe. Mafic rocks associated with the ultramafic schists have up to 58%

SiO_2 and are poor in Ti and Zr, interpreted to resemble some boninites of the western Pacific (Hynes and Gee, 1986, Cranney, 2011).

Jeffery (2013) completed a geochemical study of regional basalts comparing them to the geochemical signature of basalts at DeGrussa. Results indicate that basalt surrounding the DeGrussa deposit are comparable to Killara Formation and part of an REE enriched group of rocks forming the basal part of the Narracoota Formation, rimming the Bryah Basin and extensively underlying the Yerrida Basin. Additionally, geochemistry for the Narracoota Formation is the same as that of the Killara basalts. Samples of the Killara Formation collated by the GSWA include all basalt and dolerite cropping out in the Yerrida Basin and could include post basin mafic dykes and sills.

Local mine scale geochemistry was completed for the Fortnum region (Gotthard, 2005), and Horseshoe Lights (Gillies, 1988). A co-funded GSWA/Sipa Resources drillhole THD001 (Mueller, 2011) (see chapter 3) identified unknown mafic rocks within Johnson Cairn Formation stratigraphy that were geochemically analysed and compared to the Killara Formation basalts and that of the Johnson Cairn basalt at DeGrussa (Drill hole DGDD347, see Ch. 3 Section 3.2.4.). Studies undertaken and funded by Sandfire Resources NL include a geochemical study of the mafic rocks of the Narracoota Formation (Jeffery, 2013), that of Adamczyk (2013) and the Loiseau (2014) study of the differentiation within the DeGrussa dolerites.

Loiseau (2014) collected 180 samples of dolerite and classified them as either equigranular or ophitic. Equigranular dolerites were richer in Ti, and suggested to be a more primitive magma. Ophitic dolerites were richer in Zr indicating a more evolved magma. This study identified that magmas were from a single magmatic source and insitu differentiation of the intrusions occurred. A classification diagram by Loiseau (2014) highlights 3 different phases present in each sill: 1. Primitive phase; 2. Differentiated phase (Zr-rich phase), and 3. Mafic Ti-rich phase.

A preliminary internal report by Cranney (2011) utilised a number of geochemical data from GSWA reports in an effort to interpret the host rock unit and comparison with the Narracoota and Killara Formation rocks. Cranney (2011) noted the location of boninitic rocks along the trace of

both the Murchison and Jenkin Faults and interpreted that rifting would have occurred perpendicular to these trends (Figure 5.1). Samples from the Narracoota and Killara Formations were reanalysed by the GSWA in 2011 and analysis and discussion of regional trends are presented in section 5.9.

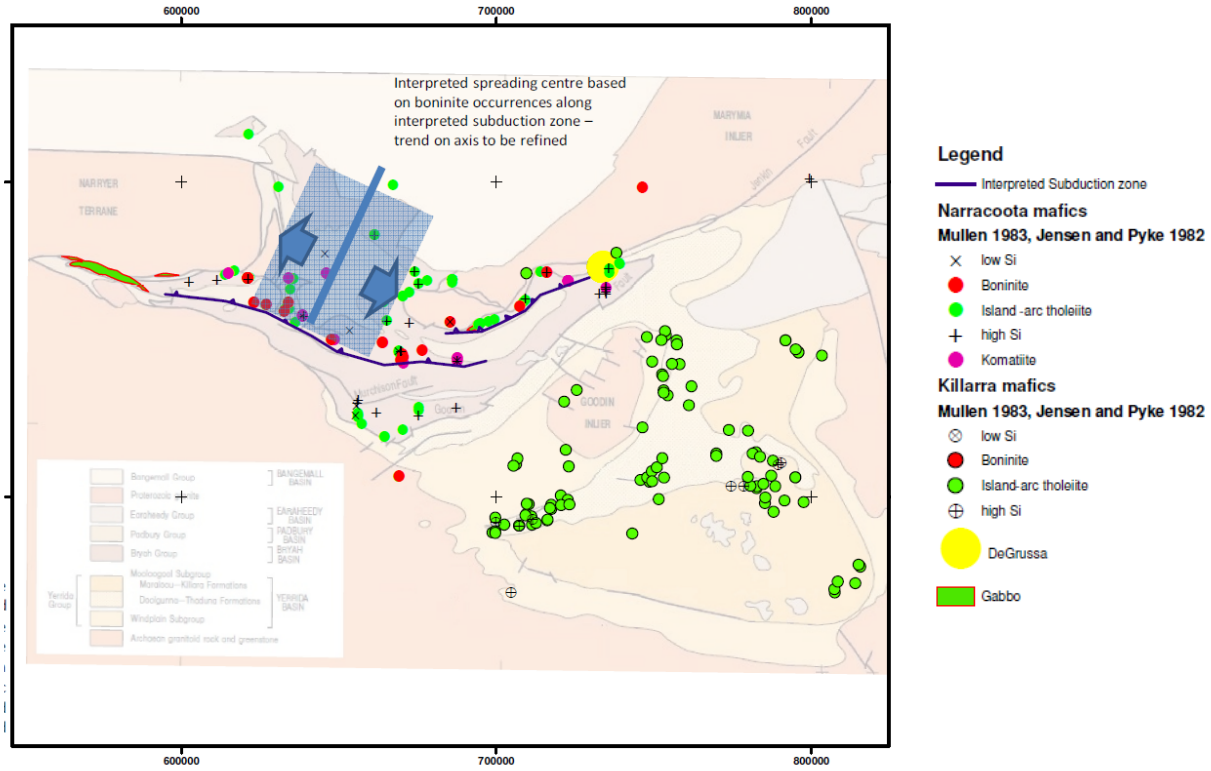

Figure 5.1. Interpretation of the Bryah Basin with relation to boninites, subduction zones and spreading centres according to Cranney (2011). Cranney (2011) suggests that a lack of data precludes accurately locating the interpreted subduction zone, especially to the south, however the boninites are interpreted as closer to the trench that all other volcanic rocks. Volcanic rocks at Fortnum and Horseshoe Lights are interpreted as distal from the trench.

5.3. Sampling and Analytical Methods

A total of 52 mafic rock samples from unweathered drill core at DeGrussa, 3 samples from the Johnson Cairn Formation below DeGrussa, 3 samples from Archean basement proximal to DeGrussa, and 12 samples from regional surface samples of Killara and Narracoota Formaton were selected for geochemical analysis. Figure 5.2 shows the distribution of samples across the Bryah and Yerrida Basins. Samples collected were as fresh as possible from available drill holes and were approximately 10-30cm lengths of quarter core. Schistose rocks were often the only samples available in the vicinity of Horseshoe Lights and Fortnum due to high levels of deformation in those areas. Geochemical results were calculated to 100% (i.e. calculate to 100% using the formula: (element/sum(all elements))*100. See also Appendix 5.1).

Geochemistry from the DeGrussa dolerites and basalts (Table 5.1, 5.2), as well as the Killara Formation and Narracoota Formation mafic rocks were compiled from GSWA and open file mine department reports, this resulted in 38 samples of Killara Formation and 46 samples of Narracoota Formation being used in this study. 26 samples of mafic rock were compiled from the THD001 study of Mueller (2011). Samples with >55% SiO_2 were removed from the dataset. Descriptions of mafic rock samples from DeGrussa, the Narracoota Formation and the Killara Formation are located in Chapters 2 and 3. A full dataset can be found in Appendix 5.3.

Samples collected at DeGrussa were contrasted with previous data from GSWA reports and published papers including studies by Hynes and Gee (1986), Gillies (1988), Pirajno and Adamides (1998), Adamides (1998), Pirajno et al. (2000), Pirajno and Adamides (2000), Sheppard et al. (2004), Gotthard (2005) and Muller (2011), and provided in Appendix 5.1. The Johnson Cairn Formation is split into two – that of the DeGrussa footwall, and that from THD001(Mueller, 2011).

DeGrussa sample analytical methods: Major elements were analysed using the X-ray fluorescence (XRF) facility at the University of Tasmania. Rock samples were crushed using a steel jaw crusher, then ground in a tungsten-carbide ring mill to produce a rock powder (<200μm). Minor and trace elements were analysed by Pico-Trace Solution ICP-MS. Samples

were analysed over 3 separate analytical runs on a 7700x Agilent ICP-MS instrument with an active He collision cell. Results were compiled from 2 sets of data so that known interferences could be adequately dealt with and analytical errors minimised. All concentrations and detection limits quoted are in ppm in the whole rock, all analytical errors are quoted in % value of the concentration (Ian Little, pers. comm, 2011).

Geochemical plots were generated using IoGas-64 v 5.2 by methods provided by cited references. Detection limits for data can be found in Appendix 5.2.

GSWA data: There is limited sampling in this study of the Killara and Narracoota Formation mafic rocks, but ample collated from GSWA data. The quality of the GSWA data is questionable. The newest data (analysed 2011) was provided directly by the GSWA and utilised more modern techniques on the original samples (before c. 2000). Some locations and rock types are unknown. These data are used for geochemical maps of section 5.7 and supplement the known data by giving an indication of the high geochemical variability of the Narracoota and Killara Formation basalts and dolerites, as well as allowing identification of geochemical trends on a basin wide scale, not only restricted to the DeGrussa area. Rocks of unknown type are not used in major and trace element bivariate plots. The following steps were undertaken to make best use of the data:

1. Where the same sample had previously been analysed and provided in existing explanatory notes, location and rock type were correlated. Where these could not be resolved, location was left blank (i.e. no co-ordinates), and rock type was listed as 'Unknown Mafic' for either Killara or Narracoota Formations. It is presumed that the majority of these rocks are basalt or dolerite due to past studies focusing on them.
2. For the Narracoota Formation, REE trace element patterns were compiled and samples were subdivided into one of four categories: Type 1 - most MORB-like patterns (nil to slight elevated REE), Type 2 -LREE enriched, Type 3 - LREE depleted, and Type 4 - HREE depleted.
3. Maps could then be made across the basins using Iogas and MapInfo to demonstrate each elements distribution as well as the type of tectonic setting based on the REE patterns.

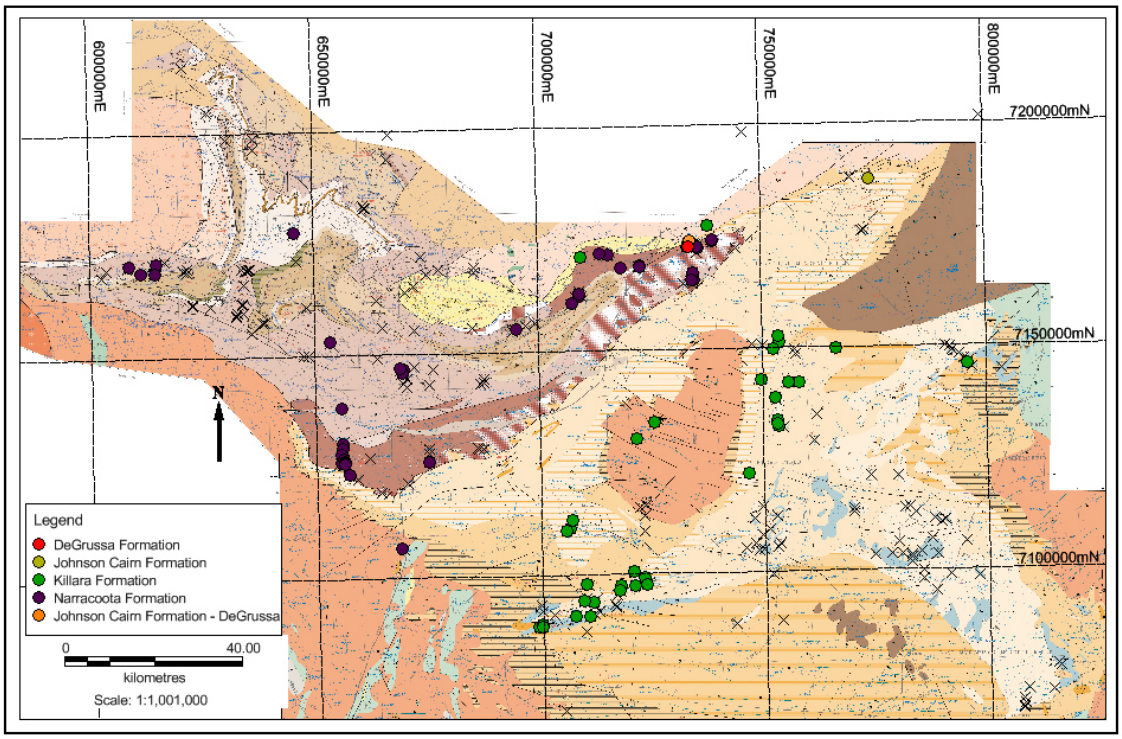

Figure 5.2. Approximate locations of samples compiled from across the Bryah and Yerrida Groups – DeGrussa and Footwall Johnson Cairn Formation (this study), Killara Formation (Pirajno and Adamides, 2000), Narracoota Formation(Hynes and Gee, 1986)(Pirajno et al., 2000), Johnson Cairn Formation (Mueller, 2011). Black crosses show location of samples of unknown composition not plotted in this study.

Table 5.1 Major element data collected for this study for DeGrussa and regional rocks. Analysis by XRF (Italics not plotted).

Sample #	Classification	SiO2 %	TiO2 %	Al2O3 %	Fe2O3 %	MnO %	MgO %	CaO %	Na2O %	K2O %	P2O5 %	Loss %	SO3 %	S %	Total
DeGrussa															
DGMH006	Dolerite	50.7	1.47	13.18	16.43	0.25	4.25	7.31	3.64	0.24	0.16	2.38	0.09		100.02
DGMH010	Dolerite	50.9	0.63	15.55	9.72	0.16	7.19	9.43	3.22	0.39	0.07	2.64	0.03		99.89
DGMH013	Dolerite	43.04	0.97	13.11	14.53	0.23	7.44	13.89	0.83	0.22	0.09	5.69	<0.01		100.04
DGMH017	Dolerite	50.16	1.2	14.1	14.37	0.22	6.38	7.56	3.43	0.08	0.12	2.67	0.02		100.28
DGMH020	Dolerite	49.29	0.73	12.97	11.18	0.19	8.81	12.51	2.27	0.18	0.06	1.99	0.02		100.17
DGMH021	Dolerite	50.46	1.28	13.69	14.39	0.21	6.14	7.65	3.35	0.11	0.16	2.47	0.03		99.9
DGMH030	Dolerite	51.37	1.2	13.99	13.44	0.2	5.33	8.79	3.12	0.21	0.12	2.16	0.2		99.94
DGMH041	Dolerite	50.17	1.18	13.77	14.06	0.22	6	8.48	3.33	0.14	0.12	2.46	0.09		99.94
DGMH042	Dolerite	51.59	1.34	14.25	14.77	0.2	4.93	6.78	3.96	0.19	0.13	2.33	0.19		100.47
DGMH043	Dolerite	48.7	1.56	13.78	16.73	0.25	4.44	7.85	3.3	0.23	0.17	2.52	0.17		99.53
DGMH044	Dolerite	50.74	1.49	13.07	16.2	0.23	4.41	8.03	3.04	0.27	0.15	2.13	0.12		99.76
DGMH045	Dolerite	47.05	1.61	12.9	17.82	0.24	4.94	9.89	2.55	0.21	0.11	2.22	<0.01		99.55
DGMH046	Dolerite	50.48	0.89	15.64	11.76	0.18	6.38	7.48	3.54	0.31	0.08	2.78	0.03		99.51
DGMH047	Dolerite	47.38	0.66	13.38	11.46	0.19	9.72	12.44	1.87	0.15	0.06	2.5	0.02		99.8
DGMH048	Dolerite	49.18	2.6	12.31	18.65	0.3	3.25	7.5	2.36	0.46	0.24	3.17	0.02		100.02
DGMH049	Dolerite	50.63	0.77	14.56	11.1	0.18	7	10.86	2.92	0.2	0.08	2.32	0.04		100.61
DGMH050	Dolerite	50.91	1.08	13.66	13.59	0.21	6.43	8.64	3.37	0.2	0.11	2.11	0.11		100.32
DGMH058	Dolerite	50.45	1.17	13.62	14.07	0.2	5.97	10.54	2.28	0.35	0.12	1.92	0.02		100.67
DGMH060	Dolerite	52.29	2.2	12.62	17.13	0.27	2.78	6.09	3.62	0.49	0.21	2.59	0.15		100.29
DGMH062	Dolerite	49.8	1	13.61	12.78	0.2	7.69	11.13	2.38	0.14	0.09	1.9	<0.01		100.73
DGMH063	Dolerite	50.03	1.09	13.49	13.6	0.23	6.47	8.29	3.39	0.38	0.11	2.86	0.12		99.95
DGMH065	Dolerite	50.59	0.93	13.63	12.55	0.2	8.13	8.68	3.43	0.03	0.08	2.3	0.07		100.56
DGMH070	Dolerite	44.93	1.35	16.62	17.14	0.25	5.33	3.37	2.49	0.07	0.17	8.2	0.07		99.9
DGMH080	Basalt	50.37	1.57	12.23	17.9	0.22	4.99	7.73	2.41	0.09	0.08	2.53	0.46		100.1
DGMH084	Basalt	54.12	0.248	15.06	10.47	0.161	6.29	8.14	3.65	0.16	0.043	2.24	<0.01	0.01	100.58
DGMH096	Dolerite	49.30	1.251	14.31	14.28	0.181	7.32	4.26	2.30	0.68	0.124	5.52	0.19	0.49	99.72
Narracoota - Regional															
DGMH147	Basalt	49.35	0.797	14.93	10.93	0.170	8.88	9.15	3.18	0.08	0.075	2.81	<0.01	0.00	100.36
FTMH003c	*Ultramafic*	*79.81*	*0.259*	*10.66*	*2.12*	*0.030*	*0.98*	*0.51*	*0.56*	*2.62*	*0.055*	*1.86*	*<0.01*	*0.00*	*99.47*
FTMH004	*Basalt*	*47.22*	*0.862*	*12.95*	*9.11*	*0.166*	*5.38*	*9.21*	*4.06*	*0.02*	*0.092*	*9.29*	*0.77*	*1.92*	*99.10*
FTMH006	*Basalt*	*57.19*	*0.614*	*16.72*	*7.51*	*0.068*	*5.16*	*2.18*	*7.03*	*0.03*	*0.134*	*3.22*	*0.01*	*0.03*	*99.87*
FTMH010	*Ultramafic*	*38.65*	*0.104*	*6.26*	*7.84*	*0.153*	*20.54*	*8.61*	*0.00*	*0.00*	*0.010*	*17.57*	*<0.01*	*0.02*	*99.75*
438851A	Granodiorite	72.07	0.343	14.76	2.13	0.006	1.13	0.22	2.76	4.58	0.111	2.22	<0.01	0.00	100.32
CS001	*Mafic Schist*	*52.02*	*0.185*	*4.49*	*9.19*	*0.040*	*25.97*	*0.02*	*0.29*	*0.02*	*0.001*	*7.36*	*<0.01*	*0.01*	*99.57*
CS002	*Mafic Schist*	*25.54*	*0.325*	*18.73*	*27.79*	*0.248*	*15.38*	*1.56*	*0.36*	*0.01*	*0.001*	*9.67*	*<0.01*	*0.02*	*99.62*
CS003	*Mafic Schist*	*82.37*	*0.087*	*6.90*	*3.82*	*0.038*	*0.51*	*0.65*	*3.82*	*0.06*	*0.000*	*1.33*	*0.28*	*0.69*	*99.87*
Johnson Cairn Formation - mafic rock															
DGMH137	Basalt	48.29	2.526	14.65	12.40	0.091	13.34	0.52	1.45	0.01	0.307	6.31	0.12	0.29	100.01
DGMH138	Basalt	46.30	2.404	13.73	11.71	0.149	9.49	3.61	2.96	0.02	0.295	8.39	0.16	0.40	99.22
DGMH140	Basalt	51.67	2.593	15.07	12.67	0.068	10.26	0.44	0.00	1.58	0.328	5.57	0.02	0.05	100.27
Archean Basement															
DGMH142	*Dolerite*	*57.68*	*0.718*	*11.68*	*13.00*	*0.088*	*9.01*	*0.83*	*1.31*	*0.06*	*0.092*	*5.08*	*0.57*	*1.43*	*100.11*
DGMH144	*Dolerite*	*45.87*	*0.708*	*12.07*	*11.24*	*0.154*	*8.29*	*8.26*	*1.79*	*0.53*	*0.053*	*9.55*	*0.12*	*0.31*	*98.64*
DGMH145	*Basalt*	*37.81*	*1.336*	*17.59*	*18.76*	*0.149*	*15.03*	*0.68*	*0.00*	*0.90*	*0.093*	*7.66*	*<0.01*	*0.00*	*100.00*
Killara Formation															
KL001	Basalt	97.21	0.081	1.02	0.18	0.002	0.02	0.10	0.06	0.02	0.004	0.82	0.02	0.05	99.52
KL003	*Basalt*	*50.32*	*0.619*	*14.61*	*10.42*	*0.183*	*8.86*	*11.38*	*1.70*	*0.23*	*0.045*	*1.78*	*0.05*	*0.14*	*100.20*
KL004	*Basalt*	*51.00*	*0.807*	*13.94*	*11.54*	*0.186*	*7.55*	*11.22*	*1.77*	*0.34*	*0.070*	*1.95*	*0.06*	*0.14*	*100.43*

Table 5.2. Trace element data collected for DeGrussa and regional rocks. Analysis by ICP-MS (Italics not plotted).

Sample #	Li ppm	Be ppm	Sc ppm	Ti ppm	V ppm	Cr ppm	Mn ppm	Co ppm	Ni ppm	Cs ppm	Zn ppm	Ga ppm	As ppm	Rb ppm
DeGrussa														
DGMH006	6.583	0.650	37.54	8660.121	386.910	5.407	1895.539	55.320	25.204	166.718	100.811	18.393	<2	11.390
DGMH010	14.276	0.235	40.22	3770.630	207.142	63.413	1211.898	56.047	80.001	308.896	234.809	14.829	<2	6.736
DGMH013	10.946	0.904	42.21	5616.221	327.779	142.035	1738.330	55.685	78.328	0.680	81.932	23.283	<2	3.634
DGMH017	12.190	0.586	40.47	7100.620	345.493	44.202	1641.876	53.916	54.395	136.670	89.737	16.565	<2	1.112
DGMH020	12.342	0.342	47.61	4329.900	257.198	183.958	1409.449	66.078	120.184	126.136	93.338	12.887	<2	3.216
DGMH021	11.561	0.450	38.73	7727.616	335.186	23.458	1597.654	51.521	44.832	218.562	95.997	15.817	<2	1.942
DGMH030	9.375	0.399	39.90	6423.184	310.445	18.682	1492.194	54.155	37.813	180.328	81.808	17.504	<2	2.727
DGMH041	8.012	0.487	44.77	6737.143	332.600	39.513	1646.547	51.170	50.718	145.948	95.508	16.860	<2	2.137
DGMH042	8.700	0.673	40.02	7606.950	363.637	4.466	1451.599	68.239	28.988	190.205	84.007	17.803	<2	5.505
DGMH043	6.787	0.593	45.16	9213.043	409.684	2.052	1812.855	59.851	27.201	139.934	94.411	19.797	<2	10.736
DGMH044	5.974	0.594	41.39	8621.847	382.972	1.707	1679.376	52.494	24.683	232.880	96.776	19.130	<2	11.871
DGMH045	5.102	0.462	47.42	8932.095	567.886	<0.6	1752.821	59.277	19.883	9.476	77.470	19.529	<2	10.048
DGMH046	14.026	0.208	37.85	4632.110	264.590	6.677	1282.419	47.414	39.440	224.191	75.306	15.548	<2	4.462
DGMH047	13.322	0.211	51.43	3401.388	241.082	140.619	1446.490	61.773	127.620	108.556	64.746	13.490	<2	2.743
DGMH048	5.318	0.840	52.81	14404.952	30.433	2.109	2220.708	52.130	1.175	36.436	86.501	19.281	<2	21.943
DGMH049	9.591	0.297	44.79	4018.732	271.762	75.190	1307.225	51.280	75.064	180.138	67.587	14.425	<2	2.712
DGMH050	5.854	0.390	44.98	5529.291	308.022	36.008	1550.316	57.250	53.139	162.161	107.516	15.756	3.18	3.615
DGMH058	8.060	0.452	43.65	6674.511	330.267	38.364	1442.058	50.456	52.569	70.913	76.675	18.655	<2	5.596
DGMH060	3.013	0.722	41.71	12385.855	24.701	1.381	2007.546	47.779	0.377	19.591	110.745	18.005	<2	20.183
DGMH062	8.799	0.312	43.42	5665.930	283.175	114.374	1501.838	57.320	84.454	30.419	68.616	15.073	3.22	2.611
DGMH063	9.318	0.501	41.73	6292.703	305.509	50.425	1700.688	54.662	58.350	122.566	105.255	15.771	37.44	6.467
DGMH065	11.425	0.371	46.62	5407.389	278.625	134.977	1581.158	72.375	101.956	67.186	89.347	13.026	2.52	0.626
DGMH070	13.183	0.761	44.73	7976.498	347.431	62.439	1866.529	85.890	94.476	138.829	1203.278	20.293	32.31	0.925
DGMH080	4.895	0.386	34.75	9479.074	549.046	N/A	1617.016	110.182	7.908	149.118	104.840	17.116	<2	3.240
DGMH084	14.031	0.209	46.00	1484.346	244.400	106.600	1247.009	46.752	95.721	5.187	64.873	10.333	-	5.052
DGMH096	21.911	1.332	47.30	7497.780	404.600	60.500	1399.131	50.958	66.799	161.200	186.496	17.013	2.66	17.397
Narracoota - Regional														
DGMH147	15.416	0.152	45.00	4776.763	282.300	398.000	1314.296	54.051	119.394	71.800	89.239	10.855	0.34	1.854
FTMH003c	*3.764*	*0.896*	*21.85*	*1552.298*	*17.500*	*16.000*	*232.913*	*70.116*	*771.051*	*34.320*	*32.488*	*4.613*	*0.66*	*0.211*
FTMH004	*6.579*	*0.277*	*43.90*	*5167.216*	*298.200*	*25.200*	*1287.149*	*19.821*	*20.276*	*125.700*	*71.849*	*13.047*	*1.10*	*75.242*
FTMH006	*6.905*	*0.719*	*33.10*	*3679.965*	*239.500*	*114.300*	*524.055*	*42.547*	*103.955*	*132.400*	*67.580*	*15.447*	*8.60*	*1.574*
FTMH010	*9.944*	*0.026*	*23.30*	*623.317*	*142.900*	*2019.000*	*1181.203*	*40.793*	*1005.275*	*24.300*	*54.043*	*14.508*	*0.70*	*0.758*
438851A	9.989	1.141	3.22	2055.746	31.200	11.000	126.149	29.231	26.349	8.624	46.442	17.326	1.98	147.162
CS001	*14.385*	*0.122*	*19.00*	*1108.784*	*97.400*	*3321.800*	*307.778*	*102.111*	*1026.066*	*21.100*	*49.253*	*3.870*	*0.80*	*0.514*
CS002	*76.462*	*0.302*	*76.90*	*1947.864*	*267.200*	*865.200*	*1921.066*	*190.370*	*309.292*	*0.698*	*298.539*	*26.511*	*1.08*	*0.669*
CS003	*1.993*	*0.087*	*5.12*	*521.428*	*45.900*	*168.600*	*294.224*	*107.127*	*18.012*	*4.089*	*5.940*	*2.804*	*0.53*	*1.082*
Johnson Cairn Formation - mafic rock														
DGMH137	24.627	1.263	32.70	15139.402	381.800	210.000	705.043	50.754	95.000	2.185	113.293	20.666	11.20	0.771
DGMH138	18.299	1.109	34.10	14410.398	379.700	245.500	1157.040	49.344	92.221	90.200	91.009	18.683	3.64	0.588
DGMH140	28.280	2.001	34.20	15540.961	388.800	274.400	524.055	48.269	101.691	58.500	99.235	20.353	18.88	74.781
Archean Basement														
DGMH142	*23.176*	*0.528*	*25.20*	*4303.282*	*238.600*	*475.500*	*682.350*	*64.096*	*277.076*	*24.000*	*121.102*	*23.484*	*2.71*	*2.656*
DGMH144	*17.885*	*0.746*	*41.60*	*4241.128*	*322.000*	*529.100*	*1192.665*	*56.097*	*176.312*	*236.100*	*98.298*	*13.569*	*0.55*	*23.257*
DGMH145	*41.684*	*0.701*	*56.30*	*8007.221*	*302.900*	*527.400*	*1156.248*	*66.983*	*136.068*	*1.041*	*171.605*	*28.286*	*0.49*	*42.999*
Killara Formation														
KL001	8.796	0.032	0.61	485.468	6.804	12.700	9.021	42.972	4.205	5.673	2.255	2.259	0.12	0.525
KL003	*14.363*	*0.279*	*36.80*	*3709.933*	*205.200*	*92.200*	*1419.476*	*62.073*	*115.483*	*120.900*	*64.873*	*14.299*	*0.26*	*7.566*
KL004	*12.371*	*0.407*	*41.60*	*4836.697*	*246.800*	*93.600*	*1441.386*	*59.010*	*77.091*	*103.000*	*83.199*	*13.569*	*0.51*	*13.659*

Table 5.2. (cont.)

Sample #	Sr ppm	Y ppm	Zr ppm	Cd ppm	Sn ppm	Sb ppm	Te ppm	Cu ppm	Nb ppm	Mo ppm	Ag ppm	Ba ppm	La ppm	Ce ppm	Pr ppm	Nd ppm
DeGrussa																
DGMH006	150.130	31.94	97.721	0.061	0.88	1.041	<0.1	3.017	6.361	0.79	<0.1	131.539	10.887	21.732	2.878	13.131
DGMH010	142.255	13.89	44.826	0.126	0.51	2.061	<0.1	0.044	2.481	0.25	<0.1	121.341	4.706	10.794	1.365	6.240
DGMH013	709.574	21.87	59.285	0.050	1.41	0.536	<0.1	0.074	3.130	0.41	<0.1	57.546	4.890	12.273	1.638	7.792
DGMH017	106.193	25.72	75.259	0.016	0.58	4.289	<0.1	0.080	4.185	0.28	<0.1	41.982	6.467	15.950	2.110	9.859
DGMH020	122.162	15.21	39.082	0.059	0.47	5.593	<0.1	0.032	2.049	0.23	<0.1	49.243	3.487	8.632	1.162	5.612
DGMH021	117.229	26.47	81.501	0.029	1.08	2.909	<0.1	0.054	4.787	0.37	<0.1	50.306	9.195	19.267	2.536	11.456
DGMH030	112.480	25.69	77.380	0.054	0.86	0.113	<0.05	0.117	3.932	0.44	0.0	80.086	6.114	14.789	2.071	9.791
DGMH041	124.765	26.10	73.077	0.034	0.54	1.432	<0.05	0.043	3.928	0.42	0.0	48.792	6.478	15.524	2.114	10.015
DGMH042	147.216	27.33	83.978	0.047	0.70	0.253	0.1	0.642	4.337	0.53	0.1	52.299	6.544	15.786	2.185	10.313
DGMH043	139.165	34.96	106.515	0.061	0.90	0.067	<0.05	1.436	5.637	0.30	0.0	55.331	9.041	21.768	2.989	14.075
DGMH044	139.874	31.44	93.980	0.090	0.80	0.051	<0.05	1.486	5.523	1.27	0.0	60.635	7.437	17.815	2.468	11.770
DGMH045	158.016	24.09	65.561	0.028	0.85	0.034	<0.05	1.299	3.639	0.25	0.0	47.299	5.526	13.382	1.869	8.897
DGMH046	130.928	18.76	51.499	0.057	0.46	0.082	<0.05	0.044	2.721	0.74	0.0	73.946	3.976	9.854	1.403	6.784
DGMH047	116.726	15.46	37.230	0.083	0.41	0.087	<0.05	0.045	1.900	0.15	0.0	31.695	3.069	7.550	1.079	5.244
DGMH048	150.591	34.53	93.803	0.050	0.46	0.666	<0.05	2.984	5.771	0.59	0.0	146.515	7.746	19.163	2.756	13.380
DGMH049	213.966	17.24	48.594	0.069	0.39	0.885	<0.05	0.033	2.279	0.06	0.0	70.125	3.854	9.319	1.318	6.299
DGMH050	131.102	24.35	69.077	0.086	0.73	5.465	<0.05	0.098	3.648	0.29	0.0	76.781	5.449	13.281	1.873	8.912
DGMH058	185.185	26.13	75.947	0.109	1.04	0.307	<0.05	0.093	4.055	0.20	0.0	92.453	6.067	14.665	2.055	9.654
DGMH060	106.349	35.66	106.859	0.045	1.53	0.046	<0.05	2.926	5.862	0.22	0.0	82.686	8.260	20.398	2.884	13.827
DGMH062	133.730	19.37	54.708	<0.05	0.50	0.890	<0.05	0.019	3.006	0.09	<0.05	36.704	4.510	11.010	1.499	7.232
DGMH063	155.686	23.13	71.616	<0.05	0.67	3.065	<0.05	0.124	4.070	0.26	0.1	114.081	5.793	14.074	1.884	8.939
DGMH065	131.541	19.16	55.676	<0.05	0.53	1.047	<0.05	0.092	3.084	0.26	<0.05	32.876	4.856	11.730	1.551	7.409
DGMH070	230.412	23.64	96.261	0.053	1.22	8.896	0.1	0.063	6.186	0.56	0.1	29.503	10.394	24.018	2.994	13.380
DGMH080	62.400	16.94	50.373	0.060	0.57	0.050	<0.05	0.465	2.862	0.37	<0.05	25.200	3.890	9.648	1.311	6.323
DGMH084	59.430	16.28	16.100	0.024	0.16	0.048	N/A	0.026	1.121	0.00	-	296.663	2.622	5.329	0.630	2.809
DGMH096	35.144	24.81	80.900	0.023	1.61	4.496	0.1	0.179	4.028	0.54	0.0	135.322	6.503	15.229	2.148	10.015
Narracoota - Regional																
DGMH147	62.827	19.47	49.500	0.025	0.51	0.038	0.0	0.029	2.263	0.19	0.0	13.375	3.415	9.054	1.340	6.714
FTMH003c	*22.281*	*6.18*	*133.300*	*0.060*	*0.07*	*0.795*	-	*0.070*	*0.077*	*0.00*	-	*828.859*	*0.150*	*0.399*	*0.078*	*0.489*
FTMH004	*74.470*	*9.04*	*73.800*	*N/A*	*1.17*	*0.528*	-	*0.887*	*5.790*	*0.03*	*0.0*	*20.063*	*20.525*	*39.305*	*4.744*	*18.068*
FTMH006	*95.214*	*22.44*	*89.900*	*0.122*	*0.85*	*0.668*	*0.1*	*0.045*	*4.164*	*0.42*	*0.1*	*26.832*	*7.133*	*15.713*	*2.101*	*9.476*
FTMH010	*34.110*	*14.97*	*84.581*	*0.023*	*0.60*	*0.345*	*0.0*	*0.046*	*6.230*	*0.10*	*0.2*	*13.166*	*7.037*	*15.790*	*1.949*	*8.310*
438851A	72.308	9.24	144.300	0.073	1.16	0.112	0.0	3.490	6.409	0.11	0.1	679.326	27.219	49.834	5.435	18.854
CS001	*4.899*	*2.57*	*25.400*	*0.023*	*0.24*	*0.253*	-	*0.019*	*3.518*	*0.07*	-	*3.528*	*1.864*	*4.235*	*0.510*	*2.080*
CS002	*13.732*	*17.45*	*49.000*	*0.046*	*0.39*	*0.476*	*0.1*	*0.141*	*3.341*	*0.06*	-	*4.426*	*19.983*	*39.557*	*4.319*	*15.698*
CS003	*11.364*	*0.72*	*12.000*	-	*0.11*	*0.308*	*0.3*	*0.054*	*0.341*	*0.12*	*0.0*	*27.169*	*0.888*	*1.775*	*0.197*	*0.748*
Johnson Cairn Formation - mafic rock																
DGMH137	26.815	26.41	156.200	0.017	2.30	0.216	0.1	0.410	30.478	0.47	0.0	14.262	35.001	68.172	8.368	33.189
DGMH138	73.563	20.68	138.700	0.022	2.21	0.155	0.0	0.145	29.932	0.76	0.0	25.554	24.358	52.522	6.722	27.640
DGMH140	8.070	24.43	147.700	-	1.57	0.198	-	1.278	32.554	0.87	-	495.936	29.979	64.521	7.989	33.226
Archean Basement																
DGMH142	*30.619*	*15.83*	*82.200*	*0.039*	*0.98*	*0.228*	*0.0*	*0.182*	*4.216*	*2.26*	*0.0*	*11.077*	*25.788*	*49.108*	*5.536*	*20.953*
DGMH144	*289.644*	*18.89*	*39.800*	*0.024*	*0.52*	*0.090*	*0.0*	*0.778*	*2.516*	*0.42*	*0.1*	*1334.304*	*2.294*	*6.171*	*0.947*	*4.989*
DGMH145	*5.774*	*45.77*	*74.600*	*N/A*	*0.96*	*0.133*	*0.0*	*1.127*	*4.033*	*0.24*	-	*273.987*	*4.932*	*10.380*	*1.339*	*5.827*
Killara Formation																
KL001	6.044	0.40	13.700	N/A	0.26	0.032	-	0.021	0.708	0.25	-	64.160	0.176	0.756	0.075	0.342
KL003	*162.555*	*12.88*	*37.700*	*0.082*	*0.46*	*0.042*	*0.0*	*0.144*	*2.872*	*0.13*	*0.1*	*120.483*	*5.038*	*10.903*	*1.402*	*6.257*
KL004	*153.729*	*16.60*	*56.000*	*0.091*	*0.55*	*0.023*	*0.0*	*0.259*	*4.091*	*0.21*	*0.0*	*171.686*	*7.305*	*15.435*	*2.017*	*8.775*

Table 5.2. (cont.)

Sample #	Sm ppm	Eu ppm	Gd ppm	Tb ppm	Dy ppm	Ho ppm	Er ppm	Tm ppm	Yb ppm	Lu ppm	Hf ppm	Ta ppm	W ppm	Tl ppm	Pb ppm	Bi ppm	Th ppm	U ppm
DeGrussa																		
DGMH006	3.824	1.401	4.690	0.882	5.663	1.247	3.618	0.528	3.362	0.509	2.685	0.417	93.555	0.112	3.368	<0.1	1.153	0.304
DGMH010	1.851	0.724	2.260	0.417	2.664	0.576	1.655	0.242	1.546	0.232	1.232	0.246	90.306	0.182	5.101	<0.1	0.521	0.120
DGMH013	2.463	1.162	3.183	0.593	3.838	0.835	2.428	0.346	2.222	0.341	1.595	0.226	32.662	0.052	2.882	<0.1	0.586	0.150
DGMH017	2.962	1.083	3.742	0.699	4.549	0.999	2.921	0.422	2.713	0.409	2.048	0.299	52.702	0.058	1.350	<0.1	0.871	0.222
DGMH020	1.799	0.748	2.281	0.433	2.809	0.621	1.790	0.263	1.655	0.251	1.094	0.217	98.464	0.185	5.448	<0.1	0.454	0.118
DGMH021	3.341	1.015	4.117	0.752	4.786	1.052	3.028	0.438	2.813	0.425	2.233	0.353	45.408	0.087	2.268	<0.1	0.955	0.271
DGMH030	2.960	1.038	3.720	0.704	4.540	1.012	2.963	0.431	2.746	0.427	2.145	0.330	82.627	0.055	2.008	0.0	0.930	0.234
DGMH041	2.982	1.044	3.793	0.720	4.561	1.017	2.916	0.429	2.751	0.426	2.037	0.327	60.561	0.037	3.094	0.0	0.884	0.220
DGMH042	3.159	1.215	3.960	0.744	4.757	1.068	3.104	0.457	2.923	0.453	2.296	0.330	45.217	0.402	3.092	0.1	1.010	0.258
DGMH043	4.196	1.458	5.154	0.965	6.097	1.367	3.983	0.586	3.757	0.574	2.900	0.432	63.810	0.052	2.034	0.0	1.221	0.321
DGMH044	3.557	1.351	4.531	0.854	5.386	1.210	3.538	0.530	3.316	0.510	2.564	0.411	44.007	0.077	1.344	0.0	1.108	0.274
DGMH045	2.714	1.081	3.459	0.649	4.214	0.950	2.757	0.404	2.592	0.402	1.842	0.286	62.372	0.042	1.233	0.0	0.776	0.201
DGMH046	2.138	0.811	2.712	0.516	3.291	0.746	2.161	0.312	2.001	0.308	1.443	0.215	48.448	0.036	1.161	0.0	0.597	0.156
DGMH047	1.681	0.638	2.214	0.423	2.724	0.614	1.774	0.261	1.651	0.252	1.083	0.168	52.312	0.021	0.965	0.0	0.423	0.106
DGMH048	4.107	1.535	5.218	0.977	6.141	1.371	3.931	0.572	3.625	0.556	2.640	0.465	89.761	0.062	2.054	0.0	0.895	0.226
DGMH049	1.954	0.884	2.503	0.470	3.012	0.683	1.952	0.285	1.790	0.269	1.364	0.200	64.625	0.026	1.275	0.0	0.470	0.129
DGMH050	2.737	0.983	3.514	0.666	4.260	0.964	2.777	0.402	2.577	0.403	1.929	0.291	53.135	0.059	2.656	0.0	0.718	0.187
DGMH058	2.962	1.144	3.679	0.720	4.565	1.022	2.959	0.451	2.816	0.442	2.082	0.319	57.867	0.052	2.480	0.0	0.891	0.232
DGMH060	4.204	1.541	5.246	0.979	6.253	1.394	4.051	0.590	3.760	0.581	2.946	0.478	85.244	0.174	0.873	0.0	1.025	0.255
DGMH062	2.286	0.866	2.979	0.563	3.551	0.772	2.275	0.337	2.094	0.327	1.477	0.188	36.452	0.031	1.226	0.0	0.528	0.127
DGMH063	2.729	1.027	3.505	0.654	4.235	0.905	2.750	0.398	2.524	0.389	1.888	0.198	28.970	0.128	6.107	0.0	0.716	0.183
DGMH065	2.298	0.760	2.969	0.551	3.529	0.763	2.300	0.333	2.125	0.322	1.511	0.240	104.098	0.016	2.471	0.0	0.635	0.163
DGMH070	3.674	1.218	4.260	0.745	4.539	0.930	2.717	0.383	2.449	0.389	2.598	0.187	12.107	0.442	5.511	0.0	2.008	0.566
DGMH080	2.002	0.907	2.569	0.477	3.100	0.674	2.022	0.294	1.904	0.291	1.346	0.163	39.296	0.076	0.965	0.0	0.453	0.115
DGMH084	0.835	0.337	1.421	0.277	2.386	0.576	1.937	0.335	2.172	0.314	0.445	0.112	70.064	0.016	0.478	N/A	0.218	0.045
DGMH096	2.993	1.115	3.777	0.704	4.477	0.946	2.821	0.430	2.742	0.418	2.183	0.250	7.864	0.873	3.110	0.1	0.883	0.224
Narracoota - Regional																		
DGMH147	2.088	0.628	2.725	0.509	3.264	0.700	2.096	0.319	2.038	0.313	1.408	0.149	36.577	N/A	0.721	-	0.396	0.098
FTMH003c	*0.265*	*0.155*	*0.527*	*0.118*	*0.874*	*0.213*	*0.731*	*0.122*	*0.887*	*0.158*	*0.168*	*0.029*	*26.240*	-	*0.676*	-		-
FTMH004	*3.310*	*0.616*	*2.290*	*0.305*	*1.606*	*0.314*	*0.951*	*0.151*	*1.020*	*0.163*	*3.552*	*0.544*	*148.074*	*0.274*	*6.052*	*0.1*	*9.223*	*1.459*
FTMH006	*2.715*	*0.883*	*3.298*	*0.628*	*3.938*	*0.860*	*2.594*	*0.405*	*2.573*	*0.405*	*1.950*	*0.350*	*48.847*	*N/A*	*3.767*	*0.1*	*1.087*	*0.335*
FTMH010	*2.160*	*0.797*	*2.448*	*0.447*	*2.757*	*0.572*	*1.686*	*0.255*	*1.599*	*0.240*	*2.176*	*0.513*	*57.227*	*N/A*	*3.618*	*0.1*	*1.186*	*0.366*
438851A	3.070	0.711	2.199	0.307	1.552	0.295	0.827	0.128	0.788	0.125	3.873	1.244	231.993	0.707	7.461	0.0	9.066	1.078
CS001	*0.450*	*0.106*	*0.404*	*0.067*	*0.416*	*0.090*	*0.284*	*0.045*	*0.322*	*0.052*	*0.629*	*0.288*	*2.551*	-	*0.737*	*0.0*	*0.514*	*0.090*
CS002	*2.616*	*0.955*	*2.275*	*0.406*	*2.796*	*0.637*	*1.921*	*0.267*	*1.567*	*0.220*	*1.364*	*0.270*	*21.802*	-	*1.725*	*N/A*	*1.528*	*0.516*
CS003	*0.155*	*0.052*	*0.127*	*0.025*	*0.121*	*0.027*	*0.090*	-	*0.106*	*0.021*	*0.309*	*0.214*	*563.730*	-	*2.094*	*0.2*	*0.218*	*0.175*
Johnson Cairn Formation - mafic rock																		
DGMH137	6.201	1.914	5.644	0.911	5.295	1.056	2.889	0.399	2.306	0.343	3.830	1.634	11.693	0.006	6.781	0.3	5.556	0.804
DGMH138	5.751	1.923	5.197	0.802	4.392	0.814	2.158	0.304	1.809	0.272	3.435	2.134	25.681	0.004	2.587	0.0	4.191	0.602
DGMH140	6.790	2.108	6.011	0.909	4.998	0.933	2.505	0.344	2.073	0.307	3.873	1.746	8.203	0.281	0.858	0.0	4.376	0.752
Archean Basement																		
DGMH142	*3.763*	*1.076*	*3.051*	*0.490*	*2.926*	*0.577*	*1.648*	*0.240*	*1.500*	*0.214*	*2.264*	*0.294*	*44.048*	*0.026*	*8.736*	*0.7*	*3.668*	*1.716*
DGMH144	*1.775*	*0.599*	*2.504*	*0.491*	*3.230*	*0.697*	*2.115*	*0.323*	*2.132*	*0.332*	*1.217*	*0.168*	*26.535*	*0.137*	*6.309*	*0.3*	*0.251*	*0.072*
DGMH145	*1.872*	*0.928*	*3.646*	*0.881*	*6.460*	*1.507*	*4.645*	*0.697*	*4.131*	*0.587*	*2.214*	*0.211*	*27.496*	*0.181*	*0.428*	*0.0*	*0.367*	*0.287*
Killara Formation																		
KL001	0.108	0.042	0.105	0.022	0.145	0.025	0.107	0.023	0.141	0.017	0.310	0.172	260.076	-	0.449	0.0	0.145	0.240
KL003	*1.670*	*0.606*	*1.913*	*0.342*	*2.145*	*0.449*	*1.335*	*0.202*	*1.300*	*0.201*	*1.081*	*0.236*	*49.366*	*0.058*	*1.872*	-	*1.099*	*0.223*
KL004	*2.329*	*0.833*	*2.656*	*0.496*	*2.959*	*0.629*	*1.851*	*0.293*	*1.811*	*0.285*	*1.597*	*0.262*	*39.238*	*0.059*	*2.564*	*0.0*	*1.456*	*0.208*

5.4. Results

5.4.1. Alteration geochemistry

Intensive alteration can change major and trace element compositions. Relict crystal textures are visible in thin section of DeGrussa rocks, although much of the primary minerals have been replaced (by chlorite, tremolite/actinolite, mica, epidote and carbonate). Rocks at DeGrussa have been subjected to subsea-floor alteration and this has been overprinted with later greenschist metamorphism. Visual observations indicate that there was some sea water alteration along the edges of the dolerite units only. Variation diagrams of the volatile (H_2O, CO_2) loss (%) versus significant major and trace elements (Fig. 5.3) indicates most samples contain low volatile content, between 2 and 4 %, and no clear relationship can be distinguished between the element ratios. Hence alteration and metamorphism is inferred to have not affected the rock geochemisty significantly. Major elements of Al_2O_3, TiO_2 and P_2O_5, transition elements, HFSE, REE and Th are generally immobile (Piercey et al., 2002) and are used throughout this chapter.

Major and trace element variability can help to establish the effects of alteration on rock forming processes. The Al_2O_3/Na_2O ratio represents the alteration of feldspars, and was used by Piercey et al. (2002) to identify the effect of alteration on mafic rocks of the Yukon-Tanana terrane. Al is immobile, while Na is mobile, and both are compatible with feldspar. With the exception of CaO there are no correlation between the major elements and the Al_2O_3/Na_2O ratio, suggesting that the major elements are not mobile in alteration and can be used for rock classification studies as they will provide fractionation trends (Piercey et al., 2002) (Figure 5.4).

The DeGrussa dolerite have a distinct magma composition with low Al_2O_3/Na_2O: CaO ratios and high Fe_2O_3, in comparison to the Killara Formation mafic rocks which have a shallower fractionation gradient. These are the result of magmatic processes rather than alteration and may reflect the fractionation of feldspars of different composition.

Cs is highly mobile in aqueous fluids and a sensitive tracer of alteration linked to seafloor hydrothermal alteration (Hawkins, 1995, Ottolini et al., 2012). Enrichment in a magmatic source can occur during dehydration of a subducting slab which results in a primitive tholeiitic basalt

bearing a subducted slab signature (Arculus, 1994, Pirajno, 2009). It can also substitute into feldspars during fractional crystallisation. The high Cs (Fig. 5.4) associated with low Mg numbers, low Cr and Ni, high Zr and TiO_2 (Fig. 5.7) in DeGrussa samples suggests this is a result of fractional crystallisation with Cs concentrated into the most fractionated rocks.

Negative Ce anomalies are seen in several samples of the Killara Formation mafic rocks (Fig. 5.8A). Ce behaviour is largely controlled by oxidation state (Trail et al., 2011). Negative anomalies may be due to either low-temperature interaction of rocks with hydrothermal fluids (de Baar, 1991, Shikazono, 2003), or from later weathering of rocks (Koppi et al., 1996). As the anomalous data were not accessible as rock samples, it is interpreted these are the result of weathering.

Alteration of mafic rocks in the Bryah group are affected by dolerite/ankerite and chlorite/carbonate alteration (Fig. 5.6) as per the alteration box plot of Large et al. (2001). This plot considers the relationship between the AI (or Ishikawa Index) against the CCPI (chlorite-carbonate-pyrite index). The AI relates to the replacement of plagioclase by sericite and chlorite during hydrothermal alteration, and the CCPI measures the intensity of chlorite, carbonate and pyrite alteration. Most DeGrussa data, as well as some Killara and Narracoota Formation data, lie within the least altered basalt field. From here, data are offset upwards with the majority forming a cluster just outside the least altered basalt box, suggesting that some hydrothermal alteration has affected the rocks. From the main cluster of data, few samples of Narracoota, DeGrussa and the footwall Johnson Cairn Formation trend towards chlorite-pyrite alteration, and a few samples of Narracoota, Killara and DeGrussa samples trend towards epidote-carbonate alteration. This could be expected if hydrothermal alteration related to mineralisation has passed through the Johnson Cairn Formation rocks.

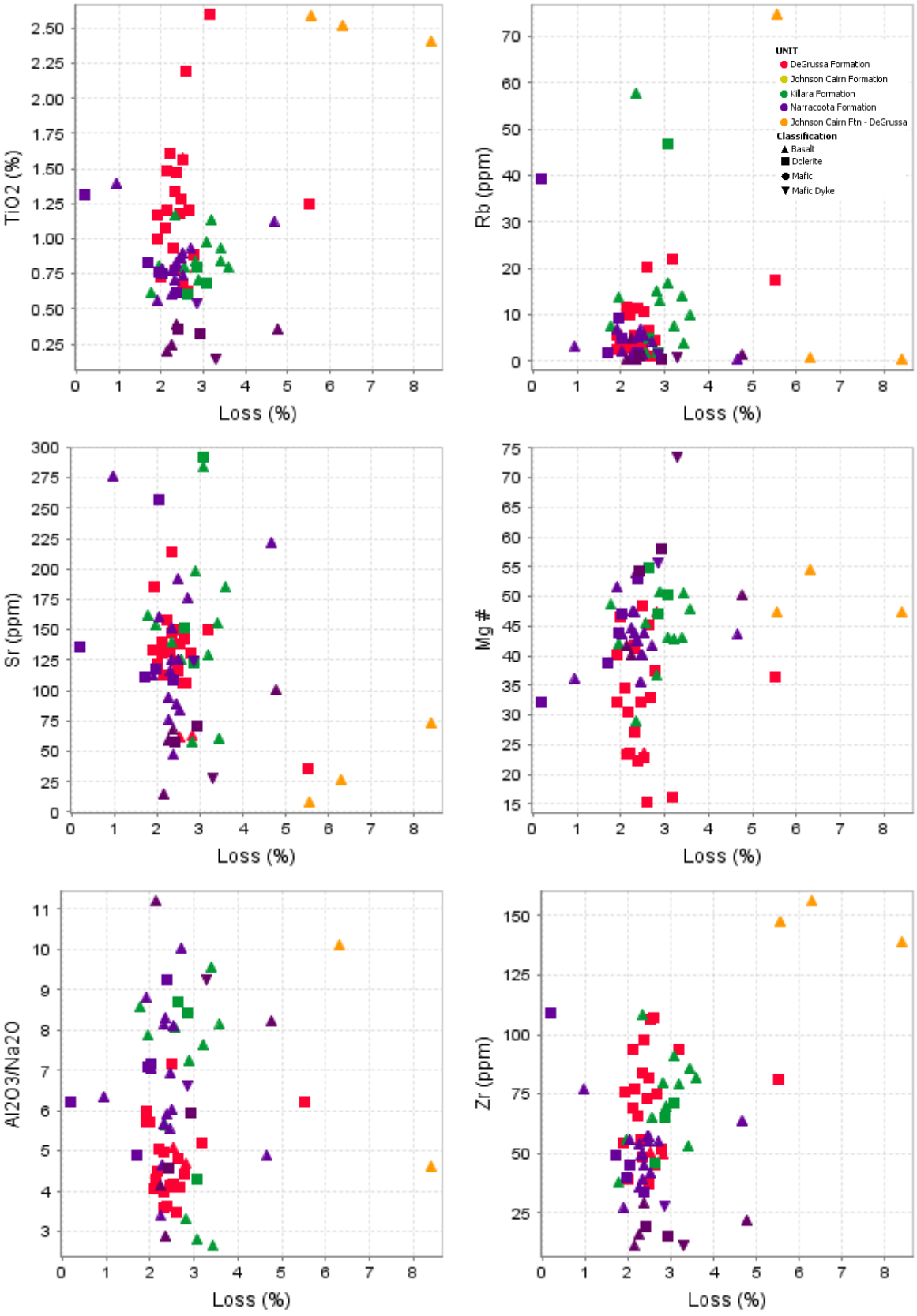

Figure 5.3. There is no relationship between key elements and the Loss (%) indicating that alteration has not significantly affected the rocks. Most rocks have loss between 2-4%.

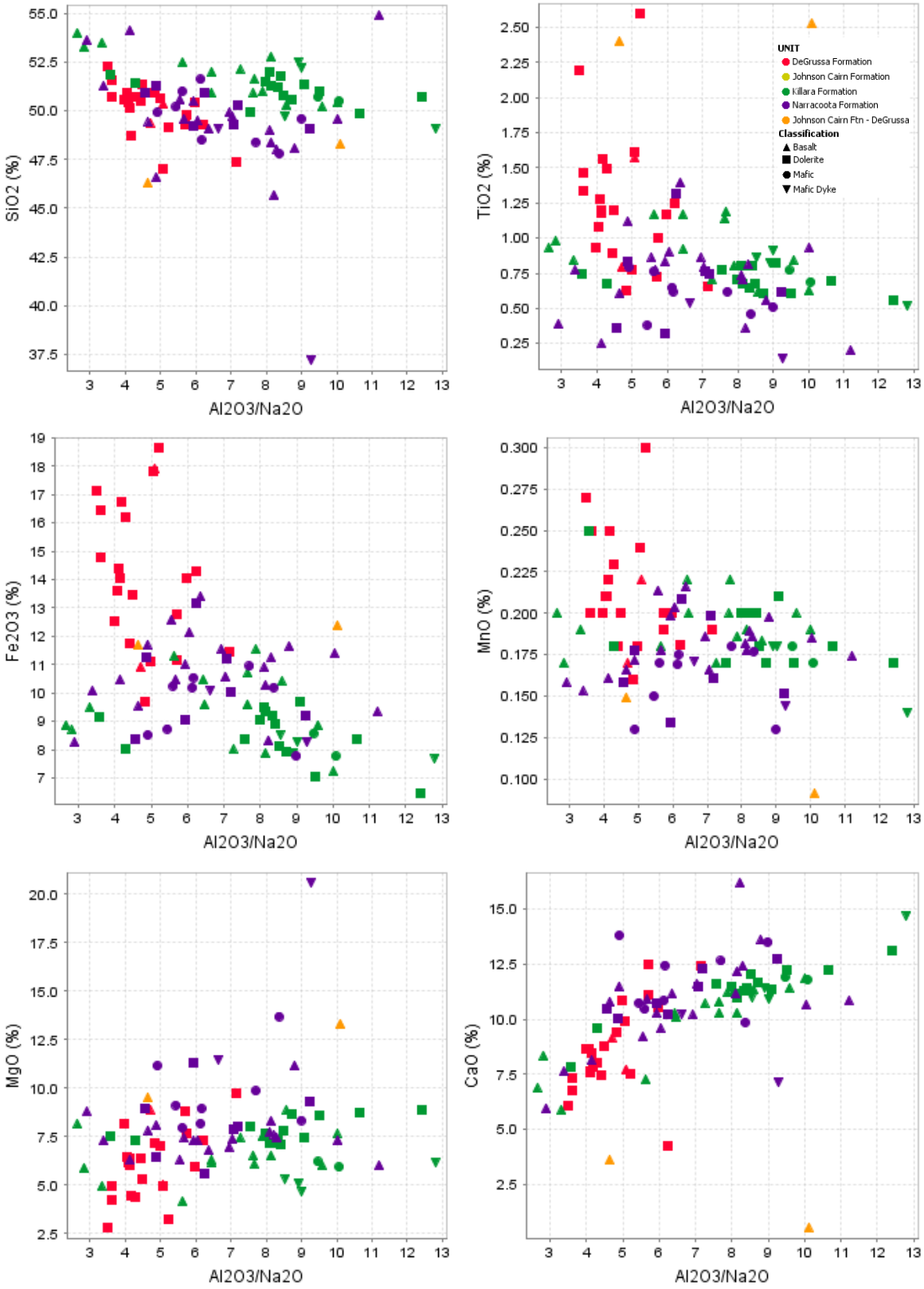

Figure 5.4. Al_2O_3/Na_2O vs. **A.** SiO_2, **B.** TiO_2, **C.** Fe_2O_3, **D.** MnO, **E.** MgO, **F.** CaO. With the exception of CaO, there are no correlation between the major elements and the Al_2O_3/Na_2O ratio. CaO represents magmatic processes and the fractionation of feldspars – the DeGrussa dolerites interpreted to crystallise from a different source composition to that of the Narracoota and Killara Formation. Dolerites associated with DeGrussa have higher TiO_2, Fe_2O_3, MnO and P_2O_5 compared with rocks of the Narracoota and Killara Formations. Two samples of DeGrussa dolerite and two samples of DeGrussa footwall Johnson Cairn Formation have high (>2% TiO_2) indicating they are more fractionated.

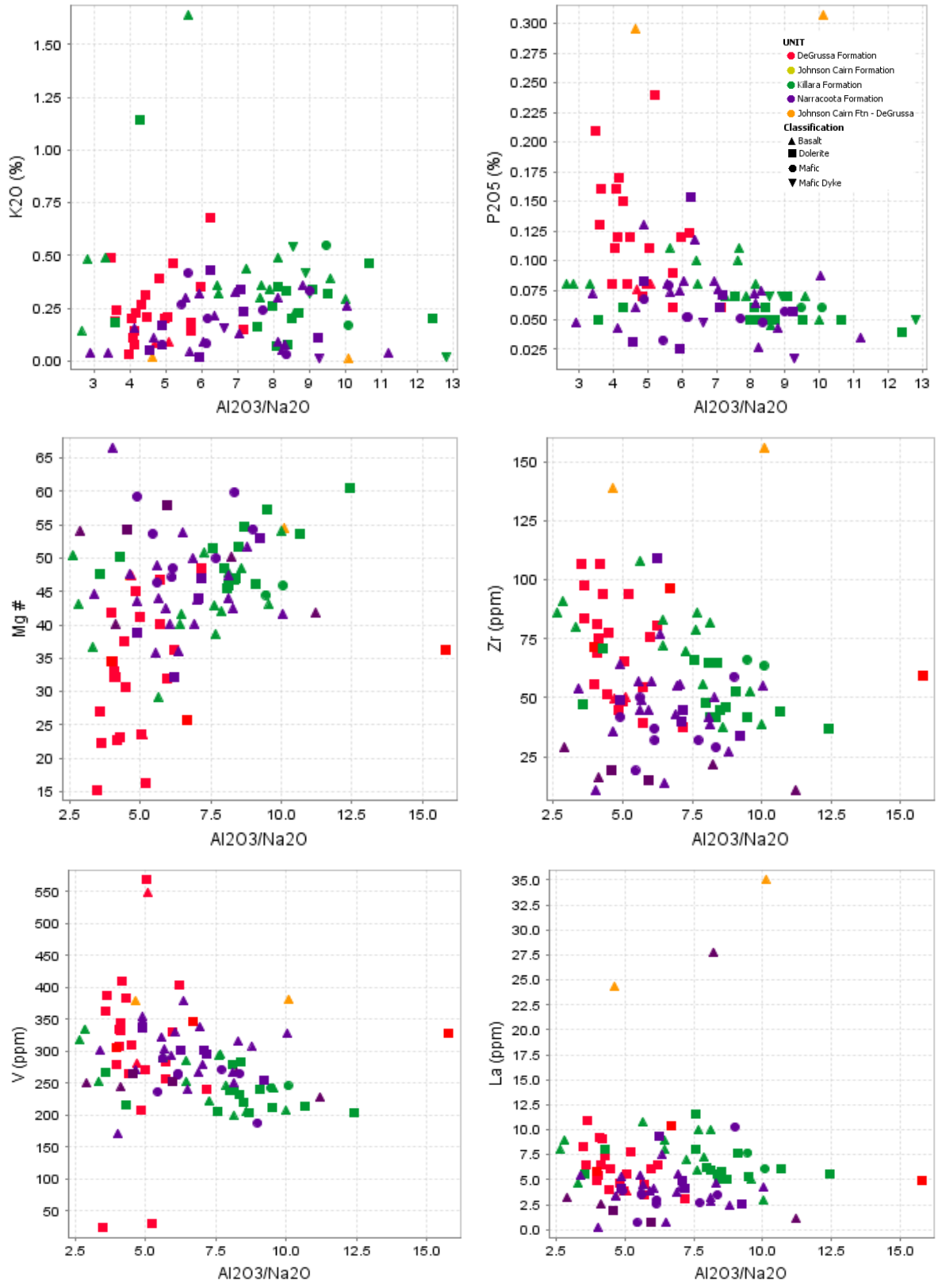

Figure 5.5. Al_2O_3/Na_2O **A.** K_2O, and **B.** P_2O_5. **C.** Mg number, **D.** Zr (ppm), **E.** V (ppm), and **F.** La (ppm).

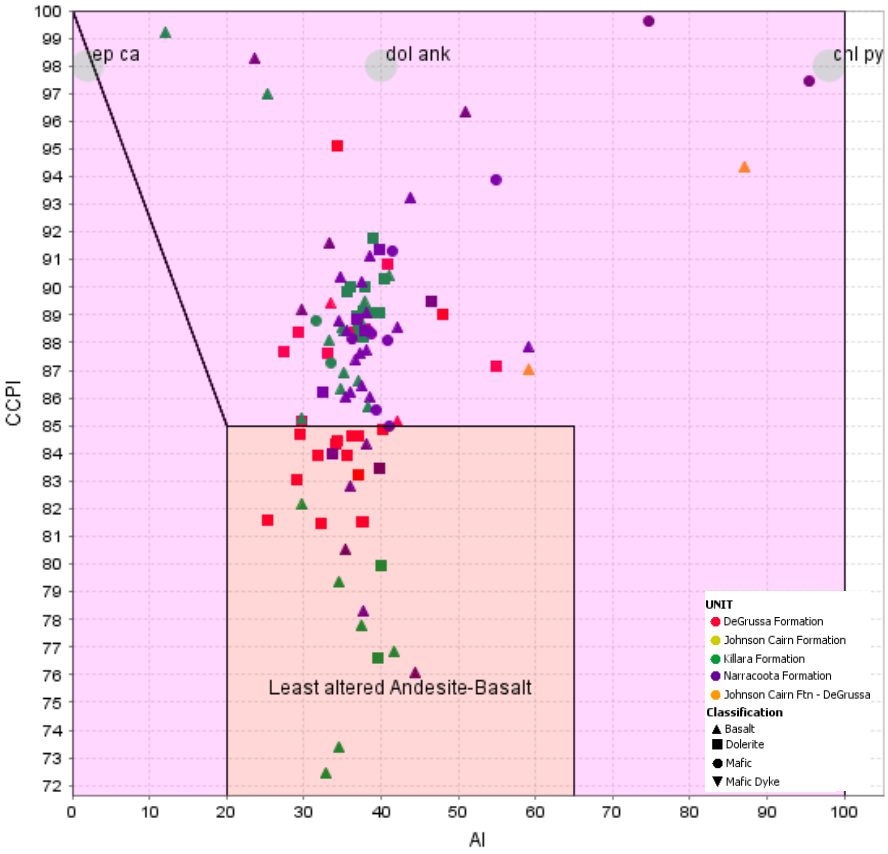

Figure5.6. Alteration of mafic rocks in the Bryah group trends towards dolerite/ankerite and chlorite/carbonate alteration as per the alteration box plot of Large et al. (2001). This is consistent with the alteration visible in hand sample and thin section and indicates that the rocks samples are only weak-moderately altered.

5.4.2. Mafic rock classifications and tectonic environments

Trace and rare earth element geochemistry is utilised to determine the tectonic setting of the DeGrussa deposit and how it is associated with the Narracoota, Killara and Johnson Cairn Formation mafic rocks. Bivariate plots (Fig. 5.4, 5.5, 5.7, 5.8) display the characteristics of each rock formation, their relationship to each other and proximity to VHMS mineralisation.

The Mg number was chosen for variation diagrams due to the greater variability in Mg numbers and its resistance to alteration. It forms an index of crystal fractionation in basaltic liquids (Rollinson, 2013). DeGrussa rocks have low Mg-numbers (23-40, mean =32.7, n=52, with outliers to as low as 15) in comparison to rocks of the Narracoota (40-53, mean = 46.6, n= 46) and Killara Formation (46-56, mean =51.3, n = 9). Primitive rocks have higher Cr and Ni contents, and in the DeGrussa rocks this correlates with higher Mg numbers (Fig. 5.7E, F). The Mg number

has negative correlation with TiO_2, Fe_2O_3, MnO and P_2O_5, and a positive correlation with MgO (Fig. 5.4). The two samples with Mg number <20 (samples DGMH048 and DGMH060) correlate with high Ti, low V and represent highly fractionated rocks, possibly cumulates (Irvine, 1981), and are also coincident with the high Ce (and other REE), Zr and strongly elevated Cs end members of the DeGrussa mafic rocks. There are no distinguishing visual differences between the two high TiO_2 outliers and the rest of the DeGrussa samples.

The footwall Johnson Cairn Formation mafic rock data clusters with Mg numbers (47-54, mean = 49.7, n = 3) similar to those of the Narracoota Formation and Killara Formation, but with very different TiO_2, MnO, CaO and P_2O_5 contents. They form the very enriched REE end member (Figure 5.8A), indicating that these rocks are even more highly fractionated than DeGrussa, or evolved from a different magma source.

The Narracoota Formation mafic rocks form the low REE content end member (e.g. Ce, La), grading into the DeGrussa and Killara Formation mafic rocks. The Johnson Cairn Formation mafic rocks forming the high REE end member (Fig. 5.8A).

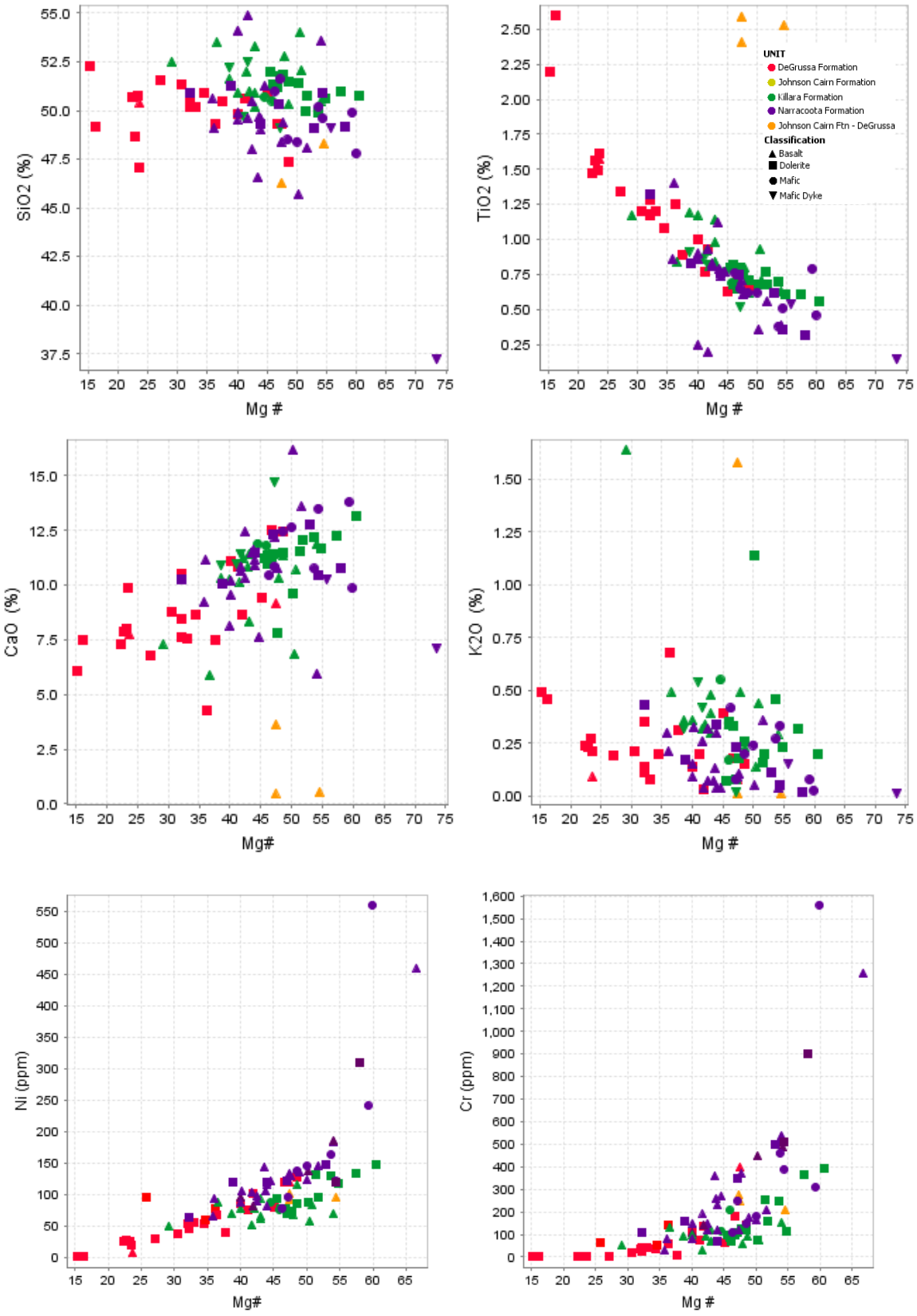

Figure 5.7. Selected major element bivariate plots. The Mg number (100x(MgO/(MgO+FeO)) is the magnesium to iron ratio, used as an index of crystal fractionation in basaltic liquids. **A.** Mg# vs. SiO2, no correlation, **B.** Mg# vs. TiO_2(%). Johnson Cairn Formation mafic rocks (footwall of DeGrussa) have elevated TiO_2, MgO and P_2O_5 in comparison to most DeGrussa rocks. The Narracoota Formation mafic rocks have similar geochemistry to DeGrussa, but a spread of values. Mafic rocks of the Killara Formation are slightly lower in both TiO_2(%) and MgO(%) than DeGrussa mafic rocks. **C.** Mg# vs. CaO(%) bivariate plot. **D.** Mg# vs. K_2O(%) bivariate plot. **E.** Mg # vs. Ni. Representing olivine fractionation, **F.** Mg # vs. Cr representing spinel fractionation

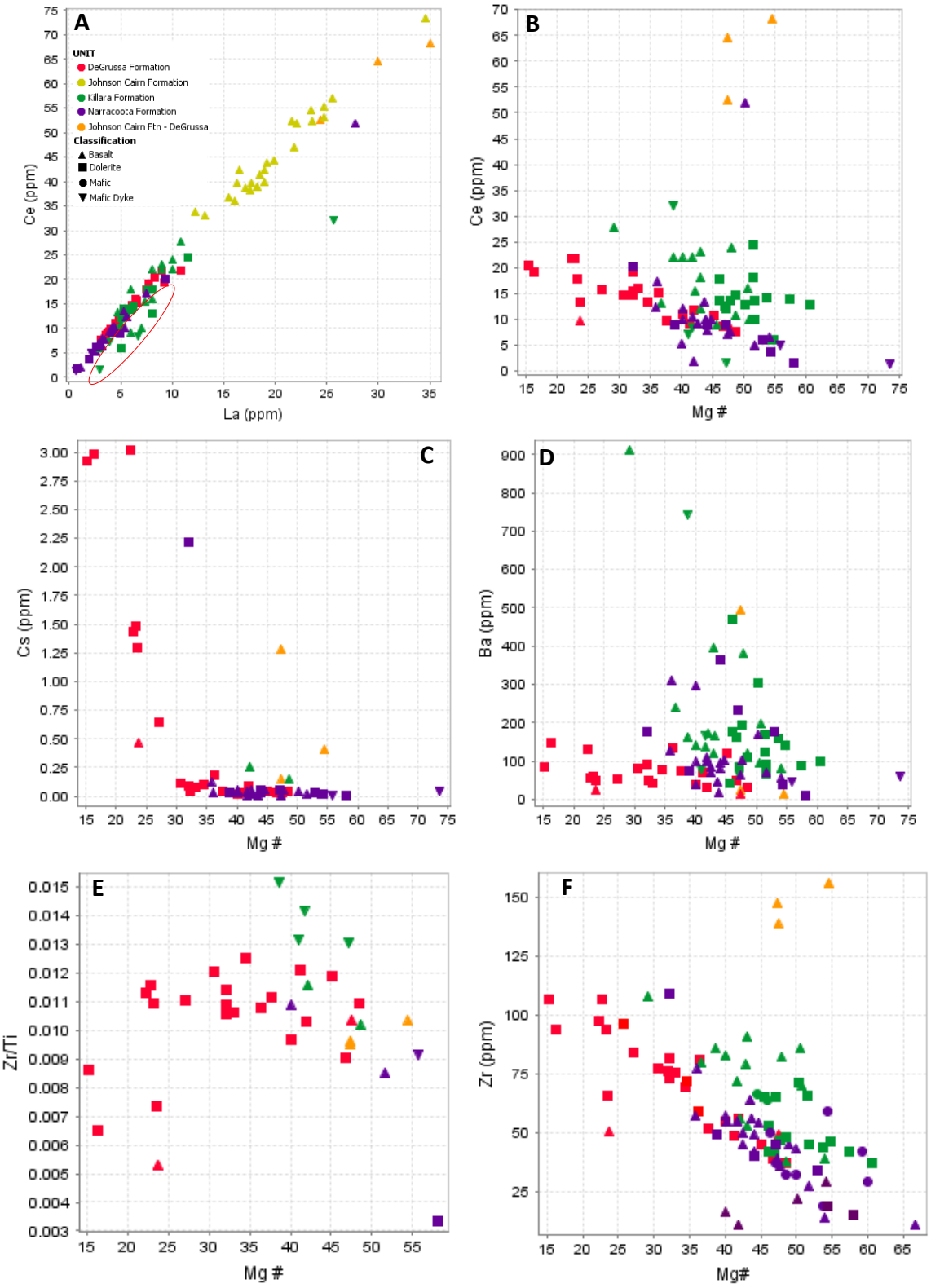

Figure 5.8. Trace element bivariate plots for **A.** La vs. Ce - incompatible LREE all show similar positive linear relationships. Killara Formation data below the main trendline represent weathering and mobility of Ce (circled). Johnson Cairn Formation mafic rocks contain higher LREE contents than those of the Narracoota and Killara. **B.** Mg # vs. Ce**.** Negative relationship for DeGrussa and Narracoota rocks, with no compatibility for the Killara Formation. **C.** Mg # vs. Cs. High Cs values of DeGrussa data at low Mg numbers, suggesting Cs was preferentially partitioned into feldspar. **D.** Mg # vs. Ba. No correlation and probably indicates hydrothermal alteration, **E.** Mg # vs. Zr. DeGrussa and Narracoota together show a negative relationship, the DeGrussa dolerites having higher Zr and low Mg numbers similar to relationships shown by P2O5 suggesting zircon fractionation.

5.4.2.1. Rock Classifications

Data for all units fall within the sub-alkaline field on a Na_2O+K_2O vs. SiO_2 plot (Irvine and Baragar, 1971). DeGrussa, Narracoota and Killara Formation mafic rocks are defined as 'gabbro' on a TAS plutonic plot (Cox et al. (1979), adapted by Wilson (1989)) (Fig 5.9). Killara Formation rocks are much lower in Na_2O+K_2O compared with the DeGrussa and some of the Narracoota Formation rocks.

The Ti vs Zr classification (Pearce and Cann, 1973) is used as both are immobile during alteration and metamorphism (Fig. 5.10A). During hydrothermal alteration, mass changes of mobile components influence the concentration of immobile elements and these variations generate a spread of data along the linear trend with net mass gains moving the rocks toward the origin and net mass losses moving them in the opposite direction (Pierre et al., 2016). A compatible positive trend is made overall between the DeGrussa, Narracoota and Killara Formations. Johnson Cairn Formation data are scattered but mostly of MORB composition. The Johnson Cairn Formation in the DeGrussa footwall have similar Zr but much higher Ti concentrations. Killara Formation mafic rocks are transitional from IAT to calc-alkaline basalts. DeGrussa dolerites define a mixed source between IAT and MORB. Narracoota mafic rocks are mostly IAT and form the lower end member to the DeGrussa mafic rocks. DeGrussa data form a linear trend, with the exception of four samples (DGMH045, 048, 060 and 080) which are offset to higher Ti/Zr ratios, representing the more fractionated dolerites in the DeGrussa dolerite sequence.

A modified Pearce (1996) after Winchester and Floyd (1977) Nb/Y:Zr/Ti plot (Fig. 5.10B) shows the similar sub-alkaline classification of the mafic rocks of the DeGrussa mine sequence, the Narracoota Formation and Killara Formation. The Johnson Cairn Formation mafic rocks are geochemically distinct from the DeGrussa, Killara and Narracoota Formation, with higher Nb/Y ratios. There is limited occurrence and sampling of the Johnson Cairn Formation basalts in the DeGrussa footwall (3 samples) and no major element analysis completed on samples from THD001 (Mueller, 2011).

On the Ti/1000 vs. V classification of Shervais (1982), the mafic rocks of the DeGrussa mine sequence are transitional between island arc basalts (IAB) and mid ocean ridge basalts (MORB) (Fig. 5.10C). The relative enrichment of V relative to Ti is strongly influenced by oxygen fugacity, hence Ti/V ratio can determine the oxidation state (Ti/V = 20-50 low fO_2 conditions, Ti/V = 10-20 more oxidised environment) (Hawkins, 1995). Oxidised magma, or interaction with oxidised fluids, is indicated from the Ti/V ratios of DeGrussa (14-23), Narracoota (10-17) and Killara (18 – 1 sample) Formations, whereas the Johnson Cairn Formation (37-46) and footwall Johnson Cairn Formation samples (37-40) indicate more reduced magmas. The two high V DeGrussa samples (DGMH045 and DGMH080 have Ti/V ratios of 15 and 17 bare interpreted as a result of fractional crystallisation in an oxidised magma. Two DeGrussa samples plot at low V, high Ti values (DGMH048 and DGMH060 with Ti/V of 473 and 501 respectively). Narracoota and Killara Formation mafic rocks are classified as IAB with consistent with the major element classification scheme of Irvine and Baragar (1971) and similar in composition to some DeGrussa mafic rocks. Johnson Cairn Formation mafic rocks form a linear trend within the MORB field, with the Johnson Cairn mafic rocks at DeGrussa form the Ti- and V-rich end member.

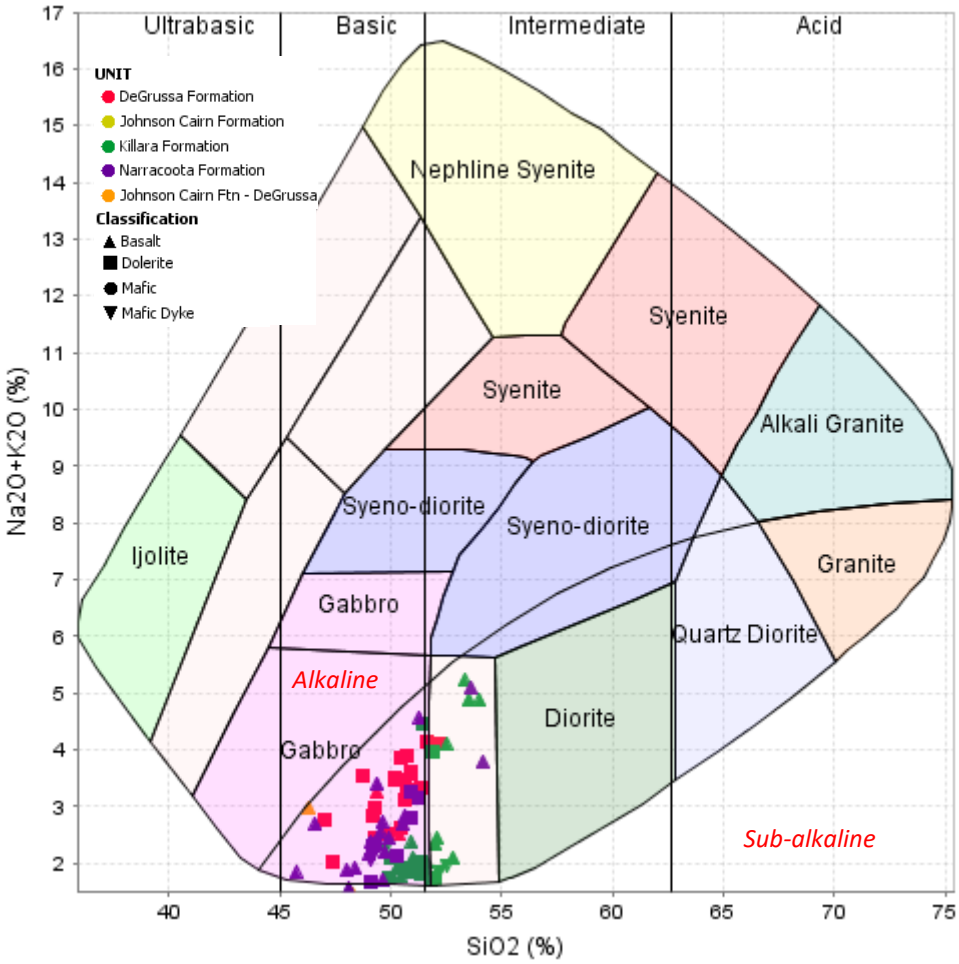

Figure 5.9. TAS plutonic plot (Cox et al. (1979), modified by Wilson (1989)). DeGrussa mafic rocks, as well as the majority of the Yerrida and Bryah Group mafic rocks, are classified as 'gabbro'. Curved line through the graph is the volcanic alkaline-subalkaline curve (Irvine and Baragar, 1971). DeGrussa mafic rocks, as well as the mafic rocks of the Yerrida and Bryah Groups, are classified as subalkaline.

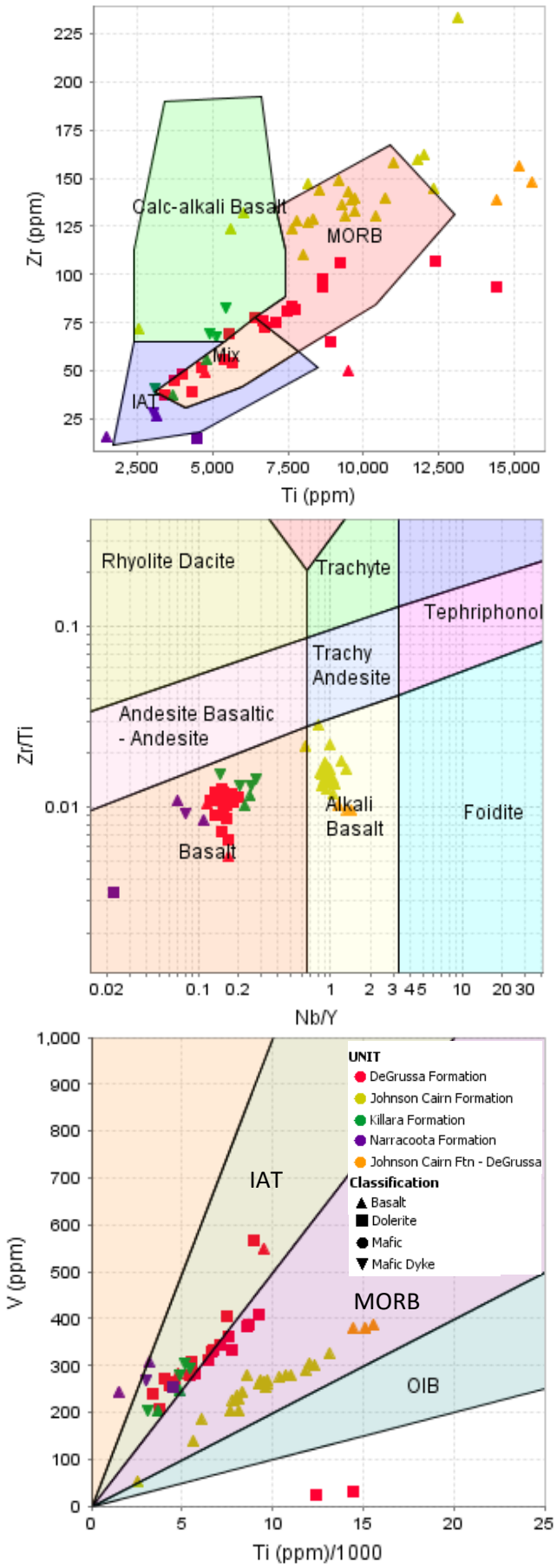

Figure 5.10. A. Basalt Ti vs Zr classification (Pearce and Cann, 1973). Johnson Cairn Formation mafic rocks are of MORB composition, with those mafic rocks of the Johnson Cairn Formation in the footwall of DeGrussa being geochemically similar to the Johnson Cairn Formation mafic rocks but higher in Ti, forming one end member to the geochemical suite. Killara Formation mafic rocks are transitional from IAT to calc-alkaline basalts. DeGrussa dolerites definie a mixed source between IAT and MORB. Narracoota mafic rocks are mostly IAT and form the lower end member to the DeGrussa mafic rocks. **B.** A modified Pearce (1996) after Winchester and Floyd (1977) Nb/Y:Zr/Ti plot comparing DeGrussa dolerites and basalts with the Killara Formation, Narracoota Formation, and Johnson Cairn Formation Basalts (of THD001, and in the Johnson Cairn Formation stratigraphically below DeGrussa). Mafic rocks of the DeGrussa mine sequence, as well as the Narracoota Formation and Killara Formation are classified as sub-alkaline basalts. Johnson Cairn Formation Basalts are alkali basalts and geochemically distinct, although this is not consistent with the classification of Irvine and Baragar (1971). **C.** Ti/1000 vs. V classification of Shervais (1982). The mafic rocks of the DeGrussa mine sequence are transitional between island arc basalts (IAB) and mid ocean ridge basalts (MORB). Narracoota Formation and Killara Formation mafic rocks are classified as IAB with similar composition to some DeGrussa mafic rocks. Johnson Cairn Formation mafic rocks form a linear trend within the MORB field, with the Johnson Cairn mafic rocks at DeGrussa form the Ti- and V-rich end member.

5.4.3. Trace element geochemistry

The origin of the mafic magmatism in the Bryah and Yerrida basin is problematic. This section utilises the Th/Yb vs. Nb/Yb crustal input (Pearce, 2008), and Nb/Yb vs. TiO_2/Yb depth of melting diagrams (Pearce, 2008), REE spider diagrams, and trace element geochemistry to help identify the rock forming processes and source regions associated with each mafic rock unit. For this section, REE graphs were plotted for the Narracoota and Killara Formation, and samples with incompatible or 'spikey' data patterns were removed from the dataset.

The Th/Yb vs. Nb/Yb proxy for crustal input of Pearce (2008) can assist in identifying the tectonic setting a suite of rocks originated in, as well as the amount of crustal input affecting the rocks (Fig. 5.11A). Primary mantle compositions are affected by crustal input, and original MORB and OIB compositions are displaced upwards due to the increased Th concentration gained from crustal rocks.

The Nb/Yb vs. TiO_2/Yb ratio plot of Pearce (2008) can assist in defining the depth of melting (Fig. 5.11B). This diagram is less sensitive to crust-magma interaction in comparison to the Th-Nb plot, because Th is sensitive to crustal input. Hence, replacing it with immobile TiO_2 makes this diagram more robust. The ratio of Nb/Yb reflects all source and melting variables other than crustal input, and the TiO_2/Yb ratio is explainable in terms of garnet residues during melting (Pearce, 2008). It is important to note that, for OIB samples, the more contaminated by crustal material samples are, the more the samples will trend towards the MORB field. For this reason, it is best to use samples which are unaffected by contamination (within or just above the MORB-OIB array of the Th/Yb vs. Nb/Yb diagram). Johnson Cairn Formation samples, the most OIB-like, lie just above the MORB-OIB field hence should be reflected accurately on the Nb/Yb vs. TiO_2/Yb plot.

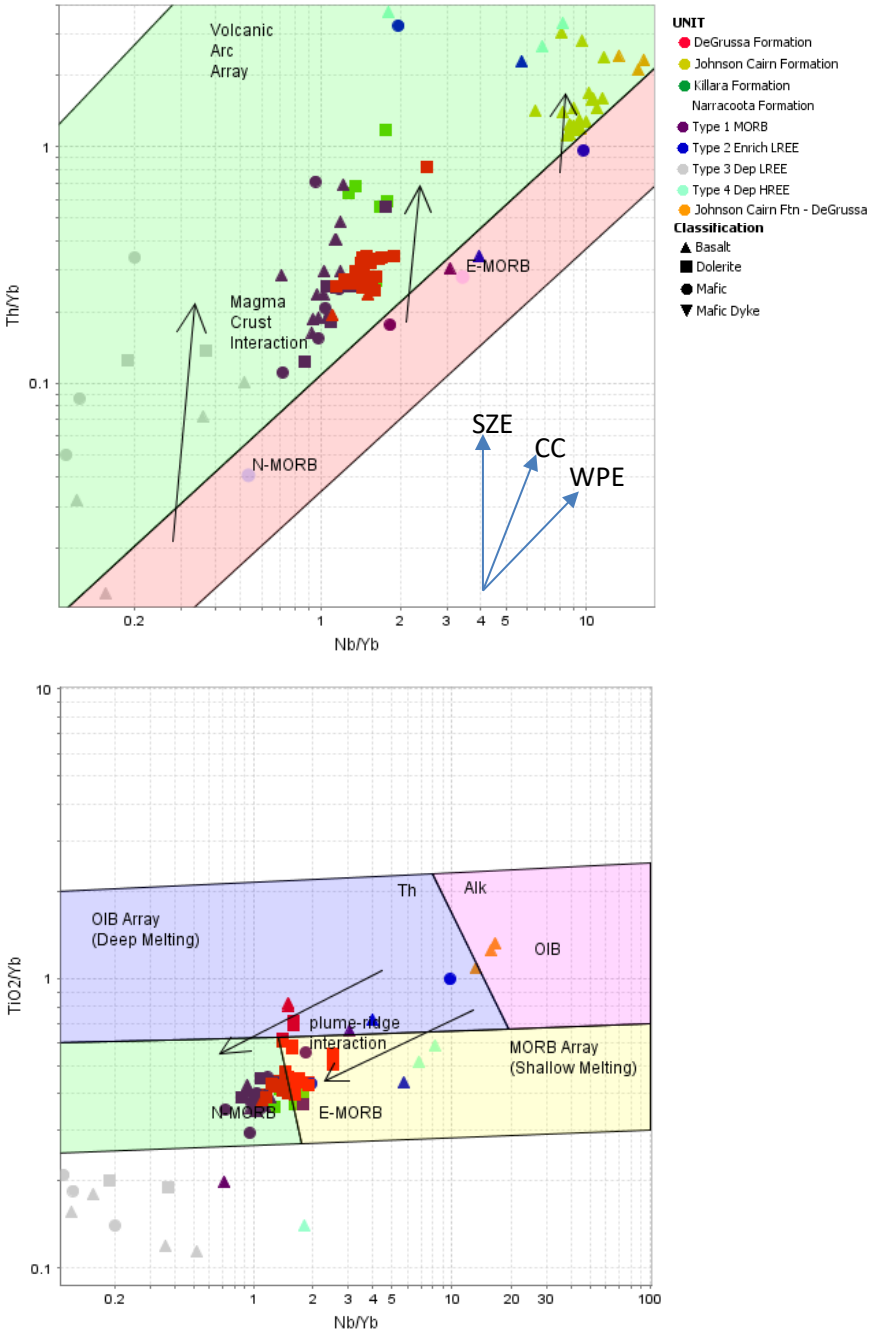

Figure 5.11. Nb/Yb vs. Th/Yb bivariate plot of Pearce (2008)for crustal input, divided into oceanic basalts and volcanic arc basalts field. MORB - Mid-Oceanic Ridge Basalt, OIB - Ocean-Island Basalt, N-MORB - Normal-MORB, E-MORB - Plume-MORB. SZE – subduction zone enrichment, CC – Crustal contamination, WPE – within plate enrichment. **A.** DeGrussa data cluster above the E-MORB to N-MORB array representing interaction of magmas with crustal material. Killara Formation data group at higher Th/Yb ratios but at similar Nb/Yb ratios to DeGrussa suggesting Killara rocks were derived from the same enriched source, but with more crustal contamination. Narracoota Formation data form a linear trend upwards from an N-MORB composition suggesting crustal input from a subduction origin. Johnson Cairn Formation data lie slightly above the MORB-OIB boundary suggesting crustal interaction, and a separate magma source compared with other units. **B.** On the Nb/Yb vs. TiO_2/Yb ratio plot(Pearce, 2008), DeGrussa, and Killara data cluster on the NMORB-EMORB boundary with an upwards trend to higher TiO_2/Yb for DeGrussa. Narracoota Formation MORB plot at slightly lower Nb/Yb values within the NMORB field, while data that plot at low values of both Nb/Yb and TiO_2/Yb have depleted REE patterns (type 4) and boninitic affinities (circle represents boninite rocks field from Piercey et al. (2001). Johnson Cairn Formation data plot within the OIB field confirming the different magma composition

5.4.3.1. Johnson Cairn Formation: The rock/chondrite REE trace element patterns of Johnson Cairn Formation basalts mafic rocks is elevated 40-100 times (Fig. 5.12), with LREE being slightly more enriched than the HREE. A week negative Eu anomaly is present in some Johnson Cairn Formation samples, indicating feldspar fractionation.

The Johnson Cairn Formation basalts represent the initial phases of rifting in the Yerrida/Bryah Basins. The Th/Yb vs. Nb/Yb proxy for crustal input of Pearce (2008) shows the alkali mafic rocks of the Johnson Cairn Formation have much higher Nb/Yb ratios (6.4-11.7, n=24) than the DeGrussa (1.2-1.8, n=23) and Narracoota (0.2-1.9, n=32) Formation, with the three samples of the footwall Johnson Cairn Formation forming a discreete group at higher Nb/Y values (13.2-16.5, n=3) (Fig. 5.11). Data plot just above the E-MORB to OIB array, suggesting they derived from OIB composition but are affected by crustal input. The upwards trend of the Johnson Cairn Formation data, pushing the Th/Nb ratio to higher values, while Nb/Yb remains constant indicates subduction zone interaction. Pearce (2008) indicates that alkalic basalts which are displaced from the MORB-OIB array can usually be explained by recycled crust in the mantle source rather than magma-crust assimilation. The OIB composition is supported by the Nb/Yb vs. TiO_2/Yb ratio plot of Pearce (2008), where footwall Johnson Cairn Formation data plot in the OIB field. THD001 data is not plotted on the 'depth of melting' graph due to a lack of major element data.

Interpretation: The REE patterns for both Johnson Cairn Formation locations, are comparatively similar to that of rift settings, in particular, the Baikal rift zone, the Red Sea Rift and the Ethiopian Plateau (Pearce, 2008, Georoc, 2014). The enrichment of immobile trace elements (.eg. Zr, Ti, LREE), increased Th/Yb ratios at similar Nb/Yb ratios indicates the presence of crustal contamination(Pearce, 2008), and given the stratigraphic setting this is likely to be due to the assimilation of crustal material during ascent. These trends are consistent with those of Piercey et al. (2002) described for the Yukon-Tanana alkaline rocks, and hence the derivation of Johnson Cairn Formation rocks may be consistent with asthenospheric or sub-continental lithospheric sources.

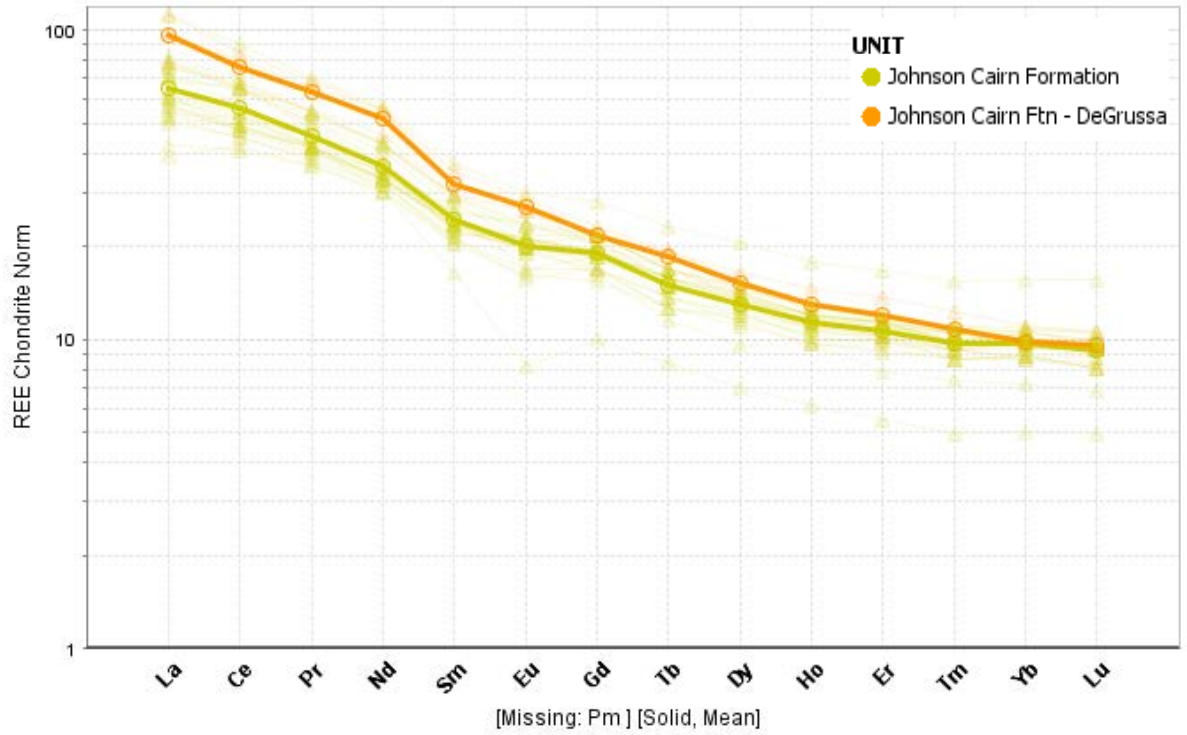

Figure 5.12. REE chondrite patterns (Boynton, 1984) for Johnson Cairn Formation mafic rocks showing REE enrichment, especially in the LREE. Bold lines are the average of each unit. The lowest sample (521976, (Muller, 2011)) is a carbonate altered basalt.

5.4.3.2. DeGrussa: The REE patterns of DeGrussa dolerites and basalts are relatively flat with elevated REE 10-40 times that of chondrite (Fig. 5.13). Both weak positive and negative Eu anomalies are present in some samples, indicative of feldspar fractionation.

DeGrussa mafic rocks form a cluster, similar to E-MORB melt compositions with some crustal contamination evident from the elevated Th/Yb ratios of the crustal input diagram (Pearce, 2008) (Fig. 5.11). The tight cluster of data likely reflects the small area sampled relative to the rest of the Bryah and Yerrida basins. Combined with the Narracoota and Killara Formation data, a more pronounced upwards displacement of Th/Yb is seen. If a rift setting is proposed, magma compositions are likely to have initially had high Th/Yb ratios, evident of the involvement of crustal sources, evolving to lesser Th/Yb ratios as progressive rifting leads to more pure MORB sourced magmas(Pearce, 2008).

DeGrussa data straddle the boundary of N-MORB and E-MORB on the Nb/Yb vs. Ti/Yb ratio plots of Pearce (2008) with a couple of samples (DGMH048 and DGMH080) displaced upwards to higher TiO_2/Yb ratios into the OIB array.

Interpretation: DeGrussa mafic rocks are derived from enriched mantle sources, with a component of crustal contamination, when combined with data from the Narracoota Formation, and interpreted to be influenced by subduction processes. The TiO_2/Yb ratios support a EMORB-NMORB source. Positive Eu anomalies may reflect feldspar fractionation as cumulates, with the negative Eu anomalies reflecting the remaining melt composition.

When compared with a range of mafic rock geochemistry from tectonic settings around the world, DeGrussa rocks show closest similarities to oceanic plateau and seamount rocks such as the Cocos/Nazca-Panama plate and Central Atlantic magmatic province, or arc environments such as Kermadec and with Archean crust (see Appendix 5.4).

5.4.3.3. Killara Formation: The Killara Formation tholeiites have compositions of enriched REE, 10 times that of chondrite and are similar to the DeGrussa and Narracoota Formation MORB REE patterns (Fig. 5.13). Killara rocks also display moderate positive Eu anomalies. Samples with negative Ce anomalies were removed from the REE plots because of the incomplete datasets or irregular patterns made between trace elements allowing dominant trace element trends to be interpreted from the E-MORB type REE patterns.

The Th/Yb vs. Nb/Yb proxy for crustal input of Pearce (2008) (Fig 5.8) constrains the Killara Formation data to a cluster at elevated Th/Yb ratios but similar Nb/Yb ratios as that of DeGrussa. This indicates that Killara mafic rocks were derived from the same enriched source as DeGrussa, but with greater amounts of crustal contamination, possibly influenced by subduction processes. The Nb/Yb vs. TiO_2/Yb ratio plot of Pearce (2008) shows data of the Killara Formation clustering with DeGrussa data on the NMORB - EMORB boundary (Fig 5.8) implying that they are derived from the same mantle source, and may even be the same mafic unit.

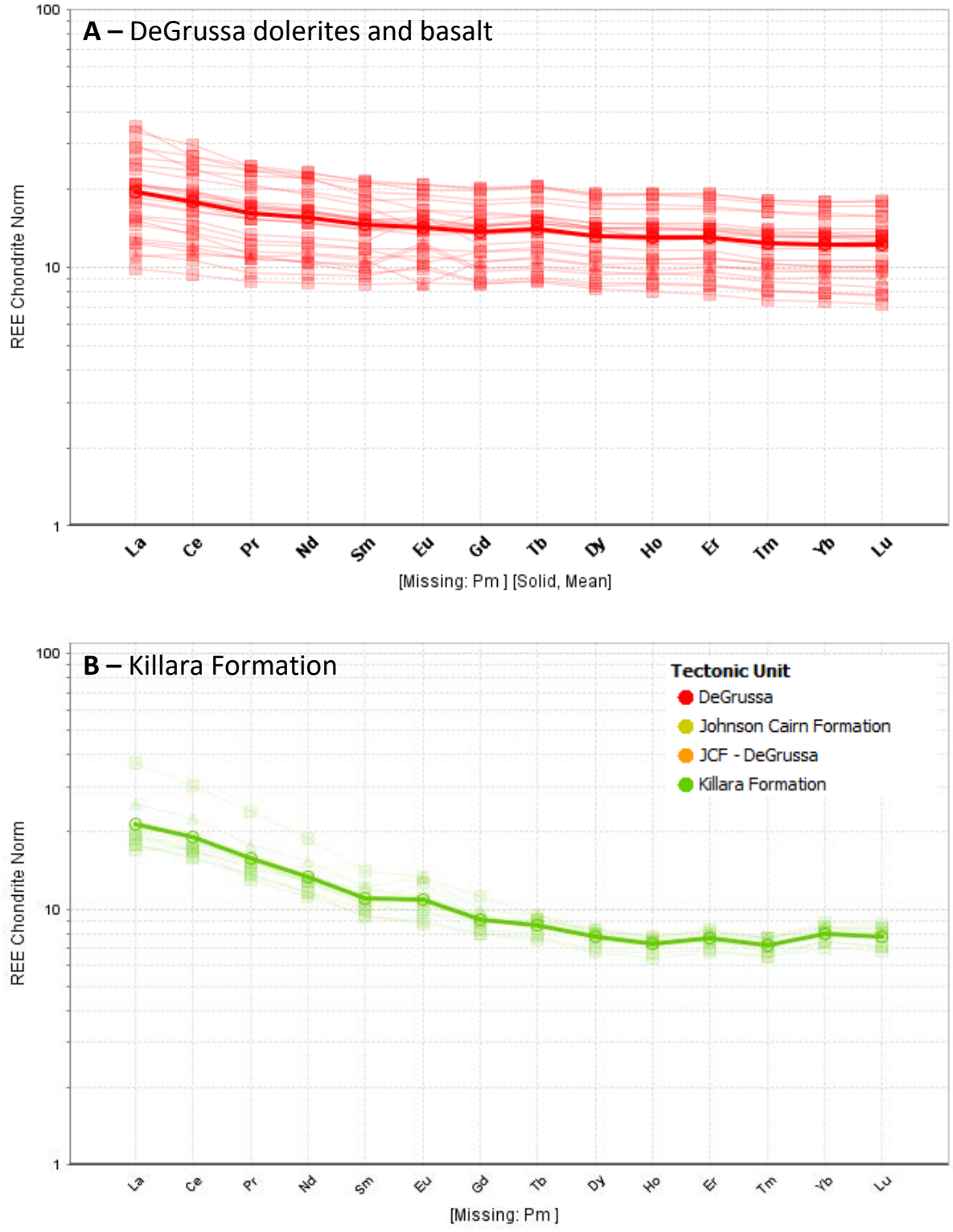

Figure 5.13 A. REE chondrite Norm (Boynton, 1984) for DeGrussa mafic rocks. Bold lines are the average of each unit. **B.** REE chondrite (Boynton, 1984) patterns for Killara Formation mafic rocks showing REE enrichment.

Interpretation: The REE trace elements combined with the enrichments in Th/Nb indicate crustal contamination from either an asthenospheric or continental lithosphere source, probably similar to that found in the Finlayson district of Canada (Piercey et al., 2002). The weak positive Eu anomalies are consistent fractionation of feldspar, possibly as cumulates.

5.4.3.4. Narracoota Formation: Regional Narracoota Formation samples were characterised and grouped by their similar REE patterns (Fig. 5.14) (see also methods section):

Type 1 – MORB: These rocks have values similar to DeGrussa. And are located in central parts of the western Bryah, to the north of the Murchison Fault, and associated with the Horseshoe Lights and Fortnum gold deposits. The REE patterns are similar to mafic rocks in present day seamount and oceanic plateau settings (Appendix 5.4).

Type 2 – enriched-REE: Found to the west of Narracoota Formation MORB samples, to the south side of the Murchison Fault, NW of Fortnum and along the Jenkin Fault / contact with the Marymia Inlier. These are similar to values at DeGrussa and type 1 samples, but with slightly more enriched LREE.

Type 3 - depleted REE: Found at Trillbar, Noonyereena, the southern Narracoota, and associated with Fortnum mineralisation, these rocks have characteristics of boninites. The very low Ti and Zr samples of the Narracoota rocks in Figure 5.10 are coupled with low SiO_2, lower Na_2O+K_2O, high Cr and Ni, and depleted REE suggesting the boninitic characteristics of Narracoota mafic rocks. Hence, the southern Narracoota may represent a forearc setting.

Type 4 – depleted HREE: similar to the Johnson Cairn Formation basalts of THD001.

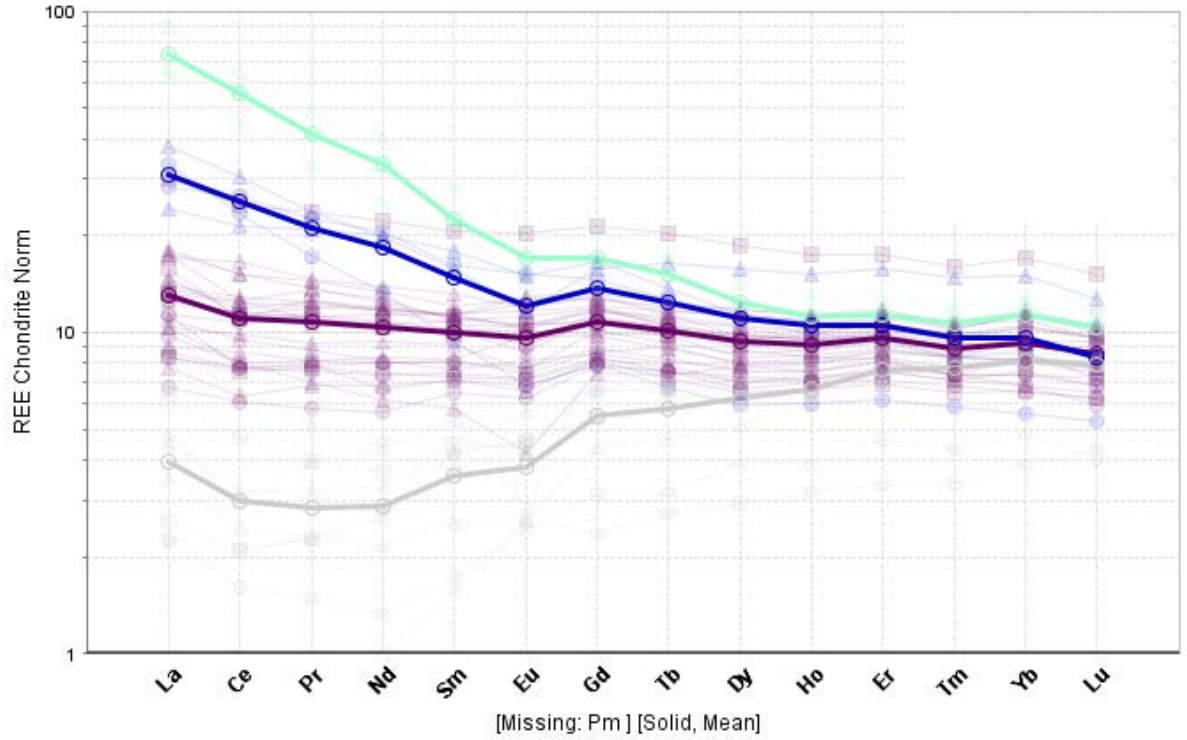

Figure5.14A. Narracoota Formation REE chondrite, separated into characteristic trace element patterns. Type 1 – MORB with slightly enriched LREE, simiar to DeGrussa and Killara rocks. Type 2 - show samples of enriched REE and are characteristic of rift settings. Type 3 – depleted REE with REE patterms comparable to that of boninites or oceanic plateau.. Type 4 - depleted HREE similar to Johnsnon Cairn Formation basalt.

All Narracoota Formation samples on the Th/Yb vs. Nb/Yb plot of Pearce (2008) lie above the MORB-OIB array (Fig 5..11). Those of Type 1 MORB form a linear trend upwards from an EMORB-NMORB composition. This reflects a crustal input to the melt and the linear trend with increasing Th/Yb reflects possible subduction zone enrichment. Type 2 MORB samples are spread to high Th/Yb ratios, and Nb/Yb ratios similar to Johnson Cairn Formation rocks.

The Nb/Yb vs. TiO_2/Yb ratio plot (Fig. 5.11) shows that the Narracoota Formation mafic rocks are mostly within the N-MORB array, plotting similarly to DeGrussa mafic rocks, but with lower Nb/Yb ratios. Some samples stray into the E-MORB and OIB array due to the higher Nb/Yb ratios in Type 2 MORB samples. Data that plot below the MORB array, at low values of both Nb/Yb and TiO_2/Yb (Type 3), have depleted REE patterns, lower Na2O+K20, higher Cr and Ni, and boninitic affinities. Geochemistry is comparable with boninitic samples from the Yukon-Tarana Province (Piercey et al., 2001).

Interpretation: The dominant mafic rock composition for Narracoota Formation rocks is MORB (Type 1) and depleted REE boninitic rocks (Type 3). REE patterns as well as the Pearce (2008)graphs suggest derivation of Type 1 MORB rocks from EMORB mantle sources, with subduction zone mantle influences. Results can be compared to oceanic plateau or seamount settings similar to those of DeGrussa mafic rocks. Depleted REE patterns plot in similar locations on a Nb/Yb vs. TiO_2/Yb graph when compared with boninites fromPiercey et al. (2001). The presence of boninitic rocks may indicate a forearc or continental rift setting.

5.5. Discussion

5.5.1. Tectonic setting

The geochemical considerations presented in this chapter leave several options for the tectonic development of the region. Table 5.3 summarises the geochemistry and preferred tectonic environment.

Table 5.3. Summary geochemistry and tectonic setting

Geochemical Plot type	Johnson Cairn Formation		DeGrussa Mafic rocks	Killara Formation	Narracoota Formation
	THD001	DeGrussa footwall			
TAS plutonic	N/A	Gabbro	Gabbro	Gabbro	Gabbro
Volcanic alkaline-subalkaline	N/A	Subalkaline	Subalkaline	Subalkaline	Subalkaline
Basalt Ti vs. Zr	MORB	Ti-rich MORB	Mix-MORB	IAT-Mix-calc-alkaline	IAT
Nb/Y:Zr/Ti	*Alkali Basalt*	*Alkali Basalt*	Basalt	Basalt	Basalt
Ti/1000 vs. V	MORB	MORB	IAT/MORB	IAT	IAT
Ta/Yb vs. Th/Yb (Pearce, 2008)	E-MORB-OIB, crustal component	E-MORB-OIB, crustal component	EMORB, crustal component	EMORB, increased crustal component	EMORB with subduction zone crustal component
Nb/Yb vs. TiO2/Yb	N/A	OIB	EMORB-NMORB transition.	EMORB-NMORB transition	NMORB, boninites
REE	Rift volcanics, sedimented backarcs		Oceanic plateau, seamounts	Oceanic plateau, seamounts	Oceanic plateau, seamounts, boninites (forearc), felsic volcanics (island arc)
Summary	OIB composition magma contaminated by crustal sources during emplacement in a sedimented rift setting.		EMORB composition similar to oceanic seamount rocks of the Cocos/Nazca Panama plate, with a crustal component		EMORB composition similar to DeGrussa but encompassing a wider range of rock suggesting island arc /subduction affiliation

The Johnson Cairn Formation mafic rocks, represent the earliest magmatic event in the region. They are geochemically distinct from the DeGrussa, Killara, and Narracoota Formation mafic rocks, and the alkali nature of the rocks is characteristic of anorogenic continental rift settings or

oceanic islands (Pearce and Cann, 1973). Elevated REE patterns (Boynton, 1984) for the Johnson Cairn Formation indicate the EMORB source, with a substantial crustal component. These REE patterns are similar to those of mafic rocks in rifted settings such as the Ethiopian Rift, Red Sea Islands and the Baikal Rift Zone (Georoc (2014)database and references within, Ap. 5.4). The crustal input diagrams of Pearce (2008) also support a rifted environment with the elevated Th/Nb ratio interpreted to reflect the addition of crustal material during ascent. The MORB-OIB nature may indicate a plume event along the northern margin of the Yilgarn.

Geological evidence in support of a continental rift tectonic setting are:

1. The presence of evaporitic rocks (Bubble Well Member, Juderina Formation, Yerrida Group) disconformably overlying Archean basement (Yilgarn and Marymia Inlier rocks) formed in a sag basin setting during the initial stages of rifting. Conglomeratic units of the Magazine Member footwall sedimentary rocks (large carbonate clasts derived from the Johnson Cairn Formation) indicate rapid subsidence. The siltstone-shale dominated turbidites of the footwall and host sedimentary rocks suggest deposition in a marine basin. Comparison can be made between the stratigraphy hosting the DeGrussa deposit and the present day stratigraphy of the Guaymas Basin, including the thick sediment sequences overlying an active spreading centre, and high heat flows (>250˚C) represented by dolerite dykes and sills (Goodfellow and Zierenberg, 1999).

2. Alkali basalt composition, a characteristic rock type in continental rifts, of the Johnson Cairn Formation mafic rocks. This is supported by the trace element geochemistry discussed above– data from the Georoc (2014) database and references within (Appendix 5.1).

3. If the contact between the Yerrida Group's Johnson Cairn Formation, and the Bryah Group's Magazine Member(Jeffery, 2013), is paraconformable or unconformable, then the DeGrussa region is most likely to have formed as a continental rift, similar to the Red Sea Rift of Africa, or the Guaymas Basin of North America (Fig. 5.15).

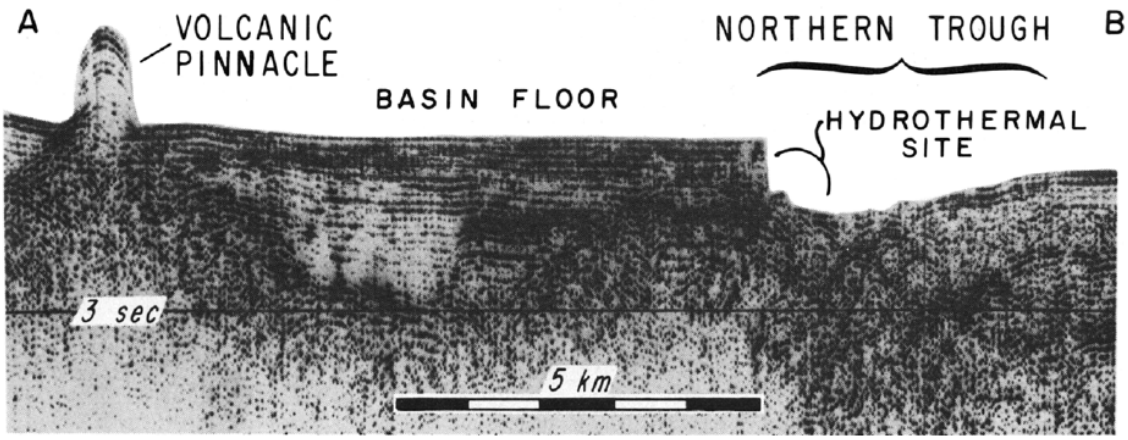

Figure 5.15. Seismic profile from Lonsdale et al. (1980) displaying the location of hydrothermal deposits in the Northern Trough of the Guaymas Basin. A basalt sill and sedimentary rock complex underlies the sea floor. Hydrothermal sites are concentrated around fault escarpments.

Although no extensive geochronological work has been completed, trace element patterns of the Killara Formation mafic rocks further suggest some interaction between a MORB source and crustal material. Pirajno and Occhipinti (1998) suggested the Killara Formation to be of continental affinity.

DeGrussa, Killara and Narracoota Formation mafic rocks are REE enriched (LREE moderately enriched above HREE) showing their similar magmatic source. Hence, the DeGrussa and Killara Formation are closely related. Narracoota Formation volcanic rocks vary from basalt through to rhyolite and dacite (Pirajno et al., 2000) indicating the different tectonic setting and magmatic processes in the western parts of the basin. The DeGrussa, Killara and Narracoota REE patterns are most similar to those of mafic rock found in the Cocos/Nazca-Panama Plate (Fig 5.16), particularly the Cocos, Carnegie and Malpelo seamount ridges, between the Galapagos Islands and the Central and South American landmass. (Figure 5.17 and Appendix 5.4). This is supported by Nb/Yb vs. TiO_2/Yb plots which show that geochemistry of DeGrussa mafic rocks can be closely compared to these seamount chains of the Panama Plate, although data sit within the MORB-OIB array (Appendix 5.4). Embley et al. (1988) identified Fe- Ti- basalt (FeO_T > 12wt%, TiO_2 >2wt%) as some of the most common rock types along the Galapagos Rift, with some highly evolved basalts containing >16% FeO_T and >3 wt% TiO_2. These values are similar to those seen in

DeGrussa mafic rocks, although TiO_2 contents in DeGrussa rocks are typically <3wt% (Fig. 5.4, 5.7).

The Cocos, Malpelo and Carnegie ridges interpreted to be hot spot traces which began to form when the Galapagos hotspot initiated (Meschede and Barckhausen, 2001). There is a lack of sedimentation in this region (10-40cm of pelagic sediments along the Galapagos rift) which is in contrast to the DeGrussa deposit area (meters of sedimentary rock). This suggests that the DeGrussa deposit may have formed in a similar tectonic setting, but in an area where a larger amount of terrigenous sediment was deposited (perhaps rapid uplift of a neighbouring terrane such as the Marymia Inlier or the Goodin Dome).

The Cocos-Nazca Plate is proximal to the Guaymas basin, and as discussed in previous chapters, may be a similar tectonic setting for the deposition of Yerrida Group evaporates, sedimentary rocks and mafic magmatism (Fig. 5.16, 5.17).

Narracoota Formation geochemistry suggests a wide variation in mafic rock geochemistry, which is characteristic of a range of tectonic settings and not restricted to a continental rift. The documented presence of boninites and/or rocks with boninitic affinities support forearc to back-arc tectonic formation. Hynes and Gee (1986), Pirajno et al. (2000) and Cranney (2011) also identified boninites in their studies. Boninites typically form in the nascent or forearc of island arc settings following the plate foundering and initiation of plate subduction (Crawford et al., 1989) allowing the position of subduction and/or basin rifting to be inferred. The location of many of the boninitic samples is along the Murchison Fault (Fig. 5.1). The lack of supporting regional geological evidence led Hynes and Gee (1986) to prefer a continental rift environment in which sub-continental mantle was locally H_2O rich with the Narracoota Formation erupted on or near continental crust that underwent rapid subsidence. Hynes and Gee (1986) proposed that the Narracoota Formation mafic rocks were erupted during rifting of an island arc. Rifting may have involved large scale melting of mantle material, some of which was similar to the source for MORB and some of which was very refractory. The refractory character of the mantle is

attributed by Hynes and Gee (1986) to a previous MORB or island arc-tholeiite-generating event, and the hydrous character is explained by dehydration of an underlying descending oceanic plate.

Boninitic rocks can be separated into both high-Ca and low-Ca suites. As defined by Crawford et al. (1989), the low Ca suite is subdivided into 3 types:

Type 1- low Ca boninites: characterised by very low CaO (<8%), low CaO/Al_2O_3 (<0.55) and low total FeO (<8%), high Al_2O_3 and alkali content.

Type 2 – low Ca boninites: characterised by <10% MgO,very low CaO/Al_2O_3 (<0.55) and low FeO (<7%) but have higher total alkalis and SiO_2 contents than type 1.

Type 3 – low Ca boninites: lower Na_2O and higher CaO and FeO* contents than types 1 or 2 lavas at any Mg# value, CaO/Al_2O_3=0.5-0.8.

High-Ca boninites – notably lower SiO_2 (52-56%), Na_2O and K_2O contents than low-Ca boninites, and have higher CaO (10-15%) and FeO* (7.5-11%) contents and grade with decreasing SiO_2 contents into low-Ti arc basalts (Crawford et al., 1989).

The eruption of boninites in a continental rift setting would require the maintenance of high temperatures during ascent to shallow depths of only 10-15km (Crawford et al., 1989). In this type of setting it is more likely that siliceous high-Mg magmas would form (Crawford et al., 1989).

Boninite is observed to have been emplaced over sialic crust in the Finlayson Lake region in the Yukon-Tanana where it is interpreted that the formation of boninite and the association with continental crust may be due to propagation of a spreading ridge into an arc built on composite basement of continental and oceanic affinity (Piercey et al., 2001). In a similar way, rifting through the Bryah basin could have affected arc magmatism in the western parts of the Narracoota where boninite as well as felsic magmatism was also intruded.

In this scenario, northward subduction may have occurred beneath the Bryah Group, along the northern margin of the Yilgarn Craton, although no volcanic rocks affiliated with island arc systems (ie. andesite and rhyolite) are identified in the southern parts of the Bryah Group. Rhyolites and andesite are found in northern parts of the Bryah Group, around the Fortnum and

Horseshoe Lights deposits, which leads to the possibility that subduction may have been south directed along the northern margin of the Bryah Basin, and north of the Marymia Inlier.

To the west of the Bryah Group, the Camel Hills Metamorphics were interpreted to have formed in a forearc or backarc basin setting along the margin of the Glenburgh Terrane during continental collision between c. 2240 and 2125 Ma (Johnson et al., 2011). The Errabiddy Shear Zone forms the boundary between the Glenburgh Terrane to the Bryah Group, and marks the northern limit of the Yilgarn Craton. The Dalgaringa Supersuite, which consists of granitic gneisses, may have formed in an Andean-type setting during north directed subduction of oceanic crust under the combined Pilbara Craton-Glenburgh Terrane until c. 1970 Ma (Sheppard et al., 2004).

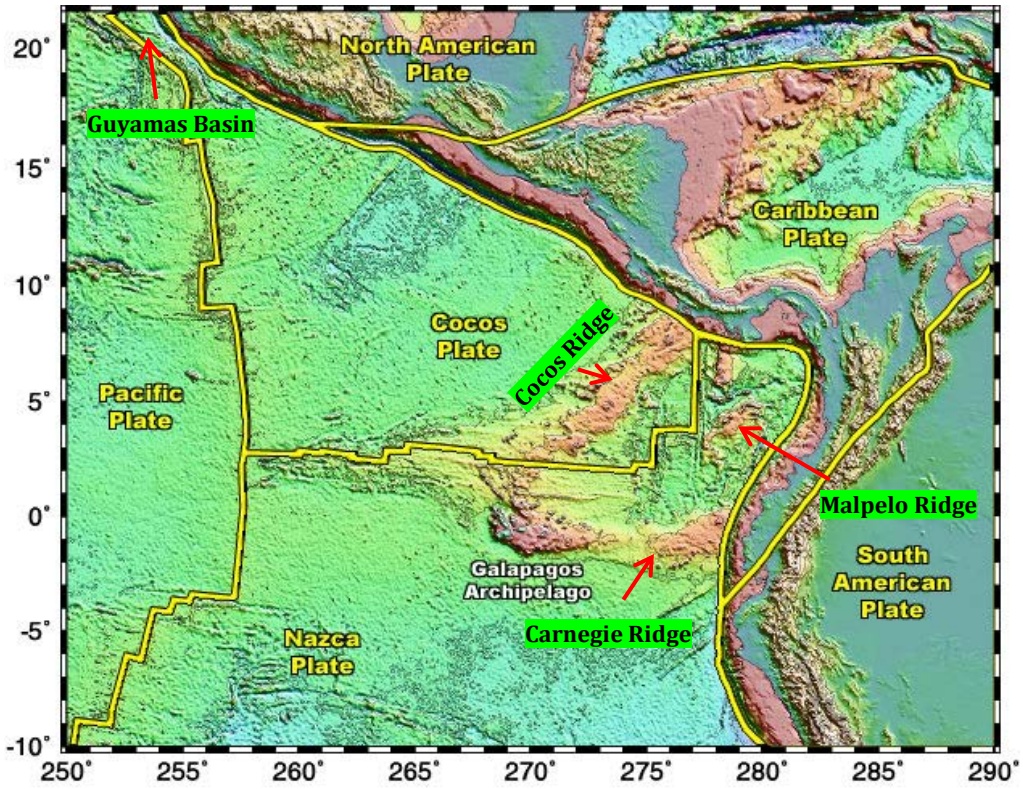

Figure 5.16. A regional view of the Cocos-Nazca, and adjacent plates showing rift axis, and seamount ridges (Cocos, Carnegie and Malpelo Ridges) which have mafic rocks that share very similar trace element characteristics and REE patterns to those associated with DeGrussa (adapted from Smith and Sandwell (1997)). This could be a present day analogy for the eastern Capricorn Orogen, in which the Guyamas basin to the north represents the Yerrida Group, the Cocos, Carnegie and Malpelo ridges and Galapagos archipelago represent a setting similar to that in which the Killara Formation and DeGrussa mafic rocks formed. The Narracoota Formation is more complex and may represent an arc-type environment, not represented in the Cocos-Nazca region. The Camel Hills Metamorphics to the east of the Bryah Group may be the equivalent of the Andean mountain range.

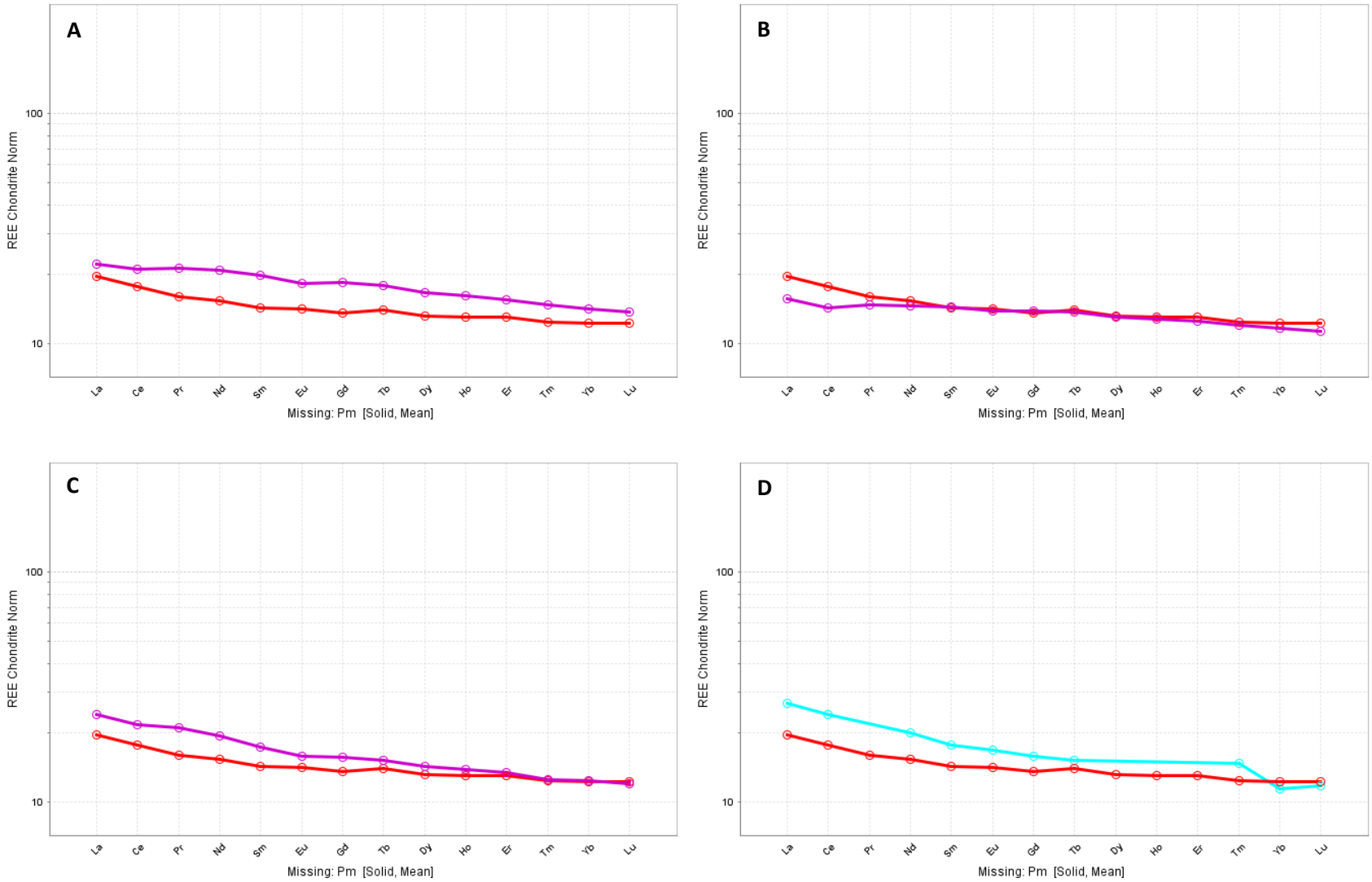

Figure 5.17. REE comparison between DeGrussa mafic rocks (red line) and **A.** Cocos Ridge Seamounts, **B.** Carnegie Ridge seamounts, **C.** Malpelo Ridge seamounts, **D.** Andean Arc

5.5.2. Geochemical maps across the Bryah Basin and regional geochemistry vectors.

Similar geochemical data for mafic rocks is examined for use as a vectoring tool to mineralisation. Geochemical maps provided in Figures 5.18-5.30 are for the Bryah Basin only.

DeGrussa is associated with mafic rocks with elevated Ti, Cu, Fe_2O_3, Mo, V, Al_2O_3, Co, Cs, and Ba. Deposits in the region have similar enriched compositions (Table 5.4) in comparison with the regional background. Several locations not associated with known economic mineralisation have anomalous geochemistry (Ruby Well and Mikhaburra) (Fig. 5.18). Regionally elevated Ti is regularly spaced to the south-east along the contact between the Killara Formation and the Yerrida Craton.

Table 5.4. Summary of deposits and locations in the Bryah Basin with anomalous geochemistry

Deposit	**Elevated in**
DeGrussa Cu-Au	Cu, Fe_2O_3, Mo, V, Al_2O_3, Ti, Co, Cs, Ba
Horseshoe Lights Cu-Au	Al_2O_3, Mo, V, Cs
Horseshoe/Cassidy Au	Cs
Yarlarweelor Au	Cs, Ba
Labouchere Au	Cs
Harmony Au	Cs
Fortnum Au	Al2O3
Ruby Well	Cu, Mo, Co, V, Tl, Cr, Ag, Hf, Ga, Pb, U, Sr, Th, Zn, Zr, TiO_2, Al_2O_3, MnO, Fe_2O_3, distal Ba
Mikhaburra	Al_2O_3, Fe_2O_3, MgO, Co, Cu, Cs

Al_2O_3 (Fig. 5.19) is spread through the area, with similar high values concurrent at DeGrussa, Horseshoe Lights and Fortnum. Co (Fig. 5.20) is elevated in several locations. The Ruby Well prospect (known Au mineralisation) is proximal to the Murchison Fault and Yerrida Group contact and also has elevated Cu, Mo, V, Tl, Cr, Ag, Co, Hf, Ga, Pb, U, Sr, Th, Zn, Zr, TiO_2, Al_2O_3, MnO, Fe_2O_3, and distal Ba (see appendix 5.1, sample #120729).

Elevated Mo (Fig. 5.23) not associated with deposits (e.g. DeGrussa and Horseshoe Lights) is found along the contact between the Peak Hill schist and Bryah Group sedimentary rocks. High V (Fig. 5.24) is widespread across the basin. Both Mo and V are likely associated with faults and major structures (e.g. along the Murchison Fault). Cs (Fig. 5.25) is elevated along the Jenkin Fault and Murchison Fault, and most deposits in the Bryah. Four locations with elevated Cs are located in the Narracoota but are not associated with any known mineralisation.

Ba (Fig. 5.26) is higher in association with the existing deposits of DeGrussa and Yarlarweelor. Elevated levels of Ba are found in rocks at THD001 (Yerrida Group), and widespread throughout the Western Bryah Group. Cr (Fig. 5.27) is low at DeGrussa, but high in mafic rocks associated with Horseshoe Lights and Fortnum. Cr is elevated (>1200ppm) in the northern and eastern parts of the Narracoota (lower values, 0-1200ppm, in the southern Narracoota) as well as variably enriched throughout the Killara Formation. These elevated values correlate with elevated Ni (Fig. 5.28) the most primitive mafic rocks of the region.

Cu (Fig. 5.21) is elevated in the Southern Narracoota and Western Killara. These locations may have potential for further VHMS mineralisation. Additionally, elevated Fe_2O_3 occur proximal to known mineralisation at DeGrussa, Harmony, Horseshoe/Cassidy, Labouchere, Mikhaburra and Ruby Well (Fig 5.22). A number of new prospects can be generated given the prospective Fe_2O_3 range (e.g. Tank Well, Narracoota Homestead/Durack Well and Mt. Fraser Creek). High Fe_2O_3 (>11%) and SiO_2 (48-52%) (Fig. 5.29) often corresponds to MgO in the range 2-10% (Fig. 5.30) within the same prospect area, although not always from the same sample. All three occurring in the one area is rare. From this preliminary study, two potential target areas for VHMS exploration are selected based on their prospective mafic rock geochemistry):

1. Ruby Well area: Located within the Narracoota Formation to the east of the Ruby Well prospect. Mafic rock samples have elevated TiO_2, Al_2O_3, Fe_2O_3, Co, Cu, Mo, V, Tl and Cr similar to DeGrussa. Ba is lower but distally has high values. This area is located north of the Goodin Fault, on the south side of the Bryah Basin, and could be inferred to be along strike from the newly discovered Monty Prospect in the northeast.

2. Mikhaburra: Located near existing prospects of Mikhaburra and Cashman within the Narracoota Formation. Mafic rock samples have elevated Al_2O_3, Fe_2O_3, MgO, Co, and Cu similar to DeGrussa mafic rocks. It is located to the west of the Ruby Well prospect within the same stratigraphy.

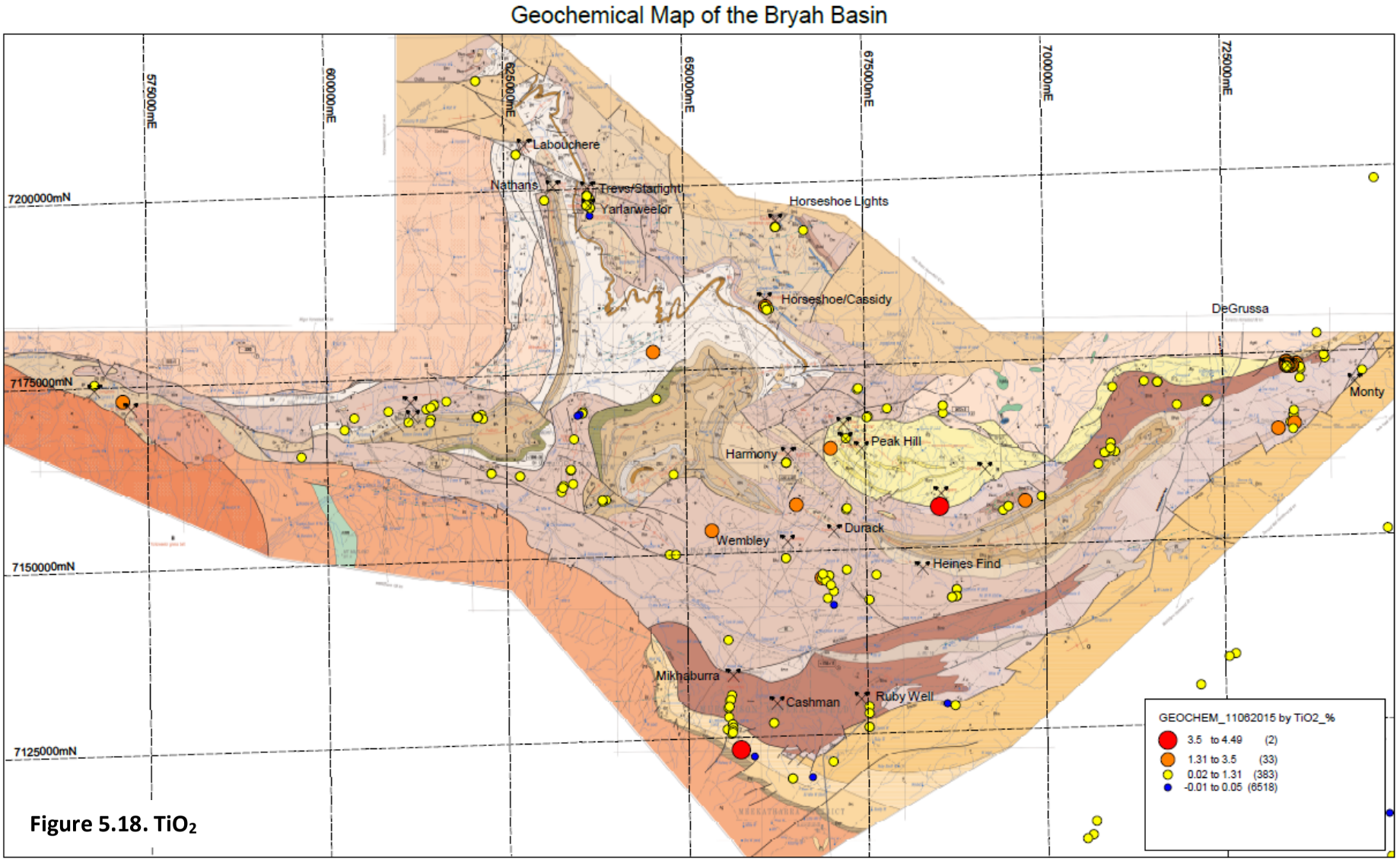

Figure 5.18. TiO_2

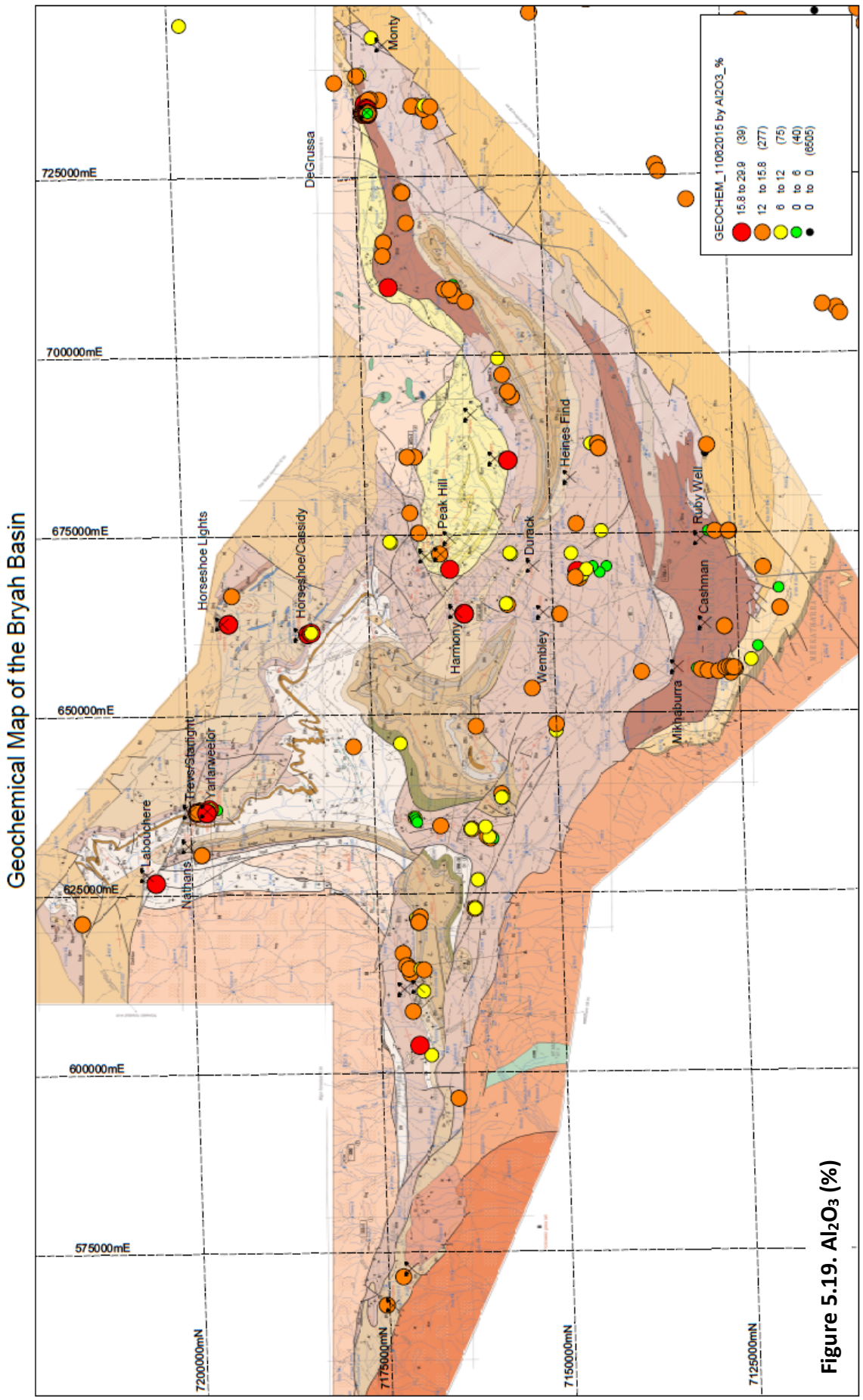

Figure 5.19. Al_2O_3 (%)

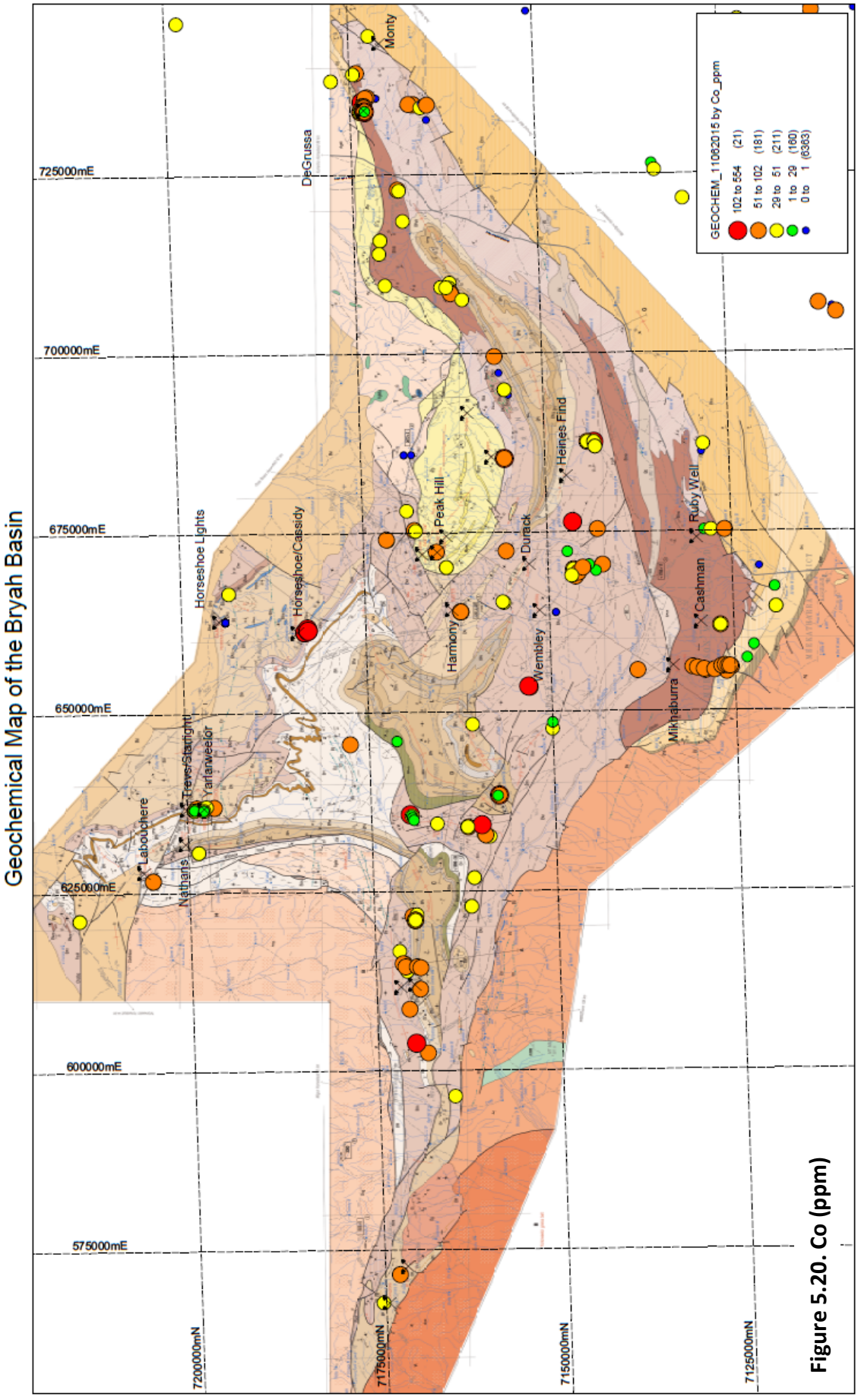

Figure 5.20. Co (ppm)

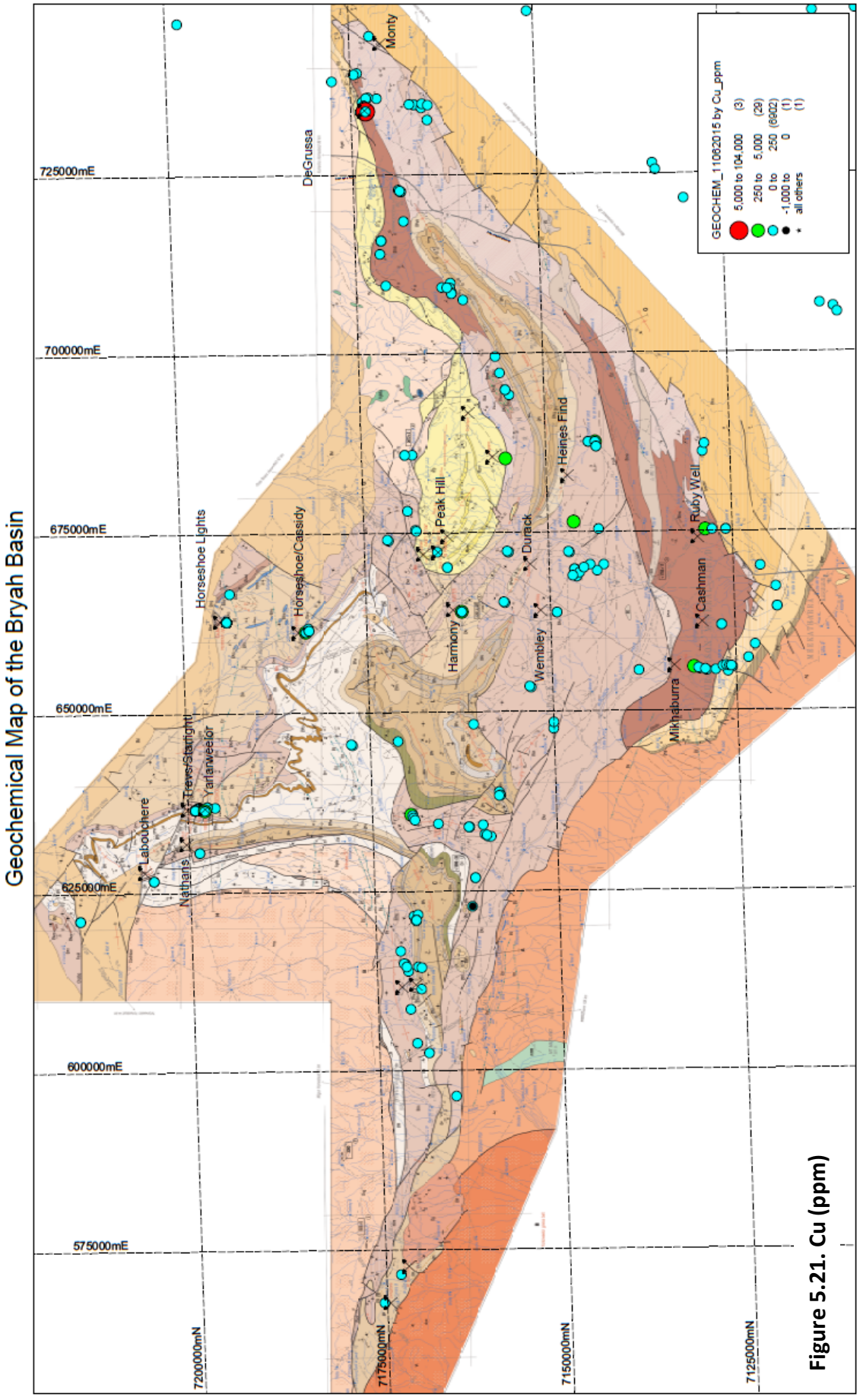

Figure 5.21. Cu (ppm)

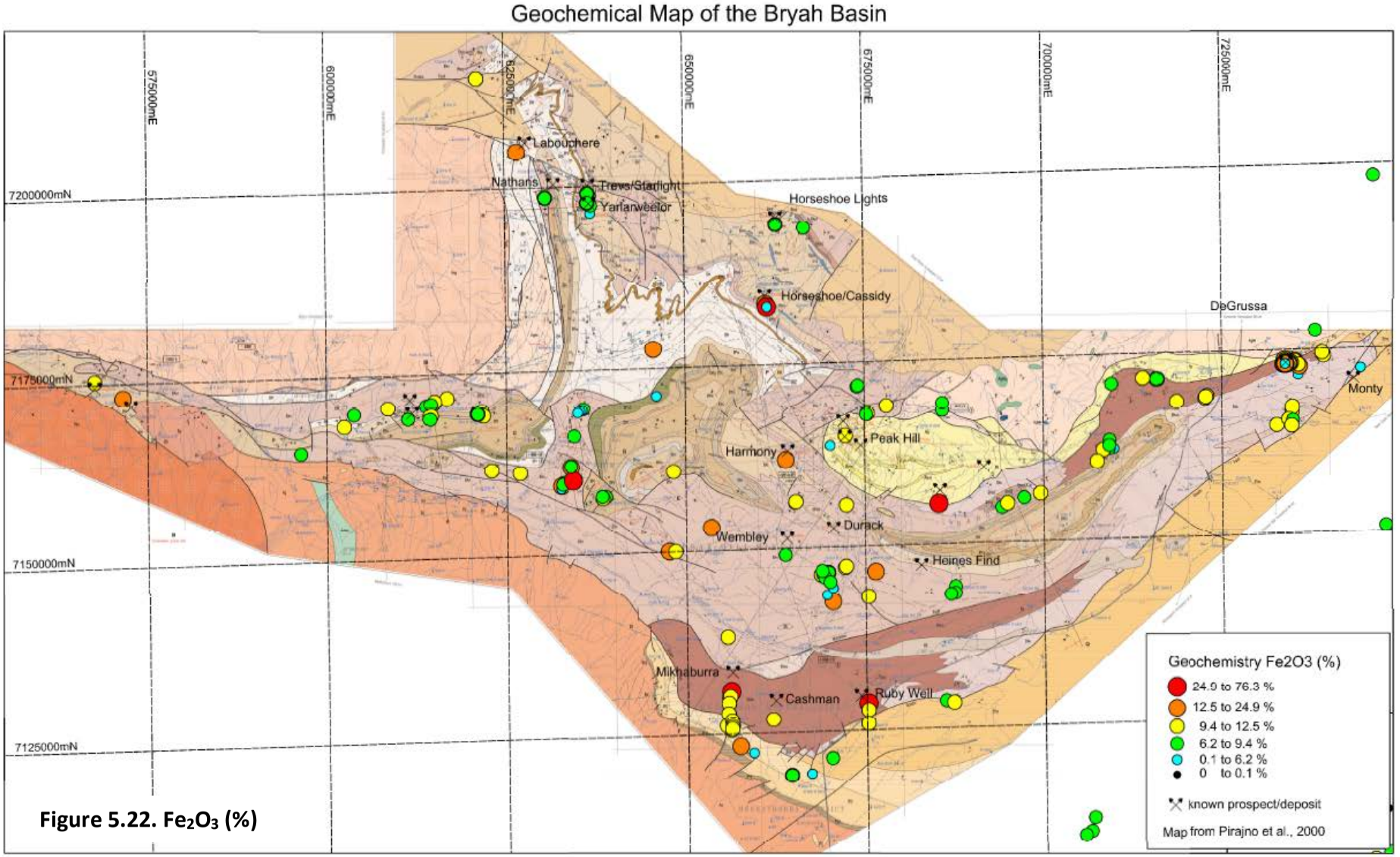

Figure 5.22. Fe_2O_3 (%)

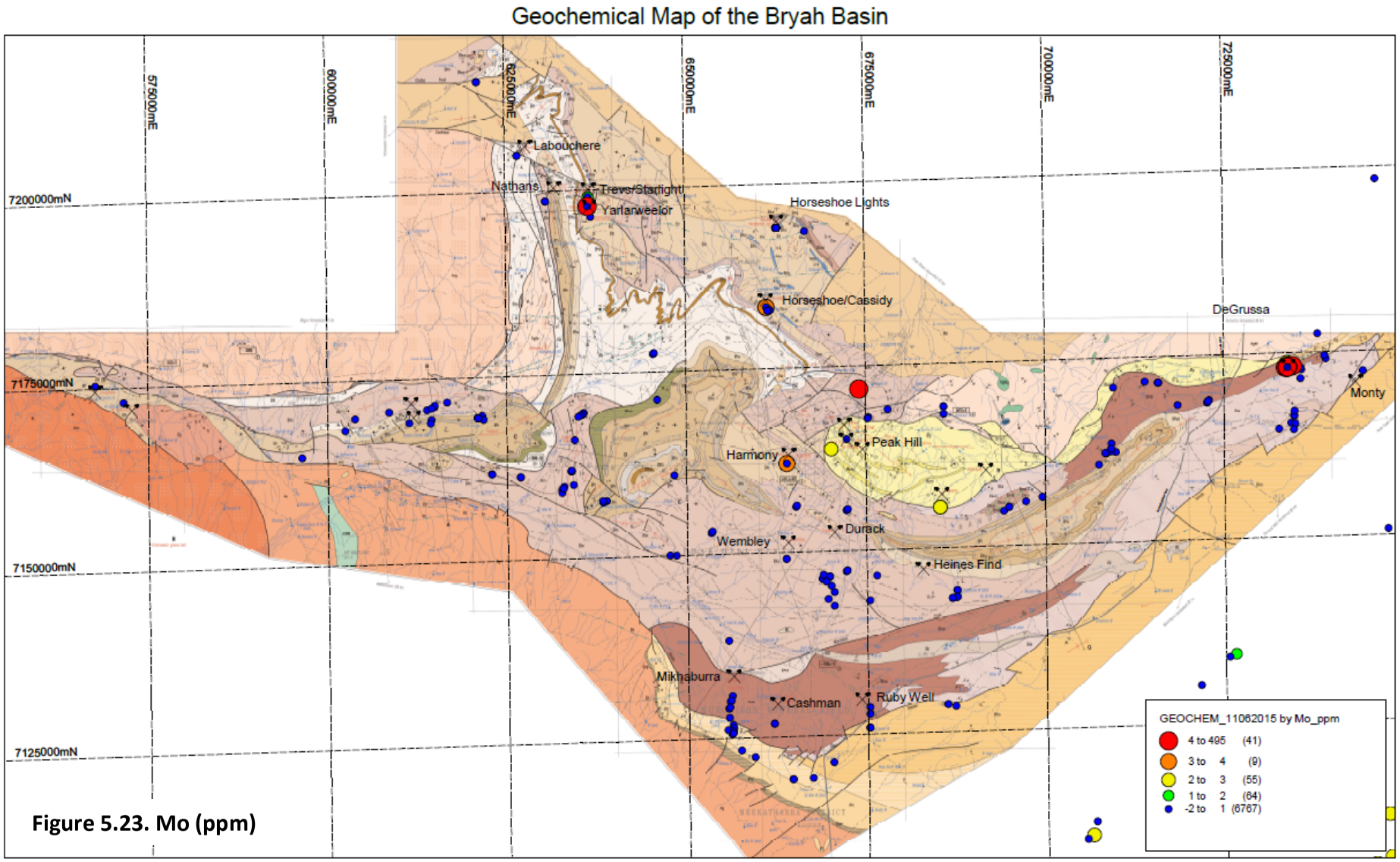

Figure 5.23. Mo (ppm)

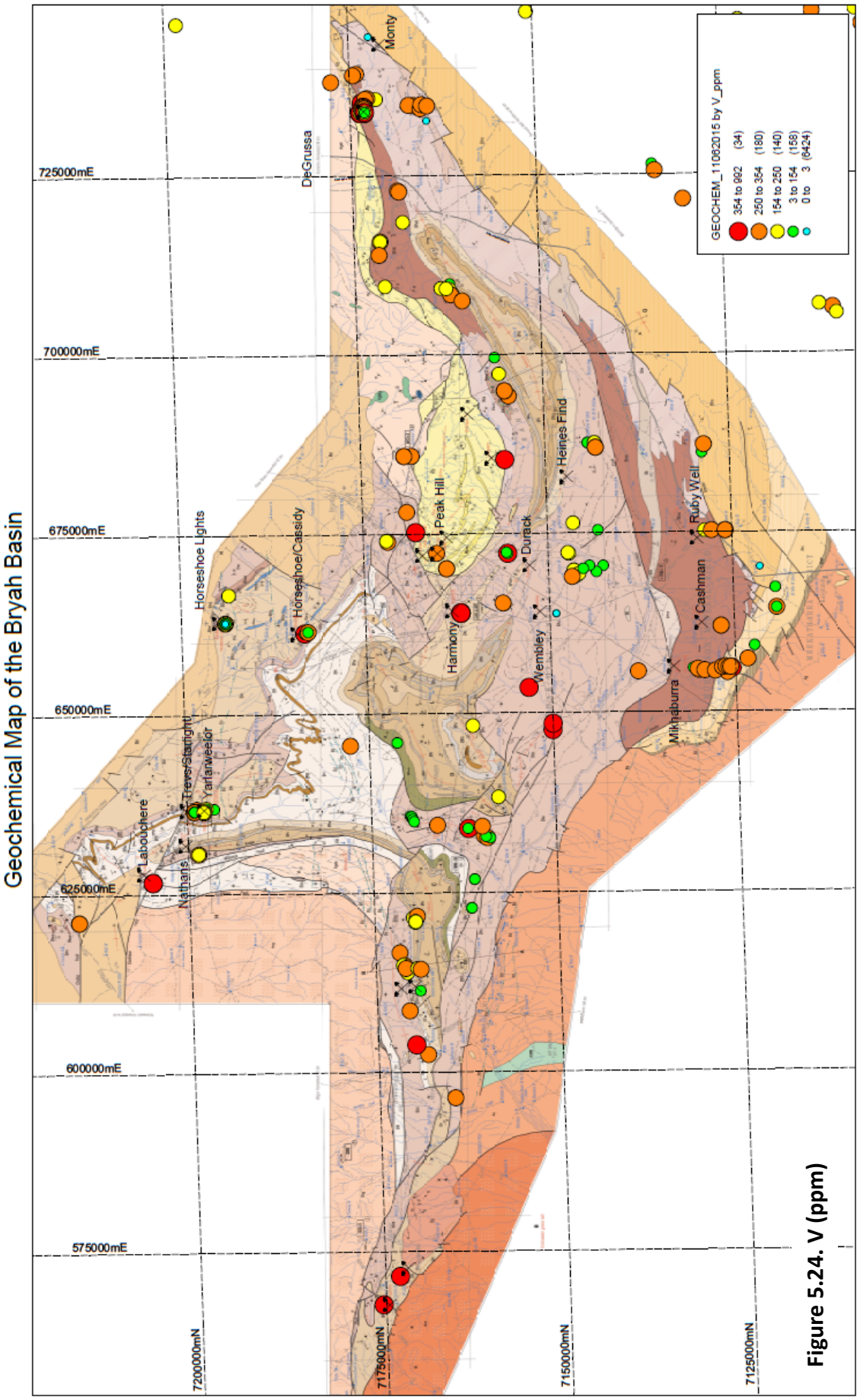

Figure 5.24. V (ppm)

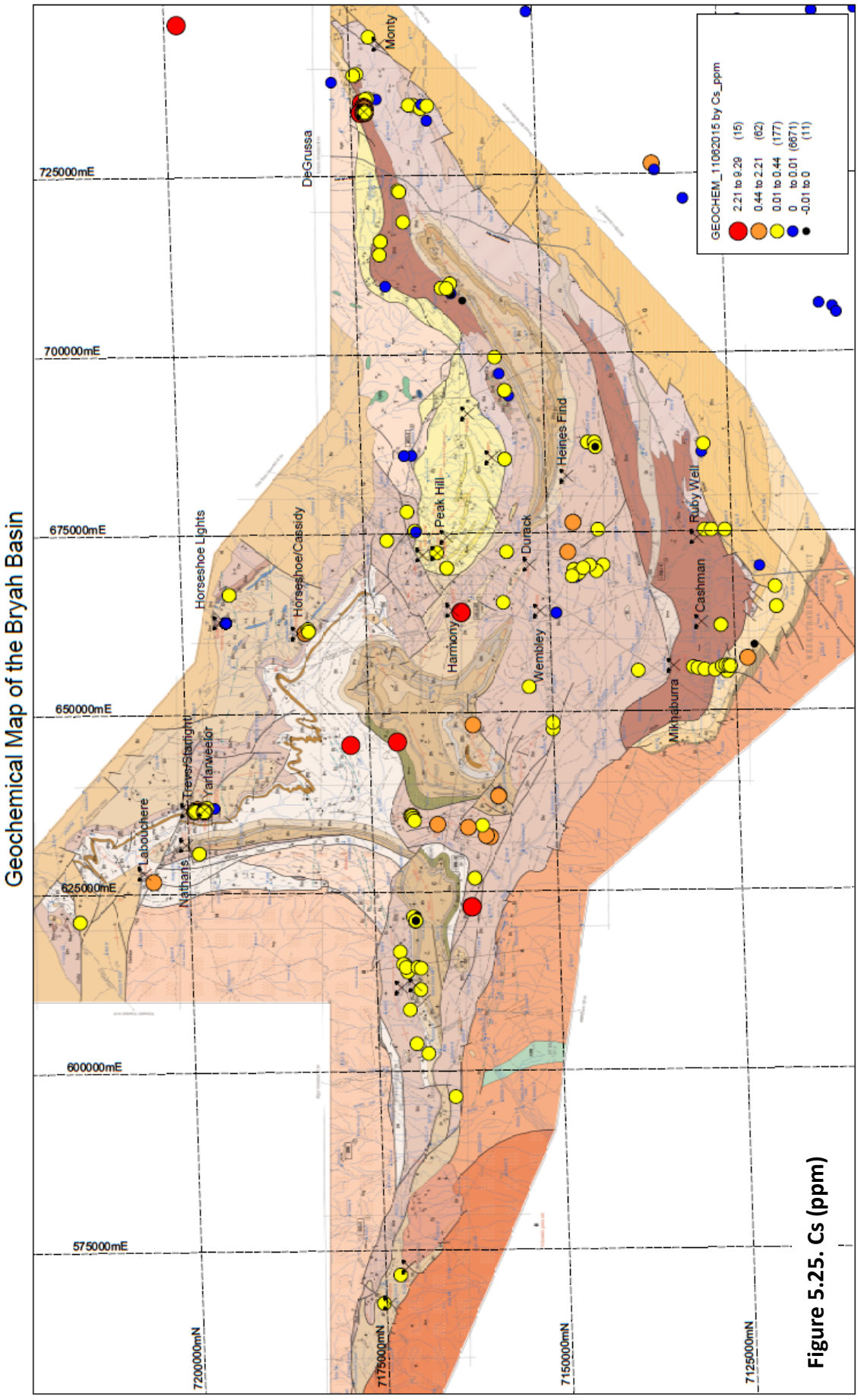

Figure 5.25. Cs (ppm)

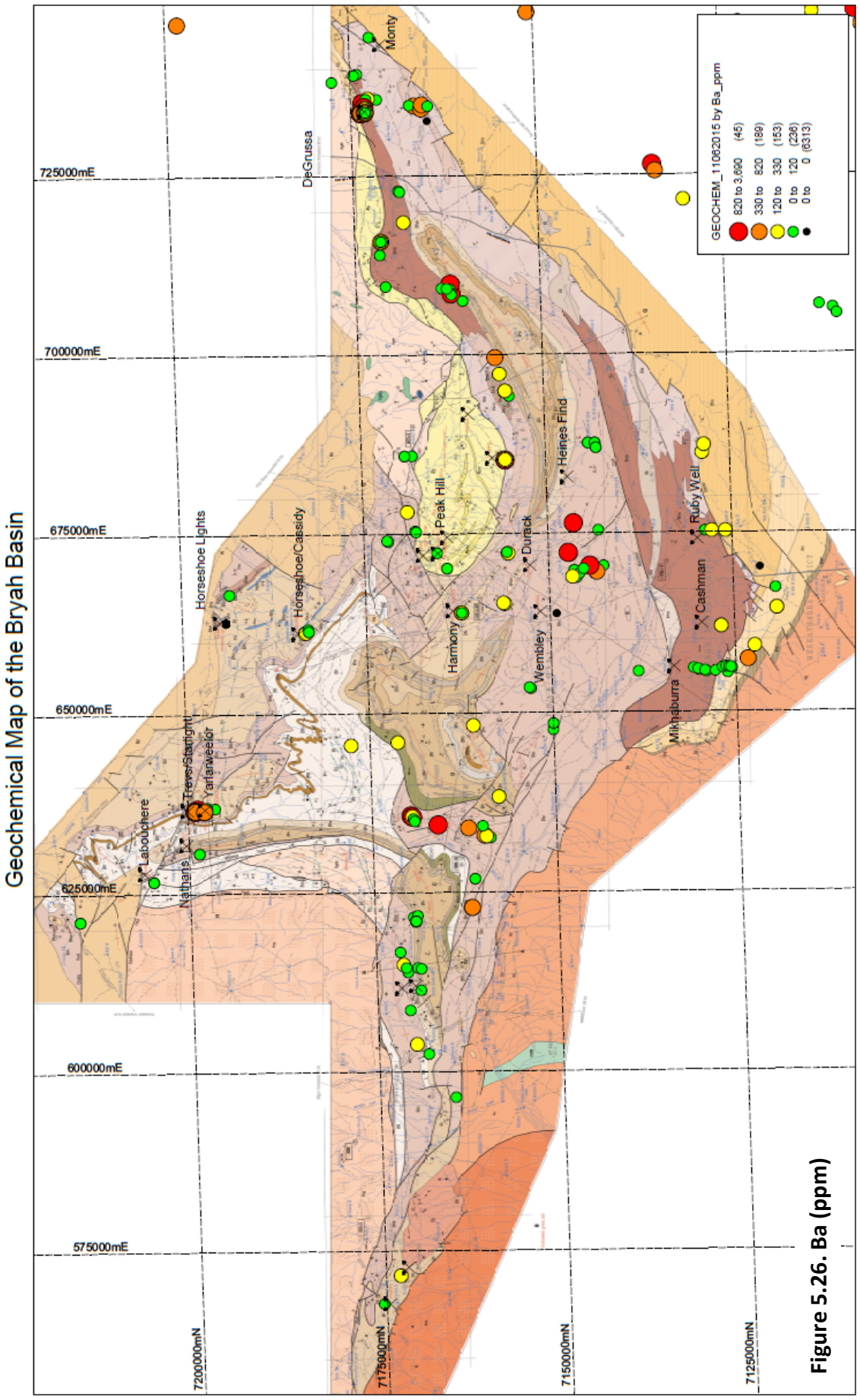

Figure 5.26. Ba (ppm)

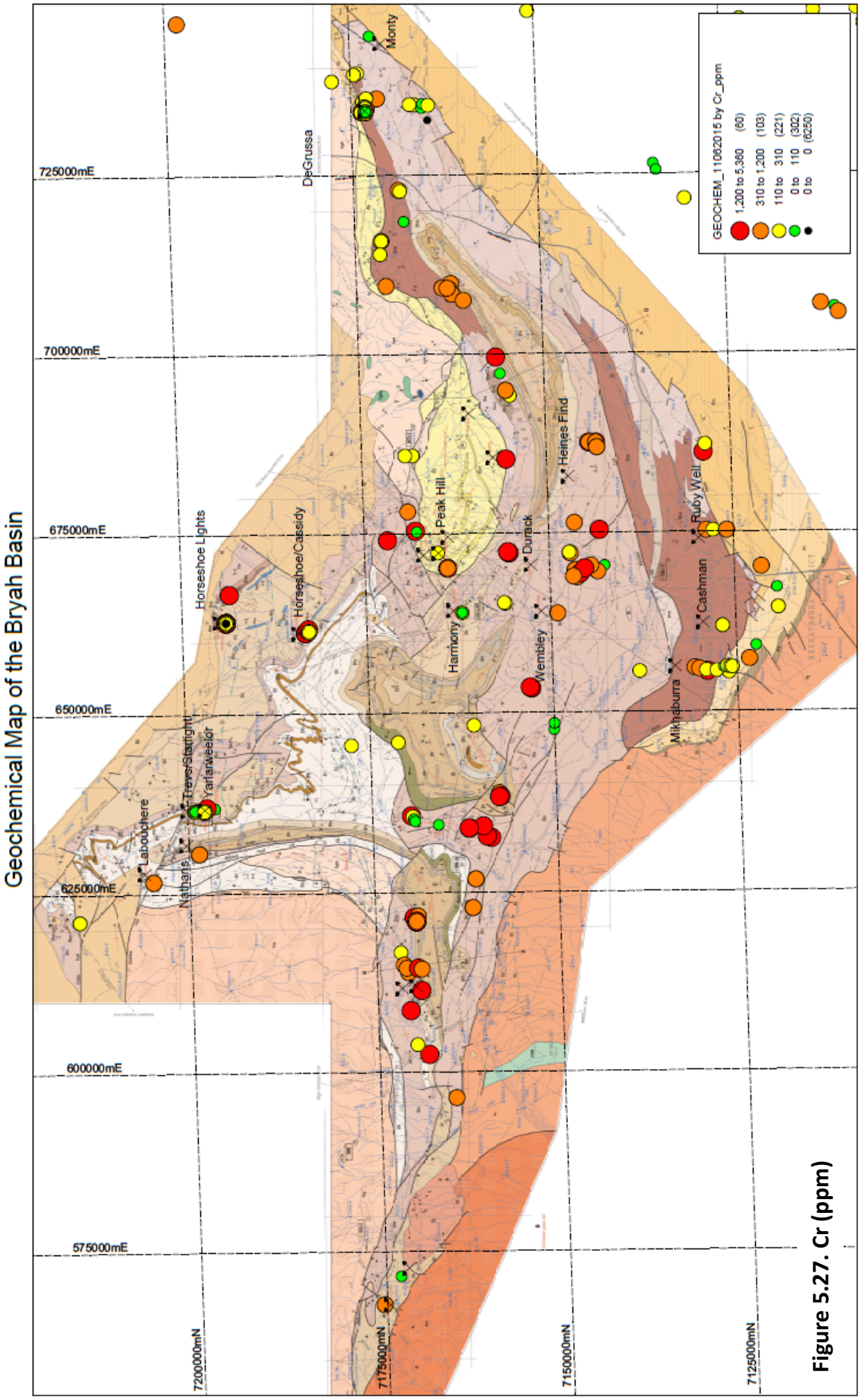

Figure 5.27. Cr (ppm)

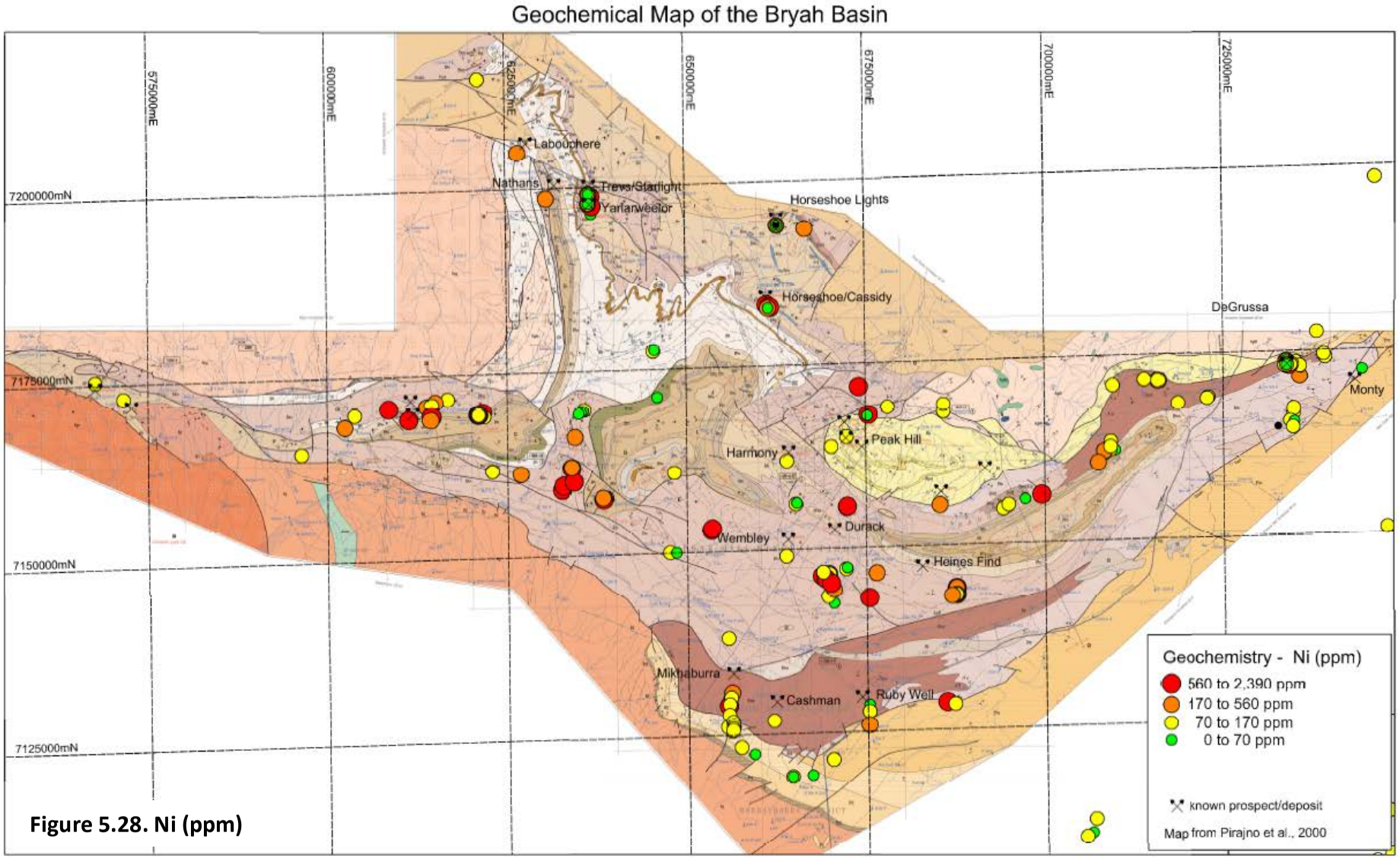

Figure 5.28. Ni (ppm)

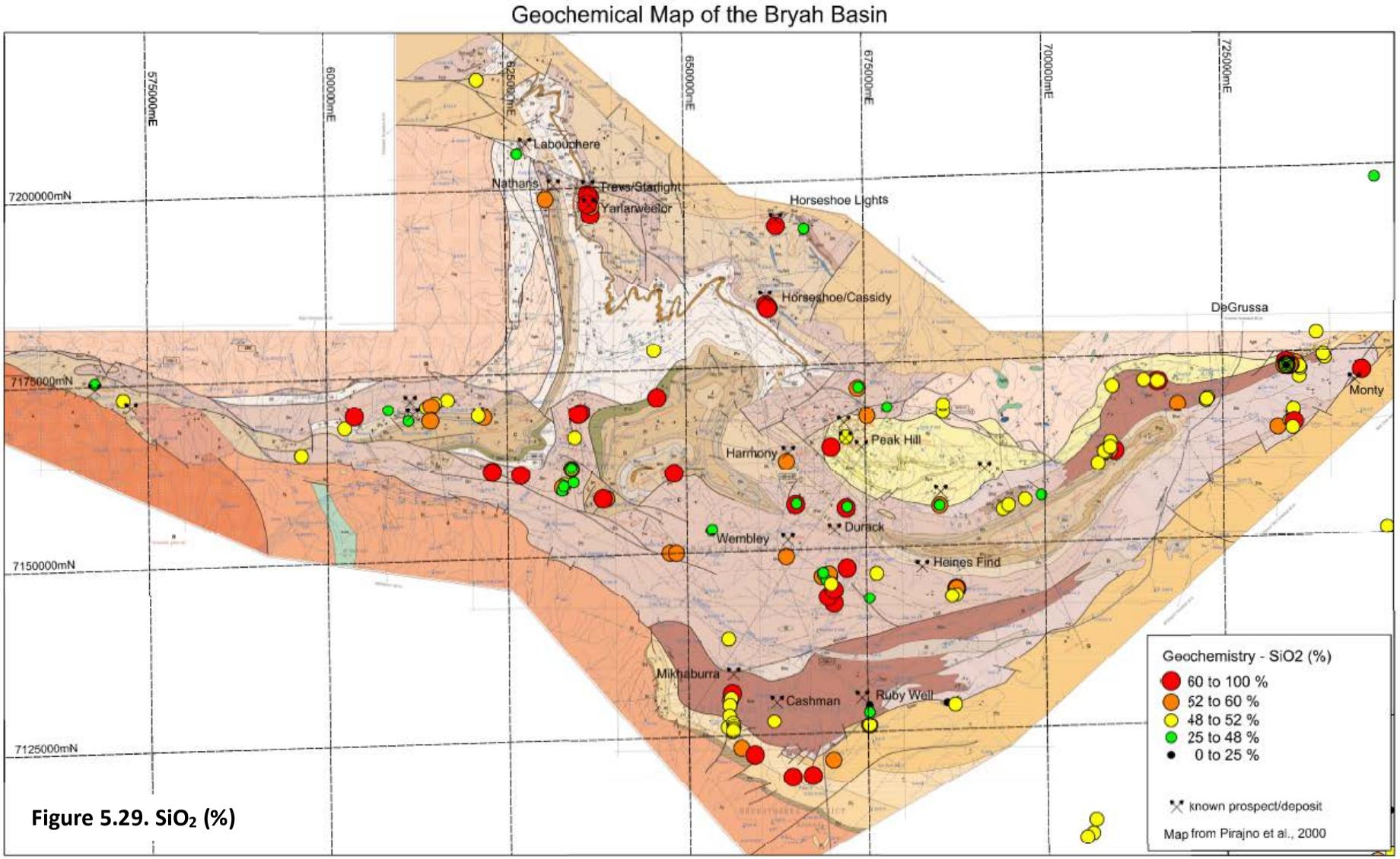

Figure 5.29. SiO_2 (%)

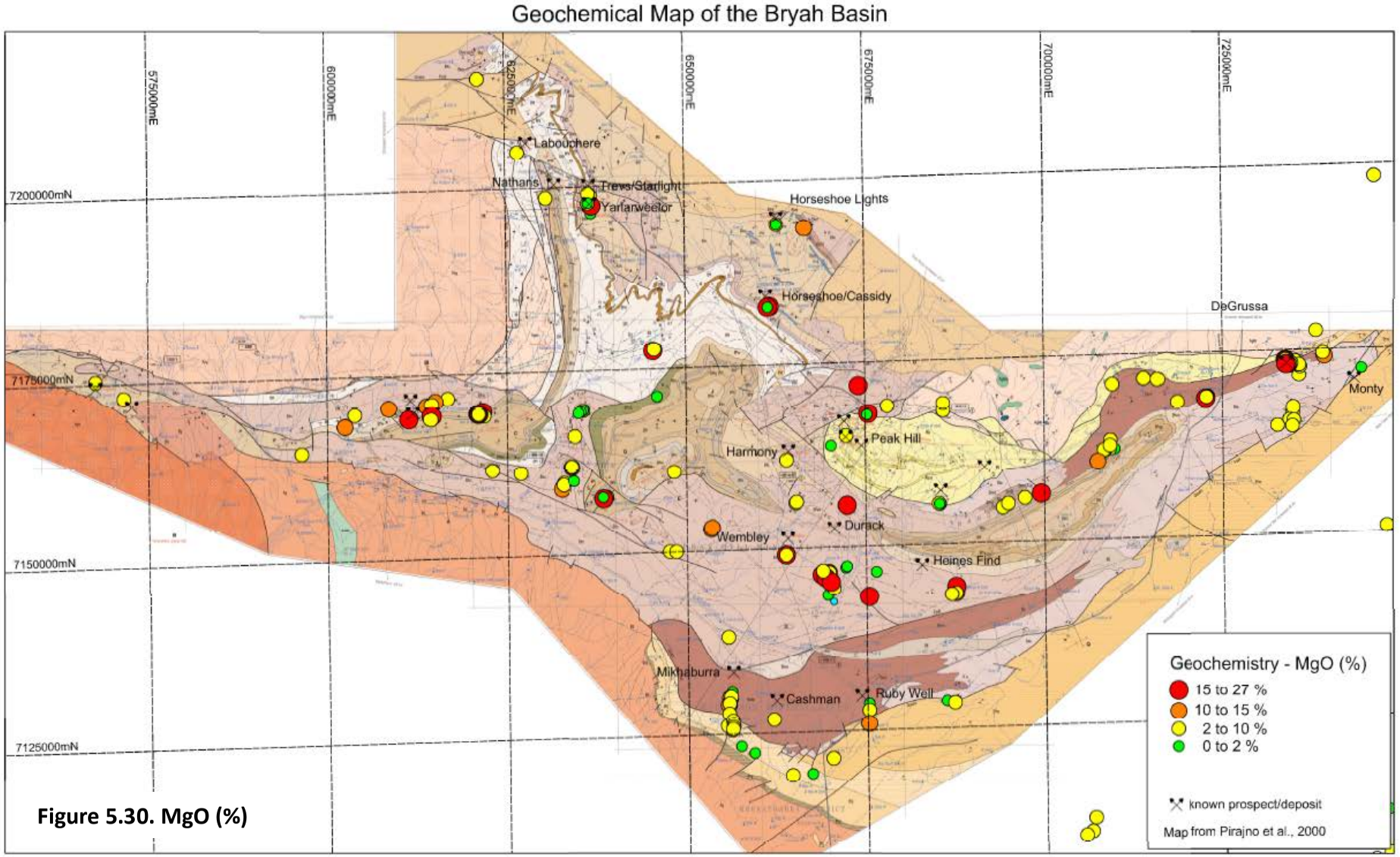

Figure 5.30. MgO (%)

5.5.3. Further work

- A detailed study on the sedimentary rocks of the hanging wall and footwall sequences, mine proximal and regional, to identify any alteration characteristic of the hydrothermal mineralising system.
- A more complete study of the geochemical features of the regions mafic rocks as well as more felsic volcanic rocks of the Narracoota Formation may help to constrain the tectonic environment.

5.6. Conclusion

The majority of geochemical data supports that the Johnson Cairn Formation to have derived from EMORB-OIB sources. The Johnson Cairn Formation mafic rocks that underlie the DeGrussa VHMS environment and represent the initiation of mafic magmatism, and are most similar to rocks found in continental rift settings (e.g. Ethiopian Rift and Red Sea Rift).

The Killara Formation and DeGrussa mafic rocks indicate the continuation of continental rifting in what was probably a submarine, sedimented rift basin (e.g. Cocos/Nazca-Panama Plate and Guaymas basin). The tholeiitic mafic rocks are of MORB composition with slight LREE enrichment suggesting association with oceanic plateau and seamount development. Geochemistry indicates rocks were initially affected by crustal contamination, evolving to more primitive MORB compositions as rifting progressed. The present day, Guaymas basin setting, Gulf of California, or the Red Sea Rift, is analogous to the DeGrussa region.

The mafic rocks of the Narracoota Formation have a large geochemical variation representing a spectrum of tectonic environments from back arc - island arc (presence of felsic volcanic rocks), forearc (presence of boninite) and oceanic rift (MORB compositions similar to DeGrussa). This could represent an evolution in basin dynamics in which an initial continental rift in the east may have first developed into an ocean rift-basin with attendant plate rifting, followed by subduction of the ocean plate and subsequent arc-related magmatism in the west.

6. Geochronology of the DeGrussa Volcanic-Hosted Massive Sulfide Deposit and Associated Mineralisation of the Yerrida, Bryah and Padbury Basins, Western Australia

Gascoyne landscapes

This chapter was published as a paper in 2015: HAWKE, M. L., MEFFRE, S., STEIN, H., HILLIARD, P., LARGE, R. & GEMMELL, J. B. 2015. Geochronology of the DeGrussa Volcanic Hosted Massive Sulfide Deposit and Associated Mineralization of the Yerrida, Bryah and Padbury Basins, Western Australia. Precambrian Research, 267, 250-284.

This chapter presents the paper in full and repeats from the previous chapters exist. The author would like to make note of the following:

1. The magazine member was held under confidentiallity and thus was not fully described in this paper.

2. The geochemistry chapter was not fully written at the time of publication, thus geochemistry does not feature. As discussed in chapter 5, although it is possible that the DeGrussa deposit formed in a back arc setting, the mafic rocks indicate an oceanic-rift setting is more likely.

6.1. Abstract

The Paleoproterozoic Yerrida, Bryah and Padbury Group sedimentary rocks are located on the northern margin of the Archean Yilgarn Craton and are host to epigenetic gold (Peak Hill,

Fortnum and Horseshoe), volcanic-hosted massive sulfide (VHMS; Horseshoe Lights, Red Bore and DeGrussa) and epithermal copper deposits (Thaduna). The DeGrussa Cu-Au-Ag VHMS deposit (12.4Mt @ 4.7% Cu and 1.8g/t Au) comprises four lenses and is hosted in turbiditic sedimentary rocks and basalts of the DeGrussa host sediments/Karalundi Formation, the lowest mafic volcano-sedimentary unit of the Bryah Group and crosscut by intrusive dolerite of Narracoota Formation age. Immediate wall rocks to the ore lenses are commonly altered to chlorite and talc-carbonate.

A number of geochronological techniques were employed to date mineralisation in the DeGrussa deposit. These include rhenium-osmium (Re-Os) of molybdenite, Pb isotopes of galena and pyrite, and U-Pb on zircon. Re-Os geochronology of molybdenite resulted in ages of 2027 ± 7 Ma and 2011 ± 7 Ma and 2013 ± 7 Ma for mineralisation, similar to Pb-Pb model ages for galena of 2060 ± 50 Ma and 2075 ± 50 Ma. U-Pb for magmatic zircons from intrusive dolerite within the mine sequence provided ages of 1991 ± 7 Ma, 1999 ± 7 Ma and 2003 ± 7 Ma with granodiorite rocks providing ages of 2014 ± 7 Ma and 2018 ± 9 Ma. Remobilisation of DeGrussa sulfides occurred at approximately 1980 Ma given Re-Os ages of pyrrhotite (1982 ± 7 Ma and 1984 ± 8 Ma) and Pb-Pb pyrite ages of 1980 ± 30 Ma.

Re-examination of the Pb isotopic evolution models for this area and the Capricorn Orogen suggests that the model of Stacey and Kramers (1975) is more appropriate than Cumming and Richards (1975); using the former model leads to revised model ages as follows: Horseshoe Lights VHMS, 2000 ± 35 Ma; Nathans 1820 ± 30 Ma, Peak Hill (Main pit: 1610 Ma, 1620 Ma, 1705 Ma, and 2070 ± 30 Ma; Fiveways: 1955 Ma; Mt. Pleasant: 1770 Ma), Horseshoe/ Cassidy, 1940 ± 30 Ma, Mikhaburra 1915 ± 30 Ma, and Labouchere 1800 ± 30 Ma. These new ages coincide with major regional orogenic events - the Glenburgh from 2005-1960 Ma, the Capricorn from 1830-1780 Ma, the Mangaroon from 1690-1620 Ma, and the Edmundian from 920-850 Ma. Although orogenic events are compressional, the Yerrida/Bryah Group sedimentary rocks, along with mineralisation at the DeGrussa and Horseshoe Lights deposits, were formed in an extensional basin setting during the Glenburgh Orogeny.

These new ages, assist in constraining stratigraphic and mineralising events of the Paleoproterozoic Yerrida, Bryah and Padbury Group with regional orogenic events and may provide guidance for exploration for significant gold and base metal mineralisation, not only in the Bryah, but also throughout the larger Capricorn Orogen.

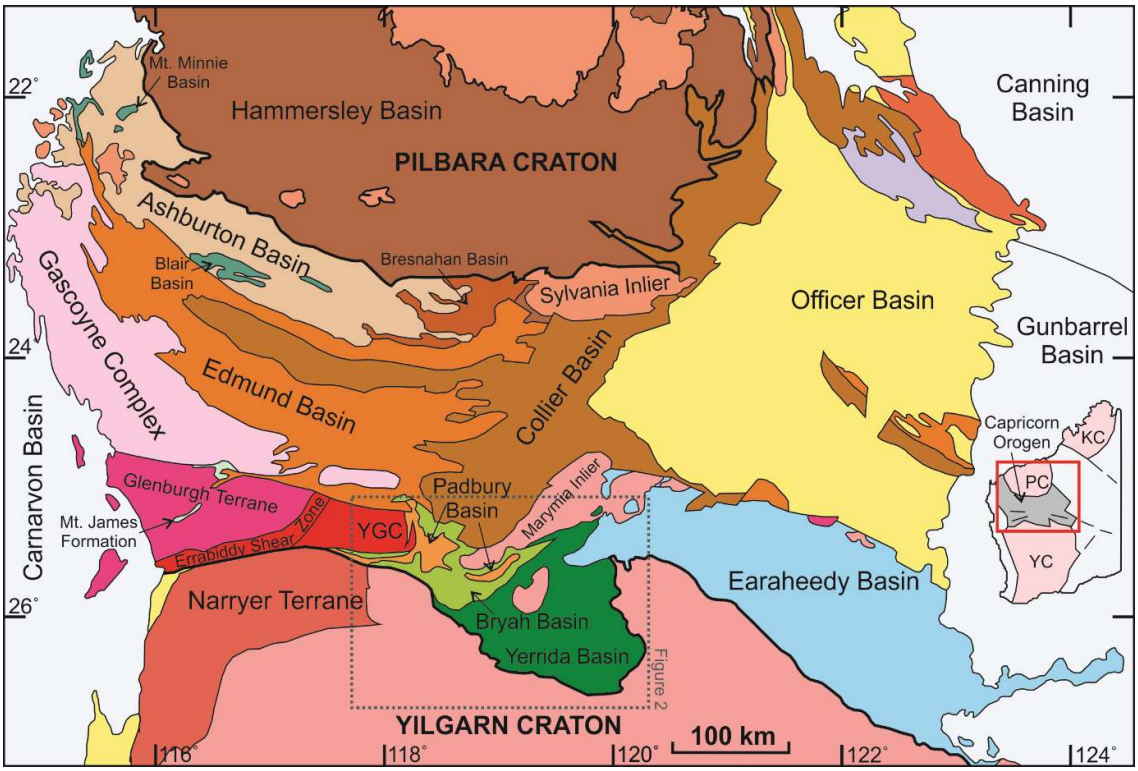

Figure 6.1. Geological Terranes of the Capricorn Orogen of Western Australia, a region of variably deformed rocks located between the Pilbara and Yilgarn Cratons which records Paleoproterozoic rifting and collision during the Opthalmian, Glenburgh and Capricorn Orogenies. It includes the deformed margins of the Pilbara and Yilgarn Cratons, as well as the Palaeoproterozoic Gascoyne Province, Errabiddy Shear Zone and the Yarlarweelor Gneiss Complex in the west, the Ashburton, Edmund and Collier Basins in the north, and the Yerrida, Bryah, Padbury and Earaheedy Basins in the south-east. Bold lines represent the extent of Palaeoproterozoic units. YGC = Yarlarweelor Gneiss Complex; KC = Kimberley Craton; PC = Pilbara Craton; YC = Yilgarn Craton.

6.2. Introduction

The Paleoproterozoic DeGrussa copper-gold–silver, volcanic-hosted massive sulfide (VHMS) deposit is located in the eastern part of the Capricorn Orogen of central Western Australia (Fig. 6.1). The DeGrussa deposit was discovered in 2009 within an interfingering sequence of

sedimentary and mafic volcanic rocks time equivalent to the Karalundi Formation and Narracoota Formation of the Bryah Group (Fig. 6.2). These rocks also host the Red Bore VHMS deposit and the Horseshoe Lights VHMS deposit. The DeGrussa deposit consists of four primary sulfide ore lenses in conjunction with a supergene enrichment of copper. Mining of the DeGrussa deposit commenced in 2012 and as of 31st December 2014, 167,000t of Cu and 98,000oz Au had been produced and the remaining resource (Taylor and Hastings, 2015) was estimated at 2.8Mt of stockpiled oxide ore averaging 1.2% Cu and 1.0g/t Au (contained metal of 33,000t Cu and 88,000oz Au) and an in-situ underground resource of 9.5Mt grading 5.7% Cu and 2.0g/t Au (contained metal of 546,000t Cu and 616,000oz Au). Paleoproterozoic rifting and collision of Archean continental terranes during three main tectonic events (the Opthalmian, Glenburgh and Capricorn) led to formation, uplift and deformation of the sedimentary basins between the Yilgarn and Pilbara cratons (Johnson, 2013)(Fig. 6.1). Ages for the supra-crustal sequences are poorly constrained. Initiation of basin rifting is estimated to have occurred around 2173 ± 64 Ma as determined by the Pb isotopic composition of carbonate from stromatolites in the lowermost Bubble Well Member of the Juderina Formation, Yerrida Group (Woodhead and Hergt, 1997). Yerrida Group sedimentary rocks underlie DeGrussa host sedimentary rocks. The Narracoota Formation in the Bryah Group had an estimated age of 1922 ± 35 Ma (Windh, 1992) from Pb isotope analysis on pyrite from the Horseshoe Lights VHMS deposit, hosted in the upper portions of the Narracoota Formation volcanic succession. Detrital zircon constrains the deposition of the Ravelstone Formation (Fig. 6.2, 6.3), which overlies Horseshoe Lights, to after c. 2014 Ma (Johnson, 2013). The Ravelstone Formation hosts several orogenic, vein-related gold deposits such as the Horseshoe/Cassidy deposits (Horseshoe/Belltop in Windh (1992)), Labouchere, and the Fortnum deposits. Detrital zircons in the lowermost Padbury Group constrain the Labouchere Formation, and hence deposition of the Padbury Group, to a maximum age of c. 1980 Ma (Johnson, 2013). Thornett (1995) completed Pb isotopic dating on the Peak Hill gold deposits (Peak Hill- main pit, Mt. Pleasant and Fiveways) located in the Archean Peak Hill Schist with ages ranging between 1548 and

1719 Ma on analysis of galena, altaite, rucklidgeite and a Bi-Pb telluride. Figure 6.3 summarises the stratigraphy as currently understood. Mineralisation ages provided by prior studies, have not often corresponded to the regional orogenic events.

With the exception of the detailed study by Adamczyk (2013) on the Conductor 5 depsit, no work has yet been published on DeGrussa. The aims of this paper are; to describe the geology of the DeGrussa depositional environment; to determine the age of the DeGrussa host rocks and mineralisation; to discuss the effects of the Stacey and Kramers (1975) and Cumming and Richards (1975) model curves when applied to age data for DeGrussa and regional mineralisation; and to compare the DeGrussa geochronology with regional mineralisation and orogenic events in order to better define the ages of sedimentary rock units in the basin which will assist in constraining district exploration models.

6.3. Regional Geological Setting

The Capricorn Orogen of Western Australia is a ~1000 km long, 500 km wide region of variably deformed rocks located between the Pilbara and Yilgarn Cratons. It records the Paleoproterozoic rifting and collision of these Archean continental terranes during three main tectonic events (the Opthalmian, Glenburgh and Capricorn) which led to deposition, uplift and deformation of the sedimentary basins between the Yilgarn and Pilbara cratons to form the West Australian Craton (Cawood and Tyler, 2004, Sheppard et al., 2010, Johnson et al., 2011a, Johnson, 2013). The Orogen includes the deformed margins of the Pilbara and Yilgarn Cratons and associated deformed continental margin rocks of the Fortescue, Hamersley, Turee Creek and lower Wyloo Groups in the Ophthalmia Fold Belt, as well as the Palaeoproterozoic Gascoyne Province, Errabiddy Shear Zone and the Yarlarweelor Gneiss Complex in the west, the Ashburton (2446-1799 Ma, (Johnson et al., 2013)), Edmund and Collier Basins (1680-1465 Ma, (Zi et al., 2015) and 1171-1070 Ma respectively, (Martin and Thorne, 2004)) in the north, and the Yerrida, Bryah, Padbury and Earaheedy Basins (c. 2174 – c. 1800 Ma, (Pirajno and Occhipinti, 2000) in the south-east (Fig. 6.1, 6.2). The Yerrida, Bryah and Padbury basins are a

series of Palaeoproterozoic volcano-sedimentary basins formed on top of each other during the Glenburgh (2005-1970 Ma) and Capricorn (1820-1770 Ma) Orogenies.

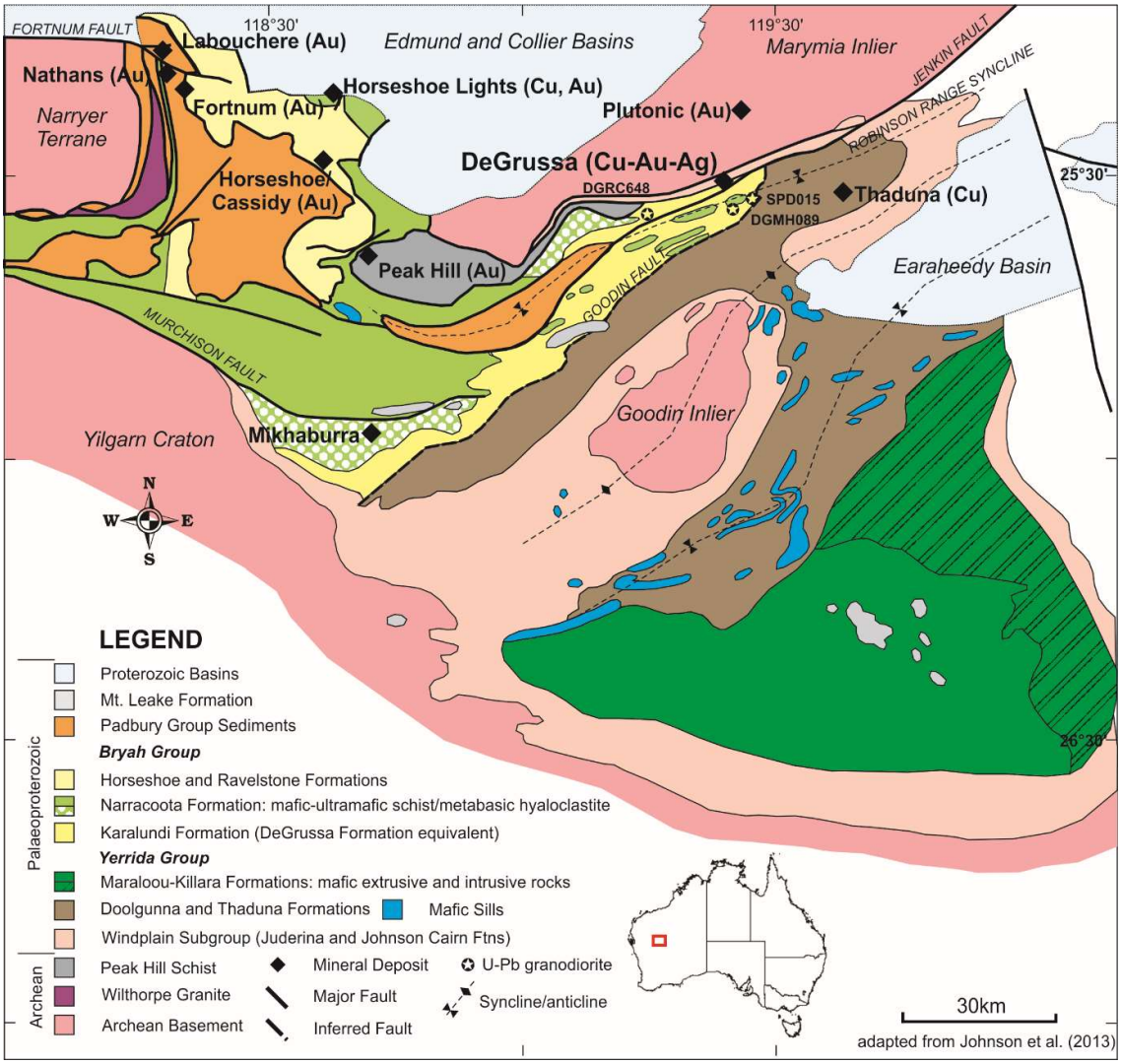

Figure 6.2. Regional Geology of the Yerrida, Bryah and Padbury groups with major mines and regional U-Pb zircon sample locations.The Bryah and Yerrida Groups are bounded to the south by the Archaean Yilgarn Craton, to the north by the Archaean Marymia Inlier and the Mesoproterozoic Edmund and Collier Basins, and to the west by the Narryer Terrane. They are unconformably overlain by the Paleoproterozoic Earaheedy Basin to the east. The Padbury Group unconformably overlies the Bryah Group. The Goodin Fault marks the southern boundary between Bryah and Yerrida Group sediments although this contact may be an unconformity (Jeffery, 2013). The DeGrussa deposit is located within sediments and mafic rocks of the DeGrussa Formation (lateral equivalent of the Karalundi Formation).

In order to put the geochronological data presented in this paper in context it is necessary to describe the major terranes and tectonic events that have formed the region. Of note is the Gascoyne Province, which comprises granitic and medium-high grade metamorphic rocks (Sheppard et al., 2010). The oldest rocks are found in the exotic Glenburgh Terrane which contains the Dalgaringa Supersuite, similar in age to rocks associated with the DeGrussa Deposit. Additional units, the Bandee, Carlathunda, MacAdam and Yarraquinn Seismic Provinces, were also identified by Johnson et al. (2013) as distinct seismic terranes of unknown age and character, not exposed at surface and located north of the Glenburgh Terrane. These were all accreted to the Pilbara Craton before c. 2775 Ma (Johnson et al., 2013).

The Glenburgh Terrane consists of metamorphosed and variably deformed intermediate to felsic granitic rocks of the Halfway Gneiss (2550-2430 Ma) and Dalgaringa Supersuite (2005-1975 Ma), as well as meta-sedimentary rocks of the Moogie Metamorphics (2240-2125 Ma) and the Camel Hills Metamorphics (2000-1955 Ma) (Sheppard et al., 2010, Johnson et al., 2011a, Sheppard et al., 2004).

The Moogie Metamorphics overlie the Halfway Gneiss in the south of the Gascoyne Province, and contain detrital zircons (3510 – 2239 Ma) derived from the southern Pilbara and the Halfway Gneiss (Johnson et al., 2010, Johnson et al., 2011a). The unit is dominated by psammitic schists (the Mumba Psammite) and minor intercalated calc-silicate gneiss and marble. The unit was deposited between c. 2240 and c. 2125 Ma, likely as part of the Opthalmian foreland basin system (Johnson et al., 2011a)

The Dalgaringa Supersuite comprises massive, foliated and gneissic granitic rocks. It forms, and is exposed in, the southern part of the Gascoyne Province. Recent magnetotelluric data obtained by Dentith et al. (2014) suggests an unknown unit beneath the Edmund and Collier Basins may correlate to the Dalgaringa Supersuite. The Dalgaringa Supersuite formed during two episodes of magmatism, which are separated by a regional high-grade tectonometamorphic event. The rocks consist of 2005-1985 Ma foliated and gneissic diorite to monzogranite with interleaved amphibolite, and c. 1975 Ma tonalite and granodiorite plutons of the Nardoo Granite

(Sheppard et al., 2004). The granites have whole rock major, trace and rare earth element concentrations consistent with formation in a supra-subduction zone setting. Whole-rock Nd isotopic signatures indicate the involvement of late Archean granitic gneisses, suggesting that magmatism occurred in a continental margin arc as an Andean-type batholith (Sheppard et al., 2004). This is supported by Hf isotope data which demonstrates that the Yilgarn Craton crust cannot be involved in the generation of these magmatic rocks instead fitting a two component system of depleted mantle and Halfway Gneiss Johnson et al. (2010), Johnson et al. (2011c).

The Camel Hills Metamorphics form fault-bounded units within the Errabiddy Shear Zone between the Gascoyne Province and Narryer Terrane of the Yilgarn Craton. The unit comprises the Quartpot Pelite and the Petter Calc-silicate, as well as undivided amphibolite and metamorphosed banded iron-formation, with all units affected by amphibolite to granulite facies metamorphism. The Quartpot Pelite consists largely of biotite– plagioclase–quartz (–K-feldspar–garnet–sillimanite) pelitic gneiss, migmatitic pelitic gneiss, and psammitic schist, interlayered with minor quartzite, calc-silicate gneiss, and amphibolite. U–Pb SHRIMP dating of detrital zircons yield a range of ages between c. 2892 and c. 1985 Ma, but are dominated by zircons in the 2080 – 2000 Ma range (Johnson et al., 2010). The package was deposited sometime after 2001 ± 26 Ma or 1985 ± 28 Ma, but before the growth of metamorphic zircon rims at 1955 ± 7 Ma and 1952 ± 14 Ma.

The Petter Calc-silicate is composed of clinopyroxene–plagioclase (–epidote– quartz ± hornblende ± grossular) calc-silicate schist and gneiss, interlayered with quartzite and quartz–diopside rock, and minor pelitic schist or migmatitic pelitic gneiss and amphibolite. The peak mineral assemblages have been overprinted and retrogressed during the Capricorn Orogeny. The unit has solely Archean detritus (c. 3148 and c. 2603 Ma) and may have been deposited along the Yilgarn Margin sometime after 2608 ± 4 Ma (Johnson et al., 2011a).

Rocks of the Camel Hills Metamorphics are interpreted to have formed in a forearc or backarc basin setting along the margin of the Glenburgh Terrane in response to uplift of the southern margin of the Pilbara during continental collision between c. 2240 and 2125 Ma

(Johnson et al., 2011a). The Camel Hills Metamorphics are the meta-sedimentary rocks equivalent to the intrusive rocks of the Dalgaringa Supersuite.

The Errabiddy Shear Zone separates the Glenburgh Terrane from early to late Archean granitic gneisses and foliated granites of the Narryer Terrane (3730 – 2920 Ma) (Fig. 1) and marks the northern limit of the Yilgarn Craton. Subduction in a northerly direction occurred along this margin until ca. 1970 Ma (Sheppard et al., 2004).

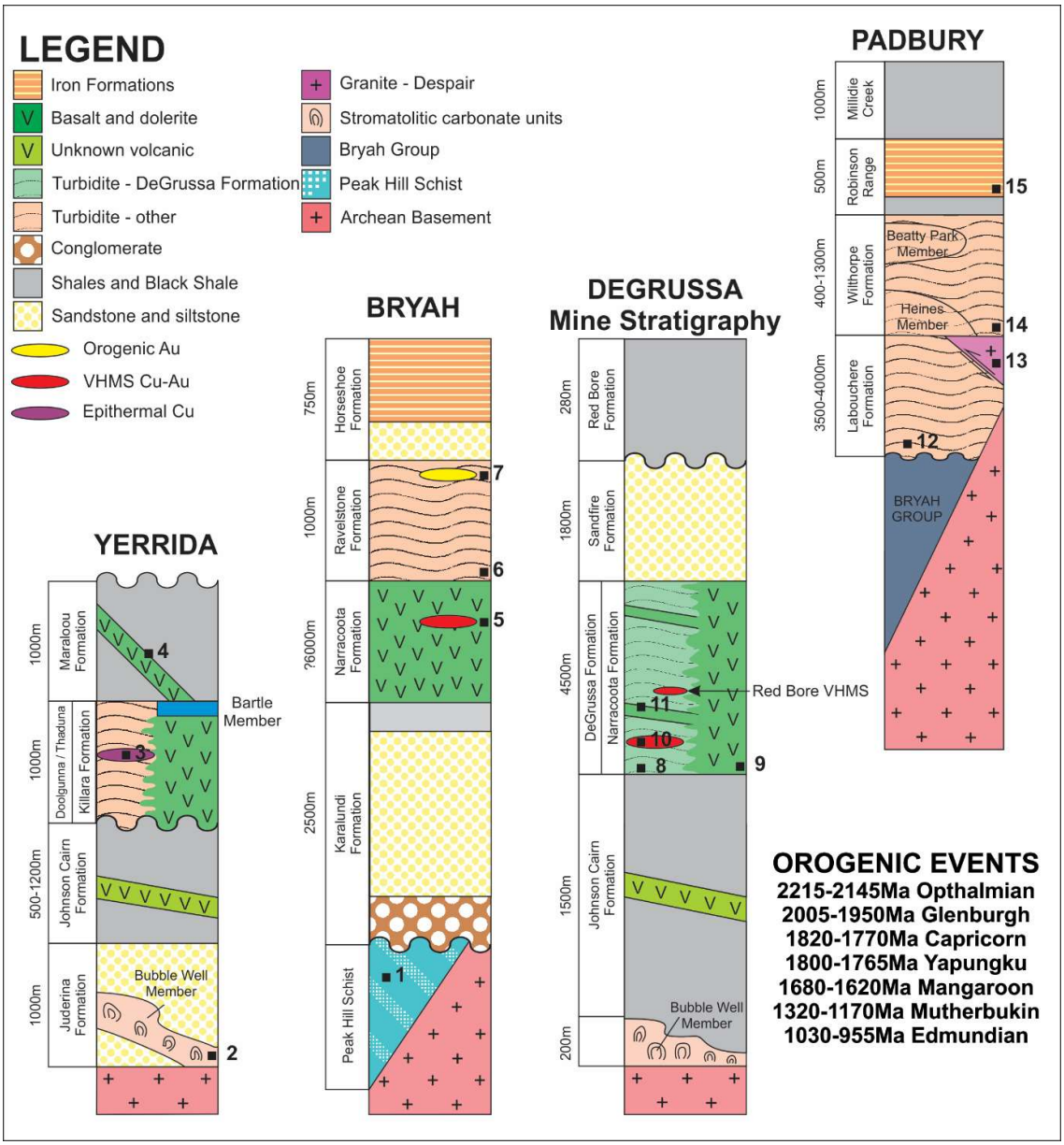

Figure 6.3. Stratigraphic column for the Yerrida, Bryah, and Padbury Group sediments with respect to the position of DeGrussa mine stratigraphy (adapted from Johnson (2013)). **1.** Peak Hill Mineralisation: main pit: 1610 Ma, 1620 Ma, 1705 Ma and 2070 ± 30 Ma; Fiveways: 1955 Ma; Mt. Pleasant: 1770 Ma (Thornett, 1995). **2.** The Bubble Well Member stromatolites at 2173 ± 64 Ma (Woodhead and Hergt, 1997). **3.** Thaduna Copper Deposit mineralisation dated at 1475 ± 50 Ma hosted in the Thaduna Formation sediments. **4.** The Maraloou Formation shales of age 1843 ± 10 Ma (Rasmussen and Fletcher, 2002). **5.** Horseshoe Lights Cu-Au mineralisation, originally dated at 1922 ± 35 Ma (Windh, 1992) but reanalysed to 2000 ± 35 Ma and hosted at the top of the Narracoota Formation. Orogenic gold at Mikhaburra (Windh, 1992), located in Narracoota Formation hyaloclastite retains a mineralisation age of 1915 ± 30 Ma. **6.** The Ravelstone Formation has a maximum age of <2014 Ma (Nelson, 1997) from detrital zircons. **7.** Orogenic gold hosted within the Ravelstone Formation: Horseshoe/Cassidy 1940 ± 30Ma (Windh, 1992), Labouchere 1800 ± 30 Ma (Windh, 1992), Nathans 1820 ± 30 Ma (Windh, 1992) and Fortnum-Starlight 920 ± 50 Ma. **8.** DeGrussa Formation/Karalundi Formation sediments detrital zircons with a maximum age of <2262 ± 40 Ma. **9.** Regional granodiorites with a magmatic zircon age of 2018 ± 9 Ma. **10.** DeGrussa deposit sulfides with a mineralisation age of 2027 ± 7 Ma from Re-Os on molybdenite. **11.** Intrusive dolerite sills and dykes of the DeGrussa mine stratigraphy of 1991 ± 7 Ma to 2003 ± 7 Ma. **12.** Labouchere Formation detrital zircons provide a maximum age of c. 1980 Ma (Johnson, 2013). **13.** The Despair Granite, in faulted contact with the Padbury group with an Archean age of 2650 Ma (Occhipinti et al., 1998). **14.** The Wilthorpe Formation with detrital zircons providing a maximum age of deposition at 1996 Ma (Nelson, 1997). **15.** The Frere Formation iron formations in the Earaheedy Group were dated at 1891 ± 8 Ma by Rasmussen et al. (2012). Zircon ages from tuff interbedded between the iron formations, is extrapolated to also be the age of the Robinson Range Iron Formations of the Padbury Basin

6.4. East Capricorn Geology and the Yerrida, Bryah and Padbury Basins

The Yerrida, Bryah and Padbury Basins form the eastern part of the Capricorn Orogen and are relatively understudied in comparison with the western parts of the Capricorn Orogen. The Yerrida Basin forms a ~4 km thick succession of mixed siliciclastic and carbonate rocks and although poorly dated, appears to be the oldest. Where undeformed it is unconformably overlain by units of the Bryah and Padbury Groups. The Bryah Basin represents a 10km thick sequence of intrusive and extrusive volcanic rocks, volcanoclastic rocks and sedimentary rocks which host significant amounts of gold and copper mineralisation. The Padbury Basin (~6 – 7 km thick) developed as a foreland basin, unconformably overlying the Bryah Basin and consists of a succession of clastic and chemical sedimentary rocks.

6.4.1. The Archean Marymia and Goodin Inliers

The Marymia Inlier is a fragment of Archean granite-greenstone basement. Rocks are mainly granitic but also include small enclaves of calc-silicate rock, ortho-amphibolite and minor metamorphosed banded iron formation. The south-western end of the Marymia Inlier comprises the Peak Hill Schist, a strongly deformed portion of Archean rocks comprising phyllonite, quartz-muscovite schist, calc-silicate schist, sericite (-quartz) schist, quartz-muscovite-biotite-chlorite schist and mylonite. They are faulted and tectonically interleaved along the contact with Bryah group sedimentary rocks (Occhipinti et al., 1997, Pirajno et al., 2000). The Peak Hill schist hosts the Peak Hill, Fiveways and Mt. Pleasant orogenic gold deposits (locations in Appendix 6.1). Rocks of the Yerrida and Bryah groups are mostly in tectonic contact with the Marymia Inlier, although north of the DeGrussa deposit it appears unconformable onto Archean basement (Jeffery, 2013).

The origin of the Marymia is controversial. Stratigraphic correlations between the Marymia Inlier and the Youanmi Terrane have been made, but more recent studies have favoured correlation with the Eastern Goldfields Superterrane (Gazley, 2011). The Marymia was suggested by Gee (1979) as an in situ remnant of Archean basement. Krapez and Martin (1999)

suggested it as a rotated and separated portion of the Yilgarn. Pirajno et al. (2004) inferred it to be a stable remnant rifted from the northern margin of the Yilgarn during the Capricorn Orogeny. Most recent magnetotelluric transects of Dentith et al. (2014) show the Marymia Inlier as a wedge-shaped, fault bounded unit, the southern contact corresponding to the Jenkin fault (Fig. 6.2). In this interpretation, the Marymia Inlier is interpreted as a para-autochthonous fragment separated from the Eastern Goldfields Superterrane of the Yilgarn Craton during continental rifting and deposition of the Windplain Group of the Yerrida Basin at c. 2174 Ma (Dentith et al., 2014).

The Goodin Inlier (2624 ± 8 Ma (Nelson, 1997)) outcrops from within the Yerrida Group sedimentary rocks. It is interpreted as a tectonically reactivated block of the Archaean Yilgarn Craton on which the Yerrida Group unconformably lies (Pirajno and Adamides, 2000a). The Goodin Inlier is suggested to be a part of the Youanmi Terrane, implying that the Ida Fault, which divides the Youanmi and Eastern Goldfields Superterrane from each other, passes to the east of the Goodin Inlier (Dentith et al., 2014).

6.4.2. Yerrida Group

The Yerrida Group consists of the Windplain Subgroup and the Mooloogool Subgroup (Pirajno and Adamides, 2000a). The Windplain Subgroup comprises the basal Finlayson sandstone, the carbonaceous and stromatolitic Juderina Formation and the siliciclastic siltstones and shales of the Johnson Cairn Formation. The overlying Mooloogool Subgroup (comprising siliciclastic sedimentary rocks of the Thaduna and Doolgunna Formations, the mafic Killara Formation and the black shale rich Maraloou Formation) is absent from stratigraphy in the DeGrussa area. The Mooloogool Subgroup is suggested to represent a change to a rift-basin setting (Pirajno et al., 1996). Initially the contact between the two subgroups was identified as transitional by Pirajno et al. (1996). Later studies suggest there is a hiatus between the Windplain (2.17 Ga) and Mooloogool groups, due to a monazite age date of 1843 ± 10 Ma for intrusion of mafic sills of the Killara Formation into Maraloou Formation

rocks (Rasmussen and Fletcher, 2002). Lower greenschist facies metamorphism has affected all rocks in the Yerrida group (Pirajno and Adamides, 2000a).

Juderina Formation: The Juderina Formation is largely observed as unconformable on Archean granite-greenstone basement and consists of the lower Finlayson member and upper Bubble Well Member. , The Finlayson Member, as identified by Pirajno and Adamides (2000a), consists of quartz arenite and subordinate siltstone, chert breccia and pebble beds. It is not present in drill holes proximal to the DeGrussa Stratigraphy (Jeffery, 2011).

The Bubble Well Member consists of dolomite, cherty microbial laminites and stromatolitic carbonate with interbeds of dolomitic shale. In the DeGrussa area, the Bubble Well Member is located above the Archean Marymia Inlier and consist of approximately 100m of stromatolitic mats, mudstones and evaporite(Grey, 1984, Gee and Grey, 1993, Grey, 1994, Russell, 1992, Grey and Pirajno, 2012). Pb-Pb dating of carbonate by Woodhead and Hergt (1997) provides an age of 2174 ± 64 Ma for the unit at the southern edges of the Yerrida Basin. The 2.22 to 2.06 Ga Lomagundi-Jatulian (Lomagundi) Event, a large positive C isotope excursion of up to +12‰, was preserved in these rocks (El Tabakh et al., 1999, Lindsay and Brasier, 2002, Melezhik et al., 2007, Bekker et al., 2008).

Johnson Cairn Formation: The Johnson Cairn Formation consists of varicoloured, iron-rich shale with graded silty layers and dolomite bands (Pirajno and Adamides, 1998). The boundary with the underlying Juderina Formation is conformable and is taken as the topmost bed of quartz arenite. The Johnson Cairn Formation is present in stratigraphic drill holes within the footwall of the DeGrussa Deposit. The siliciclastic mudstone and pyritic organic rich shale of the Johnson Cairn Shale is suggested by Krapez and Martin (1999) to represent rapid deposition in a transgressive marine environment.

Thaduna Formation: Prior works have defined the Thaduna Formation by varied names and positions in stratigraphy across both the Bryah and Yerrida Basins (MacLeod, 1970, Gee, 1979, Gee, 1987). Occhipinti et al. (1997) defined the unit as the "Thaduna Formation" with the type locality at the Thaduna Copper Mine where it is host to the mineralisation (Pirajno and Adamides, 2000a). Pirajno et al. (1996) sub-divided the Thaduna "Greywacke" into the Thaduna Formation within the Yerrida Basin, and similar sediments of the Bryah Group into the "Ravelstone Formation". This is the currently accepted stratigraphy (Fig. 6.3). The Thaduna Formation interfinger with the overlying Doolgunna Formation, Karalundi Formation and Narracoota Formation, suggesting that it is contemporaneous with these units. It eventually overlies the Narracoota Formation in the west of the basin.

The Thaduna Formation was described by Gee (1987) as a thick turbidite sequence of graded fine to coarse grained lithic, feldspathic and mafic wacke with subordinate interbedded slaty mudstone, containing a variety of sedimentary structures such as single and multiple-graded cycles, shale, intraclasts, flute masks, load casts, convolute lamination and slump folds. Lithic fragments are altered basalt, jasper and ferruginous shale. Field and petrographic analysis (Pirajno et al., 2004) provide evidence that the Thaduna and Doolgunna Formations are both composed of granite, greenstone and mafic volcanic lithic fragments. Detrital zircons have an Archaean age of 2.65 Ga (Pirajno et al., 2004).

The Thaduna Formation within the Yerrida Basin is interpreted as a product of a high energy environment, which resulted in a sequence of turbidites deposited in a deep northeast-trending rift concurrently with the volcanic activity that produced the adjacent Killara Formation (Pirajno and Adamides, 1998, Gee, 1987, Pirajno et al., 2004).

Doolgunna Formation: The Doolgunna Formation consists of thick bedded arkosic sandstone, quartz siltstone, and subordinate pebble beds, conglomerates, arkosic turbidite rocks and megabreccia units (containing large blocks and fragments up to 3m across of Bubble Well Member rocks and Archean granitic rocks)(Pirajno and Adamides, 1998, Pirajno et al.,

2004). All beds characteristically display angular to sub rounded quartz and subordinate chert clasts and feldspar in a matrix of kaolinitic clays. Low-grade metamorphism resulted in the partial conversion of kaolinite to illite or fine grained sericite.

As with the Thaduna Formation, the Doolgunna Formation is interpreted to have been deposited in a northeast-trending rift (or 'Doolgunna Graben' (Pirajno, 1996)) concurrently with the volcanic activity of the Killara Formation (Pirajno and Adamides, 1998, Gee, 1987). Pirajno and Adamides (1998) suggest that these turbidite rocks are predominately the result of terrigenous sedimentation sourced from the uplifted Goodin Dome and Marymia Inlier. Megabreccia units are suggested to be a result of mass-wasting. In comparison, Krapez and Martin (1999) suggest the Juderina Formation, Johnson Cairn Shale and the lower Doolgunna Formation resemble lagoonal mud and barrier bar sands and a late lowstand systems tract consistent with a shallow sea or large lake with barrier bar shorelines.

Killara Formation: The Killara Formation volcanic rocks are composed of flat lying to shallow dipping low Ti subalkaline, unmetamorphosed intrusive and extrusive rocks as well as high-Fe, high-Mg tholeiitic to calc-alkaline basalts and basaltic andesites emplaced as sub aerial and subaqueous lava flows, intrusive sheets, sills and dykes (Pirajno and Adamides, 1998, Pirajno and Adamides, 2000a, Pirajno et al., 2004). The dolerite and basalt contain augite, plagioclase, secondary epidote, quartz, leucoxene, carbonate, sericite, chlorite and sulfides (pyrite, pyrrhotite and lesser chalcopyrite, either replacing plagioclase crystals or forming along microfractures). Trace element geochemistry is suggestive of crustal contamination or alternately an enriched mantle source (Pirajno, 1996, Pirajno and Occhipinti, 2000) possibly representing formation in a continental rift setting (Pirajno and Davy, 1996). The end of volcanic activity is marked by the Bartle Member, a chemical-evaporitic unit consisting of chertified microbial laminites with barite and anhydrite nodules, massive chert, and chert breccia (Pirajno and Adamides, 2000a, Pirajno and Adamides, 1998). The rocks are interpreted by Pirajno and Adamides (2000a) to have been volcanoclastic, chemical sedimentary rocks and

evaporates indicative of an evaporitic-pyroclastic-thermal-spring environment associated with rifting (Pirajno and Grey, 2002).

The unit is overlain conformably by the Maraloou Formation with peperitic contacts observed in eastern parts of the Yerrida Basin associated with dolerite emplacement. The Yelma Formation of the Earaheedy Group unconformably overlies in the east. The lower contact interfinger with the Johnson Cairn, Thaduna and Doolgunna Formations (Pirajno and Adamides, 2000a). The western extensions of the formation are lenses mainly of tholeiitic basalt intercalated with rocks of the Thaduna and Johnson Cairn Formations. The Killara Formation mafic rocks are possibly a time equivalent of the Narracoota Formation and mafic rocks that host the DeGrussa deposit, however age dating of the Yerrida Group is scarce and correlations cannot be clearly defined.

Maraloou Formation: The Maraloou Formation is considered a basin-fill facies of the uppermost Yerrida Group, and could be laterally equivalent to the Labouchere Formation 150 km to the northwest (Gee, 1979, Gee, 1987, Gee and Grey, 1993). Lithologies range from siltstone, laminated siltstone, black sulfidic shale and ferruginous shale, intercalated with subordinate marl beds, dolostone, laminated chert and chert breccias deposited in below wave base conditions with evidence of microbial origin (Pirajno and Adamides, 2000a, Pirajno and Adamides, 1998). A small number of gossans with anomalous Cu, Pd, Ba and Zn are present throughout (Pirajno and Occhipinti, 2000).

The contact between the Killara and Maraloou Formations is transitional or locally discordant consisting of intercalated mafic lavas and sills and black shale. Rasmussen and Fletcher (2002) provide a minimum age of 1843 ± 10 Ma for the Maraloou Formation based on SHRIMP U-Pb analysis of monazite in contact metamorphosed shale against a Killara Formation related dolerite sill in the southwest of the Yerrida Basin.

6.4.3. Bryah Group

The Bryah Group preserves a sequence of intrusive and extrusive volcanic, volcanoclastic and sedimentary rocks (Pirajno et al., 2000). It consists of the Karalundi, Narracoota, Ravelstone and Horseshoe Formations. With the exception of the volcanic Narracoota Formation, all other formations consist of siliciclastic shales, siltstones and sandstone sequences. Additionally, the Horseshoe Formation contains a prominent iron formation which hosts the Horseshoe and Mt. Padbury Manganese deposits. Stratigraphy is often cross cut by late mafic dykes and sills of unknown age. The majority of the Bryah Group is affected by low to medium grade greenschist facies regional metamorphism as well as a retrogressive hydrothermal greenschist facies metamorphism (Pirajno et al., 2000).

The Bryah Group is in faulted contact with the Yarlarweelor Gneiss Complex, the Marymia Inlier, and the Palaeoproterozoic Yerrida Group. The Goodin Fault, a north easterly trending, high-angle reverse fault, marks the divide between the Bryah Group and the Yerrida Group (Pirajno et al., 2000, Dentith et al., 2014) (Fig. 6.2). However, more recent work by Jeffery (2013) indicates the contact as unconformable and in keeping with the original geological interpretations of Gee (1987).

Karalundi Formation: The Karalundi Formation's position within stratigraphy and distribution across the basin is problematic. It was first described by Gee (1979) and Gee (1987) as a mixed sequence of clastic, carbonate, chert and tuff about 1500m thick in a stratigraphic position conformable between the underlying Doolgunna Formation and the overlying Narracoota Formation. Bunting (1986) went on to describe it as a shale sequence with minor amounts of quartz wacke, chert, tuff and carbonate. Gee and Grey (1993) recognised the unit in thrust slices around the southern margin of the Goodin Inlier and then, for the purposes of their study, amalgamated the Karalundi with the Doolgunna Formation.

Two distinctive rocks were assigned to this sequence by Gee (1979) and Gee (1987); 1. A medium to fine-grained, poorly sorted, ferruginous sandstone with upward-fining beds,

convolute lamination and low-angle cross-bedding, and; 2. A hematite-magnetite jasper which occurs as steeply inclined pipes up to 20m in diameter, interpreted as colloidal hydrothermal deposits formed in fumarolic pipes associated with basic volcanism.

Pirajno et al. (2000) re-assigned the Karalundi Formation to form the base of the Bryah Group. It is placed in faulted contact with the Doolgunna Formation to the south-east along the Goodin Fault although this contact is questionable (Jeffery, 2013). To the north it is in faulted contact with the Peak Hill Schist. It is intercalated with volcanoclastic rocks of the Narracoota Formation in the western Bryah Basin. Pirajno et al. (2000) described the Karalundi as an immature clastic with lesser siltstone, calcareous siltstone, cross-bedded arenite, ferruginous arenite, litharenite, minor dolomite and purple, green and black shales. Basaltic water-lain tuff and minor carbonated beds appear in the upper part of the formation. They also make note of the hematite-magnetite jasperoidal chert and agree with the Gee (1979) interpretation. Overall the formation is interpreted to represent a transition from deep-water arkosic turbidites to shallow-water marine or even fluvial conditions and records the commencement of basaltic volcanism (Gee, 1987). SHRIMP U-Pb analyses of detrital zircons at the base of the Karalundi yield two ages of ca. 2.0 and 2.7Ga (Halilovic et al., 2004) indicating derivation of sediments from both the Yilgarn and possibly Dalgaringa Supersuite aged rocks, but possibly also reworked volcanic and sedimentary rocks of the underlying Yerrida Group.

Narracoota Formation: The 6000m thick Narracoota Formation forms the bulk of the Bryah Group and is intercalated with sedimentary rocks of the Karalundi Formation (Hynes and Gee, 1986). Its upper contact is both disconformable and interfingering with the Ravelstone Formation. In places it is in tectonic contact with the Padbury Group and also the Horseshoe Formation (Pirajno et al., 2000).

The Narracoota Formation comprises peridotitic and high-Mg basalt, mafic volcanoclastic rocks including pillow structured meta-basalts, mafic intrusive rocks and mafic to ultramafic schists (Pirajno and Occhipinti, 1998). More felsic volcanic rocks (basaltic andesite, andesite

and rhyolite) appear to be largely restricted to western portions of the basin proximal to the Horseshoe Lights and Fortnum mine sites (Pirajno, 1996) whereas mafic volcanic compositions predominate towards the east in the proximity of DeGrussa. Mid-greenschist and locally amphibolite facies metamorphism has affected the rocks, with almost complete replacement of the primary mafic mineralogy resulting in a mineral assemblage of albite + actinolite + chlorite + clinozoisite (epidote) + quartz + leucoxene (sphene) and relict pyroxenes. Mafic rocks are commonly aphyric, but pseudomorphs of actinolite after probable clinopyroxene and of albite/saussurite after plagioclase occur. Sheafs and plumose bundles of actinolite needles replacing former pyroxene and other metamorphic minerals including actinolite, epidote, clinozoisite, albite and calcite (Hynes and Gee, 1986). Rocks have undergone sea floor metasomatism dominated by albitisation (Hynes and Gee, 1986, Pirajno et al., 2000).

An oceanic depositional environment is supported by widespread occurrence of pillow structures and volcaniclastic rocks in eastern parts of the Bryah Basin around Noonyereena Hill and DeGrussa. Chemically, mafic rocks are similar to low-potash tholeiite from mid-ocean ridges but with slightly lower Ti and Zr contents representative of boninites (Hynes and Gee, 1986) This suggests that the Narracoota volcanics were erupted as an island arc, with rocks having more similarities to the boninites of forearc regions in the western Pacific than to any other modern tectonic environment. However, the current interpretations favour the Narracoota Formation as an oceanic plateau, accreted to the north-west margin of the Yilgarn Craton given the similar chondrite normalised REE patterns (Pirajno, 2004, Pirajno et al., 2004). Hyaloclastite in the southern Bryah Basin resulted from explosive volcanic activity in a shallow-water setting and were emplaced unconformably on the Archean granites of the Yilgarn (Hynes and Gee, 1986, Pirajno and Occhipinti, 2000) contrasting with the oceanic setting of the metabasites of the Narracoota Formation further north.

Ravelstone Formation: The 1000m thick Ravelstone Formation comprises a succession of lithic and quartz wacke, shale and siltstone with upwards fining graded bedding and a

provenance from nearby granitic or felsic precursors, and mafic material derived from the underlying Narracoota Formation (Pirajno et al., 2000, Pirajno et al., 2004, Pirajno and Occhipinti, 2000). It contains lenses of chert in the north. SHRIMP U-Pb ages on detrital zircons give a maximum age of 2.01 Ga (Nelson, 1997). The Ravelstone Formation is interpreted to represent a rift-fill succession that was deposited on top of the Narracoota Formation (Pirajno et al., 2004). The lower contact with the Narracoota Formation is disconformable, and sometimes interfinger. The upper contact with the Horseshoe Formation is conformable (Pirajno et al., 2000).

Horseshoe Formation: The Horseshoe Formation is approximately 100m thick, defined as including finely laminated (hematitic) shale and siltstone, fine grained quartz-wacke with interleaved iron formation and chert, graded quartz wacke, manganiferous shale, garnetiferous biotite-chlorite schist and garnetiferous iron-formation (Pirajno et al., 2000, Pirajno et al., 2004). A prominent iron-formation member, host to the Horseshoe and Mt. Padbury manganese deposits (Pirajno et al., 2000), occurs in the stratigraphic centre of the unit consisting of three bands of 40m thick iron formation intercalated with alternating layers of chert-magnetite-stilpnomelane rock, chloritic shale and chert (Gee, 1987). The contact between the underlying Ravelstone Formation is gradational and conformable, although in places the Horseshoe Formation directly overlies the Narracoota Formation in conformable or tectonic contact.

Deposition of the Horseshoe Formation was interpreted by Gee (1987) and Pirajno et al. (2004), to mark deposition and filling of a deep submarine trough followed by a cessation of sedimentation and a period of quiet shallow-water sedimentation during which chemical sediments (Banded Iron Formations and manganese deposits) precipitated in isolated depressions.

6.4.4. Padbury Group

The Padbury Group unconformably overlies the Bryah Group and consists of a succession of clastic and chemical sedimentary rocks deposited in a foreland basin (Pirajno et al., 2000)(Fig. 6.1, 6.2). It consists of a sequence of tightly infolded conglomerate, iron-formation and calcareous sedimentary rocks (Gee, 1987). Stratigraphic units are the Labouchere, Wilthorpe, Robinson Range and Millidie Creek Formations. The Labouchere and Wilthorpe Formations consist of upwards coarsening deep water turbidites with detrital zircons dated at c. 1980 Ma (Pirajno et al., 2004). The Robinson Range and Millidie Creek Formations are fine grained banded iron formations, ferruginous shales and siltstones deposited in a shallowing submarine environment. These iron formations could be correlated with the granular iron formation of the Frere Formation (Earaheedy Group) dated at 1891 ± 8 Ma (Rasmussen et al., 2012). The Padbury Group remains a clearly definable sequence of rocks separate from the Yerrida and Bryah Basin sedimentary sequences.

6.4.5. Regional Intrusive Rocks

Granodioritic intrusive rocks in the eastern parts of the Bryah Basin are related to the Narracoota Formation and result with Palaeoproterozoic U-Pb ages of 2012-2018 Ma (section 4.2.). Drillhole observations suggest that the granodiorite bodies are portions of dolerite sills that differentiated by crystal fractionation. Similar dolerite and basalt sills in the DeGrussa mine were contemporaneous with mineralisation.

The 1965-1945 Ma Bertibubba Supersuite granites and dykes are the first common magmatic elements of the northern margin of the Yilgarn, Yarlarweelor Gneiss Complex, Errabiddy Shear Zone and the Glenburgh Terrane (Paradise Zone) (Sheppard et al., 2004, Sheppard et al., 2010). No intrusive rocks of this age have been yet identified in the eastern Capricorn Orogen. Deformed rocks of the Padbury Group are intruded by granite (Martin, 1994) that are correlated with c. 1800 Ma granites (the Moorarie Supersuite) in the region.

6.5. Tectonic and Orogenic Events across the Capricorn Orogen

The Glenburgh terrane is an exotic micro-continent between the Pilbara and Yilgarn Cratons. Collision with the Pilbara occurred during the Opthalmian Orogeny at c. 2240 and 2125 Ma. The Moogie Metamorphics meta-sedimentary rocks were deposited concurrently in a foreland basin system (Johnson et al., 2010, Johnson et al., 2011a). In the eastern Capricorn Orogen, continental rifting of the northern Yilgarn margin may have led to separation of the Marymia Inlier and subsequent deposition of Yerrida Group sediments in a sag basin setting (Pirajno et al., 1995, Pirajno and Adamides, 2000b, Dentith et al., 2014).

Continental-margin arc-magmatic activity was initiated along the southern margin of the combined Gascoyne-Pilbara Terranes with the intrusion of the Dalgaringa Supersuite magmatic rocks in a continental margin arc as an Andean-type batholith c. 2005 to 1975 Ma (Sheppard et al., 2004). Oceanic plate subduction, and hence closure between the Gascoyne and Yilgarn, was initiated at c. 2080 Ma (Sheppard et al., 2004) along the proto-Dalgaringa arc, toward the north and under the southern leading edge, of the Glenburgh Terrane. This is opposite to the present-day dip of the suture zone (Johnson et al., 2011a). Rocks of the overlying Camel Hills Metamorphics (Petter Calc-silicate and Quartpot Pelite) are interpreted to have formed in a forearc or backarc basin setting along the southern margin of the Glenburgh Terrane, between approximately 2000 and 1955 Ma as the meta-sedimentary rocks equivalent to the intrusive rocks of the Dalgaringa Supersuite (Johnson et al., 2011a).

In contrast, rocks of the Bryah Group, in particular the Narracoota Formation, have most recently been interpreted to represent a fragment of oceanic plateau accreted to the Archean Yilgarn Craton margin during oceanic basin closure between the Pilbara and Yilgarn Cratons (Pirajno, 2004). Previous works however have suggested a range of tectonic environments from intracontinental basins to back arc rifts (Bunting et al. (1977), Gee (1979), Hynes and Gee (1986), Tyler and Thorne (1990), Windh (1992), Gee and Grey (1993), Myers (1993), Martin (1994), Pirajno et al. (1994), Myers et al. (1996), Pirajno (1996), Pirajno and Occhipinti (2000), and Pirajno et al. (2000)). Myers et al. (1996) and Hynes and Gee (1986) suggested that the

Bryah Group could represent a back-arc formed during south directed subduction beneath the northern margin of the Yilgarn Craton. Occhipinti et al. (2004) suggested that remnants of cordilleran-like magmatic suites related to this subduction, may be buried beneath the Edmund and Collier basins, to the north of the Bryah and Padbury Basins. Geochronological data presented in sections 4--6 suggests the DeGrussa host sedimentary rocks were deposited between c. 2080 and 2030 Ma coincident with deposition of the Camel Hills Metamorphics and magmatism within the Dalgaringa Arc. Closure and collision of the combined Pilbara Craton-Glenburgh Terrane and the Yilgarn Craton led to development of the Errabiddy Shear Zone and east directed emplacement of the Bryah Group over the Yerrida Group during the latter part of the Glenburgh Orogeny (c. 1965 and c. 1950 Ma)(Occhipinti et al., 2004, Sheppard et al., 2004, Johnson et al., 2011a). Conversely, drill core observations by Jeffery (2011) suggest the contact between the DeGrussa host sedimentary rocks unconformably overlie the Johnson Cairn Formation rocks of the Yerrida Group.

Several later orogenic and tectonic events have affected the region. The 1820 – 1770 Ma Capricorn Orogeny, associated with granite plutonism, affected this margin and was coincident with the Yapungku Orogeny (c. 1790 Ma) which records the onset of collision between the West Australian Craton and the North Australian Craton (Johnson, 2013). The Mangaroon Orogeny (1680-1620 Ma) was related to reworking of crust in the northern Gascoyne and the coeval intrusion of voluminous granites, followed by reactivation of faults and shear zones and intrusion of granite plutons over a wide area of the Gascoyne Province (Sheppard et al., 2005) The Mutherbukin Tectonic Event (1320-1170 Ma, (Korhonen et al., 2015)) is a tectonothermal event with no significant magmatism or sedimentation and is largely confined to the Gascoyne Province and overlying parts of the Edmund Group. The event is characterised by faulting and amphibolite facies metamorphism (Korhonen et al., 2015). The Edmundian Orogeny (1030-955 Ma) was responsible for intracontinental reworking along a NW-SE striking corridor with greenschist-amphibolite facies metamorphism and deformation followed by pegmatite intrusion and coeval granite magmatism (Sheppard et al., 2007).

6.6. DeGrussa Deposit Geology

The DeGrussa deposit is located in a sedimentary rock sequence with mafic intrusive rocks that are difficult to reconcile with the GSWA stratigraphy (Jeffery, 2013). It could be assigned to either the Narracoota Formation or to the Killara Formation and has been assigned the informal stratigraphic name of DeGrussa Formation around the DeGrussa deposit area. Future studies may be able to place it into one of the formally defined stratigraphic units. Descriptions of host sedimentary rock and mafic rock sequences of the DeGrussa deposit have been determined from drill core, underground and petrographical observations, geological logging, and geochemical studies made by the author between 2009 and 2014.

The DeGrussa VHMS deposit is located on the northern limb of the Robinson Range syncline (Fig. 6.2). Apart from some small scale open folds related to the major synclinal structure, and soft sediment deformation within host sedimentary rocks, the deposit appears largely undeformed. The deposit is composed of four lenses (Fig. 6.4) – DeGrussa, Conductor 1 (C1), Conductor 4 (C4) and Conductor 5 (C5) – variably hosted within turbiditic sedimentary rocks and shales, basaltic breccia, chlorite and talc-carbonate schists. Mineralisation is hosted by sedimentary rocks and basalts with contacts often displaying replacement features (Adamczyk, 2013). The lenses occur as massive pyrite and/or chalcopyrite, sphalerite, pyrrhotite and magnetite. Oxidation is present to a depth of approximately 100m, with shallow levels of the DeGrussa and Conductor 1 ore bodies rich in chalcocite and native copper. DeGrussa occurs as a ~200m long sub vertical northeast-southwest striking lens. Conductor 1 has an east west strike of ~400m and is separated from the DeGrussa lens by a dolerite sill. Conductors 4 and 5 have much shallower dips. Two large faults displace the ore lenses from each other. The Shiraz fault, a northward splay from the long-lived and deep crustal Jenkin Fault, is the most significant with reverse sinistral displacement of 500-600m (Fig. 6.4). The Shiraz Fault truncates the southern side of the DeGrussa and C1 ore lenses, separating them from C4 and C5. The Merlot Fault splays off the Shiraz Fault in a south-westerly direction, approximately 500 m north east of the DeGrussa and C1 ore lenses. It displaces C5 from C4 by approximately 80m. The Jenkin Fault

(Fig. 6.2) transects the DeGrussa and Narracoota Formation stratigraphy, placing it in faulted contact with the Red Bore Formation, possibly an equivalent to Padbury Group sediments (Jeffery, 2011).

Sedimentary rocks and chlorite or talc-rich units have acted as loci for strain during deformation. In drill core, contacts between different units are often fractured or sheared, destroying primary features. In underground exposure, margins of the ore body form sheared contacts within the C1 and DeGrussa ore lenses. C4 and C5 are less deformed. Peperite is present where basalts have intruded wet, unconsolidated sedimentary rocks and are a significant feature of the host sequence.

Figure 6.4. Local geological setting of the DeGrussa ore lodes in plan and section view. DeGrussa and Conductor 1 crop out into the weathered zone. Conductor 4 and 5 are interpolated to surface. The Shiraz Fault truncates the DeGrussa and Conductor 1 lodes on their southern edge, offsetting Conductor 4 and Conductor 5 ore lodes. The DeGrussa Formation sedimentary rocks and dolerites are in unconformable contact with the underlying Johnson Cairn Formation in the vicinity of the DeGrussa deposit.

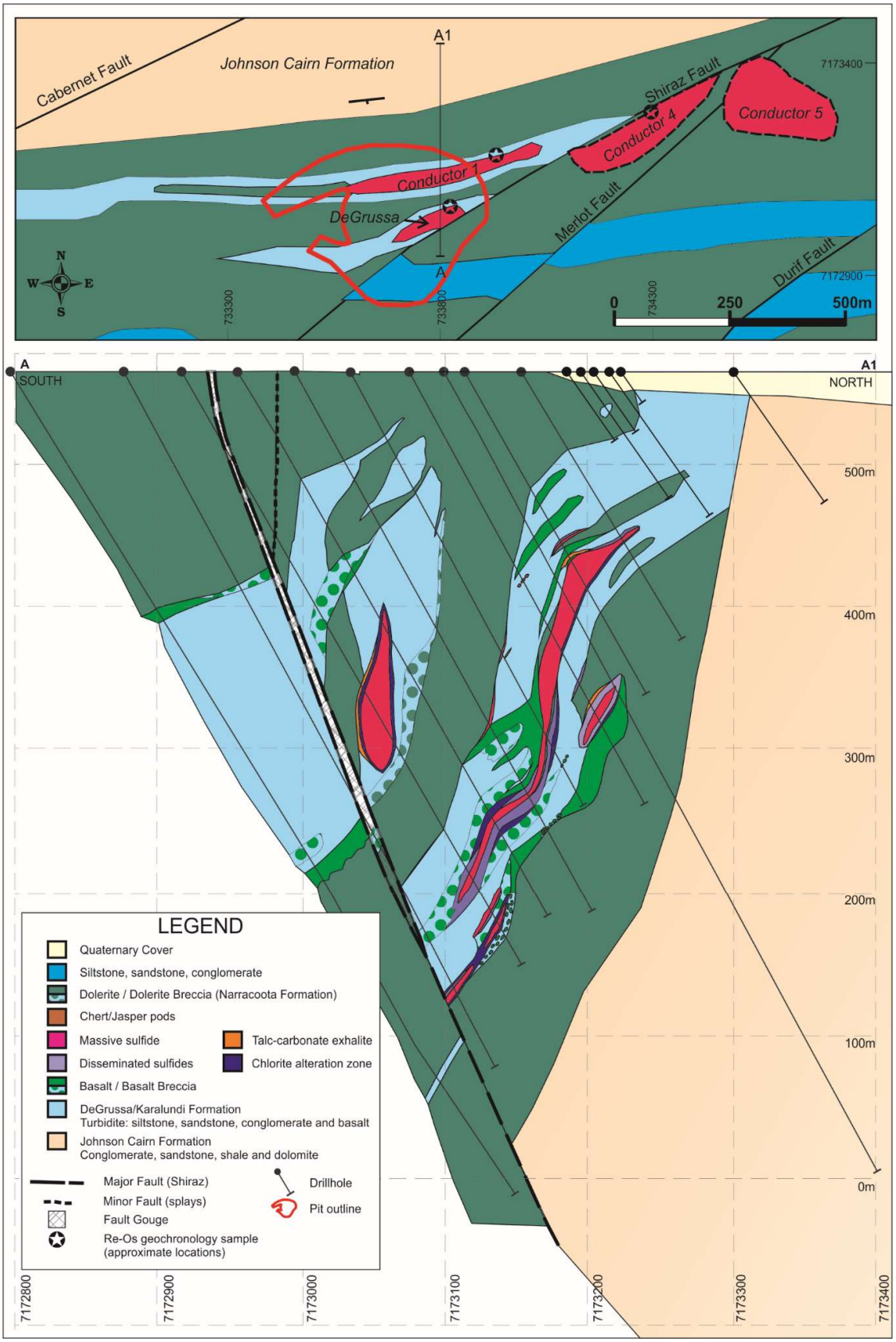
Cabernet Fault
Johnson Cairn Formation
A1
Shiraz Fault
7173400
Conductor 5
Conductor 4
Conductor 1
DeGrussa
Merlot Fault
Durif Fault
7172900
N
W
E
S
A
733300
733800
734300
0
250
500m
A
SOUTH
A1
NORTH
500m
400m
300m
200m
100m
0m
LEGEND
Quaternary Cover
Siltstone, sandstone, conglomerate
Dolerite / Dolerite Breccia (Narracoota Formation)
Chert/Jasper pods
Massive sulfide
Talc-carbonate exhalite
Disseminated sulfides
Chlorite alteration zone
Basalt / Basalt Breccia
DeGrussa/Karalundi Formation
Turbidite: siltstone, sandstone, conglomerate and basalt
Johnson Cairn Formation
Conglomerate, sandstone, shale and dolomite
Major Fault (Shiraz)
Minor Fault (splays)
Fault Gouge
Re-Os geochronology sample
(approximate locations)
Drillhole
Pit outline
7172800
7172900
7173000
7173100
7173200
7173300
7173400

6.6.1. Footwall Sequence

Stratigraphy in the DeGrussa deposit area has been documented from the Paleoproterozoic host sequence down to the Archean basement. The basal Finlayson Member occurs as thin lenses along the northern contact between the Yerrida Group and the Marymia Inlier, but is largely absent from stratigraphy in the DeGrussa deposit area leaving the Bubble Well Member (Juderina Formation) in unconformable contact with the Marymia Inlier (Fig. 6.3). The Bubble Well Member preserves a ~100m thick sequence of stromatolitic material, alternating with mudstone and evaporite layers. Several of the Bubble Well Member stromatolite species described by Grey (1994), including *Segosia finlaysonensis*, *Stromatolite form 1* and *Stromatolite form 2* are found in drill core below DeGrussa. The Johnson Cairn Formation conformably overlies the Bubble Well Member and is approximately 1500 meters thick comprising sandstone, siltstones, mudstones and black carbonaceous/graphitic shales. It also hosts a basalt unit previously unidentified in the literature, and is geochemically similar to basalts seen in co-funded GSWA/SIPA Resources drill hole THD001 which also contains a sequence of volcaniclastic material (Muller, 2011, Hawke, in prep) (Fig. 6.3). The upper contact is unconformable against the DeGrussa host sedimentary rocks (Jeffery, 2013) with lower stratigraphic levels of the DeGrussa host sedimentary rocks containing large fragments of Yerrida Group carbonate (Hawke, in prep). No units of the Mooloogool Subgroup (the Thaduna, Doolgunna, Killara and Maraloou Formations) are present. This may reflect a progressive non-deposition of Yerrida Group stratigraphy towards the west (Jeffery, 2011).

6.6.2. Host Sedimentary rocks

Mineralisation is hosted by sedimentary rocks and lesser basalt in the lowermost units of the Bryah Group (Fig. 6.4). Identified locally as the DeGrussa Formation it is considered to be a lateral equivalent of the Karalundi Formation. Dolerite and gabbro sills form the other dominant rock type in the mine stratigraphy and are interpreted to postdate sedimentation and mineralisation due to the intrusive contacts.

The DeGrussa Formation is largely turbiditic and variably dolomitic, consisting of graded units from quartz-rich sandstone and siltstone to fine grained mudstones with soft sediment deformation. Occasional conglomerate bands including small sub angular clasts of basalt occur at the base of turbidite lenses. Sedimentary rocks have experienced carbonate alteration with lesser chlorite and clay. Epidote is rare. Quartz, carbonate, and quartz-carbonate veins both laminar and stockwork, with or without trace amounts of sulfides (pyrite > chalcopyrite), dominate through the sedimentary units.

6.6.3. Mafic rocks

Basalt morphology includes pillow basalts, peperite and irregular deformation of adjacent sedimentary rocks. This suggests the basalts are partly intrusive and the sedimentary rocks were unconsolidated at the time of basalt emplacement. Basalts are pale green-grey to dark blue-black, fine grained and flecked with white-grey titanite crystals up to 0.5mm.

Basalts interfinger with sedimentary rocks of the DeGrussa host sedimentary rocks. Geochemically, host basalts and intrusive dolerites are indistinguishable from each other suggesting that they derive from the same magmatic source. Dolerites are in the order of meters to hundreds of meters thick. Contacts range from brecciated, sheared, faulted and contact metamorphosed with host sedimentary rocks. They are interpreted as sills and dykes, post-dating the sedimentary rocks and mineralisation. Grain size within intrusive units varies from fine grained microdolerite at the margins, gradational or with sharp contacts, to medium grained dolerite and occasional coarse grained gabbro and pegmatite. Similar observations were made by Adamczyk (2013) of the Conductor 5 ore lens stratigraphic sequence.

Alteration intensity varies between cases where textures and original mineral composition are largely preserved to cases where primary mineralogy is obliterated, yet original textures are preserved. Typical mafic mineralogy consists of plagioclase (40-70%), hornblende (≤40%), clinopyroxene (≤30%), magnetite and/or titanite (sphene) and occasional trace sulfides (pyrite and chalcopyrite). Rocks are largely altered pervasively to Fe-Mg clays, chlorite (clinochlore

and/or chamosite) and carbonate. These observations of the mineral assemblage are consistent with that of Hynes and Gee (1986) with the almost complete replacement of primary mineralogy a widespread characteristic of the basin. Infrequent alteration minerals include talc, actinolite, epidote, albite, titanite and stilpnomelane, both replacing primary phenocrysts and around grain margins. The similar petrological characteristics of the Narracoota Formation rocks of Hynes and Gee (1986) are indicated as typical of quenched submarine basalts. Alteration assemblages (both groundmass and veins) vary with distance through the mafic intrusions. Carbonate and clay alteration are pervasive at the edges, with chlorite, epidote and albite becoming dominant towards the intrusive centre. When present, pyrite appears related to chlorite-carbonate veins.

There are no felsic volcanic units present within the DeGrussa stratigraphy, however they become more frequent within the western succession of the Narracoota Formation, proximal to the Horseshoe Lights copper-gold VHMS and Fortnum orogenic gold deposits.

6.6.4. Ore lenses

Mineralisation is characterised by massive pyrite, chalcopyrite and pyrrhotite units with lesser sphalerite, marcasite, magnetite, galena and molybdenite. Ore textures are varied and display primary features (e.g. bedded sulfides and primary sedimentary breccias), deformational textures (breccia, remobilisation and recrystallisation textures, sheared contacts with host rocks and schist) and replacement textures (Fig. 6.5) (e.g. preferential replacement of basalt breccia as evidenced by Adamczyk (2013)). Underground exposures of the C1 ore display sheared marginal contacts with surrounding host sedimentary rocks, banded sulfides, brecciated contacts where sulfides wrap around basalt breccia clasts, pyrite clast breccia, disseminated sulfide horizons forming stringers with carbonate association in sedimentary rocks, chlorite schist and talc-carbonate-chlorite-schist. Possible chimney structures have been identified in drill core and hand sample from DeGrussa and C1 (Fig. 6.5).

Figure 6.5. Mineralisation features. **A.** Chalcopyrite replacing basalt clasts with stringers of pyrite associated with chlorite sedimentary rock in Conductor 1 (DGDD173, 278.08m). **B.** Banded pyrite and pyrrhotite in sedimentary host rocks from the Conductor 5 ore (DGDD219, 534.0-534.4m). **C.** Brecciated massive sulfide with angular clasts of pyrite. Chalcopyrite infilling fractures in a host chloritic sedimentary rock from Conductor 5 (DGDD277, 577.8-578.2m). **D.** Possible chimney structure. Central core of carbonate rimmed with bands of pyrite and chalcopyrite (DGUG755, 57-59m). **E.** Possible chimney structures from underground exposure in the Conductor 1 ore lode. Central core of chlorite, rimmed with chalcopyrite within pyrite-rich massive sulfide. **F.** Cut slab of interbedded pyrite-rich ore, chalcopyrite-rich ore and mudstone from Conductor 1. Chalcopyrite and chlorite remobilised into tension gashes during deformation (photo courtesy Sandfire Resources). **G.** Feeder pipe – silicified unit with disseminations and stringers of pyrite and chalcopyrite (DGUG0569, 69.5-69.75m). Sample locations are in Appendix 6.6.

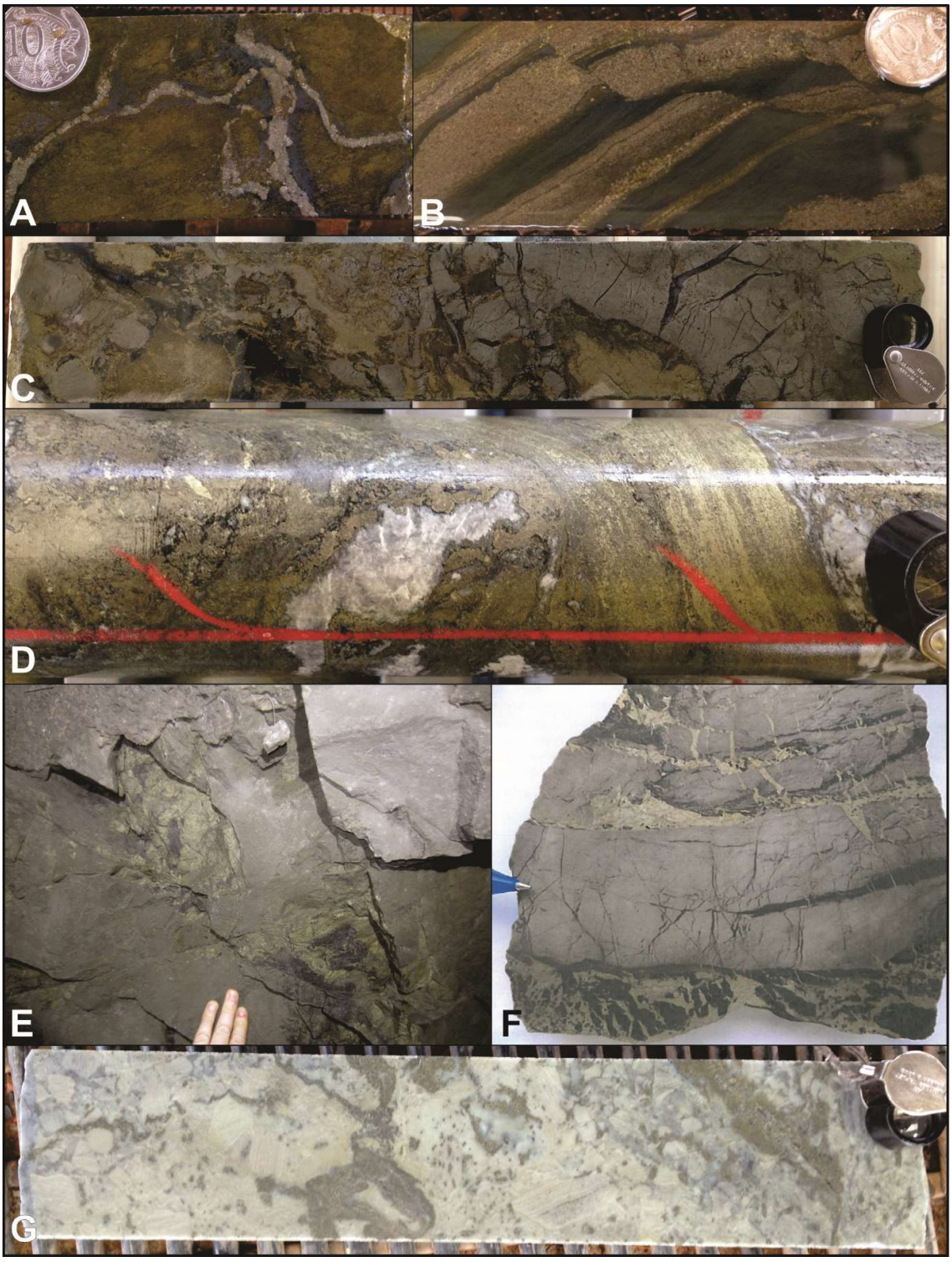
A
B
C
D
E
F
G

Figure 6.6. **A.** Typical VHMS model and zoning (Lydon, 1984). and **B.** VHMS zoning for a siliciclastic-mafic deposit (Galley et al., 2007). **C.** VHMS model for the DeGrussa deposit displaying characteristics of Besshi-type deposits and both sea floor and sub seafloor ore lenses.

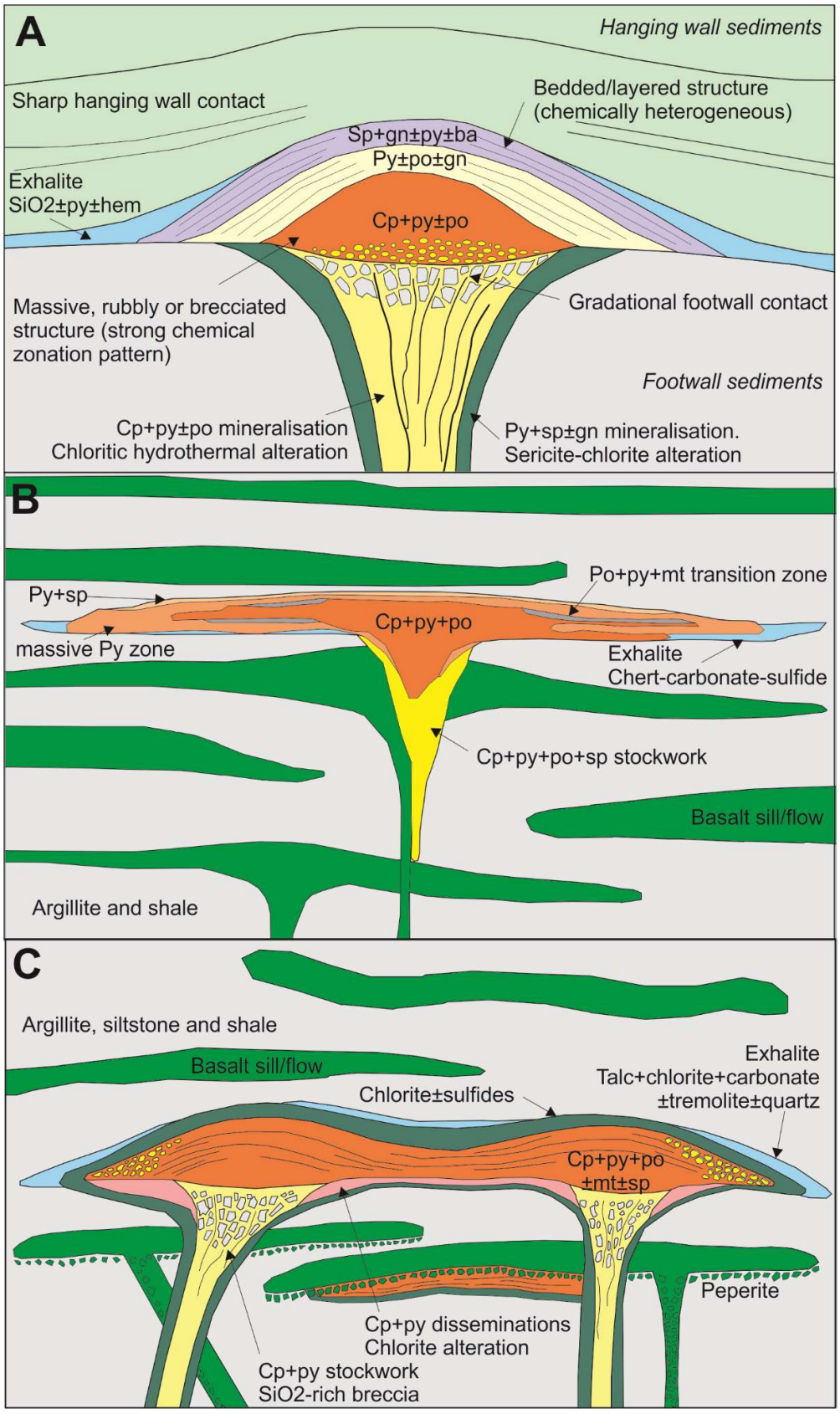
A
Hanging wall sediments
Sharp hanging wall contact
Bedded/layered structure
(chemically heterogeneous)
Sp+gn±py±ba
Py±po±gn
Exhalite
SiO2±py±hem
Cp+py±po
Massive, rubbly or brecciated
structure (strong chemical
zonation pattern)
Gradational footwall contact
Footwall sediments
Cp+py±po mineralisation
Chloritic hydrothermal alteration
Py+sp±gn mineralisation.
Sericite-chlorite alteration
B
Po+py+mt transition zone
Py+sp
Cp+py+po
massive Py zone
Exhalite
Chert-carbonate-sulfide
Cp+py+po+sp stockwork
Basalt sill/flow
Argillite and shale
C
Argillite, siltstone and shale
Basalt sill/flow
Exhalite
Talc+chlorite+carbonate
±tremolite±quartz
Chlorite±sulfides
Cp+py+po
±mt±sp
Peperite
Cp+py disseminations
Chlorite alteration
Cp+py stockwork
SiO2-rich breccia

Figure 6.7. Mineralisation textures. **A.** Coarse chalcopyrite, sphalerite, rare pyrite. Black crystals of minnesotaite in sulfides and forming veins (field of view 600μm) (DGRC105, 138-140m). **B**. Extensive chalcopyrite with scattered pyrite and flakes of minnesotaite (field of view 600μm) (DGRC105, 138-140m). **C.** Low magnification (field of view 2mm) showing gross characteristics of sulfide (+magnetite) mineralisation. Left side of photo is intricately mixed, extremely fine chalcopyrite and pyrite enclosing patches of grey magnetite. Right hand is mixed chalcopyrite > pyrite incorporating random flakes/fibres of minnesotaite and rarer grey magnetite (DGRC104, 183-184m). **D.** Framboidal pyrite with centres of needles (DGRC104, 183-184m)(field of view 1.2mm). **E.** Fine grained, banded massive sulfide (DGRC104, 120-127m) (field of view 5mm). **F.** Light pink pyrrhotite intergrown with pyrite, chalcopyrite and stilpnomelane crystals from the Conductor 5 ore lode (DGMH091: DGDD219, 538.87-538.93m) (field of view 600μm). **G.** Massive fine grained pyrite with chalcopyrite and minor stilpnomelane with age of 2060 Ma (DGMH090: DGDD047, 240.28-240.39m)(field of view 500μm). **H.** Sample from sulfide-rich lamina in meta-sediment, illustrating primary concentric colloform microtexture of intergrown sulfides (chalcopyrite, pyrite and galena) in a spheroidal aggregate. The primary texture survived the metamorphic recrystallization event. Pyrite is approximately 300μm diameter (DGMH038: DGDD125, 562.82-562.92m). Sample locations are in Appendix 6.6.

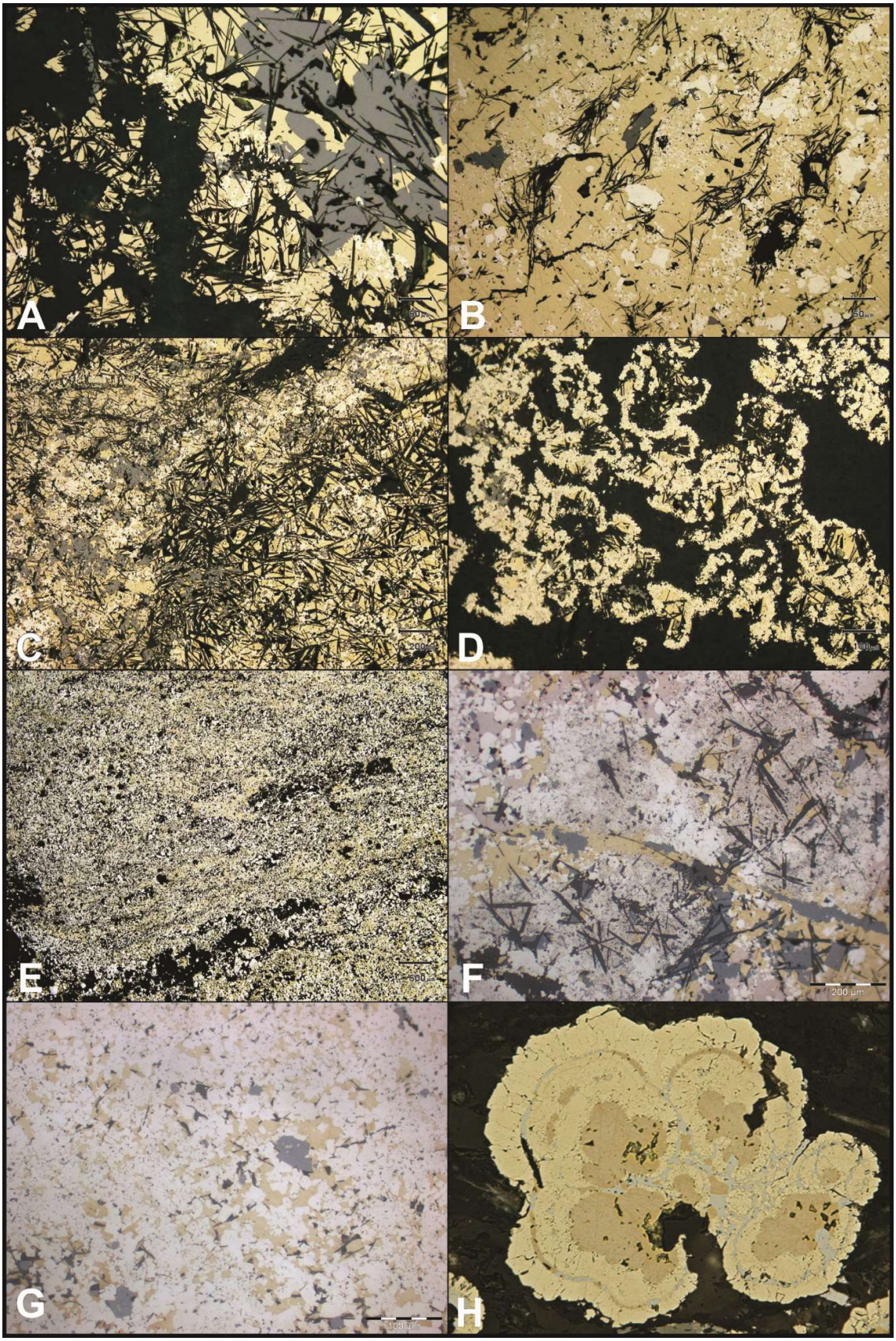
A
B
C
D
E
F
200 µm
G
H

Volcanic-hosted massive sulfide deposits generally display zonation, progressing from an inner core of chalcopyrite + pyrite ± pyrrhotite ± magnetite to pyrite ± sphalerite ± galena and an outer shell of sphalerite ± galena ± pyrite ± barite (Large, 1977, Lydon, 1984, Franklin et al., 2005, Galley et al., 2007) The DeGrussa deposit however, shows no such zoning and instead has a metal content comparable only to the central core of chalcopyrite + pyrite ± pyrrhotite in typical VHMS model (Fig. 6.6). Barium values are elevated within the hanging wall and footwall of the massive sulfide lenses, yet rare barite has been observed.

Pyrite is the dominant ore mineral. It is fine grained, but takes on a range of larger scale morphologies, including small globular aggregates and larger breccia fragments and is intimately intergrown with other sulfides (Fig. 6.7). Chalcopyrite is the only copper bearing mineral forming in massive, fine grained bands, alternating with pyrite and pyrrhotite. Some chalcopyrite has an association with carbonate and its mobility during deformation is exemplified by its presence in tension gashes (Fig. 6.5). Sphalerite is intricately intergrown with the other sulfides, but localised in patches and more dominant in thick parts of the ore deposit. Galena is fine grained and localised to thin horizons within the ore body intricately associated with pyrite, chalcopyrite, sphalerite and pyrrhotite. Galena is also found in later quartz-carbonate extensional veins formed during later orogenic events. Molybdenite occurs in thin (~10cm) horizons as small fine grained aggregates between other sulfides, or in association with chalcopyrite mineralisation in disseminated sulfide zones above and below massive ore.

The DeGrussa lens is located higher in the stratigraphy, separated from the C1 ore lenses by a thick dolerite sill (Fig. 6.4). Mineralisation in the DeGrussa lens is massive, fine grained pyrite, chalcopyrite, pyrrhotite and sphalerite. Disseminated sulfide stringers of chalcopyrite, pyrite and molybdenite are present within talc-carbonate alteration.

Drill core displays evidence of small and restricted feeder pipes of intensely silicified sedimentary rock breccia, with pyrite-chalcopyrite-rich sulfide mineralisation as stringers and disseminations in the footwall of the DeGrussa lenses (Fig. 6.5). This is bounded by a green-black chlorite-rich alteration zone, sometimes schistose with or without sulfides. Outward of

this is a zone of chlorite-sericite alteration and finally sericite dominant sedimentary rocks. Sericite altered sedimentary rocks are commonly associated with peperitic basalt. Peperitic basalt may have been a dominant precursor lithology to sulfide mineralisation, with remnant clast textures apparent throughout the alteration halo, including the silicified core. It is postulated that the feeder structures for the host basalts may have provided the pathway for hot, hydrothermal metal-bearing fluids which would explain the association of chalcopyrite + sphalerite + magnetite-rich massive sulfide above the feeder pipes. There is no evidence of feeder structures or related alteration within units underlying the DeGrussa host sedimentary rocks, although drill holes and mine exposure to this depth are limited. The lack of any footwall alteration supports a tectonic nature between the DeGrussa fof the lower contact with the Johnson Cairn Formation. A schematic model of how the DeGrussa deposit may have formed is presented in Figure 6.8.

Wall rock alteration: Chlorite schist occurs in contact with the massive sulfide lenses. The chlorite is green-black, in comparison to light green regional chlorite alteration, suggesting this chlorite could be related to mineralisation. Talc-chlorite-carbonate(±tremolite ± quartz) alteration (up to ~2m thick) has a schistose texture and could have an origin comparable to talc zones formed around the Stirling VMS, Nova Scotia Canada (Kontak, 1998). The unit forms lenses, inconsistent along both upper and lower contacts of the ore bodies and separated only by chlorite schist. Often it occurs interbedded within the ore deposit and occasionally contains significant amounts of pyrite and chalcopyrite. Disseminated pyrites, exhalative jaspers and hematite-rich sediments are present in sedimentary rocks above and peripheral to the ore lenses.

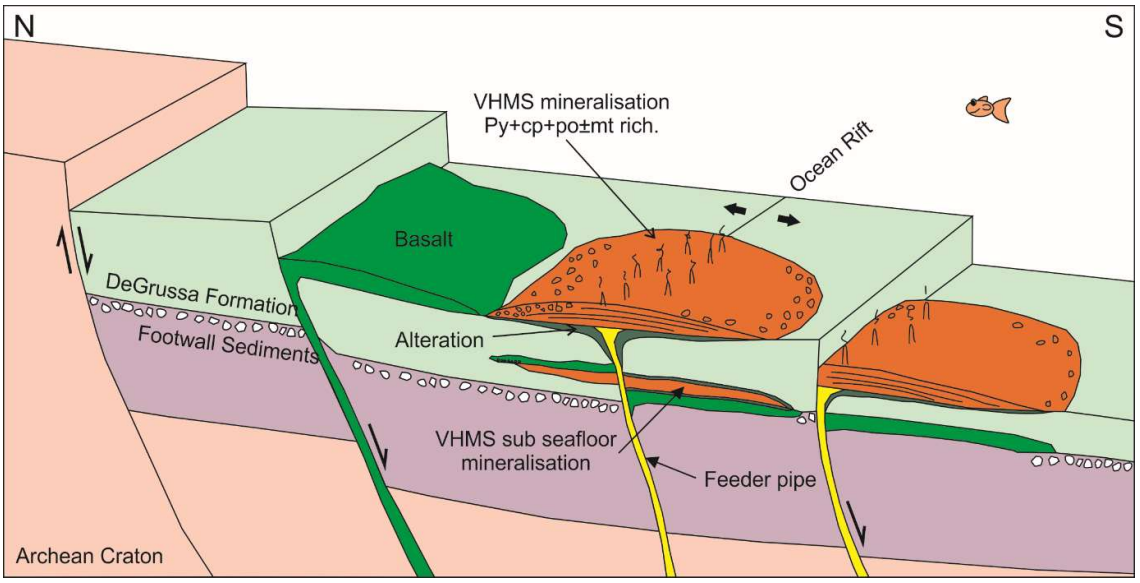

Figure 6.8. Schematic representation of the depositional environment of the DeGrussa VHMS mineralisation. VHMS mineralisation forms as sub-seafloor mineralisation, exemplified by replacement of basalt clasts and sedimentary rocks, and also as sea floor mound. The feeder pipe is formed from siliceous replacement of sediment and basalt clasts, stringers and disseminations of pyrite and chalcopyrite throughout. VHMS alteration comprises a strong chlorite alteration zone with sulfide stringers and disseminations proximal to ore lenses.

6.7. U-Pb Zircon Geochronology

Three samples from coarse grained dolerites and gabbro (DGMH032, 061 and 082) from within the hanging wall sequence of the DeGrussa mine were collected for U-Pb dating of zircons.

Another two igneous samples of the regional granodiorite bodies which are portions of dolerite sills that differentiated by crystal fractionation (referred to in this paper as regional granodiorites), were collected from outside the DeGrussa deposit area (SPD015 and DGRC648). These were identified as granodiorite or leucogranite from modal mineralogy in thin section. These granodiorite/dolerite sills intrude DeGrussa host sedimentary rocks and/or Karalundi Formation rocks. U, Th and Pb isotopes in the zircons were analysed by laser mass spectrometry (LA-ICPMS) at the University of Tasmania in Hobart (see Appendix 6.2 for methods). Representative cathodoluminescence (CL) images of zircons from these samples are presented in Figure 6.9. All data is located in Appendix 6.3. Wetherill plots are presented within the text and Terra-Wasserburg plots are provided in Appendix 6.4.

6.7.1. DeGrussa Dolerites

All three of the mafic rocks intruding the DeGrussa hanging wall (DGMH032, 061 and 082) sequence contained euhedral, zoned zircons which provided concordia ages of 1991 ± 7, 1999 ± 7 and 2003 ± 7 Ma (2σ, Fig. 6.10). Zircons are elongate, lath shaped crystals, approximately 40-60 μm width and 100 μm length with small outer rims approximately 10 μm width. These are interpreted as primary magmatic zircons, formed insitu in the mafic melt. Most of the zircons are concordant or slightly reversely discordant suggesting that only slight Pb mobility occurred within the crystals. The standard used before and after these analysis (e.g. 91500, Appendix 6.4) is concordant which indicates reverse discordance in samples such as DGMH032 and DGMH061 are due to geological factors, in this case the crystal has undergone considerable radiation damage leading to redistribution of radiogenic lead on the few micron scale within the crystal analysed. Dark zones in some zircon CL images (Fig. 6.9) representing high U metamict zones which may have contributed some radiogenic Pb along cracks in the crystal. The data is uncorrected for common lead, however the data plots in the direction of radiogenic Pb and not common Pb (Fig. 6.10).

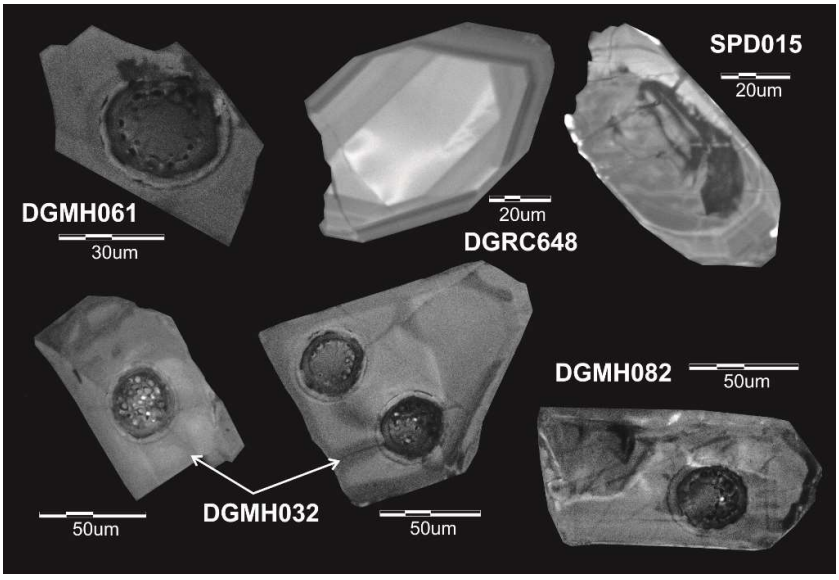

Figure 6.9. Representative cathodoluminescence images for zircons analysed.

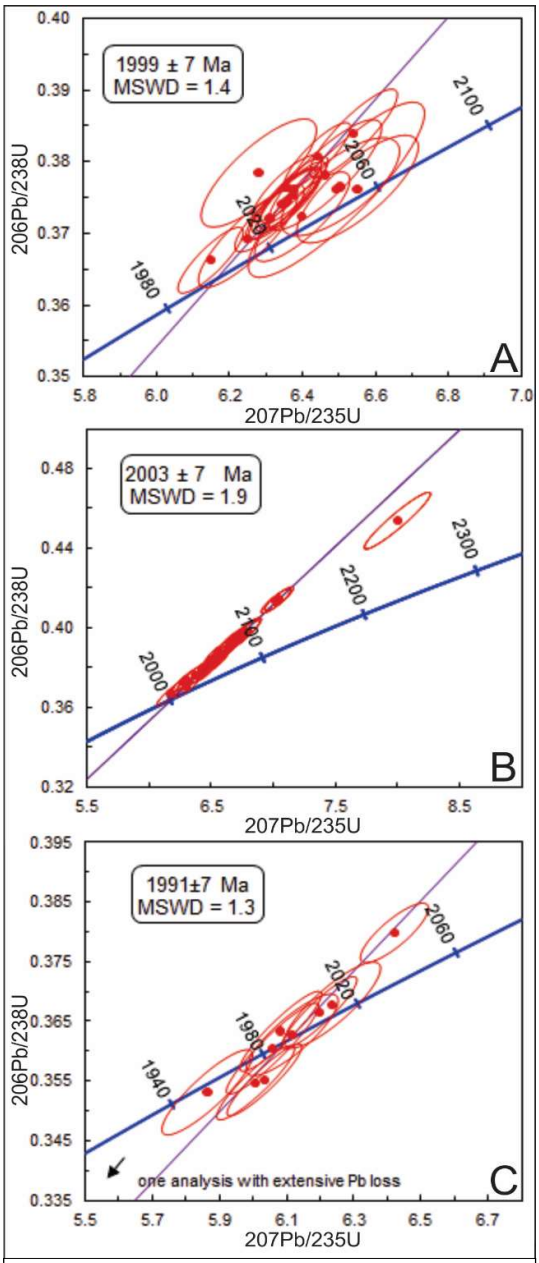

Figure 6.10. U-Pb zircon geochronology for three dolerite samples within DeGrussa mine stratigraphy. **A.** DGMH032 (DGDD125, 390.74-391.0m) from the hanging wall of Conductor 1 with age of 1999 ± 7 Ma, **B.** DGMH061 (DGDD203, 369.78-369.9m) from dolerite in the hanging wall to Conductor 4 with age of 2003 ± 7 Ma, and **C.** DGMH082 (DGDD243, 113.32-113.7m) from dolerite 500m east of Conductor 5 with an age of 1991 ± 7 Ma. Sample locations are in Appendix 6.6.

6.7.2. Regional Granodiorite

The zircons from a leucogranite in diamond drillhole SPD015, have $^{207}Pb/^{206}Pb$ age clustering at 2014 ± 7 Ma with 6 of the analyses indicating extensive Pb loss (see Appendix 6.3, 6.4). CL images of zircons display two types of zircon. The first are small and fragmented and very similar to those of the DeGrussa dolerites displaying clear, elongate, lath shaped crystals with think zoning around the rims. The second show inherited cores with younger rims, approximately 40 µm width and 80 µm length. The SPD-015 leucogranite/fractionated dolerite is located on the southern side of the Robinson Range syncline (Fig. 6.2) intruding the Karalundi Formation. Dolerite chips collected from RC drill hole DGRC648, to the west of the DeGrussa deposit contained a unimodal zircon population of clear, zoned crystals 60 µm width and 100 µm length with an average $^{207}Pb/^{206}Pb$ age of 2018 ± 9 Ma. Both of these samples provide ages which are slightly older than previous age constraints from this area of 1922 ± 35 Ma provided by Pb isotopic analysis of Horseshoe Lights pyrite (Windh, 1992).

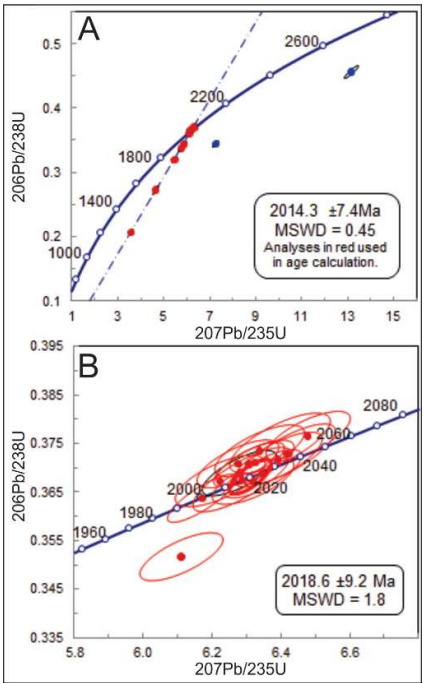

Figure 6.11. U-Pb zircon geochronology for granodiorites. **A.** DGRC648 (DGRC648, 96.0-97.0m) located southwest of the DeGrussa deposit with resulting age of 2018 ± 9 Ma, **B.** SPD015 (SPD015, 75.2-78.9m) a leucogranite from the Narracoota Formation, intrusive into Karalundi Formation, located in the southeast of the Bryah Group. This resulted in an age of 2014 ± 7 Ma. Sample locations are in Appendix 6.6.

6.7.3. Detrital zircons

Detrital zircons were also separated from 2 samples from the C4 ore lens host sedimentary rocks (DGMH033 and DGMH040). DGMH033 contained 47 zircons and resulted with populations at 2560 Ma, 2600-2700 Ma and 2900 Ma a youngest $^{207}Pb/^{206}Pb$ age at 2262 ± 40 Ma (95% conf.) and the average age of the 3 youngest zircons at 2307 Ma. DGMH040 contained fewer zircons (6), with ages, 2173, 2456,, 2604-2666 and 2801-2802 Ma. These ages suggest that the host sedimentary rocks were largely derived from the Archean Marymia and rocks of the northern Yilgarn Craton. As a check, a sample of Marymia granite (DGMH115) approximately 800m below the DeGrussa deposit, contains insitu magmatic zircons with ages between 2479 to 3224 Ma with the largest population between 2635 and 3045 Ma compatible with ages of detrital zircons in DeGrussa host sediments (Appendix 6.3, 6.4). Younger zircons provide ages similar to that of the Glenburgh Terrane in the western Capricorn Orogen, in particular with the 2555-2430 Ma Halfway Gneiss (Johnson et al., 2011c). These ages are all older than that of the dolerites proximal to the DeGrussa deposit which suggest that there was little or no reworking of synsedimentary zircon-bearing magmatic rocks.

SHRIMP U-Pb analyses by Halilovic et al. (2004)_for detrital zircons at the base of the Karalundi Formation yield two ages of ca. 2.0 and 2.7Ga. If the Karalundi Formation is supposed to be older than the Narracoota Formation, and the DeGrussa dolerites are the equivalent of the Narracoota Formation, this suggests that the DeGrussa host sediments are not the Karalundi Formation and the Karalundi Formation was deposited syn- or post-Narracoota Formation.

Table 6.1. U-Pb radiogenic ages for magmatic zircon bearing dolerites and detrital zircons (*) from host sediments within the DeGrussa mine sequence and regional Narracoota Formation.

Sample	Drill hole	Co-ordinates (GDA94)	Description	Age (Ma)	Error (±Ma)
DGMH032	DGDD125, 390.74-391.0m	734206.94mE, 7173080.97mN	DeGrussa, hanging wall to C1	1999	7
DGMH061	DGDD203, 369.78-369.9m	734400.14mE, 7173101.04mN	DeGrussa, hanging wall to C4	2003	7
DGMH082	DGDD243, 113.32-113.7m	735200mE, 7173425mN	DeGrussa, 500m east of C5	1991	7
SPD015	SPD015, 75.2-78.9m	744396mE, 7172283mN	Leucogranite, Regional Narracoota Formation	2014	7
DGRC648	DGRC648, 96.0-97.0m	724230.2mE, 7169852.36mN	Regional Narracoota, granodiorite	2018	9.2
DGMH033*	DGDD125, 543.83-544.02m	734206.94mE, 7173080.97mN	Host turbiditic sediment above C4 ore lens	2262	40
DGMH040*	DGDD125, 577.42-577.71m	734206.94mE, 7173080.97mN	Host turbiditic sediment below C4 ore lens	2173	87
*detrital zircon maximum age					

Table 6.2. Re-Os data for DeGrussa Cu-Au VHMS deposit, Western Australia. Sample locations are in Appendix 6.6.

AIRIE Run #	Sample Name	Comments	Ore Lens	Re, ppm	^{187}Os, ppb	Age, Ma
MD-1207	DGDD125, 568.8-569.0m (MH035)	banded cp+py+po massive sulfide; dark grey layers targeted as potential Mo-Re-rich material, though may not be molybdenite	base of Conductor 4	0.2497 (5)	5.275 (4)	***1984 ± 8***
MD-1215	DGDD125, 568.8-569.0m (b) (MH035)		base of Conductor 4	0.3503 (3)	7.390 (6)	***1982 ± 7***
MD-1212	DGDD141, 187.08-187.25m (MH001)	visible molybdenite together with chalcopyrite in a talc-chlorite schist; molybdenite and talc define schistose fabric and locally wrap chalcopyrite	base of DeGrussa	164 (1)	3495 (3)	1998 ± 15
MD-1218	DGDD141, 187.08-187.25m (b) (MH001)		base of DeGrussa	133.28 (9)	2878 (2)	***2027 ± 7***
MD-1281	DGDD106, 279.36-279.44m (MH011A)	massive cp extracted; Re concentration suggests associated molybdenite, though rarely visible in binocular scope; mostly massive sulfide in chloritic host; cannot discern host rock	Conductor 1	11 (2)	239.4 (2)	2007 ± 321
MD-1293	DGDD106, 279.36-279.44m (b) (MH011A)		Conductor 1	35.34 (4)	757.6 (6)	***2013 ± 7***
MD-1283	DGDD125, 569.45-569.55m (MH036)	sparse visible molybdenite in a fine-grained chlorite phyllite host	base of Conductor 4	57.88 (4)	1239 (1)	***2011 ± 7***

Carius tube digestion using mixed-double Os spike; designation of (b) denotes a NEW mineral separate; boldface ages for comparison with radiometric ages by other methods.
All uncertainties at two-sigma and shown in parentheses for the last digit indicated; age calculation for assumed initial $^{187}Os/^{188}Os = 0.20$.
Second age determination provided for one sample (MD-1207 and MD-1215) based on a second mineral separate from the core; age replicates well.
Second Re-Os analyses (MD-1218 and MD-1293) to correct Re spiking; note decrease in Re error and age uncertainty with correct spiking; use second analyses for reporting.
For all samples, common Os is insignificant relative to radiogenic ^{187}Os.
Re and Os blanks are in the low picogram range, and insignificant to age calculations in all cases.
Sample size varies from 20-220 milligrams depending on Re concentration.

6.8. Re-Os Geochronology

Molybdenite is one of the most robust minerals for isotopic dating (Stein et al., 2001, Stein, 2006). Molybdenite samples were collected from three different locations representing different ore lenses in the DeGrussa Deposit:

1. In the chalcopyrite-rich stringer zone of DeGrussa (e.g. DGMH001) as thick stringers within basal talc-chlorite schist.
2. Rimming sulfides within massive sulfide lenses.
3. Small, fine grained, micron-sized clusters associated with chalcopyrite both within massive sulfide (Conductor 1, DGMH011A and Conductor 4, DGMH035) and in chloritised sedimentary rock with disseminated sulfides (base of Conductor 4, DGMH036).

Four samples were analysed, with two giving robust age dates, including a replicate age for one sample. Sample DGDD141 (187.08-187.25m) consists of crystalline molybdenite in the fabric of talc-chlorite schist. It resulted in the oldest molybdenite age and was run twice because the first run (MD-1212) was extremely underspiked. The uncertainty in the Re concentration is propagated into the uncertainty reported on the Re-Os age. A replicate sample (MD-1218), with the correct spiking, obtained a precise age of 2027 ± 7 Ma. An additional two molybdenite samples, DGDD106 (279.36-279.44m) from Conductor 1 and DGDD125 (569.45-569.55m) from Conductor 4 gave age dates of 2013 ± 7 Ma and 2011 ± 7 Ma respectively. These 2011, 2013 and 2027 Ma dates correlate with the Pb-Pb date for galena, discussed in the next section and represent the age of primary mineralisation.

Sample DGDD125 (568.8-569.0m) provides a younger age of 1984 ± 8 Ma. The low Re concentration for DGDD125 (568.8-569.0m) is not unusual for molybdenite, but the age obtained could be linked to other sulfides with a LLHR (Low Level Highly Radiogenic) Re-Os isotopic composition (Stein et al., 2000). Thin section observations of DGDD125 (568.8-569.0m), indicates a pyrrhotite dominated zone with little to no molybdenite throughout, and hence the age date of 1984 ± 8 Ma suggest a radiogenic pyrite or pyrrhotite source for the Re-Os. As a check, DGDD125 (568.8-569.0m) was run a second time with a new mineral separate

(MD-1207 and MD-1215) resulting in a repeat age of 1982 ± 7 Ma. The acquisition of a new mineral separate is a check for geologic accuracy. This age correlates with the youngest ages of dolerite intrusion (DGMH082) at 1991 ± 7 Ma. A summary of Re-Os results is compiled in Table 6.2.

6.9. Pb-Pb Isotope Geochronology of Galena and Pyrite

Pb-Pb isotopic determination was performed on two galena-rich samples from the DeGrussa and Conductor 5 ore lenses as well as three pyrite samples from Conductor 1 and Conductor 4 (Table 6.3) from within Pb-rich massive sulfide horizons. Further analyses were performed on a late stage galena + quartz ± carbonate vein that cuts across the Conductor 1 ore lens in the underground workings. Analysis was by solution according to methods outlined by Townsend et al. (1998) for the two galena samples from DeGrussa and C5, and by LA-ICPMS for all other samples and completed at the University of Tasmania, Hobart. Details of the methods used are provided in Appendix 6.2 and data located in Appendix 6.5.

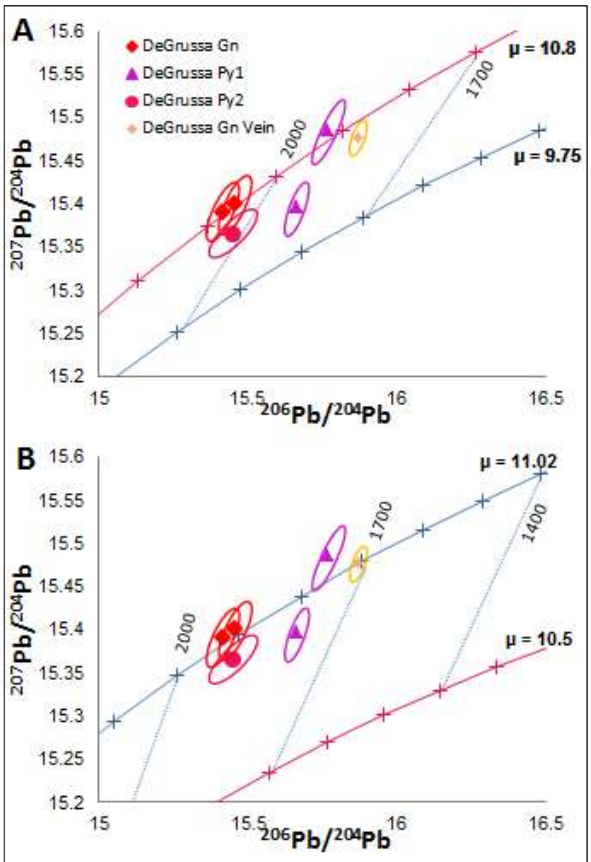

Figure 6.12. Comparison of Pb isotopic data for pyrite and galena at the DeGrussa deposit with respect to the (A) Stacey and Kramers (1975) (μ=9.75 and 10.8) curve and (B) Cumming and Richards (1975) (μ=11.02) growth curves showing the 150 million year age difference between the two model curves.

The isotopic composition of high Pb low U minerals such as galena changed through time in a systematic manner as the result of addition from U and Th. This temporal change provides the basis for Pb-Pb model ages. A number of different models have been used to determine Pb model ages for ore deposits. These include the single

stage model of Cumming and Richards (1975) which has the U to Pb ratio ($^{238}U/^{204}Pb$) in the crust increasing through time (referred to as Model III in the original publication). This model implies a relatively young apparent age for the Earth of 4.5 Ga (Dickin, 2005) but the curve has been developed based on a model which involves the least number of assumption and describes the average behaviour of Pb.

In comparison, Stacey and Kramers (1975) break terrestrial Pb evolution into two parts using Canyon Diablo Pb and average modern Pb to anchor the ends of a composite growth curve. It defines the age of the earth to be 4.57 Ga with a stage 1 closed system Pb evolution from 4.57 Ga to time t_1 and stage 2 closed system with different μ value from t_1 to present (where t_1 = 3700 Ma, selected at the point at which the plot yields the best fit of model ages to accepted ages for conformable galenas worldwide).

Although both models have their merits, the Stacey and Kramers (1975) model curve is used for DeGrussa mineralisation, rather than the Cumming and Richards (1975) model used widely across the region, due to its comparability with age constraints provided by the Re-Os and U-Pb methods discussed above.

The Pb isotopic compositions of the DeGrussa and Yerrida/Bryah Group mineralisation plot above the average growth curves implying higher $^{238}U/^{204}Pb$ (μ) in the source of the mineralisation fluids. High μ values such as these are typically interpreted to represent Pb source from upper crustal sedimentary rocks (Zartman and Doe, 1981) rather than the average crust in the models discussed above. Previous studies, such as Richards and Gee (1985)'s Pb isotope data for the Earaheedy basin, have modelled this by increasing the μ value of Cumming and Richards (1975) Model III growth curve to 11.12. In this study both the Cumming and Richards (1975) and Stacey and Kramers (1975) models with increased μ value were evaluated against the Re-Os ages for mineralisation.

The Pb isotopic composition indicates that galena crystallised between 2060 ± 50 Ma and 2075 ± 50 Ma on the Stacey and Kramers (1975) curve with μ at 10.8 (Fig. 6.12a). One pyrite sample plotted near the two galenas (DGMH090), however two pyrite samples (DGMH085 and

DGMH088) had slightly more radiogenic Pb isotopic composition giving model ages of 1920 ± 50 Ma and 1900 ± 50 Ma respectively. The model of Cumming and Richards (1975) at this age and this μ value is offset from the Stacey and Kramers (1975) model by 150 million years and provides a model age of 1915 Ma for galena and the least radiogenic pyrite and 1760 Ma and 1810 Ma for the two more radiogenic pyrites (Fig. 6.12b.) (Table 6.3). Again, an elevated μ value of 11.02 is required to fit the data to the Cumming and Richards (1975) modelled curve. The ages calculated using the Stacey and Kramers (1975) model are within error of the Re-Os mineralisation ages but those calculated using the Cumming and Richards (1975) model are significantly offset.

6.10. Geochronology of Regional Mineralisation

As discussed earlier, the regional geochronology of sedimentary rocks and mineralisation within the Yerrida, Bryah and Padbury Group sedimentary rocks is not well defined. In the past, Pb isotope data on pyrite and galena had been collected in association with gold mineralisation at Fortnum-Nathans, Labouchere, and Horseshoe Lights. In these studies, sulfides were handpicked, dissolved and analysed by methods described by Ho et al. (1994) and preferred the Cumming and Richards (1975) model curve for age calculations.

A compilation of Pb isotope data from the Yerrida, Bryah, and Padbury Groups (Dyer, 1991, Windh, 1992, Thornett, 1995) as well as reanalysed samples, and newly sampled deposits (Fig. 6.13, Appendix 6.5) shows the majority of data conforms to the same high μ growth curve as DeGrussa Pb, suggesting this isotopic composition is characteristic of the Paleoproterozoic basins. However, the Horseshoe Lights pyrite samples sit below the average crustal growth curve and require a μ value of 10.0 to 10.1 to conform. With a μ value of 10.0 in the Stacey and Kramers (1975) model the Pb isotopic data from the Horseshoe Lights deposit cluster around 1985 Ma, and correlate with the age of the DeGrussa deposit. With a best fit μ of 10.1 the age is 2000 Ma (Table 6.4).

Table 6.3. Pb isotope results for pyrite and galena in the DeGrussa deposit (see also Appendix 6.5). Mineral analysed denoted by *Galena and ^Pyrite. DGMH19 and DGMH54 analysed by solution with error correlation coefficients ρ = 0.16 on 207Pb/204Pb and 206Pb/204Pb. All other samples analysed by LA ICP MS with error correlation coefficient ρ = 0.8 between the 206Pb/204Pb, 207/204 and 208/204Pb. Sample locations are in Appendix 6.6.

Sample #	Details	Ore Lense	206/204	±1σ	207/204	±1σ	208/204	±1σ	207/206	208/206	Stacey and Kramers age μ=10.8	Cumming and Richards age μ=11.02
DGMH19*	DGDD173, 145.35-145.57m	DeGrussa	15.42	0.032	15.39	0.025	35.04	0.102	0.998	2.272	**2075**	1925
DGMH54*	DGDD219, 546.0-546.16m	Conductor 5	15.46	0.032	15.4	0.025	35.09	0.102	0.996	2.27	**2060**	1905
DGMH104*	UG sample	Conductor 1 - Qtz-Carb vein	15.872	0.031	15.476	0.033	36.074	0.066	0.976	2.273	**1820**	1705
DGMH085^	DGDD202, 457.98-458.06m	Conductor 4	15.77	0.026	15.484	0.024	35.56	0.069	0.981	2.252	**1920**	1760
DGMH088^	DGDD106, 279.62-279.83m	Conductor 1	15.664	0.019	15.396	0.019	35.476	0.045	0.982	2.263	**1970**	1810
DGMH090^	DGDD057, 240.28-240.39m	Conductor 1	15.453	0.024	15.364	0.021	35.071	0.051	0.995	2.269	**2060**	1910

Table 6.4. Massive pyrite samples from Horseshoe Lights (Windh, 1992) data and new model age for Stacey and Kramers (1975) curve. Windh (1992) data was calculated with high μ (=10) to obtain an age with 1922 Ma the generally accepted age in the literature. For Windh (1992) data, all analytical uncertainty in isotopic ratios is ±0.15% (2σ) recalculated here to ±1σ (see also Appendix 6.5).

UWA no.	206/204	±1σ	207/204	±1σ	208/204	±1σ	Age C+R calculated by Windh (1992)	S+K age u=10	S+K age u=10.1
115311	15.528	0.011646	15.285	0.011464	34.83	0.026123	1775	1875	1900
115311	15.428	0.011571	15.282	0.011462	34.873	0.026155	1840	1925	1945
115312	15.374	0.011531	15.271	0.011453	34.835	0.026126	1867	1950	1970
115310	15.589	0.011692	15.308	0.011481	34.92	0.026190	1754	1850	1865
113347	**15.302**	**0.011477**	**15.278**	**0.011459**	**34.903**	**0.026177**	**1922**	**1985**	**2000**

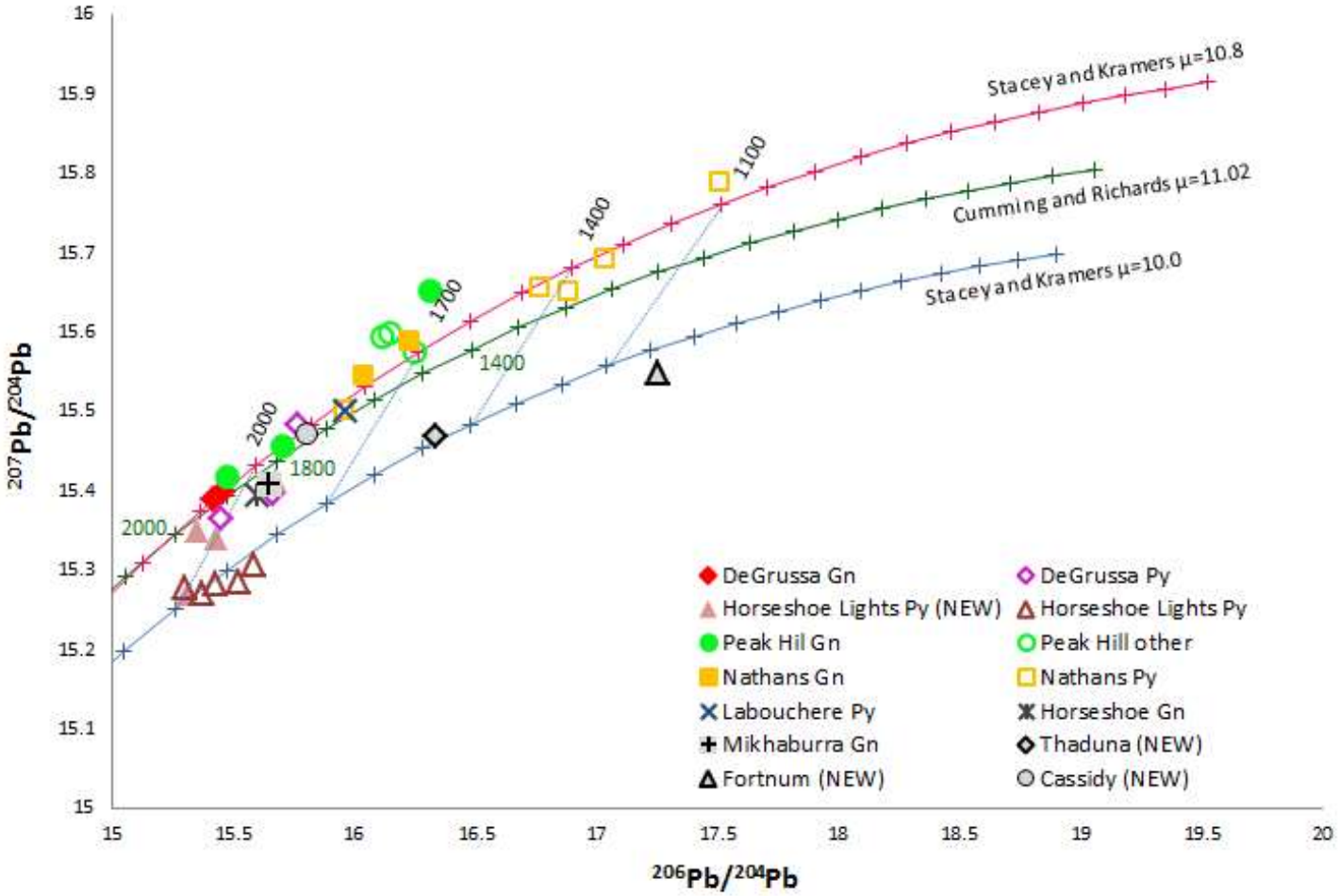

Figure 6.13. Comparison of Pb isotopic data for regional mineralisation across the Bryah and Yerrida Groups. Data is plotted with respect to the Stacey and Kramers (1975) (μ=10.0 and 10.8) curve and Cumming and Richards (1975) (μ=11.02) growth curves. The Stacey and Kramers (1975) μ=10.8 growth curve forms the best fit to the majority of the regional data (exceptions of Horseshoe Lights, Thaduna and Fortnum-Starlight). Sample locations are in Appendix 6.6.

The timing of the major orogenic and tectonic events that have affected the Paleoproterozoic basins of the Capricorn Orogen have recently been reviewed and redefined by Johnson (2013) (see Fig. 6.3). If the old model Pb ages are recalculated using the Stacey and Kramers (1975) Pb model, the main gold deposits shift approximately 150 Ma in age to become better correlated with major orogenic events (Table 6.5): the Glenburgh Orogeny can be related to the oldest age for mineralisation at Peak Hill (Main pit: 2070 Ma and Fiveways: 1955 Ma); the Capricorn Orogen to Labouchere (1800 ± 30 Ma), Nathans (1820 ± 30 Ma), Mt. Pleasant (1770 ± 30 Ma); and the Mangaroon Orogen to secondary events at Peak Hill (Main pit ages of 1705 ± 30 Ma, 1610 ± 30 Ma and 1620 ± 30 Ma). A cluster of ages occur around ~1900-1940 Ma including ages for Mikhaburra (1915 ± 30 Ma), Horseshoe/Cassidy (1940 ± 30 Ma), and remobilisation events at Horseshoe Lights (1900 ± 30 Ma and 1945 ± 30 Ma).

6.11. Revised deposit ages

Pyrite samples from the orogenic gold deposits of Horseshoe/Cassidy and Fortnum-Starlight, the Horseshoe Lights Cu-Au VHMS and the epithermal Thaduna Copper Deposit were analysed by LA-ICPMS at the University of Tasmania, Hobart (see Appendix 6.2). Samples were collected from the field, with the exception of Horseshoe Lights samples which were obtained from the University of Western Australia archive. No geochronological work had previously been completed on Fortnum-Starlight or the Thaduna Copper Deposit. Horseshoe/Cassidy provides an age of 1910 ± 50 Ma, within error of the original 1940 ± 30 Ma age of Windh (1992). Euhedral pyrite from Fortnum-Starlight obtains an age of 920 ± 50 Ma which correlates with the Edmundian Orogeny (1030-955 Ma). Horseshoe Lights samples from Gillies (1988), not previously dated, were analysed and resulted with ages of 1900, 1980, 1990 and 2075 (± 50 Ma; see Table 6.5 and Appendix 6.5). These ages are within the range of those provided by a Stacey and Kramers (1975) model curve using Pb isotope data from Windh (1992). The Thaduna copper deposit, hosted in the Thaduna Formation sedimentary rocks of the Yerrida group, has a pyrite Pb isotope model age of 1475 ± 50 Ma.

Table 6.5. Summary of geochronological results for DeGrussa and regional mineralisation. Pb isotope ages for published ages and their recalculated ages, as well as galena samples from DeGrussa were analysed by solution. New ages were analysed by LA-ICPMS (Appendix 6.5).

Deposit	Mineral	Method	Published Age (Ma) (C&R)	Recalculated Age (Ma) (S&K)	This study Age (Ma) (S&K)	Comparative Age (Ma) (C&R)	Tectonic Event
DeGrussa	Mo	Re-Os[1]	-	-	**2027±7**	-	Glenburgh
			-	-	**2011, 2013±7**	-	
	Gn	Pb-Pb[1]	-	-	**2060, 2075±50**	1905, 1925	
	Py	Pb-Pb[1]	-	-	**1885-2010±50**	1770, 1885	
Horseshoe Lights	Py	Pb-Pb[2]	1922±35	**2000±35**	1900, 1980, 1990, **2075±50**	1785, 1910, 1890, 1950±50	Glenburgh
Nathans	Gn	Pb-Pb[3]	1652	**1820, 1730**	-	-	Capricorn
	Py	Pb-Pb[3]	945, 1149, 1206, 1286	**1130, 1300, 1360, 1450**	-	-	Mutherbukin
Fortnum-Starlight	Py	Pb-Pb[1]	-	-	**920±50**	870±50	Edmundian
Peak Hill – Main Pit	Te	Pb-Pb[4]	1548±30	**1705±30**	-	-	Mangaroon
	Alt		1629±30	**1620±30**			
	Ruck		1656±30	**1610±30**			
	Gn		1719±30	**2070±30**			Glenburgh
Fiveways	Gn		1799±30	**1955±30**			
Mt. Pleasant	Gn		1568±30	**1770±30**			Capricorn
Horseshoe/Belltop (Cassidy)	Gn	Pb-Pb[2]	-	**1940±30**	-	-	Glenburgh
	Py	Pb-Pb[1]			1910±50	1740±50	
Mikhaburra	Gn	Pb-Pb[2]	-	**1915±30**	-	-	Glenburgh
Labouchere	Py	Pb-Pb[3]	1662±30	**1800±30**	-	-	Capricorn
Thaduna Copper	Py	Pb-Pb[1]	-	-	**1475±50**	1395±50	-

[1] M Hawke (this study)
[2] Windh (1992)
[3] Dyer (1991)
[4] Thornett (1995)

6.12. Discussion

Re-Os geochronology provides the most accurate method for dating mineralisation at the DeGrussa deposit and forms the basis for Pb isotope comparisons. In the Paleoproterozoic basins of the Capricorn Orogen, the Stacey and Kramers (1975) model curve falls within error of the Re-Os data, and is 150 million years in difference to the Cumming and Richards (1975) curve used in previous studies. The Cumming and Richards (1975) model curve has been used successfully by Vielreicher et al. (2002) and Gazley (2011) to date mineralisation at the Plutonic deposits within the Marymia Inlier, approximately 40km to the northeast of DeGrussa. If the Plutonic data is analysed on the Stacey and Kramers (1975) model, ages are 100-250 million years older - older than the host rocks themselves - than those provided by the Cumming and Richards (1975) model curve (Gazley, 2011).

If the Cumming and Richards (1975) model curve is used to interpret DeGrussa data, the resulting ages suggests formation of the DeGrussa deposit during the Capricorn Orogeny and of comparable age to the Horseshoe Lights volcanic-hosted massive sulfide 1922 ± 35 Ma age of Windh (1992). However, the intrusive relationships between sedimentary rocks and dolerite intrusions indicate a Capricorn Orogeny related time of formation is too young. Reanalysis of the Horseshoe Lights data (Table 6.4), fitting it to the Stacey and Kramers (1975) growth curve with elevated μ, results in an age of 1980 ± 35 Ma (see also Fig. 6.13 and Appendix 6.5).

6.12.1. Regional Mineralisation

As previously stated, Pb isotope analysis shows that with the exception of the Horseshoe Lights samples, the majority of data conforms to a high μ=10.8 growth curve indicating that this isotopic composition is characteristic of the Paleoproterozoic basins. The Horseshoe Lights samples require a lower μ value of 10.0 to 10.1 to conform and may reflect a different source for this mineralisation. The newly analysed Horseshoe Lights samples with ages of 1900, 1980, 1990 and 2075 (± 50 Ma) were analysed using LA-ICPMS and hence have higher precision than those age dates obtained in the original work (where sulfide species were analysed by solution

and hence the different phases of pyrite formation could not be separated). The maximum age of 2075 ± 50 Ma age required a best fit μ value of 10.6 (Appendix 6.5), although most Horseshoe Lights samples require μ values closer to 10.1. Elevated μ values are a feature of the region, implying higher source $^{238}U/^{204}Pb$ (μ) for mineralising fluids. Hence a lesser contribution of Pb sourced from upper crustal sedimentary rocks may contribute to Pb isotopes at Horseshoe Lights in comparison with DeGrussa mineralisation. The LA-ICPMS Horseshoe Lights ages are similar to the DeGrussa sulfides and hence could preserve a primary age for Horseshoe Lights mineralisation at c. 2075 Ma and remobilisation ages at c. 1980 Ma and c. 1900 Ma. Regional magmatic events around c. 1980 Ma include the intrusion of DeGrussa associated dolerites (1991 – 2003 Ma) and the end of Dalgaringa Supersuite intrusion (2005 – 1980 Ma) and Nardoo Granite (c. 1975 Ma) of the Glenburgh Terrane.

Horseshoe/Cassidy provides an age of 1910 ± 50 Ma, within error of the original 1940 ± 30 Ma age of Windh (1992). Euhedral pyrite from Fortnum-Starlight obtains an age of 920 ± 50 Ma which roughly correlates with the Edmundian Orogeny (1030-955 Ma) although the euhedral nature of these sulfides suggests that this is not the primary age of mineralisation. The cluster of orogenic gold ages for Horseshoe/Cassidy, Mikhaburra and late pyrite at DeGrussa and Horseshoe Lights between ~1900-1940 Ma does not relate to any known orogenic event currently identified in the region, although metamorphic events are recorded on rims of zircon in the Moogie Metamorphics and Camel Hills Metamorphics of the Glenburgh Terrane at a similar time (c. 1966-1952 Ma and c. 1955-1944 Ma respectively (Johnson et al., 2011a)).

The Thaduna copper deposit, hosted in the Thaduna Formation sedimentary rocks of the Yerrida group, has a pyrite Pb isotope model age of 1475 ± 50 Ma. Thaduna mineralisation cannot be correlated with any orogenic event currently identified in the region. There is correlation with a reset age of Nathans pyrite (≤1460 Ma) and with c. 1465 Ma dolerite sills of the western Bangemall Supergroup (Edmund and Collier Basins) to the north (Morriss and Pirajno, 2005).

The Peak Hill deposits are located in strongly deformed Archean rocks at the western end of the Marymia Inlier, and were once believed to be Palaeoproterozoic in age. The oldest Stacey and Kramers (1975) 2070 ± 30 Ma age for mineralisation at Peak Hill main pit perfectly correlates with Pb isotope ages of DeGrussa mineralisation and hence may reflect a hydrothermal event related to rifting in the Bryah Group. The 1955 ± 30 Ma age for the Fiveways deposit correlates with the end of the Glenburgh Orogeny. The younger ages between 1610 ± 30 Ma, 1620 ± 30 Ma fit roughly with the end of the Mangaroon Orogeny and the 1770 ± 30 Ma age for the Mt. Pleasant deposit correlates with the end of the Capricorn Orogeny. If the Cumming and Richards (1975) age dates are used, ages are restricted between 1548 ± 30 Ma and 1799 ± 30 Ma. Neither of these scenarios is implausible, however the Stacey and Kramers (1975) model curve appears to better resolve the mineralising ages with orogenic events. A summary of all these ages is located in Table 6.5 and Figure 6.14.

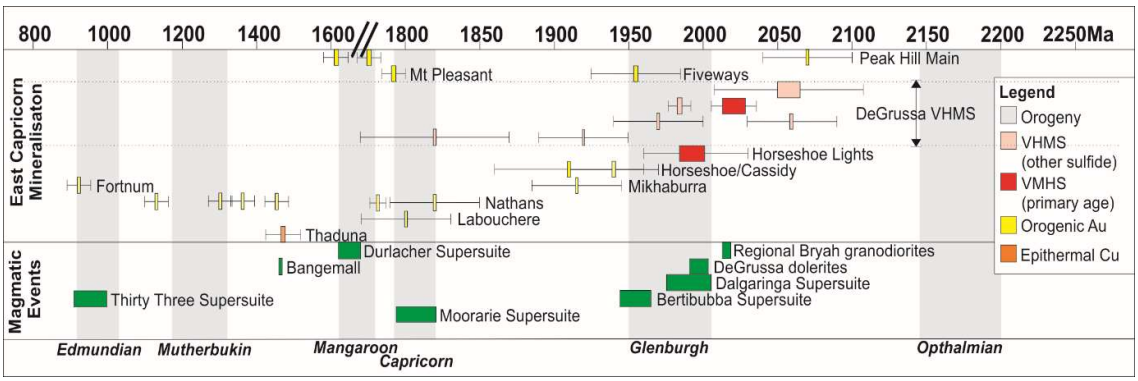

Figure 6.14. Correlation between mineralisation events in the Paleoproterozoic basins of the Capricorn Orogen, major regional mafic magmatic events across the Capricorn Orogen and regional orogenic events. All mineralisation ages use the Stacey and Kramers (1975) model curve with the exception of the Re-Os (molybdenite and pyrrhotite) ages for the DeGrussa VHMS. Mineralisation mostly ages cluster around the major orogenic events. with the exception of a cluster of orogenic gold ages around ~1900-1920 Ma.

6.12.2. DeGrussa Stratigraphy

North-northwest directed extension led to rifting of the Yilgarn Craton and the development of the intracratonic Yerrida sag basin (Pirajno et al., 2004) with siliciclastic sediments of the Yerrida Basin deposited in a shallow epicontinental sea. The Juderina Formation was deposited

on a shallow evaporitic margin, such as a sabkha, as evidenced from stromatolites, algal mats and evaporite textures in the Bubble Well Member (El Tabakh et al., 1999, Pirajno et al., 2004). Deepening of the Yerrida Basin resulted in deposition of the Johnson Cairn Formation, including initial volcanism in the lower part of the Johnson Cairn Formation. The contact between the Johnson Cairn Formation and the DeGrussa host sedimentary rocks (DeGrussa Formation) is unclear and may be unconformable underneath DeGrussa and Conductor 1, but in tectonic contact below Conductor 4 and 5 where the Shiraz Fault displaces the ore body.

The tectonic environment for the Bryah group sedimentary rocks remains controversial. The favoured interpretation by Pirajno (2004) for the Narracoota Formation is currently that of an oceanic plateau formed at c. 2.0 Ga and accreted to the northern Yilgarn Craton margin at c. 1960 Ma. However, boninites identified within the Narracoota Formation (Hynes and Gee, 1986) suggest an island arc environment, and the apparent restricted nature of the DeGrussa Formation, suggests that DeGrussa mineralisation may have formed between c. 2027 and c. 2011 Ma in a back-arc sub basin - oceanic rift tectonic setting, similar to that of the present day Lau Basin of the Western Pacific (Clift et al., 1994, Knittel and Oles, 1994). Back arc basins can reach depths of up to 2500-3000m, contain restricted sub-basins of only 2-5km width and ~10km length before being offset by transverse faults (Clift et al., 1994). Turbidites at DeGrussa are also not well developed although graded bedding is evident with localised folding, slumping and chaotic bedding. Most sediments are fine grained clays grading to medium grained at the base. Rarely do coarse or conglomeratic bands occur. Where sediments appear reversely graded, this is interpreted as due to local slump folding as folds are often not traceable between drill holes. Conversely, it may be due to intrusion of dolerite sills into unconsolidated sediments. There is no volcanic material evident within DeGrussa host sedimentary rocks, however this may be due to the extensive alteration reducing the rock to a clay dominated assemblage.

Mineralisation was likely contemporaneous with regional magmatism between 2018 and 2014 Ma, during deposition of the DeGrussa Formation/Karalundi Formation sedimentary

rocks and associated basalts. This magmatism may have acted as a heat source for circulation of metal bearing hydrothermal fluids which formed the DeGrussa deposit. Given the restricted mineralisation assemblage of pyrite, chalcopyrite and pyrrhotite, the deposit is interpreted to have formed at temperatures of 270-350°C (Large, 1977). The style of VHMS mineralisation at DeGrussa best fits the siliciclastic- mafic type of Barrie and Hannington (1999), or 'Besshi' type (Fox, 1984, Peter and Scott, 1999). All four lenses are interpreted to have initially been part of the same ore system and display features associated with both sea floor deposition and subsea floor replacement. Besshi-type, or siliciclastic- mafic type deposits are characteristically found in back-arc rift settings (Peter and Scott, 1999, Franklin et al., 2005).

Following mineralisation, the ore lenses were buried by turbidites and basalt flows. The turbiditic sedimentary host rocks suggest a submarine depositional environment. Dolerite sills and dykes, interpreted to derive from the same magmatic source as the Narracoota Formation basalts, intruded the host stratigraphy between 2003 ± 7 Ma and 1991 ± 7 Ma. These ages, combined with the stratigraphic relationships between host sedimentary rocks, basalts and dolerites, suggest that the dolerites were slightly later than mineralisation, inflating stratigraphy and detaching DeGrussa from the C1 ore lens. Additionally, populations of detrital zircons within the DeGrussa host sediments provide ages similar to that of the 2555-2430 Ma Halfway Gneiss of the Glenburgh Terrane in the western Capricorn Orogen (Johnson et al., 2011a) although Yilgarn aged zircons form the dominant population. There are no zircons of Narracoota Formation age, reinforcing that the dolerites postdate sedimentary rocks. Deformation of the sulfides is reflected in the earlier group of ages recorded by the pyrite Pb isotopes at 1920-1975 ± 50 Ma and Re-Os ages at c. 1982-1984 Ma and could be contemporaneous with the intrusive dolerite event.

Deformation in a southwest to northeast direction (Pirajno et al., 2000), related to closure of the late Paleoproterozoic basins during the Glenburgh Orogeny is likely to have caused faulting and folding across the region. Deformation and reworking (of both rocks and pre-existing mineralisation) during the 1820-1770 Ma Capricorn Orogeny was related to intracratonic

orogenesis (Sheppard et al., 2010). Quartz + carbonate ± galena veins transect the ore deposit around 1820 ± 50 Ma (model Pb age) which is interpreted to reflect deformation during the Capricorn Orogeny and correlates with orogenic gold mineralisation at the Labouchere deposit (1800 ± 30 Ma) and Nathans (1820 ± 30 Ma).

6.12.3. Correlations of Capricorn Orogen Stratigraphy, Orogenesis and Mineralising Events

In the west, collision of the Glenburgh Terrane with the Pilbara occurred during the Opthalmian Orogeny between c. 2240 and 2125 Ma. The Moogie Metamorphics meta-sedimentary rocks were deposited concurrently in a foreland basin system (Johnson et al., 2010, Johnson et al., 2011a). In the east, continental rifting may have led to separation of the Marymia Inlier from the northern Yilgarn's Eastern Goldfields Superterrane (Gazley, 2011) and subsequent deposition of Yerrida Group sedimentary rocks in an evaporitic sag basin setting from c. 2174 Ma (Pirajno et al., 1995, Woodhead and Hergt, 1997, Pirajno and Adamides, 2000a, Dentith et al., 2014)

Geochronological data presented in section 6 suggests the DeGrussa sedimentary rocks were deposited at c. 2080 to 2030 Ma coincident with the Camel Hills Metamorphics meta-sedimentary rocks (2000 and 1955 Ma) and initiation of continental-margin arc-magmatic activity along the southern margin of the combined Gascoyne-Pilbara terranes and intrusion of the Dalgaringa Supersuite magmatic rocks c. 2005 to 1975 Ma (Sheppard et al., 2004, Johnson et al., 2011a)). Rocks of the overlying Camel Hills Metamorphics are interpreted to have formed in a forearc or backarc basin setting along the southern margin of the Glenburgh Terrane, as the meta-sedimentary rocks equivalent to the intrusive rocks of the Dalgaringa Supersuite (Johnson et al., 2011a).

The revised age of the Narracoota Formation based on the igneous zircons of dolerites (1991 ± 7 Ma to 2003 ± 7 Ma) and associated granodioritic (fractionated dolerite) rocks (2014 ± 10 Ma, 2018 ± 9 Ma) of the DeGrussa deposit stratigraphy were intruded at a similar time to the

2005-1975 Ma Dalgaringa Supersuite. The Dalgaringa Supersuite consists of granitic gneisses which may have formed in an Andean-type setting during northward subduction of oceanic crust under the combined Pilbara Craton - Glenburgh Terrane (Sheppard et al., 2004). Geochronological work presented by Sheppard et al. (2004) resulted in the following SHRIMP U-Pb ages for the Dalgaringa Supersuite: 2002 ± 2 Ma for tonalite, 1989 ± 4 Ma for diorite, 1999 ± 5 Ma for a monzogranite, 2002 ± 3 Ma for granodiorite and monzogranite sheets, and 1987 ± 4 Ma for foliated monzogranite sheets. These ages are all very similar to those presented here for DeGrussa associated dolerite intrusions and hence further reinforces a correlation between the Narracoota Formation and Dalgaringa Supersuite. Recent interpretation of magnetotelluric transects of the eastern Capricorn Orogen by Dentith et al. (2014) suggest that the Glenburgh Terrane, or a similar oceanic crustal terrane with equivalent rocks of the Dalgaringa Supersuite, may underlie the Edmund and Collier Basins to the north of the Bryah Group and Marymia Inlier.

The Bryah and Padbury Basins were likely developed to the west or north-west of the Yilgarn Craton (Pirajno and Occhipinti, 2000) and, in contrast to the oceanic plateau interpretation, the rock associations presented here suggest the tectonic setting of the DeGrussa sedimentary and mafic rocks formed in a back-arc tectonic setting, similar to those of the western Pacific (Clift et al., 1994) and possibly within or on the margin of the Yilgarn Craton. Additionally, boninites identified by Hynes and Gee (1986) are only found in island arc tectonic settings. This suggests that there has been a change in subduction dynamics from the western Capricorn Orogen where northward subduction occurs beneath the Glenburgh Terrane–Pilbara Craton; to the eastern Capricorn where subduction was possibly south directed. Development of the DeGrussa volcanic-hosted massive sulfide, and possibly the Horseshoe Lights mineralisation, developed from hydrothermal fluids as a response to subduction and back-arc rifting along the northern margin of the Yilgarn Craton.

Closure and collision of the combined Pilbara Craton - Glenburgh Terrane and the Yilgarn Craton led to development of the Errabiddy Shear Zone during the latter part of the Glenburgh

Orogeny between c. 1965 and c. 1950 Ma (Occhipinti et al., 2004, Sheppard et al., 2004, Johnson et al., 2011a). The Glenburgh Orogeny can be related to mineralisation ages at Peak Hill (Fiveways: 1955 Ma) and remobilisation ages of sulfides at DeGrussa (c. 1970-1980 Ma), Horseshoe Lights (c. 1980 Ma), and Horseshoe/Belltop (c. 1940 Ma). Ages for Mikhaburra (1915 ± 30 Ma), Horseshoe/Cassidy (1940 ±30 Ma), and remobilisation events at Horseshoe Lights (1900 ± 30 Ma and 1945 ± 30 Ma) and DeGrussa (1920 ± 50 Ma) may also be associated with final stages of the Glenburgh Orogeny (Fig. 6.14).

The Capricorn Orogeny is associated with granite plutonism (Johnson, 2013). Mineralisation ages which correlate to this orogeny include Labouchere (1800 ± 30 Ma), Nathans (1820 ± 30 Ma), and Mt. Pleasant (1770 ± 30 Ma) as well as a late stage galena + quartz ± carbonate vein that cuts across the Conductor 1 ore lens at 1820 ± 50 Ma.

Secondary mineralisation events at Peak Hill (Main pit ages of 1705 ± 30 Ma, 1610 ± 30 Ma and 1620 ± 30 Ma) could be related to the Mangaroon Orogeny (1680-1620 Ma). The Mutherbukin Tectonic Event (1320-1170 Ma) is characterised by faulting, amphibolite facies metamorphism and deformation (Johnson et al., 2013, Johnson et al., 2011b) with some mineralisation ages at Nathans gold deposit (1130 ± 30 Ma, 1300 ± 30 Ma, 1360 ± 30 Ma) correlating to this event. The Edmundian Orogeny (1030-955 Ma) may be associated with metamorphism of sulfides at Fortnum-Starlight (920 ± 50 Ma) although original mineralisation is likely to be much older.

6.13. Conclusion

The DeGrussa deposit is a siliciclastic - mafic style VHMS deposit located in the lowermost stratigraphy of the Bryah Group (Karalundi/DeGrussa Formation equivalent sedimentary and mafic volcanic rock). Mineralisation was dated to between 2011 ± 7 Ma and 2027 ± 7 Ma (Re-Os) and 2060 ± 50 Ma and 2075 ± 50 Ma (Pb model ages) constraining the maximum deposition age for the Bryah Group rocks at c. 2075 Ma.

Bryah Group rocks were likely deposited within a back arc rift, formed concurrently with subduction and rifting as recorded by the Camel Hills Metamorphics and Dalgaringa Supersuite in the western Capricorn Orogen. DeGrussa mineralisation was deposited in a submarine environment both directly onto the seafloor and as sub-seafloor replacement. Dolerites post-date the DeGrussa mineralisation (2003 ± 7 Ma to 1991 ± 7 Ma) and regional granodiorites (fractionated dolerites) provide the first age for the Narracoota Formation of 2014 ± 7 Ma and 2018 ± 9 Ma.

Limitations of the Pb isotopic models are indicated by the large discrepancy in ages between the Cumming and Richards (1975) method used in previous studies, and the Stacey and Kramers (1975) method used for the DeGrussa deposit. Comparable ages obtained between the Re-Os and Stacey and Kramers (1975) ages suggests that the Stacey and Kramers (1975) model curve provides more adhesive ages. This allows a new age of 2000 ± 35 Ma for Horseshoe Lights pyrite (or 2075 ± 50 Ma by LA-ICPMS), indicating that this deposit may have developed at a similar time to that of DeGrussa. Furthermore, applying the Stacey and Kramers (1975) model to basin mineralisation provides ages that correlate with the major regional orogenic events: the Glenburgh from 2005-1960 Ma (DeGrussa and Horseshoe Lights forming in an extensional basin rift setting during deposition of Bryah Group sediments, while Peak Hill – main pit and Fiveways formed under compression in the Archean Peak Hill Schist), the Capricorn from 1830-1780 Ma (Labouchere, Mt. Pleasant and Nathans), the Mangaroon from 1690-1620 Ma (Peak Hill- Main pit), the Mutherbukin Tectonic Event between 1320 and 1170 Ma (Nathans), and the Edmundian from 1030-955 Ma (Fortnum-Starlight deposit). The only age for mineralisation of 1475 ± 50 Ma is provided for the Thaduna Copper deposit.

These new ages assist in constraining stratigraphy and mineralising events of the Paleoproterozoic Yerrida, Bryah and Padbury Group sediments and their associations with regional orogenic events. Identification of prospective time periods and stratigraphy associated with major mineralising events will assist in exploration for significant gold and base metal mineralisation in the Capricorn Orogen.

6.14. Acknowledgements

Thanks to Sandfire Resources NL for funding of this work, and in particular Shannan Bamforth, John Evans and Bob Jeffery for their continuous encouragement and support. Additionally, to the geologists at RNI, Ventnor Resources and Talisman Resources for access to drill core and field sites, the University of Western Australia and the Geological Survey of Western Australia for access to their rock sample collections and providing valuable ideas and input to the final product. To the Central Science Laboratory (CSL) at the University of Tasmania for assistance in CL imaging of zircons. And to reviewers Simon Johnson and Randall Parish for their invaluable comments which have improved this manuscript substantially.

Chapter 7. Source of Mineralising Fluids

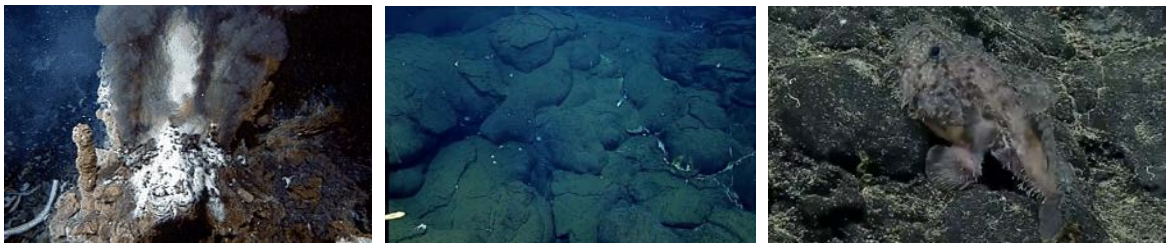

7.1. Introduction

Volcanic-hosted massive sulfide deposits are considered to be produced from either leaching of metals from sea water or from sedimentary/volcanic rocks in a hydrothermal cell. This hydrothermal cell may be driven by a magmatic, mantle derived pluton which, in some VHMS deposits, are considered to supply substantial amounts of metals (Franklin et al., 1981, Huston et al., 2001, Galley et al., 2007, Huston et al., 2010).

The Panorama VHMS district of Western Australia is an example of a mineralising system in which the reduction of sea water sulfate and metal leaching from the volcanic pile is considered to provide enough metal to produce mineralisation (Huston et al., 2001). In contrast, the Neves Corvo deposit, Portugal, hosted in a volcano-sedimentary rock package of similar tectonic setting to that of the Bryah/Yerrida groups, has high Sn and Cu contents inferred to include a hydrothermal-magmatic source component (Relvas et al., 2001, Huston et al., 2010). Furthermore, studies by Huston et al. (2010) suggest that high $\delta^{18}O$ >5‰, as well as the HFSE-rich nature of Neves Corvo cassiterite and presence of diagnostic metals in cassiterite of Nb, Ta, Zr, Sc, Ti, W and Fe indicate a magmatic source for mineralisation. Similar to the Neves Corvo deposit, Kidd Creek in Canada is a Cu-Zn-rich deposit with significant Sn (0.14%) credits. In most respects, features are typical of a bimodal mafic VMS system, however, parts of the deposit are characterised by unusual geochemical assemblages such as bornite-rich zones with Cu-Co-Bi-Se-Ag-As-Ni metal assemblages which are interpreted to have formed from either leaching of new Cu from basement rocks as a result of deepening hydrothermal circulation, condensation of a metal-rich brine into a deep geothermal reservoir, or a direct contribution from a felsic magma

source (Hannington et al., 1999). The importance of these characteristics with respect to fluid source are interpreted from studies on present day VHMS systems (e.g. PACMANUS, Manus Basin (Herzig et al., 2003) and the Brothers deposits in the Kermadec Arc (de Ronde et al., 2011, Berkenbosch et al., 2015) in which a hydrothermal-magmatic component is proposed.

This chapter discusses three aspects related to understanding fluid sources:

1. DeGrussa associated dolerite geochemistry,
2. Sulfur isotopes of sulfides, and
3. Pb isotopes of sulfides.

Using a combination of laser geochemical analysis of DeGrussa associated dolerite samples, sulfur isotopes and Pb isotopes, this chapter aims to evaluate the source of some of the components in mineralising fluids at DeGrussa, as well as other sulfide occurrences in the basin. These geochemical methods are also used to constrain the environmental conditions that were present at the time of mineralisation in the basin (e.g. temperature of mineralising fluids).

7.2. Cu-rich mafic rocks as a source for mineralisation

7.2.1. Introduction

Dolerite forms one of the dominant rock types in the DeGrussa mine stratigraphy. In thin section, dolerites consist of plagioclase (40-70%), hornblende (≤40%), clinopyroxene (≤30%), titanate (sphene), and occasional trace sulfides (pyrite and chalcopyrite). Rocks are altered to clay minerals, chlorite (chamosite) and carbonate, lesser talc, actinolite, epidote, albite and stilpnomelane replacing primary phenocrysts and around grain margins. Titanite alters to leucoxene and clays and carbonate replaces plagioclase and chlorite. Talc and actinolite replace pyroxenes and amphibole. Dolerites are intrusive in nature, displaying peperitic contacts.

The dolerites in the DeGrussa formation have Fe_2O_3 > 11 wt%, compared with other Narracoota Formation and Killara Formation mafic rocks which nearly all have < 11 % (Fig. 7.1). The dolerites surrounding DeGrussa are also higher in Cu (>125ppm on average in comparison to regional mafic rocks of mostly <125ppm) in comparison to regional mafic rocks of the

Narracoota and Killara Formations (as collected by the GSWA). Similar observations have been made for geochemical data for drill holes at Monty, which show the Monty dolerites in the hanging-wall and footwall also have > 11% Fe_2O_3 with most analyses ranging from 12 to 14.5 % Fe_2O_3 (Large, 2016).

Textures recently identified in dolerite, which show small chalcopyrite blebs within the outlines of altered crystals, and correlating high Cu and Fe contents suggest that these rocks may be the source of metals for DeGrussa mineralisation. Several scenarios are possible depending on the relative timing of dolerite emplacement with respect to DeGrussa mineralisation:

1. *Pre-mineralisation:* leaching of Cu-rich dolerites to contribute to the ore deposit.
2. *Syn-mineralisation:* dolerites were both a contributor to the Cu-rich hydrothermal-magmatic fluids, and also able to reabsorb Cu-rich hydrothermal fluids.
3. *Post-mineralisation:* dolerites either were emplaced with high Cu contents, or they absorbed Cu from the nearby ore deposit during emplacement.

There are three possible ways for metals to be transported into a VHMS deposit (Franklin et al., 1981):

1. Leaching of rocks, including sedimentary and magmatic rocks.
2. Direct input as a volatile component of crystallising magma, or indirectly by a hydrothermal convection cell involved in the direct cooling of a magma body coeval with mineralisation.
3. High T reduction of seawater as it circulates through the rocks, or organic reduction of ambient seawater at the site of deposition.

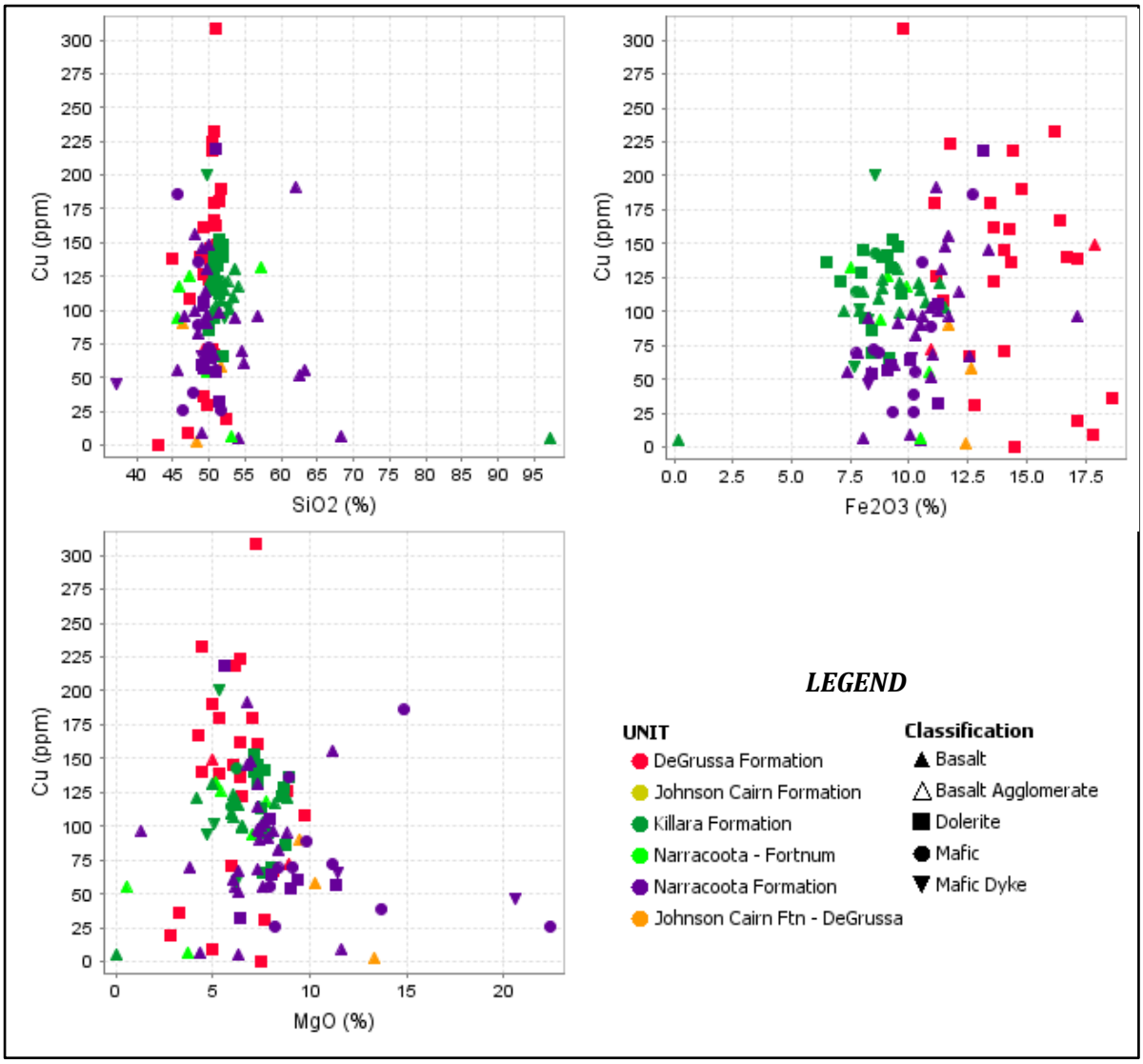

Figure 7.1. Copper content of DeGrussa and regional mafic rocks versus **A.** SiO_2 (max SiO_2 = 48 – 52 wt%) **B.** Fe_2O_3, with the DeGrussa mafic rocks showing that Fe_2O_3 >11 wt% is a suitable source rock, and **C.** MgO (DeGrussa mafic rocks with 2-10%). Mafic rocks within the DeGrussa mine sequence typically higher copper content.

Studies by Huston et al. (2010) hypothesised that the following characteristics of ore deposit isotopes and geochemistry support a magmatic input for mineralising hydrothermal fluids;

1. Geological criteria, including Cu-Mo, Cu-Sn-Zn, Au-Cu mineralisation assemblages with Mo, Sn and Au interpreted to reflect a hydrothermal-magmatic contribution to hydrothermal systems. Higher temperature alteration, and the presence of advanced argillic alteration assemblages are considered indicative of a magmatic input (Williams and Davidson, 2004). Conversely, the presence of quartz-chlorite-sericite assemblages is not considered to be diagnostic of the

presence or absence of a hydrothermal-magmatic contribution to VHMS systems (Huston et al., 2010).

2. Geochemical: A majority of the world's Mo, Sn and W resources also appear to have a hydrothermal-magmatic source, with diagnostic high levels of the elements Nb, Ta, Zr, Sc, Ti, W and Fe as trace elements in cassiterite are considered diagnostic of a hydrothermal-magmatic source in the Neves Corvo VHMS deposit, Portugal (Huston et al., 2010).

3. Isotopic characteristics including;

- Sulfur Isotopes consistently > 0 ‰, $\delta^{34}S_{sulfate}$ different from that of coeval seawater and $\Delta^{34}S_{sulfate\text{-}sulfide} \sim 20 - 30$ ‰. And sulfur isotopes of sulfide in the range -3 to +1‰ (see section 7.3)
- Oxygen Isotopes: deposits with ^{18}O-enriched ($\delta^{18}O > 5$ ‰) ore fluids where only low grade metamorphic processes have occurred. Higher metamorphic conditions can overprint primary $\delta^{18}O$ to higher values.
- Pb isotope with μ values higher than average reflect input from crustal material whereas μ values below average reflect a mantle source for Pb (see section 7.4).

Huston et al. (2010) interprets Cu in both VHMS and porphyry deposits to derive directly from degassing magmas and that this forms a direct hydrothermal-magmatic contribution for a large proportion of global Cu resources. Other authors consider that the bulk of Cu in transported in the brine (Candela and Holland, 1986, Candela, 1989, Cline and Bodnar, 1991, Archibald et al., 2002).

As previously discussed in earlier chapters, mineralisation at DeGrussa was likely emplaced in the sub seafloor and seafloor environments, in sedimentary rock dominated stratigraphy, with dolerites syn- to post- mineralisation (see chapters 3, 4, 6). Hence, Cu-bearing mafic rocks are considered to be rare in the host stratigraphy. There are three possible sources for metals in the DeGrussa deposit: 1. A magmatic input of Cu could be the cause of the high Cu grades found in the DeGrussa deposit, 2. A mafic dominant composition of the host and footwall sedimentary

rocks may be responsible, or 3. a sea water source either by reduction as it circulates through the rocks, or at the seawater-hydrothermal fluid interface.

7.2.2. Aim

This section will examine the hypothesis that the Cu-rich dolerites surrounding DeGrussa or a related doleritic magma at depth are responsible for the Cu-rich mineralisation. Furthermore, that the Cu-rich nature of the DeGrussa dolerites could be used as an exploration vector in the Bryah basin.

7.2.3. Methods

Three polished mounts of mafic rocks from DeGrussa associated rocks were selected from samples collected for this PhD study (see Table 7.1 and 7.2). These included high (308ppm), medium (218ppm) and low (9ppm) Cu samples. Two of these samples were from dolerite between the DeGrussa and Conductor 1 lenses, and one from the footwall dolerite.

Areas for laser mapping were selected from thin section and polished mount observations (see Appendix 7.1). Features that were targeted included exsolution textures where remnant crystal shapes are visible and flecks of chalcopyrite remain and veins with associated fine grained sulfides. Laser maps of selected areas (max 3 x 3 mm areas) with a spot size of 23µm was undertaken in order to identify the location of different elements in the rock (see Appendix 7.2. for analytical settings).

Table 7.1. Rock type and sample description for samples selected for geochemical laser mapping

Sample #	Hole #	Interval (m)	Collar (mE)	Collar (mN)	Classification	Description
DGMH010	DGDD057	118.33-118.5	733877	7173120	Dolerite (middle gabbro)	Plagioclase 50%, hornblende/pyroxene 40% (altering to fibrous hornblende 20%), Opaque 10% (chalcopyrite and pyrite?). Strong carbonate alteration of feldspar + hornblende. albite alteration ~70% of rock. Interlocking grains, no tectonic fabric, largely undeformed, just altered. Crosscutting veinlets with fibrous hornblende. ?calcite vein
DGMH021	DGDD173	330.72-330.9	733895	7173060	Altered dolerite, (footwall gabbro)	Plagioclase (20%) + amphibole (blue-green)(60%) + opaque (18%) + orthopyroxene (<2%). Feldspar overprinted by clay alteration. Original twinning of crystals still present in places. Amphibole altering to chlorite and tremolite (green- blue pleochroism). Chlorite mid-green pleochroic.
DGMH045	DGDD219	197.6-197.74	734598	7173197	Altered, fine-grained dolerite (middle-lower gabbro)	Fine-grained dolerite with interlocking crystals, plagioclase (20%) altered to clay minerals (40%), hornblende/pyroxene (5%) altered to chlorite (20%), opaque (magnetite/leucoxene+trace pyrite) (5%). Clay alteration of feldspars almost entire and pervasive through rock.

Table 7.2. Whole rock geochemistry of samples selected for laser mapping

Sample #	SiO2 (%)	TiO2 (%)	Al2O3 (%)	Fe2O3 (%)	MgO (%)	Ag (ppm)	Ba (ppm)	Co (ppm)	Cr (ppm)	Cu (ppm)	Mn(ppm)	Ni (ppm)	Pb (ppm)	Sb (ppm)	Sc (ppm)	Ti (ppm)	V (ppm)	Zn (ppm)
DGMH010	49.50	0.61	15.25	9.54	7.05		121	56	63	309	1212	80	5	2	40	3771	207	235
DGMH021	49.16	1.25	13.43	14.12	6.02		50	51	23	219	1598	45	2	3	389	7728	335	96
DGMH045	45.79	1.57	12.65	17.48	4.85	0.015	47	59		9	1753	20	1	0	47	8932	568	77

7.2.4. Results

Laser maps of the geochemistry in ppm (data located in Appendix 7.2) and SEM identification (full data and images located in Appendix 7.3 and table of minerals identified in each sample located in Appendix 7.4) was completed to assess the dolerite as a possible source of Cu for the DeGrussa ore lenses.

7.2.4.1. DGMH010 (308ppm Cu)

DGMH010 is a high Cu (308ppm) sample with lower Fe and Ti and higher Ba, Ni, Pb and Zn than DGMH021 and 045 (see Table 7.3). This sample is largely replaced by albite alteration, and is originally likely to have consisted of feldspar, hornblende, titanite and clinopyroxene (augite). Primary minerals are now altered to chlorite (chamosite), actinolite, albite and epidote.

SEM images (Fig. 7.2) identify clusters of fine-grained chalcopyrite and traces of sphalerite within outlines of remnant crystals, now composed of chamosite and actinolite. Small amounts of hornblende suggest that this could have been the original grain. The black crystal phase seen in Fig. 7.2, which correlates with the black clast to the left of the image in laser maps (see Figure 7.3), is identified as a Zn-rich augite-aegerine.

Mineral maps (Fig 7.3 and 7.4) show chalcopyrite forming patches associated with elevated Ni, Pb, Zn, Co and Fe. The area is also associated with high Mg, Al and Mn. The large black clast (augite-aegerine) mentioned above contains slightly elevated Cu, Ti and Zn compared with the groundmass alteration, as well as similarly high Mg, Al, Mn, Fe, Co and Ni. The best fit mineral composition appears to be 'jeffersonite', a dark green variety of augite-aegerine enriched in Mg and Zn (Anonymous, 2016).

Clasts with high Ti are titanate/sphene and contain small amounts of REE (Ta, Hf, Gd) and sometimes Pb. High Hf may also indicate the presence of zircon.

The laser map for DGMH010 shown in Figure 7.4 presents sulfide minerals within a vein crosscutting through the centre of the image. There are two different locations for Cu within the image. Within the vein, elevations of Cu correlate with elevated Ni, As, K, Co, Te and Pb, but with

depletions of Fe and no Na, Mg, Ca or Ti. Cu is also found in patches, similar to that in Figure 7.3, within chlorite (chamosite) and actinolite alteration, and in association with the black Zn-rich aegerine-augite. This same augite is associated with high Mg, Al, Mn, Fe as well as elevated Zn and Ni.

In map DGMH010a (Fig. 7.3) K is present, but not a substantial element related to chalcopyrite/sphalerite mineralisation in this sample. In map DGMH010b (Fig. 7.4), K is found in the vein and is most likely to be orthoclase ($KAlSi_3O_8$). No Fe is associated with Cu mineralisation within the vein in DGMH101b (Fig. 7.4), perhaps indicating that this is native Cu with inclusions of trace metals.

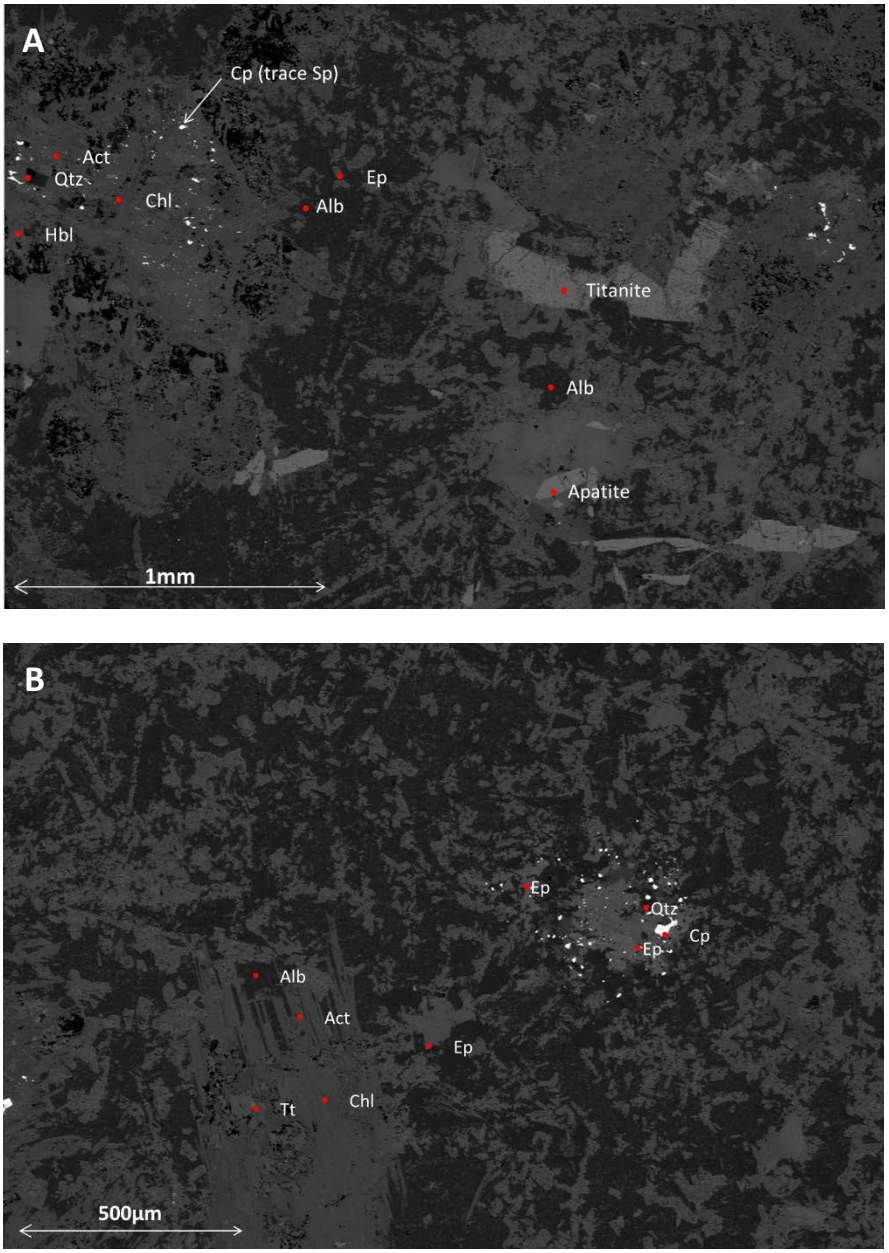

Figure 7.2. SEM image of DGMH010, Site 5 and 6 (See Appendix 7.3 for full spectrum) high Cu (308ppm) sample. **A.** Chalcopyrite in a remnant crystal grain of hornblende/amphibole, now altering to chlorite (chamosite) and actinolite. Interstitial alteration minerals between clasts include epidote and albite. Titanite and apatite form two of the other crystals. **B.** Site 4 Chalcopyrite cluster associated with epidote and quartz. Albite altered host rock, with pervasive epidote and large crystals of actinolite and chlorite (chamosite).

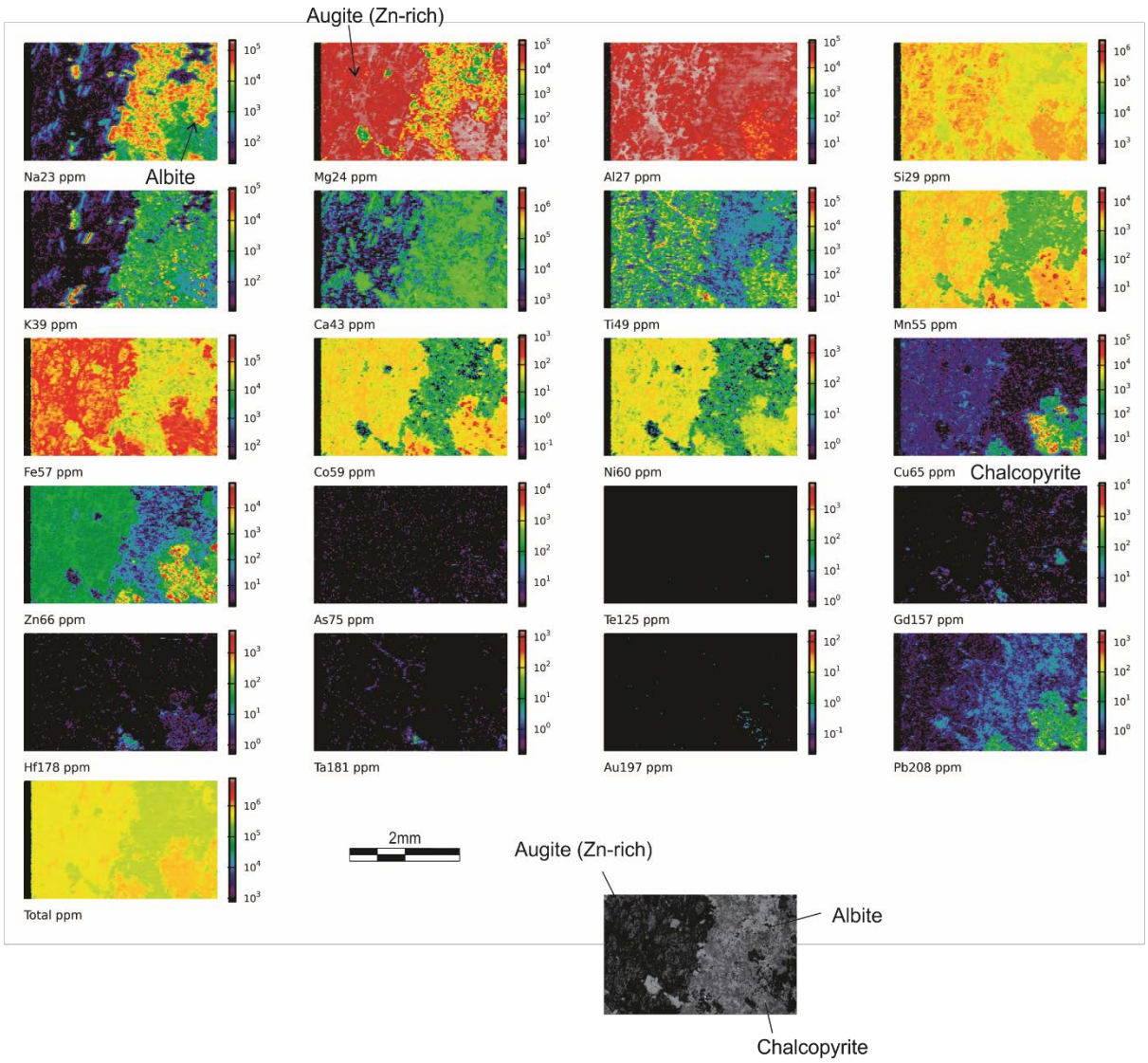

Figure 7.3. DGMH010a Laser ablation ICPMS Map and associated petrographic image

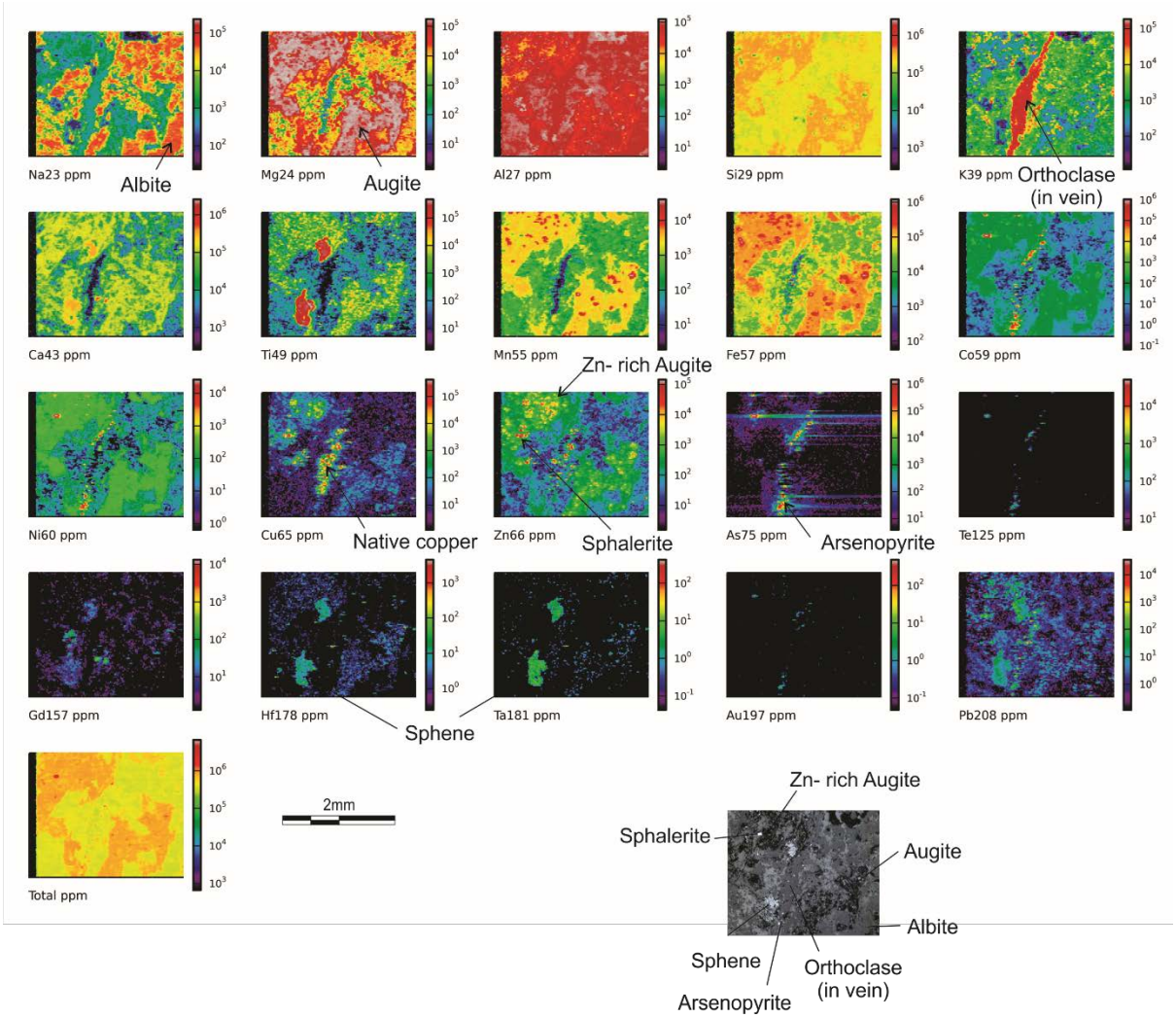

Figure 7.4. DGMH010b Laser ablation ICPMS Map and associated petrographic image

7.2.4.2. DGMH021 (218ppm Cu)

A medium Cu (218ppm) sample from the altered dolerite within the footwall of the DeGrussa deposit consisting of interlocking laths of albite, hornblende, augite and titanate/sphene as the main mineral phases. Albite alters to epidote, and hornblende/augite to chlorite and actinolite. Titanite is intergrown with hornblende (Fig. 7.5a). Minor quartz is present.

High Mg, Si, Ca, Mn and Fe, with lesser elevations in Co, Ni and Zn (Fig. 7.6) are in hornblende/augite crystals, which are altered to chlorite and actinolite. Albite contains high Na, Mg, Al and low Ca. Pb may be associated with fine-grained carbonate alteration. High Ti, associated with elevated Ta, Hf and Ca, indicates titanate/sphene.

Cu in chalcopyrite forms clusters of blebby grains coincident with elevated Gd, Pb, Fe, lesser K and Au, and low Ni, Co, Na and Mg. Chalcopyrite clusters correlate with the hornblende/augite (Fig. 7.6), although SEM images show that chalcopyrite may also occur in veins that contain carbonate, quartz, epidote and chlorite (Fig. 7.5).

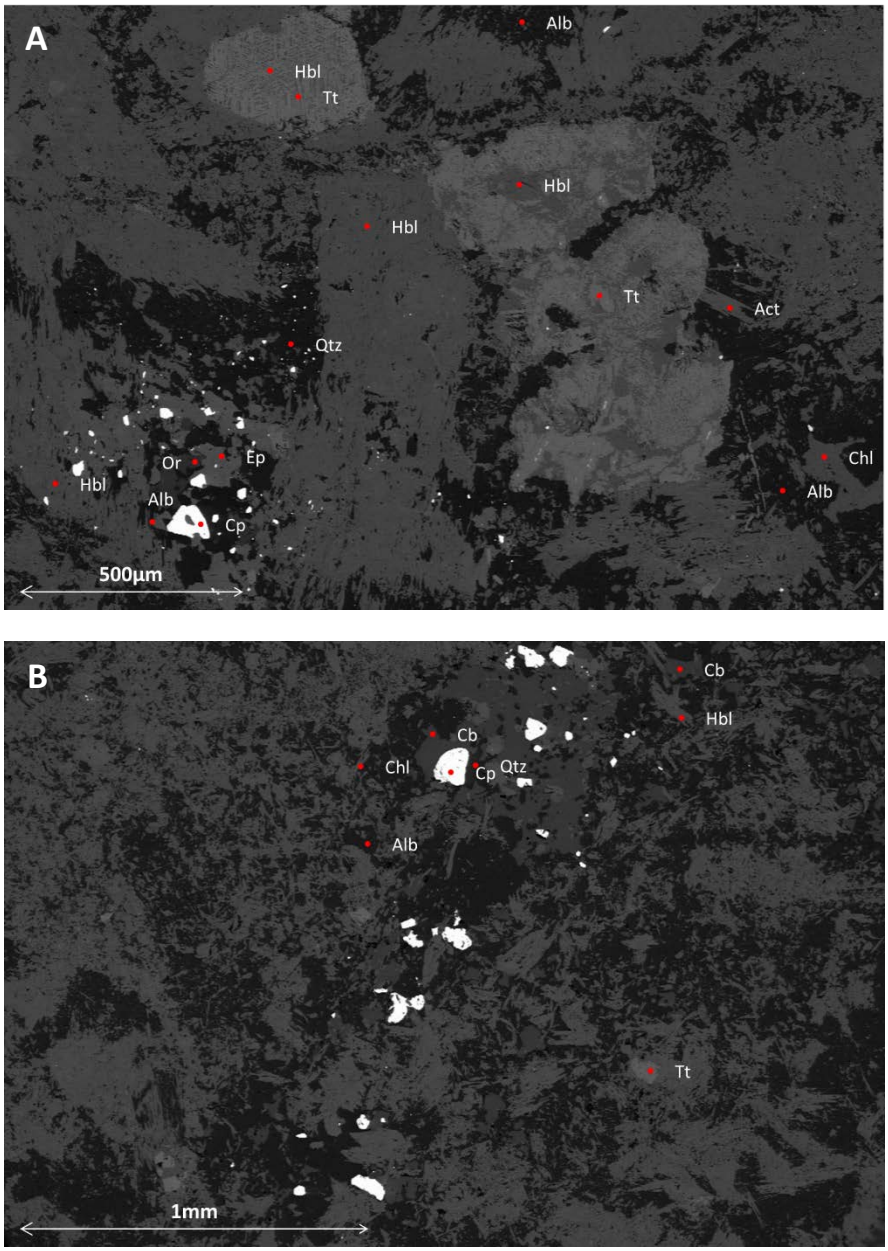

Figure 7.5. SEM image of DGMH021 (218ppm Cu) **A.** Site 3, large hornblende and titanite crystals (weathering to actinolite?). Albite widespread, chlorite (chamosite alteration), chalcopyrite crystals associated with epidote, quartz and albite alteration, some orthoclase feldspars in proximity. **B.** Site 1, vein containing chalcopyrite, carbonate, quartz with outer zone of chlorite (chamosite) and albite. Albite and hornblende with lesser titanite make up the main mineralogy away from the vein.

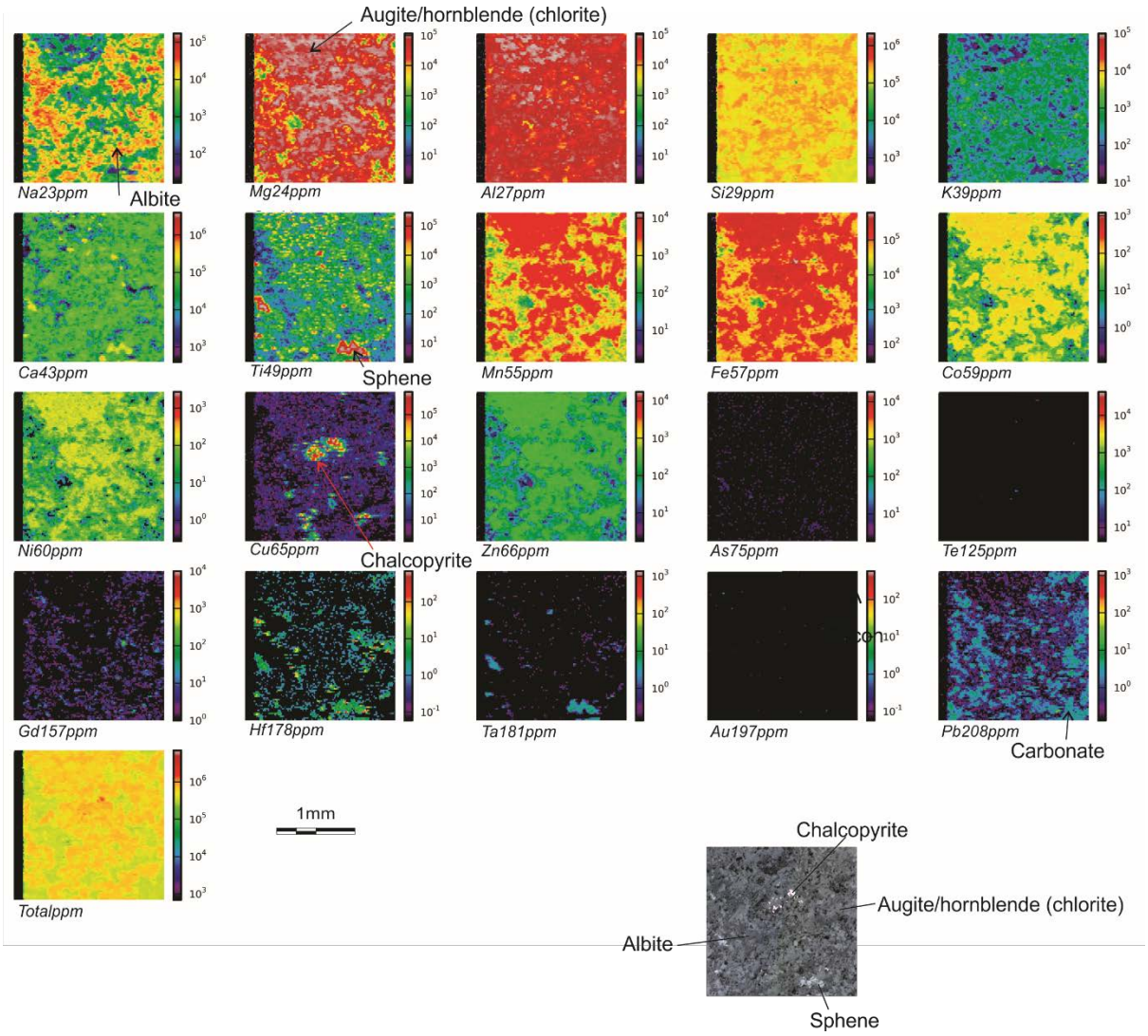

Figure 7.6. DGMH021b (218ppm Cu) laser ablation ICPMS maps and associated petrographic image

7.2.4.3. DGMH045 (9ppm Cu)

A low Cu (9ppm) sample with occasional small blebby crystals of chalcopyrite and pyrite. A fine-grained, highly altered rock in which the remnant interlocking nature of crystals can be seen, but now largely replaced by chlorite (chamosite), albite and epidote (Fig. 7.7).

Small apatite crystals are observed. Larger titanate/sphene crystals are a notable component. Hornblende is abundant. Little to no augite is seen although it may have been altered to chlorite.

Laser maps (Fig. 7.8) show albite laths, represented by high Na, Mg, Al and low Ca with variable amounts of Zn, Co and Ni. Titanite/sphene is associated with high Ti, Ta, Hf and Ca. Orthoclase is indicated by patches of high K, low Mg and Na. Areas of high Ca, Si, Ti, Mn, Fe, Co, Ni and Zn represent remnant hornblende (and possibly augite), now altered largely to chlorite (chamosite). Cu found throughout this rock also correlates with hornblende/chlorite. High Hf indicates zircon (see also appendix 7.4).

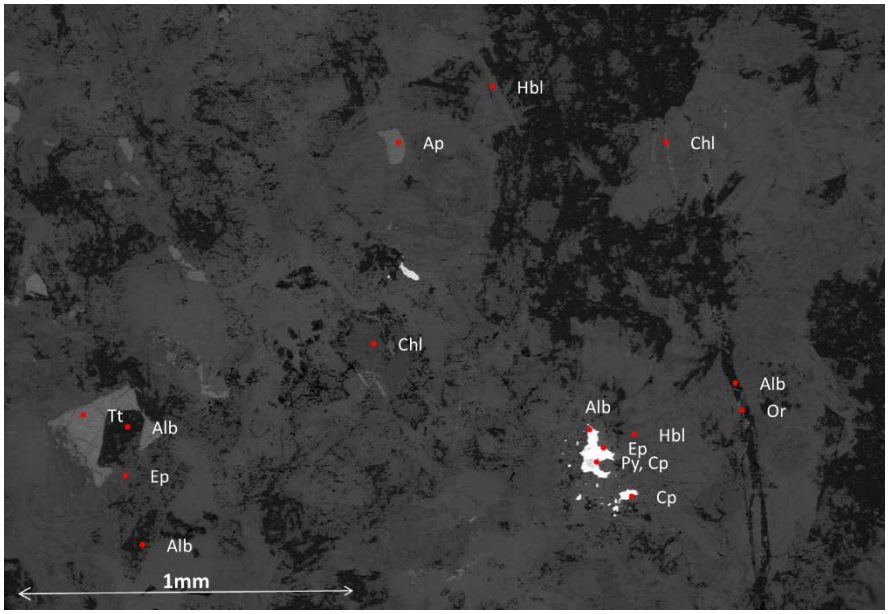

Figure 7.7. SEM image of DGMH045 (Site 1) with minimal sulfides (pyrite + chalcopyrite). Hornblende, albite and titanite and alterationproducts of chlorite and epidote.

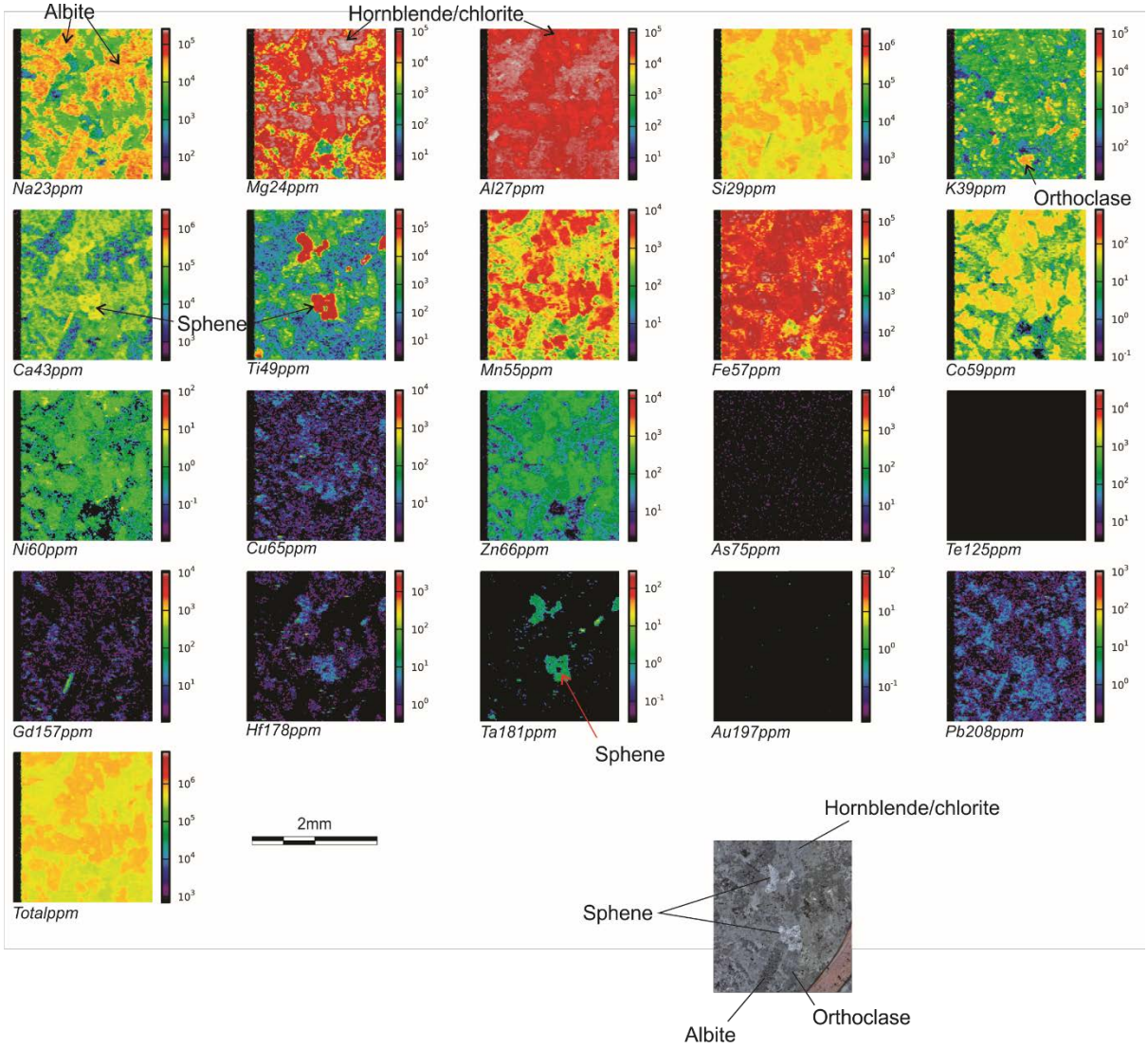

Figure 7.8. Laser ablation ICPMS map and associated petrographic image: DGMH045 (9ppm Cu). Little chalcopyrite is present with higher Cu values restricted to titanate and amphibole.

7.2.4.4. Whole Rock Geochemistry

In addition to the analysis of mafic dolerites above, some features of the whole rock geochemistry need to be noted.

1. The alteration box plot of Large et al. (2001) displays the distribution of mafic rocks and sedimentary host rocks of the DeGrussa deposit and underlying Johnson Cairn Formation sedimentary rocks (Fig. 7.?). Data is limited, however the trend towards the sericite-chlorite-pyrite alteration fields, away from least altered rock, may indicate favourable stratigraphy, proximity to mineralisation and hydrothermal leaching.

2. Loss (%) vs Cu for mafic rocks indicates scattered data, indicating that copper is independent of volatile content, and hence was probably introduced to the mafic rock during alteration unrelated to mineralisation (Fig. 7.9).

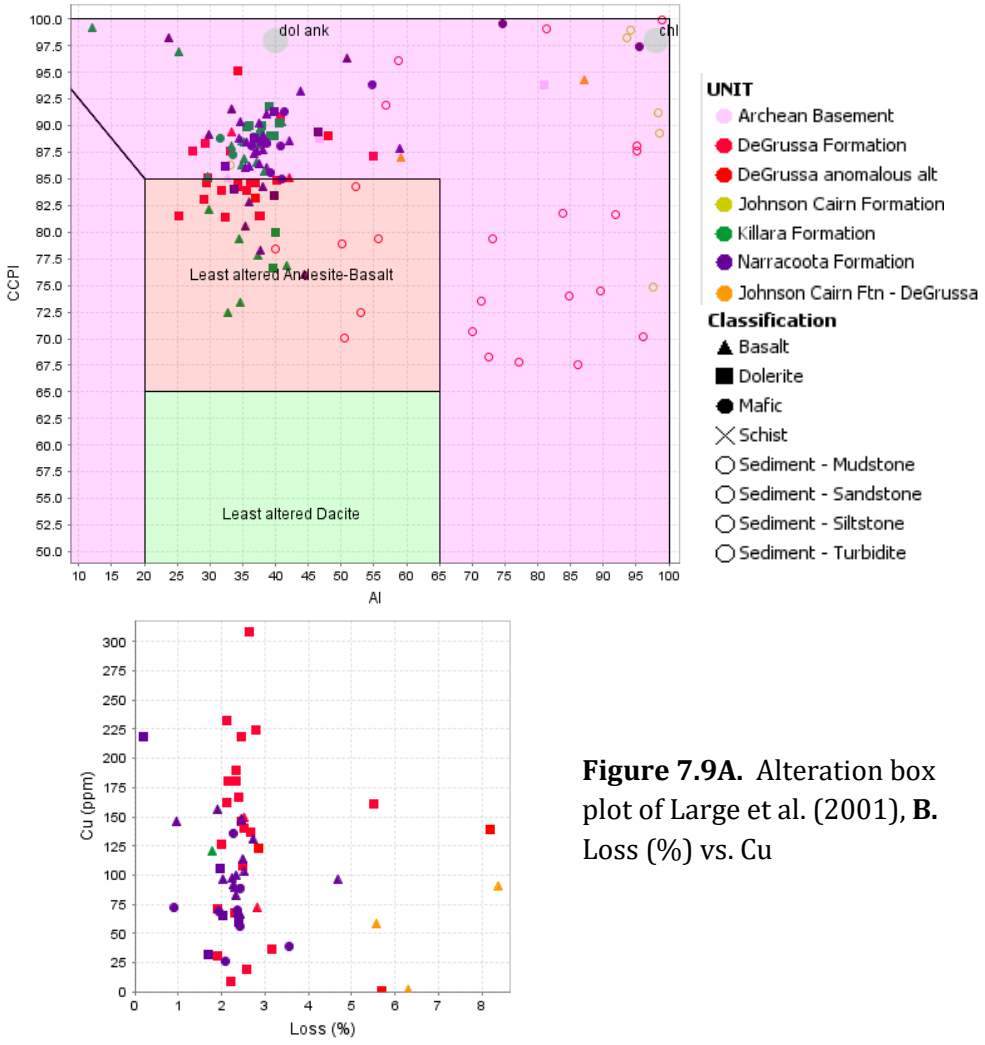

Figure 7.9A. Alteration box plot of Large et al. (2001), **B.** Loss (%) vs. Cu

7.2.5. Discussion

The Cu in the high Cu sample (DGMH010) is located within chalcopyrite that is clustered within relict crystals of amphibole (hornblende), now replaced by chlorite-chamosite and actinolite. The Cu in sample DGMH021 is similarly associated with chalcopyrite in amphibole. The small, discreet clusters of chalcopyrite are also associated with minor sphalerite, which possibly represent exsolution textures as a result of partial melting of an original basaltic rock. Studies by Stanton (1994) show that Cu is highest in spinel (145-295ppm) which also contain high TiO_2, FeO* and V, when compared with other minerals found in mafic volcanic rock. In rocks from the Solomon Islands Young Volcanic suite, Stanton (1994) also noted that clinopyroxene has 30-67ppm Zn and 31ppm Cu, hornblende 39ppm Cu and 111ppm Zn, and olivine 36ppm Cu and 156ppm Zn. Similar minerals correlate with the areas in which Cu and zinc are hosted by the DeGrussa dolerites. Pyroxene (i.e. augite) is present, although rare in most mafic rocks around DeGrussa. The host of Zn within the dolerites may be a Zn-rich augite-aegerine ('jeffersonite') member of the pyroxene group (Frondel and Ito, 1966) or 'frankilinite' ($Zn^{2+}Fe_2^{3+}O_4$) a Zn-rich spinel both found in the Franklin mining district of New Jersey. However, the extent of alteration throughout the rock makes it difficult to interpret whether chalcopyrite in the dolerite is sourced from crystal phases within the dolerite (e.g. hornblende), or was introduced during emplacement, or formed as a result of alteration due to the close proximity of the DeGrussa mineralisation. Chalcopyrite visible in SEM images in sample DGMH021 (Fig 7.5b, Appendix 7.3, site 1) appears associated with carbonate veining, which is likely post dolerite intrusion and DeGrussa mineralisation.

Cu is also hosted in a potassium-rich orthoclase vein (DGMH010b, Fig. 7.4), with little to no iron association and may be native Cu. Arsenopyrite is also located in veins as indicated by increased As and Fe, but not in association with Cu. This vein likely postdates the dolerite intrusion and DeGrussa mineralisation.

The low Cu in DGMH045 is associated with titanite and amphibole/chlorite regions. This suggests that Cu may be sourced from these phases. Two possibilities exist: 1. the lack of any

significant Cu-bearing metal in DGMH045 favours that Cu-bearing metals were introduced to the dolerite by way of hydrothermal alteration and metamorphism. 2. Lack of a significant amount of Cu-bearing source mineral (i.e. hornblende) resulted in a lack of Cu being retained in the dolerite.

The similar patterns of chalcopyrite and carbonate through the ore deposit suggest that these may have been mobilised throughout the deposit using the same conduits (both often being found along faults, fractures and shear zones). Chalcopyrite deposits in response to changes in temperature and pH (Xiao et al., 1998) and this allows sulfide to precipitate due to temperature and pH changes when the hydrothermal fluid interacts with sea water. Carbonate alteration and veining is extensive on the outer edges of the dolerite intrusions. This suggests interaction between dolerite and sea water, or given the peperitic contacts, unconsolidated wet sedimentary rock (see chapter 3). Carbonate precipitating from this seawater may have transported Cu and to a lesser extent Pb (see Fig. 7.7 and 7.8).

It is plausible that metals were released directly from the dolerites proximal to DeGrussa, although this is highly dependent on whether the dolerites are syn- or post- mineralisation (see chapter 6). Mineralisation may have comprised a significant exhalative volcanogenic component, with Cu- and Au-rich hydrothermal-magmatic fluids produced at depth. For example, deposition rates of Fe on the east Pacific Rise are up to 40 times greater than in surrounding areas of the Pacific, suggesting local volcanism to be the source of the iron (Stanton, 2015a). Fe-rich hydrothermal discharges associated with the Brothers volcano of the southern Tonga-Kermadec arc, is considered by de Ronde et al. (2011) to be indicative of direct exsolution of an Fe-rich liquid brine, possibly coincident with magmatic degassing.

Similarly, the DeGrussa dolerites may have been emplaced from a magmatic source which was also responsible for the metal-bearing, hydrothermal fluids responsible for DeGrussa mineralisation. It is plausible that a mode of metal-bearing volatile loss, supported by several authors (Archibald et al., 2002, Williams-Jones and Heinrich, 2005, Marques et al., 2011, Scher et al., 2013, Stanton, 2015a, Stanton, 2015b), may have occurred and contributed to the

mineralisation at DeGrussa. The mafic-dominant volcanism may have limited the amount of metals being exsolved into a mineralising fluid (i.e. in comparison to bimodal volcanic systems with a large felsic component), however the small amount of fractionation from mafic dolerite to granodiorite – leucogranite composition found in the region may provide a similar effect on a much smaller scale. No advanced argillic alteration, characteristic of a magmatic input is present, however the dominant quartz-chlorite-sericite alteration assemblage does not exclude a hydrothermal-magmatic input (Huston et al., 2010). The restricted suite of mafic rocks in the eastern Bryah may reflect the small size of deposits (i.e. not as much degassing/volatile loss in larger bimodal districts). This leaves the more bimodal Western Bryah basin area open for larger sized deposits.

Leaching of metals from the basement can not be discounted, and given the alteration of DeGrussa sedimentary rocks and Johnson Cairn Formation rocks, some input from hydrothermal leaching seems likely. No mass balance calculations have been carried out for the rocks around DeGrussa, and these may assist in further identification of hydrothermal alteration related to mineralisation in the footwall.

The enrichment of Cu in VMS deposits is suggested to be because Cu is trapped more efficiently than Zn and Fe. This results from the replacement of pyrite and sphalerite by chalcopyrite in the sulfide piles and feeder stockworks as hot vent fluids continue to pass through, and Fe and Zn is dissolved and discharged into the ocean (Cathles, 2011). The emplacement of sills likely helped to focus mineralising fluids and trap heat in the hydrothermal system, retaining the Cu. As mentioned in chapter 4, the giant Rio Tinto massive sulfide deposit formed in a restricted basin, hosted by a sediment-sill package of rocks, and massive sulfide mineralisation in the Guaymas basin, is forming in response to the intrusion of mafic sills into a sedimentary rock package (Gieskes et al., 1982). At DeGrussa, the dolerites may have provided a mechanism to keep the system hot, and trap the Cu.

Further work on the dolerites at DeGrussa and across the Bryah basin, where samples can be better assessed for a project of this nature, is required to assess the characteristics, if any, that may be associated with base metal mineralisation.

7.2.6. Conclusion

Cu and Zn bearing minerals are found in the DeGrussa dolerites, although it is unclear how much effect these have had on the source of mineralisation. The host of Zn within the dolerites is likely augite-aegerine. However, the chalcopyrite may be sourced by crystal phases such as hornblende, or formed as a result of alteration due to the close proximity of the DeGrussa mineralisation. Chalcopyrite visible in SEM images appears associated with carbonate veining, likely post dolerite intrusion and DeGrussa mineralisation, hence supporting an alteration source, rather than a primary source for Cu precipitation in dolerites. Preliminary geochemical plots show that leaching of sedimentary rocks of the DeGrussa host rock package, the underlying footwall and Johnson Cairn Formation may have occurred, with the sedimentary rocks likely to comprise material derived of other mafic terranes and the Yilagarn Craton.

7.3. Sulfur Isotopes

7.3.1. Introduction and Aims

This is a preliminary study of the characteristics of the east Capricorn mineralisation including DeGrussa. Access to regional samples was difficult. Apart from the extensive amount of samples from DeGrussa mineralisation, this meant that fewer samples were obtainable for other deposits in the district. The samples collected are shown in Table 7.3.

Table 7.3. Samples collected for sulfur isotope analysis from DeGrussa and across the east Capricorn Orogen.

Deposit	Sample #	Sample Type	Age (Ma)
DeGrussa	87	Core, offcuts from (Condon, 2015)	2027 ± 7
Horseshoe Lights	5	Grab samples from (Gillies, 1988)	2000 ± 35
Fortnum (Yarlarweelor and Starlight/Trevs)	8	Core from Yarlarweelor, Grab sample from Starlight pit	920 ± 50
Cassidy/Horseshoe	4	Grab sample stockpile	1940 ± 30
Thaduna	16	Diamond drill core	1475 ± 50

Sulfur isotopes are utilised in this study to:

1. Characterise the $\delta^{34}S$ isotope values at DeGrussa, in particular evaluating for sulfides of different type and morphology throughout DeGrussa and Conductor 1 mineralisation;

2. Compare $\delta^{34}S$ isotopes to regional mineralisation and so make a judgement on sulfur sources in the basin;

3. Identify whether $\delta^{34}S$ isotopes can be used as an exploration vector for different styles of mineralisation (VHMS, orogenic and epithermal) in the region; and

4. Determine the origin and evolution of sulfur in the DeGrussa ore body.

7.3.2. Methods

DeGrussa samples were collected by Condon (2015) from the DeGrussa and Conductor 1 ore lenses for use in her masters study. and were selected based on their different textures (massive, disseminated, veined, stringer, framboidal, etc. See chapter 4 section 4.2.2. for a summary of textures identified by Condon (2015)), and mineralogical variation (i.e. chalcopyrite, pyrite and sphalerite). Thin section off cuts from this work are used for this doctoral study. Sample numbers and locations can be found in Appendix 7.5a and b. They were selected from throughout the ore lenses in order to best represent the range of textures. No samples from Conductor 4 or 5 were collected.

Additional sulfide samples were collected from mineral deposits in the district including Fortnum (Orogenic), Cassidy/Horseshoe (Orogenic), Horseshoe Lights (VHMS) and Thaduna (Epithermal) in order to compare these to the DeGrussa mineralisation. Short summaries of the

geology and style of mineralisation are provided in Chapter 2. Samples for Horseshoe Lights were donated by the University of Western Australia from the material collected by Gillies (1988). Samples from Fortnum were both grab samples from a site visit to the Starlight pit, as well as from core samples from a cofounded GSWA/RNI drill hole below the Yarlarweelor pit. Thaduna samples were from core provided by Ventnor Resources, and Cassidy/Horseshoe samples were grab samples from the old stockpile near the pit (access was not possible to the pit).

Samples were checked petrographically for purity before drilling. Approximately 30µg of sulfide was collected by carefully drilling out the sulfides from the rock using a micro drill with a 300 micron diamond bit (see Appendix 7.6 for location of sample on each rock, descriptions and values). These were stored in small vials. Between each sample the drill bit was cleaned with limestone block to remove any contamination that may occur from the drill bit.

Samples were analysed using flash combustion isotope ratio mass spectrometry (varioPYRO cube coupled to Isoprime100 mass spectrometer) at the Central Science Laboratory, University of Tasmania (Appendix 7.7). The analytical precision of the $\delta^{34}S$ values, determined by repetitive measurements of three international standards, is around 0.2‰ (Dietz, 2016).

7.3.3. Sulfur Isotopes through the Archean and Proterozoic

The Earth's atmosphere and oceans were in a transitional phase between 3.2 and 1.0 Ga (Canfield and Raiswell, 1999, Huston and Logan, 2004, Poulton et al., 2004, Canfield, 2005, Bekker and Holland, 2012). The Earth's atmospheric and hydrospheric (oceanic) compositions transitioned during the Archean and the Palaeoproterozoic, and the sulfur isotope compositions varied in response to these changes (Fig. 7.10). These variations in sulfur isotope are summarised here with respect to both mass dependent and mass independent fractionation of sulfur through time. However, this thesis forms a preliminary study and only $\delta^{34}S$ sulfur isotopes have been analysed. Sulfur fractionation processes (MID) in the Archean are summarised in Figure 7108. Palaeoproterozoic and Proterozoic sulfur fractionation processes and environments are shown in Figure 7.11.

7.3.3.1. Sulfur mass independent vs. mass dependent fractionation

Mass independent fractionation (MIF) of sulfur occurs as a result of photolysis of SO_2 by UV radiation in the 190–220 nm spectral region (Farquhar et al., 2001). Short-wave radiation can only penetrate deep into the atmosphere at low ozone and oxygen levels (Pavlov and Kasting, 2002) (Fig. 7.10). Sulfur MIF processes dominated in the Archean up until ~2.3 Ga, indicating that the Archean oxygen levels must have been at least one to two orders of magnitude lower than at present (Pavlov and Kasting, 2002, Farquhar et al., 2001). Experimental work by Farquhar et al. (2001) and Pavlov and Kasting (2002) provide strong evidence for an almost completely anoxic Archean atmosphere. Sulfur isotope MIF could only have occurred under reduced atmospheric conditions when sulfur was being removed from the atmosphere in a variety of different oxidation states (Pavlov and Kasting, 2002).

Mass dependent fractionation (MDF) of sulfur occurs as a result of thermodynamic, kinetic, or biological processes in aqueous solution or solid phase fractionation of isotopes in a mass-dependent way (Pavlov and Kasting, 2002). Biological fractionation of sulfate to sulfide reduces the $\delta^{34}S$ by 22 ‰ and requires an oxygenated hydrosphere, sulfate in the oceans, and temperatures of less than 120°C (Rollinson, 2013). Inorganic fractionation of sulfate to sulfide can occur either in the presence of hydrocarbons, or at temperatures greater than 250°C, by reduction with ferrous iron and is an important process at mid-ocean ridges (Rollinson, 2013).

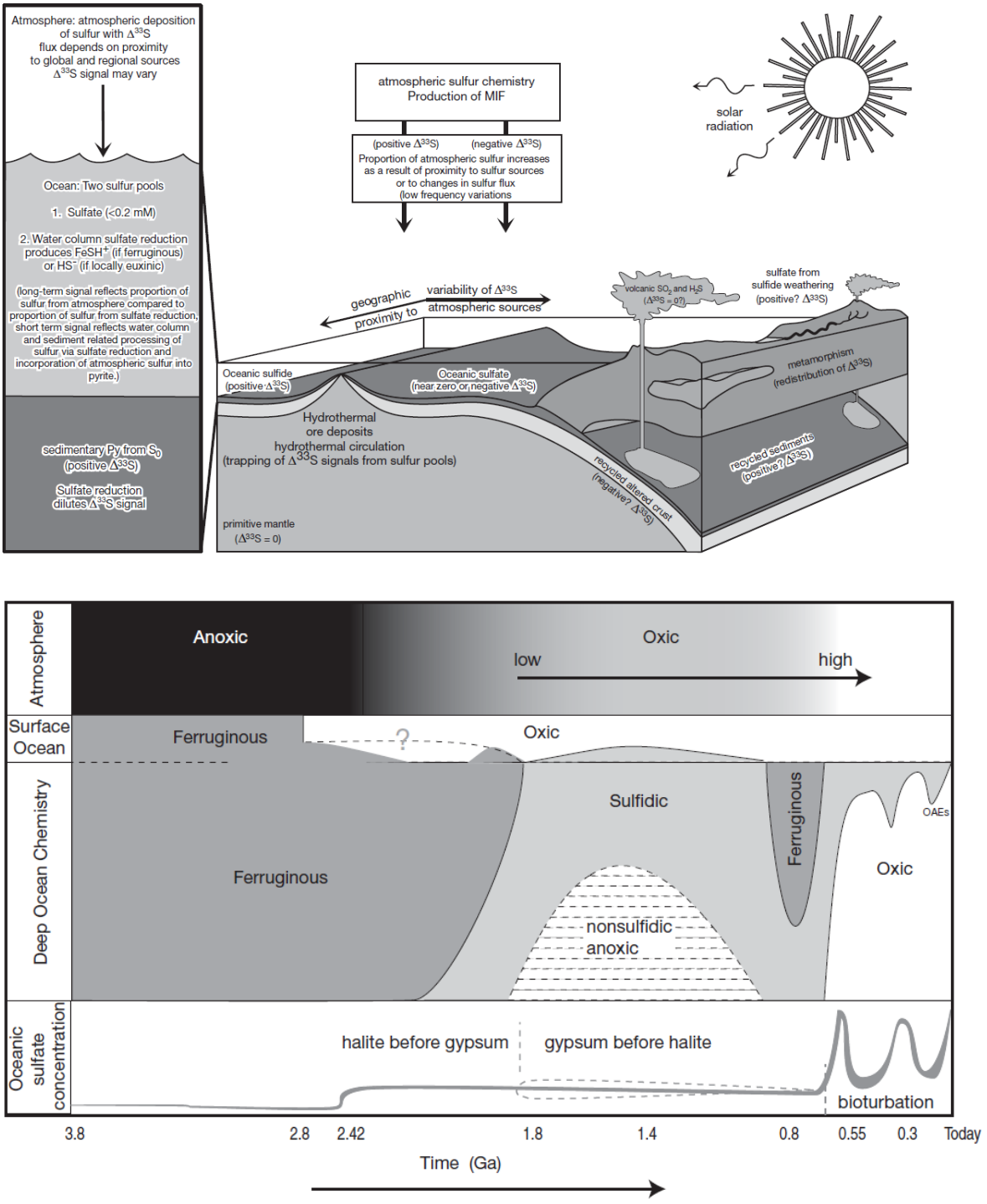

Fig 7.10. A. Archean sulfur cycle model of Farquhar et al. (2010). The MIF signal is of atmospheric origin and the transfer of this signal to the sediments includes components related to atmospheric, water column and sedimentary processes. **B.** Composition of the earth's oceans and atmosphere through time as presented by Farquhar et al. (2010)

MDF dominated after the great oxidation event (G.O.E.) at ~ 2.3 Ga due to increasing amounts of sulfate in fresh and ocean water produced by oxidation of sulfide (Ueda et al., 1990). As discussed in chapter 4, depositional temperatures for mineralising fluids were greater than 120°C, and the low-sulfate oceans make biological fractionation unlikely. Hence, inorganic fractionation of sulfur is the preferred explanation that will be discussed for the observed range of DeGrussa $\delta^{34}S$ isotope values. Figure 7.11 summarises the changing atmospheric conditions through time.

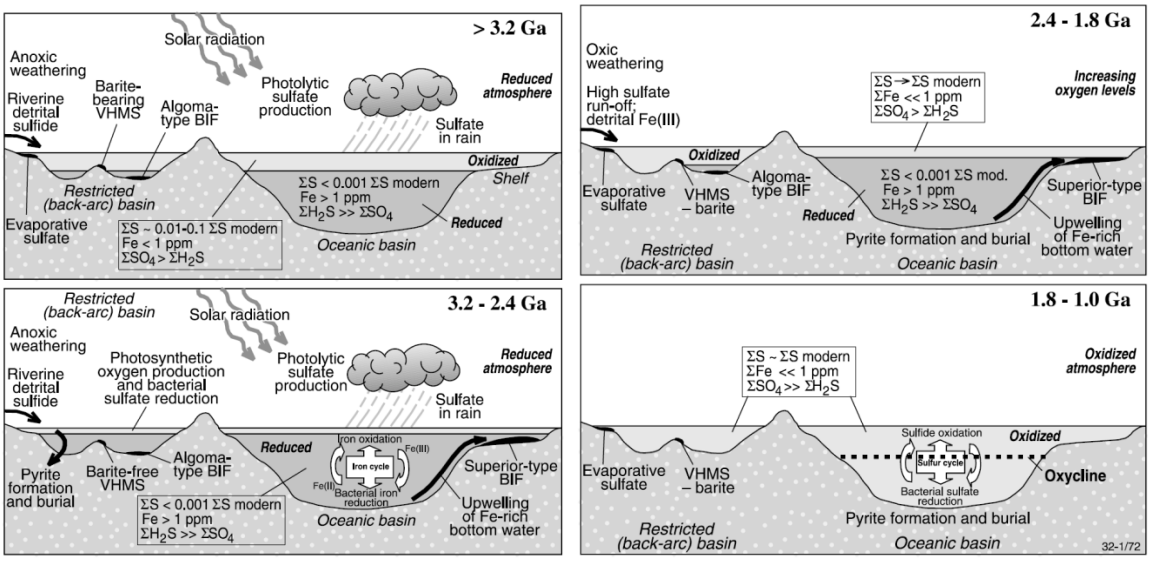

Figure 7.11. Earth's hydrospheric composition through time and potential location of VHMS and BIF formation (Huston and Logan, 2004).

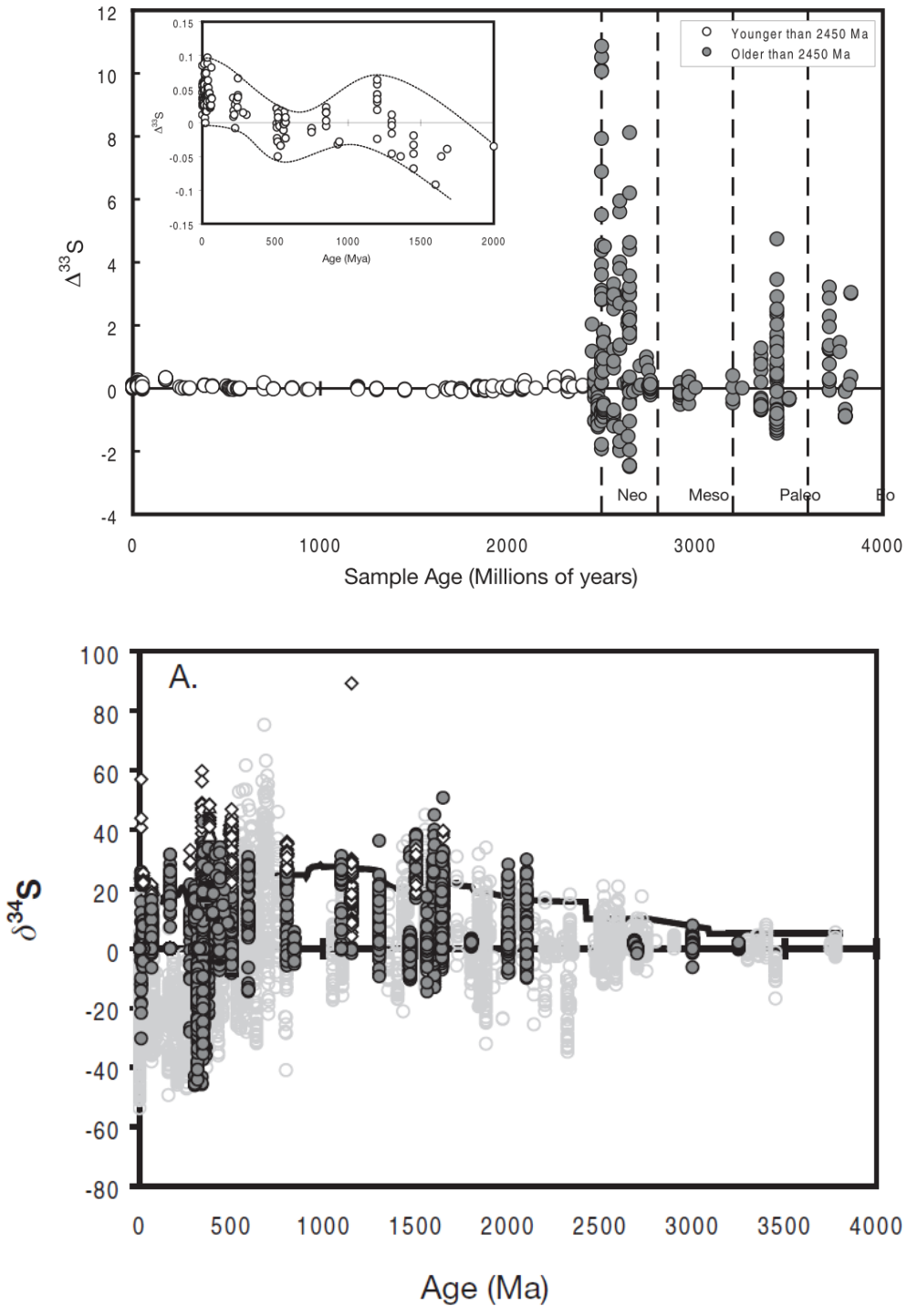

Figure 7.12. A. Plot of Δ33S versus sample age from a compilation of values. Grey filled circle symbols are samples older than 2.45 Ga and reflect mass independent reactions and preservation of isotopic signals in the rock record. White filled circle symbols are for samples younger than 2.45 Ga and are interpreted to carry a mass conservation-type signal associated with mass-dependent fractionation by BSR and other sulfur cycle processes (see inset for sulfate) (Farquhar et al., 2010). B. Evolution of the atmosphere, surface ocean, and deep oceanic sulfate concentration as inferred by Farquhar et al. (2010). The solid black line represents the average seawater sulfate curve, which at 2.0 Ga is ~ 20 ‰.

7.3.3.2. Archean (>2.4 Ga)

At >3.2 Ga, the hydrosphere is considered to be sulfur-poor and the oceans stratified (surface waters oxidised, with deeper waters anoxic and Fe-rich) (Huston and Logan, 2004, Farquhar et al., 2010) (Fig. 7.11). H_2S and SO_2 were stabilised in the atmosphere and could undergo photolytic reactions, producing mass-independent sulfur isotope fractionation and large variation in $\Delta^{33}S$ (Fig. 7.11). This produced oxidised, sulfur-bearing gases, such as SO_3 (Huston and Logan, 2004, Farquhar et al., 2010).

Between 3.2 and 2.4 Ga the oxidised top waters of the ocean were slowly reduced leading to a deep reduced ocean. The majority of the geologic evidence supports low oxygen levels prior to 2.3 Ga, however, photosynthesis was likely operative as early as 2.7 Ga in some areas of the world's oceans (Pavlov and Kasting, 2002). Variation in $\Delta^{33}S$ decreased after 3.2 Ga, but some MIF and photolytic reactions of H_2S and SO_2 were still ongoing in the atmosphere due to the lack of ozone layer development (Fig. 7.12) (Huston and Logan, 2004). The $\delta^{34}S$ value of Archean seawater sulfate was close to 0‰ consistent with limited biological sulfur isotope fractionation (MID), and sulfate concentrations <200µm/L (Ueda et al., 1990, Strauss, 1993, Gellatly and Lyons, 2005, Schröder et al., 2008). The most likely explanation for low concentrations of sulfate in the Archean is the limited oxidative weathering of pyrite on land under reduced concentrations of atmospheric O_2 (Canfield, 2005).

This was a major period of Banded Iron Formation (BIF) formed by mixing of deep reduced, and shallow oxygenated ocean layers. Oceans would have had high concentrations of Fe^{2+} in the bottom waters (Huston and Logan, 2004) (Fig. 7.10, 7.11, 7.13).

7.3.3.3. Palaeoproterozoic (2.4-1.8 Ga)

Oceans were transitional to sulfur-rich (oxidised sulfur species), although oxidised conditions are interpreted to occur only in surface/shallow waters. The advent of free oxygen in the atmosphere ended photochemical oxidation of reduced sulfur-bearing gases (Huston and Logan, 2004). There is a lack of mass independent fractionations in pyrite from ~2.4 Ga indicating a

significant rise in O_2 (> 10^{-5} PAL) occurred although limited amounts of MIF still persisted (Canfield, 2005, Williford et al., 2011, Luo et al., 2016).

Compared with the Archean, in oxidised layers of water, the mobility of S and Fe during weathering of sulfides and oxidising of iron changed due to the changed solubility of these elements under the new conditions (Huston and Logan, 2004). Sulfur became increasingly mobile as an oxidised species in water, with oxidative weathering of terrestrial sulfides producing soluble sulfate, and, thereby, increasing sulfate concentrations in seawater. Increasing flux of sulfate derived from oxidative weathering, swamped the buffering capacity of atmospheric and volcanic sulfur reservoirs (Ueda et al., 1990, Huston and Logan, 2004). The evolution and/or radiation of microbial sulfate reduction, coupled with higher sea water sulfate levels, led to larger isotopic fractionation between SO_4 and H_2S of pyrite ($\Delta^{34}S_{sulfate\text{-}sulfide}$) and the shallow levels of the oceans became more oxidised and sulfate-rich (Huston and Logan, 2004). The presence of iron formations indicate that the bottom waters remained reduced, sulfide poor and iron-rich. Small, closed basins would experience sulfate concentration rises at a faster rate compared with open basins (Scott et al., 2014, Lyons and Severmann, 2006). Biological sulfate reduction would have been an active process in shallow ocean waters and the sulfide produced would have been sequestered by the Fe^{2+}-rich bottom waters to form pyrite, keeping the lower ocean virtually sulfate-free (Huston and Logan, 2004).

Evidence for an anoxic atmospheric and oceanic environment prior to 2.4 Ga is discussed by Canfield (2005). Canfield (2005) presents evidence such as the preservation of uraninite, pyrite and siderite as detrital placers in river deposits older than 2.3 Ga and their lack of preservation after 2.3 Ga to indicated a change from an anoxic to an oxidated atmosphere at this time. The presence of iron-rich palaeosols after 2.3 Ga and the appearance of red bed deposits at 2.2 Ga also indicates a change to an oxygenated atmosphere (Canfield, 2005, Bekker and Holland, 2012).

At ~2.3 Ga there is a change to sulfides with $\delta^{34}S$ isotopic values that vary to a positive range. Schröder et al. (2008) identified that early Paleoproterozoic sulfates have elevated $\delta^{34}S$ values of ~10‰ suggesting that bacterial sulfate reduction and pyrite formation in anoxic settings might

have driven seawater $\delta^{34}S$ values towards the $\delta^{34}S$ of seawater sulfate. For instance, sulfate from the 2.0-2.3 Ga Gordon Lake Formation, Ontario; Malmani Formation, Transvaal; and the Kona Dolomite, Michigan, have uniform $\delta^{34}S$ values of +14 ± 3‰. Palaeoproterozoic seawater sulfate $\delta^{34}S$ is estimated at 10 to 18‰ (Scott et al., 2014).

The overall average $\delta^{34}S$ values of Proterozoic sedimentary pyrite remained near zero, as shown by Farquhar et al. (2010) and is interpreted to imply high fractions of pyrite burial, and a missing ^{34}S-depleted sulfur pool. Leaching of sulfur from Proterozoic rocks would precipitate new sulfur bearing minerals with the same $\delta^{34}S$ value as that of the Proterozoic rocks from which they were derived because the efficiency of sulfate reduction was very high.

The major positive $\delta^{13}C$ excursion of the Lomagundi-Jatuli event (2.22 to 2.06 Ga) (Fig. 7.12) is recorded in rocks of the Bubble Well Member (see chapter 2 and 3) (Russell, 1992, Karhu and Holland, 1996, El Tabakh et al., 1999, Lindsay and Brasier, 2002, Melezhik et al., 2007, Schröder et al., 2008, Master et al., 2010). This worldwide event corresponded with tectonic reorganisation which likely influenced the ocean circulation and redox state and potentially ended the conditions that promoted high burial of organic matter with sediments during the Lomagundi excursion (Lindsay and Brasier, 2002, Master et al., 2010). Low oxygen levels in the Palaeoproterozoic atmosphere and the occurrence of ocean anoxia until the late Precambrian resulted (Aharon, 2005). The resulting $\delta^{34}S$ values at DeGrussa should reflect inorganic fractionation of $\delta^{34}S$ isotopes due to a lack biological fractionation.

A lack of Banded Iron Formations (BIF) after 2.4 Ga is consistent with an oxygenated surface environment at this time although their presence at ~1.8 Ga in the Frere Formation in the Earaheedy Group, Western Australia (postulated to also be similar in age to the undated Robinson Range Formation of the Padbury Group) suggests that, at least locally, Fe-containing bottom waters returned between 2.0 and 1.8 Ga (Hall and Goode, 1978, Canfield, 2005, Rasmussen et al., 2012). BIF deposits in shallow shelf environments (Fig. 7.1, 7.13), in oceans containing dissolved Fe(II) which is consistent with the low concentrations of atmospheric O_2 and low concentrations of sea water sulfate (Canfield, 2005). Low concentrations of atmospheric O_2 would allow for an

anoxic deep ocean, whereas low concentrations of seawater sulfate would suppress rates of sulfate reduction and hence sulfide production, allowing dissolved Fe to persist (Canfield, 2005).

The 1.8 Ga Frere Formation in the Earaheedy Group, Western Australia shows evidence that the Fe-oxides precipitated in the high energy region of shoaling waves near the seashore (Hall and Goode, 1978, Canfield, 2005, Rasmussen et al., 2012). For the transport of Fe^{2+} into near-shore environments, it is suggested that O_2 levels of about 0.1% PAL (present atmospheric level) are required. Canfield (2005) suggests that the global ocean experienced extensive periods of anoxic-sulfidic conditions during the middle Proterozoic, with an upper limit for atmospheric O_2 at 40% PAL.

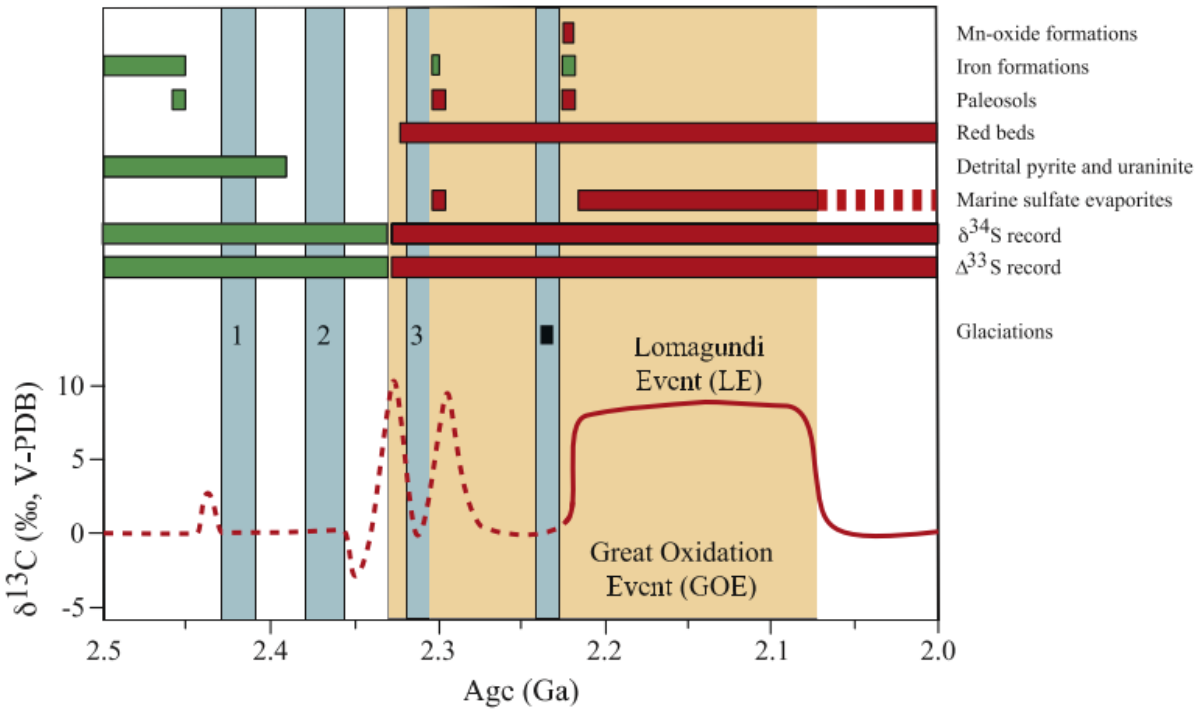

Figure 7.13. C isotope values between 2.5-2.0 Ga and indicators for the oxidation state of the atmosphere-ocean system. Blue bars mark Palaeoproterozoic glacial events (from(Bekker and Holland, 2012)).

7.3.3.4. Proterozoic 1.8-1.0Ga

It is suggested by Huston and Logan (2004) that the deep oceans changed from anoxic, sulfide-free to sulfidic conditions at ~1.8 Ga responding to the final removal of free-Fe (Poulton et al., 2004, Canfield and Raiswell, 1999) (Fig. 7.11). However, Slack et al. (2007) suggest that deep water, open-marine sediments associated with VHMS deposits show that the redox state of the ocean was in a transitional, suboxic state with low levels of dissolved O_2 and no H_2S. The presence of jasper/iron formations in some VHMS deposits, located in variable water depths, suggest that the ocean was, at least locally, oxygenated and non-sulfidic during this time.

7.3.4. Sulfur Isotopes in VHMS deposits

7.3.4.1. Modern VHMS systems

VHMS deposits are associated with large-scale hydrothermal circulation systems that involve seawater and sulfur leached from igneous and other crustal rocks, or from reduction of seawater sulfate (Franklin et al., 1981, Franklin et al., 2005). Seafloor sulfides from modern black smokers are the present day analogy for VHMS deposit formation with studies showing that sulfides in these environments are derived mostly from leaching of juvenile sources (73-89%) and a lesser amount (11-27%) from reduction of seawater sulfate at the site of deposition (Farquhar et al., 2010). Present day sulfides of the Guaymas Basin, Gulf of California have $\delta^{34}S$ values of -11.06 to 7.31‰ interpreted by Lonsdale et al. (1980) and Gieskes et al. (1982) as having a contribution of both hydrothermal sulfide and biogenic sulfide. Sulfide formation may occur from mixing or cooling of metal- and sulfide-bearing fluids and be dependent on the metal/sulfide ratio with the efficiency of precipitation increased in the presence of sulfidic bottom waters (Farquhar et al., 2010). Anhydrite may precipitate at recharge zones but is lost once systems cool (due to reverse solubility in anhydrite) and tends not to be preserved in older deposits. Barite forms when sulfate solutions mix with a barium-rich solution (Humphris et al., 1995, Farquhar et al., 2010).

Studies of present day VHMS systems resulted in the following basic steps for the formation of a deposit (Figure 7.14) and the transport of sulfur (Rollinson, 2013):

1. Cold seawater sulfate is drawn down into seafloor sediments and basalts, and heated in vicinity of magma and high temperature hydrothermal discharge zones.
2. Some sulfate precipitates as anhydrite, and some is reduced to sulfide with reaction with basalt and sediments.
3. Both magmatic and reduced sulfur is leached from the sub seafloor by hot, reduced convecting seawater. The sulfide and metal-bearing hydrothermal fluid is vented back onto the seafloor at temperatures of 350°C.
4. Through both lithostatic pressure changes (forming vein stockworks) and mixing with circulating colder seawater sulphides are precipitated near, or on the seafloor.

$\delta^{34}S$ isotopic compositions of sulfide and sulfate in VHMS deposits compared with the sedimentary record is shown in Figure 7.15A. This indicates a narrow range of $\delta^{34}S$ values for sulfide and sulfate for Archean samples, and a broader range for Proterozoic samples which is dominated by positive $\delta^{34}S$ values. Phanerozoic $\delta^{34}S$ values exhibit greater range again (Farquhar et al., 2010) due to increased sulfur input into the oceans creating S-rich oceans. The processing of sulfur (e.g. sulfur in barite caps) in VHMS deposits reflects Rayleigh fractionation that contributes to the variability. These distributions differ from those of the sedimentary record insofar as the mean values are generally positive for both sulfate and sulfide, which reflects the role played by sulfate and leaching of igneous sulfur, ultimately of juvenile origin, as sources of sulfur rather than of pyrite produced from reduced sulfur contributed by sulfate reducers (Farquhar et al., 2010). Isotopic studies of present day hydrothermal systems suggest that the fraction of sulfur derived from sulfate, is less than 40 % of the total sulfur and the remainder is derived from leaching of igneous sulfides (Farquhar et al., 2010). The resulting $\delta^{34}S$ values are a combination of these mixing and fractionation patterns, and are not straightforward because ore-forming processes can also influence the $\delta^{34}S$ values of sulfide and sulfate (Farquhar et al., 2010). In contrast, the Paleozoic VHMS deposits of the Prince of Wales Island, Alaska ($\delta^{34}S$ of 5.9 to 17.4‰, average of 11.5±2.7‰) reflect a sea water sulfate source of the sulfides that is linked to $\delta^{34}S$ of contemporary sea water sulfate (Slack et al., 2005).

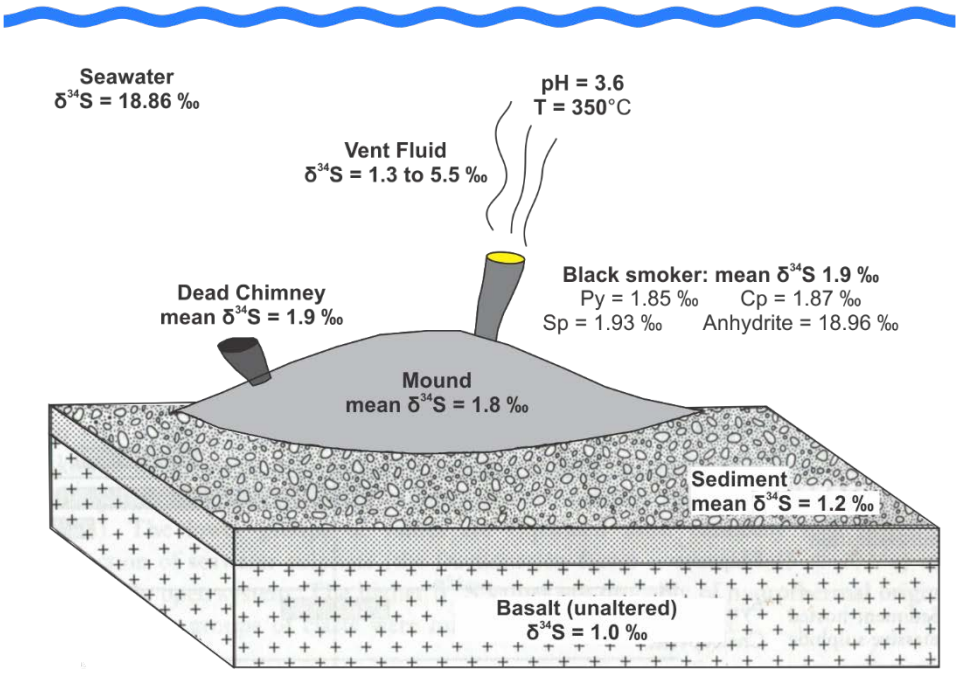

Figure 7.14. Schematic representation of $\delta^{34}S$ values in a modern mid-ocean ridge hydrothermal vent system (adapted from Rollinson (2013) and references within).

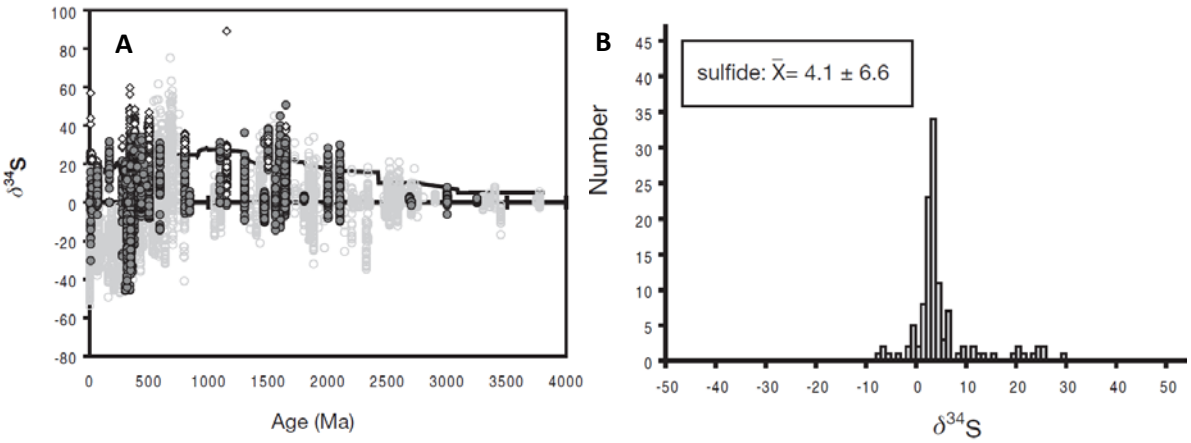

Figure 7.15A. Compilation from Farquhar et al. (2010) of $\delta^{34}S$ vs time for base metal sulfides (filled grey circle symbols), sulfate (unfilled diamond symbols) and sedimentary pyrite (unfilled light grey circle symbols). The black line is the seawater sulfate curve. **B.** Histogram of the frequency of observations of sulfide for Proterozoic VHMS deposits (Farquhar et al., 2010).

7.3.4.2. VHMS deposits in the Archean and Proterozoic

Archean VHMS deposits (e.g. Golden Grove (Sharpe, 1999), Panorama (Brauhart, 1999), Flin Flon (Sangster, 1972), and Windy Craggy (Peter and Scott, 1999)) display mineralogical and textural features as well as Cu, Pb and Zn sulfide mineralisation and barite that is similar to younger Phanerozoic deposits (Farquhar et al., 2010, Huston et al., 2010) – although exceptions occur, with no reported barite exhalite present above the ~2.8-2.7 Ga Teutonic Bore VHMS deposit (Vaasjoki, 1985, Hallberg and Thompson, 1985, Bonnici, 2016). Barite suggests that barium was mobilised in the sub seafloor hydrothermal system and that sufficient sulfate was present at the site of deposition to precipitate barite (Vearncombe et al., 1995, Farquhar et al., 2010). Early oceans may have had high sulfate concentrations, which is likely to indicate an oxygenated atmosphere/ocean system. However, sulfate can be formed by photochemical pathways from volcanic emissions in a reducing atmosphere, with the precipitation of sulfate requiring only that the solubility product for barite be exceeded (Vanderwood and Thiemens, 1980, Farquhar et al., 2010).

The ~3.0 Ga Gossan Hill Cu-Zn VHMS deposit of the Yilgarn Craton in Western Australia is interpreted to have $\delta^{34}S$ values which reflect a uniform reduced S source dominated by leached igneous rock S and minor magmatic sulfur (-1.6 to 3.4‰) at the base, with an upper zone explained by the mixing of hydrothermal fluids containing $\delta^{34}S$ values leached from rocks that preserve an Archean sea water $\delta^{34}S$ value ($\delta^{34}S$ of 2 to 3‰ near the palaeo-seafloor) (Sharpe and Gemmell, 2000).

Neoarchean VHMS deposits do not contain significant barite, similar to observations at the DeGrussa deposit (Farquhar et al., 2010, Hilliard, 2013, Hawke et al., 2015). Lower sulfate conditions may have prevailed, or the nature of the hydrothermal circulation systems may have influenced the chemistry of the overlying water making barite precipitation unlikely (Farquhar et al., 2010). As discussed in chapter 4, the presence of sulfide breccia indicates that anhydrite may have existed and was not preserved during cooling of mound. Anoxic conditions in the Neoarchean would reduce the amount of sulfate available in sea water, and as shown in Figure

7.11, sulfate bearing Archean VHMS deposits may derive from smaller restricted sea basins, in which sulfur oxidation was more extensive than the open ocean (Huston and Logan, 2004).

Oxygen in the Palaeoproterozoic deep ocean (present day VHMS deposits form in water depths of >1000m, with the DeGrussa deposit considered to be located at depths consistent with these observations (see chapter 4) is interpreted by Farquhar et al. (2010) to be low (anoxic), but still variable over many orders of magnitude. A change in ocean chemistry is postulated by Slack and Cannon (2009) to have occurred at 1850 Ma with the Sudbury impact event. Iron associated with exhalites of VHMS deposits at this time changed from a sulfidised iron to an oxidised iron (Farquhar et al., 2010). The presence of hematite in jasper associated with the deep water (>1000m) Jerome VHMS deposit, Arizona (~1740 Ma), was inferred by (Slack et al., 2007) to indicated the oceans were locally oxygenated in the stability field of hematite, and extrapolate these conditions over a time interval of 1792-1241 Ma.

7.3.5. Results

7.3.5.1. DeGrussa

At the time of sample collection, the C4 and C5 ore lenses were not well defined, hence samples were collected only from the DeGrussa and C1 ore lenses. DeGrussa samples were collected by Condon (2015) from the DeGrussa and Conductor 1 ore lenses for use in her masters study. and were selected based on their different textures, and mineralogical variation (i.e. chalcopyrite, pyrite and sphalerite) with the thin section off cuts from this work are used for this phd study. There is no consistent spatial distribution through the ore deposit. Feeder zone samples, which would provide the best representation for the source of sulfides, were not collected as this was not identified at the time of sample collection.

Chalcopyrite displays $\delta^{34}S$ values between +0.3 and +6.3‰ (n=25; mean 2.1‰), pyrrhotite between +0.9 and +3.3‰ (n=7; mean = +1.6‰). Limited samples of sphalerite returned values of +1.2 and +3.5‰ (n=2; mean +2.4‰). Pyrite has $\delta^{34}S$ values of +0.7 to +10.5‰ (n=52; mean=+3.6‰) (Fig. 7.16, 7.17.). Pyrite samples with the highest $\delta^{34}S$ values were framboidal in

nature (Fig. 7.18) with associated chalcopyrite also displaying positive values. There were no common textural features for the samples with the lightest $\delta^{34}S$ values (Fig. 7.29) although lighter values were mostly found in chalcopyrite-rich samples. Most of the data lies between +1.0 and +4.0‰, with a distinct skew towards values as high as ~+10.0‰. The overall median for all data (n=82) is +3.0‰.

7.3.5.1.1. Barite

As previously mentioned, there is little to no barite present in or around the DeGrussa deposit, although barium is elevated in the hanging wall of the deposit. Only one sample with high barium, DGDD281- 855m (737800mE, 7172800mN), contained visible barite in the form of a large vein. This was drilled using the same method as above, for $\delta^{34}S$ analysis. The vein is located in lower parts of DeGrussa host stratigraphy, approximately 4kms east of the DeGrussa ore lenses and may potentially represent the sea water composition at the time of DeGrussa deposition (2030Ma); this will be reviewed in the discussion. Two analyses were performed resulting in an average value of 38.1‰ (37.9 and 38.3‰) (Appendix 7.5b).

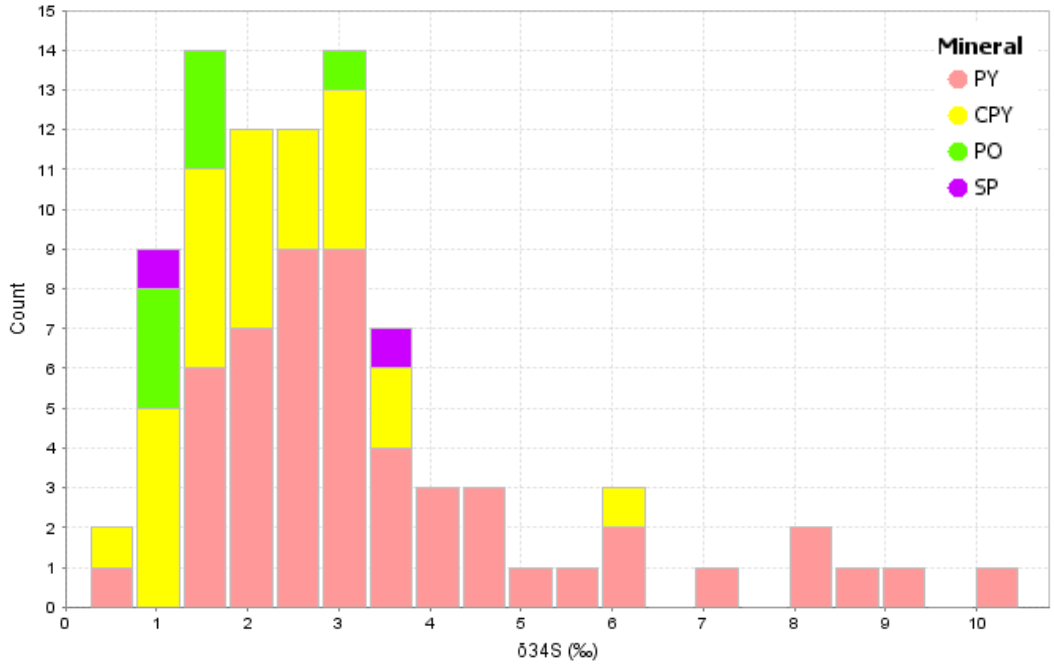

Figure 7.16. Sulfur $\delta^{34}S$ for DeGrussa sulfides (chalcopyrite – cpy, pyrhotite – po, pyrite – py and sphalerite – sp). Chalcopyrite, pyrrhotite and sphalerite characteristically have $\delta^{34}S$ values of 0 - +4.0‰ with pyrites displaying a large range of $\delta^{34}S$ values between 0 and +11.0‰. Higher values of $\delta^{34}S$, above +8.0‰, could be indicative of sea water/biological fractionation.

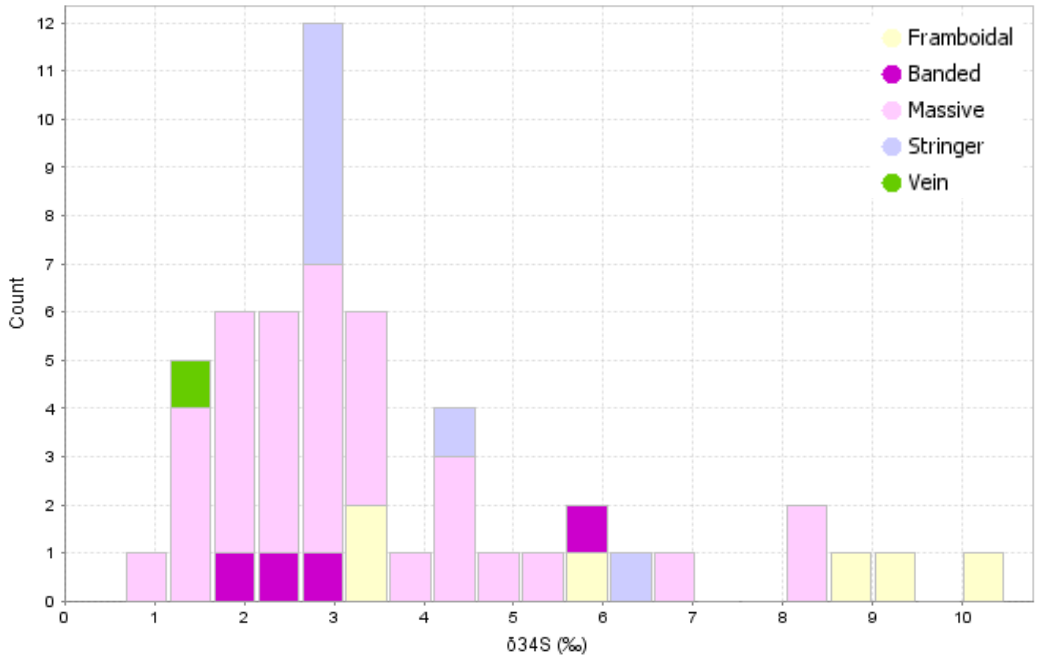

Figure 7.17. $\delta^{34}S$ for pyrite samples at DeGrussa according to texture (banded, framboidal, massive, stringer or vein). All samples of pyrite are fine-grained. Framboidal pyrites are believed to be primary sulfides and plot with heavy $\delta^{34}S$ values of between +8.0 and +11.0‰ (outliers with values of +3.1, +3.2 and +6.0‰). Other sulfides, presumed recrystallised or remobilised, have values largely constrained to between 0 and +5.0‰. As DeGrussa sulfides are fine-grained, thin section analysis is required to distinguish the morphology of individual samples.

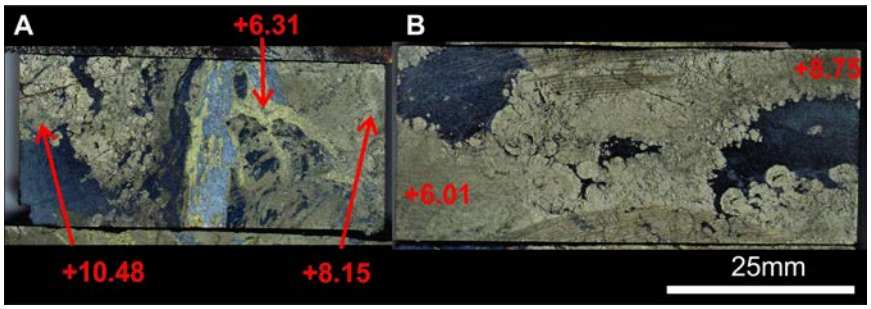

Figure 7.18. Thin section offcuts of heavy $\delta^{34}S$ samples **A.** DGDD053-404.2m, C1 lens (pyrite +7.0 - +10.5‰ and chalcopyrite +6.3‰) and **B.** DGDD014-182.2m from DeGrussa lens (pyrite +6.0 - +8.6‰).

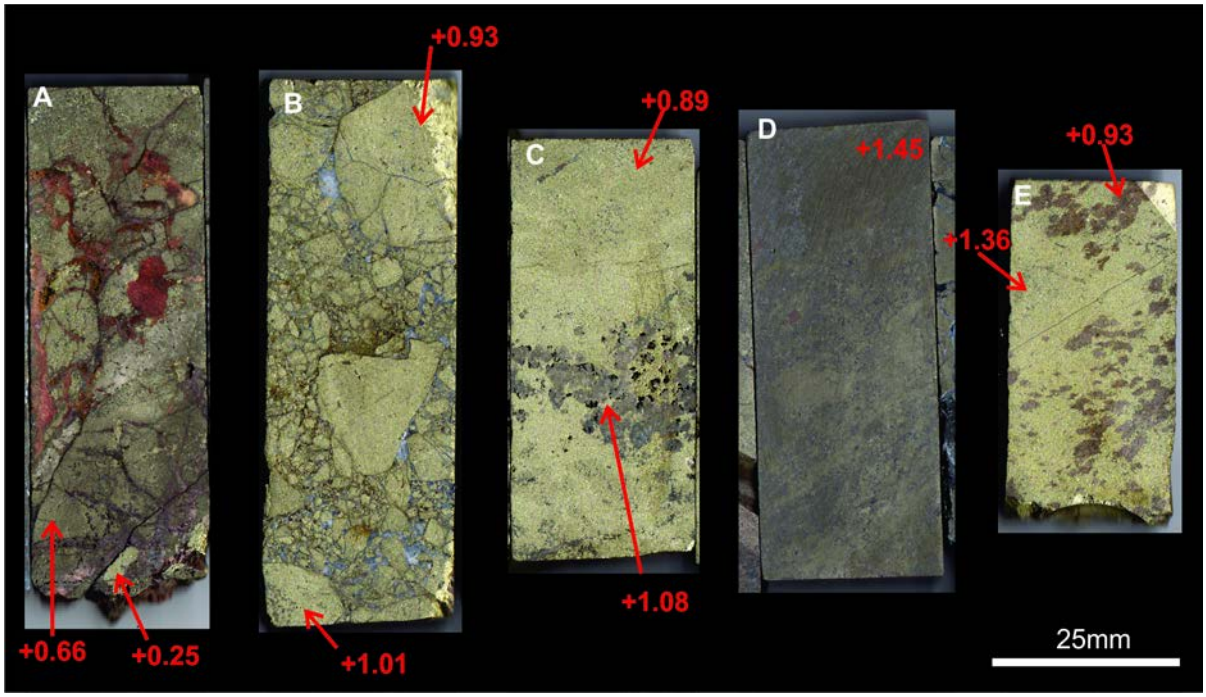

Figure 7.19. The light $\delta^{34}S$ values were found in samples **A.** DGDD015-277.8m (DeGrussa lens, pyrite 0.7‰, chalcopyrite 0.3‰), **B.** DGDD015-285m, a chalcopyrite breccia with carbonate matrix from the DeGrussa lens with values 0.9-1.0‰, **C**. DGDD015-288.1 with chalcopyrite (0.9‰) and sphalerite (1.1‰) from the DeGrussa lens, **D**. DGDD014-315.05m Conductor 1 pyrite (1.5‰), and **E.** DGDD012-282.8m Conductor 1 pyrite (0.9‰,).

7.3.5.2. Horseshoe Lights

The geology of the Horseshoe Lights deposit is provided in Chapter 2 (section 2.9.1.1). Four hand samples were provided by the University of Western Australia, and one from Horseshoe Mining. From these, eight analyses were collected of pyrite and chalcopyrite minerals. Two populations of sulfides were encountered (Fig. 7.20, 7.23), and their disparate character indicated that the full variation at the site is not yet understood. One population contains $\delta^{34}S$ values of +7.3 to 12.4‰. The second contains two analysis from #106878 which have abnormally heavy values of +44.7 to +45.8‰ and are associated with a silicic/chert rich 'sandy' ore (Gillies, 1988). These later two results were repeated, with the same elevated results.

Sulfide textures (Figure 7.21, 7.22, 7.23) included massive pyrite sometimes with chalcopyrite rims in a cherty matrix with consistently heavy $\delta^{34}S$ values of +44.7 to +45.8‰ (106878; Fig 7.21); irregular and angular-subangular pyrites ($\delta^{34}S$ +12.2 to +12.3‰) in quartz-muscovite-epidote-schist with chalcopyrite and chalcocite located in pressure shadows (106855; Fig 7.21; 106875, Fig. 7.23). As discussed in chapter 2, the Horseshoe Lights deposit is highly deformed.

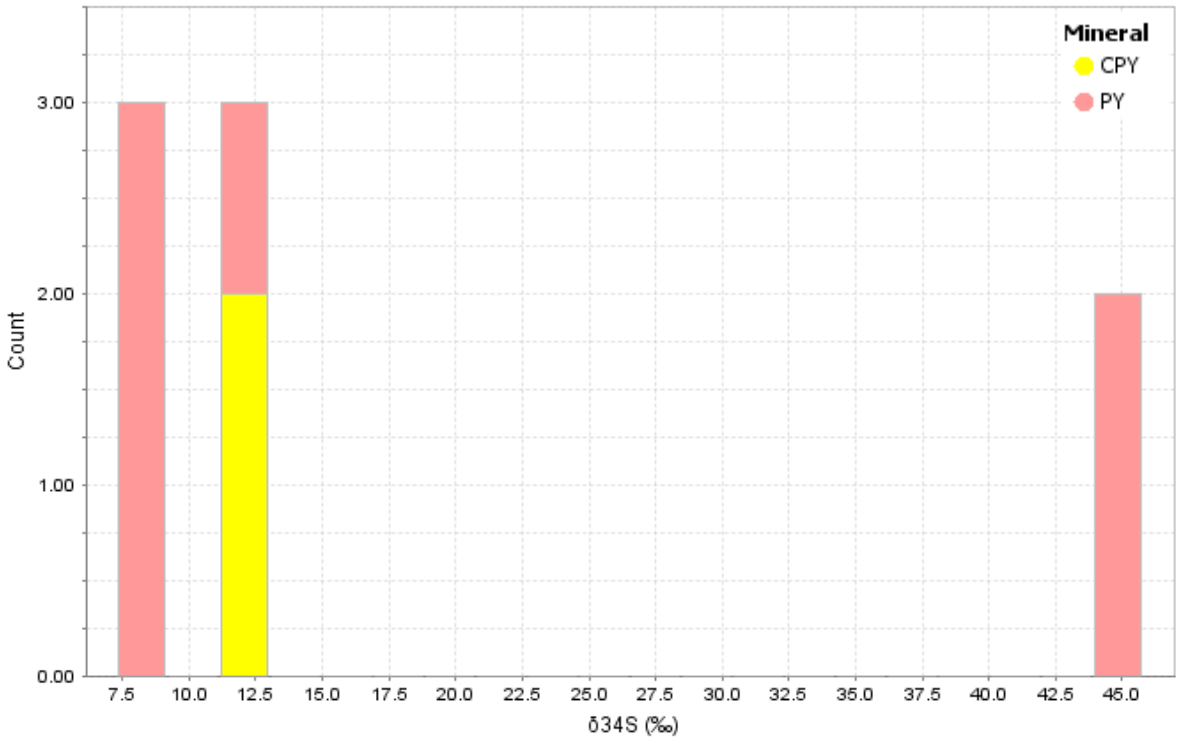

Figure 7.20. Chalcopyrite and pyrite samples analysed for Horseshoe Lights. The majority of samples have $\delta^{34}S$ values of +7.0 to 12.5‰. Two samples from #106878 have abnormally heavy values of 44.6 to 45.8‰.

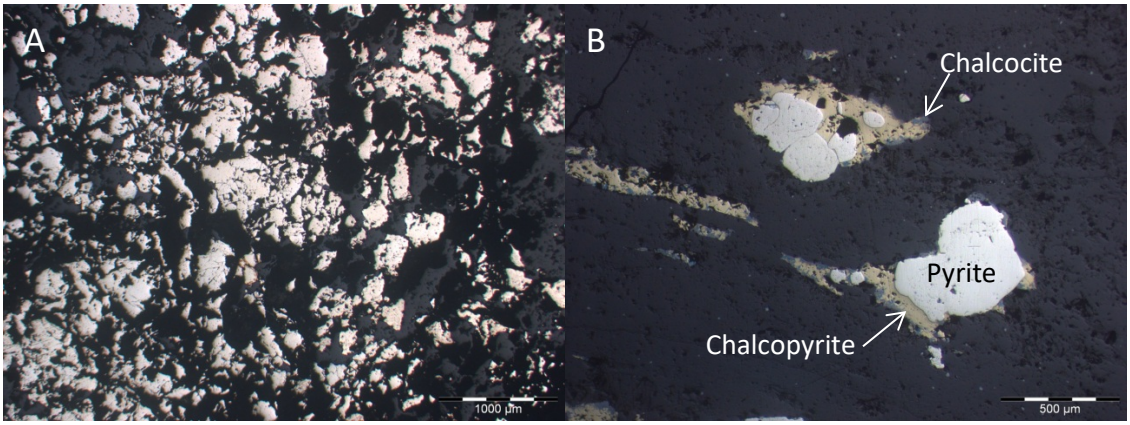

Figure 7.21. Pyrites sampled from the Horseshoe Lights deposit. A. Sample 106878 pyrite with irregular and angular-subangular pyrites. This sample had consistently heavy $\delta^{34}S$ of +44.6 to +45.8‰. **B.** Sample 106855 with chalcopyrite located in pressure shadows of pyrite ($\delta^{34}S$ +12.2 to +12.3‰) grains. Chalcocite is secondary and rims the chalcopyrite. Only pyrite was sampled.

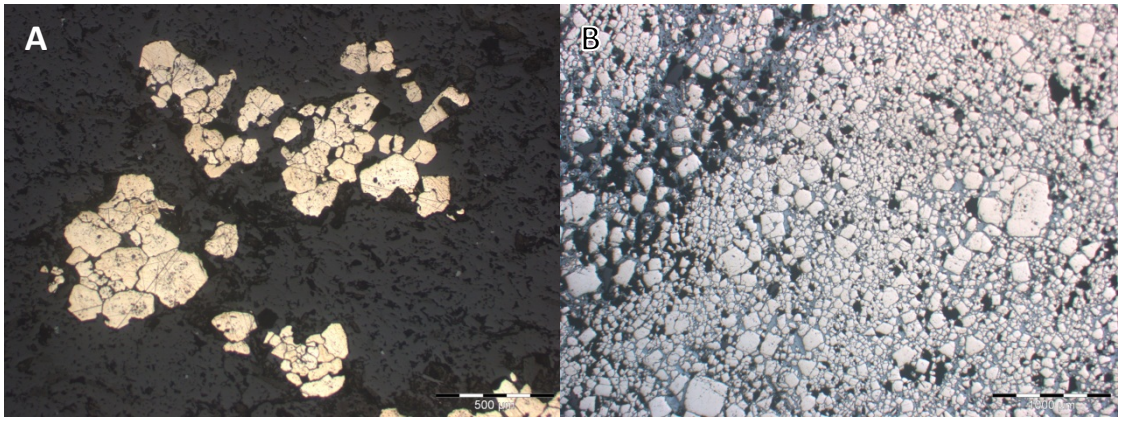

Figure 7.22. Horseshoe Lights pyrite samples. **A.** Pyrites from sample 106875 ($\delta^{34}S$ +12.4‰). **B.** Pyrite from 106865 ($\delta^{34}S$ +8.4 to 9.0‰) fine-grained and fragmental.

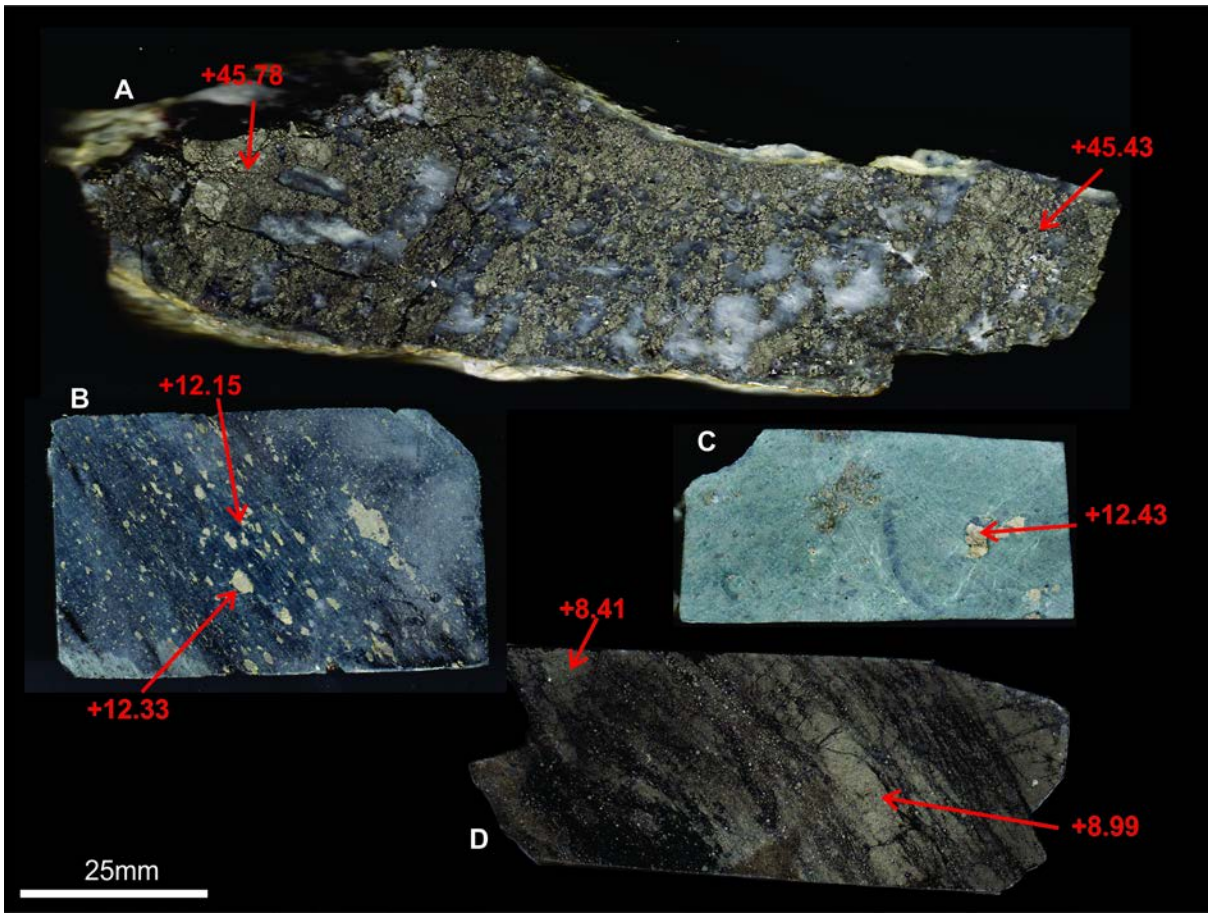

Figure 7.23. Horseshoe Lights sulfur isotope samples in hand sample showing differing textures for different sulfur isotopes **A.** 106878 heavy S isotopes ($\delta^{34}S$ +44.6 to +45.8‰), **B.** 106855 schistose sample (pyrite $\delta^{34}S$ +12.2 to +12.3‰), **C.** Disseminated sulfides in 106875 ($\delta^{34}S$ +12.4‰ in chalcopyrite), and **D.** banded sulfide in 106865 ($\delta^{34}S$ +8.4 to +9.0‰).

7.3.5.3. Thaduna Cu Deposit

The Thaduna Cu deposit (geological summary in Chapter 2, section 2.9.1.2) has primary chalcocite, bornite, chalcopyrite and pyrite. $\delta^{34}S$ values for 16 samples are constrained between +18.6 and +26.7‰ (Fig 7.24). Pyrite is rare in the Thaduna deposit but where present it contains heavier $\delta^{34}S$ values (above +23.5‰; n = 2; mean = +24.3‰) than the main ore bearing chalcopyrite ($\delta^{34}S$ values between +18.6 and +23‰; n = 7; mean = 20.7). Further sampling is needed in future to properly define populations.

Sulfide textures (Fig 7.25) include massive chalcopyrite, carbonate ± quartz vein hosted chalcopyrite, blebby bornite associated with pervasive carbonate alteration and chalcopyrite, and pyrite stringers. Chalcocite is in association with bornite and chalcopyrite, with all three considered primary (Reid, 2013).

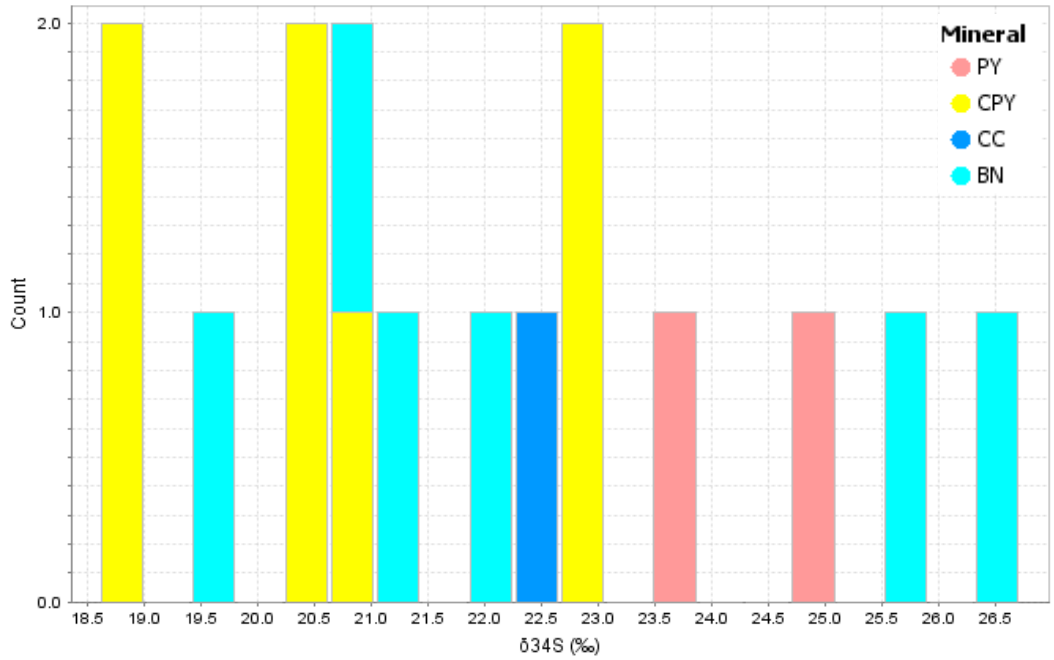

Figure 7.24. $\delta^{34}S$ values of +18.6 to +26.7‰ for bornite, chalcocite, chalcopyrite and pyrite mineralisation at Thaduna Cu deposit. Chalcopyrite has a lighter isotopic signature than pyrite, with bornite displaying a range of values.

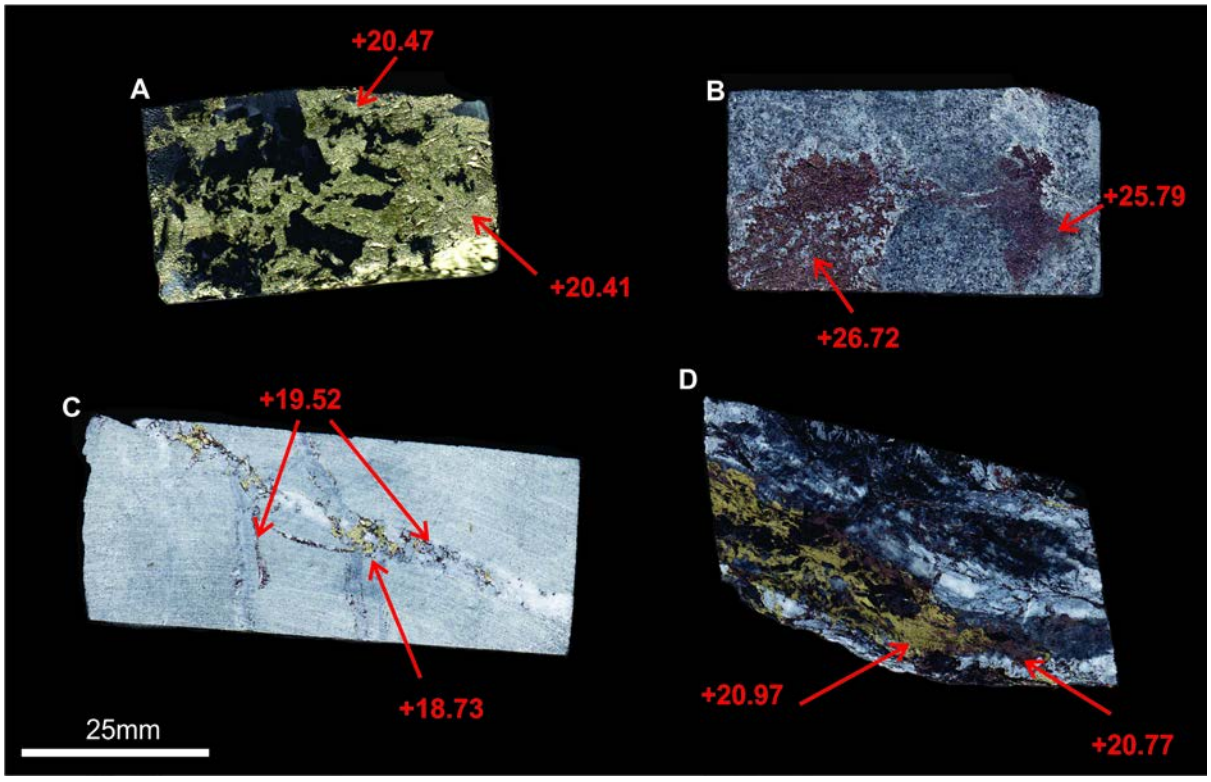

Figure 7.25. Thaduna sulfide samples **A.** Massive crystalline chalcopyrite ($\delta^{34}S$ +20.5‰) from THD003-270.61m, **B.** Bornite ($\delta^{34}S$ +26.7‰) with associated carbonate alteration and the highest $\delta^{34}S$ values in THD220-499.4m, **C.** Carbonate vein hosting chalcopyrite ($\delta^{34}S$ +18.7‰) and bornite ($\delta^{34}S$ +19.5‰) mineralisation in sample THD220-508m, **D.** Chalcopyrite ($\delta^{34}S$ +21.0‰), bornite ($\delta^{34}S$ +20.8‰) and carbonate stringers in sample THD220-525m.

7.3.5.4. Fortnum and Cassidy

Eight samples were analysed for $\delta^{34}S$ at Fortnum (Yarlarweelor and Starlight/Trevs) and three from the Cassidy/Horseshoe open pits. Both deposits have similar geological formation described as 'orogenic' by Groves (1996) and are hosted by ultramafic-mafic rocks of the Narracoota Formation (see chapter 2). Pyrite at Fortnum and Cassidy is euhedral, varying from millimetres to centimetres both in quartz-carbonate veins and in the surrounding wall rock (Fig. 7.26, 7.27).

The Fortnum deposits and Cassidy have $\delta^{34}S$ values between +0.1 and +8.4‰ (n=12; mean = +3.6‰). Fortnum is at the lighter end with $\delta^{34}S$ values between +0.1 and +7.6‰ with an overlap of Cassidy values of +2.3 to +8.4‰ (Fig. 7.27).

Samples from the Starlight deposit display two styles. One sample was banded and consisted of small pyrite grains 0.1-0.2mm in diameter and subeuhedral in shape. These grains have $\delta^{34}S$ values of +4.1 and +5.2‰. Conversely, the large euhedral pyrites (up to 20mm in size) varied in $\delta^{34}S$ values (+0.1 to +7.6‰) but when associated with quartz-carbonate veining typically had decreased $\delta^{34}S$ values (0 to +1.0‰). The highest value (+7.6‰) was from a Starlight euhedral pyrite. The lone Yarlarweelor sample (FTMH009, Fig. 7.26) is associated with carbonate veining and has a light value (+0.3‰).

Cassidy pyrite proximal to quartz-carbonate veins has light $\delta^{34}S$ values (+3.3‰) in comparison to smaller pyrite grains throughout the host rock (+5.2 to +8.4‰). Massive pyrite from the Cassidy deposit has $\delta^{34}S$ values similar to that found associated with quartz-carbonate veins (+2.3‰).

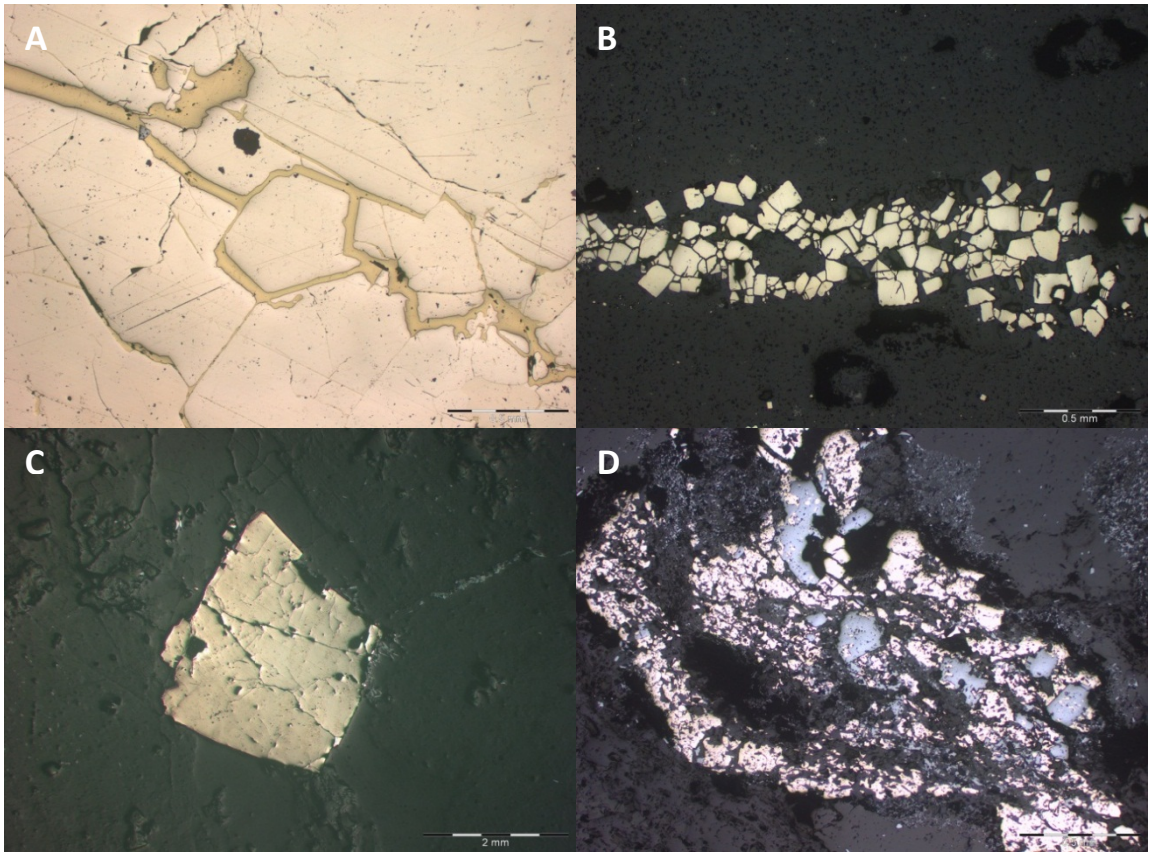

Figure 7.26A. FHMH009A Fortnum massive pyrite from GSWA co-funded drill hole below the Yarlarweelor deposit. Sample contains pyrite with chalcopyrite in fractures. **B.** Pyrite bands in basalt from the Starlight deposit. **C.** Cassidy CS003 large, euhedral pyrite grains. **D.** Cassidy pyrite with chalcocite.

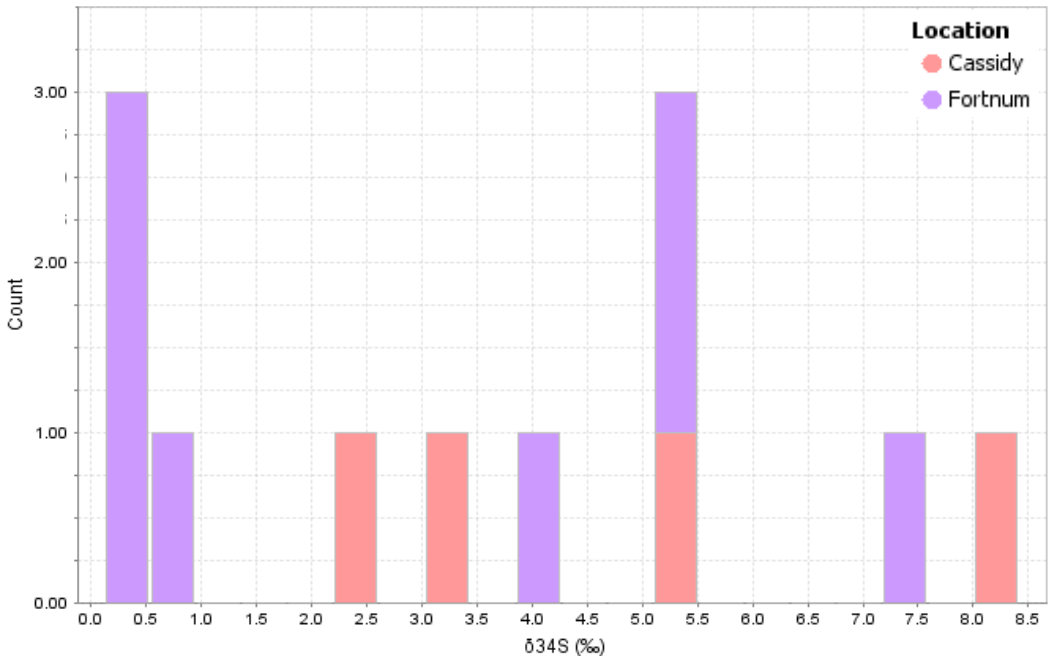

Figure 7.27. $\delta^{34}S$ values of +0.1 and +8.4‰. Fortnum is at the lighter end with $\delta^{34}S$ values between +0.1 and +7.6‰ with an overlap of Cassidy values of +2.3 to +8.4‰

7.3.6. Discussion

7.3.6.1. DeGrussa

As mentioned previously, there was no selective sampling completed for a comprehensive sulfur isotope study on the DeGrussa deposit, and no samples collected from the stringer zone. Hence, the data presented in this thesis can be best used to characterise the ore deposits of the region, and any distinctive features that may assist in later exploration. It has formed a preliminary study of the DeGrussa $\delta^{34}S$ only with a more detailed study required to properly understand the DeGrussa mineralising system.

The DeGrussa pyrites can be split into two morphologies, framboidal and euhedral, with a range of variations between. Heavier $\delta^{34}S$ values are found in the framboidal pyrites – these textures appear to have experienced less deformation. Pyrites with lighter $\delta^{34}S$ values, are fragmental to euhedral, and may have been affected by a secondary sulfur source that added sulfur during recrystallisation. Chalcopyrite has lighter $\delta^{34}S$ values.

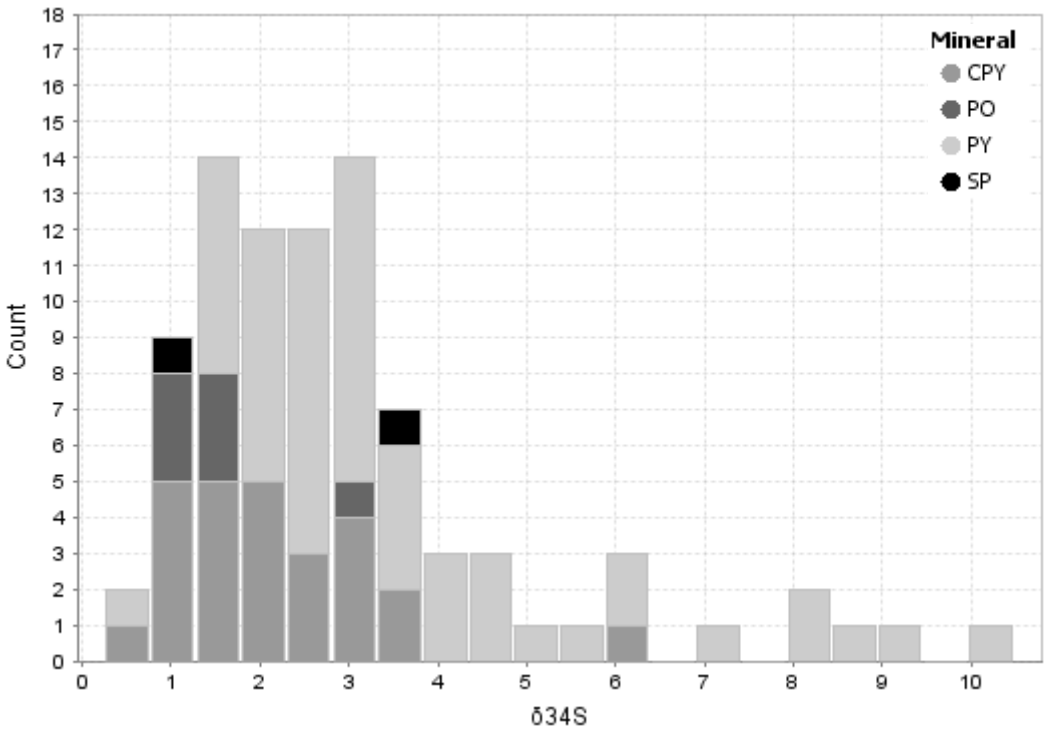

Figure 7.28. Sulfur isotopes for DeGrussa pyrite, chalcopyrite, pyrrhotite and sphalerite.

Reduced sea water sulfate, and sulfur leached from volcanic and sedimentary rocks in the surrounding substrate appear to be the most important in mid ocean ridge environments, whereas a hydrothermal-magmatic sulfur source is the most important in arc environments (Huston et al., 2010). Palaeoproterozoic to Palaeoarchaean deposits have a restricted range for $\delta^{34}S_{sulfide}$ of +1.0 ± 2.6‰, interpreted to indicate that dissolved rock sulfide or hydrothermal-magmatic H_2S were the dominant source or sources of ore sulfur. This would be consistent with very low total sulfur concentrations (2ppm) in Palaeoproterozoic oceans (Ueda et al., 1990, Strauss, 1993, Gellatly and Lyons, 2005, Schröder et al., 2008, Huston et al., 2010). VHMS deposits which are proven to be derived from igneous fluid have $\delta^{34}S_{H_2S} < 0$ ‰, and many down to -10 ‰, and are associated with very acidic alteration assemblages (Huston et al., 2010).

The pyrite, pyrrhotite, chalcopyrite dominant mineralogy of the DeGrussa deposit suggests high temperatures for deposition (pyrite at >350˚C, chalcopyrite at 270-350˚C (Huston and Large, 1989)). Sphalerite may also be coprecipitated depending on the oxygen fugacity, pH and temperature of the system, all which flux between high and low. Sphalerite and chalcopyrite can be coprecipitated, or high temperature minerals can reabsorb sphalerite during high heat flow. At temperatures over 120˚C there are no bacterial reactions, although hot fluids which leak out through the sediments or chimney vents may disperse, leading to bacterial reactions in the cooler surrounding waters and subsurface. Given the consistently positive $\delta^{34}S$ values, and the observed push to more negative values, au significant amount of bacterial reduction acting on an initial fluid of magmatic composition can be discounted as a possible effect for DeGrussa samples.

The range of $\delta^{34}S$ values for the DeGrussa sulfides (+0.3 to 10.5‰) with a peak at 1.0 – 3.0‰ (reflected in chalcopyrite ($\delta^{34}S$ +0.3 to +6.3‰), pyrrhotite (+0.9 and +3.3‰) and sphalerite (+1.2 and +3.5‰)) suggests that the dominant source sulfur is probably igneous (0 ± 3‰; (Chaussidon and Lorand, 1990)) (Fig. 7.28), although skewed values to +10.5‰ require a second source (perhaps an evaporitic or seawater source), or an insitu fractionation mechanism of the input sulfur. All sulfide minerals group closely, so the best interpretation is for a uniform $\delta^{34}S$ of dominantly igneous-sourced sulfur, with temperature and minor seawater sulfate reduction

producing the heavy tail via chimney growth (Peter and Shanks III, 1992, Rollinson, 2013). The $\delta^{34}S$ data are considered to be consistent with a reduced, metal-bearing, hydrothermal fluid, initially of acidic composition (pH 3-5), which leached footwall and host sedimentary and basaltic rocks, and deposited sulfide onto the seafloor and sub seafloor at a pH of 5-8 at temperatures of 270-350°C.

Sulfur isotope geothermometry is based on the equilibrium sulfur isotope fractionations between co-existing sulfur-bearing compounds. The sulfur isotopic fractionations among other important sulfur species in hydrothermal solutions and sulfur-bearing minerals are given in Figure 7.29 (Rye and Ohmoto, 1974). In reduced solutions it can be seen that the major ore minerals in the DeGrussa deposit - pyrite, chalcopyrite, pyrrhotite and sphalerite - show negligible to small isotopic changes due to temperature and even galena is only shifted 2 to 4 ‰ more negative than source H_2S across the DeGrussa VHMS fluid depositional range of 250 - 350°C.

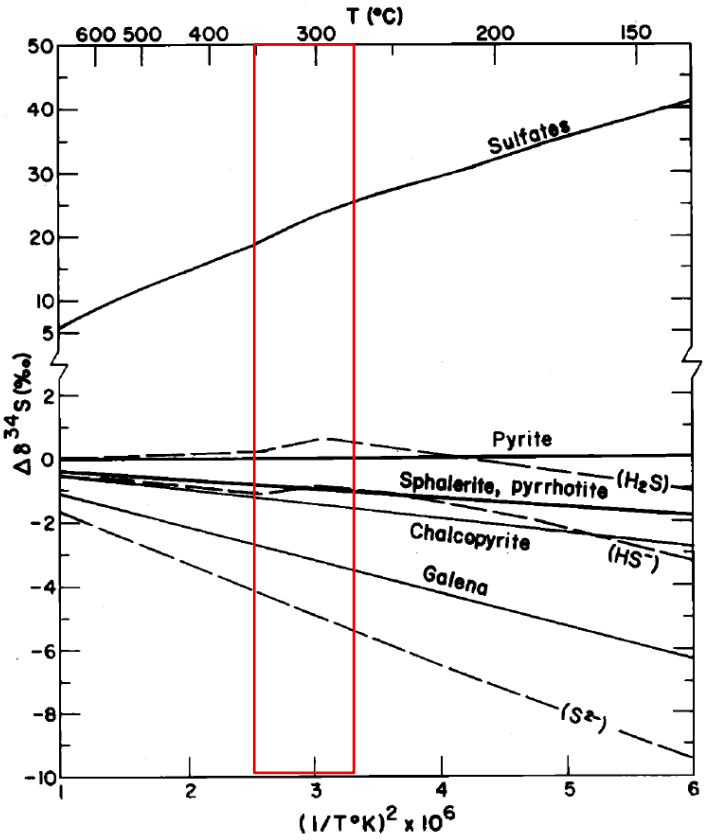

Figure 7.29. The effect of temperature on sulfur fractionation. Sulfur isotope fractionations plotted with respect to pyrite. Dashed lines indicate species in solution. Solid lines indicate minerals (Rye and Ohmoto, 1974). Red lines indicated estimated temperature range for DeGrussa sulfide deposition.

The effect of temperature on the resulting sulfur isotopes for DeGrussa chalcopyrite compared with pyrite should be ~ +1.0 to +1.5‰ lighter, and pyrrhotite/sphalerite ~ +1.0‰ lighter, at temperatures between 270-350°C (Rye and Ohmoto, 1974). The observed differences between mean sulfur isotope values in the DeGrussa deposit are pyrite (+3.6‰)-chalcopyrite (+2.1‰) = +1.5‰; pyrite-sphalerite (+2.4‰) = +1.2‰; and pyrite-pyrrhotite (+1.6‰) = +2.0‰. These values are consistent with work by Rye and Ohmoto (1974) and suggest that the sulfides precipitated from the same sulfur source. The sphalerite and pyrrhotite have a slightly higher difference reflecting either deposition at a lower temperature, or reflecting the small sample size.

Chalcopyrite-rich VHMS deposits are also found at the Brothers volcano, Kermadec Arc, Lau basin (de Ronde et al., 2011). These present day deposits are interpreted to form from magamatic volatiles exsolved from magma with some mixing with ambient sea water directly in the sub seafloor. Cu isotope studies by Berkenbosch et al. (2015) interpret δ^{36}Cu values of -0.03 to 1.4‰ to represent a mantle source for the Cu in the Brothers deposit. This is supported by the δ^{34}S values presented by de Ronde et al. (2011) for sulfides in the chalcopyrite rich NW caldera in the Brothers hydrothermal field that range from -0.6 to -5.7‰ (average -3.0‰) suggested to reflect a high temperature, hydrothermal-magmatic source for sulfur under oxidised conditions.

The Guaymas basin is another present day location, which perhaps formed in a tectonically similar setting to the DeGrussa deposit. The Guaymas is a sedimented (>500m thick sediments), active rift basin in which a complex of basaltic sills and dikes has intruded the sedimentary rocks (Peter and Shanks III, 1992). The δ^{34}S values for talc-pyrrhotite (lesser sphalerite, galena and chalcopyrite) –rich deposits of the southern Guaymas basin are between -3.7 and 4.5‰. These values are interpreted by Peter and Shanks III (1992) as a result of several sulfur sources; the dissolution of sulfide in basalt rocks, the thermal reduction of seawater sulfate during sediment alteration reactions to give positive δ^{34}S values, and entrainment or leaching of isotopically light bacteriogenic sulfide from sediments underlying the deposit giving negative δ^{34}S values. DeGrussa may have similar sources for the sulfur seen in sulfide mineralisation, although bacteriogenic sulfide reduction is considered unlikely.

Volcanic rocks proximal to DeGrussa mineralisation are dolerite and basalt. Some basalt is believed to be part of the host rock sequence, however dolerite is syn- to post- mineralisation (See chapter 6. Intrusive dolerite within the DeGrussa host sequence is 1991 to 2003 Ma). Recent work by Hilliard et al. (in prep) suggests the footwall dolerite is also intrusive, although its emplacement age is unknown and mafic volcaniclastic rocks of the Magazine member are also believed to have been present at the time of mineralisation. Carbonate alteration at the edges of dolerite sills indicates some alteration of dolerite on contact with surrounding wet sediments in likely, although the amount of copper this is likely to contribute to mineralising fluids is minor. However the composition of the sedimentary rock in the footwall and Johnson Cairn Formation is likely derived from mafic rock sources as well as the Yilgarn craton, indicating this as a possible source for the S isotopes seen in DeGrussa mineralisation. The model in Figure 7.30 summarises the potential sulfur sources and $\delta^{34}S$ values of the hydrothermal-mineralising components. It is important to note that;

1. There is no value for seawater locally. The DeGrussa basin may or may not be restricted at the time of mineralisation. If it is restricted, the $\delta^{34}S$ of seawater sulfate may not follow that of the oceans. The average palaeoproterozoic seawater $\delta^{34}S$ values are +10 to +18 ‰ (Scott et al., 2014).

2. The $\delta^{34}S$ values of the sediments interacting with any mineralising hydrothermal fluid are unknown. Footwall sedimentary rocks, and host sedimentary rocks are derived from the Archean Yilgarn Craton and Marymia Inlier. As such, it is assumed that the $\delta^{34}S$ values of these rocks will reflect the Archean seawater $\delta^{34}S$ values of 0 ‰.

3. We can presume that the basalt (and dolerite) present within the host rock sequence has $\delta^{34}S$ values of ~ +1 ‰.

4. Some magmatic input is plausible ($\delta^{34}S$ values of -3 to +1 ‰), although no negative $\delta^{34}S$ values are present. Mixing of magmatic values with seawater values (+10 to +18 ‰) could form the resulting spread of $\delta^{34}S$ values in DeGrussa mineralisation.

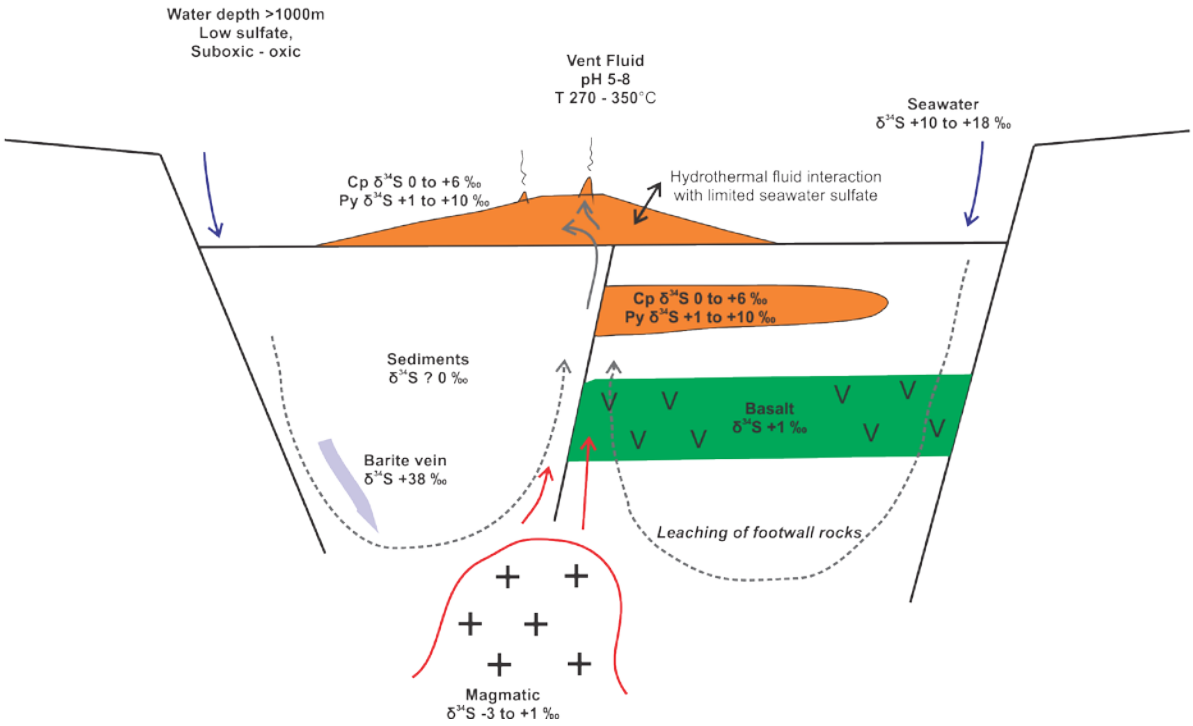

Figure 7.30. Schematic representation of the DeGrussa deposit and the transport and distribution of known $\delta^{34}S$ values. Leaching of footwall mafic rock (+1 ‰) and sedimentary rock (~ 0 ‰) with some hydrothermal-magmatic input is likely. A small amount of interaction between mineralising hydrothermal fluids and sea water sulfate is likely to explain the heavy tail to $\delta^{34}S$ histogram values. The barite vein may be related to the hydrothermal system but is more likely to reflect a different sulfur source such as metamorphic fluids.

The $\delta^{34}S$ values for pyrite and chalcopyrite could then represent a mix of leached rock sulfur (basalt and sediments from the footwall and host rock sequence), igneous sulfur, and minor seawater sulfate. Most $\delta^{34}S$ values for sulfides are ~ 0 to +3‰ indicating that the sulfur comes from leaching of rocks (0 to +1 ‰) with minor addition of seawater (+10 to +18 ‰) reflected in the skew to heavy $\delta^{34}S$ values. A dominantly leached igneous sulfur source is supported by a lack of lead-bearing minerals in the deposit (i.e. pyrite contains minimal Pb and there is scarce galena through the deposit, with that present likely derived from sedimentary rocks (see also chapter 6)). This is similar to mineralogy seen in present day VHMS deposit of the Galapagos Spreading Ridge (Embley et al., 1988).

DeGrussa was formed at approximately 2.03 Ga in a transitional atmospheric and oceanic environment. The lack of sulfate minerals in the ore, but the presence of peripheral jasper, suggests that DeGrussa formed in a sub-oxic to oxic, low sulfate oceanic sub-basin from reduced, metal-bearing fluids. The latter scenario produces barite-poor, Cu-Zn deposits in modern mid-ocean ridge basins (Huston and Logan, 2004). Hydrospheric conditions of the deep basin water globally were probably Fe-rich and sulfate free, leading to the lack of a sulfate-bearing exhalite. In the place of a barium exhalite typical of VHMS deposits in later eras, is a talc-carbonate rock (see chapter 3) which may have originated as a Si-Ca-Mg rich unit.

The barite vein, with average $\delta^{34}S$ value of +38.1‰ (n = 2), is a candidate to represent the basin water composition at the time of DeGrussa deposition, and sits close to the pyrite $\delta^{34}S$ curve provided by Kump (2012), but is almost twice as heavy as the average seawater sulfate curve provided by Farquhar et al. (2010) (Fig. 7.31). Sangster (1968) identified that in Palaeozoic deposits, $\Delta^{34}S_{\text{seawater sulfate – ore sulfate}}$ was ~ 17‰ lower than coeval seawater sulfate (Large, 1992, Huston et al., 2010). The $\Delta^{34}S_{\text{seawater sulfate – ore sulfide}}$ between the barite vein and the DeGrussa sulfide median is +29.3‰. The only comparable value to the heavy $\delta^{34}S$ values of the barite vein are those of pyrite at Horseshoe Lights. It may be that the barite vein has no association with $\delta^{34}S$ seawater compositions, and that it reflects an unknown heavy $\delta^{34}S$ source.

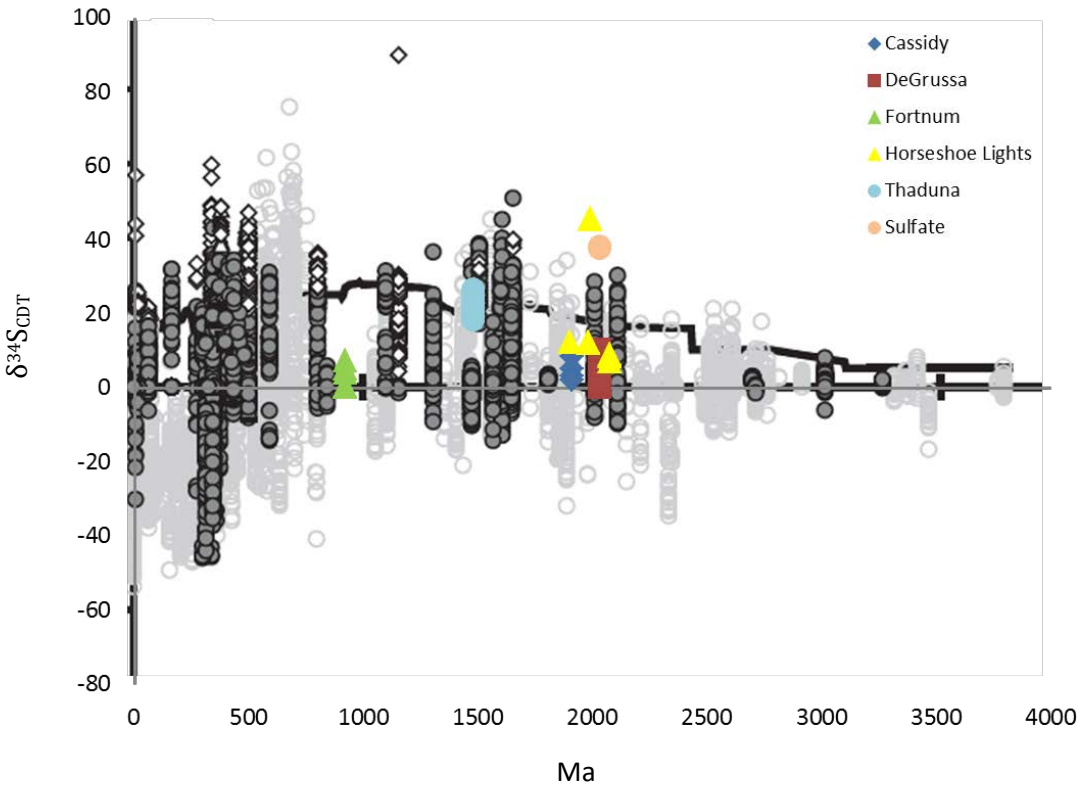

Figure 7.31. Approximate range of $\delta^{34}S$ values (‰) base metal sulfides (filled grey circle symbols), sulfate (unfilled diamond symbols) and sedimentary pyrite (unfilled light grey circle symbols) from Farquhar et al. (2010) with the Bryah/Yerrida sulfide and sulfate values in colour. The black line is the $\delta^{34}S$‰ seawater sulfate curve. With the exception of the heavy Horseshoe Lights samples which sits above the curve at 2000 Ma, $\delta^{34}S$ values of DeGrussa and regional deposit sulfide sit between 0‰ and the seawater sulfate curve, and with similar values in comparison to other deposits of similar age. The barite (orange), potentially associated with DeGrussa, sits well above the seawater sulfate curve and has more similarity to the anomalously high $\delta^{34}S$‰ at Horseshoe Lights.

7.3.6.2. Horseshoe Lights

Positive Horseshoe Lights pyrite values come from a rock (sample #106878) that contained pyrite and quartz with some chalcocite. Horseshoe Lights end member values of +45.0‰ provide evidence of a ^{34}S-enriched source or a closed system mode of sulfur fractionation, capable of isolating extremely ^{34}S enriched H_2S. On the basis of high temperatures needed to form the chalcopyrite-pyrite-gold assemblage, surface weathering processes can be discounted for Horseshoe Lights.

Apart from the anomalous high values in one sample, all other samples fall within a defined range of $\delta^{34}S$ values (+7.3 to 12.4‰). In sample 106855 (Fig. 7.21, 7.22) both chalcopyrite and pyrite have similar $\delta^{34}S$ values of 12.2 and 12.3‰ respectively. The presence of small amounts of chalcocite on the rims of chalcopyrite and pyrite, although avoided if possible, appears to have

had no effect on the $\delta^{34}S$ in the samples. There is no sample of pure chalcopyrite analysed for the deposit. The $\delta^{34}S$ values are significantly higher (10‰) than DeGrussa sulfide samples, and are interpreted to require a greater proportion of ^{34}S-enriched sulfur source.

The heavier $\delta^{34}S$ values (+44‰), from silicic/chert rich 'sandy' ore (Gillies, 1988) could be compared with $\delta^{34}S$ of sulfidic chert at the Hellyer deposit in Western Tasmania, where $\delta^{34}S$ of sulfide in paragenetically early veins in the outer stringer envelope zone have values of 11.9 to 40.7‰ as well as high barite $\delta^{34}S$ (barite cap: 32.4 to 46.0‰ and footwall stringer veins: 19.1-49.5‰)(Gemmell and Fulton, 2001). In the footwall of Hellyer, sulfur isotope variations are explained by a model in which hydrothermal fluids initially consist of totally to partially reduced seawater sulfate that evolves into a fluid dominated by igneous rock sulfur as the convection system intensifies and penetrates deeper into the footwall (Gemmell and Fulton, 2001).

The depositional conditions at Horseshoe Lights are similar to that at DeGrussa although further sampling is required to fully characterise the Horseshoe Lights deposit. As discussed in Chapter 5, the tectonic setting may have been a continental-oceanic rift setting, with the rift being more developed and associated with island-arc activity at Horseshoe Lights. Without further data about the tectonic setting and nearby geology, reasons for the unique isotopic values cannot be easily determined, but the high overall $\delta^{34}S$ values require a seawater sulfate-type component, despite the fact that Palaeoproterozoic seawater sulfate abundance was much lower than in today's oceans.

7.3.6.3. Thaduna

The Thaduna copper deposit is believed to be an example of a fault-controlled Cu deposit (see chapter 2)(Pirajno and Adamides, 2000), in contrast to the VHMS style Cu mineralisation widely found throughout the Bryah Group. The Thaduna Cu deposit is hosted in the Thaduna Formation of the Yerrida Basin, located stratigraphical above the evaporites of Bubble Well Member of the Juderina Formation, although original evaporite minerals in the Bubble Well Member have been replaced by chert and minor barite (El Tabakh et al., 1999).

Mobilisation of saline fluids derived from the Bubble Well Member along the faults by hydrothermal circulation may have transported the Cu. The host rocks for Thaduna mineralisation are pre- to syn- DeGrussa host rock deposition and mineralisation (2.1 - 2.0 Ga), and the estimated age of Thaduna mineralisation is 1475 ±50 Ma (Chapter 6, (Hawke et al., 2015)). At this time, the $\delta^{34}S$ of ocean sea water was approximately +20 to +25‰ (Farquhar et al., 2010) (Fig. 7.31).

The large range (+18.6 and +26.7‰) and characteristic very heavy $\delta^{34}S$ values of the Thaduna pyrite-chalcopyrite-chalcocite-bornite mineralisation are very likely to have required a large component of a sea water source for sulfur. Further sampling is needed in future to properly define populations, although comparisons can be made with sedimentary-hosted Cu deposits. Sedimentary rock-hosted stratiform Cu deposits form by movement of oxidized, Cu-bearing fluids across a reduction front that results in the precipitation of Cu sulfides (Hitzman et al., 2010). Evaporites, basinal brines and sulfidic hydro-carbons may be some of the sources for sulfur, and generally form in continental rift settings (Farquhar et al., 2010). $\delta^{34}S$ values of Neoproterozoic seawater were +18.6‰ to +21.0‰ V_{CDT} (El Desouky et al., 2010). If Thaduna formed from seawater sulfate, the very positive $\delta^{34}S$ values require large amounts of inorganic sulfate reduction (i.e. quantitative conversion of seawater sulfate or it's buried evaporate equivalent). The $\delta^{34}S$ values for Thaduna chalcopyrite, bornite and chalcocite, may reflect a heavy sulfur source combined with $\delta^{34}S$ values leached of the host rocks of the Thaduna Formation, underlying evaporate rocks of the Bubble Well Member and a possible seawater sulfate component.

7.3.6.4. Fortnum and Cassidy/Horseshoe

Further sampling is needed to properly characterise the Fortnum and Cassidy/Horseshoe gold deposits and their relationship to VHMS mineralisation, as no clear peaks in the data form from the small sample size (n=12). These deposits are highly deformed and geochronological work (chapter 2) identifies the mineralisation as much younger than DeGrussa. (Fortnum-Starlight, 920 ± 50 Ma; Cassidy/Horseshoe, 1940 ± 30 Ma; no age for Fortnum-Yarlarweelor). Fortnum

$\delta^{34}S$ pyrite values between +0.1 and +7.6‰ overlap with Cassidy $\delta^{34}S$ pyrite values of +2.3 to +8.4‰. The Fortnum and Cassidy $\delta^{34}S$ values (between +0.1 and 8.4‰), comparable to igneous values, and could represent leaching of the host Narracoota Formation rocks (estimated at 0 to +1 ‰ similar to estimated values of the DeGrussa host rock sequence) or Archean basement sulfur. As with DeGrussa, the heavy tail may indicate mixing with $\delta^{34}S$ values of host rocks which have preserved the seawater sulfate at the time of their deposition (c. 2.0 Ga, and $\delta^{34}S$ of seawater of +10 to +18 ‰). This interpretation is limited as no $\delta^{34}S$ data has been collected for the host rocks or sea water in the Fortnum or Cassidy/Horseshoe deposit regions.

Lighter $\delta^{34}S$ values may indicate metamorphic effects on the Fortnum gold deposits (due to the euhedral nature of the pyrite analysed and possible homogenisation of S isotope with metamorphic fluids), however, parts of the Fortnum deposits, are described as 'jasperoid' (Gotthard, 2005) and potentially may represent a VHMS related exhalite and hence similar $\delta^{34}S$ values to that of DeGrussa could result.

Additionally, pyrite samples associated with carbonate veining in these deposits have lighter $\delta^{34}S$ values (0 to +1‰) than pyrite samples taken from within the host sedimentary rocks (+4.06 to 8.41‰). It is postulated here, that sulfur may have been stripped from the surrounding ultramafic and mafic rocks during deformation and redeposited in veins. The ultramafic and mafic rocks would presumably have $\delta^{34}S$ comparable to igneous-rock values (~0 to 1‰). A second, minor source of sulfur may account for the heavier $\delta^{34}S$ values, up to +8.4‰ at Cassidy and +7.6‰ at Fortnum-Starlight. The Ravelstone Formation, a sequence of lithic and quartz wacke, shale and siltstone deposited as 'rift-fill' (Pirajno et al., 2004), forms the major sedimentary rock unit around these mines. The possibility exists that the sulfur was sourced from hydrothermal leaching of this sedimentary rock unit. Sea water at ~1940 Ma (the age of Cassidy mineralisation) is approximately 20‰ and at ~920 Ma (the age of Fortnum mineralisation) $\delta^{34}S$ is approximately 25-30‰ ((Farquhar et al., 2010), see Fig. 7.31).

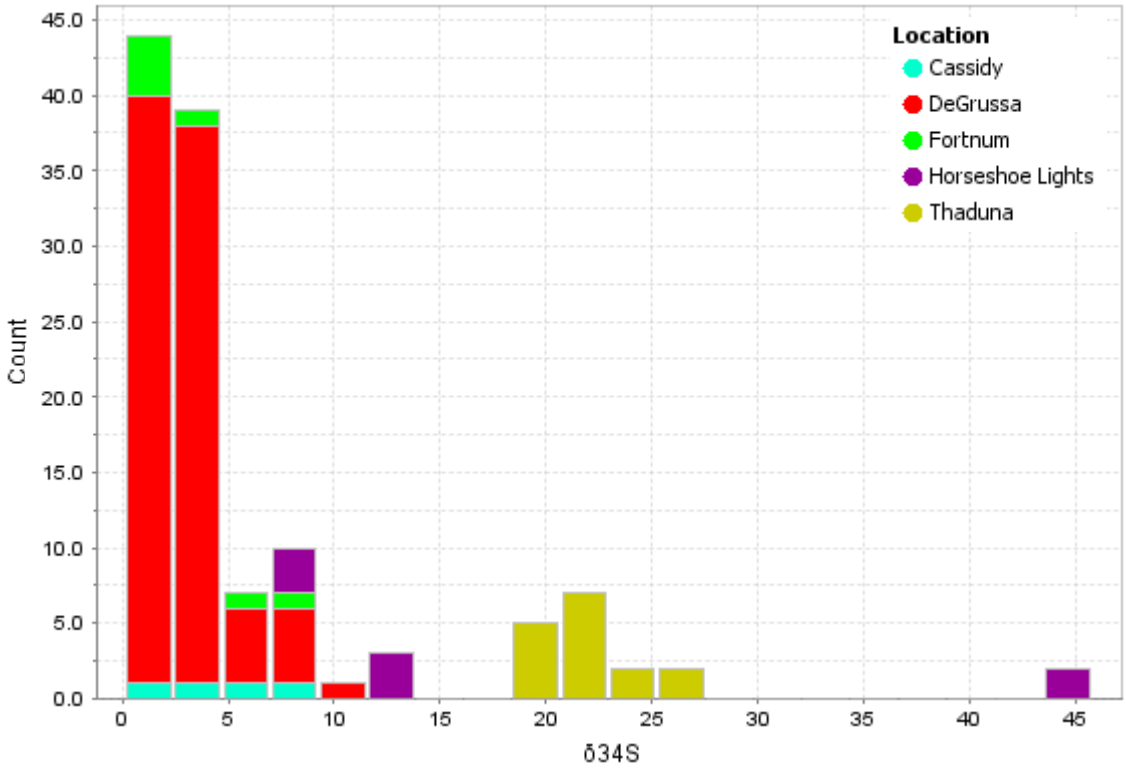

Figure 7.32. Comparison of S isotopes by deposit. Cassidy, Fortnum and DeGrussa are indistinguhisable from each other, with the exception of DeGrussa having a range of S isotopes to heavy values in framboidal pyrites. Horseshoe Lights displays two different populations of S isotope. A population similar to the framboidal pyrites of DeGrussa with $\delta^{34}S$ values of +7 - +15‰, and a second heavy population at +43 - +46‰. Thaduna Cu Mine forms a discreet population at values of +18 - +27.5‰ suggesting a source from evaporitic fluids.

7.3.6.5. Deposit Comparisons

Used as an exploration indicator, there is no unequivocal value at which a DeGrussa-style VHMS can be distinguished from the orogenic gold deposits of Fortnum and Cassidy, although the Fortnum-Cassidy/Horseshoe population lacks the very distinct $\delta^{34}S$ peak of DeGrussa, possibly as a function of the small sample size (Fig. 7.32). The few $\delta^{34}S$ values at DeGrussa above +8.5‰ somewhat separates the DeGrussa deposit from Fortnum and Cassidy/Horseshoe, although the Horseshoe Lights isotopes then fall into this range.

Deposits of Thaduna Cu-type, can be clearly defined from all other deposits, with values between +18.6 to 26.7‰, not overlapping with any other deposit analysed in the district. These values reflect a saline evaporite sulfur source or modified contemporary sea water sulfate. Cu occurrences throughout the Yerrida Group sedimentary rocks, may result in similar results, however, a wider regional study, with better sample context, needs to be completed.

It is unclear whether obtaining sulfur isotopes on regional sulfides of unknown affiliation would enhance prospectivity ranking in the basin on its own. However, combined with other geological evidence, such as rock type and tectonic setting, they may provide a better indication. Given the overlap between the different types of deposit in the Bryah Basin, sulfur isotopes are much more useful for determining the source of sulfur and mineralising processes, rather than the type of deposit the mineralisation is from.

7.3.7. Summary and future work

1. S isotopes can clearly distinguish the fault-controlled Thaduna copper deposit from VHMS ores and orogenic gold deposits across the rest of the region. Fortnum and Cassidy are not easily distinguished isotopically from the DeGrussa deposit at the current extent of sampling. The Horseshoe Lights deposit is comparable with the higher range of DeGrussa values, however, it has very distinct high values >+40‰ which are highly distinctive but require further sampling to properly understand their significance.

2. It is suggested that DeGrussa was deposited into a deep (>1000m), oxidised, low-sulfate ocean basin or sub-basin as seafloor and sub seafloor mineralisation. $\delta^{34}S$ data are considered to be consistent with a reduced, metal-bearing, hydrothermal fluid, initially of acidic composition (pH 3-5), which leached footwall and host sedimentary and basaltic rocks, and deposited sulfide onto the seafloor and sub seafloor at a pH of 5-8 at temperatures of 270-350°C. A hydrothermal-magmatic component cannot be ruled out, however, $\delta^{34}S$ values of a magmatic component cannot be distinguished from other sulfur sources. The heavy tail to the DeGrussa $\delta^{34}S$ data is comparable to those seen in VHMS systems with a chimney component (e.g. the Guaymas Basin (Peter and Shanks III, 1992).

3. This study was a preliminary sulfur isotope study and was based on samples collected by Condon (2015) which focused on different ore textures. A study which focuses specifically on sulfur isotope distributions throughout the DeGrussa deposit – including the stringer/feeder

zone, and alteration halo is required to confirm any differences between sulfides in different parts of the ore lens.

7.4. Pb Isotopes

7.4.1. Aim

In addition to the geochronology shown in Chapter 6, this section uses Pb isotopes to determine the likely source of Pb in DeGrussa mineralisation in relation to the models discussed above. Comparisons of the Pb isotopes will be made between DeGrussa with deposits in the east Capricorn region as well as other Western Australian VHMS deposit. Comparisons will also be made with VHMS deposits around the world in order to identify any similarities or differences in the sources for lead in these deposits.

7.4.2. Introduction

The Pb isotopic composition of the crust and mantle changed through time in a systematic manner as the result of addition from U and Th. This temporal change provides the basis for Pb-Pb model ages. A number of different models have been used to determine Pb model ages for ore deposits. These include the single stage model of Cumming and Richards (1975) which has the U to Pb ratio ($^{238}U/^{204}Pb$) in the crust increasing through time (referred to as Model III in the original publication). This model implies a relatively young apparent age for the Earth of 4.5 Ga (Dickin, 2005) but the curve has been developed based on a model which involves the least number of assumption and describes the average behaviour of Pb.

In comparison, Stacey and Kramers (1975) break terrestrial Pb evolution into two parts using Canyon Diablo Pb and average modern Pb to anchor the ends of a composite growth curve. It defines the age of the earth to be 4.57 Ga with a stage 1 closed system Pb evolution from 4.57 Ga to time t_1 and stage 2 closed system with different μ value from t_1 to present (where t_1 = 3700 Ma, selected at the point at which the plot yields the best fit of model ages to accepted ages for conformable galenas worldwide).

The Plumbotectonics model of Zartman and Doe (1981) attempts to model the geochemical behaviour of U, Th and Pb among the four major terrestrial reservoirs – 1. the lower crust, 2. mantle (<500 km depth), 3. orogene and 4. upper crust. Because continental accretion began at approximately 4.0 Ga and frequent orogenies mixed mantle and crustal sources to form differentiated crustal blocks, they modelled orogenies at 400 million year intervals with decreasing mantle contribution through time. Crustal contributions represented erosion and continental foundering. Orogenies are a mix of U, Th and Pb extracted from the lower crust, mantle and upper crust (Fig. 7.33).

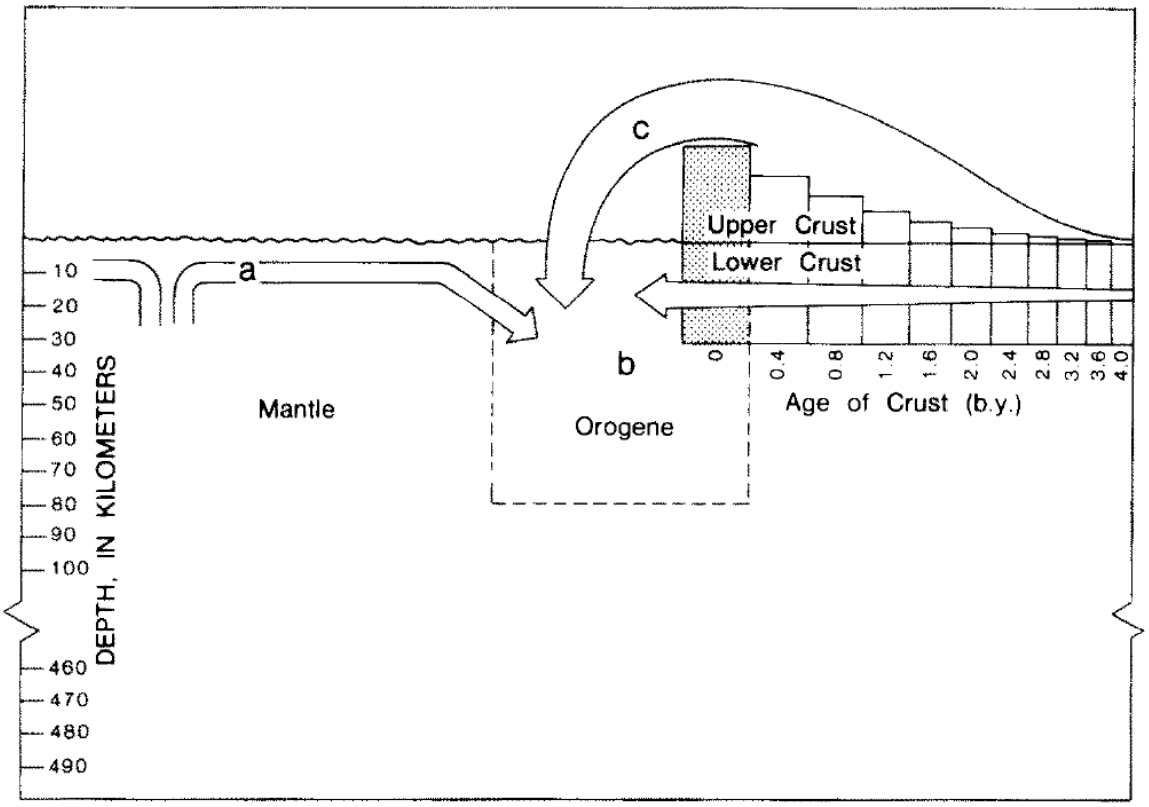

Figure 7.33. Configuration of reservoirs showing locations of mantle, upper crust, lower crust and orogene. The arrows represent the transport of material into the orogene during the last orogenic cycle which produced the stippled block of new crust (Zartman and Doe, 1981). The orogene composition generated by the plumbotectonics model was constrained empirically to fit galena ores. The upper crust develops radiogenic Pb, which is balanced by the development of an unradiogenic lower-crustal reservoir due to preferential retention of Pb relative to U during granulite-facies metamorphism of the lower crust.

Pb isotopic ratios from high Pb low U minerals in hydrothermal ore deposits reflect the source region for mineralising fluids and the timing of mineral formation in respect to growth curves. Data which plot above the average crustal growth curves implies higher $^{238}U/^{204}Pb$ (μ) in the source of the mineralising fluids which are typically interpreted to represent a Pb source from upper crustal sedimentary rocks (Zartman and Doe, 1981). Conversely data that plots below the average crustal growth curve are interpreted to represent a mantle origin for the Pb.

Sato and Sasaki (1980) described the Pb isotope characteristics of the Besshi deposits of Japan (comparable in host rocks, mineralogy and morphology to that of the DeGrussa deposit), with low $^{207}Pb/^{204}Pb$:$^{206}Pb/^{204}Pb$ ratios in comparison to the Cumming and Richards (1975) ore lead curve suggesting retarded Pb evolution, probably due to enrichment of Pb (relative to U) of the sub-arc mantle wedge during long lived subduction, followed by tapping of that Pb during the melting of the supra-subduction zone mantle.

7.4.3. Method

Pb-Pb isotopic determination was performed on two galena-rich samples from the DeGrussa and Conductor 5 ore lenses as well as three pyrite samples from Conductor 1 and Conductor 4 (See chapter 6, Table 6.?) from within Pb-rich massive sulfide horizons. Analysis was undertaken using the solution method outlined by Townsend et al. (1998) for the two galena samples from DeGrussa and C5, and by LA-ICPMS for all other samples. All of the work was undertaken at the University of Tasmania, Hobart. More details of the methods are provided in chapter 6 (Appendix 6.2 and data located in Appendix 6.5).

Pb isotope data was also compiled from studies of VHMS deposits around the world (e.g. Besshi, Japan (Sato and Sasaki, 1980); Iberian Pyrite Belt, Portugal/Spain (Marcoux, 1998, Relvas et al., 2001); Norwegian VHMS deposits(Fox et al., 1988); Roseberry, Hercules, Que River, Hellyer, Australia (Gulson and Porritt, 1987); Abitibi-Wawa belt, Canada (Thorpe, 1999); Flin Flon, Canada (Sangster, 1972); Windy Craggy, Canada (Peter and Scott, 1999); Chahgaz, Iran (Mousivand et al., 2011), Alaskan VHMS deposits (Ayuso et al., 2007); Skellefte district, Sweden

(Billstrom and Vivallo, 1994, Rickard and Svensson, 1984); Panorama (Vearncombe et al., 1995), Teutonic Bore (Vaasjoki, 1985), the Kalgoorlie Super Pit (Steadman et al., 2015) and Golden Grove (Browning et al., 1987) in Western Australia. Appendix 7.8 contains a compilation of this data.

7.4.4. Results

As was presented in Chapter 6, the DeGrussa sulfides require elevated μ values (10.8) using the Stacey and Kramers (1975) growth curve (Fig. 7.34). There is little lead in the DeGrussa deposit, but the high μ ($^{238}U/^{204}Pb$) Pb isotopes reflect a crustal source, potentially from hydrothermal fluids scavenging Pb from host and footwall rocks, in particular the sedimentary rocks of the footwall, Johnson Cairn and Juderina Formations.

The Stacey and Kramers (1975) growth curve was chosen over the Cumming and Richards (1975) growth curve based on the resulting age and its fit with the stratigraphic relationships of the Bryah Group. A Cumming and Richards (1975) μ value of ~11.0 is the best fit for DeGrussa data (see Ch. 6) but provides an age for DeGrussa Pb isotopes ~100Ma younger than that of the Stacey and Kramers (1975) growth curve, and does not fit with the geological relationships of the Bryah Group.

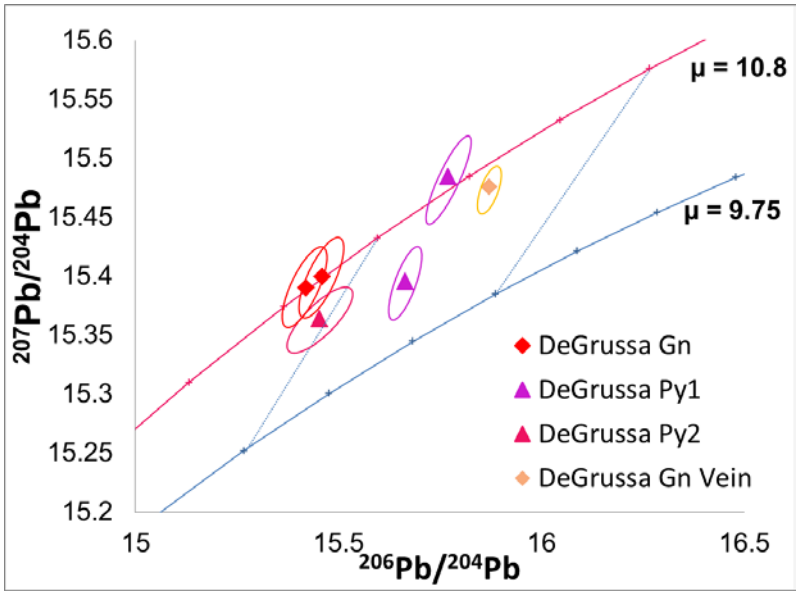

Figure 7.34. DeGrussa galena and pyrite Pb isotope results with respect to both the original μ=9.75 of Stacey and Kramers (1975) and elevated μ=10.8 required to fit the DeGrussa data to the growth curve. As discussed in chapter 6, the high μ values are typically interpreted to represent Pb source from upper crustal sedimentary rocks.

Part of the age discrepancy between the different models arises due to the steeper gradient on isochrons (lines joining different μ values at a single time period) in the Cumming and Richards (1975) model in comparison to Stacey and Kramers (1975) and Zartman and Doe (1981) models. (Fig. 7.35). A Stacey and Kramers (1975) μ value 9.0 approximates the Zartman and Doe (1981) 'mantle' growth curve. A Stacey and Kramers (1975) μ value 9.75 approximates the Zartman and Doe (1981) 'orogene' growth curve although the two curves differ by ~100Ma . A Stacey and Kramers (1975) μ value 10.8 approximates the Zartman and Doe (1981) 'upper crust' growth curve at ages older that ~2000Ma (Stacey and Kramers, 1975) but the two diverge at younger ages.

As the DeGrussa data fits best with the Stacey and Kramers (1975) model curve, along with its stratigraphic age constraints in the Bryah Basin, it is used for reference for all Pb isotope data for Australian and worldwide VHMS deposit presented in this section.

East Capricorn Regional Sulfides: The Magellan Pb deposit and lead in carbonates from the 'Sweetwaters Well Member' in the Earaheedy basin has Pb isotopic composition which plot on a high μ (10.8) growth curve of Stacey and Kramers (1975) indicating a crustal component in the source of the mineralising fluids. Gold deposits of Nathans, Peak Hill and Labouchere also conform to the high μ (10.8) growth curve indicating that the high μ is a characteristic of the district (Fig 7.36).

The Fortnum gold and Thaduna Cu deposits are coincident with the Stacey and Kramers (1975) growth curve with μ values of ~ 9.75 to 10.0 respectively. Lead occurrences in the Frere Formation (Earaheedy Basin) also conform to a Stacey and Kramers (1975) μ ~10 growth curve as does the Horseshoe Lights VHMS deposit (μ ~10).

The Plutonic gold deposit formed from different pulses of mineralisation, largely conform to the μ = 9.75 growth curve for part of the mineralisation that is relatively radiogenic (Palaeoproterozoic model ages), but display high μ ≥ 10.8 for the part of the mineralisation with the least radiogenic Pb isotopes (Archean model ages).

Western Australia Pb isotopes: The oldest VHMS deposit in Western Australia are those of the Panorama district in the Pilbara (model ages of 3262-3084Ma using Cumming and Richards (1975) growth curve) (Vearncombe et al., 1995, Brauhart, 1999). The Panorama district has Pb isotope ratios comparable to Stacey and Kramers (1975) high μ values (~10.8) similar of the DeGrussa district. Similarly, the Golden Grove VMS deposit in the Murchison/Youanmi Terrane of the Yilgarn, has Pb isotopes which plot on a high μ (~14 Stacey and Kramers (1975)) growth curve . Mineralisation of the Patterson Orogen forms a Pb isotope array at 1000Ma with μ values between 9.75 and 10.8 Stacey and Kramers (1975) (Fig. 7.36).

The exception for Western Australian VHMS deposits is Teutonic Bore in the Eastern Goldfields Province. Teutonic Bore displays Pb isotopes which are lower than the average Pb growth curve (μ =9.75 Stacey and Kramers (1975)).

Palaeoproterozoic VHMS deposit Pb isotopes: Very few VHMS deposits of Palaeoproterozoic age exist. Those that are known, include those of the Skellefte district (e.g. Boliden, Näsliden etc.) (Rickard and Svensson, 1984, Billstrom and Vivallo, 1994) in Sweden, and those of the Flin Flon mineral belt in Canada (Sangster, 1972).

In comparison to DeGrussa and the Bryah Basin region, the Skellefte and Flin Flon VHMS districts have much lower μ values (~8.8 – 9.75 Stacey and Kramers (1975)) (Fig. 7.37).

World-wide VHMS deposit Pb isotopes: Deposits of the Iberian Pyrite Belt (including Neves Corvo,), the Besshi deposits of Japan, Windy Craggy in Canada and the VHMS deposits of Alaska, Norwegian VHMS deposits, Tasmanian deposits and Chagaz in Iran, Pb isotopes are displayed in comparison to DeGrussa (Fig. 7.38).

Unlike the DeGrussa deposit, none of these deposits plot on high μ growth curves. The deposits of Alaska, Norway and Japan (Besshi) plot as arrays between Stacey and Kramers (1975) growth curves of μ=9 to 9.75. Tasmania VHMS deposits have similar Pb ratios to those of the Iberian Pyrite Belt and Windy Craggy and sit conformable with the Stacey and Kramers (1975) μ=9.75 average crustal growth curve.

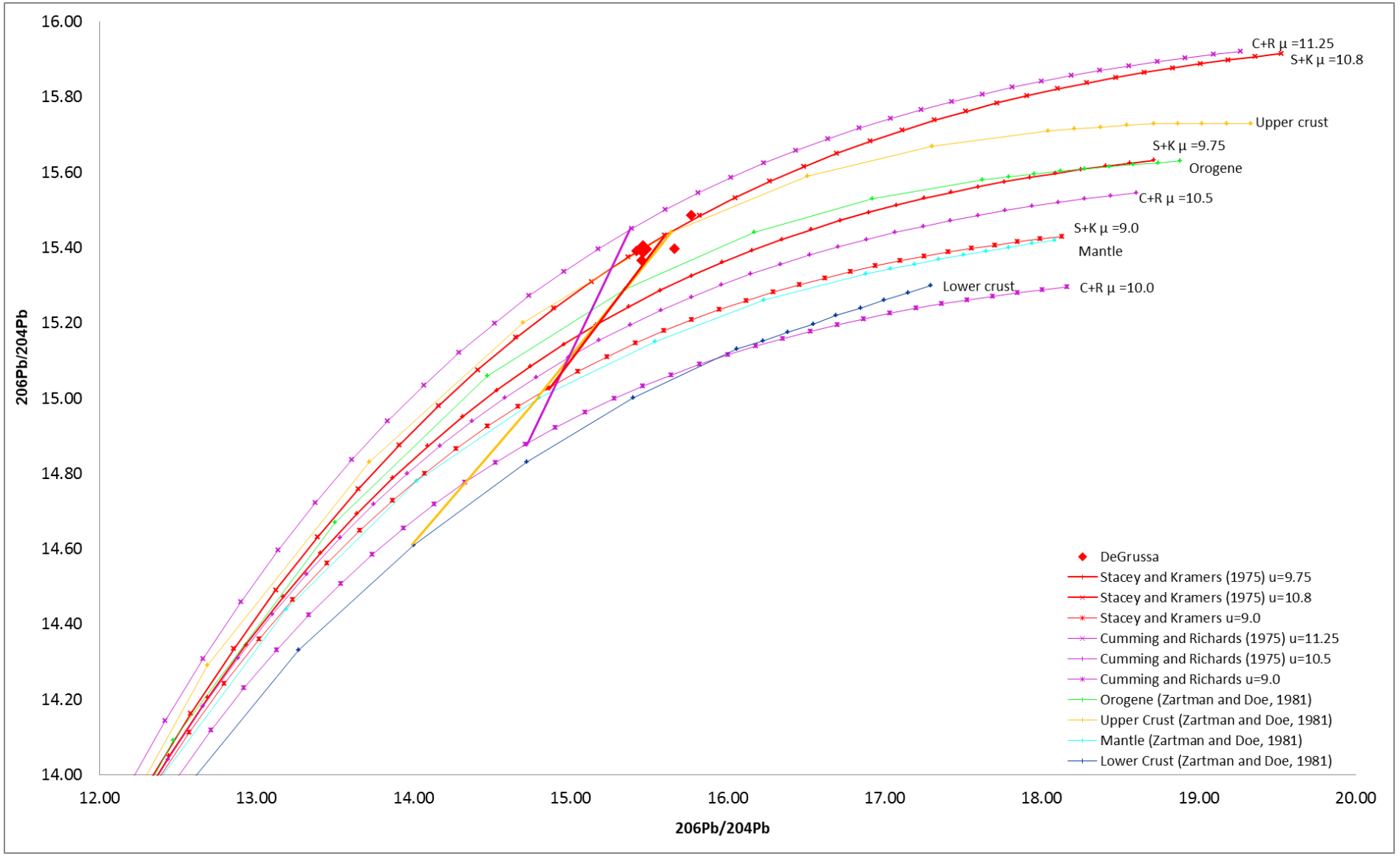

Figure 7.35. Comparison of different Pb growth curves and different μ values with solid lines connecting different μ values at equivalent time (2000Ma)- Stacey and Kramers (1975) (red), Cumming and Richards (1975) (purple) and Zartman and Doe (1981) (orange).

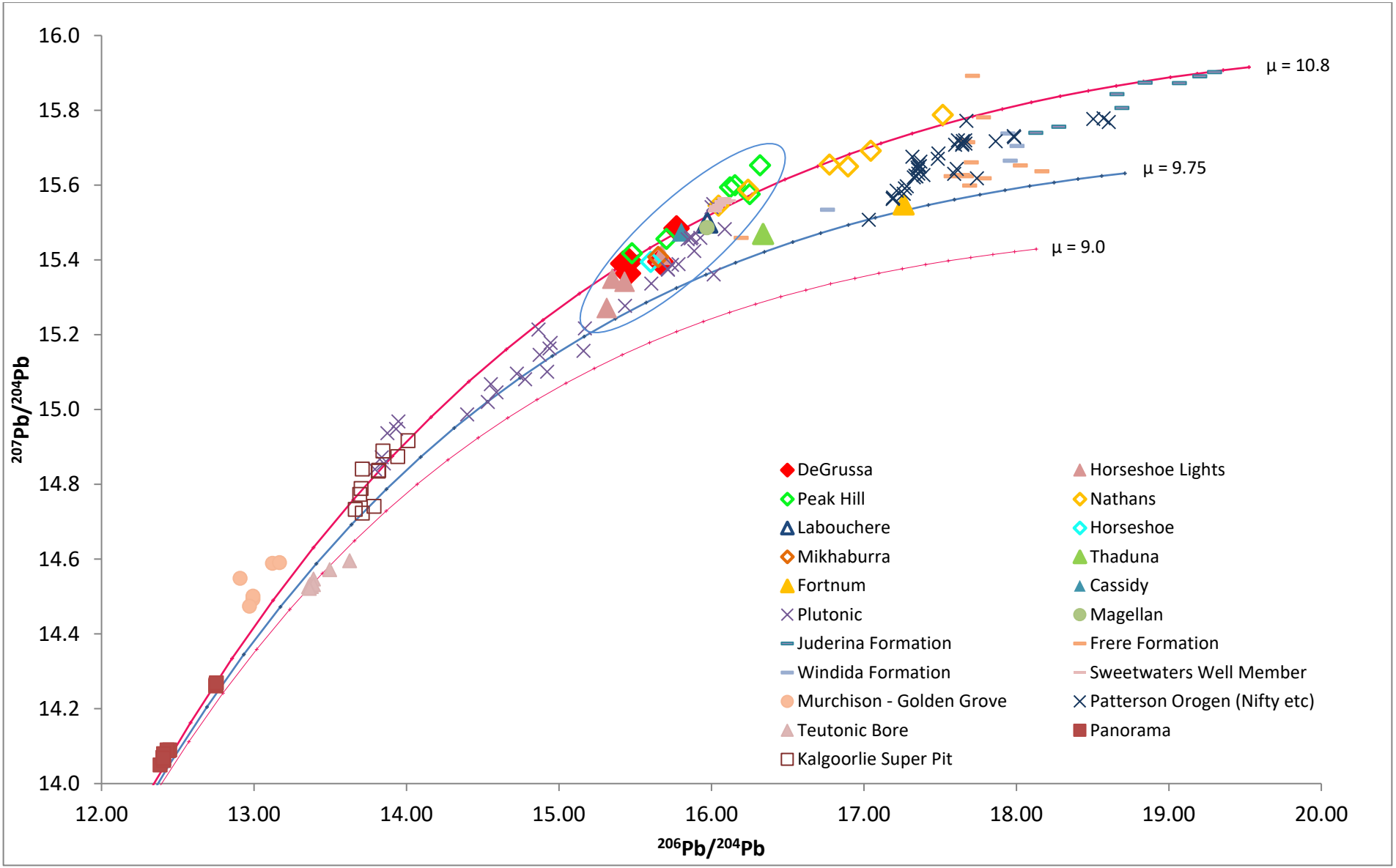

Figure 7.36. Comparison of Pb isotopic data for regional mineralisation across the Bryah and Yerrida Groups. Data is plotted with respect to the Stacey and Kramers (1975) (μ=9.0, 9.75 and 10.8) growth curves. The Stacey and Kramers (1975) μ=10.8 growth curve forms the best fit to the majority of the regional data (exceptions of Horseshoe Lights, Thaduna and Fortnum-Starlight which require μ=10). DeGrussa data in comparison with Pb isotopes from the eastern Capricorn, and around Western Australia including the VHMS deposits of Golden Grove, Teutonic Bore and Panorama as well as deposits of the Patterson Orogen. With the exception of Teutonic Bore all deposits display characteristically elevated μ.

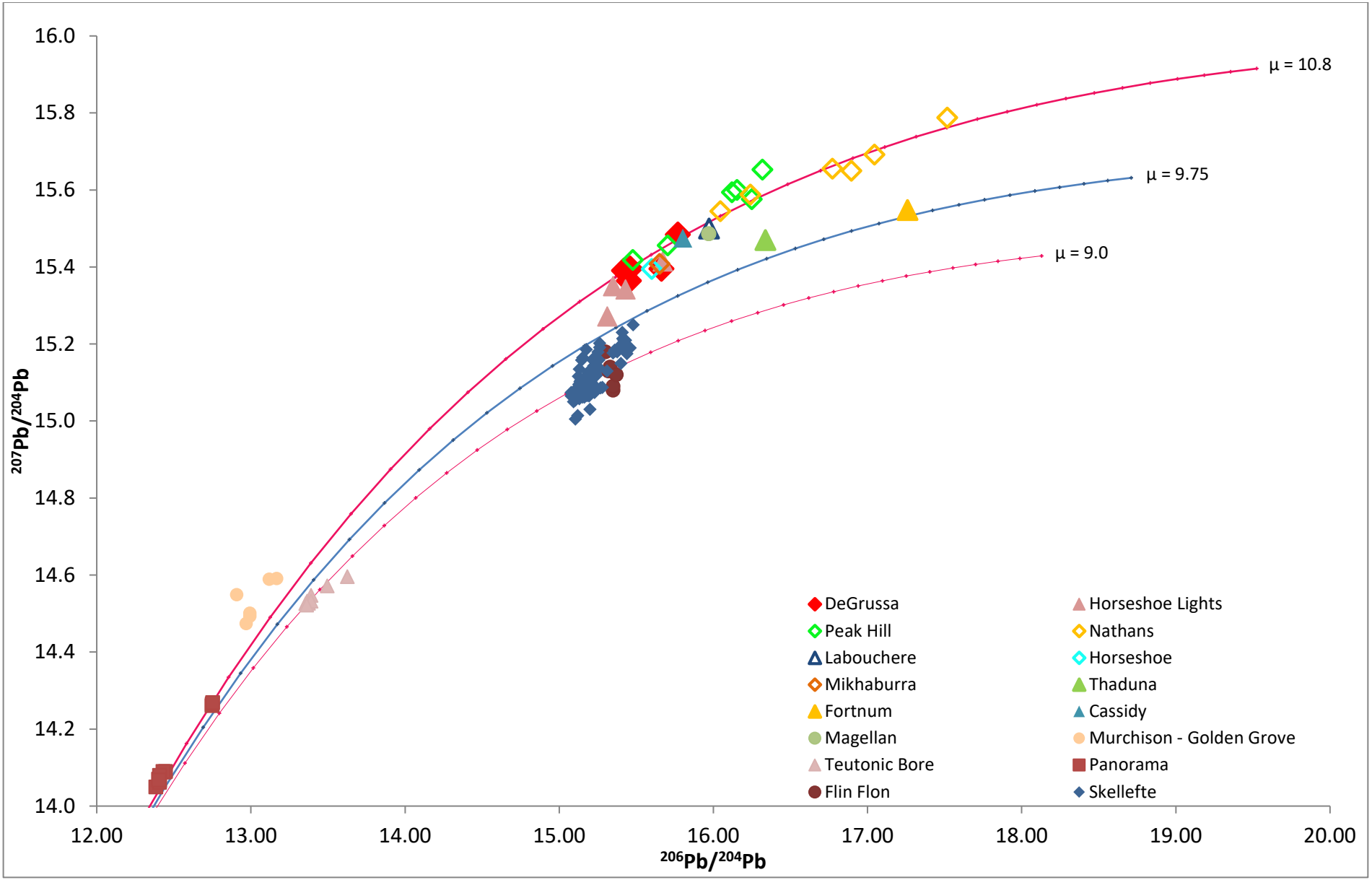

Figure 7.37. $^{206}Pb/^{204}Pb$ vs. $^{207}/^{204}Pb$ with Stacey and Kramers (1975) model curves in comparison with DeGrussa and Archean WA VHMS deposits and Paleoproterozoic deposits of similar age to DeGrussa (Skellefte district, Scandanavia and Flin-Flon, Canada).

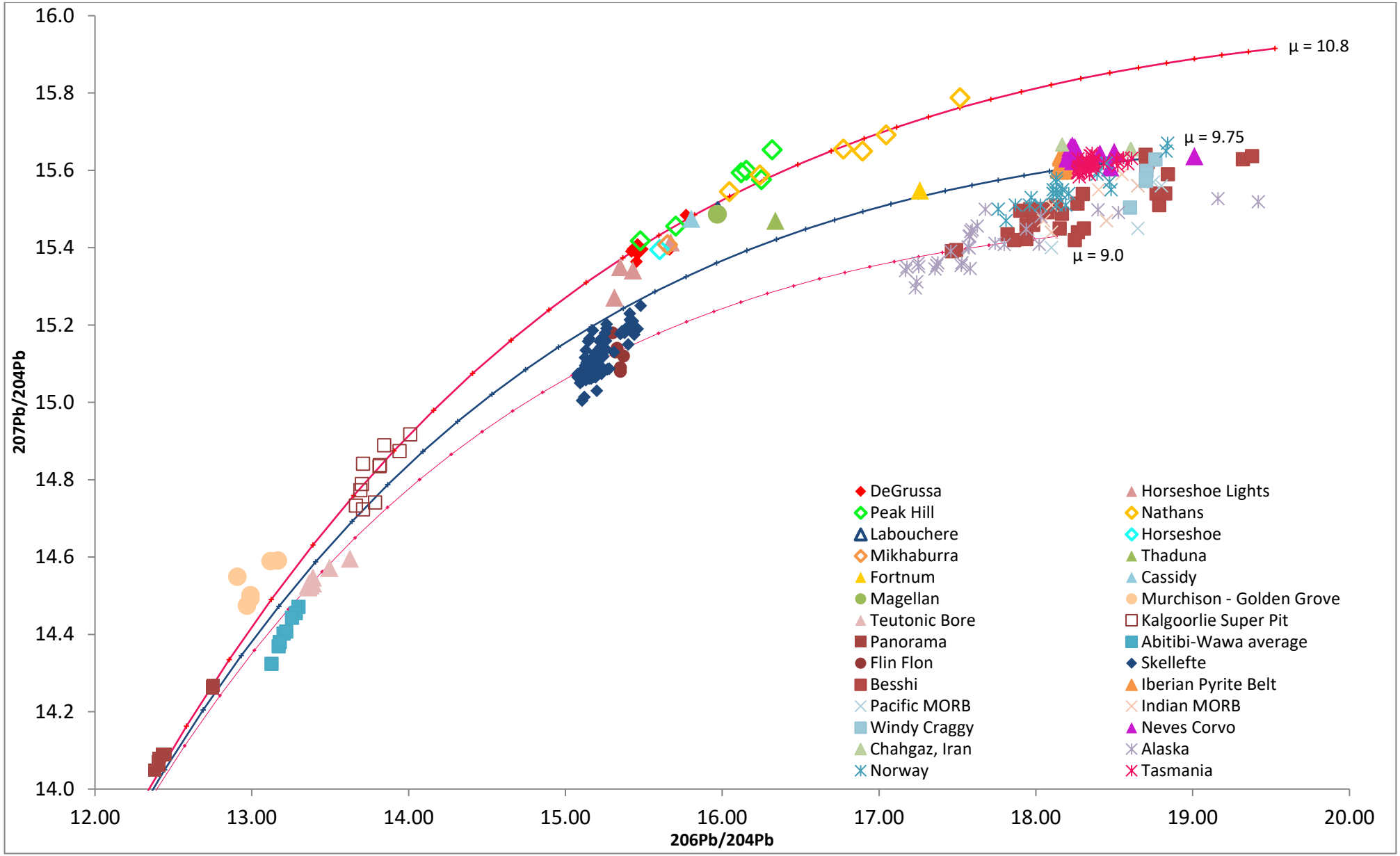

Figure 7.38. $^{206}Pb/^{204}Pb$ vs. $^{207}Pb/^{204}Pb$ for VHMS deposits around the world in comparison to DeGrussa.

7.4.5. Discussion

East Capricorn Regional Sulfides: DeGrussa Pb isotopes may be derived from the same high μ source as that of Archean VHMS deposits in the Youanmi Terrane. Underlying basement rocks to the Bryah and Yerrida groups most likely belong to the Youanmi terrane, with northward directed underthrusting of the Yilgarn Craton below rocks of the Bryah Group and Glenburgh terrane. Pb isotopes of Bryah basin deposits could reflect fluids that have interacted with high μ reservoirs in the Pilbara and Yilgarn (crustal signature).

In comparison with the high μ values of VHMS deposit in the Youanmi terrane, VHMS deposits of the Eastern Yilgarn Superterrane have lower μ values as represented by the Teutonic Bore VHMS deposit. In comparison, Pb isotopes of pyrite in black shales and the Kalgoorlie Super Pit have similar high μ, although a larger compilation of Pb isotopes from across the Yilgarn is needed to determine if either high or low μ is typical of this section of Yilgarn crust.

The supergene Magellan lead deposit, hosted within the high μ Yerrida group, likely recycles Pb by leaching the surrounding sedimentary host rocks, and preserving the high μ Pb isotope. In a similar way, high μ Pb isotope are retained in the Nathans, Labouchere, Peak Hill and Plutonic gold deposits.

Western Australia Pb isotopes: Comparing the Yilgarn and Pilbara Pb isotopic trends which these Pb isotope evolution curves suggests that high μ crustal values for Pb in the Western Australian Archean Cratons and Palaeoproterozoic basins is a characteristic of this area (Fig. 7.37).

Except in the case of Teutonic Bore, Pb isotope ratios all display high μ values. One possibility is that the high μ values reflect the underlying Archean craton from which the lead could have been derived. Pb in the DeGrussa and Horseshoe Lights VHMS deposits is scare and could be interpreted to be due to a lack of Pb in the magmatic source.

Secondary Pb deposits such as the Magellan Pb mine in the south of the Yerrida Basin require similar high μ values. Lead in carbonates within the younger Earaheedy basin, and the pre-DeGrussa, Juderina Formation in the Yerrida Group also plot above the average growth curves

implying higher $^{238}U/^{204}Pb$ (μ) in the source of the mineralisation fluids. High μ values such as these are typically interpreted to represent Pb sourced from upper crustal sedimentary rocks (Zartman and Doe, 1981) rather than the average crust. Although the Bryah Basin has been interpreted to be an oceanic rift setting with associated sea mount and MORB type magmas (see chapter 5) late during its tectonic history, the basin began as a continental rift, containing sedimentary rock derived from erosion of Archean crustal material. Hence, it is plausible that the Pb in the DeGrussa deposit, found either as galena or in other sulfides, was leached from Archean basement rocks and basin sedimentary rocks derived from the Archean Yilgarn and Pilbara Cratons.

Palaeoproterozoic VHMS deposit Pb isotopes: The Pb isotopic composition of ore samples from the Skellefte district tend to show mixing arrays between the mantle and lower crustal growth curves suggesting that at least some of the Pb in the Skellefte district originated from a mantle reservoir (Billstrom and Vivallo (1994)). Similarly, the deposits of the Flin Flon mineral belt plot near the low μ mantle curves. The difference in Pb isotope ratios between these deposits may reflect the different tectonic settings in which the Skellefte and Flin Flon districts formed. The Skellefte district is interpreted as either an island arc or an intra-arc rift within a continental margin (Rickard and Svensson, 1984, Montelius, 2005). The deposits were interpreted by Billstrom and Vivallo (1994) to have a Pb source which involved mixing of a mantle source with lower crustal material at approximately 2.0Ga.

As previously mentioned, the DeGrussa deposit is likely formed in what began as a continental rift along the northern margin of the Yilgarn Craton and later developed into an oceanic rift with sea floor spreading and magmatism and accompanied by large amounts of sedimentation.

World-wide VHMS deposit Pb isotopes: Interestingly, the Neves Corvo VHMS deposit of Portugal, indicated by several authors (e.g. Huston et al. (2010);) as having Pb sourced from magmatic rocks, which derived their lead from interaction with the crust or subduction of crustal sedimentary rocks. Neves Corvo Pb values are consistent with a slightly higher μ curve than most other VHMS samples. Neves Corvo is believed to have a large magmatic component due to

enrichments in Sn and Cu (cassiterite and chalcopyrite ores). $^{206}Pb/^{204}Pb$–$^{207}Pb/^{204}Pb$ diagrams of Neves Corvo sulfides provided by Huston et al. (2010) indicate that sulfide and tin ore deposition involved ore-forming solutions with two distinct isotopic sources. Relvas et al. (2001) interpreted one of these sources, characterised by less radiogenic Pb and less evolved Nd, to have been derived from sedimentary and volcanic rocks stratigraphically underlying the ores. Relvas et al. (2001) interpreted the second source, which is preserved in the Sn-rich ores and was characterised by highly radiogenic Pb and evolved Nd, to have been derived from an external source, not present in other Iberian Pyrite Belts ores, and interpreted to be magmatic–hydrothermal fluids, basinal brines or metamorphic fluids that have circulated deeply through older basement rocks.

Again, these observations reinforce the high $^{238}U/^{204}Pb$ (μ) in the source hydrothermal fluids in the eastern Capricorn Orogen relative to most VHMS deposits. Given the spread of Pb isotope compositions found in a range of VHMS deposits throughout time, it is more likely that they are derived of leaching of surrounding host and basement rocks. The nature of these rocks and their characteristic Pb isotopes is reflected in the ore deposit Pb isotopes.

7.4.6. Further work

It is plausible that Pb isotopic compositions may vary across the different terranes of the Yilgarn. For example, higher $^{238}U/^{204}Pb$ (μ) in the mineralising source in the Youanmi/Murchison Province may reflect in the Golden Grove deposit, whereas lower $^{238}U/^{204}Pb$ (μ) may prevail in the Eastern Goldfields Province and be reflected in mineralisation at Teutonic Bore.

The origin of the Marymia Inlier is still controversial, with the favoured interpretation that it belongs to the Eastern Goldfields Superterrane with the Ida Fault interpreted to divide this province from the western Youanmi Terrane below the Bryah Basin (Gazley, 2011). A comparative study could be made with a larger dataset of Pb isotopes throughout the Eastern Goldfields Superterrane and the Youanmi Terrane with those of the Marymia Inlier. This could possibly distinguish which of the terranes the Marymia is derived from.

7.4.7. Conclusion

The Pb isotopic compositions of the DeGrussa mineralisation plot above the average growth curve of Stacey and Kramers (1975) implying higher $^{238}U/^{204}Pb$ (μ) in the source of the mineralising fluids. High μ values such as these are typically interpreted to represent Pb source from upper crustal sedimentary rocks and is typical of lead and ore deposits across the Capricorn Orogen as well as the Yilgarn and Pilbara Cratons. Hence it is likely that Pb was derived from leaching of Archean basement and sedimentary host rocks in the Bryah Basin.

7.5. Summary

The characteristics of the geology and hydrothermal-magmatic mineralising system at DeGrussa is summarised as follows:

- The lack of a strong alteration halo, indicating that minimum interaction between hydrothermal fluids and host rocks has occurred in the immediate environment of the deposit. Feeder zones are narrow and appear constrained to fault zones indicating that fluid flow was focused along these faults. A broader, more cryptic alteration may be present below the deposit but has not been described by this study.
- Syn-deposition of sulfide minerals indicated by the interlocking textures of the sulfide ore (chapter 4).
- Co-incident magmatism (2018 Ma) with mineralisation (2011-2018 Ma) as discussed in Chapter 6. Additionally, the age provided by Re-Os geochronology for mineralisation is within error of the U-Pb dolerite intrusions and hence dolerites may have contributed to the hydrothermal systems heat source.
- The presence of a talc-carbonate zone is similar to the talc deposits seen along the Guaymas spreading centre, deposit which result from high temperature hydrothermal-magmatic fluids (Lonsdale et al., 1980).
- Enrichment of Cu in basalts and dolerites proximal to the DeGrussa deposit in comparison with dolerites sampled across the Bryah Group. The high Cu content in both the dolerites and

DeGrussa mineralisation may indicate that the same magmatic source was responsible for the dolerites and Cu-rich hydrothermal fluids, and the carbonate alteration suggests some alteration of dolerite has occurred during intrusion of the dolerite although not enough to account for the metal contents of the deposit.

- The range of $\delta^{34}S$ values for the DeGrussa sulfides (+0.3 to 10.5‰) with a peak at 1.0 – 3.0‰ sugests that the dominant source sulfur resembles $\delta^{34}S$ values similar to an igneous sulfur source (0 ± 3.0‰).
- High $^{207}Pb/^{206}Pb$ values for DeGrussa sulfides plot above that of the standard Stacey and Kramers (1975) growth curve implying higher $^{238}U/^{204}Pb$ (μ) in the source of the mineralizing fluids. This indicates a crustal source (Zartman and Doe, 1981) for Pb in the DeGrussa deposit, which could only be obtained from leaching of surrounding host rocks. There is little Pb throughout the DeGrussa deposit due to the high temperatures of mineralisation leading to a lack of Pb and Zn. Galena-bearing horizons are restricted to small zones in the ore lenses. It is likely that the small amount of Pb in the surrounding host rocks was stripped via hydrothermal fluids and re-precipitated into the ore deposit.

7.5.1. Environmental Constraints

Between 2.4 and 1.8 Ga the oceans were transitional to sulfur-rich and oxidised conditions (Ueda et al., 1990, Huston and Logan, 2004). Hematite-rich sedimentary rocks in the footwall of DeGrussa (the Magazine Member/Karalundi Formation) indicate that either the depositional environment was oxidised or the hydrothermal fluid responsible for the hematite alteration was oxidised. Hematite alteration is widespread across the basin and in the hanging wall of the DeGrussa deposit towards the west.

The lack of sulfate minerals in the ore, but the presence of peripheral jasper, suggests that DeGrussa formed in an sub-oxic to oxic, low sulfate oceanic sub-basin from reduced, low-Ba, metal-bearing fluids (Huston and Logan, 2004). Hydrospheric conditions of the deep basin water

were Fe-rich and sulfate free, leading to the high content of Fe-rich minerals (pyrite, minnesotaite, stilpnomelane, Fe-Mg chlorite) and the lack of a sulfate-bearing exhalite.

The water depth necessary to allow venting of sufficiently high-temperature fluids, allowing metal transport and deposition of massive sulfides is >1000m, with present day examples including the Brothers Cu-rich deposits, Lau Basin, (Berkenbosch et al., 2015) and PACMANUS, Manus Basin (Glasby et al., 2008). The presence of turbidites as well as conglomerates and mass flows suggests a below wave base, off shelf location for the formation of DeGrussa mineralisation.

7.6. Conclusion

The DeGrussa deposit was formed along a deep marine, sub-oxic to oxic, low sulfate oceanic rift setting at 2027Ma. Mineralisation is a result of reduced, hydrothermal fluids (initial pH 3-5) which leached sedimentary and basaltic rocks of igneous sulfur composition ($\delta^{34}S$ values of +0.3 to +6.3‰). Cu, and Au may be derived from a hydrothermal-magmatic fluid ($\delta^{34}S$ values of -3 to +1‰) although it is likely this too was derived from leaching and interaction with sea water sulfate (producing the heavy $\delta^{34}S$ in pyrite up to +9.8‰). Lead isotopes however, indicate a crustal source of lead. Mineralisation deposited on the seafloor and sub seafloor at a pH of 5-8 and a temperature of 250-350°C.

8. Genetic Model

8.1. Genetic model for DeGrussa mineralisation

The formation of the Bryah Basin is presented in schematic form and largely summarises and combines prior work not limited to those by Pirajno et al. (1995), Occhipinti et al. (1997), Sheppard et al. (2004), Occhipinti et al. (2004), Johnson et al. (2011a), and Dentith et al. (2014). The tectonic processes that operated to the north of the Marymia Inlier, along the southern margin of the Pilbara Craton, are postulated only. No geological evidence exists due to the area being buried beneath the Edmund and Collier Basins.

Prior to the Opthalmian Orogeny (>2245Ma), several terranes of the Capricorn Orogen were accreted. These include the collision of the Pilbara and Ashburton Basin, the Pilbara with the Gascoyne Terrane, and the collision of several other small terranes such as the Bandee Seismic Province and the Carthalunda Seismic Province (Johnson et al., 2013, Dentith et al., 2014).

1. 2240-2125Ma: Opthalmian Orogeny - rifting of the northern Yilgarn Craton (Fig. 8.1)

Continental rifting led to separation of the Marymia Inlier from the northern Yilgarn's Eastern Goldfields Superterrane (Gazley, 2011) and subsequent deposition of Yerrida Group sedimentary rocks in an evaporitic sag basin setting from c. 2174 Ma (Pirajno et al., 1995, Woodhead and Hergt, 1997, Pirajno and Adamides, 2000, Dentith et al., 2014).

Except in the DeGrussa area, the Finlayson member sandstone and conglomerate form the lowermost unit of the Yerrida Group, deposited unconformably onto Archean basement.

Stromatolite growth in the Bubble well member, interbedded with evaporite deposits indicate the saline, shallow water environment (El Tabakh et al., 1999, Grey, 1984), open to the ocean at one end of the basin (west from DeGrussa). The Bubble Well member preserves the Lomagundi event with positive carbon isotope excursions of up to +7‰, correlating with an increase in atmospheric oxygen and an early explosion in life (Russell, 1992, Lindsay and Brasier, 2002, Bekker and Holland, 2012).

Progressive rifting of crustal material and deepening of the rift basin caused the deposition of the carbonaceous Johnson Cairn Formation's turbiditic sandstones, pale-dark grey siltstones, mudstones, and black shales in an anoxic submarine basin. Minor amounts of alkaline basalt related to early rifting are found in the Johnson Cairn Formation.

In the west, collision of the Glenburgh Terrane with the "Pilboyne" (accreted Pilbara/Gascoyne Terrane) occurred during the Opthalmian Orogeny between c. 2240 and 2125 Ma with the Moogie Metamorphics meta-sedimentary rocks deposited concurrently in a foreland basin system (Johnson et al., 2010, Johnson et al., 2011a).

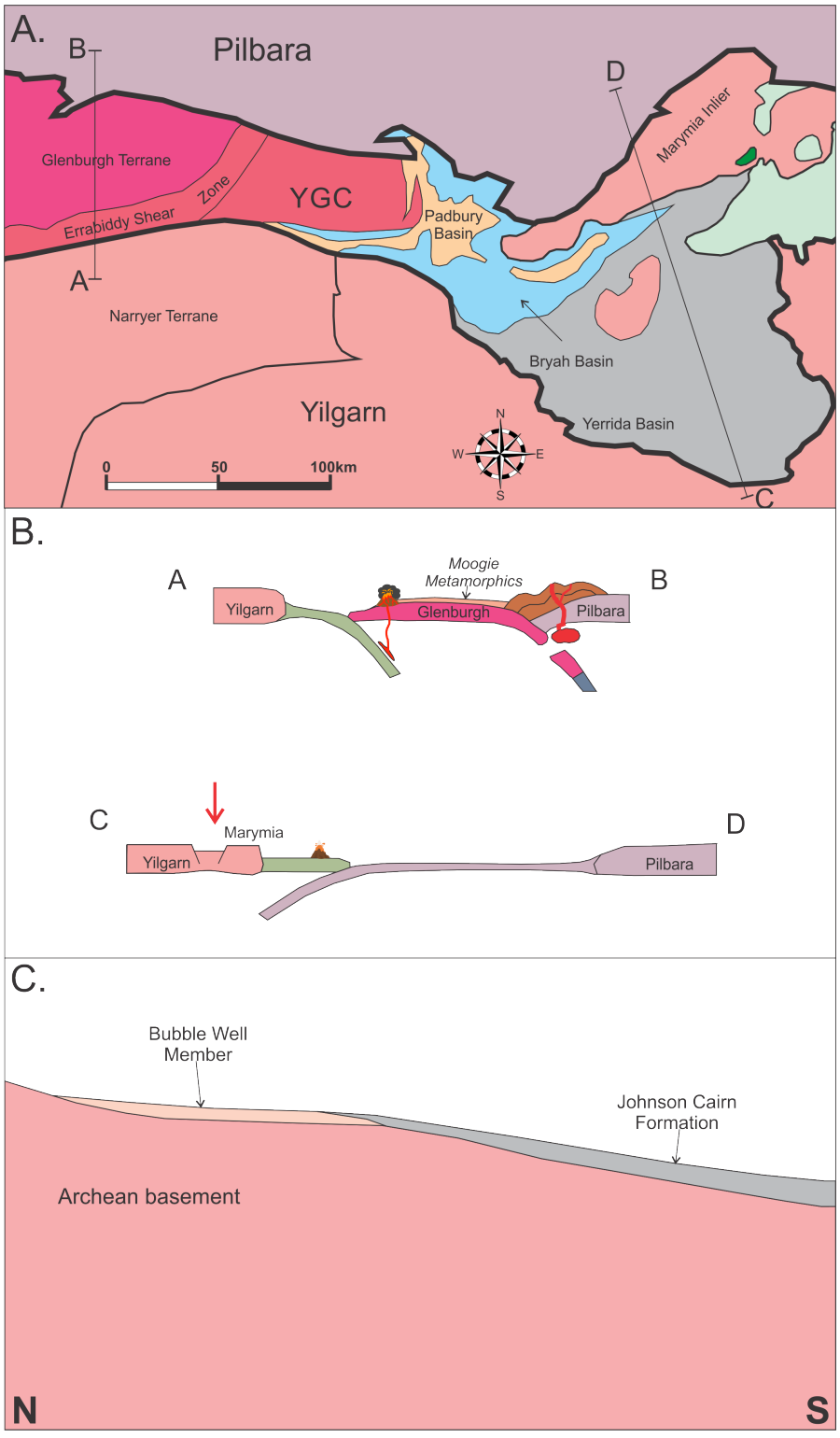

Figure 8.1A. Plan view of the Capricorn Orogen and Archean Cratons in their present day configuration. **B.** Sections as presented in 8.1a through the eastern Capricorn Orogen, and the western Capricorn Orogen where the DeGrussa deposit formed at 2240-2125Ma. Red arrow indicates the position that DeGrussa mineralisation will form. **C.** Schematic cross section through the DeGrussa area during deposition of the Bubble Well Member and Johnson Cairn Formation at 2240-2125Ma.

2. Deposition of the Magazine Member (Fig. 8.2)

The Magazine member (a possible lateral equivalent to the Karalundi Formation) is deposited during continental rifting and extension along the northern margin of the Yilgarn Craton. It comprises conglomerate (carbonate-dolomite breccia), hematitic, mudstone-rich turbidite rocks, volcanic conglomerate and polymict conglomerate. The Magazine Member represents proximal volcanic activity to DeGrussa, although the extent of the unit in the Bryah Basin is not known. The contact between the Yerrida Group sedimentary rocks (Johnson Cairn Formation) and Magazine Member is likely to be paraconformable (Jeffery, 2013). The non-deposition of the upper units of the Yerrida Group (Mooloogool sub-group: Killara, Doolgunna, Thaduna and Maraloou Formations) may reflect either a hiatus in sedimentation, or a progression across the basin of sedimentation, magmatic activity and rifting (Jeffery, 2013).

Pervasive hematite alteration throughout the footwall Magazine Member (Karalundi Formation equivalent) sedimentary rocks indicates the oxidised submarine environment of deposition, in a deepening submarine basin as evidenced from mass flow deposition of carbonate breccia. Large clasts and boulders of carbonate (now silicified) rocks found in the lower footwall units of the Magazine member, formed as a result of bank-margin collapse from seismic activity related to rifting events.

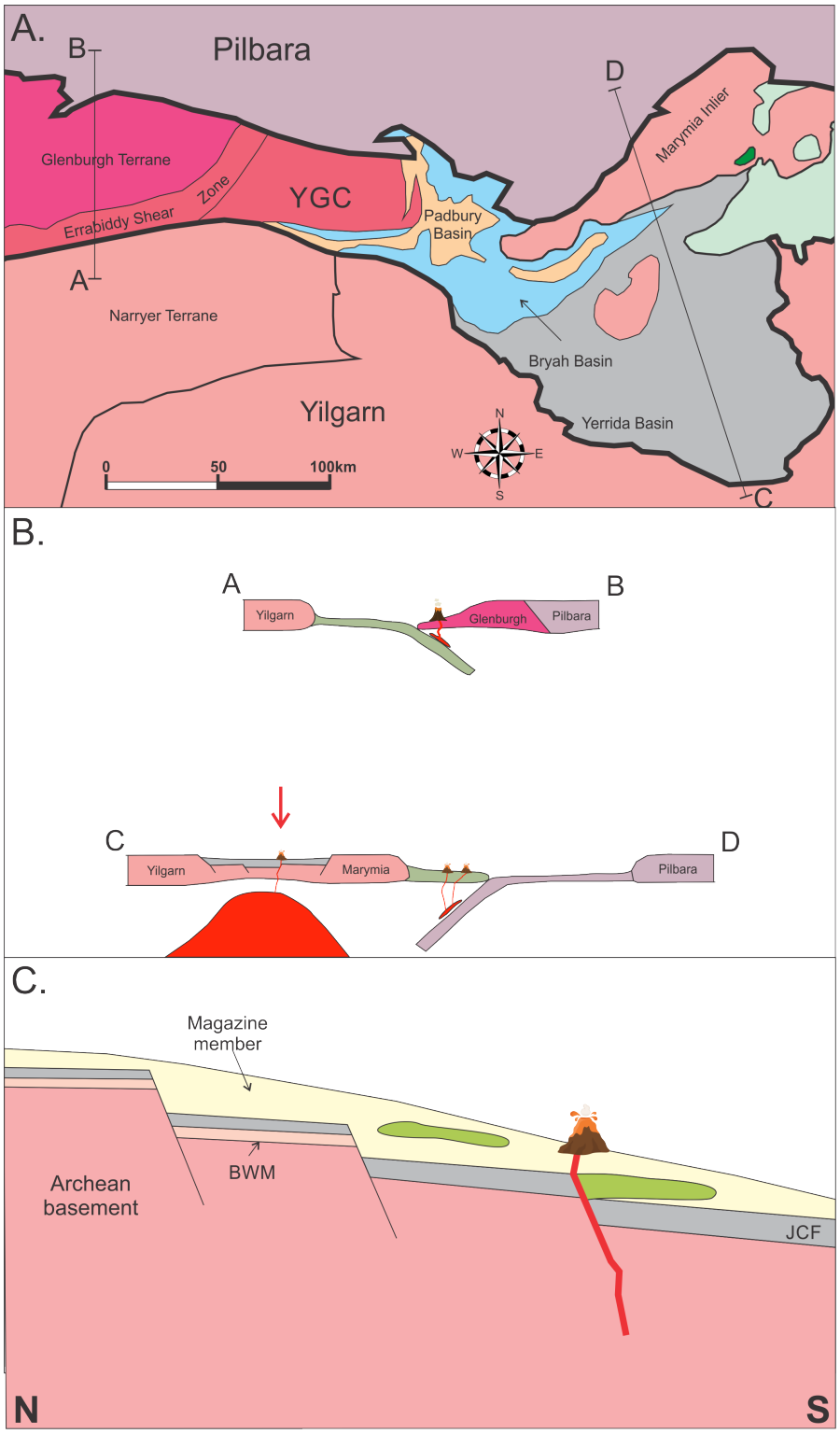

Figure 8.2A. Plan view of the Capricorn Orogen and Archean Cratons in their present day configuration. **B.** Sections as presented in 8.32a through the eastern Capricorn Orogen, and the western Capricorn Orogen at the time of early rifting in the eastern Capricorn, and deposition of the Magazine member. Red arrow indicates the position that DeGrussa mineralisation will form. **C.** Schematic cross section through the DeGrussa area during deposition of the Magazine member. Volcano depicts volcanic activity associated with the Magazine Member.

3. 2080-2000Ma: VHMS mineralisation at DeGrussa and around the Bryah Basin (Fig. 8.3)

Dolerite and basalts, syn- to post- DeGrussa mineralisation. The Killara Formation and DeGrussa mafic rocks and the Killara Formation indicate the continuation of continental rifting in what was probably a submarine, sedimented rift basin (e.g. Cocos/Nazca-Panama Plate and Guaymas basin). The present day, Guaymas basin setting, Gulf of California, or the Red Sea Rift, is analogous to the DeGrussa region.

The presence of Archean aged zircons within DeGrussa host sedimentary rocks suggests that detrital material was sourced from the Marymia Inlier, Goodin Dome or Yilgarn Craton as well as the underlying Yerrida Group rocks. Their composition may reflect why metal content and mineralogy more closely resembles mafic-type/ophiolitic VHMS deposits.

Mineralisation was contemporaneous with regional magmatism between 2018 and 2014 Ma (Mo-Re and U-Pb geochronology), during deposition of the DeGrussa host sedimentary rocks, basalts and fractionated dolerite. This magmatism triggers hydrothermal circulation.

It is suggested that DeGrussa was deposited into a deep, oxidised, low-sulfate ocean basin or sub-basin as seafloor and sub seafloor mineralisation. Magmatic-hydrothermal fluids are transported upwards via extensional faults in the seafloor. $\delta^{34}S$ isotope values support a leached igneous rock source, and Pb isotopes indicate leaching of a crustal source. Hence, leaching of footwall, Johnson Cairn and Juderina Formation sedimentary and mafic rocks is likely to contribute the metal contents present in the DeGrussa deposit. The $\delta^{34}S$ data are considered to be consistent with a reduced, metal-bearing, hydrothermal fluid, initially of acidic composition (pH 3-5), which leached footwall and host sedimentary and basaltic rocks, and deposited sulfide onto the seafloor (chimney structures and sea floor mound breccia) and sub seafloor (evidenced by features such as replacement of peperitic basalt clasts) at a pH of 5-7 at temperatures of 250-350°C. Interaction of the hydrothermal fluid with sea water during sulfide deposition led to the heavy $\delta^{34}S$ tail, comparable to those seen in VHMS systems with a chimney component (Peter and Shanks III, 1992).

Pb appears to be sourced from the surrounding rocks given the high μ values of the Pb isotopes which indicate a crustal component, and supported by the rare occurrence of galena and low lead contents of the ore. Penecontemporaneous magmatism and dolerite intrusion may have focused the hot hydrothermal fluids, concentrating mineralisation into favourable sites. Feeder zones are restricted to narrow, fault controlled upflow pipes, zoned by chlorite and sericite alteration. These is no indication of the feeder zone continuing into the underlying Magazine Member or Yerrida Group rocks. Anhydrite may have formed an exhalative cap, but is not preserved due to dissolution during cooling of the hydrothermal system.

The DeGrussa mineralisation was deposited into a deep submarine setting (>1000m), below wave base, possibly in a constrained basin similar to the setting of hydrothermal sites in the northern trough of the Guaymas basin, at the bottom of horst blocks/ fault escarpments. The lack of sulfate minerals in the ore, but the presence of peripheral jasper, suggests that DeGrussa formed in a sub-oxic to oxic, low sulfate oceanic sub-basin from reduced, low-Ba, metal-bearing fluids.

4. 2000-1975Ma: Intrusion of dolerites (Fig. 8.4)

Following mineralisation, the ore lenses were buried by turbidites and basalt flows, with occasional small ore lenses found higher in stratigraphy (e.g. the Red Bore deposit). Dolerite sills and dykes intruded and inflated the host stratigraphy. This detached the DeGrussa ore lens from the C1 ore lens between 2003 ± 7 Ma and 1991 ± 7 Ma.

The Narracoota Formation was emplaced dominantly in western parts of the Bryah Basin, perhaps as a result of rifting progressing from east to west across the Bryah Basin. The mafic rocks of the Narracoota Formation have a large geochemical variation representing a spectrum of tectonic environments from back arc - island arc (presence of felsic volcanic rocks), forearc (presence of boninite) and oceanic rift (MORB compositions similar to DeGrussa). The Horseshoe Lights Cu-Au VHMS deposit was formed at ~2000Ma from similar fluid compositions and temperatures to that of DeGrussa.

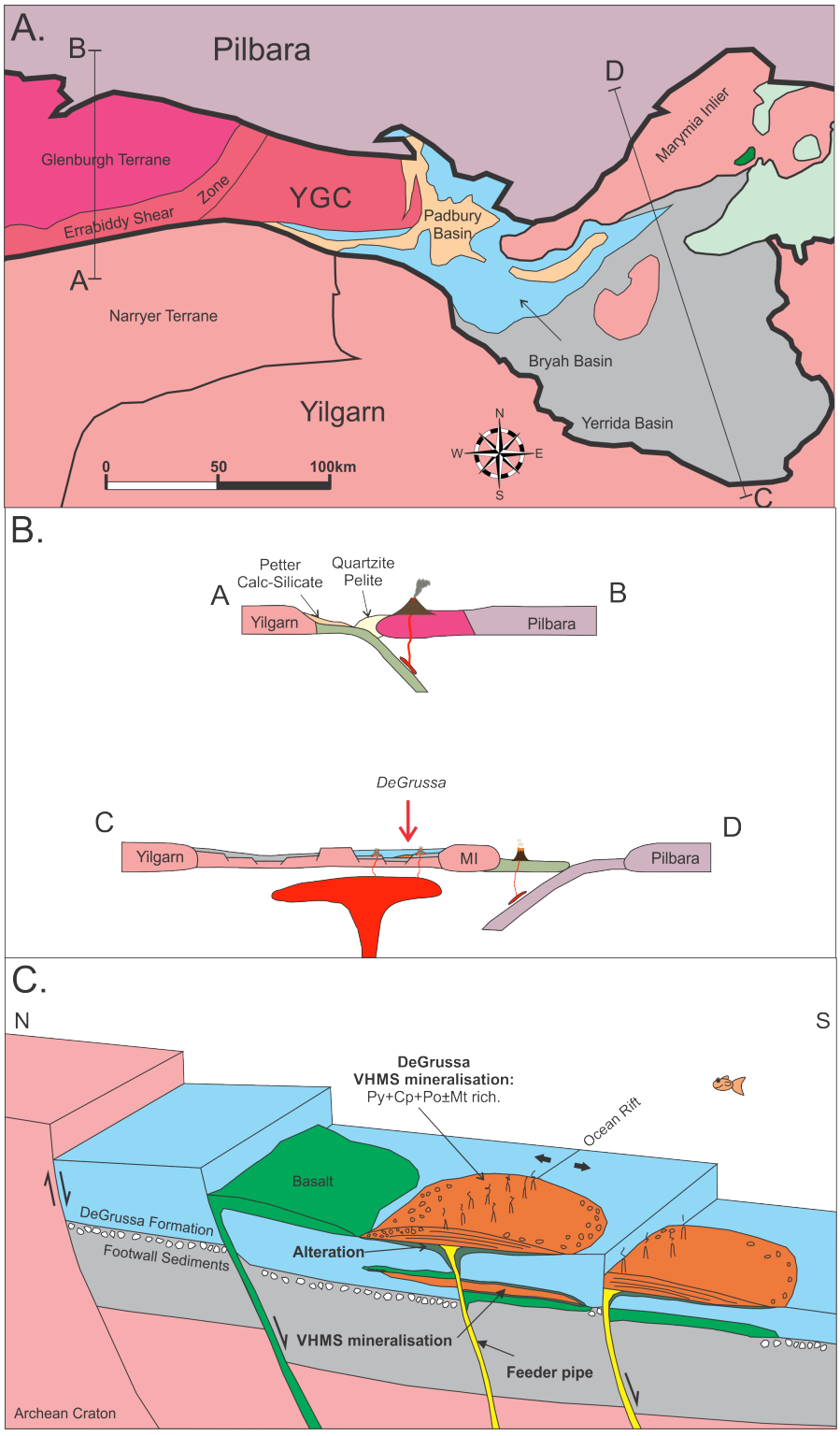

Figure 8.3A. Plan view of the Capricorn Orogen and Archean Cratons in their present day configuration. **B.** Sections as presented in 8.3a through the eastern Capricorn Orogen, and the western Capricorn Orogen at the time of early rifting in the eastern Capricorn at 2080-2000Ma. At this time, the DeGrussa mineralisation was formed in a submarine rift setting along with accompanying magmatism. In the western Capricorn Orogen, northward subduction of the Yilgarn Craton below the Glenburgh Terrane led to the eruption of the Dalgaringa Supersuite and deposition of the Petter calc-silicate and Quartzite pelite in a forearc setting. **C.** Schematic cross section through the DeGrussa mineralisation.

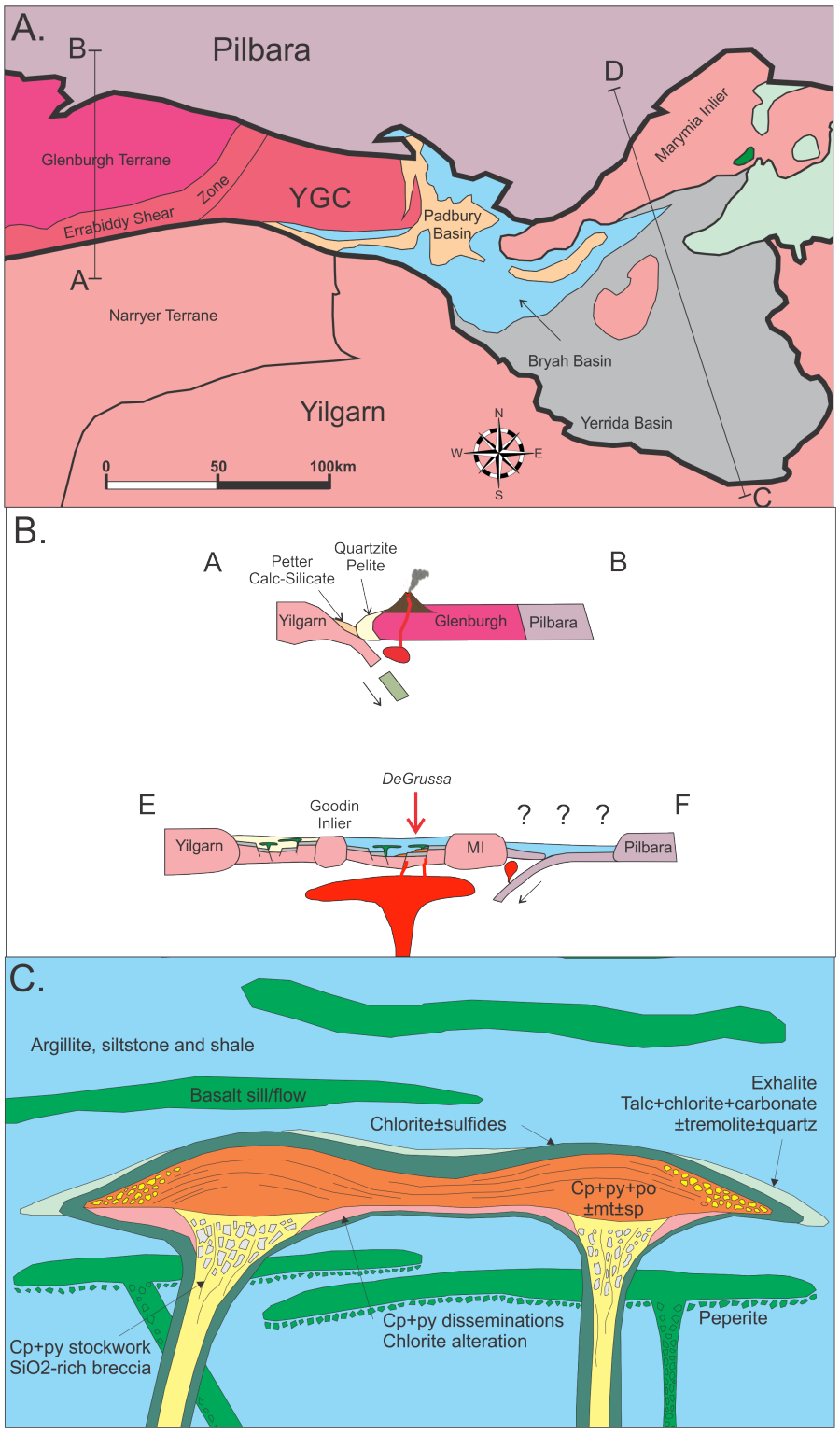

Figure 8.4A. Plan view of the Capricorn Orogen and Archean Cratons in their present day configuration. **B.** Sections as presented in 8.4a through the eastern Capricorn Orogen, and the western Capricorn Orogen at the time of early rifting in the eastern Capricorn at 2000-1975Ma. At this time, the DeGrussa mineralisation and the host sedimentary rocks were intruded by dolerites. Some remobilisation and metamorphism of sulfides within DeGrussa occurred. In the western Carpricon Orogen, subduction below the Glenburgh Terrane ceased leading to the amalgamation of the Glenburgh Terrane and Yilgarn Craton. **C.** Schematic cross section of DeGrussa mineralisation showing the chlorite- and talc-rich alteration halos and feeder pipes. Peperite is associated with basaltic rocks, possibly allowing a conduit for hydrothermal-fluids.

5. ***1980-1880Ma: Development of the Errabiddy Shear Zone, end of the Glenburgh Orogeny (Fig. 8.5)***

Younger pyrite Pb isotope ages at 1920-1975 ± 50 Ma, and correlating Re-Os ages at c. 1982-1984 Ma are interpreted to reflect deformation. Southwest to northeast directed deformation (Pirajno et al., 2000), related to closure of the late Paleoproterozoic basins caused faulting and folding across the region. Closure and collision of the combined Pilbara Craton - Glenburgh Terrane and the Yilgarn Craton led to development of the Errabiddy Shear Zone during the latter part of the Glenburgh Orogeny between c. 1965-1950 Ma (Occhipinti et al., 2004, Sheppard et al., 2004, Johnson et al., 2011a). The DeGrussa deposit was tilted during deformation of the basin.

The Padbury Group sedimentary rocks developed in a forearc basin c. 1940 Ma. This included deposition of the banded iron formations of the Robinson Range Formation, and similarly aged Frere Formation (Earaheedy Group).

The final stages of the Glenburgh Orogeny can be related to mineralisation ages at Peak Hill (Fiveways: 1955 Ma), Horseshoe/Belltop (c. 1940 Ma), Mikhaburra (1915 ± 30 Ma), and Horseshoe/Cassidy (1940 ±30 Ma), and remobilisation ages of sulfide at DeGrussa (c. 1970-1980 Ma, 1920 ± 50 Ma), and Horseshoe Lights (c. 1980 Ma, 1945 ± 30 Ma and 1900 ± 30 Ma).

Figure 8.5A. Plan view of the Capricorn Orogen and Archean Cratons in their present day configuration. **B.** Sections as presented in 8.5a through the eastern Capricorn Orogen, and the western Capricorn Orogen at the time of early rifting in the eastern Capricorn at 1980-1880Ma. DeGrussa mineralisation and host stratigraphy was folded into synclinal folds, the DeGrussa deposit lying in the northern limb of the Robinson Syncline. In the western Capricorn Orogen, the Glenburgh Terrane is now sutured to the Yilgarn and Pilbara Craton. **C.** Schematic cross section of DeGrussa mineralisation tilted to the south and separated by a large intrusive dolerite sill.

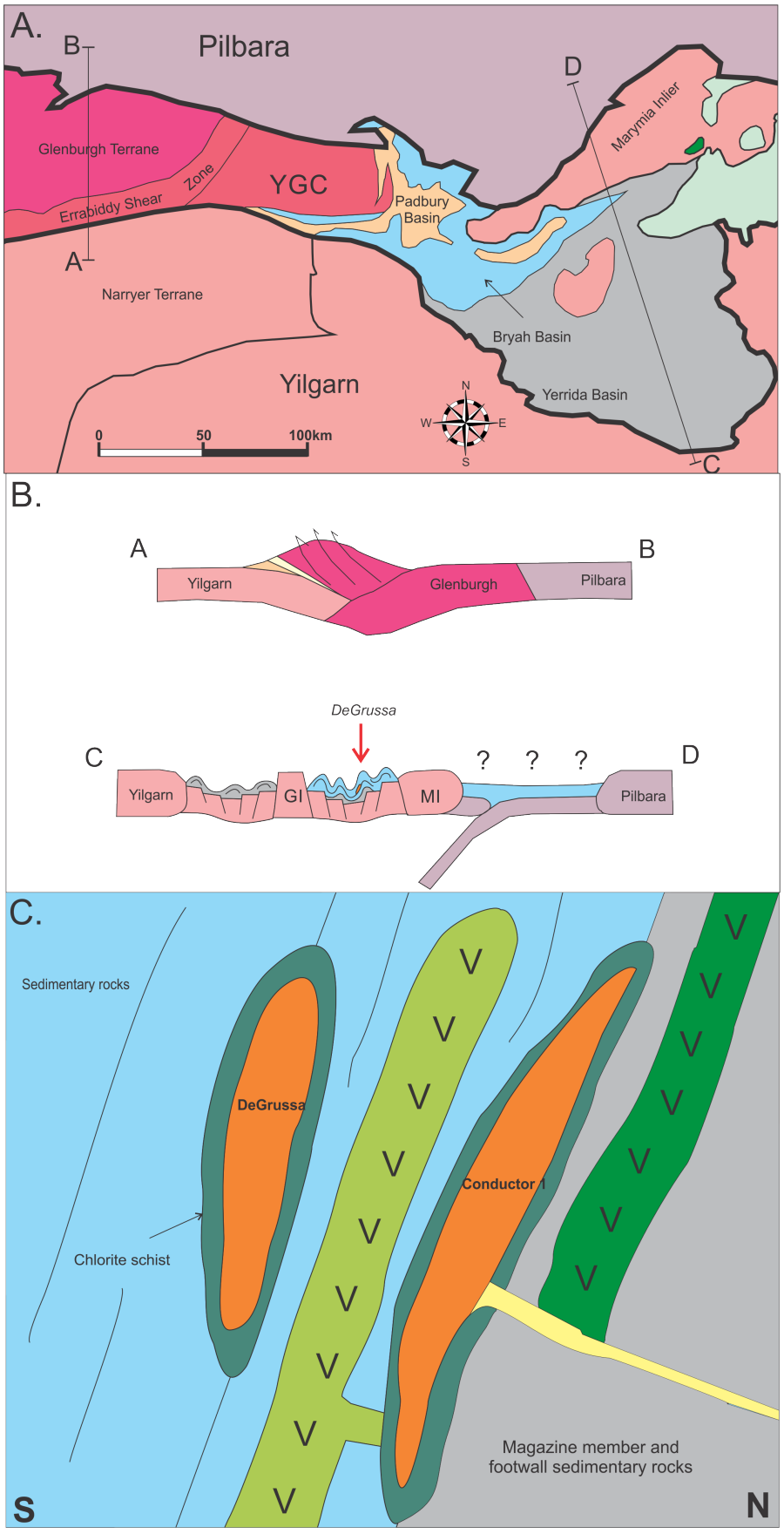
A.
B
Pilbara
D
Glenburgh Terrane
Errabiddy Shear
Zone
YGC
Padbury Basin
Marymia Inlier
A
Narryer Terrane
Bryah Basin
Yilgarn
Yerrida Basin
N
W
E
S
0
50
100km
C
B.
A
B
Yilgarn
Glenburgh
Pilbara
DeGrussa
C
? ? ?
D
Yilgarn
GI
MI
Pilbara
C.
Sedimentary rocks
DeGrussa
Conductor 1
Chlorite schist
Magazine member and
footwall sedimentary rocks
S
N

6. 1820-1770Ma (Capricorn Orogen): Deformation of DeGrussa deposit (Fig. 8.6)

Granite plutonism associated with the Capricorn Orogen, was coincident with the Yapungku Orogeny (c. 1790 Ma), which records the onset of collision between the West Australian Craton and the North Australian Craton (Johnson, 2013). Deformed rocks of the Padbury Group are intruded by granite (Martin, 1994) that are correlated with the c. 1800 Ma Moorarie Supersuite granites which intrude the region.

Quartz + carbonate ± galena veins transect the DeGrussa ore deposit at 1820 ± 50 Ma (model Pb age), interpreted to reflect intracratonic orogenesis and subsequent deformation during the Capricorn Orogeny. Orogenic gold mineralisation at the Labouchere (1800 ± 30 Ma), Nathans (1820 ± 30 Ma) and Mt. Pleasant (1770 ± 30 Ma) deposits occurred at this time. The DeGrussa deposit was folded and transected by three major SE-NW faults – the Shiraz, Merlot and Cabernet faults - dividing the deposit into three lenses.

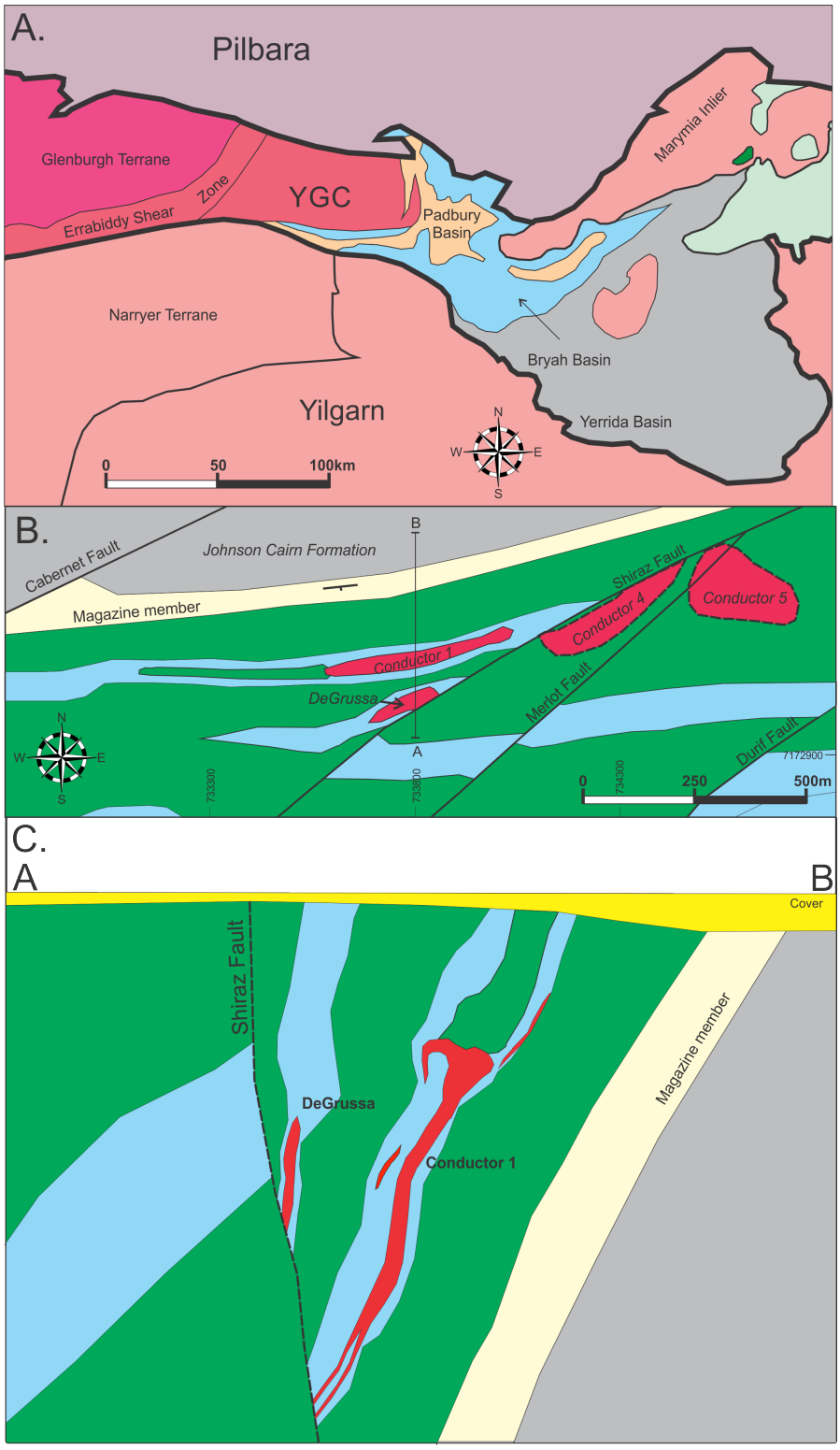

Figure 8.6A. Plan view of the Capricorn Orogen and Archean Cratons in their present day configuration. **B.** Plan view of the DeGrussa deposit and it's 4 ore lenses (DeGrussa, Conductor 1, Conductor 4 and Conductor 5. These ore lenses were displaced from each other by three SE-NE faults by up to 500m. **C.** Schematic cross section of DeGrussa and Conductor 1 ore lenses along a section from A-B (Fig 8.7b), showing the DeGrussa and Conductor 1 ore lenses terminating along the Shiraz Fault (modified from Hilliard (2013))

7. Later Orogenic Events

Subsequent orogenic events affecting the eastern Capricorn Orogen include:

1. The 1680-1620Ma Mangaroon Orogeny: This is related to secondary mineralisation events at Peak Hill (Main pit ages of 1705 ± 30 Ma, 1610 ± 30 Ma and 1620 ± 30 Ma).

2. The 1320-1170Ma Mutherbukin Tectonic Event: This event is characterised by faulting, amphibolite facies metamorphism and deformation across the Capricorn Orogen (Johnson et al., 2011b, Johnson et al., 2013). Some mineralisation ages at Nathans gold deposit (1130 ± 30 Ma, 1300 ± 30 Ma, 1360 ± 30 Ma) correlate to this event.

3. The 1030-955Ma Edmundian Orogeny: This period may be associated with metamorphism of sulfides at the Fortnum-Starlight deposit (920 ± 50 Ma) although, as discussed previously, original mineralisation could be much older.

Supergene weathering of the DeGrussa deposit resulted in oxidation of sulfide minerals, and dispersal of metals through the regolith environment. Chalcocite-rich mineralisation developed throughout the upper parts of the DeGrussa and Conductor 1 ore lenses, within ~200m of the surface. Copper minerals forming within the supergene environment (within ~100m from surface) include chalcocite, cuprite, tennantite, malachite, azurite, chrysocolla, and native copper.

The deposit and host sedimentary and doleritic rocks are buried by lateritic alluvial and colluvial sediments.

9. Conclusion

9.1. Conclusions

- The Paleoproterozoic DeGrussa copper-gold–silver, volcanic-hosted massive sulfide (VHMS) deposit is located in the eastern part of the Capricorn Orogen of central Western Australia.
- The DeGrussa deposit consists of four primary sulfide ore lenses (DeGrussa, Conductor 1, Conductor 4 and Conductor 5) in conjunction with supergene enrichment of copper. Production to February 2015 totalled 137,000 tonnes of copper and 98,000 ounces of gold. The resource estimate consists of an underground primary sulfide of 9.5Mt @ 5.7% Cu, and 2.0g/t Au, for a contained metal content of 546,000 tonnes Cu and 616,000 ounces of Au; stockpiled oxide resource estimate of 2.8Mt @ 1.2% Cu and 1.0g/t Au, for a total metal resource of 33,000t Cu and 88,000 ounces Au; contributing to a total resource of 12.4Mt @ 4.7% Cu and 1.8g/t Au, with a metal resource of 579,000t Cu and 704,000 ounces Au (Taylor and Hastings, 2015).
- DeGrussa is located in the lowermost stratigraphy of the Bryah Group and is classified as a siliciclastic - mafic style, VHMS deposit although it shares characteristics with mafic/ophiolitic type deposits. The Bryah Group comprises an interfingering sequence of sedimentary and mafic volcanic rocks, equivalent to the c. 2000 Ma Karalundi Formation and Narracoota Formation of the Bryah Group. These rocks also host the Red Bore VHMS and Horseshoe Lights VHMS deposits.
- The DeGrussa ore deposit sits on the northern limb of the Robinson Range syncline. No significant parasitic folding has been documented at the DeGrussa deposit. Two large faults crosscut and displace the DeGrussa ore lodes from each other. The north east – south west orientated Shiraz Fault (500-600m displacement) truncates the southern side of the DeGrussa and C1 ore lodes, separating them from C4 and C5 which are on the south side of the fault. The Merlot Fault splays off the Shiraz Fault in a south-west direction, approximately

500 m north east of DeGrussa and C1 ore lenses. It displaces C5 from C4 by approximately 80m.

- Geological and geochemical evidence supports that the deposit formed in a submarine continental rift setting, most likely within a small, ~2km wide, graben structure. DeGrussa host sedimentary rocks, including the Magazine Member, overlie rocks of the Yerrida Group (Bubble Well Member and Johnson Cairn Formation) and are in paraconformable contact. The upper units of the Yerrida Group (Doolgunna and Maraloou Formations) are not identified east of the Gascoyne along the northern Bryah Basin margin, and are not deposited in the DeGrussa area although are regionally extensive. Mafic rocks of the Johnson Cairn Formation are alkalic, and are most similar to rocks found in continental rift settings and Killara Formation mafic rocks have similar trace element geochemistry characteristics and are also considered to have formed in a continental rift setting (e.g. Ethiopian Rift and Red Sea Rift).
- The Magazine Member marks the beginning of rifting and volcanic activity in the Bryah Group. The upper portion of the Magazine Member is intruded by dolerite and it is separated from the DeGrussa host sedimentary rocks by a thick dolorite sill.
- Dolerites within the DeGrussa host sedimentary rock sequence are tholeiitic and of MORB composition with slight REE enrichment suggesting association with seamount and oceanic rift magmatism. The comparable mafic rocks of the Bryah Group, in particular, the Narracoota Formation, have a large geochemical variation but are most similar to EMORB compositions of DeGrussa, and boninites. Killara Formation rocks similarly have EMORB patterns. All three units show evidence of a subduction influence indicating that the basin may have progressed from continental rift to an ensialic back arc or sedimented oceanic rift setting. Subduction along margins of the Bryah basin is possible given the potential boninitic affinities of some mafic rocks of the Narracoota Formations.
- DeGrussa proximal alteration includes chlorite and talc-carbonate. Chlorite schist surrounds the contacts of the massive sulfide lenses. The unit is generally strongly sheared although

less deformed variations contain abundant disseminated sulfide (pyrite and chalcopyrite). Talc-chlorite-carbonate(±sulfide) schist occurs as lenses, along either the upper or lower contacts of the ore bodies and separated from mineralisation only by chlorite schist, or interbedded within the ore deposit.

- Magnetite forms in the hottest, central core of the deposit in association with pyrite and lesser chalcopyrite and pyrrhotite. Sphalerite and galena form in rare horizons throughout the ore lenses.
- Geological evidence indicates that reduced, hydrothermal, mineralising fluids deposited a pyrite-chalcopyrite-pyrrhotite dominant mineral assemblage via fault controlled feeder structures at temperatures of 250-350°C and pH of 5-7. Replacement textures indicate parts of the deposit were formed in the sub seafloor environment, although seafloor textures and chimney structures are present in parts of the deposit and the heavy $\delta^{34}S$ tail indicates mixing of the metal-bearing hydrothermal fluid with some sea water sulfate. The lack of sulfate minerals in the ore, but the presence of peripheral jasper, suggests that DeGrussa formed in a sub-oxic to oxic, low sulfate oceanic sub-basin.
- The $\delta^{34}S$ data are considered to be consistent with a reduced, metal-bearing, hydrothermal fluid, initially of acidic composition (pH 3-5), which mixed with a possible magmatic-hydrothermal component, leaching the footwall and host sedimentary and basaltic rocks and depositing sulfide onto the seafloor and sub seafloor under changing temperature and pH. The $\delta^{34}S$ values of +0.3 to +6.3‰ of DeGrussa sulfides are comparable to igneous values and could form by leaching of volcanic S.
- The low contents of Pb and Zn present in the deposit may be sourced from leaching of the surrounding low Pb, low Zn sedimentary and mafic rocks. Lead isotopes indicate a crustal source of lead, and higher $\delta^{34}S$ for pyrite (up to +9.8‰) suggest mixing with a secondary seawater sulfur source.
- Sulfur isotopes can clearly distinguish the fault-controlled Thaduna Copper Deposit from VHMS ores and orogenic gold deposits across the rest of the region. Fortnum and Cassidy are

not easily distinguished isotopically from the DeGrussa deposit at the current extent of sampling. The Horseshoe Lights deposit is comparable with the higher range of DeGrussa values, however has very distinct high values >+40‰ which require further sampling to properly understand the significance.

- The copper-rich dolerites at DeGrussa did not contribute any significant metal content to mineralisation and appearing to be syn- post-date mineralisation, perhaps keeping the mineralising system hot.
- Bryah Group rocks were likely deposited concurrently with subduction and rifting as recorded by the Camel Hills Metamorphics and Dalgaringa Supersuite in the western Capricorn Orogen. DeGrussa mineralisation was dated to between 2011 ± 7 Ma and 2027 ± 7 Ma (Re-Os) and 2060 ± 50 Ma and 2075 ± 50 Ma (Pb model ages) constraining the maximum deposition age for the Bryah Group rocks at c. 2075 Ma. Dolerites post-date the DeGrussa mineralisation (2003 ± 7 Ma to 1991 ± 7 Ma) and regional granodiorites (fractionated dolerites) provide the first age for the Narracoota Formation of 2014 ± 7 Ma and 2018 ± 9 Ma.
- Limitations of the Pb isotopic models are indicated by the large discrepancy in ages between the Cumming and Richards (1975) method used in previous studies, and the Stacey and Kramers (1975) method used for the DeGrussa deposit. Comparable data obtained between the Re-Os and Stacey and Kramers (1975) ages suggests that the Stacey and Kramers (1975) model curve provides more robust ages. This allows a new age of 2000 ± 35 Ma for Horseshoe Lights pyrite (or 2075 ± 50 Ma by LA-ICPMS), indicating that this deposit may have developed at a similar time to that of DeGrussa. Furthermore, applying the Stacey and Kramers (1975) model to basin mineralisation provides ages that correlate with the major regional orogenic events: the Glenburgh from 2005-1960 Ma (DeGrussa and Horseshoe Lights forming in an extensional basin rift setting during deposition of Bryah Group sediments, while Peak Hill – main pit and Fiveways formed under compression in the Archean Peak Hill Schist), the Capricorn from 1830-1780 Ma (Labouchere, Mt. Pleasant and Nathans), the Mangaroon from 1690-1620 Ma (Peak Hill- Main pit), the Mutherbukin Tectonic Event between 1320 and 1170

Ma (Nathans), and the Edmundian from 1030-955 Ma (Fortnum-Starlight deposit). An age for mineralisation of 1475 ± 50 Ma is interpreted for the Thaduna Copper deposit.

- These new ages assist in constraining stratigraphy and mineralising events of the Paleoproterozoic Yerrida, Bryah and Padbury Group sedimentary rocks and their associations with regional orogenic events. Identification of prospective time periods and stratigraphy associated with major mineralising events will assist in exploration for significant gold and base metal mineralisation in the Capricorn Orogen.

9.2. Exploration Implications

As was discussed by Galley et al. (2007), the exploration model for VHMS deposits requires areas of focused heat flow caused by tectonic extension, mantle depressurisation, and the resultant formation of high-T mantle melts, crustal melts and common bimodal volcanic successions. The most prospective VHMS districts are characterised by bimodal volcanic successions that have a tholeiitic to transitional tholeiitic-calc alkaline composition (Galley et al., 2007). The Yerrida-Bryah region fits this description, with the Johnson Cairn Formation basalts being calc-alkaline in the Yerrida Group and the Killara, DeGrussa and Narracoota tholeiitic. Felsic volcanism is present towards the west in the vicinity of the Horseshoe Lights and Fortnum deposits.

The presence of the dolerite sills and dykes around DeGrussa suggests that this is an area of high heat flow favourable for VHMS formation, similar to prospective areas suggested by Galley et al. (2007). Similar areas with abundant dikes could be the target for further exploration.

Whether the copper in the dolerite sills and dikes associated with DeGrussa is a primary feature of the magma, or a result of proximal Cu-rich mineralisation, the identification of copper-rich dolerites could still indicate proximity to a major copper-rich VHMS deposit. and may assist to constrain target areas for deposits.

Trace sulfides could be analysed for Pb isotopes to identify if they are part of the same mineralising hydrothermal system as DeGrussa. As shown for the other deposits in the district,

those that are not of the same type and age have different lead isotope compositions. Further work, however, should be done into exploration around the Fortnum gold deposits and the relationship of gold bearing cherts to possible VHMS mineralisation as resetting of pyrite Pb isotope ages may be possible in this region.

Sulfur isotope data does not clearly distinguish the DeGrussa deposit from the orogenic gold deposits in the west of the basin. However, the heavier $\delta^{34}S$ values, also similar to those seen at Horseshoe Lights and inferring interaction of hydrothermal sulfur with sea water sulfur at the sea floor interface, could indicate the unique depositional environment of the VHMS deposits in the district.

9.3. Further work

Some of the areas in which more work could be attempted are as follows:

1. Studies into constraining the stratigraphy of the Bryah Group and its relationship to the Yerrida Group rocks. Comparison of the Eastern Capricorn Orogen and its relationship to the Dalgaringa supersuite and the location of all sedimentary basins at the time of DeGrussa deposition. Identification of what lies under the Earaheedy Group and the Bangemall (Edmund and Collier) Basins as it may be a continuation of the Bryah Group or similar aged rift succession with potential for VHMS mineralisation.
2. Identification of the DeGrussa host unit across the district and its potential for mineralisation.
3. A more widespread and well-spaced study of the dolerites at DeGrussa and across the Bryah basin is required to assess the characteristics, if any, that may be associated with base metal mineralisation.
4. A widespread and detailed study of the geochemistry of mafic and felsic volcanic rocks in the region to identify the changes across the Bryah and Yerrida Groups to better constrain the tectonic environment of emplacement, and identify if there is any relationship to mineralisation.

5. Studies of the chert and jasper exhalite and their relationship to mineralisation both at DeGrussa and other deposit across the Bryah Basin.
6. The region has a characteristically high μ of 10.8 indicating a crustal source of Pb, which preliminary studies suggest is a feature of other Proterozoic basins of Western Australia, as well as the Archean Craton. A widespread study could be attempted of the Pb isotopes across the district and the Yilgarn terrane (E.g. The Youanmi and the Eastern Goldfields terranes that underlie the eastern Bryah Basin and DeGrussa). Are there any comparisons that can be made for the Pb ratios of VHMS and other deposits across the district?
7. A systematic and widespread study of the sulfur isotopes at DeGrussa and within the surrounding host rocks to assess any changes due to position in the ore deposit or distance from the ore deposit. Could any characteristic patterns be then seen in support of a magmatic-hydrothermal or sea water source of sulfur.
8. Multiple sulfur isotope studies ($\Delta^{33}S$) of the DeGrussa mineralisation and the host stratigraphy may be able to identify if any mass independent fractionation of sulfur was occurring at the time. Additionally, the identification of any Archean sulfur incorporated into the footwall and host rock sequence may be possible.
9. As discussed in Chapter 7, more data needs to be collected for the orogenic gold deposits to properly define their sulfur isotope populations. The small number of samples, but similar heavy $\delta^{34}S$ values suggest that these deposits may also have a sea water component (although sea water at ~2.0 Ga is 0‰) and the presence of hematitic chert at this time suggests a possible exhalative formation. Similarly, a more controlled sampling program for DeGrussa sulfides may better define the sulfur isotope distribution for mineralisation formed in the sub seafloor and seafloor environments.

10. References

ADAMCZYK, K. 2013. Understanding the context of volcanogenic massive sulphide deposits in the Paleo-Proterozoic and Archean Basins: The stratigraphic and faces architecture and origins of the Paleo-Proterozoic DeGrussa volcanogenic massive sulphide deposit host-rock succession, Western Australia. *Honours Thesis, School of Geosciences, Monash University*.

ADAMIDES, N. G. 1998. Geology of the Doolgunna 1:100 000 Sheet. *Geological Survey of Western Australia Explanatory Notes*.

AHARON, P. 2005. Redox stratification and anoxia of the early Precambrian oceans: Implications for carbon isotope excursions and oxidation events. *Precambrian Research*.

AMES, D. E., FRANKLIN, J. M. & HANNINGTON, M. 1993. Mineralogy and geochemisry of active and inactive chimneys and massive sulfide, middle valley, northern Juan de Fuca ridge: an evolving hydrothermal system. *The Canadian Mineralogist,* 31**,** 997-1024.

ANONYMOUS 2014. DeGrussa Sulphide textures and open cut observations. *CSA Report No: R121.2014*.

ANONYMOUS. 2015. *Thunderlarra Resources - Red Bore Project* [Online]. Available: http://www.thundelarra.com/projects/doolgunna-wa/red-bore/ [Accessed 21/05/2015].

ANONYMOUS 2016a. Maiden high-grade mineral resource for Monty VMS deposit: 99,000t copper and 55,000 oz gold. *Sandfire Resources NL ASX Announcement 13 April 2016*.

ANONYMOUS. 2016b. *Mindat.org* [Online]. Available: http://www.mindat.org/min-2085.html [Accessed].

ARCHIBALD, S. M., MIGDISOV, A. A. & WILLIAMS-JONES, A. E. 2002. An experimental study of the stability of copper chloride complexes in water vapor at elevated temperatures and pressures. *Geochimica et Cosmochimica Acta,* 66**,** 1611-1619.

ARCULUS, R. J. 1994. Aspects of magma genesis in arcs. *Lithos,* 33**,** 189-208.

AYUSO, R. A., KARL, S. M., SLACK, J. F., HAEUSSLER, P. J., BITTENBENDER, P. E., WANDLESS, G. A. & COLVIN, A. S. 2007. Oceanic Pb-isotopic sources of Proterozoic and Palaeozoic volcanogenic massive sulfide deposits on Prince of Wales Island and Vicinity, Southeastern Alaska. *US Geological Survey Professional Paper*.

BAGAS, L. 1999. Early tectonic history of the Marymia Inlier and correlation with the Archaean Yilgarn Craton, Western Australia. *Australian Journal of Earth Sciences,* 46**,** 115-125.

BAKER, J., PEATE, D., WAIGHT, T. & MEYZEN, C. 2004. Pb isotopic analysis of standards and samples using a Pb-207-Pb-204 double spike and thallium to correct for mass bias with a double-focusing MC-ICP-MS. . *Chemical Geology,* 211**,** 275-303.

BAKER, W. 2015. Lithostratigraphy and Facies Architecture of the Footwall to the DeGrussa Volcanic Hosted Massive Sulphide Deposit, Western Australia. *Honours Thesis, CODES, School of Earth Sciences, University of Tasmania*.

BARRIE, C. T. & HANNINGTON, M. D. 1999. Classification of Volcanic-Associated Massive Sulfide Deposits Based on Host-Rock Composition. *Reviews in Economic Geology,* 8**,** 1-11.

BEKKER, A. & HOLLAND, H. D. 2012. Oxygen overshoot and recovery during the early Paleoproterozoic. *Earth and Planetary Science Letters,* 317-318**,** 295-304.

BEKKER, A., HOLMDEN, C., BEUKES, N. J., KENIG, F., EGLINTON, B. & PATTERSON, W. P. 2008. Fractionation between inorganic and organic carbon during the Lomagundi (2.22–2.1 Ga) carbon isotope excursion. *Earth and Planetary Science Letters,* 271**,** 278-291.

BERKENBOSCH, H. A., DE RONDE, C. E. J., PAUL, B. T. & GEMMELL, J. B. 2015. Characteristics of Cu isotopes from chalcopyrite-rich black smoker chimneys at Brothers volcano, Kermadec arc, and Niuatahi volcano, Lau basin. *Miner Deposita,* 50**,** 811-824.

BEST, M. G. (ed.) 2002. *Igneous and Metamorphic Petrology.*: Blackwell Publishers.

BILLSTROM, K. & VIVALLO, W. 1994. Synvolcanic mixing of ore lead and the development of lead isotopic provinces in the Skellefte district, Sweden. *Mineralium Deposita,* 29**,** 111-119.

BINNS, R. A. 2004. Eastern Manus Basin, Papua New Guinea: guides for volcanogenic massive sulphide exploration from a modern seafloor analogue.

BLACK, L. P. & GULSON, B. L. 1978. The age of the Mud tank Carbonatite, Strangways Range, Northern Territory. *BMR Journal of Australian Geology and Geophysics* 3**,** 227-232.

BLACK, L. P., KAMO, S. L., ALLEN, C. M., DAVIS, D. W., ALENINIKOFF, J. N., VALLEY, J. W., MUNDIL, R., CAMPBELL, I. H., KORSCH, R. J., WILLIAMS, I. S. & FOUDOULIS, C. 2004. Improved 206Pb/238U microprobe geochronology by the monitoring of a trace-element related matrix effect; SHRIMP, ID-TIMS, ELA-ICP-MS, and oxygen isotope documentation for a series of zircon standards. *Chemical Geology* 205.

BLACK, L. P., KAMOS, L., ALLEN, C. M., ALEINIKOFF, J. N., DAVIS, D. W., KORSCH, R. J. & FOUDOULIS, C. 2003. TEMORA 1: a new zircon standard for Phanerozoic U–Pb geochronology. *Chemical Geology* 200**,** 155-170.

BODON, S. B. & VALENTA, R. K. 1995. Primary and tectonic features of the Currawong Zn-Cu-Pb ()-Au) massive sulfide deposit, Benambra, Victoria: Implications for ore genesis. *Economic Geology,* 90**,** 1694-1721.

BONNICI, N. 2016. Personnal communication re. lack of Teutonic Bore barite cap 27/07/16.

BOULTER, C. A. 1993. Comparison of Rio Tinto, Spain, and Guaymas Basin, Gulf of California: An explanation of a supergiant massive sulfide deposit in an ancient sill-sediment complex. *Geology,* 21**,** 801-804.

BOYNTON, W. V. 1984. Geochemistry of rare earth elements: meteorite studies. *Rare earth element geochemistry (ed. Henderson, P.)***,** 63-114.

BRAUHART, C. W. 1999. Regional alteration systems associated with Archean volcanogenic massive sulfide deposits at Panorama, Pilbara, Western Australia. *PhD thesis, University of Western Australia*.

BROWNING, P., GROVES, D. I., BLOCKLEY, J. G. & ROSMAN, K. J. R. 1987. Lead isotopes on the Age and Source of Gold Mineralization in the Archean Yilgarn Block, Western Australia. *Economic Geology,* 82**,** 971-986.

BUNTING, J. A. 1986. Geology of the eastern part of the Nabberu Basin, Western Australia. *Geological Survey of Western Australia Bulletin No. 131*.

BUNTING, J. A., COMMANDER, D. P. & GEE, R. D. 1977. Preliminary synthesis of Lower Proterozoic stratigraphy and structure adjacent to the northern margin of the Yilgarn. *Geological Survey of Western Australia Annual Report 1976***,** 43-48.

CANDELA, P. A. 1989. Calculation of magmatic fluid contributions to porphyry-type ore systems: predicting fluid inclusion chemistries. *Geochemical Journal,* 23**,** 295-305.

CANDELA, P. A. & HOLLAND, H. D. 1986. A mass transport model for copper and molybdenum in magmatic hydrothermal systems: the origin of porphyry-type ore deposits. *Economic Geology,* 81**,** 1-19.

CANFIELD, D. E. 2005. The early history of atmospheric oxygen: Homage to Robert M. Garrels. *Annu. Rev. Earth Planet. Sci.,* 33**,** 1-36.

CANFIELD, D. E. & RAISWELL, R. 1999. The evolution of the sulfur cycle. *Americal Journal of Science,* 299**,** 697-723.

CATHLES, L. M. 2011. What processes at mid-ocean ridges tell us about volcanogenic massive sulfide deposits. *Mineralium Deposita,* 46**,** 639-657.

CAWOOD, P. A. & TYLER, I. M. 2004. Assembling and reactivating the Proterozoic Capricorn Orogen: lithotectonic elements, orogenies, and significance. *Precambrian Research,* 128**,** 201-218.

CHANG, Z., VERVOORT, J. D., MCCLELLAND, W. C. & KNAACK, C. 2006. U-Pb dating of zircon by LA-ICP-MS. *Geochemistry, Geophysics, Geosystems,* 7.

CHAUSSIDON, M. & LORAND, J. P. 1990. Sulphur isotope composition of orogenic spinel lherzolite massifs from Ariege (N.E. Pyrenees, France): An ion microprobe study. *Geochimica et Cosmochimica Acta,* 54**,** 2835-2846.

CLIFT, P. D., PARSON, L. M., HAWKINS, J. W., ALLAN, J. F., ABRAHAMSEN, N., BEDNARZ, U., BLANC, G., BLOOMER, S. H., BOEL, R., BRUNS, T. R., BRYAN, W. B., CHAPRONIERE, G. C. H., EWART, A., FOWLER, M. G., HERGT, J. M., HODKINSON, R. A., LAVOIE, D., LEDBETTER, J. K., MACLEOD, C. J., NILSSON, K., NISHI, H., PRATT, C. E., QUINTERNO, P. J., REYNOLDS, R. R., ROTHWELL, R. G., SAGER, W. W., SCHOPS, D., SOAKAI, S. & STYZEN, M. 1994. Volcanism and sedimentation in a rifting island arc terrain: an example from Tonga, SW Pacific. *Geological Society Special Publication Classics: Volcanism associatied with extension at consuming plate margins***,** 29-52.

CLINE, J. S. & BODNAR, R. J. 1991. Can economic porphyry copper mineralization be generated by a typical calc-alkaline melt? *Journal of Geophysical Research,* 96**,** 8113-8126.

CLOUTIER, J., PIERCEY, S. J., LAYNE, G., HESLOP, J., HUSSEY, A. & PIERCEY, G. 2015. Styles, textural evolution, and sulfur isotope systematics of Cu-rich sulfides from the Cambrian Whalesback volcanogenic massive sulfide deposit, central Nerfoundland, Canada. *Economic Geology,* 110**,** 1215-1234.

COMPSTON, W. 1999. Geological age by instrumental analysis: the 29th Hallimond Lecture. *Mineralogical Magazine,* 63**,** 297-311.

CONDON, J. 2015. Ore types of DeGrussa and Conductor 1 ore lenses of the DeGrussa VHMS deposit, Western Australia. *Masters Thesis, CODES, University of Tasmania*.

COX, K. G., BELL, J. D. & PANKHURST, R. J. 1979. The interpretation of igneous rocks. *George Allen and Unwin, London*.

CRAIG, J. R. & VAUGHAN, D. J. 1994. *Ore Microscopy and Ore Petrography, Second Edition,* United States of America, John Wiley & Sons, Inc.

CRAIG, J. R. & VOKES, F. M. 1993. The metamorphism of pyrite and pyritic ores: an overview. *Mineralogical Magazine,* 57**,** 3-18.

CRANNEY, P. 2011. A review of the geochemistry of the Bryah and Yerrida Basins in relation to the DeGrussa mineralisation. *Sandfire Resources NL Internal Report*.

CRAWFORD, A. J., FALLOON, T. J. & GREEN, D. H. 1989. Classification, petrogenesis and tectonic setting of boninites. . *IN Boninites*.

CUMMING, G. L. & RICHARDS, J. R. 1975. Ore lead isotope ratios in a continuous changing earth. *Earth and Planetary Science Letters,* 28**,** 155-171.

DE BAAR, H. 1991. On cerium anomalies in the Sargasso Sea. *Geochimica et Cosmochimica Acta,* 55**,** 2981-2983.

DE RONDE, C. E. J., MASSOTH, G. J., BUTTERFIELD, D. A., CHIRSTENSON, B. W., ISHIBASHI, J., DITCHBURN, R. G., HANNINGTON, M. D., BRATHWAITE, R. L., LUPTON, J. E., KAMENETSKY, V. S., GRAHAM, I. J., ZELLMER, G. F., DZIAK, R. P., EMBLEY, R. W., DEKOV, V. M., MUNNIK, F., LAHR, J., EVANS, L. J. & TAKAI, K. 2011. Submarine hydrothermal activity and gold-rich mineralization at Brothers Volcano, Kermadec Arc, New Zealand. *Miner Deposita,* 46**,** 541-584.

DENTITH, M. C., JOHNSON, S. P., EVANS, S., AITKEN, A. R. A., JOLY, A., THIEL, S. & TYLER, I. M. 2014. A magnetotelluric traverse across the eastern part of the Capricorn Orogen. *Geological Survey of Western Australia,* Report 135.

DICKIN, A. P. 2005. *Radiogenic Isotope Geology*, Cambridge University Press, New York.

DIETZ, C. 2016. *RE: personal communication - email 19/05/16 (CSL staff, University of Tasmania).*

DIXON, K. 2000. Red Bore Project, Peak Hill District, 26 March 1999 to 25 March 2000, Exploration Licence 52/1130. *Troy Resources NL report TR009/00 GSWA Open File Report*

DOYLE, M. G. & ALLEN, R. L. 2003. Subsea-floor replacement in volcanic-hosted massive sulfide deposits. *Ore Geology Reviews,* 23**,** 183-222.

DYER, F. L. 1991. The nature and origin of gold mineralization at the Fotnum, Nathan's and Labouchere Deposits, Glengarry Basin, Western Australia. *Thesis (Honours), University of Western Australia*.

EASTOE, C. J. & GUSTIN, M. M. 1996. Volcanogenic massive sulfide deposits and anoxia in the Phanerozoic oceans. *Ore Geology Reviews,* 10**,** 179-197.

EBERLI, G. P. 1987. Carbonate turbidite sequences deposited in rift-basins of the Jurrasic Tethy Ocean (eastern Alps, Switzerland). *Sedimentology,* 34**,** 363-388.

EL DESOUKY, H. A., MUCHEZ, P., BOYCE, A. J., SCHNEIDER, J., CAILTEUX, J. L. H., DEWAELE, S. & VON QUADT, A. 2010. Genesis of sediment-hosted stratifrom copper-cobalt mineralization at Luiswishi and Kamoto, Katanga Copperbelt (Democratic Republic of Congo). *Miner Deposita,* 45**,** 735-763.

EL TABAKH, M., GREY, K., PIRAJNO, F. & CHARLOTTE SCHREIBER, B. 1999. Pseudomorphs after evaporitic minerals interbedded with 2.2 Ga stromatolites of the Yerrida basin, Western Australia: Origin and significance. *Geology,* 27**,** 871.

ELDRIDGE, C. S., BARTON JR., P. B. & OHMOTO, H. 1983. Mineral textures and their bearing of formation of the Kuroko orebodies. *Economic Geology,* Monograph 5**,** 241-281.

EMBLEY, R. W., JONASSON, I. R., PERFIT, M. R., FRANKLIN, J. M., TIVEY, M. A., MALAHOFF, A., SMITH, M. F. & FRANCIS, T. J. G. 1988. Submersible investigation of an extinct hydrothermal system on the Galapagos Ridge: Sulfide mounds, stockwork zone, and differentiated lavas. *Canadian Mineralogist,* 26**,** 517-539.

EVANS, W. J. 2009. 27% copper intersected over 8 metres at Doolgunna. *Sandfire Resources NL, ASX Release*.

FALLON, M., PORWAL, A. & GUJ, P. 2010. Prospectivity analysis of the Plutonic Marymia Greenstone Belt Western Australia. *Ore Geology Reviews,* 38**,** 208-218.

FARQUHAR, J., SAVARINO, J., AIRIEAU, S. & THIEMENS, M. H. 2001. Observation of wavelength-sensitive mass-independant sulfur isotope effects during SO2 photolysis: Implications for the early atmosphere. *Journal of Geophysical Research,* 106**,** 32829-32839.

FARQUHAR, J., WU, N., CANFIELD, D. E. & ODURO, H. 2010. Connections between sulfur cycle evolution, sulfur isotopes, sediments, and base metal sulfide deposits. *Economic Geology,* 105**,** 509-533.

FOX, J. S. 1984. Besshi-type volcanogenic sulphide deposits - a review. *CIM Bulletin,* 77**,** 57-68.

FOX, J. S., FARQUHAR, R., RUI, I. & COOK, N. 1988. Genesis of basalt hosted massive sulphide deposits from the Trondhein and Sulitjelma districts Norway ore lead isotopic considerations. *Mineralium Deposita,* 23**,** 276-285.

FRANKLIN, J. M., GIBSON, H. L., JONASSON, I. R. & GALLEY, A. G. 2005. Volcanogenic Massive Sulfide Deposits. *Economic Geology 100th Anniversary Volume***,** 523-560.

FRANKLIN, J. M., LYDON, J. W. & SANGSTER, D. F. 1981. Volcanic-Associated Massive Sulfide Deposits. *Economic Geology 75th Anniversary Volume,* 485-627.

FRONDEL, C. & ITO, J. 1966. Zincian Aegerine-augite and Jeffersonite from Franklin, New Jersey. *The American Mineralogist,* 51**,** 1406-1413.
FRYER, B. J., JACKSON, S. E. & LONGERICH, H. P. 1993. The Application of Laser Ablation Microprobe-Inductively Coupled Plasma-Mass Spectrometry (Lam-Icp-Ms) to in situ (U)-Pb Geochronology. *Chemical Geology,* 109**,** 1-8.
GALLEY, A. G., HANNINGTON, M. D. & JONASSON, I. R. 2007. Volcanogenic massive sulphide deposits. *in Goodfellow, W., ed., Mineral deposits of Canada: A synthesis of major deposit types, district metallogeny, and the evolution of geological provinces, and exploration methods, 5: St. Johns, Geological Association of Canada, Mineral Deposits Division, Special Publication 5***,** 141–162.
GALLEY, A. G. & KOSKI, R. A. 1999. Setting and Characteristics of Ophiolite-Hosted Volcanogenic Massive Sulfide Desposits. *Reveiws in Economic Geology,* 8**,** 221-246.
GAZLEY, M. F. 2011. Metamorphism, geochronology and stratigraphy of an amphibolite-facies greenstone-hosted gold deposit: Plutonic Gold Mine, Marymia Inlier, Western Australia. *PHD thesis, Victoria University of Wellington*.
GEE, R. D. 1979. The geology of the Peak Hill Area., Western Australia. *Department of Mines. Annual Report, 1978***,** 99-106.
GEE, R. D. 1986. Explanatory Notes on the Peak Hill 1:250 000 Geological Sheet, Western Australia, Second Edition. *Geological Survey of Western Australia Record 1986/11*.
GEE, R. D. 1987. Peak Hill Western Ausatralia. *Geological Survey of Western Australia 1: 250 000 Geological Series - Explanatory Notes*.
GEE, R. D. 1990. Nabberu Basin. *Geology and Mineral Resources of Western Australia, Geological Survey of Western Australia Memoir 3***,** 202-210.
GEE, R. D. & GREY, K. 1993. Proterozoic Rocks on the Glengarry 1:250 000 sheet - stratigraphy, structure and stromatolite biostratigraphy. *Geological Survey of Western Australia Report 41*.
GELLATLY, A. M. & LYONS, T. W. 2005. Trace sulfate in mid-Proterozoic carbonates and the sulfur isotope record of biospheric evolution. *Geochimica et Cosmochimica Acta,* 69**,** 3813-3829.
GEMMELL, J. B. & FULTON, R. 2001. Geology, genesis, and exploration implications of the footwall and hanging-wall alteration associated with the Hellyer Volcanic-Hosted Massive Sulfide deposit, Tasmania, Australia. *Economic Geology,* 96**,** 1003-1035.
GEOROC. 2014. *Georoc: Geochemistry of Rocks of the Oceans and Continents* [Online]. Max Planck Institute for Chemistry Mainz, Germany Available: http://georoc.mpch-mainz.gwdg.de/georoc/ [Accessed].
GIBSON, H. L., MORTON, R. L. & HUDAK, G. 1999. Submarine Volcanic Processes, Deposits And Environments Favorable For The Location Of Volcanic-associated Massive Sulfide Deposits. *In Barrie, C.T., and Hannington, M.D. (Eds) Volcanic-associated massive sulfide deposits: Processes and examples*
in modern and ancient settings. Reviews in Economic Geology, 8**,** 13-51.
GIESKES, J. M., KASTNER, M., EINSELE, G., KELTS, K. & NIEMITZ, J. 1982. 55. Hydrothermal Activity in the Guaymas Basin, Gulf of California: A Synthesis.
GILLIES, S. L. 1988. Horseshoe Lights, Western Australia: A Proterozoic gold- and copper-rich massive sulphide deposit. *Thesis (Honours), University of Western Australia*.
GLASBY, G. P., IIZASA, K., HANNINGTON, M., KUBOTA, H. & NOTSU, K. 2008. Mineralogy and composition of Kuroko deposits from northeastern Honshu and their possible modern analogues from the Izu-Ogasawara (Bonin) Arc south of Japan: Implications for mode of formation. *Ore Geology Reviews,* 34**,** 547-560.
GOODFELLOW, W. D. & ZIERENBERG, R. A. 1999. Genesis of Massive Sulfide Deposits at Sediment-Covered Spreading Centers. *Reveiws in Economic Geology,* 8**,** 297-324.
GOTTHARD, R. 2005. Whole-rock multi-element geochemistry study. *Gleneagle Gold Ltd Company Report*.
GREY, K. 1984. Biostratigraphical studies of stromatolites from the Proterozoic Earaheedy Group, Nabberu Basin, Western Australia. *Geological Survey of Western Australia Bulletin No. 130*.
GREY, K. 1994. Stromatolites from the Palaeoproterozoic (Orosirian) Glengarry Group, Glengarry Basin, Western Australia. *Alcheringa: An Australasian Journal of Palaeontology,* 18**,** 275-300.
GREY, K. 2012a. personal communication. GSWA biostratigraphy and stromatolite expert.
GREY, K. 2012b. Yerrida Group poster prep IGC. *personal notes K. Grey*.
GREY, K. & PIRAJNO, F. 2012. The Lomagundi-Jatulian event in the Bubble Well Member, Juderina Formation, Yerrida Basin, Western Australia. *IGC 23*.
GROVES, I. M. 1996. Cassidy, Horseshoe and the Pod Mines: A Geological and Structural Interpretation, Appendix 1.
GRUNER, J. W. 1944. The composition and structure of minnesotaite, a common iron silicate in iron formations.

GUILLONG, M., KUHN, H. R. & GUNTHER, D. 2003. Application of a particle separation device to reduce inductively coupled plasma-enhanced elemental fractionation in laser ablation-inductively coupled plasma-mass spectrometry. *Spectrochimica Acta - Part B Atomic Spectroscopy,* 58**,** 211-220.

GULSON, B. L. & PORRITT, P. M. 1987. Base metal exploration of the Mount Read volcanics, Western Tasmania: Pt. II. Lead isotope signatures and genetic implications. *Economic Geology,* 82**,** 291-307.

HALILOVIC, J., CAWOOD, P. A., JONES, J. A., PIRAJNO, F. & NEMCHIN, A. A. 2004. Provenance of the Earaheedy Basin: implications for assembly of the Western Australian Craton. *Precambrian Research,* 128**,** 343-366.

HALL, W. D. M. & GOODE, A. D. T. 1978. The Early Proterozoic Nabberu Basin and associated iron formations of Western Australia. *Precambrian Research,* 31**,** 107-132.

HALLBERG, J. A. & THOMPSON, J. F. H. 1985. Geologic Setting of the Teutonic Bore Massive Sulfide Deposit, Archcan Yilgarn Block, Western Australia. *Economic Geology,* 90**,** 1953-1964.

HALPIN, J. A., JENSEN, T., MCGOLDRICK, P., MEFFRE, S., BERRY, R. F., EVERARD, J. L., CALVER, C. R., THOMPSON, J., GOEMANN, K. & WHITTAKER, J. M. 2014. Authigenic monazite and detrital zircon dating from the Proterozoic Rocky Cape Group, Tasmania: Links to the Belt-Purcell Supergroup, North America. *Precambrian Research,* 250**,** 50-67.

HANNINGTON, M., GALLEY, A. G., HERZIG, P. M. & PETERSEN, S. 1998. Comparison of the TAG mound and stockwork complex with Cyprus-type massive sulfide deposits. *in Herzig, P. M., Humphris, S. E., Miller, D. J., and Zierenberg, R. A. (Eds.), 1998 Proceedings of the Ocean Drilling Program, Scientific Results,* 158**,** 389-415.

HANNINGTON, M. D., BLEEKER, W. & KJARSGAARD, I. 1999a. Sulfide mineralogy, geochemistry and ore genesis of the Kidd Creek Deposit: Park 1. North, central, and south orebodies. *Economic Geology Monograph 10***,** 163-224.

HANNINGTON, M. D., BLEEKER, W. & KJARSGAARD, I. 1999b. Sulfide mineralogy, geochemistry, and ore genesis of the Kidd Creek deposit: Part II. The bornite zone. *Economic Geology Monograph 10***,** 225-266.

HARLEY, S. L. & KELLY, N. M. 2007. Zircon: Tiny but timely. *Elements,* 3**,** 13-18.

HARPER, M., HILL, M. G., RENTON, J. I. & THORNETT, S. E. 1998. *Gold Deposits of the Peak Hill area, Western Australia*, Australasian Institute of Mining and Metallurgy, Monograph 14.

HASS, J. 1999. Genesis of Late Cretaceous toe-of-slope breccias in the Bakony Mts, Hungary. *Sedimentary Geology,* 128**,** 51-66.

HAWKE, M. L. in prep. The Geology of the DeGrussa Cu-Au-Ag Volcanic-Hosted Massive Sulfide Deposit. *PhD thesis, University of Tasmania*.

HAWKE, M. L., MEFFRE, S., STEIN, H., HILLIARD, P., LARGE, R. & GEMMELL, J. B. 2015. Geochronology of the DeGrussa Volcanic Hosted Massive Sulfide Deposit and Associated Mineralization of the Yerrida, Bryah and Padbury Basins, Western Australia. *Precambrian Research,* 267**,** 250-284.

HAWKINS, J. W. 1995. The Geology of the Lau Basin. *In: Taylor, B. Backarc Basins: Tectonics and Magmatism***,** 63-138.

HERZIG, P. M., PETERSEN, S., KUHN, T., HANNINGTON, M. D., GEMMELL, J. B. & SKINNER, A. C. 2003. Shallow drilling of seafloor hydrothermal systems: The missing link. *Mineral Exploration and Sustainable Development, Eliopoulos et al, (eds), Millpress, Rotterdam*.

HILLIARD, P. 2013a. DeGrussa Copper Mine, Geology Presentation: Geological Evolution, Stratigraph and Structure. October 2013. *Sandfire Resources NL Internal Presentation*.

HILLIARD, P. 2013b. Personal Communication (Sandfire Resources Geologist).

HILLIARD, P. 2015. Personal Communication: Email correspondance 21 October (Sandfire Resources Geologist).

HILLIARD, P., ADAMCZYK, K. & HAWKE, M. L. in prep. DeGrussa Copper-gold deposit. *Australian Ore Deposits Monograph*.

HINE, A. C., LOCKER, S. D., TEDESCO, L. P., MULLINS, H. T., HALLOCK, P., BELKNAP, D. F., GONZALES, J. L., NEUMANN, A. C. & SNYDER, S. W. 1992. Megabreccia shedding from modern, low-relief carbonate platforms, Nicaraguan Rise. *Geological Society of America Bulletin,* 104**,** 928-943.

HITZMAN, M., SELLEY, D. & BULL, S. 2010. Formation of sedimentary rock-hosted straiform copper deposits through earth history. *Economic Geology,* 105**,** 627-639.

HO, S. E., MCNAUGHTON, N. J. & GROVES, D. I. 1994. Criteria for determining initial lead isotopic compositions of pyrite in Archean lode-gold deposits: a case study at Victory, Kambalda, Western Australia. *Chemical Geology,* 111.

HUMPHRIS, S. E., HERZIG, P. M., MILLER, D. J., ALT, J. C., BECKER, K., BROWN, D., BRUGMANN, G., CHIBA, H., FOUQUET, Y., GEMMELL, J. B., GUERIN, G., HANNINGTON, M. D., HOLM, N. G., HONNOREZ, J. J.,

ITURRINO, G. J., KNOTT, R., LUDWIG, R., NAKAMURA, K., PETERSEN, S., REYSENBACH, A. L., RONA, P. A., SMITH, S., STURZ, A. A., TIVEY, M. K. & ZHAO, X. 1995. The Internal Structure Of An Active Sea-floor Massive Sulfide Deposit. *Nature,* 377**,** 713-716.

HUSTON, D. & LARGE, R. R. 1989. A chemical model for the concentration of gold in volcanogenic massive sulphide deposits. *Ore Geology Reviews,* 4**,** 171-200.

HUSTON, D. & LOGAN, G. 2004. Barite BIFs and bugs: evidence for the evolution of the Easrth's early hydrosphere. *Earth and Planetary Science Letters,* 220**,** 41-55.

HUSTON, D. L., BRAUHART, C. W., DRIEBERG, S. L., DAVIDSON, G. J. & GROVES, D. I. 2001. Metal leaching and inorganic sulfate reduction in volcanic-hosted massive sulfide mineral systems: Evidence from the paleo-Archean Panorama district, Western Australia. *Geology,* 29**,** 687-690.

HUSTON, D. L., RELVAS, J. M. R. S., GEMMELL, J. B. & DRIEBERG, S. 2010. The role of granites in volcanic-hosted massive sulphide ore-forming systems: an assessment of magmatic–hydrothermal contributions. *Mineralium Deposita,* 46**,** 473-507.

HYNES, A. & GEE, R. D. 1986. Geological setting and petrochemistry of the Narracoota Volcanics, Capricorn Orogen, Western Australia. *Precambrian Research,* 31**,** 107-132.

INVERNO, C. M. C., SOLOMON, M., BARTON, M. D. & FODEN, J. 2008. The Cu Stockwork And Massive Sulphide Ore Of The Feitais Volcanic-Hosted Massive Sulphide Deposit, Aljustrel, Iberian Pyrite Belt, Portugal: A Mineralogical, Fluid Inclusion and Isotopic Investigation. *Economic Geology,* 103**,** 241-267.

IRVINE, T. N. 1981. Terminology for Layered Intrusions. *Journal of Petrology,* 23**,** 127-162.

IRVINE, T. N. & BARAGAR, W. R. A. 1971. A guide to the Chemical Classification of the Common Volcanic Rocks. *Canadian Journal of Earth Sciences,* 8**,** 523-548.

JACKSON, S. E., PEARSON, N. J., GRIFFIN, W. L. & BELOUSOVA, E. A. 2004. The application of laser ablation-inductively coupled plasma-mass spectrometry to in situ U–Pb zircon geochronology. *Chemical Geology* 211**,** 47-69.

JAN M. PETER & SCOTT, S. D. 1999. Windy Craggy, Northwestern Britsih Colombia: The World's Largest Besshi-Type Deposit. *Reveiws in Economic Geology,* 8**,** 261-295.

JEFFERY, R. G. 2011. Sandfire Resources NL Geological Mapping Report. *Internal Sandfire Report*.

JEFFERY, R. G. 2013. Addendum to geological mapping report - Doolgunna Project. *Sandfire Resources NL Internal Report*.

JOHNSON, S. P. 2013. The birth of supercontinents and the Proterozoic assembly of Western Australia. *Geological Survey of Western Australia***,** 78.

JOHNSON, S. P., SHEPPARD, S., RASMUSSEN, B., WINGATE, M. T. D., KIRKLAND, C. L., MUHLING, J. R., FLETCHER, I. R. & BELOUSOVA, E. A. 2010. The Glenburgh Orogen as a record of Palaeoproterozoic continent-continent collision. *Geological Survey of Western Australia Record 2010/5*.

JOHNSON, S. P., SHEPPARD, S., RASMUSSEN, B., WINGATE, M. T. D., KIRKLAND, C. L., MUHLING, J. R., FLETCHER, I. R. & BELOUSOVA, E. A. 2011a. Two collisions, two sutures: Punctuated pre-1950Ma assembly of the West Australian Craton during the Opthalmian and Glenburgh Orogenies. *Precambrian Research,* 189**,** 239-262.

JOHNSON, S. P., SHEPPARD, S., THORNE, A. M., RASMUSSEN, B. & FLETCHER, I. R. 2011b. The role of the 1280 to 1250 Ma Mutherbukin tectonic event in shaping the crustal architecture and mineralisation history of the Capricorn Orogen. *GSWA 2011 extended abstracts: promoting the prospectivity of Western Australia. Geological Survey of Western Australia, Record 2011/2***,** 1-3.

JOHNSON, S. P., SHEPPARD, S., WINGATE, M. T. D., KIRKLAND, C. L. & BELOUSOVA, E. A. 2011c. Temporal and Hafnium Isotopic Evolution of the Glenburgh Terrane Basement: an exotic crustal fragment in the Capricorn Orogen. *Geological Survey of Western Australia, Report 110***,** 27p.

JOHNSON, S. P., THORNE, A. M., TYLER, I. M., KORSCH, R. J., KENNETT, B. L. N., CUTTEN, H. N., GOODWIN, J., BLAY, O., BLEWETT, R. S., JOLY, A., DENTITH, M. C., AITKEN, A. R. A., HOLZSCHUH, J., SALMON, M., READING, A., HEINSON, G., BOREN, G., ROSS, J., COSTELLOE, R. D. & FOMIN, T. 2013. Crustal architecture of the Capricorn Orogen Western Australia and associated metallogeny. *Australian Journal of Earth Sciences: An International Geoscience Journal of the Geological Society of Australia,* 60**,** 681-705.

KARHU, J. A. & HOLLAND, H. D. 1996. Carbon isotopes and the rise of atmospheric oxygen. *Geology* 24**,** 867–870.

KEITH, M., HAASE, K. M., KLEMD, R., KRUMM, S. & STRAUSS, H. 2016. Systematic variations of trace element and sulfur isotope compositions in pyrite with stratigraphic depth in the Skouriotissa volcanic-hosted massive sulfide deposit, Troodos ophiolite, Cyprus. *Chemical Geology,* 423**,** 7-18.

KNITTEL, U. & OLES, D. 1994. Basaltic volcanism associated with extensional tectonics in the taiwan-Luzon island arc: evidence for non-depleted sources and subduction zone enrichment. *Geological Society*

Special Publication Classics: Volcanism associatied with extension at consuming plate margins, 77-94.
KONTAK, D. J. 1998. Geology of the Stirling Zn-Pb-Cu-Ag-Au VMS deposit, southeast Cape Breton, Nova Scotia: reinterpretation of the quartz-talc-carbonate (QTC) rock with implications for mineral exploration. *Geological Association of Canada-Mineralogical Association of Canada, Program with Abstracts,* 23, A94.
KOPPI, A. J., EDIS, R., FIELD, D. J., GEERING, H. R., KLESSA, D. A. & COCKAYNE, D. J. H. 1996. Rare earth element trends and cerium-uranium-manganese associations in weathered rock from Koongarra, Northern Territory, Australia. *Geochimica et Cosmochimica Acta,* 60, 1695-1707.
KORHONEN, F. J., JOHNSON, S. P., FLETCHER, I. R., RASMUSSEN, B., SHEPPARD, S., MUHLING, J. R., DUNKLEY, D. J., WINGATE, M. T. D., ROBERTS, M. P. & KIRKLAND, C. L. 2015. Pressure-temperature-time evolution of the Mutherbukin Tectonic Event, Capricorn Orogen. *Geological Survey of Western Australia,* Report 146, 64p.
KOSLER, J. 2001. Laser-ablation ICPMS study of metamorphic minerals and processes. *In: Sylvester P. J. ed. Laser-ablation-ICPMS in the earth sciences; principles and applications Mineralogical Association of Canada Short Course Handbook 29*, 185-202.
KOSLER, J. & SYLVESTER, P. J. 2003. Present trends and the future of zircon in geochronology; laser ablation ICPMS. *Reviews in Mineralogy and Geochemistry* 53, 243-275.
KRAPEZ, B. & MARTIN, D. M. 1999. Sequence stratigraphy of the Palaeoproterozoic Nabberu Province of Western Australia. *Australian Journal of Earth Sciences,* 46, 89-103.
KUMP, L. R. 2012. Sulfur Isotopes and the stepwise oxygenation of the biosphere. *Perspective Magazine*.
LARGE, R. 2016. Personal communication
LARGE, R. R. 1977. Chemical Evolution And Zonation Of Massive Sulfide Deposits In Volcanic Terrains. *Economic Geology,* 72, 549-572.
LARGE, R. R. 1992. Australian Volcanic-Hosted Massive Sulfide Deposits: Features, Styles, and Genetic Models. *Economic Geology,* 87, 471-510.
LARGE, R. R., GEMMELL, J. B. & PAULICK, H. 2001. The alteration box plot: A simple approach to understanding the relationship between alteration mineralogy and lithogeochemisrty associated with volcanic-hosted massive sulfide deposits. *Economic Geology,* 96, 957-971.
LEHURAY, A. P. 1984. Lead and Sulfur Isotopes and a Model for the Origin of the Ducktown Deposit, Tennessee. *Economic Geology,* 79, 1561-1573.
LINDSAY, J. F. & BRASIER, M. D. 2002. Did global tectonics drive early biosphere evolution? Carbon isotope record from 2.6 to 1.9Ga carbonates of Western Australian basins. *Precambrian Research,* 114, 1-34.
LOISEAU, J. 2014. Lithogeochemistry Project - DeGrussa, Proposed model of differentiation of the dolerites and Characterization of the geochemical signature of the host horizon. *Sandfire Resources NL Internal Presentation*.
LONSDALE, P. F. & BECKER, K. 1985. Hydrothermal plumes, hot springs, and conductive heat flow in the Southern Trough of Guaymas Basin. *Earth and Planetary Science Letters,* 73, 211-225.
LONSDALE, P. F., BISCHOFF, J. L., BURNS, V. M., KASTNER, M. & SWEENEY, R. E. 1980. A high-temperature hydrothermal deposit on the seabed at a Gulf of California spreading center. *Earth and Planetary Science Letters,* 49, 8-20.
LUDWIG, K. R. 2003. Isoplot 3.00: A Geochronological Toolkit for Microsoft Excel. *Berkeley Geochronological Centre Special Publication no. 4*.
LUO, G., ONO, S., BEUKES, N. J., WANG, D. T., XIE, S. & SUMMONS, R. E. 2016. Rapid oxygenation of Earth's atmosphere 2.33 billion years ago. *Science Advances,* 2.
LYDON, J. W. 1984. Ore Deposit Models-8 Volcanogenic Massive Sulphide Deposits Part 1: A Descriptive Model. *Geocscience Canada,* 11, 195-202.
LYONS, T. W. & SEVERMANN, S. 2006. A critical look at iron paleoredox proxies: New insights from modern euxinic marine basins. *Geochimica et Cosmochimica Acta,* 70, 5698-5722.
MACLEOD, W. N. 1970. Peak Hill, WA (1st edition). *Geological Survey of Western Australia 1: 250 000 Geological Series - Explanatory Notes*.
MARCOUX, E. 1998. Lead isotope systematics of the giant massive sulphide deposits in the Iberian Pyrite Belt. *Mineralium Deposita,* 33, 45-58.
MARCOUX, E., BELKABIR, A., GIBSON, H. L., LENTZ, D. & RUFFET, G. 2008. Draa Sfar, Morocco A Visean (331 Ma) Pyrrhotite-Rich, Polymetallic Volcanogenic Massive Sulphide Deposit In A Hercynian Sediment-Dominant Terrane. *Ore Geology Reviews,* 33, 307-328.

MARQUES, A. F. A., SCOTT, S. D. & GUILLONG, M. 2011. Magmatic degassing of ore-metals at the Menez Gwen: Input from the Azores plume into an active Mid-Atlantic Ridge seafloor hydrotheral system. *Earth and Planetary Science Letters,* 310**,** 145-160.

MARTIN, D. M. 1994. Sedimentology, sequence stratigraphy, and tectonic setting of a Palaeoproterozoic turbidite complex, lower Padbury Group, Western Australia. *Thesis (Ph.D.), University of Western Australia*.

MARTIN, D. M. & THORNE, A. M. 2004. Tectonic setting and basin evolution of the Bangemall Supergroup in the northwestern Capricorn Orogen. *Precambrian Research,* 128**,** 385-409.

MASLENNIKOV, V. V., MASLENNIKOVA, S. P., LARGE, R. R. & DANYUSHEVSKY, L. V. 2009. Study of Trace Element Zonation in Vent Chimneys from the Silurian Yaman-Kasy Volcanic-Hosted Massive Sulfide Deposit (Southern Urals, Russis) Using Laser Ablation-Inductively Coupled Plasma Mass Spectrometry (LA-ICPMS). *Economic Geology,* 104**,** 1111-1141.

MASLENNIKOV, V. V., MASLENNIKOVA, S. P., LARGE, R. R., DANYUSHEVSKY, L. V., HERRINGTON, R. J. & STANLEY, C. J. 2013. Tellurium-bearing minerals in zoned sulfide chimneys from Cu-Zn massive sulfide deposits of the Urals, Russia. *Mineralogy and Petrology,* 107**,** 67-99.

MASON, D. R. 2011. Petrographic Descriptions for Twenty-one Rock Samples from the DeGrussa VMS Deposit (Doolgunna Project, Peak Hill Region, Western Australia) Full Report. *Mason Geoscience Internal Report #3723*.

MASTER, S., BEKKER, A. & HOFMANN, A. 2010. A review of the stratigraphy and geological setting of the Palaeoproterozoic Magondi Supergroup, Zimbabwe – Type locality for the Lomagundi carbon isotope excursion. *Precambrian Research,* 182**,** 254-273.

MCKNIGHT, S. W. 2009. Report on Drill Core Samples DGDD001, 024, 035, 102 DeGrussa (SAN00016845). *Internal Sandfire Report*.

MCKNIGHT, S. W. 2010. Mineralogical Report on Drill-Core Samples Submitted by Sandfire Resources NL. *Internal Sandfire Report SAN00018281*.

MCKNIGHT, S. W. 2011. Mineralogical Report on Drill-Core Samples Submitted by Sandfire Resources NL. *Internal Sandfire report by McKnight Mineralogy*.

MEFFRE, S., LARGE, R. R., SCOTT, R., WOODHEAD, J., CHANG, Z., GILBERT, S. E., DANYUSHEVSKY, L. V., MASLENNIKOV, V. & HERGT, J. M. 2008. Age and pyrite Pb-isotopic composition of the giant Sukhoi Log sediment-hosted gold deposit, Russia. *Geochimica et Cosmochimica Acta,* 72**,** 2377-2391.

MELEKESTSEVA, I. Y., ZAYKOV, V. V., NIMIS, P., TRET'YAKOV, G. A. & TESSALINA, S. G. 2013. Cu–(Ni–Co–Au)-bearing massive sulfide deposits associated with mafic–ultramafic rocks of the Main Urals Fault, South Urals: Geological structures, ore textural and mineralogical features, comparison with modern analogs. *Ore Geology Reviews,* 52**,** 18-36.

MELEZHIK, V. A., HUHMA, H., CONDON, D. J., FALLICK, A. E. & WHITEHOUSE, M. J. 2007. Temporal constraints on the Paleoproterozoic Lomagundi-Jatuli carbon isotopic event. *Geology,* 35**,** 655.

MERCIER-LANGEVIN, P., HANNINGTON, M. D., DUBÉ, B. & BÉCU, V. 2010. The gold content of volcanogenic massive sulfide deposits. *Mineralium Deposita,* 46**,** 509-539.

MESCHEDE, M. & BARCKHAUSEN, U. 2001. The relationship of the Cocos and Carnegie ridges: age constraints from paleogeographic reconstructions. *International Journal of Earth Sciences,* 90**,** 386-392.

MIYANO, T. & KLEIN, C. 1989. Phase equilibria in the system K2O-FeO-MgO-Al2O3-SiO2-H2O-CO2 and the stability limit of stilpnomelane in metamorphosed Precambrian iron-formations. *Contributions to Mineralogy and Petrology,* 102**,** 478-491.

MONTELIUS, C. 2005. The Genetic Relationship Between Rhyolitic Volcanism And Zn-Cu-Au Deposits In The Maurliden Volcanic centre, Skellefte District, Sweden. *PhD thesis, Luleå University of Technology, Sweden*.

MORRISS, P. A. & PIRAJNO, F. 2005. Mesoproterozoic sill complexes in the Bangemall Supergroup, Western Australia: geology geochemistry and mineralization potential. *Western Australia Geological Survey Report 99*.

MOUSIVAND, F., RASTAD, E., MEFFRE, S., PETER, J. M., SOLOMON, M. & ZAW, K. 2011. U–Pb geochronology and Pb isotope characteristics of the Chahgaz volcanogenic massive sulphide deposit, southern Iran. *International Geology Review,* 53**,** 1239-1262.

MUELLER, D. H. A. 2011. Final report on drilling of THD001, a 1017.8m vertical core hole of E52/1673 drilled pursuant to a funding agreement, Royalties for Regions, co-funded Government-Industry drilling program 2010/11, Application number DAG2010/00000021. *Geological Survey of Western Australia Reference C144/2005*.

MULLER, D. H. A. 2011. Final Report on drilling of THD001, a 1017.8m vertical core hole on E52/16783 drilled pursuant to a funding agreement, royalties for regions, co-funded government-industry drilling program 2010/11. *SIPA Resources NL Report GSWA Reference C144/2005*.

MYERS, J. S. 1993. Precambrian history of the Western Australian craton and adjacent orogens. *Annual Review of Earth and Planetary Sciences,* 21**,** 453-485.

MYERS, J. S., SHAW, R. D. & TYLER, I. M. 1996. Tectonic Evolution of Proterozoic Australia. *Tectonics,* 15**,** 1431-1446.

NELSON, D. R. 1997. Compilation of Shrimp U-Pb Zircon Geochronology Data, 1996. *Geological Survey of Western Australia Record 1997/2*.

OCCHIPINTI, S., GREY, K., PIRAJNO, F. & AL, E. 1997a. Stratigraphic revision of Palaeoproterozoic rocks of the Yerrida, Bryah and Padbury Basins (former Glengarry Basin). *Geological Survey of Western Australia Record 1997/3*.

OCCHIPINTI, S. A., GREY, K., PIRAJNO, F., ADAMIDES, N. G., BAGAS, L., DAWES, P. & LE BLANC SMITH, G. 1997b. Stratigraphic revision of the Palaeoproterozoic rocks of the Yerrida, Byah and Padbury Basins (former Glengarry Basin). *Geological Survey of Western Australia Record 1997/3*.

OCCHIPINTI, S. A. & MYERS, J. S. 1999. Geology of the Moorarie 1: 100 000 sheet. *Western Australia Geological Survey 1: 100 000 Geological Series Explanatory Notes***,** 20p.

OCCHIPINTI, S. A., MYERS, J. S. & SWAGER, C. P. 1998. Geology of the Padbury 1:100 000 Sheet Geological Survey of Western Australia. *Explanatory Notes* 1**,** 29p.

OCCHIPINTI, S. A., SHEPPARD, S., PASSCHIER, C., TYLER, I. M. & NELSON, D. R. 2004. Palaeoproterozoic crustal accretion and collision in the southern Capricorn Orogen: the Glenburgh Orogeny. *Precambrian Research,* 128**,** 237-255.

OHMOTO, H. 1996. Formation of volcanogenic massive sulfide deposits: The Kuroko perspective. *Ore Geology Reviews,* 10**,** 135-177.

OTTOLINI, L. P., RAFFONE, N., FRIDLEIFSSON, G. O., TONARINI, S., D'ORAZIO, M. & GIANELLI, G. 2012. A geochemical investigation of trace elements in well RN-17 at Reykjanes geothermal system, SW-Iceland. *EMAS 2011: 12th European Workshop on Modern Developments in Microbeam Analysis. IOP Conf. Series: Materials Science and Engineering,* 32**,** 1-39.

PAGE, R. W., STEVENS, B. P. J. & GIBSON, G. M. 2005. Geochronology of the sequence hosting the Broken Hill Pb-Zn-Ag orebody. *Australia. Econ. Geol.,* 100**,** 633-661.

PATON, C., WOODHEAD, J. D., HELLSTROM, J. C., HERGT, J., GREIG, A. & MAAS, R. 2010. Improved laser ablation U-Pb zircon geochronology through robust down-hole fractionation correction. *Geochemistry, Geophysics, Geosystems,* 11**,** 1525-2027.

PAVLOV, A. A. & KASTING, J. F. 2002. Mass-Independant Fractionation of Sulfur Isotopes in Archean Sediments: Strong Evidence for an Anoxic Archean Atmosphere. *Astrobiology,* 2**,** 27-41.

PEARCE, J. A. 1996. A user's guide to basalt discrimination diagrams. *In: Wyman, D. A. (ed.) Trace Element Geochemistry of Volcanic Rocks: Applications for Massive Sulphide Exploration. Geological Association of Canada, Short Course Notes 12***,** 79-113.

PEARCE, J. A. 2008. Geochemical fingerprinting of oceanic basalts with applications to ophiolite classification and the search for Archean oceanic crust. *Lithos,* 100**,** 14-48.

PEARCE, J. A. & CANN, J. R. 1973. Tectonic setting of basic volcanic rocks determined using trace element analyses. *Earth and Planetary Science Letters,* 12**,** 339-349.

PELTONEN, P., KONTINEN, A., HUHMA, H. & KURONEN, U. 2008. Outokumpu revisited: New mineral deposit model for the mantle peridotite-associated Cu–Co–Zn–Ni–Ag–Au sulphide deposits. *Ore Geology Reviews,* 33**,** 559-617.

PETER, J. M. & SCOTT, S. D. 1999. Windy Craggy, Northwestern British Columbia: The World's Largest Besshi-Type Deposit. *Reviews in Economic Geology,* 8**,** 261-296.

PETER, J. M. & SHANKS III, W. C. 1992. Sulfur, carbon, and oxygen isotope variations in submarine hydrothermal deposits of Guayams Basin, Gulf of California, USA. *Geochimica et Cosmochimica Acta,* 56**,** 2025-2040.

PETRUS, J. A. & KAMBER, B. S. 2012. VizualAge: a novel approach to laser ablation ICP-MSU–Pb geochronology data reduction. *Geostandards and Geoanalytic Research,* 36**,** 247-270.

PIERCEY, S. J., MORTENSEN, J. K., MURPHY, D. C., PARADIS, S. & CREASER, R. A. 2002. Geochemistry and tectonic significance of alkalic mafic magmatism in the Yukon-Tanana terrane, Finlayson Lake region, Yukon. *Canadian Journal of Earth Sciences,* 39**,** 1729-1744.

PIERCEY, S. J., MURPHY, D. C., MORTENSEN, J. K. & PARADIS, S. 2001. Boninitic magmatism in a continental margin setting, Yukon-Tanana terrane, southeastern Yukon, Canada. *Geology,* 29**,** 731-734.

PIERRE, S., JEBRAK, M., FAURE, S. & ROY, G. 2016. Depositional setting and structural evolution of the Archean Perseverance volcanogenic massive sulfide deposit, Matagami Mining District, Quebec, Canada. *Economic Geology,* 111.

PIRAJNO, F. 1996. Models for the geodynamic evolution of the Palaeoproterozoic Glengarry Basin Western Australia. *Geological Survey of Western Australia 1995-96 Annual Review*.

PIRAJNO, F. 2004. Oceanic plateau accretion onto the northwestern margin of the Yilgarn Craton, Western Australia. *Journal of Geodynamics,* 37**,** 205-231.

PIRAJNO, F. 2009. Hydrothermal Processes and Mineral Systems. *Springer SciencebBusiness Media B.V.***,** 1250.

PIRAJNO, F. & ADAMIDES, N. G. 1998. Geology of the Thaduna 1: 100 000 sheet. *Geological Survey of Western Australia 1: 100 000 Geological Series - Explanatory Notes*.

PIRAJNO, F. & ADAMIDES, N. G. 2000a. Geology and Mineralization of the Palaeoproterozoic Yerrida Basin Western Australia. *Geological Survey of Western Australia Report 60*.

PIRAJNO, F. & ADAMIDES, N. G. 2000b. Iron-manganese oxides and glauconite-bearing rocks of the Earaheedy Group: implications for the base metal potential of the Earaheedy Basin. *Geological Survey of Western Australia Technical Papers*.

PIRAJNO, F., ADAMIDES, N. G., OCCHIPINTI, S., SWAGER, C. P. & BAGAS, L. 1995. Geology and tectonic evolution of the Early Proterozoic Glengarry Basin Western Australia. *Geological Survey of Western Australia 1994-95 Annual Review*.

PIRAJNO, F., BAGAS, L., SWAGER, C. P., OCCHIPINTI, S. A. & ADAMIDES, N. G. 1996. A reappraisal of the stratigraphy of the Glengarry Basin, Western Australia. *Geological Survey of Western Australia 1995–96 Annual Review***,** 81-87.

PIRAJNO, F. & DAVY, R. 1996. Mafic volcanism in the Palaeoproterozoic Glengarry Basin, Western Australia, and implications for its tectonic evolution. *Abstracts - Geological Society of Australia,* 41**,** 343.

PIRAJNO, F. & GREY, K. 2002. Cherts in the Palaeoproterozoic Bartle Member, Killara Formation, Yerrida Basin, Western Australia: a rift-related playa lake and thermal spring environment. *Precambrian Research,* 113**,** 169-192.

PIRAJNO, F., JONES, J. A., HOCKING, R. M. & HALILOVIC, J. 2004. Geology and tectonic evolution of Palaeoproterozoic basins of the eastern Capricorn Orogen, Western Australia. *Precambrian Research,* 128**,** 315-342.

PIRAJNO, F. & OCCHIPINTI, S. 1998. Geology of the Bryah 1:100 000 map sheet. *Geological Survey of Western Australia Explanatory Notes***,** 41p.

PIRAJNO, F. & OCCHIPINTI, S. 2000. Three Palaeoproterozoic basins - Yerrida, Bryah and Padbury - Capricorn Orogen, Western Australia. *Australian Journal of Earth Sciences,* 47**,** 675-688.

PIRAJNO, F., OCCHIPINTI, S., SMITH, G. L. B. & ADAMIDES, N. 1994. Pillow lavas in the Peak Hill and Glengarry terranes. *Geological Survey of Western Australia 1993-94 Annual Review*.

PIRAJNO, F., OCCHIPINTI, S. A. & SWAGER, C. P. 2000. Geology and Mineralization of the Palaeoproterozoic Bryah and Padbury Basins Western Australia. Geological Survey of Western Australia Report 59.

PONTIFEX, I. R. 2009. Mineralogical Report No. 9556 (SAN00019949). *Internal Sandfire Report*.

POULTON, S. W., FRALICK, P. W. & CANFIELD, D. E. 2004. The transition to a sulphidic ocean ~ 1.84 billion years ago. *Nature,* 431**,** 173-177.

RASMUSSEN, B. & FLETCHER, I. R. 2002. Indirect dating of mafic intrusions by SHRIMP U-Pb analysis of monazite in contact metamorphosed shale: an example from the Palaeoproterozoic Capricorn Orogen Western Australia. *Earth and Planetary Science Letters,* 197**,** 287-299.

RASMUSSEN, B., FLETCHER, I. R., BEKKER, A., MUHLING, J. R., GREGORY, C. J. & THORNE, A. M. 2012. Deposition of 1.88-billion-year-old iron formations as a consequence of rapid crustal growth. *Nature,* 484**,** 498-501.

REID, D. 2013a.

REID, D. 2013b. *RE: Personal communication, re. mineralogy of the Thaduna copper mine (Ventnor Resources Geologist).*

RELVAS, J. M. R. S., TASSINARI, C. C. G., MUNHA, J. & BARRIGA, F. J. A. S. 2001. Multiple sources for ore-forming fluids in the Neves Corvo VHMS Deposit of the Iberian Pyrite Belt (Portugal): strontium, neodymium and lead isotope evidence. *Mineralium Deposita,* 36**,** 416-427.

RICHARDS, J. R. & GEE, R. D. 1985. Galena lead isotopes from the eastern part of the Nabberu Basin, Western Australia. *Australian Journal of Earth Sciences,* 32**,** 47-54.

RICKARD, D. & SVENSSON, S.-A. 1984. Ore lead isotope variations in the Proterozoic massice pyrite deposit at Nasliden, Skellefte District, Sweden. *Mineralium Deposita,* 19**,** 145-151.

ROADHOUSE, R. 2012. *Ventnor Resources enters Dragon Territory* [Online]. Available: http://www.resourcesroadhouse.com.au/_blog/Resources_Roadhouse/post/Ventnor_Resources_enters_Dragon_country/ [Accessed 22/09/2015].
ROLLINSON, H. 2013. *Using geochemical data: Evaluation, Presentation, Interpretation*, Routledge.
ROWE, R. J., AWAN, A. W., MCCUAIG, T. C., SAUTER, P. C. & VICKERY, N. M. 2002. Structural Geology of the Plutonic Gold Mine. *Applied Structural Geology for Mineral Exploration and Mining International Symposium, Kalgoorlie, WA*, 180–185.
RUSSELL, J. 1992. Investigation of the potential of Pb-Pb radiometric dating for the direct age determination of carbonates. *Ph.D. thesis, Oxford University*.
RYE, R. O. & OHMOTO, H. 1974. Sulfur and carbon isotopes and ore genesis: A review. *Economic Geology,* 69, 826-842.
SACK, P. J., BERRY, R. F., MEFFRE, S., FALLOON, T. J., GEMMELL, J. B. & FRIEDMAN, R. M. 2011. In situ location and U–Pb dating of small zircon grains in igneous rocksusing laser ablation-inductively coupled plasma-quadrupole mass spectrometry. *Geochemistry Geophysics Geosystems,* 12.
SANGSTER, D. F. 1968. Relative suphur isotope abundances of ancient seas and stratabound sulphide deposits. *Geological Association of Canada Procedings,* 17, 79-91.
SANGSTER, D. F. 1972. Isotopic studies of Ore-leads in the Hanson Lake-Flin Flon-Snow Lake mineral belt, Saskatchewan and Manitoba. *Canadian Journal of Earth Sciences,* 9, 500-513.
SATO, K. & SASAKI, A. 1980. Lead isotope feature of the Besshi-type deposits and its bearing on the ore lead evolution. *Geochemical Journal,* 14, 303-315.
SCHER, S., WILLIAMS-JONES, A. E. & WILLIAMS-JONES, G. 2013. Fumarolic activity, acid sulfate alteration, and high sulfidation epithermal precious metal mineralization in the crater of Kawah Ijen volcano, Java, Indonesia. *Economic Geology,* 108, 1099-1118.
SCHRÖDER, S., BEKKER, A., BEUKES, N. J., STRAUSS, H. & VAN NIEKERK, H. S. 2008. Rise in seawater sulphate concentration associated with the Paleoproterozoic positive carbon isotope excursion: evidence from sulphate evaporites in the ~2.2–2.1 Gyr shallow-marine Lucknow Formation, South Africa. *Terra Nova,* 20, 108-117.
SCOTT, C., WING, B. A., BEKKER, A., PLANAVSKY, N. J., MEDVEDEV, P., BATES, S. M., YUN, M. & LYONS, T. W. 2014. Pyrite multiple-sulfur isotope evidence for rapid expansion and contraction of the early Paleoproterozoic seawater sulfate reservoir. *Earth and Planetary Science Letters,* 389, 95-104.
SHANKS III, W. C. & THURSTON, R. 2012. Volcanogenic massive sulfide occurrence model. *US Geological Survey Scientific Investigations Report 2010-5070*, 345.
SHARPE, R. 1999. The Archean Cu-Zn magnetite-rich Gossan Hill VHMS deposit, Western Australia: Evidence of a structurally-focussed, exhalative and sub-seafloor replacement mineralising system. *PhD thesis, University of Tasmania*.
SHARPE, R. & GEMMELL, J. B. 2000. Sulfur isotope characteristics of the Archean Cu-Zn Gossan Hill VHMS deposit, Western Australia. *Miner Deposita,* 35, 533-550.
SHEPPARD, S., JOHNSON, S. P., WINGATE, M. T. D., KIRKLAND, C. L. & PIRAJNO, F. 2010. Explanatory Notes for the Gascoyne Province: Geological Survey of Western Australia. 336p.
SHEPPARD, S., OCCHIPINTI, S. A. & NELSON, D. R. 2005. Intracontinental reworking in the Capricorn Orogen Western Australia the 1680-1620Ma Mangaroon Orogeny. *Australian Journal of Earth Sciences,* 52, 443-460.
SHEPPARD, S., OCCHIPINTI, S. A. & TYLER, I. M. 2004. A 2005-1970 Ma Andean-type batholith in the southern Gascoyne Complex, Western Australia. *Precambrian Research,* 128, 257-277.
SHEPPARD, S., RASMUSSEN, B., MUHLING, J. R., FERRELL, T. R. & FLETCHER, I. R. 2007. Grenvillian-ages orogenesis in the Palaeoproterozoic Gascoyne Complex, Western Australia: 1030-950 Ma reworking of the Proterozoic Capricorn Orogen. *Journal of Metamorphic Geology,* 25, 477-494.
SHERVAIS, J. W. 1982. Ti-V plots and the petrogenesis of modern and ophiolitic lavas. *Earth and Planetary Science Letters,* 59, 101-118.
SHIKAZONO, N. 2003. Geochemical and Tectonic Evolution of Arc-Backarc Hydrothermail Systems: Implication for the origin of Kuroko and epithermal vein-type mineralizations and the global geochemical cycle. *Elsevier*.
SIPA. 2015. *Thaduna Copper Project* [Online]. Available: http://www.sipa.com.au/thaduna.html [Accessed 22/09/2015].
SLACK, J. F. & CANNON, W. F. 2009. Extraterrestrial demise of banded iron formations 1.85 billion years ago. *Geology,* 37, 1011-1014.
SLACK, J. F., GRENNE, T., BEKKER, A., ROUXEL, O. J. & LINDBERG, P. A. 2007. Suboxic deep seawater in the late Paleoproterozoic: Evidence from hematitic chert and iron formation related to seafloor-

hydrothermal sulfide deposits, central Arizona, USA. *Earth and Planetary Science Letters,* 255**,** 243-256.
SLACK, J. F., SHANKS III, W. C., KARL, S. M., GEMERY, P. A., BITTENBENDER, P. E. & RIDLEY, W. I. 2005. Geochemcial and sulfur-isotopic signatures of volcanogenic massive sulfide deposits on Prince of Wales Island and Vicinity, Southeastern Alaska. *US Geological Survey Professional Paper,* 1732-C.
SLÁMA, J., KOŠLER, J., CONDON, D. J., CROWLEY, J. L., GERDES, A., HANCHAR, J. M., HORSTWOOD, M. S. A., MORRIS, G. A., NASDALA, L., NORBERG, N., SCHALTEGGER, U., SCHOENE, B., TUBRETT, M. N. & WHITEHOUSE, M. J. 2008. Plešovice zircon - a new natural reference material for U-Pb and Hf isotopic microanalysis. *Chemical Geology,* 249**,** 1-35.
SMITH, W. H. F. & SANDWELL, D. T. 1997. Global Seafloor Topography from Satellite Altimetry and Ship Depth Soundings. *Science,* 277**,** 1956-1962.
SPENCE, G. H. & TUCKER, M. E. 1997. Genesis of limestone megabreccias and their significance in carbonate sequence stratigraphic models. *Sedimentary geology,* 112**,** 163-163.
STACEY, J. S. & KRAMERS, J. D. 1975. Approximation of Terrestrial Lead Isotope Evolution by a Two-stage model. *Earth and Planetary Science Letters,* 26**,** 207-221.
STANTON, R. L. 1994. *Ore elements in arc lavas,* Oxford, Clarendon Press.
STANTON, R. L. 2015a. The 'orogenic andesite' puzzle of C. E. TIlley: 1 - Is the volatile phase the missing piece? *Australian Journal of Earth Sciences,* 62**,** 625-641.
STANTON, R. L. 2015b. The 'orogenic andesite' puzzle of C. E. Tilley: 2 - Some exploratory experiments and their possible implications. *Australian Journal of Earth Sciences,* 62**,** 643-655.
STEADMAN, J. A., LARGE, R. R., MEFFRE, S., OLIN, P. H., DANYUSHEVSKY, L., GREGORY, D. D., BELOUSOV, E., IRELAND, T. R. & HOLDEN, P. 2015. Synsedimentary to early diagenetic gold in black shale-hosted pyrite nodules at the Golden Mile Deposit, Kalgoorlie, Western Australia. *Economic Geology,* 110**,** 1-35.
STEIN, H. J. 2006. Low-rhenium molybdenite by metamorphism in northern Sweden: Recognition, genesis, and global implications. *Lithos,* 87**,** 300-327.
STEIN, H. J., MARKEY, R. J., MORGAN, J. W., HANNAH, J. L. & SCHERSTEN, A. 2001. The remarkable Re-Os chronometer in molybdenite: how and why it works. *Terra Nova,* 13**,** 479-486.
STRAUSS, H. 1993. The sulfur isotopic record of Precambrian sulfates: new data and a critical evaluation of the existing record. *Precambrian Research,* 63**,** 225-246.
TALBOT, H. W. B. & FARQUHARSON, R. A. 1920. Geology and Mineral Resources of the North-West, Central and Eastern Divisions. *Geological Survey of Western Australia Bulletin No. 83*.
TAYLOR, E. & HASTINGS, N. 2015. *Sandfire Resources NL Reserves and Resources* [Online]. Available: http://www.sandfire.com.au/ [Accessed 27/02/2015].
THORNETT, S. 1995. The nature, origin and timing of gold mineralisation in Proterozoic rocks of the Peak Hill District, Western Australia. *Thesis (M.Sc.) University of Western Australia*.
THORPE, R. I. 1999. The Pb isotope linear array for volcanogenic massive sulfide deposits of the Abitibi and Wawa subprovinces, Canadian Shield. *Economic Geology Monograph 10*.
TORMANEN, T. O. & KOSKI, R. A. 2005. Gold enrichment and the Bi-Au association in pyrrhotite-rich massive sulfide deposits, Escanaba Trough, Southern Gorda Ridge. *Economic Geology,* 100**,** 1135-1150.
TOWNSEND, A. T., YU, Z., MCGOLDRICK, P. & HUTTON, J. A. 1998. Precise lead isotope ratios in Australian galena samples by high resolution inductively coupled plasma mass spectrometry. *Journal of Analytical Atomic Spectrometry,* 13**,** 809-813.
TRAIL, D., WATSON, E. B. & TAILBY, N. D. 2011. The oxidation state of Haden magmas and implications for early Earht's atmosphere. *Nature,* 480**,** 79-83.
TYLER, I. M. & THORNE, A. M. 1990. The northern margin of the Capricorn Orogen, Western Australia - an example of an early Proterozoic collision zone. *Journal of Structural Geology,* 12**,** 685-701.
UEDA, A., CAMERON, E. M. & KROUSE, H. R. 1990. 34S-enriched sulphate in the Belcher Group, N. W. T., Canada: evidence for dissimilatory sulphate reduction in the early Proterozoic ocean. *Precambrian Research,* 49**,** 229-233.
VAASJOKI, M. 1985. The Teutonic Bore deposit, Western Australia: a lead isotope study of an ore and its gossan. *Mineralium Deposita,* 20**,** 266-270.
VANDERWOOD, T. B. & THIEMENS, M. H. 1980. The fate of hydroxyl radical in the earth's primitive atmosphere and implications for the production of molecular-oxygen. *Journal of Geophysical Research - Oceans and Atmospheres,* 85**,** 1605-1610.
VEARNCOMBE, S., BARLEY, M. E., GROVES, D. I., MCNAUGHTON, N. J., MIKUCKI, E. J. & VEARNCOMBE, J. R. 1995. 3.26 Ga black smoker-type mineralization in the Strelley Belt, Pilbara Craton, Western Australia. *Journal of the Geological Society, London,* 152**,** 587-590.

VIELREICHER, N. & MCNAUGHTON, N. 2002. SHRIMP U-Pb geochronology of magmatism and thermal events in the Archaean Marymia Inlier, central Western Australia. *International Journal of Earth Sciences,* 91**,** 406-432.

VIELREICHER, N., RIDLEY, J. & GROVES, D. 2002. Marymia: an Archean, amphibolite facies-hosted, orogenic lode-gold deposit overprinted by Palaeoproterozoic orogenesis and base metal mineralisation, Western Australia. *Mineralium Deposita,* 37**,** 737-764.

WAGNER, T., BOYCE, A. J., JONSSON, E. & FALLICK, A. E. 2004. Laser microprobe sulphur isotope analysis of arsenopyrite: experimental calibration and application to the Boliden Au-Cu-As massive sulphide deposit. *Ore Geology Reviews,* 25**,** 311-325.

WATTS, K. F. 1990. Mesozoic carbonate slope facies marking the Arabian platform margin in Oman: depositional history, morphology and palaeogeography. *The Geology and Tectonics of the Oman Region, Geological Society Special Publication,* 49**,** 139-159.

WIEDENBECK, M., ALLE, P., CORFU, F., W.L., G., MEIER, M., OBERLI, F., A., V., RODDICK, J. C. & W., S. 1995. 3 Natural Zircon Standards for U-Th-Pb, Lu-Hf, Trace-Element and REE Analyses. *Geostandards Newsletter,* 19**,** 1-23.

WILLIAMS-JONES, A. E. & HEINRICH, C. A. 2005. 100th Anniversary special paper: Vapour transport of metals and the formation of magmatic-hydrothermal ore deposits. *Economic Geology,* 100**,** 1287-1312.

WILLIAMS, N. C. & DAVIDSON, G. J. 2004. Possible submarine advanced argillic alteration at the Basin Lake prospect, Western Tasmania, Australia. *Economic Geology,* 99**,** 987–1002.

WILLIFORD, K. H., VAN KRANENDONK, M. J., USHIKUBO, T., KOZDON, R. & VALLEY, J. W. 2011. Constraining atmospheric oxygen and seawater sulfate concentrations during Paleoproterozoic glaciation: In situ sulfur three-isotope microanalysis of pyrite from the Turee Creek Group, Western Australia. *Geochimica et Cosmochimica Acta,* 75**,** 5686-5705.

WILSON, M. 1989. Igneous petrogenesis. *Unwin Hyman, London*.

WINCHESTER, J. A. & FLOYD, P. A. 1977. Geochemical discrimination of different magma series and their differentiation products using immobile elements. *Chemical Geology,* 20**,** 325-343.

WINDH, J. 1992. Tectonic evolution and metallogensis of the Early Proterozoic Glengarry Basin, Western Australia. *Thesis (Ph.D.), University of Western Australia*.

WOODHEAD, J. 2002. A simple method for obtaining highly accurate Pb isotope data by MC-ICP-MS. *Journal of Analytical Atomic Spectrometry,* 17**,** 1381-1385.

WOODHEAD, J., HERGT, J., MEFFRE, S., LARGE, R. R., DANYUSHEVSKY, L. & GILBERT, S. 2009. In situ Pb-isotope analysis of pyrite by laser ablation (multi-collector and quadrupole) ICPMS. *Chemical Geology,* 262**,** 380-390.

WOODHEAD, J. D. & HERGT, J. M. 1997. Application of the 'double spike' technique to Pb-isotope geochronology. *Chemical Geology,* 138**,** 311-321.

WRIGHT-HOLFELD, A., MERCIER-LANGEVIN, P. & DUBÉ, B. 2010. Contrasting Alteration Mineral Assemblages Associated With The Westwood Deposit Ore Zones, Doyen-Bousquet-LaRonde Mining Camp Abitibi, Quebec. *Geological Survey of Canada, Current Research 2010-9***,** 1-24.

XIAO, Z., GAMMONS, C. H. & WILLIAMS-JONES, A. E. 1998. Experimental study of copper(I) chloride complexing in hydrothermal solutions at 40 to 300C and saturated water vapor pressure. *Geochimica et Cosmochimica Acta,* 62**,** 2949-2964.

YUI, S. 1983. Textures of Some Japanese Besshi-Type Ores and Their Implications for Kuroko Deposits. *Economic Geology,* Monograph 5**,** 231-240.

ZARTMAN, R. E. & DOE, B. R. 1981. Plumbotectonics - the model. *Tectonophysics,* 75**,** 135-162.

ZI, J., RASMUSSEN, B., MUHLING, J. R., FLETCHER, I. R., THORNE, A. M., JOHNSON, S. P., CUTTEN, H. N., DUNKLEY, D. J. & KORHONEN, F. J. 2015. In situ U-Pb geochronology of xenotime and monazite from the Abra polymetallic deposit in the Capricorn Orogen, Australia: Dating hydrothermal mineralisation and fluid flow in a long-lived crustal structure. *Precambrian Research,* 260**,** 91-112.

ZIERENBERG, R. A., SHANKS III, W. C., SEYFRIED JR., W. E., KOSKI, R. A. & STRICKLER, M. D. 1988. Mineralisation, alteration and hydrothermal metamorphism of the ophiolite-hosted Turner-Albright sulfide deposit, southwestern Oregon. *Journal of Geophysical Research,* 93**,** 4657-4674.

11. Appendices

3.1.	Thin section descriptions	(Digital)
3.2.	Cross sections	(Digital)
3.3.	Drill hole logs	(Digital)
3.4.	Terraspec analysis	(Digital)
3.5.	QXRD	(Digital)
4.1.	Downhole assay data (Sandfire Resources)	(Digital)
4.2.	Drill hole logs – stringer zone.	(Digital)
4.3.	DeGrussa deposit graphic logs	(Digital)
4.4.	Core photos	(Digital)
4.5.	Alteration box plots	(Digital)
4.6.	Selected assay data from DeGrussa section 733800 and other mineralised drill holes for downhole assay interpretation.	(Digital)
5.1.	Geochemical Data (all compiled)	(Digital)
5.2.	DeGrussa assay data collected for this study	(Digital)
5.3.	GSWA geochemistry for the Narracoota and Killara Formations and boninite Analysis	(Digital)
5.4.	Narracoota Formation REE comparison with world locations	(Digital)

Appendix 6.1. Deposit locations referred to in the text. All coordinates in GDA_94, Zone 50.					
Deposit	**Commodity**	**Easting (mE)**	**Northing (mN)**	**Latitude (S)**	**Longitude (E)**
DeGrussa	Cu-Au	734151	7173265	-25°, 32', 22"	119°, 19', 49"
Horseshoe Lights	Cu-Au	662788	7194047	-25°,21',41.117''	118°, 37, .4.197''
Nathans (Deep south mine)	Au	631853	7198965	-25°, 19', 12.268''	118°, 18', 35.947''
Fortnum	Au	636512	7197780	-25°, 19', 49.275''	118°, 21', 22.978''
Trevs/Starlight	Au	636552	7199040	-25°, 19', 8.31''	118°, 21', 23.952''
Yarlarwheelor	Au	636863	7196576	-25°, 20', 28.291''	118°, 21', 35.968''
Peak Hill (opencut)	Au	672330	7163156	-25°, 38', 21.054''	118°, 42', 59.736''
Mt. Pleasant	Au	674427	7162053	-25°, 38', 56.007''	118°, 44', 15.427''
Fiveways	Au	672368	7163416	-25°, 38', 12.612''	118°, 43', 0.962''
Horseshoe/Cassidy	Au	661359	7183130	-25°, 27', 36.439''	118°, 36', 17.789''
Mikhaburra	Au	656392	7130549	-25°, 56', 7.075''	118°, 33', 42.243''
Labouchere	Au	627870	7204863	-25°, 16', 1.814''	118°, 16', 11.518''
Thaduna Copper	Cu	772872	7176217	-25°, 30', 22.225''	119°, 42', 52.937''

Appendix 6.2.

U-Pb Zircon Methods: The LA-ICPMS method is now widely used for measuring U, Th and Pb isotopic data (e.g. Kosler and Sylvester (2003), Black et al. (2004), Jackson et al. (2004), Chang et al. (2006), Harley and Kelly (2007), Fryer et al. (1993), Compston (1999), Black et al. (2003). Approximately 100g of rock was repeatedly sieved and crushed in a Cr-steel ring mill to a grain size <400 micron. Non-magnetic heavy minerals were then separated using a gold pan and a Fe-B-Nd hand magnet. The zircons were hand-picked from the heavy mineral concentrate under the microscope in cross-polarised transmitted light. The selected crystals were placed on double sided sticky tape and epoxy glue was then poured into a 2.5 cm diameter mould on top of the zircons. The mount was dried for 12 hours and polished using clean sandpaper and a clean polishing lap. The samples were then washed in distilled water in an ultrasonic bath.

Analysis, data reduction and reproducibility are as per Halpin et al. (2014): U–Pb zircon analyses were performed on an Agilent 7500csquadrupole ICPMS with a 193 nm Coherent Ar–F gas laser and the Resonetics S155 ablation cell at the School of Earth Sciences, University of Tasmania. Each analysis was pre-ablated with 5 laser pulses to remove the surface contamination then the blank gas was analysed for 30 s followed by 30 s of zircon ablation at 5 Hz and ~2 J/cm2using a spot size of 32 μm; keeping U and Th in the pulse counting mode of detection on the electron multiplier. Representative analyses of the sedimentary matrix (mean values, n ≥ 3) were carried out under the same conditions with a spot size of 80–110 μm for common Pb corrections (see below). A flow of He carrier gas at a rate of 0.35 l/min carried particles ablated by the laser out of the sample chamber to be mixed with Ar gas before transfer to the plasma. Elements measured include 49Ti, 56Fe, 90Zr, 178Hf, 202Hg, 204Pb, 206Pb, 207Pb, 208Pb, 232Th and 238U with each element being measured sequentially every 0.16 s with longer counting time on the Pb isotopes compared to the other elements.. The down hole fractionation, instrument drift and mass bias correction factors for Pb/U and Pb/Th ratios on zircons were calculated using two analyses on the primary standard (91500 of Wiedenbeck et al. (1995) and one analysis on each of the secondary standard zircons (TEMORA 1 of Black et al. (2003); GJ-1 of Jackson et al. (2004)

analysed at the beginning of the session and every 16 unknowns using the same spot size and conditions as used on the samples to provide an independent control to assess accuracy and precision. Additional secondary zircon standards (Mud Tank of Black and Gulson (1978); Plešovice of Sláma et al. (2008) were also analysed. The correction factor for the 207Pb/206Pb ratio was calculated using six analyses of the international glass standard NIST610 analysed throughout analytical session and corrected using the values recommended byBaker et al. (2004).

Data reduction and reproducibility: All data reduction calculations and error propagations were done within Microsoft Excel® via Macros designed at the University of Tasmania using techniques summarized by Meffre et al. (2008) and Sack et al. (2011). Element abundances were calculated using Zr as the internal standard element for zircon, assuming stoichiometric proportions and using the NIST610 standard to correct for mass bias and drift. Interrogation of time-resolved signals allowed for identification of isotopic heterogeneity within the ablation volume. Time-resolved isotopic ratios for each analysis were scrutinised on Concordia diagrams to investigate the presence of common Pb and/or ancient Pb-loss and/or mixing of age zones, and analyses (or parts of analyses) were excluded from the dataset where a combination of these trends was detected. This approach is similar to that outlined by Petrus and Kamber (2012). Uncertainties were calculated using similar techniques to those outlined by Paton et al. (2010). Unlike Paton et al. (2010), the variance on the secondary standards is taken into account when calculating the "excess uncertainty", calculated via a 206Pb/238U ages for the secondary monazite standards MB35 and N3364-1.5m over the course of this study are 501.1 ± 3.3 Ma (n = 16, MSWD = 1.5) and 1585.1 ± 8.6 Ma (n = 11, MSWD = 1.14), within error of the reference ages of 507 ± 5 Ma (S. Meffre, unpublished data) and 1599 ± 9 Ma(Page et al., 2005), respectively. Tera-Wasserburg diagrams, probability density plots and age calculations were made using Isoplot v3.1(Ludwig, 2003).

Element abundances on zircons were calculated using the method outlined by Kosler (2001) using Zr as the internal standard element, assuming stoichiometric proportions and using the 91500 to standard correct for mass bias.

Re-Os Molybdenite Method: Because of the fine grained nature of the molybdenite mineralisation, in all but one sample assay data was used to distinguish zones of anomalous Mo, Re and Os as well as visual inspection of the core. Six samples were submitted to Dr. Holly Stein at the University of Colorado for Rhenium (Re)-Osmium (Os) dating. Samples were processed as per Stein (2006): Analyses were made using a single ^{190}Os spike plus a separate ^{185}Re spike or a double Os spike, as a mixed ^{185}Re–^{188}Os–^{190}Os solution (Table 6.2). For all samples, a Carius tube digestion was employed, where molybdenite is dissolved and equilibrated with spike in HNO_3–HCl (inverse aqua regia) by sealing in a thick-walled glass ampoule and heating for 12 hours at 230˚C. Following digestion, Os is recovered by distilling directly from the Carius tube aqua regia into HBr, and is subsequently purified by microdistillation. Re is recovered by anion exchange. Re and Os are loaded onto Pt filaments and isotopic compositions are determined using NTIMS on NBS 12-inch radius, 688 and 908 sector mass spectrometers at Colorado State University. Two in-house molybdenite standards, calibrated at AIRIE, are run routinely as an internal check. Blanks, their Os isotopic compositions, and associated uncertainties are routinely monitored. The MDID data reported in Table 6.2 are blank-corrected for jusRe=1.16F0.024 pg, total Os =1.9F0.1 pg, and 187Os/ 188Os=0.24F 0.01. The earlier CT runs have somewhat higher associated blanks, but in no instance was the blank significant to the calculated ages. For example, using the lowest Re sample (AL4) and our largest blank correction, the Re–Os age is changed by 0.5 m.y., well within the reported F6–7 m.y. analytical errors that include the 187Re decay constant uncertainty. Inclusion of the decay constant uncertainty allows direct comparison of Re–Os ages to ages determined by other isotopic systems (e.g., U–Pb).

Pb-Pb Galena Method (LA ICP MS): Analysis was completed as per Townsend et al. (1998) with the only exception being that the analysis was performed on a new ELEMENT 2 high resolution ICP-MS compared with the original ELEMENT 1 ICP-MS specified (A. Townsend, pers. comm., 2011).

The Pb isotopic analyses from galena were analysed using the quadrupole ICPMS at the University of Tasmania using a method similar to that outlined in Meffre et al. (2008) and Woodhead et al. (2009).

The analyses in this study were performed on an Agilent 7700 quadrupole ICPMS with a 193 nm excimer laser and the S155 laser ablation systems from Resonetics. The instrument drift and mass bias correction factors were calculated using 1 or 2 analyses on the primary Broken Hill galena standard (values from Townsend et al. (1998)) analysed roughly 30 min with extra standards at the beginning and end of the run. The results were checked using in house secondary standards analysed with the samples

Each analysis on the galena began with a 10 second blank gas measurement followed by a further 80 seconds of analysis time when the laser was switched on. Galenas were sampled on 17 micron spots using the laser at 3 Hz and a density of approximately 1.7 J/cm2. A flow of He carrier gas at a rate of 0.8 litres/minute carried particles out of the ablation crater to be mixed with Ar gas and carried to the plasma torch. Elements measured were ^{107}Ag, ^{202}Hg, ^{204}Pb, ^{206}Pb, ^{207}Pb, ^{208}Pb, ^{232}Th and ^{238}U with each element being measured for 5 ms with the exception of ^{204}Pb which was measured for 10 ms. The data reduction used was based on the method outlined in detail in Meffre et al. (2008) and Woodhead et al. (2009) and the isoplot software of Ludwig (2003).

Pb-Pb Pyrite Method: The Pb isotopic composition of the pyrite was determined using the quadrupole ICPMS methods similar to those used by Meffre et al. (2008) and Woodhead et al. (2009), with additional changes to obtain better precision. The method involved analysing pyrite Resonetics S155 laser ablation system coupled with an excimer 193 nm laser. Spot size and ablation conditions varied from 30 to 100 μm depending on Pb concentration. Previous experiments by Woodhead et al. (2009) have shown that changing spot size has no discernible effects on the measured Pb isotopic ratios so the spot size was adjusted to achieve count rates between 1 x10^4 and 4 x 10^6 counts per second. At very low count rates the isobaric interference

on ^{204}Hg become too large to achieve reasonable precision on ^{204}Pb. At very high count rates the electron multipliers on the Agilent 7700 quadrupole ICPMS change from pulse to analogue mode making the Pb isotopic ratios less accurate. Experiments performed prior to this study have shown that accuracy is improved if all the Pb isotopes are measured only in normal pulse mode, rather than using mixed pulse and analogue modes. All of the analyses were performed in spot mode to obtain the smoothest possible signal.

The laser repetition rate of 10Hz and a fluence of 2.5 Jcm^{-2} were used together with a mixing manifold in the interface between the laser and ICPMS to provide a smooth signal. A smooth signal is very important to achieve good precision on the quadrupole instrument as each Pb isotope is measured sequentially. If the signal varies significantly in the few milliseconds between the measurements of the two isotopes then the ratio will scatter significantly. Signal quality on the ratios on heterogeneous material can be improved by dwelling only a short period on each isotope. In this study we have used 5 ms on all isotopes (^{202}Hg, ^{206}Pb, ^{207}Pb, ^{208}Pb, ^{232}Th, ^{238}U) with the exception of ^{204}Pb where 10 ms was used to improve precision on the low signal. Additional elements were also used either to monitor that a pyrite mineral was being analysed throughout (Al, Cu, and Fe) or to look for zoning in the crystals (As). These were analysed for 2 ms. When analysing using these parameters the quadrupole sweeps through the mass range every 90 ms (including dead time) producing between 560-replicate measurements for each individual 50 s ablation (excluding blank gas measurement).

Background gas measurements were generally kept short (10s) as the Pb isotope signal intensity (1 x10^4 and 2 x 10^6 counts per second required for reasonable precision) makes the 5-15 counts per second background count rate on the Pb isotopes insignificant. The background measurements are mostly for the Hg isobaric correction on ^{204}Pb and 10 seconds of measurement was found to be sufficient for this purpose.

A further innovation used to improve signal quality was the use of particle filters in the interface to remove spikes in the signal. These spikes are caused by larger particles that flash in the plasma for a few milliseconds and cause a single isotope to be elevated above the others. The

particle filter used is very simple and was modified from Guillong et al. (2003). The filter consisted of a narrow (1 mm inside diameter) tygon tube wound 4 to 6 times around a 10 mm diameter cylinder (a pen lid). The device removes an estimated 75% of the spikes in the signal with only a small drop (5-10%) in the count rates. To minimise the potential for contamination the tygon tube is changed every day.

Instrumental mass bias and drift were corrected by a polynomial regression of the standard data for the entire day. The NIST610 glass was used as the primary standard using the reference values from Woodhead (2002). A range of published and unpublished secondary matrix matched standards were also used in every analytical run. The secondary standards used were the pyrite nodule from the Jaguar deposit in Western Australia (sample 700380 with reference values from Woodhead et al. (2009), Chatree pyrite (2625-291.6m, reference value unpublished solution multi-collector ICPMS from University of Melbourne) and the GSD1G glass (preferred values from GEOREM data base georem.mpch-mainz.gwdg.de)

Between 9 spots were analysed on each of the three mounts with each spots or lines analysed for 50s. The measurements were averaged for each sample using the weighted average function of the Isoplot software of Ludwig (2003). Typical precision on the Pb isotopic ratios at 2 sigmas is generally between 0.2%. Accuracy on the secondary standards was found to be within the range expected from the statistical analysis of the data with less than 1 in every 20 weighted average ratio falling outside the 95% confidence level relative to the reference values (see stds data sheet).

6.3.	U-Pb geochronological data	(Digital)
6.4.	Terra-Wasserberg plots for U-Pb geochronology	(Digital)
6.5.	Pb isotope data	(Digital)
6.6.	Sample locations referred to in the text	(Digital)
7.1.	Laser map data (cps) and images for high, medium and low dolerite samples from DeGrussa.	(Digital)
7.2.	Dolerite sample laser maps and data in ppm	(Digital)
7.3.	SEM analysis, reports and images.	(Digital)
7.4.	Chemical data for minerals within dolerites from SEM analysis with identification	(Digital)
7.5.	A. Sulfur isotope data for sulfide minerals,	(Digital)
	B. Sulfur isotope data for DeGrussa barite.	(Digital)
7.6.	Locations of sulfur isotope collection from rock samples/thin section offcuts.	(Digital)
7.7.	Sulfur isotope analytical methods	(Digital)
7.8.	Compilation of worldwide Pb isotope data.	(Digital)